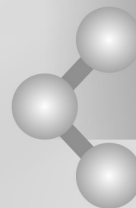


BIBLIOGRAFIA

- D. A. Skoog, D.M. West, F. J. Holler, S. R. Crouch, "Fundamentals of Analytical Chemistry" (9th ed.), Brooks/Cole, Belmont, 2014
- D. Harvey, "Modern Analytical Chemistry", McGraw-Hill, 2000
- J. R. Lakowicz, "Principles of Fluorescence Spectroscopy" (3rd ed.), Springer, Singapore, 2006
- B. Valeur and M. N. Berberan-Santos, "Molecular Fluorescence" (2nd ed.), Wiley-VCH, Singapore, 2012
- P. J. Larkin, "IR and Raman Spectroscopy: Principles and Spectral Interpretation", Elsevier, USA, 2011
- B. Stuart, "Infrared Spectroscopy: Fundamental and Applications", Wiley, Chichester, 2004
- E. Smith and G. Dent, "Modern Raman Spectroscopy: a practical approach", Wiley, Chippenham, 2005
- P. Vandenabeele, "Practical Raman Spectroscopy – An Introduction", Wiley, Chichester, 2013

Chapter 10



Spectroscopic Methods of Analysis

Before the beginning of the twentieth century most quantitative chemical analyses used gravimetry or titrimetry as the analytical method. With these methods, analysts achieved highly accurate results, but were usually limited to the analysis of major and minor analytes. Other methods developed during this period extended quantitative analysis to include trace level analytes. One such method was colorimetry.

One example of an early colorimetric analysis is Nessler's method for ammonia, which was first proposed in 1856. Nessler found that adding an alkaline solution of HgI_2 and KI to a dilute solution of ammonia produced a yellow to reddish brown colloid with the color determined by the concentration of ammonia. A comparison of the sample's color to that for a series of standards was used to determine the concentration of ammonia. Equal volumes of the sample and standards were transferred to a set of tubes with flat bottoms. The tubes were placed in a rack equipped at the bottom with a reflecting surface, allowing light to pass through the solution. The colors of the samples and standards were compared by looking down through the solutions. Until recently, a modified form of this method was listed as a standard method for the analysis of ammonia in water and wastewater.¹

Colorimetry, in which a sample absorbs visible light, is one example of a spectroscopic method of analysis. At the end of the nineteenth century, spectroscopy was limited to the absorption, emission, and scattering of visible, ultraviolet, and infrared electromagnetic radiation. During the twentieth century, spectroscopy has been extended to include other forms of electromagnetic radiation (photon spectroscopy), such as X-rays, microwaves, and radio waves, as well as energetic particles (particle spectroscopy), such as electrons and ions.²

10A Overview of Spectroscopy

The focus of this chapter is photon spectroscopy, using ultraviolet, visible, and infrared radiation. Because these techniques use a common set of optical devices for dispersing and focusing the radiation, they often are identified as optical spectroscopies. For convenience we will usually use the simpler term “spectroscopy” in place of photon spectroscopy or optical spectroscopy; however, it should be understood that we are considering only a limited part of a much broader area of analytical methods. Before we examine specific spectroscopic methods, however, we first review the properties of electromagnetic radiation.

10A.1 What Is Electromagnetic Radiation

Electromagnetic radiation, or light, is a form of energy whose behavior is described by the properties of both waves and particles. The optical properties of electromagnetic radiation, such as diffraction, are explained best by describing light as a wave. Many of the interactions between electromagnetic radiation and matter, such as absorption and emission, however, are better described by treating light as a particle, or photon. The exact nature of electromagnetic radiation remains unclear, as it has since the development of quantum mechanics in the first quarter of the twentieth century.³ Nevertheless, the dual models of wave and particle behavior provide a useful description for electromagnetic radiation.

Wave Properties of Electromagnetic Radiation Electromagnetic radiation consists of oscillating electric and magnetic fields that propagate through space along a linear path and with a constant velocity (Figure 10.1). In a vacuum, electromagnetic radiation travels at the speed of light, c , which is 2.99792×10^8 m/s. Electromagnetic radiation moves through a medium other than a vacuum with a velocity, v , less than that of the speed of light in a vacuum. The difference between v and c is small enough ($< 0.1\%$) that the speed of light to three significant figures, 3.00×10^8 m/s, is sufficiently accurate for most purposes.

Oscillations in the electric and magnetic fields are perpendicular to each other, and to the direction of the wave's propagation. Figure 10.1 shows an example of plane-polarized electromagnetic radiation consisting of an oscillating electric field and an oscillating magnetic field, each of which is constrained to a single plane. Normally, electromagnetic radiation is unpolarized, with oscillating electric and

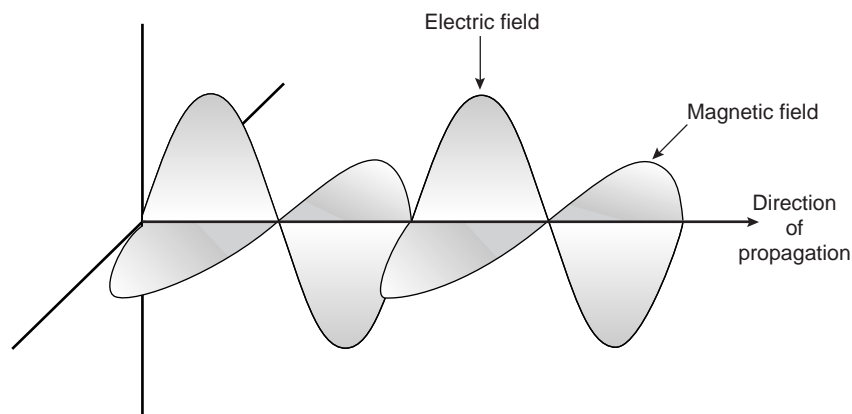
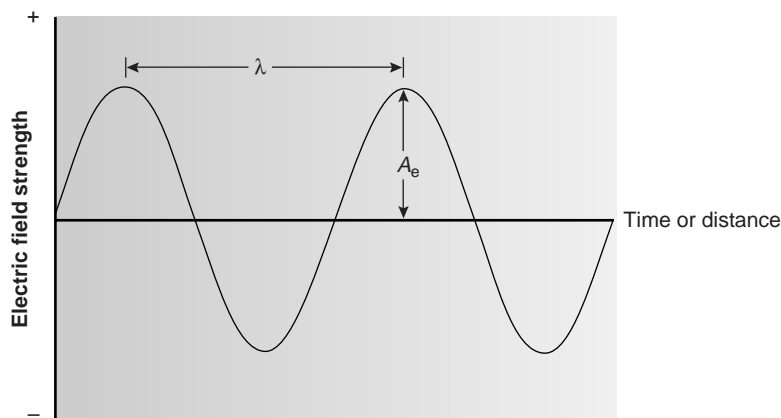


Figure 10.1

Plane-polarized electromagnetic radiation showing the electric field, the magnetic field, and the direction of propagation.

**Figure 10.2**

Electric field component of plane-polarized electromagnetic radiation.

magnetic fields in all possible planes oriented perpendicular to the direction of propagation.

The interaction of electromagnetic radiation with matter can be explained using either the electric field or the magnetic field. For this reason, only the electric field component is shown in Figure 10.2. The oscillating electric field is described by a sine wave of the form

$$E = A_e \sin(2\pi\nu t + \Phi)$$

where E is the magnitude of the electric field at time t , A_e is the electric field's maximum amplitude, ν is the **frequency**, or the number of oscillations in the electric field per unit time, and Φ is a phase angle accounting for the fact that the electric field's magnitude need not be zero at $t = 0$. An identical equation can be written for the magnetic field, M

$$M = A_m \sin(2\pi\nu t + \Phi)$$

where A_m is the magnetic field's maximum amplitude.

An electromagnetic wave, therefore, is characterized by several fundamental properties, including its velocity, amplitude, frequency, phase angle, polarization, and direction of propagation.⁴ Other properties, which are based on these fundamental properties, also are useful for characterizing the wave behavior of electromagnetic radiation. The **wavelength** of an electromagnetic wave, λ , is defined as the distance between successive maxima, or successive minima (see Figure 10.2). For ultraviolet and visible electromagnetic radiation the wavelength is usually expressed in nanometers (nm, 10^{-9} m), and the wavelength for infrared radiation is given in microns (μm , 10^{-6} m). Unlike frequency, wavelength depends on the electromagnetic wave's velocity, where

$$\lambda = \frac{v}{\nu} = \frac{c}{\nu} \quad (\text{in vacuum})$$

Thus, for electromagnetic radiation of frequency, ν , the wavelength in vacuum is longer than in other media. Another unit used to describe the wave properties of electromagnetic radiation is the **wavenumber**, $\bar{\nu}$, which is the reciprocal of wavelength

$$\bar{\nu} = \frac{1}{\lambda}$$

frequency

The number of oscillations of an electromagnetic wave per second (ν).

wavelength

The distance between any two consecutive maxima or minima of an electromagnetic wave (λ).

wavenumber

The reciprocal of wavelength ($\bar{\nu}$).

Wavenumbers are frequently used to characterize infrared radiation, with the units given in reciprocal centimeter (cm^{-1}).

Example

EXAMPLE 10.1

In 1817, Josef Fraunhofer (1787–1826) studied the spectrum of solar radiation, observing a continuous spectrum with numerous dark lines. Fraunhofer labeled the most prominent of the dark lines with letters. In 1859, Gustav Kirchhoff (1824–1887) showed that the “D” line in the solar spectrum was due to the absorption of solar radiation by sodium atoms. The wavelength of the sodium D line is 589 nm. What are the frequency and the wavenumber for this line?

SOLUTION

The frequency and wavenumber of the sodium D line are

$$\nu = \frac{c}{\lambda} = \frac{3.00 \times 10^8 \text{ m/s}}{589 \times 10^{-9} \text{ m}} = 5.09 \times 10^{14} \text{ s}^{-1}$$

$$\bar{\nu} = \frac{1}{\lambda} = \frac{1}{589 \times 10^{-9} \text{ m}} \times \frac{1 \text{ m}}{100 \text{ cm}} = 1.70 \times 10^4 \text{ cm}^{-1}$$

Two additional wave properties are **power**, P , and **intensity**, I , which give the flux of energy from a source of electromagnetic radiation.

Particle Properties of Electromagnetic Radiation When a sample absorbs electromagnetic radiation it undergoes a change in energy. The interaction between the sample and the electromagnetic radiation is easiest to understand if we assume that electromagnetic radiation consists of a beam of energetic particles called **photons**. When a photon is absorbed by a sample, it is “destroyed,” and its energy acquired by the sample.⁵ The energy of a photon, in joules, is related to its frequency, wavelength, or wavenumber by the following equations

$$E = h\nu$$

$$= \frac{hc}{\lambda}$$

$$= hc\bar{\nu}$$

where h is Planck’s constant, which has a value of $6.626 \times 10^{-34} \text{ J} \cdot \text{s}$.

Example

EXAMPLE 10.2

What is the energy per photon of the sodium D line ($\lambda = 589 \text{ nm}$)?

SOLUTION

The energy of the sodium D line is

$$E = \frac{hc}{\lambda} = \frac{(6.626 \times 10^{-34} \text{ J} \cdot \text{s})(3.00 \times 10^8 \text{ m/s})}{589 \times 10^{-9} \text{ m}} = 3.37 \times 10^{-19} \text{ J}$$

power

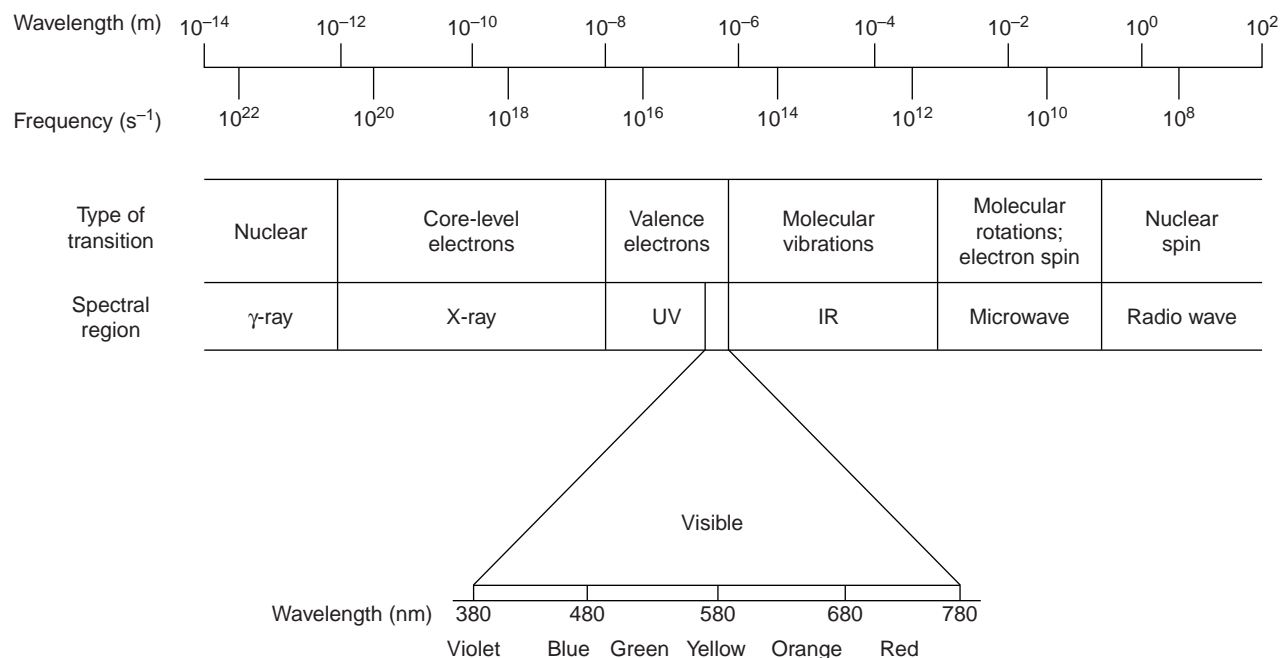
The flux of energy per unit time (P).

intensity

The flux of energy per unit time per area (I).

photon

A particle of light carrying an amount of energy equal to $h\nu$.

**Figure 10.3**

The electromagnetic spectrum showing the colors of the visible spectrum.

Colorplate 9 shows the spectrum of visible light.

The energy of a photon provides an additional characteristic property of electromagnetic radiation.

electromagnetic spectrum

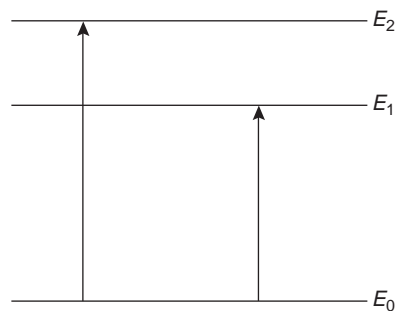
The division of electromagnetic radiation on the basis of a photon's energy.

The Electromagnetic Spectrum The frequency and wavelength of electromagnetic radiation vary over many orders of magnitude. For convenience, electromagnetic radiation is divided into different regions based on the type of atomic or molecular transition that gives rise to the absorption or emission of photons (Figure 10.3). The boundaries describing the **electromagnetic spectrum** are not rigid, and an overlap between spectral regions is possible.

10A.2 Measuring Photons as a Signal

In the previous section we defined several characteristic properties of electromagnetic radiation, including its energy, velocity, amplitude, frequency, phase angle, polarization, and direction of propagation. Spectroscopy is possible only if the photon's interaction with the sample leads to a change in one or more of these characteristic properties.

Spectroscopy is conveniently divided into two broad classes. In one class of techniques, energy is transferred between a photon of electromagnetic radiation and the analyte (Table 10.1). In absorption spectroscopy the energy carried by a photon is absorbed by the analyte, promoting the analyte from a lower-energy state to a higher-energy, or excited, state (Figure 10.4). The source of the energetic state depends on the photon's energy. The electromagnetic spectrum in Figure 10.3, for example, shows that absorbing a photon of visible light causes a valence electron in the analyte to move to a higher-energy level. When an analyte absorbs infrared radiation, on the other hand, one of its chemical bonds experiences a change in vibrational energy.

**Figure 10.4**

Simplified energy level diagram showing absorption of a photon.

Table 10.1 Representative Spectroscopies Involving an Exchange of Energy

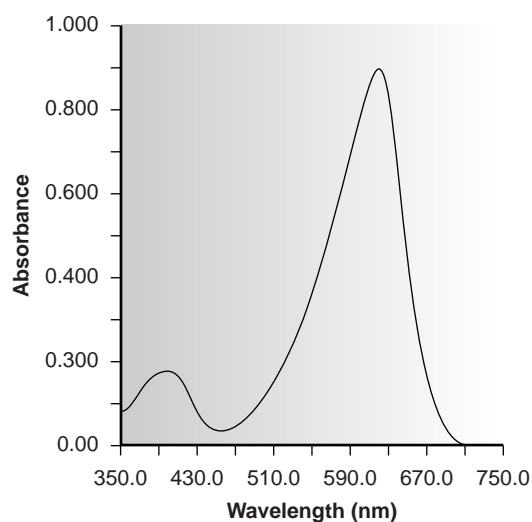
Type of Energy Transfer	Region of the Electromagnetic Spectrum	Spectroscopic Technique
absorption	γ -ray	Mossbauer spectroscopy
	X-ray	X-ray absorption spectroscopy
	UV/Vis ^a	UV/Vis spectroscopy ^b atomic absorption spectroscopy ^b
	infrared	infrared spectroscopy ^b raman spectroscopy
	microwave	microwave spectroscopy
emission (thermal excitation)	radio waves	electron spin resonance spectroscopy nuclear magnetic resonance spectroscopy
	UV/Vis	atomic emission spectroscopy ^b
photoluminescence	X-ray	X-ray fluorescence
	UV/Vis	fluorescence spectroscopy ^b phosphorescence spectroscopy ^b atomic fluorescence spectroscopy

^aUV/Vis: ultraviolet and visible ranges.

^bTechniques discussed in this text.

The intensity of photons passing through a sample containing the analyte is attenuated because of absorption. The measurement of this attenuation, which we call **absorbance**, serves as our signal. Note that the energy levels in Figure 10.4 have well-defined values (i.e., they are quantized). Absorption only occurs when the photon's energy matches the difference in energy, ΔE , between two energy levels. A plot of absorbance as a function of the photon's energy is called an **absorbance spectrum** (Figure 10.5).

Emission of a photon occurs when an analyte in a higher-energy state returns to a lower-energy state (Figure 10.6). The higher-energy state can be achieved in several ways, including thermal energy, radiant energy from a photon, or by a



absorbance

The attenuation of photons as they pass through a sample (A).

absorbance spectrum

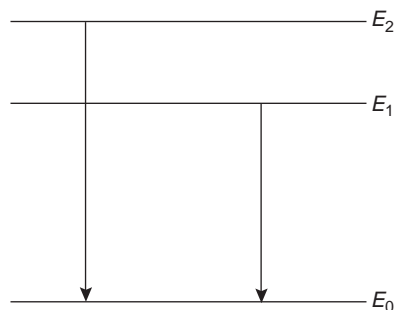
A graph of a sample's absorbance of electromagnetic radiation versus wavelength (or frequency or wavenumber).

emission

The release of a photon when an analyte returns to a lower-energy state from a higher-energy state.

Figure 10.5

Ultraviolet/visible absorption spectrum for bromothymol blue.

**Figure 10.6**

Simplified energy level diagram showing emission of a photon.

Table 10.2 Representative Spectroscopies That Do Not Involve an Exchange of Energy

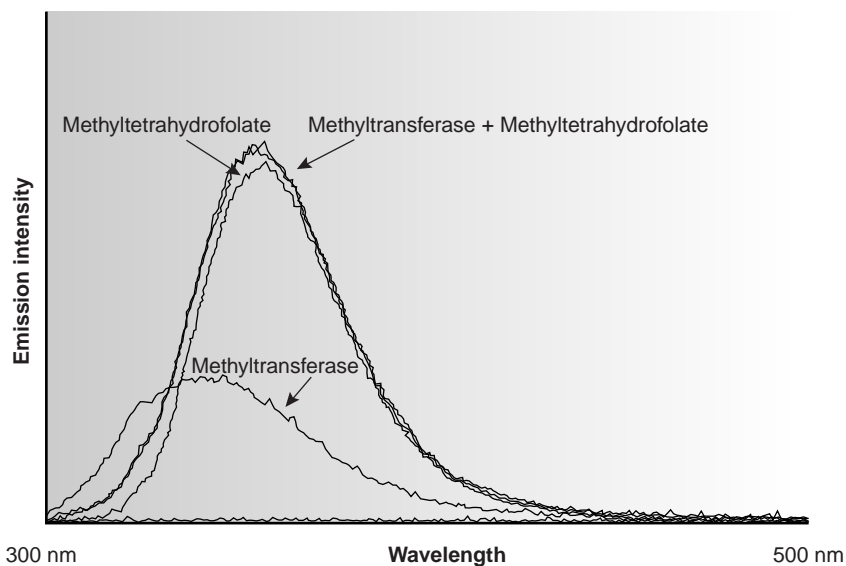
Region of the Electromagnetic Spectrum	Type of Interaction	Spectroscopic Technique
X-ray	diffraction	X-ray diffraction
UV/Vis ^a	refraction	refractometry
	scattering	nephelometry ^b turbidimetry ^b
	dispersion	optical rotary dispersion

^aUV/Vis: Ultraviolet and visible ranges.

^bTechniques covered in this text.

Figure 10.7

Photoluminescent spectra for methyltetrahydrofolate and the enzyme methyltransferase. When methyltetrahydrofolate and methyltransferase are mixed, the enzyme is no longer photoluminescent, but the photoluminescence of methyltetrahydrofolate is enhanced. (Spectra courtesy of Dave Roberts, DePauw University.)



photoluminescence

Emission following absorption of a photon.

chemiluminescence

Emission induced by a chemical reaction.

emission spectrum

A graph of emission intensity versus wavelength (or frequency or wavenumber).

chemical reaction. Emission following the absorption of a photon is also called **photoluminescence**, and that following a chemical reaction is called **chemiluminescence**. A typical **emission spectrum** is shown in Figure 10.7.

In the second broad class of spectroscopy, the electromagnetic radiation undergoes a change in amplitude, phase angle, polarization, or direction of propagation as a result of its refraction, reflection, scattering, diffraction, or dispersion by the sample. Several representative spectroscopic techniques are listed in Table 10.2.

10B Basic Components of Spectroscopic Instrumentation

The instruments used in spectroscopy consist of several common components, including a source of energy that can be input to the sample, a means for isolating a narrow range of wavelengths, a detector for measuring the signal, and a signal processor to display the signal in a form convenient for the analyst. In this section we introduce the basic components used to construct spectroscopic in-

Table 10.3 Common Sources of Electromagnetic Radiation for Spectroscopy

Source	Wavelength Region	Useful for
H ₂ and D ₂ lamp	continuum source from 160–380 nm	UV molecular absorption
tungsten lamp	continuum source from 320–2400 nm	Vis molecular absorption
Xe arc lamp	continuum source from 200–1000 nm	molecular fluorescence
Nernst glower	continuum source from 0.4–20 μm	IR molecular absorption
globar	continuum source from 1–40 μm	IR molecular absorption
nichrome wire	continuum source from 0.75–20 μm	IR molecular absorption
hollow cathode lamp	line source in UV/Vis	atomic absorption
Hg vapor lamp	line source in UV/Vis	molecular fluorescence
laser	line source in UV/Vis	atomic and molecular absorption, fluorescence and scattering

Abbreviations: UV: ultraviolet; Vis: visible; IR: infrared.

struments. A more detailed discussion of these components can be found in the suggested end-of-chapter readings. Specific instrument designs are considered in later sections.

10B.1 Sources of Energy

All forms of spectroscopy require a source of energy. In absorption and scattering spectroscopy this energy is supplied by photons. Emission and luminescence spectroscopy use thermal, radiant (photon), or chemical energy to promote the analyte to a less stable, higher energy state.

Sources of Electromagnetic Radiation A source of electromagnetic radiation must provide an output that is both intense and stable in the desired region of the electromagnetic spectrum. Sources of electromagnetic radiation are classified as either continuum or line sources. A **continuum source** emits radiation over a wide range of wavelengths, with a relatively smooth variation in intensity as a function of wavelength (Figure 10.8). **Line sources**, on the other hand, emit radiation at a few selected, narrow wavelength ranges (Figure 10.9). Table 10.3 provides a list of the most common sources of electromagnetic radiation.

Sources of Thermal Energy The most common sources of thermal energy are flames and plasmas. Flame sources use the combustion of a fuel and an oxidant such as acetylene and air, to achieve temperatures of 2000–3400 K. Plasmas, which are hot, ionized gases, provide temperatures of 6000–10,000 K.

Chemical Sources of Energy Exothermic reactions also may serve as a source of energy. In chemiluminescence the analyte is raised to a higher-energy state by means of a chemical reaction, emitting characteristic radiation when it returns to a lower-energy state. When the chemical reaction results from a biological or enzymatic reaction, the emission of radiation is called bioluminescence. Commercially available “light sticks” and the flash of light from a firefly are examples of chemiluminescence and bioluminescence, respectively.

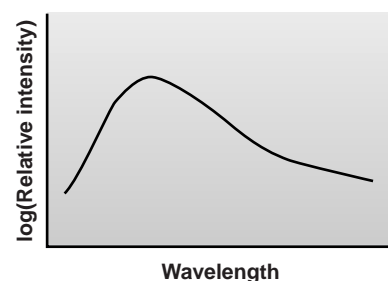


Figure 10.8
Emission spectrum from a typical continuum source.

continuum source

A source that emits radiation over a wide range of wavelengths.

line source

A source that emits radiation at only select wavelengths.

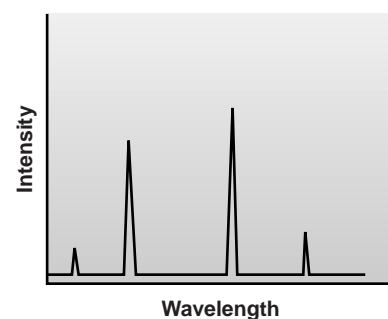


Figure 10.9
Emission spectrum from a typical line source.

10B.2 Wavelength Selection

In Nessler's original colorimetric method for ammonia, described at the beginning of the chapter, no attempt was made to narrow the wavelength range of visible light passing through the sample. If more than one component in the sample contributes to the absorption of radiation, however, then a quantitative analysis using Nessler's original method becomes impossible. For this reason we usually try to select a single wavelength where the analyte is the only absorbing species. Unfortunately, we cannot isolate a single wavelength of radiation from a continuum source. Instead, a wavelength selector passes a narrow band of radiation (Figure 10.10) characterized by a **nominal wavelength**, an **effective bandwidth**, and a maximum throughput of radiation. The effective bandwidth is defined as the width of the radiation at half the maximum throughput.

The ideal wavelength selector has a high throughput of radiation and a narrow effective bandwidth. A high throughput is desirable because more photons pass through the wavelength selector, giving a stronger signal with less background noise. A narrow effective bandwidth provides a higher **resolution**, with spectral features separated by more than twice the effective bandwidth being resolved. Generally these two features of a wavelength selector are in opposition (Figure 10.11). Conditions favoring a higher throughput of radiation usually provide less resolution. Decreasing the effective bandwidth improves resolution, but at the cost of a noisier signal. For a qualitative analysis, resolution is generally more important than the throughput of radiation; thus, smaller effective bandwidths are desirable. In a quantitative analysis a higher throughput of radiation is usually desirable.⁶

nominal wavelength

The wavelength which a wavelength selector is set to pass.

effective bandwidth

The width of the band of radiation passing through a wavelength selector measured at half the band's height.

resolution

In spectroscopy, the separation between two spectral features, such as absorption or emission lines.

filter

A wavelength selector that uses either absorption, or constructive and destructive interference to control the range of selected wavelengths.

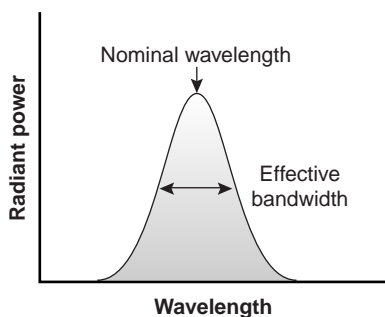


Figure 10.10

Band of radiation exiting wavelength selector showing the nominal wavelength and effective bandpass.

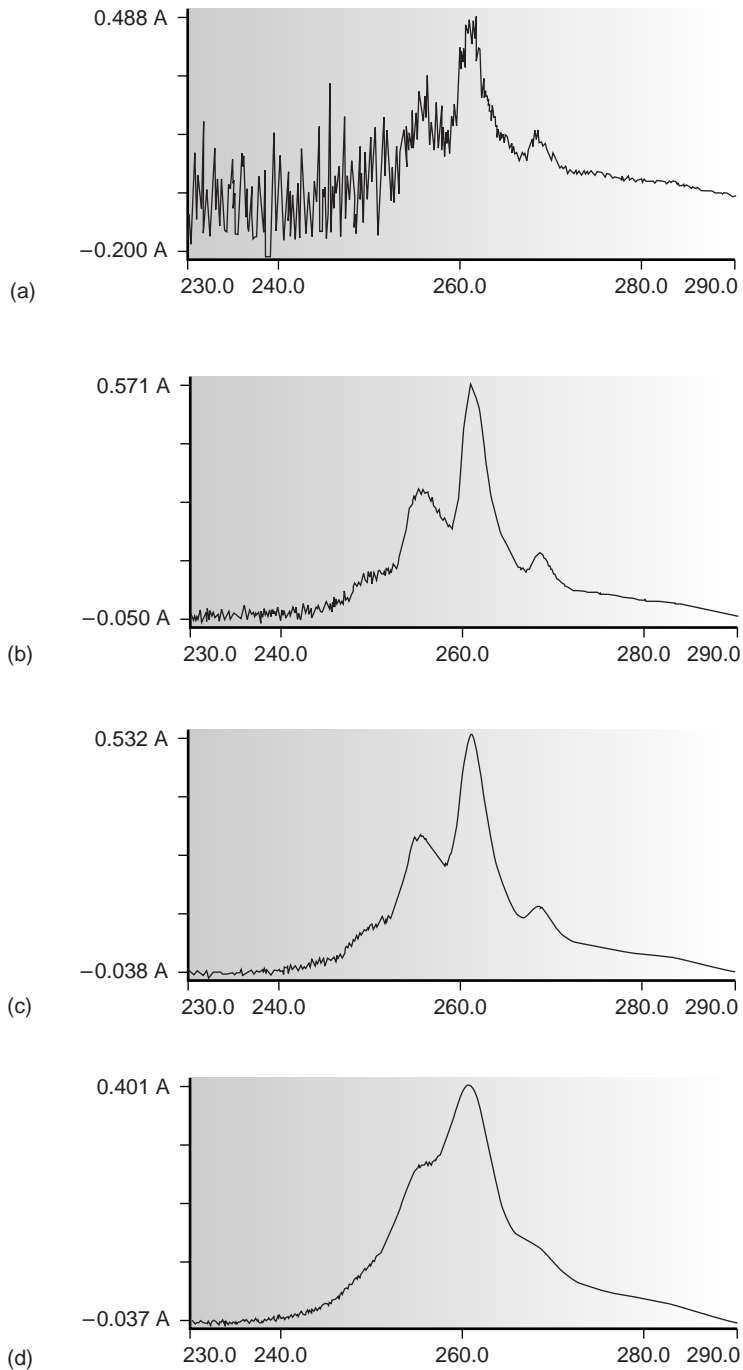
monochromator

A wavelength selector that uses a diffraction grating or prism, and that allows for a continuous variation of the nominal wavelength.

Wavelength Selection Using Filters The simplest method for isolating a narrow band of radiation is to use an absorption or interference filter. Absorption **filters** work by selectively absorbing radiation from a narrow region of the electromagnetic spectrum. Interference filters use constructive and destructive interference to isolate a narrow range of wavelengths. A simple example of an absorption filter is a piece of colored glass. A purple filter, for example, removes the complementary color green from 500–560 nm. Commercially available absorption filters provide effective bandwidths from 30–250 nm. The maximum throughput for the smallest effective bandpasses, however, may be only 10% of the source's emission intensity over that range of wavelengths. Interference filters are more expensive than absorption filters, but have narrower effective bandwidths, typically 10–20 nm, with maximum throughputs of at least 40%.

Wavelength Selection Using Monochromators One limitation of an absorption or interference filter is that they do not allow for a continuous selection of wavelength. If measurements need to be made at two wavelengths, then the filter must be changed in between measurements. A further limitation is that filters are available for only selected nominal ranges of wavelengths. An alternative approach to wavelength selection, which provides for a continuous variation of wavelength, is the **monochromator**.

The construction of a typical monochromator is shown in Figure 10.12. Radiation from the source enters the monochromator through an entrance slit. The radiation is collected by a collimating mirror, which reflects a parallel beam of radiation to a diffraction grating. The diffraction grating is an optically reflecting surface with

**Figure 10.11**

Effect of the monochromator's slit width on noise and resolution for the ultraviolet absorption spectrum of benzene. The slit width increases from spectrum (a) to spectrum (d) with effective bandpasses of 0.25 nm, 1.0 nm, 2.0 nm, and 4.0 nm.

a large number of parallel grooves (see inset to Figure 10.12). Diffraction by the grating disperses the radiation in space, where a second mirror focuses the radiation onto a planar surface containing an exit slit. In some monochromators a prism is used in place of the diffraction grating.

Radiation exits the monochromator and passes to the detector. As shown in Figure 10.12, a **polychromatic** source of radiation at the entrance slit is converted at the exit slit to a **monochromatic** source of finite effective bandwidth. The choice of

polychromatic

Electromagnetic radiation of more than one wavelength.

monochromatic

Electromagnetic radiation of a single wavelength.

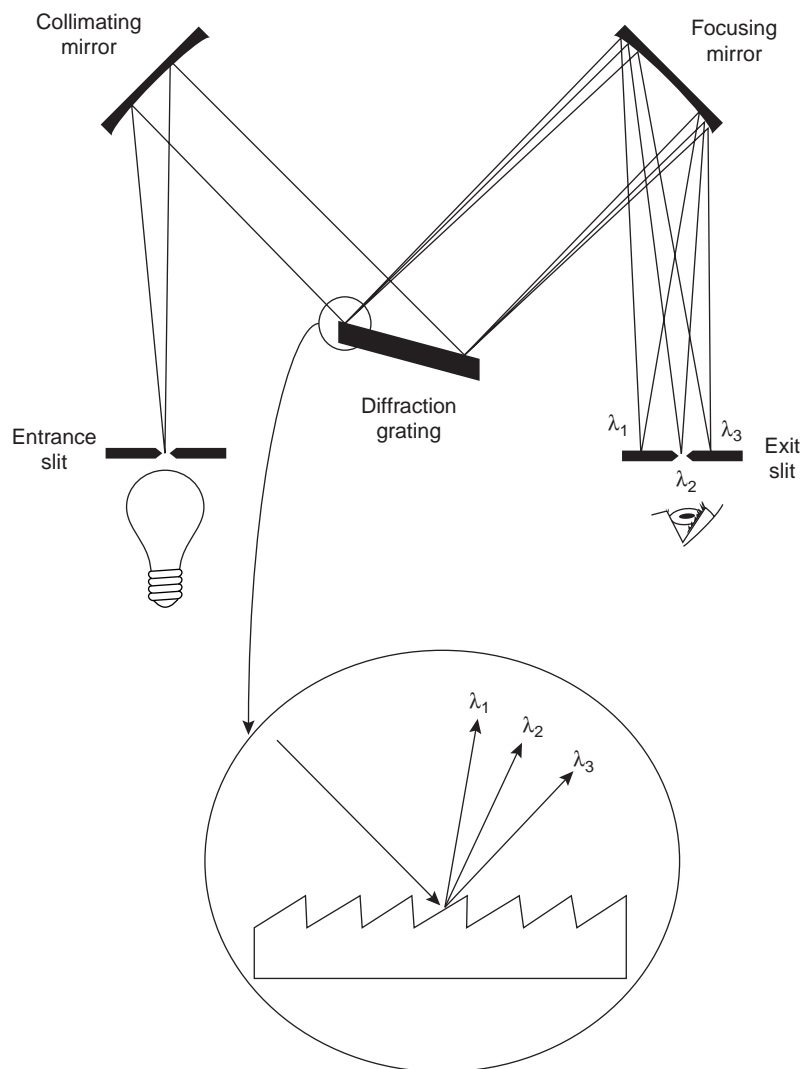


Figure 10.12
Typical grating monochromator with inset showing the dispersion of the radiation by the diffraction grating.

interferometer

A device that allows all wavelengths of light to be measured simultaneously, eliminating the need for a wavelength selector.

which wavelength exits the monochromator is determined by rotating the diffraction grating. A narrower exit slit provides a smaller effective bandwidth and better resolution, but allows a smaller throughput of radiation.

Monochromators are classified as either fixed-wavelength or scanning. In a fixed-wavelength monochromator, the wavelength is selected by manually rotating the grating. Normally, a fixed-wavelength monochromator is only used for quantitative analyses where measurements are made at one or two wavelengths. A scanning monochromator includes a drive mechanism that continuously rotates the grating, allowing successive wavelengths to exit from the monochromator. Scanning monochromators are used to acquire spectra and, when operated in a fixed-wavelength mode, for quantitative analysis.

Interferometers An **interferometer** provides an alternative approach for wavelength selection. Instead of filtering or dispersing the electromagnetic radiation, an interferometer simultaneously allows source radiation of all wavelengths to reach the detector (Figure 10.13). Radiation from the source is focused on a beam splitter that transmits half of the radiation to a fixed mirror, while reflecting the other half to a movable mirror. The radiation recombines at the beam splitter,

where constructive and destructive interference determines, for each wavelength, the intensity of light reaching the detector. As the moving mirror changes position, the wavelengths of light experiencing maximum constructive interference and maximum destructive interference also changes. The signal at the detector shows intensity as a function of the moving mirror's position, expressed in units of distance or time. The result is called an interferogram, or a time domain spectrum. The time domain spectrum is converted mathematically, by a process called a Fourier transform, to the normal spectrum (also called a frequency domain spectrum) of intensity as a function of the radiation's energy. Further details about interferometers and the mathematics of the Fourier transform can be found in the suggested readings listed at the end of the chapter.

In comparison with a monochromator, interferometers provide two significant advantages. The first advantage, which is termed Jacquinot's advantage, results from the higher throughput of source radiation. Since an interferometer does not use slits and has fewer optical components from which radiation can be scattered and lost, the throughput of radiation reaching the detector is 80–200 times greater than that achieved with a monochromator. The result is an im-

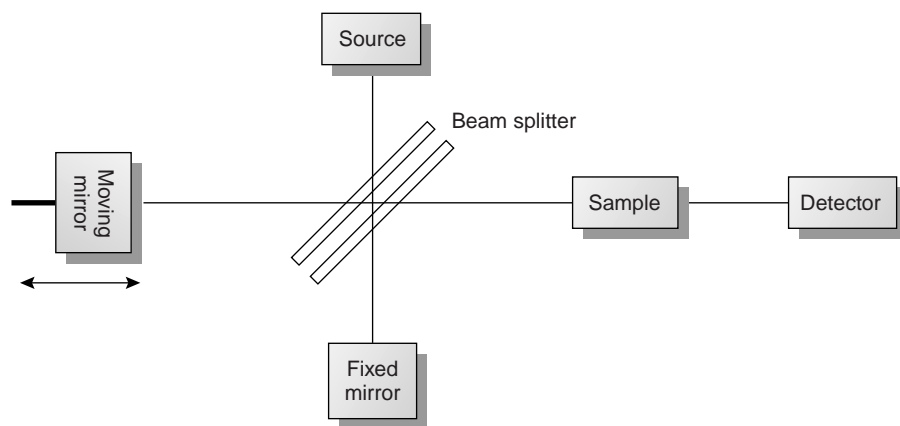


Figure 10.13

Block diagram of an interferometer.

proved **signal-to-noise ratio**. The second advantage, which is called Fellgett's advantage, reflects a savings in the time needed to obtain a spectrum. Since all frequencies are monitored simultaneously, an entire spectrum can be recorded in approximately 1 s, as compared to 10–15 min with a scanning monochromator.

10B.3 Detectors

The first detector for optical spectroscopy was the human eye, which, of course, is limited both by its accuracy and its limited sensitivity to electromagnetic radiation. Modern detectors use a sensitive **transducer** to convert a signal consisting of photons into an easily measured electrical signal. Ideally the detector's signal, S , should be a linear function of the electromagnetic radiation's power, P ,

$$S = kP + D$$

where k is the detector's sensitivity, and D is the detector's **dark current**, or the background electric current when all radiation from the source is blocked from the detector.

Photon Transducers Two general classes of transducers are used for optical spectroscopy, several examples of which are listed in Table 10.4. Phototubes and photomultipliers contain a photosensitive surface that absorbs radiation in the ultraviolet, visible, and near infrared (IR), producing an electric current proportional to the number of photons reaching the transducer. Other photon detectors use a semiconductor as the photosensitive surface. When the semiconductor absorbs photons, valence electrons move to the semiconductor's conduction band, producing a measurable current. One advantage of the Si photodiode is that it is easily miniaturized. Groups of photodiodes may be gathered together in a linear array containing from 64 to 4096 individual photodiodes. With a width of 25 μm per diode, for example, a linear array of 2048 photodiodes requires only 51.2 mm of linear space. By placing a **photodiode array** along the monochromator's focal plane, it is possible to monitor simultaneously an entire range of wavelengths.

Thermal Transducers Infrared radiation generally does not have sufficient energy to produce a measurable current when using a photon transducer. A thermal transducer, therefore, is used for infrared spectroscopy. The absorption of infrared photons by a thermal transducer increases its temperature, changing one or more of its characteristic properties. The pneumatic transducer, for example,

signal-to-noise ratio

The ratio of the signal's intensity to the average intensity of the surrounding noise.

transducer

A device that converts a chemical or physical property, such as pH or photon intensity, to an easily measured electrical signal, such as a voltage or current.

dark current

The background current present in a photon detector in the absence of radiation from the source.

photodiode array

A linear array of photodiodes providing the ability to detect simultaneously radiation at several wavelengths.

Table 10.4 Characteristics of Transducers for Optical Spectroscopy

Detector	Class	Wavelength Range	Output Signal
phototube	photon	200–1000 nm	current
photomultiplier	photon	110–1000 nm	current
Si photodiode	photon	250–1100 nm	current
photoconductor	photon	750–6000 nm	change in resistance
photovoltaic cell	photon	400–5000 nm	current or voltage
thermocouple	thermal	0.8–40 μm	voltage
thermistor	thermal	0.8–40 μm	change in resistance
pneumatic	thermal	0.8–1000 μm	membrane displacement
pyroelectric	thermal	0.3–1000 μm	current

consists of a small tube filled with xenon gas equipped with an IR-transparent window at one end, and a flexible membrane at the other end. A blackened surface in the tube absorbs photons, increasing the temperature and, therefore, the pressure of the gas. The greater pressure in the tube causes the flexible membrane to move in and out, and this displacement is monitored to produce an electrical signal.

10B.4 Signal Processors

The electrical signal generated by the transducer is sent to a **signal processor** where it is displayed in a more convenient form for the analyst. Examples of signal processors include analog or digital meters, recorders, and computers equipped with digital acquisition boards. The signal processor also may be used to calibrate the detector's response, to amplify the signal from the detector, to remove noise by filtering, or to mathematically transform the signal.

signal processor

A device, such as a meter or computer, that displays the signal from the transducer in a form that is easily interpreted by the analyst.

10C Spectroscopy Based on Absorption

Historically, the first spectroscopic studies involved characterizing the emission of visible light from the sun, from flames, and from salts added to flames. Our survey of spectroscopy, however, begins with absorption because it is the more important technique in modern analytical spectroscopy.

10C.1 Absorbance of Electromagnetic Radiation

In absorption spectroscopy a beam of electromagnetic radiation passes through a sample. Much of the radiation is transmitted without a loss in intensity. At selected frequencies, however, the radiation's intensity is attenuated. This process of attenuation is called absorption. Two general requirements must be met if an analyte is to absorb electromagnetic radiation. The first requirement is that there must be a mechanism by which the radiation's electric field or magnetic field interacts with the analyte. For ultraviolet and visible radiation, this interaction involves the electronic energy of valence electrons. A chemical bond's vibrational energy is altered by the absorbance of infrared radiation. A more detailed treatment of this interaction, and its importance in deter-

mining the intensity of absorption, is found in the suggested readings listed at the end of the chapter.

The second requirement is that the energy of the electromagnetic radiation must exactly equal the difference in energy, ΔE , between two of the analyte's quantized energy states. Figure 10.4 shows a simplified view of the absorption of a photon. The figure is useful because it emphasizes that the photon's energy must match the difference in energy between a lower-energy state and a higher-energy state. What is missing, however, is information about the types of energetic states involved, which transitions between states are likely to occur, and the appearance of the resulting spectrum.

We can use the energy level diagram in Figure 10.14 to explain an absorbance spectrum. The thick lines labeled E_0 and E_1 represent the analyte's ground (lowest) electronic state and its first electronic excited state. Superimposed on each electronic energy level is a series of lines representing vibrational energy levels.

Infrared Spectra for Molecules and Polyatomic Ions The energy of infrared radiation is sufficient to produce a change in the vibrational energy of a molecule or polyatomic ion (see Table 10.1). As shown in Figure 10.14, vibrational energy levels are quantized; that is, a molecule may have only certain, discrete vibrational energies. The energy for allowed vibrational modes, E_v , is

$$E_v = \left(v + \frac{1}{2} \right) h\nu_0$$

where v is the vibrational quantum number, which may take values of 0, 1, 2, . . . , and ν_0 is the bond's fundamental vibrational frequency. Values for ν_0 are determined by the bond's strength and the mass at each end of the bond and are characteristic of the type of bond. For example, a carbon-carbon single bond (C—C) absorbs infrared radiation at a lower energy than a carbon-carbon double bond (C=C) because a C—C bond is weaker than a C=C bond.

At room temperature most molecules are in their ground vibrational state ($v = 0$). A transition from the ground vibrational state to the first vibrational excited state ($v = 1$) requires the absorption of a photon with an energy of $h\nu_0$. Transitions in which Δv is ± 1 give rise to the fundamental absorption lines. Weaker absorption lines, called overtones, are due to transitions in which Δv is ± 2 or ± 3 . The number of possible normal vibrational modes for a linear molecule is $3N - 5$, and for a nonlinear molecule is $3N - 6$, where N is the number of atoms in the molecule. Not surprisingly, infrared spectra often show a considerable number of absorption bands. Even a relatively simple molecule, such as benzene (C_6H_6), for example, has 30 possible normal modes of vibration, although not all of these vibrational modes give rise to an absorption. A typical IR spectrum is shown in Figure 10.15.

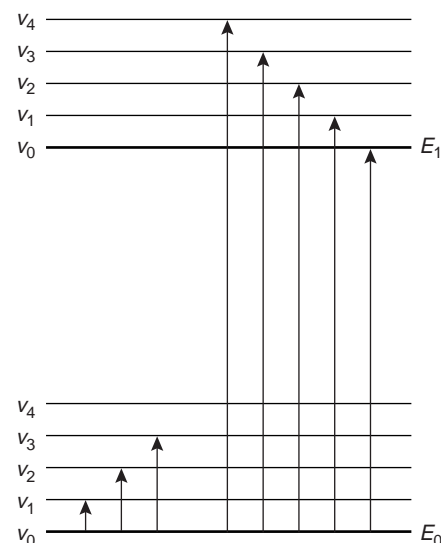


Figure 10.14

Energy level diagram showing difference between the absorption of infrared radiation (left) and ultraviolet-visible radiation (right).

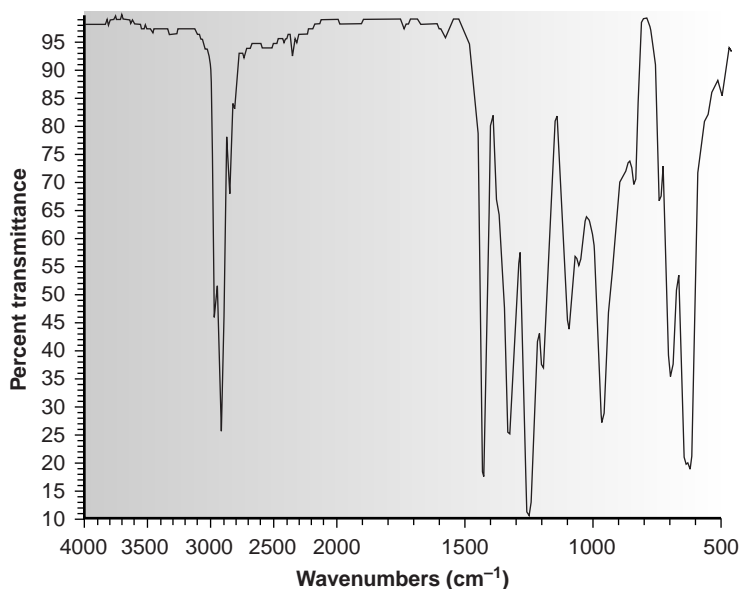


Figure 10.15

Fourier transform infrared (FT-IR) spectrum of polyvinylchloride.

Table 10.5 Electronic Transitions Involving n , σ , and π Molecular Orbitals

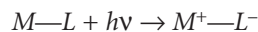
Transition	Wavelength Range (nm)	Examples
$\sigma \rightarrow \sigma^*$	< 200	C—C, C—H
$n \rightarrow \sigma^*$	160–260	H ₂ O, CH ₃ OH, CH ₃ Cl
$\pi \rightarrow \pi^*$	200–500	C=C, C=O, C=N, C≡C
$n \rightarrow \pi^*$	250–600	C=O, C=N, N=N, N=O

UV/Vis Spectra for Molecules and Ions When a molecule or ion absorbs ultraviolet or visible radiation it undergoes a change in its valence electron configuration. The valence electrons in organic molecules, and inorganic anions such as CO₃²⁻, occupy quantized sigma bonding, σ , pi bonding, π , and nonbonding, n , molecular orbitals. Unoccupied sigma antibonding, σ^* , and pi antibonding, π^* , molecular orbitals often lie close enough in energy that the transition of an electron from an occupied to an unoccupied orbital is possible.

Four types of transitions between quantized energy levels account for molecular UV/Vis spectra. The approximate wavelength ranges for these absorptions, as well as a partial list of bonds, functional groups, or molecules that give rise to these transitions is shown in Table 10.5. Of these transitions, the most important are the $n \rightarrow \pi^*$ and $\pi \rightarrow \pi^*$, because they involve functional groups that are characteristic of the analyte and wavelengths that are easily accessible. The bonds and functional groups that give rise to the absorption of ultraviolet and visible radiation are called **chromophores**.

Many transition metal ions, such as Cu²⁺ and Co²⁺, form solutions that are colored because the metal ion absorbs visible light. The transitions giving rise to this absorption are due to valence electrons in the metal ion's d -orbitals. For a free metal ion, the five d -orbitals are of equal energy. In the presence of a complexing ligand or solvent molecule, however, the d -orbitals split into two or more groups that differ in energy. For example, in the octahedral complex Cu(H₂O)₆²⁺ the six water molecules perturb the d -orbitals into two groups as shown in Figure 10.16. The resulting $d-d$ transitions for transition metal ions are relatively weak.

A more important source of UV/Vis absorption for inorganic metal–ligand complexes is charge transfer, in which absorbing a photon produces an excited state species that can be described in terms of the transfer of an electron from the metal, M , to the ligand, L .

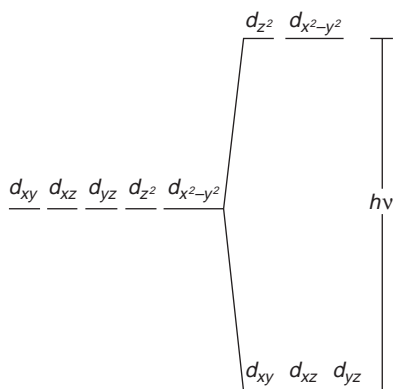


Charge-transfer absorption is important because it produces very large absorbances, providing for a much more sensitive analytical method. One important example of a charge-transfer complex is that of *o*-phenanthroline with Fe²⁺, the UV/Vis spectrum for which is shown in Figure 10.17. Charge-transfer absorption in which the electron moves from the ligand to the metal also is possible.

Comparing the IR spectrum in Figure 10.15 to the UV/Vis spectrum in Figure 10.17, we note that UV/Vis absorption bands are often significantly broader than those for IR absorption. Figure 10.14 shows why this is true. When a species

chromophore

The specific bonds or functional groups in a molecule responsible for the absorption of a particular wavelength of light.

**Figure 10.16**

Splitting of d -orbitals in an octahedral field.

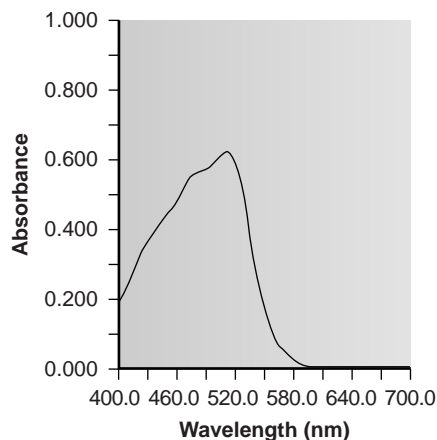


Figure 10.17
UV/Vis spectrum for $\text{Fe}(\text{o-phenanthroline})_3^{2+}$.

absorbs UV/Vis radiation, the transition between electronic energy levels may also include a transition between vibrational energy levels. The result is a number of closely spaced absorption bands that merge together to form a single broad absorption band.

UV/Vis Spectra for Atoms As noted in Table 10.1, the energy of ultraviolet and visible electromagnetic radiation is sufficient to cause a change in an atom's valence electron configuration. Sodium, for example, with a valence shell electron configuration of $[\text{Ne}] 3s^1$, has a single valence electron in its $3s$ atomic orbital. Unoccupied, higher energy atomic orbitals also exist. Figure 10.18 shows a partial energy level diagram for sodium's occupied and unoccupied valence shell atomic orbitals. This configuration of atomic orbitals, which shows a splitting of the p orbitals into two levels with slightly different energies, may differ from that encountered in earlier courses. The reasons for this splitting, however, are beyond the level of this text, and unimportant in this context.

Absorption of a photon is accompanied by the excitation of an electron from a lower-energy atomic orbital to an orbital of higher energy. Not all possible transitions between atomic orbitals are allowed. For sodium the only allowed transitions are those in which there is a change of ± 1 in the orbital quantum number (ℓ); thus transitions from $s \rightarrow p$ orbitals are allowed, but transitions from $s \rightarrow d$ orbitals are forbidden. The wavelengths of electromagnetic radiation that must be absorbed to cause several allowed transitions are shown in Figure 10.18.

The atomic absorption spectrum for Na is shown in Figure 10.19 and is typical of that found for most atoms. The most obvious feature of this spectrum is that it consists of a few, discrete absorption lines corresponding to transitions between the ground state (the $3s$ atomic orbital) and the $3p$ and $4p$ atomic orbitals. Absorption from excited states, such as that from the $3p$ atomic orbital to the $4s$ or $3d$ atomic orbital, which are included in the energy level diagram in Figure 10.18, are too weak to detect. Since the

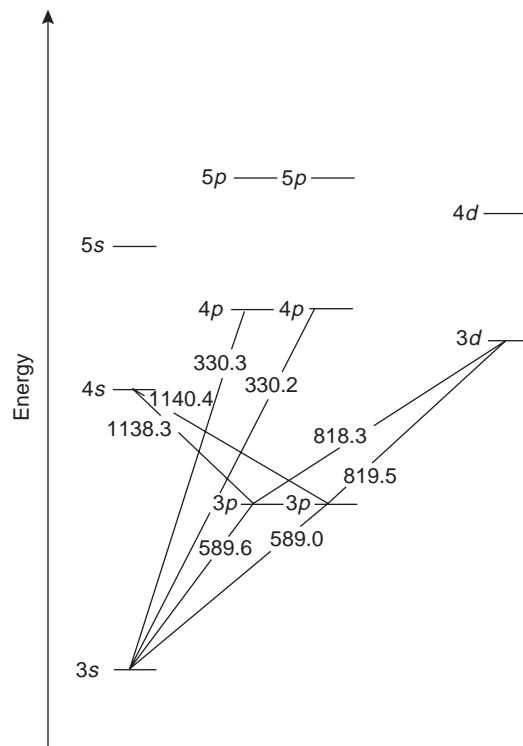


Figure 10.18
Valence shell energy diagram for sodium.

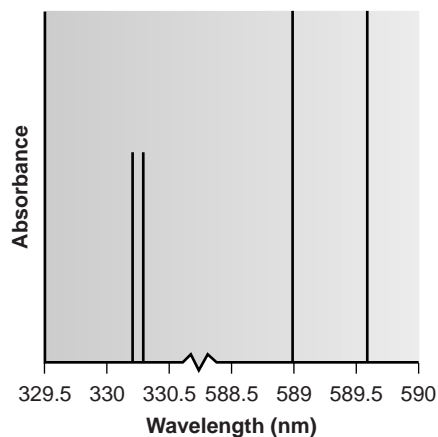


Figure 10.19
Atomic absorption spectrum for sodium.

transmittance

The ratio of the radiant power passing through a sample to that from the radiation's source (T).

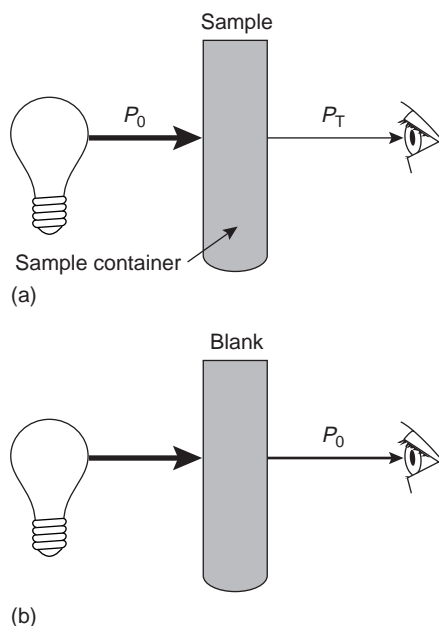


Figure 10.20

(a) Schematic diagram showing the attenuation of radiation passing through a sample; P_0 is the radiant power from the source and P_T is the radiant power transmitted by the sample. (b) Schematic diagram showing that P_0 is redefined as the radiant power transmitted by the blank, correcting the transmittance in (a) for any loss of radiation due to scattering, reflection or absorption by the cuvette, and absorption by the sample's matrix.

lifetime of an excited state is short, typically 10^{-7} – 10^{-8} s, an atom in the excited state is likely to return to the ground state before it has an opportunity to absorb a photon.

Another feature of the spectrum shown in Figure 10.19 is the narrow width of the absorption lines, which is a consequence of the fixed difference in energy between the ground and excited states. Natural line widths for atomic absorption, which are governed by the uncertainty principle, are approximately 10^{-5} nm. Other contributions to broadening increase this line width to approximately 10^{-3} nm.

10C.2 Transmittance and Absorbance

The attenuation of electromagnetic radiation as it passes through a sample is described quantitatively by two separate, but related terms: transmittance and absorbance. **Transmittance** is defined as the ratio of the electromagnetic radiation's power exiting the sample, P_T , to that incident on the sample from the source, P_0 , (Figure 10.20a).

$$T = \frac{P_T}{P_0} \quad 10.1$$

Multiplying the transmittance by 100 gives the percent transmittance (% T), which varies between 100% (no absorption) and 0% (complete absorption). All methods of detection, whether the human eye or a modern photoelectric transducer, measure the transmittance of electromagnetic radiation.

Attenuation of radiation as it passes through the sample leads to a transmittance of less than 1. As described, equation 10.1 does not distinguish between the different ways in which the attenuation of radiation occurs. Besides absorption by the analyte, several additional phenomena contribute to the net attenuation of radiation, including reflection and absorption by the sample container, absorption by components of the sample matrix other than the analyte, and the scattering of radiation. To compensate for this loss of the electromagnetic radiation's power, we use a method blank (Figure 10.20b). The radiation's power exiting from the method blank is taken to be P_0 .

An alternative method for expressing the attenuation of electromagnetic radiation is absorbance, A , which is defined as

$$A = -\log T = -\log \frac{P_T}{P_0} = \log \frac{P_0}{P_T} \quad 10.2$$

Absorbance is the more common unit for expressing the attenuation of radiation because, as shown in the next section, it is a linear function of the analyte's concentration.

EXAMPLE 10.3

A sample has a percent transmittance of 50.0%. What is its absorbance?

SOLUTION

With a percent transmittance of 50.0%, the transmittance of the sample is 0.500. Substituting into equation 10.2 gives

$$A = -\log T = -\log(0.500) = 0.301$$

Equation 10.1 has an important consequence for atomic absorption. Because of the narrow line width for atomic absorption, a continuum source of radiation cannot be used. Even with a high-quality monochromator, the effective bandwidth for a continuum source is 100–1000 times greater than that for an atomic absorption line. As a result, little of the radiation from a continuum source is absorbed ($P_o \approx P_T$), and the measured absorbance is effectively zero. For this reason, atomic absorption requires a line source.

10C.3 Absorbance and Concentration: Beer's Law

When monochromatic electromagnetic radiation passes through an infinitesimally thin layer of sample, of thickness dx , it experiences a decrease in power of dP (Figure 10.21). The fractional decrease in power is proportional to the sample's thickness and the analyte's concentration, C ; thus

$$\frac{-dP}{P} = \alpha C dx \quad 10.3$$

where P is the power incident on the thin layer of sample, and α is a proportionality constant. Integrating the left side of equation 10.3 from $P = P_0$ to $P = P_T$, and the right side from $x = 0$ to $x = b$, where b is the sample's overall thickness

$$-\int_{P=P_0}^{P=P_T} \frac{dP}{P} = \alpha C \int_{x=0}^{x=b} dx$$

gives

$$\ln\left(\frac{P_0}{P_T}\right) = \alpha b C$$

Converting from ln to log, and substituting equation 10.2, gives

$$A = abC \quad 10.4$$

where a is the analyte's absorptivity with units of $\text{cm}^{-1} \text{conc}^{-1}$. When concentration is expressed using molarity, the absorptivity is replaced by the molar absorptivity, ϵ (with units of $\text{cm}^{-1} \text{M}^{-1}$)

$$A = \epsilon b C \quad 10.5$$

The absorptivity and molar absorptivity give, in effect, the probability that the analyte will absorb a photon of given energy. As a result, values for both a and ϵ depend on the wavelength of electromagnetic radiation.

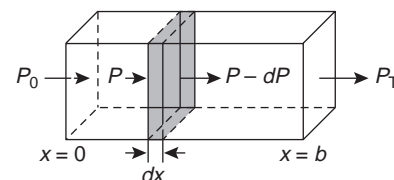


Figure 10.21
Factors used in deriving the Beer–Lambert law.

EXAMPLE 10.4

A $5.00 \times 10^{-4} \text{ M}$ solution of an analyte is placed in a sample cell that has a pathlength of 1.00 cm. When measured at a wavelength of 490 nm, the absorbance of the solution is found to be 0.338. What is the analyte's molar absorptivity at this wavelength?

SOLUTION

Solving equation 10.5 for ϵ and making appropriate substitutions gives

$$\epsilon = \frac{A}{bC} = \frac{0.338}{(1.00 \text{ cm})(5.00 \times 10^{-4} \text{ M})} = 676 \text{ cm}^{-1} \text{ M}^{-1}$$

Beer's law

The relationship between a sample's absorbance and the concentration of the absorbing species ($A = \epsilon bC$).

Equations 10.4 and 10.5, which establish the linear relationship between absorbance and concentration, are known as the Beer–Lambert law, or more commonly, as **Beer's law**. Calibration curves based on Beer's law are used routinely in quantitative analysis.

10C.4 Beer's Law and Multicomponent Samples

Beer's law can be extended to samples containing several absorbing components provided that there are no interactions between the components. Individual absorbances, A_i , are additive. For a two-component mixture of X and Y, the total absorbance, A_{tot} , is

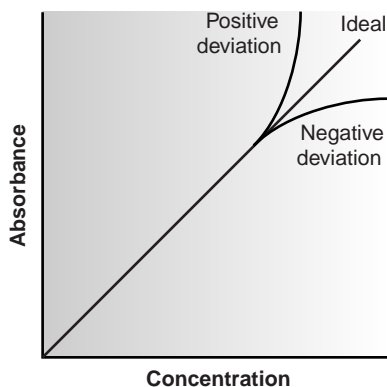
$$A_{\text{tot}} = A_X + A_Y = \epsilon_X b C_X + \epsilon_Y b C_Y$$

Generalizing, the absorbance for a mixture of n components, A_m , is given as

$$A_m = \sum_{i=1}^n A_i = \sum_{i=1}^n \epsilon_i b C_i \quad 10.6$$

10C.5 Limitations to Beer's Law

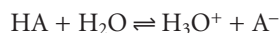
According to Beer's law, a calibration curve of absorbance versus the concentration of analyte in a series of standard solutions should be a straight line with an intercept of 0 and a slope of ab or ϵb . In many cases, however, calibration curves are found to be nonlinear (Figure 10.22). Deviations from linearity are divided into three categories: fundamental, chemical, and instrumental.

**Figure 10.22**

Calibration curves showing positive and negative deviations from Beer's law.

Fundamental Limitations to Beers Law Beer's law is a limiting law that is valid only for low concentrations of analyte. There are two contributions to this fundamental limitation to Beer's law. At higher concentrations the individual particles of analyte no longer behave independently of one another. The resulting interaction between particles of analyte may change the value of ϵ . A second contribution is that the absorptivity, a , and molar absorptivity, ϵ , depend on the sample's refractive index. Since the refractive index varies with the analyte's concentration, the values of a and ϵ will change. For sufficiently low concentrations of analyte, the refractive index remains essentially constant, and the calibration curve is linear.

Chemical Limitations to Beer's Law Chemical deviations from Beer's law can occur when the absorbing species is involved in an equilibrium reaction. Consider, as an example, an analysis for the weak acid, HA. To construct a Beer's law calibration curve, several standards containing known total concentrations of HA, C_{tot} , are prepared and the absorbance of each is measured at the same wavelength. Since HA is a weak acid, it exists in equilibrium with its conjugate weak base, A^-



If both HA and A^- absorb at the selected wavelength, then Beers law is written as

$$A = \epsilon_{\text{HA}} b C_{\text{HA}} + \epsilon_{\text{A}^-} b C_{\text{A}^-} \quad 10.7$$

where C_{HA} and C_{A^-} are the equilibrium concentrations of HA and A^- . Since the weak acid's total concentration, C_{tot} , is

$$C_{\text{tot}} = C_{\text{HA}} + C_{\text{A}^-}$$

the concentrations of HA and A^- can be written as

$$C_{\text{HA}} = \alpha_{\text{HA}} C_{\text{tot}} \quad 10.8$$

$$C_{\text{A}} = (1 - \alpha_{\text{HA}}) C_{\text{tot}} \quad 10.9$$

where α_{HA} is the fraction of weak acid present as HA. Substituting equations 10.8 and 10.9 into equation 10.7, and rearranging, gives

$$A = (\epsilon_{\text{HA}}\alpha_{\text{HA}} + \epsilon_{\text{A}} - \epsilon_{\text{A}}\alpha_{\text{HA}})bC_{\text{tot}} \quad 10.10$$

Because values of α_{HA} may depend on the concentration of HA, equation 10.10 may not be linear. A Beer's law calibration curve of A versus C_{tot} will be linear if one of two conditions is met. If the wavelength is chosen such that ϵ_{HA} and ϵ_{A} are equal, then equation 10.10 simplifies to

$$A = \epsilon_{\text{A}}bC_{\text{tot}}$$

and a linear Beer's law calibration curve is realized. Alternatively, if α_{HA} is held constant for all standards, then equation 10.10 will be a straight line at all wavelengths. Because HA is a weak acid, values of α_{HA} change with pH. To maintain a constant value for α_{HA} , therefore, we need to buffer each standard solution to the same pH. Depending on the relative values of ϵ_{HA} and ϵ_{A} , the calibration curve will show a positive or negative deviation from Beer's law if the standards are not buffered to the same pH.

Instrumental Limitations to Beer's Law There are two principal instrumental limitations to Beer's law. The first limitation is that Beer's law is strictly valid for purely monochromatic radiation; that is, for radiation consisting of only one wavelength. As we learned in Section 10B.2, however, even the best wavelength selector passes radiation with a small, but finite effective bandwidth. Using polychromatic radiation always gives a negative deviation from Beer's law, but is minimized if the value of ϵ is essentially constant over the wavelength range passed by the wavelength selector. For this reason, as shown in Figure 10.23, it is preferable to make absorbance measurements at a broad absorption peak. In addition, deviations from Beer's law are less serious if the effective bandwidth from the source is less than one tenth of the natural bandwidth of the absorbing species.^{7,8} When measurements must be made on a slope, linearity is improved by using a narrower effective bandwidth.

Stray radiation is the second contribution to instrumental deviations from Beer's law. Stray radiation arises from imperfections within the wavelength selector

stray radiation
Any radiation reaching the detector that does not follow the optical path from the source to the detector.

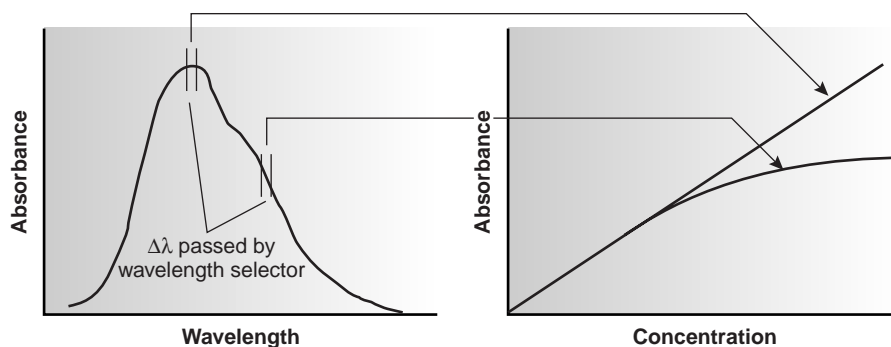


Figure 10.23
Effect of wavelength on the linearity of a Beer's law calibration curve.

that allows extraneous light to “leak” into the instrument. Stray radiation adds an additional contribution, P_{stray} , to the radiant power reaching the detector; thus

$$A = \log \frac{P_0 + P_{\text{stray}}}{P_T + P_{\text{stray}}}$$

For small concentrations of analyte, P_{stray} is significantly smaller than P_0 and P_T , and the absorbance is unaffected by the stray radiation. At higher concentrations of analyte, however, P_{stray} is no longer significantly smaller than P_T and the absorbance is smaller than expected. The result is a negative deviation from Beer’s law.

10D Ultraviolet-Visible and Infrared Spectrophotometry

The earliest routine application of molecular absorption spectroscopy, which dates to the 1830s, was colorimetry, in which visible light was absorbed by a sample. The concentration of analyte was determined visually by comparing the sample’s color to that of a set of standards using Nessler tubes (as described at the beginning of this chapter), or by using an instrument called a colorimeter. The development of visible absorption spectroscopy as a routine analytical technique was limited by the tedious nature of making visual color comparisons. Furthermore, although infrared radiation was discovered in 1800 and ultraviolet radiation in 1801, their use in optical molecular absorption spectroscopy was limited by the lack of a convenient means for detecting the radiation. During the 1930s and 1940s, advances in electronics resulted in the introduction of photoelectric transducers for ultraviolet and visible radiation, and thermocouples for infrared radiation. As a result, “modern” instrumentation for absorption spectroscopy routinely became available in the 1940s. Progress in these fields has been rapid ever since.

10D.1 Instrumentation

Frequently an analyst must select, from several instruments of different design, the one instrument best suited for a particular analysis. In this section we examine some of the different types of instruments used for molecular absorption spectroscopy, emphasizing their advantages and limitations. Methods of sample introduction are also covered in this section.

filter photometer

A simple instrument for measuring absorbance that uses absorption or interference filters to select the wavelength.

Instrument Designs for Molecular UV/Vis Absorption The simplest instrument currently used for molecular UV/Vis absorption is the **filter photometer** shown in Figure 10.24, which uses an absorption or interference filter to isolate a band of radiation. The filter is placed between the source and sample to prevent the sample from decomposing when exposed to high-energy radiation. A filter photometer has a single optical path between the source and detector and is called a single-beam instrument. The instrument is calibrated to 0% T while using a shutter to block the source radiation from the detector. After removing the shutter, the instrument is calibrated to 100% T using an appropriate blank. The blank is then replaced with the sample, and its transmittance is measured. Since the source’s incident power and the sensitivity of the detector vary with wavelength, the photometer must be recalibrated whenever the filter is changed. In comparison with other spectroscopic instruments, photometers have the advantage of being relatively inexpensive, rugged, and easy to maintain. Another advantage of a photometer is its portability, making it a useful instrument for conducting spectroscopic analyses in the field. A disadvantage of a photometer is that it cannot be used to obtain an absorption spectrum.

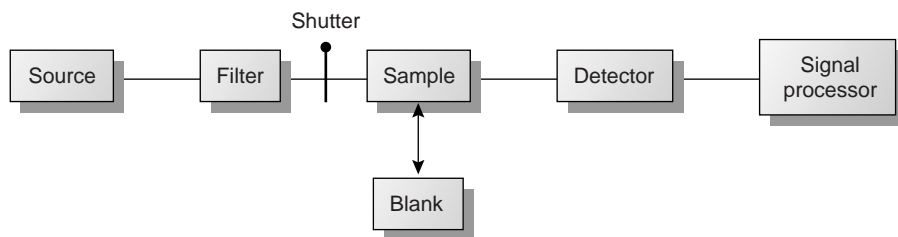


Figure 10.24

Block diagram for a filter photometer with photo showing a typical hand-held instrument suitable for field work.

Colorimeter™ is manufactured by Hach Company/photo courtesy of Hach Company.

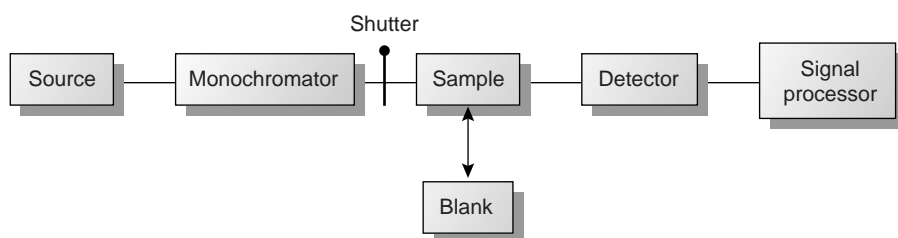


Figure 10.25

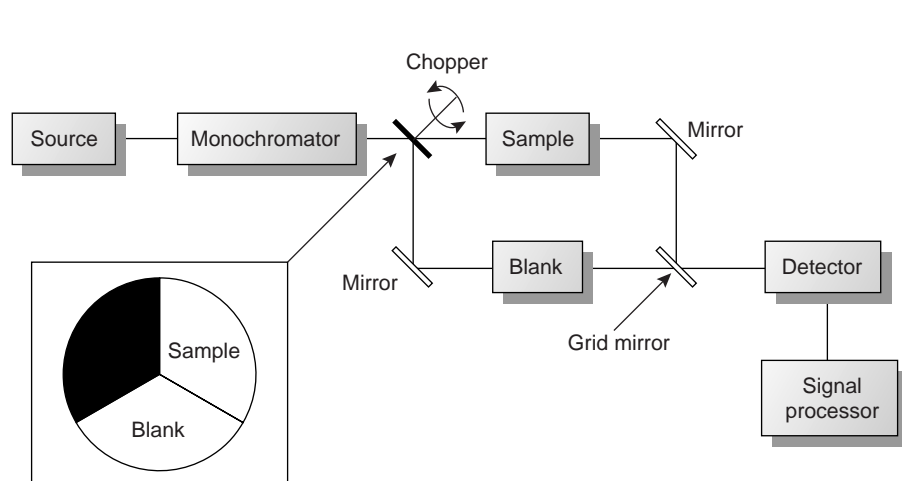
Block diagram for a single-beam fixed-wavelength spectrophotometer with photo of a typical instrument.

Photo courtesy of Fisher Scientific.

Instruments using monochromators for wavelength selection are called spectrometers. In absorbance spectroscopy, where the transmittance is a ratio of two radiant powers, the instrument is called a spectrophotometer. The simplest **spectrophotometer** is a single-beam instrument equipped with a fixed-wavelength monochromator, the block diagram for which is shown in Figure 10.25. Single-beam spectrophotometers are calibrated and used in the same manner as a photometer. One common example of a single-beam spectrophotometer is the Spectronic-20 manufactured by Milton-Roy. The Spectronic-20 can be used from 340 to 625 nm (950 nm with a red-sensitive detector), and has a fixed effective bandwidth of 20 nm. Because its effective bandwidth is fairly large, this instrument is more appropriate for a quantitative analysis than for a qualitative analysis. Battery-powered, hand-held single-beam spectrophotometers are available, which are easily transported and can be used for on-site analyses. Other single-beam spectrophotometers are available with effective bandwidths of 2–8 nm. Fixed-wavelength single-beam spectrophotometers are not practical for recording spectra since manually adjusting the wavelength and recalibrating the spectrophotometer is awkward and time-consuming. In addition, the accuracy of a single-beam spectrophotometer is limited by the stability of its source and detector over time.

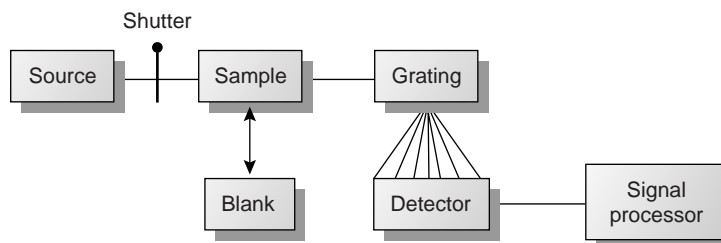
spectrophotometer

An instrument for measuring absorbance that uses a monochromator to select the wavelength.

**Figure 10.26**

Block diagram for a double-beam in-time scanning spectrophotometer with photo of a typical instrument.

Photo courtesy of Varian, Inc.

**Figure 10.27**

Block diagram for a diode array spectrophotometer.

The limitations of fixed-wavelength, single-beam spectrophotometers are minimized by using the double-beam in-time spectrophotometer as shown in Figure 10.26. A chopper, similar to that shown in the insert, controls the radiation's path, alternating it between the sample, the blank, and a shutter. The signal processor uses the chopper's known speed of rotation to resolve the signal reaching the detector into that due to the transmission of the blank (P_0) and the sample (P_T). By including an opaque surface as a shutter it is possible to continuously adjust the 0% T response of the detector. The effective bandwidth of a double-beam spectrophotometer is controlled by means of adjustable slits at the entrance and exit of the monochromator. Effective bandwidths of between 0.2 nm and 3.0 nm are common. A scanning monochromator allows for the automated recording of spectra. Double-beam instruments are more versatile than single-beam instruments, being useful for both quantitative and qualitative analyses; they are, however, more expensive.

The instrument designs considered thus far use a single detector and can only monitor one wavelength at a time. A linear photodiode array consists of multiple detectors, or channels, allowing an entire spectrum to be recorded in as little as 0.1 s. A block diagram for a typical multichannel spectrophotometer is shown in Figure 10.27. Source radiation passing through the sample is dispersed by a grating. The linear photodiode array is situated at the grating's focal plane, with each diode recording the radiant power over a narrow range of wavelengths.

One advantage of a linear photodiode array is the speed of data acquisition, which makes it possible to collect several spectra for a single sample. Individual spectra are added and averaged to obtain the final spectrum. This process of **signal averaging** improves a spectrum's signal-to-noise ratio. When a series of spectra is added, the sum of the signal at any point increases as (nS_x) , where n is the number of spectra, and S_x is the signal for the spectrum's x -th point. The propagation of noise, which is a random event, increases as $(\sqrt{n}N_x)$, where N_x is the noise level for the spectrum's x -th point. The signal-to-noise ratio (S/N) at the x -th data point, therefore, increases by a factor of \sqrt{n}

$$\frac{S}{N} = \frac{nS_x}{\sqrt{n}N_x} = \sqrt{n} \frac{S_x}{N_x}$$

where (S_x/N_x) is the signal-to-noise ratio for a single scan. The effect of signal averaging is shown in Figure 10.28. The spectrum in Figure 10.28a shows the total signal for a single scan. Although there is an apparent peak near the center of the spectrum, the level of background noise makes it difficult to measure the peak's signal. Figures 10.28b and Figure 10.28c demonstrate the improvement in signal-to-noise ratio achieved by signal averaging. One disadvantage of a linear photodiode array is that the effective bandwidth per diode is roughly an order of magnitude larger than that obtainable with a high-quality monochromator.

The sample compartment for the instruments in Figures 10.24–10.27 provides a light-tight environment that prevents the loss of radiation, as well as the addition of stray radiation. Samples are normally in the liquid or solution state and are placed in cells constructed with UV/Vis-transparent materials, such as quartz, glass, and plastic (Figure 10.29). Quartz or fused-silica cells are required when working at wavelengths of less than 300 nm where other materials show a significant absorption. The most common cell has a pathlength of 1 cm, although cells with shorter (≥ 1 mm) and longer pathlengths (≤ 10 cm) are available. Cells with a longer pathlength are useful for the analysis of very dilute solutions or for gaseous samples. The highest quality cells are constructed in a rectangular shape, allowing the radiation to strike the cell at a 90° angle, where losses to reflection are minimal. These cells, which are usually available in matched pairs having identical optical properties, are the cells of choice for double-beam instruments. Cylindrical test tubes are often used as a sample cell for simple, single-beam instruments, although differences in the cell's pathlength and optical properties add an additional source of error to the analysis.

In some circumstances it is desirable to monitor a system without physically removing a sample for analysis. This is often the case, for example, with the on-line monitoring of industrial production lines or waste lines, for physiological monitoring, and for monitoring environmental systems. With the use of a fiber-optic probe it is possible to analyze samples in situ. A simple example of a remote-sensing, fiber-optic probe is shown in Figure 10.30a and consists of two bundles of fiber-optic cable. One bundle transmits radiation from the source to the sample cell, which is designed to allow for the easy flow of sample through the cell. Radiation from the source passes through the solution, where it is reflected back by a mirror. The second bundle of fiber-optic cable transmits the nonabsorbed radiation to the wavelength selector. In an alternative design (Figure 10.30b), the sample cell is a membrane containing a reagent phase capable of reacting with the analyte. When the analyte diffuses

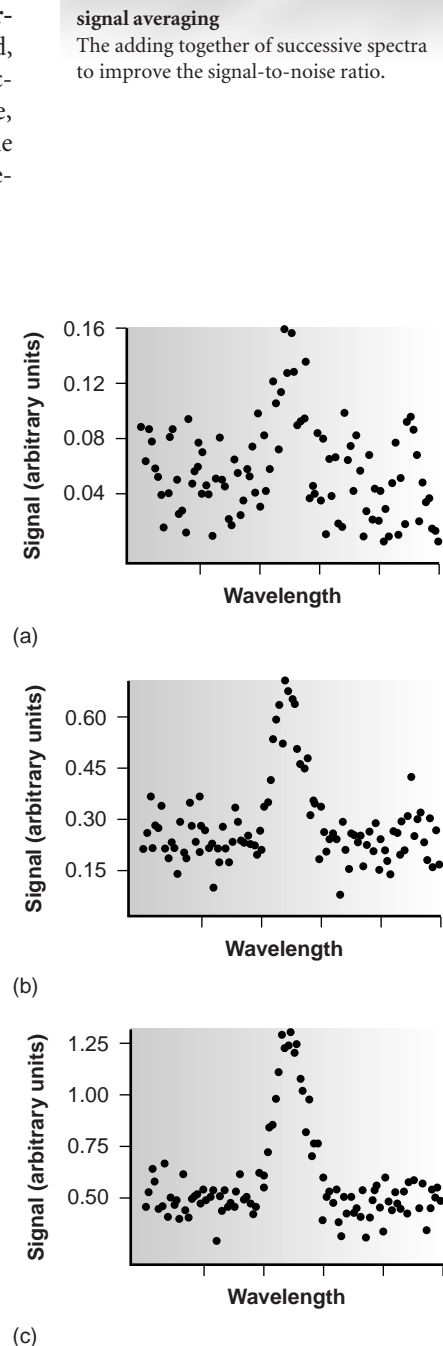


Figure 10.28

Effect of signal averaging on a spectrum's signal-to-noise ratio: (a) spectrum for a single scan; (b) spectrum after co-adding five spectra; (c) spectrum after co-adding ten spectra.



Figure 10.29
Typical cells used in UV/Vis spectroscopy.
Courtesy of Fisher Scientific.

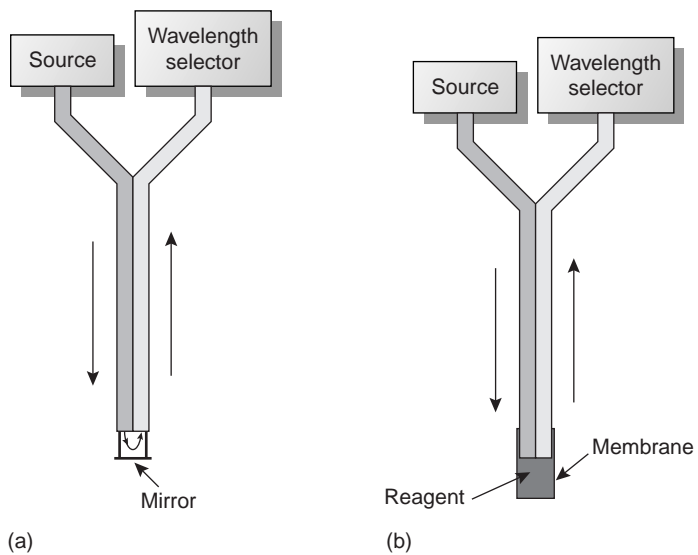


Figure 10.30
Example of fiber-optic probes.

across the membrane, it reacts with the reagent phase, producing a product that absorbs UV or visible radiation. Nonabsorbed radiation from the source is reflected or scattered back to the detector. Fiber-optic probes that show chemical selectivity are called optrodes.^{9,10}

Instrument Designs for Infrared Absorption The simplest instrument for IR absorption spectroscopy is a filter photometer similar to that shown in Figure 10.24 for UV/Vis absorption. These instruments have the advantage of portability and typically are used as dedicated analyzers for gases such as HCN and CO.

Infrared instruments using a monochromator for wavelength selection are constructed using double-beam optics similar to that shown in Figure 10.26. Double-beam optics are preferred over single-beam optics because the sources and detectors for infrared radiation are less stable than that for UV/Vis radiation. In addition, it is easier to correct for the absorption of infrared radiation by atmospheric CO₂ and H₂O vapor when using double-beam optics. Resolutions of 1–3 cm⁻¹ are typical for most instruments.

In a Fourier transform, infrared spectrometer, or FT-IR, the monochromator is replaced with an interferometer (see Figure 10.13). Because an FT-IR includes only a single optical path, it is necessary to collect a separate spectrum to compensate for the absorbance of atmospheric CO₂ and H₂O vapor. This is done by collecting a background spectrum without the sample and storing the result in the instrument's computer memory. The background spectrum is removed from the sample's spectrum by ratioing the two signals. In comparison to other IR instruments, an FT-IR provides for rapid data acquisition, allowing an enhancement in signal-to-noise ratio through signal averaging.

Infrared spectroscopy is routinely used for the analysis of samples in the gas, liquid, and solid states. Sample cells are made from materials, such as NaCl and KBr, that are transparent to infrared radiation. Gases are analyzed using a cell with a pathlength of approximately 10 cm. Longer pathlengths are obtained by using mirrors to pass the beam of radiation through the sample several times.

Liquid samples are analyzed in one of two ways. For nonvolatile liquids a suitable sample can be prepared by placing a drop of the liquid between two NaCl plates, forming a thin film that typically is less than 0.01 mm thick. Volatile liquids must be placed in a sealed cell to prevent their evaporation.

The analysis of solution samples is limited by the solvent's IR-absorbing properties, with CCl₄, CS₂, and CHCl₃ being the most common solvents. Solutions are placed in cells containing two NaCl windows separated by a Teflon spacer. By changing the Teflon spacer, pathlengths from 0.015 to 1.0 mm can be obtained. Sealed cells with fixed or variable pathlengths also are available.

The analysis of aqueous solutions is complicated by the solubility of the NaCl cell window in water. One approach to obtaining infrared spectra on aqueous solutions is to use attenuated total reflectance (ATR) instead of transmission. Figure 10.31 shows a diagram of a typical ATR sampler, consisting of an IR-transparent crystal of high-refractive index, such as ZnSe, surrounded by a sample of lower-refractive index. Radiation from the source enters the ATR crystal, where it undergoes a series of total internal reflections before exiting the crystal. During each reflection, the radiation penetrates into the sample to a depth of a few microns. The result is a selective attenuation of the radiation at those wavelengths at which the sample absorbs.

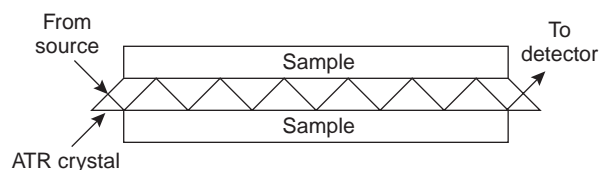


Figure 10.31
Attenuated total reflectance (ATR) cell for use in infrared spectroscopy.

ATR spectra are similar, but not identical, to those obtained by measuring the transmission of radiation.

Transparent solid samples can be analyzed directly by placing them in the IR beam. Most solid samples, however, are opaque and must be dispersed in a more transparent medium before recording a traditional transmission spectrum. If a suitable solvent is available, then the solid can be analyzed by preparing a solution and analyzing as described earlier. When a suitable solvent is not available, solid samples may be analyzed by preparing a mull of the finely powdered sample with a suitable oil. Alternatively, the powdered sample can be mixed with KBr and pressed into an optically transparent pellet.

Solid samples also can be analyzed by means of reflectance. The ATR sampler (see Figure 10.31) described for the analysis of aqueous solutions can be used for the analysis of solid samples, provided that the solid can be brought into contact with the ATR crystal. Examples of solids that have been analyzed by ATR include polymers, fibers, fabrics, powders, and biological tissue samples. Another reflectance method is diffuse reflectance, in which radiation is reflected from a rough surface, such as a powder. Powdered samples are mixed with a nonabsorbing material, such as powdered KBr, and the reflected light is collected and analyzed. As with ATR, the resulting spectrum is similar to that obtained by conventional transmission methods. Further details about these and other methods for preparing solids for infrared analysis can be found in the suggested readings listed at the end of the chapter.

10D.2 Quantitative Applications

The determination of an analyte's concentration based on its absorption of ultraviolet or visible radiation is one of the most frequently encountered quantitative analytical methods. One reason for its popularity is that many organic and inorganic compounds have strong absorption bands in the UV/Vis region of the electromagnetic spectrum. In addition, analytes that do not absorb UV/Vis radiation, or that absorb such radiation only weakly, frequently can be chemically coupled to a species that does. For example, nonabsorbing solutions of Pb^{2+} can be reacted with dithizone to form the red Pb–dithizonate complex. An additional advantage to UV/Vis absorption is that in most cases it is relatively easy to adjust experimental and instrumental conditions so that Beer's law is obeyed.

Quantitative analyses based on the absorption of infrared radiation, although important, are less frequently encountered than those for UV/Vis absorption. One reason is the greater tendency for instrumental deviations from Beer's law when using infrared radiation. Since infrared absorption bands are relatively narrow, deviations due to the lack of monochromatic radiation are more pronounced. In addition, infrared sources are less intense than sources of UV/Vis radiation, making stray radiation more of a problem. Differences in pathlength for samples and standards when using thin liquid films or KBr pellets are a problem, although an internal standard can be used to correct for any difference in pathlength. Finally, establishing a 100% T ($A = 0$) baseline is often difficult since the optical properties of NaCl sample cells may change significantly with wavelength due to contamination and degradation. This problem can be minimized by determining absorbance relative to a baseline established for the absorption band. Figure 10.32 shows how this is accomplished.

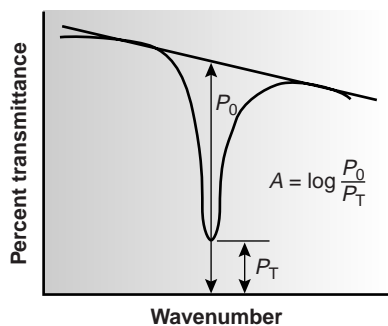


Figure 10.32

Method for determining absorbance from an IR transmission spectrum.

The applications of Beer's law for the quantitative analysis of samples in environmental chemistry, clinical chemistry, industrial chemistry and forensic chemistry are numerous. Examples from each of these fields follow.

Table 10.6 Selected Examples of the Application of UV/Vis Molecular Absorption to the Analysis of Waters and Wastewaters

Analyte	Method	λ (nm)
<i>Trace Metals</i>		
aluminum	reaction with Eriochrome cyanide R dye at pH 6 produces red to pink complex	535
arsenic	reduce to AsH_3 using Zn and react with silver diethyldithiocarbamate to form red complex	535
cadmium	extraction into $CHCl_3$ containing dithizone from sample made basic with NaOH; pink to red complex	518
chromium	oxidize to Cr(VI) and react with diphenylcarbazide in acidic solution to give red-violet product	540
copper	react with neocuprine in neutral to slightly acid solution; extract into $CHCl_3/CH_3OH$ to give yellow solution	457
iron	react with <i>o</i> -phenanthroline in acidic solution to form orange-red complex	510
lead	extraction into $CHCl_3$ containing dithizone from sample made basic with ammoniacal buffer; cherry red complex	510
manganese	oxidize to MnO_4^- with persulfate	525
mercury	extraction into $CHCl_3$ containing dithizone from acidic sample; orange complex	492
zinc	reaction with zincon at pH 9 to form blue complex	620
<i>Inorganic Nonmetals</i>		
ammonia	reaction with ammonia, hypochlorite, and phenol produces blue indophenol; catalyzed by manganous salt	630
cyanide	convert to $CNCl$ by reaction with chloramine-T, followed by reaction with a pyridine-barbituric acid to form red-blue dye	578
fluoride	reaction with red Zr-SPADNS lake results in formation of ZrF_6^{2-} and decrease in concentration of the lake	570
chlorine (residual)	oxidation of leuco crystal violet to form product with a bluish color	592
nitrate	reduction to NO_2^- by Cd, colored azo dye formed by reaction with sulfanilamide and <i>N</i> -(1-naphthyl)-ethylenediamine	543
phosphate	reaction with ammonium molybdate followed by reduction with stannous chloride to form molybdenum blue	690
<i>Organics</i>		
phenol	reaction with 4-aminoantipyrine and $K_3Fe(CN)_6$ to form antipyrine dye	460
surfactants	formation of blue ion pair between anionic surfactant and the cationic dye methylene blue, which is extracted into $CHCl_3$	652

Environmental Applications Methods for the analysis of waters and wastewaters relying on the absorption of UV/Vis radiation are among some of the most frequently employed analytical methods. Many of these methods are outlined in Table 10.6, and a few are described later in more detail.

Although the quantitative analysis of metals in water and wastewater is accomplished primarily by atomic absorption or atomic emission spectroscopy, many metals also can be analyzed following the formation of a colored metal–ligand complex. One advantage to these spectroscopic methods is that they are easily adapted to the field analysis of samples using a filter photometer. One ligand used in the analysis of several metals is diphenylthiocarbazone, also known as dithizone. Dithizone is insoluble in water, but when a solution of dithizone in $CHCl_3$ is shaken with an aqueous solution containing an appropriate metal ion, a colored metal–dithizonate complex forms that is soluble in $CHCl_3$. The selectivity

of dithizone is controlled by adjusting the pH of the aqueous sample. For example, Cd^{2+} is extracted from solutions that are made strongly basic with NaOH, Pb^{2+} from solutions that are made basic with an ammoniacal buffer, and Hg^{2+} from solutions that are slightly acidic.

When chlorine is added to water that portion available for disinfection is called the chlorine residual. Two forms of the chlorine residual are recognized. The free chlorine residual includes Cl_2 , HOCl, and OCl^- . The combined chlorine residual, which forms from the reaction of NH_3 with HOCl, consists of monochloroamine, NH_2Cl , dichlororamine, NHCl_2 , and trichloroamine, NCl_3 . Since the free chlorine residual is more efficient at disinfection, analytical methods have been developed to determine the concentration of both forms of residual chlorine. One such method is the leuco crystal violet method. Free residual chlorine is determined by adding leuco crystal violet to the sample, which instantaneously oxidizes giving a bluish color that is monitored at 592 nm. Completing the analysis in less than 5 min prevents a possible interference from the combined chlorine residual. The total chlorine residual (free + combined) is determined by reacting a separate sample with iodide, which reacts with both chlorine residuals to form HOI. When the reaction is complete, leuco crystal violet is added and oxidized by HOI, giving the same bluish colored product. The combined chlorine residual is determined by difference.

The concentration of fluoride in drinking water may be determined indirectly by its ability to form a complex with zirconium. In the presence of the dye SPADNS,* solutions of zirconium form a reddish colored compound, called a "lake," that absorbs at 570 nm. When fluoride is added, the formation of the stable ZrF_6^{2-} complex causes a portion of the lake to dissociate, decreasing the absorbance. A plot of absorbance versus the concentration of fluoride, therefore, has a negative slope.

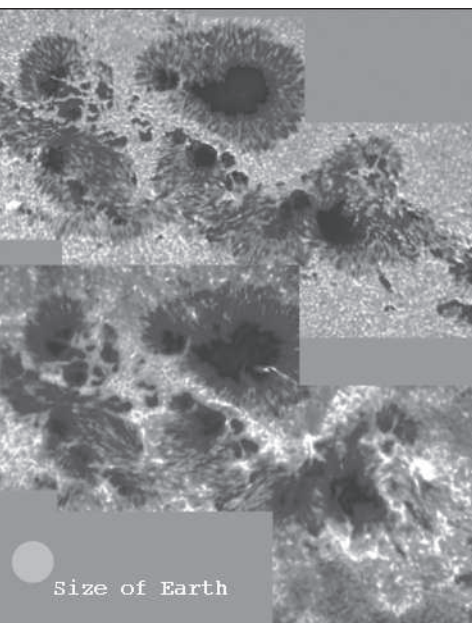
Spectroscopic methods also are used in determining organic constituents in water. For example, the combined concentrations of phenol, and ortho- and meta-substituted phenols are determined by using steam distillation to separate the phenols from nonvolatile impurities. The distillate is reacted with 4-aminoantipyrine at $\text{pH } 7.9 \pm 0.1$ in the presence of $\text{K}_3\text{Fe}(\text{CN})_6$, forming a colored antipyrine dye. The dye is extracted into CHCl_3 , and the absorbance is monitored at 460 nm. A calibration curve is prepared using only the unsubstituted phenol, $\text{C}_6\text{H}_5\text{OH}$. Because the molar absorptivities of substituted phenols are generally less than that for phenol, the reported concentration represents the minimum concentration of phenolic compounds.

Molecular absorption also can be used for the analysis of environmentally significant airborne pollutants. In many cases the analysis is carried out by collecting the sample in water, converting the analyte to an aqueous form that can be analyzed by methods such as those described in Table 10.6. For example, the concentration of NO_2 can be determined by oxidizing NO_2 to NO_3^- . The concentration of NO_3^- is then determined by reducing to NO_2^- with Cd and reacting the NO_2^- with sulfanilamide and *N*-(1-naphthyl)-ethylenediamine to form a brightly colored azo dye. Another important application is the determination of SO_2 , which is determined by collecting the sample in an aqueous solution of HgCl_4^{2-} where it reacts to form $\text{Hg}(\text{SO}_3)_2^{2-}$. Addition of *p*-rosaniline and formaldehyde results in the formation of a bright purple complex that is monitored at 569 nm. Infrared absorption has proved useful for the analysis of organic vapors, including HCN, SO_2 , nitrobenzene, methyl mercaptan, and vinyl chloride. Frequently, these analyses are accomplished using portable, dedicated infrared photometers.

*SPADNS is the acronym for the sodium salt of 2-(4-sulfophenylazo)-1,8-dihydroxy-3,6-naphthalenedisulfonic acid.

CHAPTER 24

Introduction to Spectrochemical Methods



M. Sigwarth, J. Elrod, K.S. Balasubramaniam,
S. Fletcher/NSO/AURA/NSF

Methods that use or produce UV, visible, or IR radiation are often called optical spectroscopic methods. Other useful methods include those that use the γ -ray, X-ray, microwave, and RF spectral regions.



This composite image is a sunspot group collected with the Dunn Solar Telescope at the Sacramento Peak Observatory in New Mexico on March 29, 2001. The lower portion consisting of four frames was collected at a wavelength of 393.4 nm, and the upper portion was collected at 430.4 nm. The lower image represents calcium ion concentration, with the intensity of the radiation proportional to the amount of the ion in the sunspot. The upper image shows the presence of the CH molecule. Using data like these, it is possible to determine the location and abundance of virtually any chemical species in the universe. Note that the Earth could fit in the large black core sunspot at the upper left of each of the composite images.

Measurements based on light and other forms of electromagnetic radiation are widely used throughout analytical chemistry. The interactions of radiation and matter are the subject of the science called **spectroscopy**. Spectroscopic analytical methods are based on measuring the amount of radiation produced or absorbed by molecular or atomic species of interest.¹ We can classify spectroscopic methods according to the region of the electromagnetic spectrum used or produced in the measurement. The γ -ray, X-ray, ultraviolet (UV), visible, infrared (IR), microwave, and radio-frequency (RF) regions have been used. Indeed, current usage extends the meaning of spectroscopy yet further to include techniques such as acoustic, mass, and electron spectroscopy in which electromagnetic radiation is not a part of the measurement.

Spectroscopy has played a vital role in the development of modern atomic theory. In addition, **spectrochemical methods** have provided perhaps the most widely used tools for the elucidation of molecular structure as well as the quantitative and qualitative determination of both inorganic and organic compounds.

In this chapter, we discuss the basic principles that are necessary to understand measurements made with electromagnetic radiation, particularly those dealing with the absorption of UV, visible, and IR radiation. The nature of electromagnetic radiation and its interactions with matter are stressed. The next five chapters are devoted to spectroscopic instruments (Chapter 25), molecular absorption spectroscopy (Chapter 26), molecular fluorescence spectroscopy (Chapter 27), atomic spectroscopy (Chapter 28), and mass spectrometry (Chapter 29).

¹For further study, see D. A. Skoog, F. J. Holler, and S. R. Crouch, *Principles of Instrumental Analysis*, 6th ed., Sections 2–3, Belmont, CA: Brooks/Cole, 2007; F. Settle, ed., *Handbook of Instrumental Techniques for Analytical Chemistry*, Sections III–IV, Upper Saddle River, NJ: Prentice-Hall, 1997; J. D. Ingle, Jr., and S. R. Crouch, *Spectrochemical Analysis*, Upper Saddle River, NJ: Prentice-Hall, 1988; E. J. Meehan, in *Treatise on Analytical Chemistry*, 2nd ed., P. J. Elving, E. J. Meehan, and I. M. Kolthoff, eds., Part I, Vol. 7, Chs. 1–3, New York: Wiley, 1981.

PROPERTIES OF ELECTROMAGNETIC RADIATION

24A RADIATION

Electromagnetic radiation is a form of energy that is transmitted through space at enormous velocities. We will call electromagnetic radiation in the UV/visible and sometimes in the IR region, **light**, although strictly speaking the term refers only to visible radiation. Electromagnetic radiation can be described as a wave with properties of wavelength, frequency, velocity, and amplitude. In contrast to sound waves, light requires no transmitting medium; thus, it can travel readily through a vacuum. Light also travels nearly a million times faster than sound.

The wave model fails to account for phenomena associated with the absorption and emission of radiant energy. For these processes, electromagnetic radiation can be treated as discrete packets of energy or particles called **photons** or **quanta**. These dual views of radiation as particles and waves are not mutually exclusive but complementary. In fact, the energy of a photon is directly proportional to its frequency as we shall see. Similarly, this duality applies to streams of electrons, protons, and other elementary particles, which can produce interference and diffraction effects that are typically associated with wave behavior.

24A-1 Wave Properties

In dealing with phenomena such as reflection, refraction, interference, and diffraction, electromagnetic radiation is conveniently modeled as waves consisting of perpendicularly oscillating electric and magnetic fields, as shown in **Figure 24-1a**. The electric field for a single frequency wave oscillates sinusoidally in space and time, as shown in **Figure 24-1b**. The electric field is represented as a vector whose length is proportional to the field strength. The x axis in this plot is either time as the radiation passes a fixed point in space or distance at a fixed time. Note that the direction in which the field oscillates is perpendicular to the direction in which the radiation propagates.

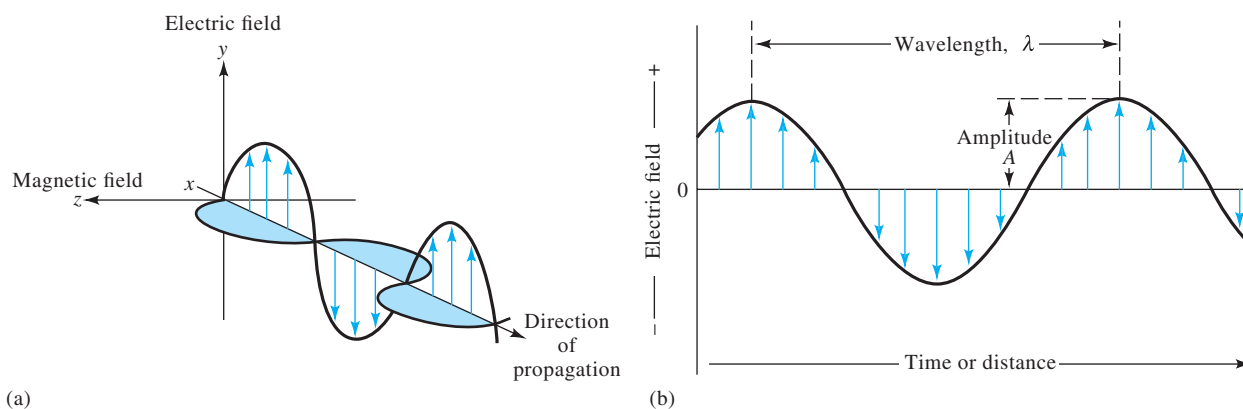


Figure 24-1 Wave nature of a beam of single frequency electromagnetic radiation. In (a), a plane-polarized wave is shown propagating along the x axis. The electric field oscillates in a plane perpendicular to the magnetic field. If the radiation were unpolarized, a component of the electric field would be seen in all planes. In (b), only the electric field oscillations are shown. The amplitude of the wave is the length of the electric field vector at the wave maximum, while the wavelength is the distance between successive maxima.



Courtesy of the Archives, California Institute of Technology

Richard P. Feynman (1918–1988) was one of the most renowned scientists of the twentieth century. He was awarded the Nobel Prize in Physics in 1965 for his role in the development of quantum electrodynamics. In addition to his many and varied scientific contributions, he was a skilled teacher, and his lectures and books had a major influence on physics education and science education in general.

Now we know how the electrons and photons behave. But what can I call it? If I say they behave like particles I give the wrong impression; also if I say they behave like waves. They behave in their own inimitable way, which technically could be called a quantum mechanical way. They behave in a way that is like nothing that you have ever seen before. — R. P. Feynman²

²R. P. Feynman, *The Character of Physical Law*, New York: Random House, 1994, p. 122.

The **amplitude** of an electromagnetic wave is a vector quantity that provides a measure of the electric or magnetic field strength at a maximum in the wave.

The **period** of an electromagnetic wave is the time in seconds for successive maxima or minima to pass a point in space.

The **frequency** of an electromagnetic wave is the number of oscillations that occur in one second.

The unit of frequency is the **hertz** (Hz), which corresponds to one cycle per second, that is, $1 \text{ Hz} = 1 \text{ s}^{-1}$. The frequency of a beam of electromagnetic radiation does not change as it passes through different media.

Radiation velocity and wavelength both decrease as the radiation passes from a vacuum or from air to a denser medium. Frequency remains constant.

Note in Equation 24-1, v (distance/time) = v waves/time $\times \lambda$ (distance/wave)

To three significant figures, Equation 24-2 is equally applicable in air or vacuum.

The **refractive index**, η , of a medium measures the extent of interaction between electromagnetic radiation and the medium through which it passes. It is defined by $\eta = c/v$. For example, the refractive index of water at room temperature is 1.33, which means that radiation passes through water at a rate of $c/1.33$ or $2.26 \times 10^{10} \text{ cm s}^{-1}$. In other words, light travels 1.33 times slower in water than it does in vacuum. The velocity and wavelength of radiation become proportionally smaller as the radiation passes from a vacuum or from air to a denser medium while the frequency remains constant.

TABLE 24-1

Wavelength Units for Various Spectral Regions

Region	Unit	Definition
X-ray	Angstrom unit, Å	10^{-10} m
Ultraviolet/visible	Nanometer, nm	10^{-9} m
Infrared	Micrometer, μm	10^{-6} m

Wave Characteristics

In Figure 24-1b, the **amplitude** of the sine wave is shown, and the wavelength is defined. The time in seconds required for the passage of successive maxima or minima through a fixed point in space is called the **period**, p , of the radiation. The **frequency**, ν , is the number of oscillations of the electric field vector per unit time and is equal to $1/p$.

The frequency of a light wave or any wave of electromagnetic radiation is determined by the source that emits it and remains constant regardless of the medium traversed. In contrast, the **velocity**, v , of the wave front through a medium depends on both the medium and the frequency. The **wavelength**, λ , is the linear distance between successive maxima or minima of a wave, as shown in Figure 24-1b. The product of the frequency in waves per unit time and the wavelength in distance per wave is the velocity v of the wave in distance per unit time (cm s^{-1} or m s^{-1}), as shown in Equation 24-1. Note that both the velocity and the wavelength depend on the medium.

$$v = \nu\lambda \quad (24-1)$$

Table 24-1 gives the units used to express wavelengths in various regions of the spectrum.

The Speed of Light

In a vacuum, light travels at its maximum velocity. This velocity, which is given the special symbol c , is $2.99792 \times 10^8 \text{ m s}^{-1}$. The velocity of light in air is only about 0.03 % less than its velocity in vacuum. Thus, for a vacuum, or for air, Equation 24-1 can be written to three significant figures as

$$c = \nu\lambda = 3.00 \times 10^8 \text{ m s}^{-1} = 3.00 \times 10^{10} \text{ cm s}^{-1} \quad (24-2)$$

In a medium containing matter, light travels with a velocity less than c because of interaction between the electromagnetic field and electrons in the atoms or molecules of the medium. Since the frequency of the radiation is constant, the wavelength must decrease as the light passes from a vacuum to a medium containing matter (see Equation 24-1). This effect is illustrated in **Figure 24-2** for a beam of visible radiation. Note that the effect can be quite large.

The **wavenumber**, $\bar{\nu}$, is another way to describe electromagnetic radiation. It is defined as the number of waves per centimeter and is equal to $1/\lambda$. By definition, $\bar{\nu}$ has the units of cm^{-1} .

EXAMPLE 24-1

Calculate the wavenumber of a beam of infrared radiation with a wavelength of $5.00 \mu\text{m}$.

Solution

$$\bar{\nu} = \frac{1}{\lambda} = \frac{1}{5.00 \mu\text{m} \times 10^{-4} \text{ cm}/\mu\text{m}} = 2000 \text{ cm}^{-1}$$

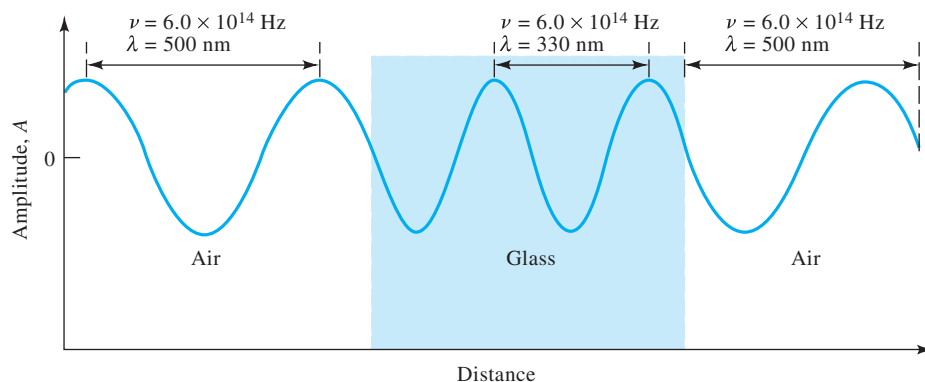


Figure 24-2 Change in wavelength as radiation passes from air into a dense glass and back to air. Note that the wavelength shortens by nearly 200 nm, or more than 30%, as it passes into glass; a reverse change occurs as the radiation again enters air.

Radiant Power and Intensity

The **radiant power**, P , in watts (W) is the energy of a beam that reaches a given area per unit time. The **intensity** is the radiant power-per-unit solid angle.³ Both quantities are proportional to the square of the amplitude of the electric field (see Figure 24-1b). Although not strictly correct, radiant power and intensity are frequently used interchangeably.

24A-2 The Particle Nature of Light: Photons

In many radiation/matter interactions, it is useful to emphasize the particle nature of light as a stream of photons or quanta. We relate the energy of a single photon to its wavelength, frequency, and wavenumber by

$$E = h\nu = \frac{hc}{\lambda} = hc\bar{\nu} \quad (24-3)$$

where h is Planck's constant (6.63×10^{-34} J·s). Note that the wavenumber and frequency in contrast to the wavelength are directly proportional to the photon energy. Wavelength is inversely proportional to energy. The radiant power of a beam of radiation is directly proportional to the number of photons per second.

EXAMPLE 24-2

Calculate the energy in joules of one photon of radiation with the wavelength given in Example 24-1.

Solution

Applying Equation 24-3, we can write

$$\begin{aligned} E &= hc\bar{\nu} = 6.63 \times 10^{-34} \text{ J} \cdot \text{s} \times 3.00 \times 10^{10} \frac{\text{cm}}{\text{s}} \times 2000 \text{ cm}^{-1} \\ &= 3.98 \times 10^{-20} \text{ J} \end{aligned}$$

³Solid angle is the three dimensional spread at the vertex of a cone measured as the area intercepted by the cone on a unit sphere whose center is at the vertex. The angle is measured in steradians (sr).

The **wavenumber** $\bar{\nu}$ in cm^{-1} (Kaysers) is most often used to describe radiation in the infrared region. The most useful part of the infrared spectrum for the detection and determination of organic species is from 2.5 to 15 μm , which corresponds to a wavenumber range of 4000 to 667 cm^{-1} . As shown below, the wavenumber of a beam of electromagnetic radiation is directly proportional to its energy and thus its frequency.

A **photon** is a particle of electromagnetic radiation having zero mass and an energy of $h\nu$.

Equation 24-3 gives the energy of radiation in SI units of **joules**, where one joule (J) is the work done by a force of one newton (N) acting over a distance of one meter.

Both frequency and wavenumber are proportional to the energy of a photon.

We sometimes speak of “a mole of photons”, meaning 6.022×10^{23} packets of radiation of a given wavelength. The energy of one mole of photons with a wavelength of 5.00 μm is $6.022 \times 10^{23} \text{ photons/mol} \times 1 \text{ mol} \times 3.98 \times 10^{-20} \text{ J/photon} = 2.40 \times 10^4 \text{ J} = 24.0 \text{ kJ}$.

24B INTERACTION OF RADIATION AND MATTER

The most interesting and useful interactions in spectroscopy are those in which transitions occur between different energy levels of chemical species. Other interactions, such as reflection, refraction, elastic scattering, interference, and diffraction, are often related to the bulk properties of materials rather than to the unique energy levels of specific molecules or atoms. Although these bulk interactions are also of interest in spectroscopy, we will limit our discussion here to those interactions in which energy level transitions occur. The specific types of interactions observed depend strongly on the energy of the radiation used and the mode of detection.

TABLE 24-2

Regions of the UV, Visible, and IR Spectrum	
Region	Wavelength Range
UV	180–380 nm
Visible	380–780 nm
Near-IR	0.78–2.5 μm
Mid-IR	2.5–50 μm

One easy way to recall the order of the colors in the spectrum is by the mnemonic **ROY G BIV**, which is short for **R**ed, **O**range, **Y**ellow, **G**reen, **B**lue, **I**ndigo, and **V**iolet.

The **visible region** of the spectrum extends from about 400 nm to almost 800 nm (see Table 24-2).

24B-1 The Electromagnetic Spectrum

The electromagnetic spectrum covers an enormous range of energies (frequencies) and thus wavelengths (see Table 24-2). Useful frequencies vary from $>10^{19}$ Hz (γ -ray) to 10^3 Hz (radio waves). An X-ray photon ($\nu \approx 3 \times 10^{18}$ Hz, $\lambda \approx 10^{-10}$ m), for example, is 10,000 times as energetic as a photon emitted by an ordinary light bulb ($\nu \approx 3 \times 10^{14}$ Hz, $\lambda \approx 10^{-6}$ m) and 10^{15} times as energetic as a radio-frequency photon ($\nu \approx 3 \times 10^3$ Hz, $\lambda \approx 10^5$ m).

The major divisions of the spectrum are shown in color in Color Plate 21. Note that the visible region, to which our eyes respond, is only a tiny fraction of the entire spectrum. Different types of radiation such as gamma (γ) rays or radio waves differ from visible light only in the energy (frequency) of their photons.

Figure 24-3 shows the regions of electromagnetic spectrum that are used for spectroscopic analyses. Also shown are the types of atomic and molecular transitions that result from interactions of the radiation with a sample. Note that the

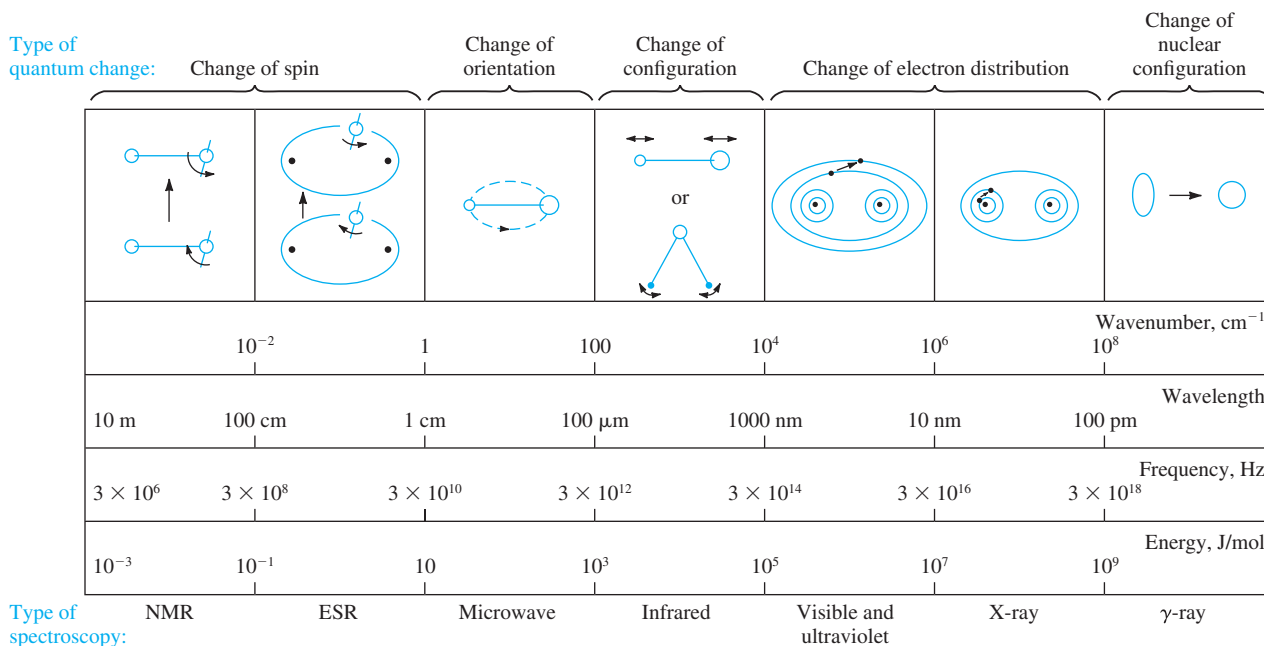


Figure 24-3 The regions of the electromagnetic spectrum. Interaction of an analyte with electromagnetic radiation can result in the types of changes shown. Note that changes in electron distributions occur in the UV/visible region. The wavenumber, wavelength, frequency, and energy are characteristics that describe electromagnetic radiation. (From C. N. Banwell, *Fundamentals of Molecular Spectroscopy*, 3rd ed., New York; McGraw-Hill, 1983, p. 7.)

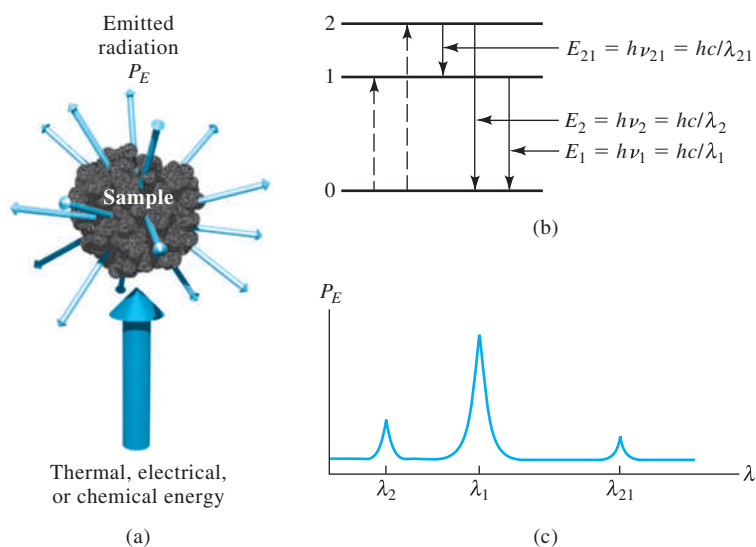
low-energy radiation used in nuclear magnetic resonance (NMR) and electron spin resonance (ESR) spectroscopy causes subtle changes, such as changes in spin; the high-energy radiation used in γ -ray spectroscopy can cause much more dramatic changes, such as nuclear configuration changes.

Spectrochemical methods that use not only visible but also ultraviolet and infrared radiation are often called **optical methods** in spite of the fact that the human eye is not sensitive to UV or IR radiation. This terminology arises from the many common features of instruments for the three spectral regions and the similarities in the way we view the interactions of the three types of radiation with matter.

24B-2 Spectroscopic Measurements

Spectroscopists use the interactions of radiation with matter to obtain information about a sample. Several of the chemical elements were discovered by spectroscopy (see Feature 24-1). The sample is usually stimulated in some way by applying energy in the form of heat, electrical energy, light, particles, or a chemical reaction. Prior to applying the stimulus, the analyte is predominately in its lowest-energy or **ground state**. The stimulus then causes some of the analyte species to undergo a transition to a higher-energy or **excited state**. We acquire information about the analyte by measuring the electromagnetic radiation emitted as it returns to the ground state or by measuring the amount of electromagnetic radiation absorbed as a result of excitation.

Figure 24-4 illustrates the processes that occur in emission and chemiluminescence spectroscopy. The analyte is stimulated by applying heat or electrical energy or by a chemical reaction. The term **emission spectroscopy** usually refers to methods in which the stimulus is heat or electrical energy, while **chemiluminescence spectroscopy** refers to excitation of the analyte by a chemical reaction. In both cases, measurement of the radiant power emitted as the analyte returns to the ground state can give information about its identity and concentration. The results of such a measurement are often expressed graphically by a **spectrum**, which is a plot of the emitted radiation as a function of frequency or wavelength.



Optical methods are spectroscopic methods based on ultraviolet, visible, and infrared radiation.

A familiar example of **chemiluminescence** is found in the light emitted by a firefly. In the firefly reaction, an enzyme luciferase catalyzes the oxidative phosphorylation reaction of luciferin with adenosine triphosphate (ATP) to produce oxyluciferin, carbon dioxide, adenosine monophosphate (AMP), and light. Chemiluminescence involving a biological or enzyme reaction is often termed **bioluminescence**. The popular light stick is another familiar example of chemiluminescence.

Figure 24-4 Emission or chemiluminescence processes. In (a), the sample is excited by applying thermal, electrical, or chemical energy. No radiant energy is used to produce excited states, and so, these are called non-radiative processes. In the energy level diagram (b), the dashed lines with upward pointing arrows symbolize these nonradiative excitation processes, while the solid lines with downward pointing arrows indicate that the analyte loses its energy by emission of a photon. In (c), the resulting spectrum is shown as a measurement of the radiant power emitted, P_E , as a function of wavelength, λ .

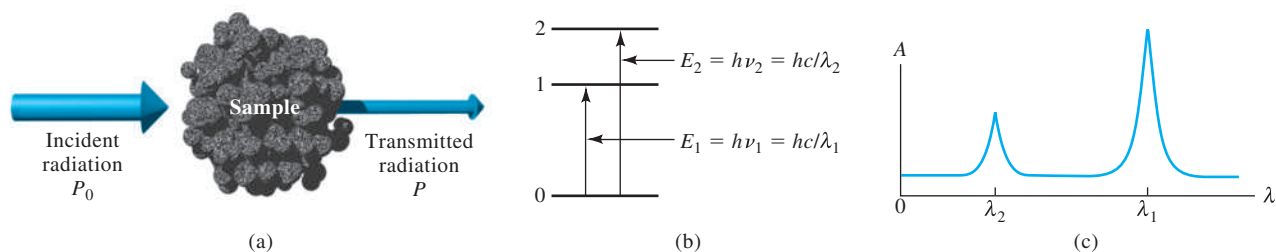


Figure 24-5 Absorption methods. In (a), radiation of incident radiant power P_0 can be absorbed by the analyte, resulting in a transmitted beam of lower radiant power P . For absorption to occur the energy of the incident beam must correspond to one of the energy differences shown in (b). The resulting absorption spectrum is shown in (c).

When the sample is stimulated by applying an external electromagnetic radiation source, several processes are possible. For example, the radiation can be scattered or reflected. What is important to us is that some of the incident radiation can be absorbed and promote some of the analyte species to an excited state, as shown in **Figure 24-5**. In **absorption spectroscopy**, we measure the amount of light absorbed as a function of wavelength. Absorption measurements can give both qualitative and quantitative information about the sample. In **photoluminescence spectroscopy** (see **Figure 24-6**), the emission of photons is measured following absorption. The most important forms of photoluminescence for analytical purposes are **fluorescence** and **phosphorescence spectroscopy**.

We focus here on absorption spectroscopy in the UV/visible region of the spectrum because it is so widely used in chemistry, biology, forensic science, engineering, agriculture, clinical chemistry, and many other fields. Note that the processes shown in Figures 24-4 through 24-6 can occur in any region of the electromagnetic spectrum; the different energy levels can be nuclear levels, electronic levels, vibrational levels, or spin levels.

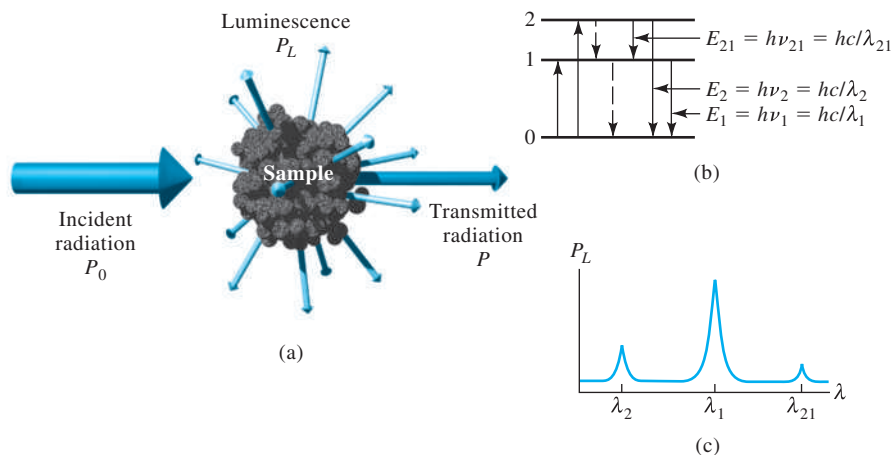


Figure 24-6 Photoluminescence methods (fluorescence and phosphorescence). Fluorescence and phosphorescence result from absorption of electromagnetic radiation and then dissipation of the energy by emission of radiation, as shown in (a). In (b), the absorption can cause excitation of the analyte to state 1 or state 2. Once excited, the excess energy can be lost by emission of a photon (luminescence shown as solid lines) or by nonradiative processes (dashed lines). The emission occurs over all angles, and the wavelengths emitted (c) correspond to energy differences between levels. The major distinction between fluorescence and phosphorescence is the time scale of emission with fluorescence being prompt and phosphorescence being delayed.

FEATURE 24-1

Spectroscopy and the Discovery of Elements

The modern era of spectroscopy began with the observation of the spectrum of the sun by Sir Isaac Newton in 1672. In his experiment, Newton passed rays from the sun through a small opening into a dark room where they struck a prism and dispersed into the colors of the spectrum. The first description of spectral features beyond the simple observation of colors was in 1802 by Wollaston, who noticed dark lines on a photographic image of the solar spectrum. These lines along with more than 500 others, which are shown in the solar spectrum of [Figure 24F-1](#), were later described in detail by Fraunhofer. Based on his observations, which began in 1817, Fraunhofer gave the prominent lines letters starting with “A” at the red end of the spectrum. The solar spectrum is shown in color plate 17.

It remained, however, for Gustav Kirchhoff and Robert Wilhelm Bunsen in 1859 and 1860 to explain the origin of the Fraunhofer lines. Bunsen had invented his famous burner (see [Figure 24F-2](#)) a few years earlier, which made possible spectral observations of emission and absorption phenomena in a nearly transparent flame. Kirchhoff concluded that

the Fraunhofer “D” lines were due to sodium in the sun’s atmosphere and the “A” and “B” lines were due to potassium. To this day, we call the emission lines of sodium the sodium “D” lines. These lines are responsible for the familiar yellow color seen in flames containing sodium or in sodium vapor lamps. The absence of lithium in the sun’s spectrum led Kirchhoff to conclude that there was little lithium present in the sun. During these studies, Kirchhoff also developed his famous laws relating the absorption and emission of light from bodies and at interfaces. Together with Bunsen, Kirchhoff observed that different elements could impart different colors to flames and produce spectra exhibiting differently colored bands or lines. Kirchhoff and Bunsen are thus credited with discovering the use of spectroscopy for chemical analysis. Emission spectra of several elements are shown in color plate 16. The method was soon put to many practical uses, including the discovery of new elements. In 1860, the elements cesium and rubidium were discovered with spectroscopy, followed in 1861 by thallium and in 1864 by indium. The age of spectroscopic analysis had begun.

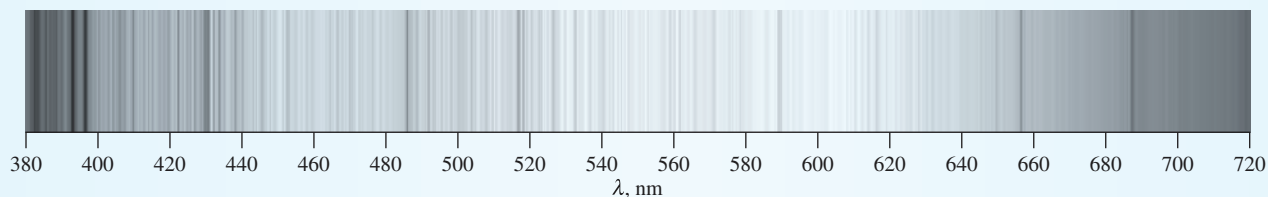


Figure 24F-1 The solar spectrum. The dark vertical lines are the Fraunhofer lines. See color plate 17 for a full-color version of the spectrum. Data for the image were collated by Dr. Donald Mickey, University of Hawaii Institute for Astronomy, from National Solar Observatory spectral data. NSO/Kitt Peak FTS data used here were produced by NSF/NOAO.

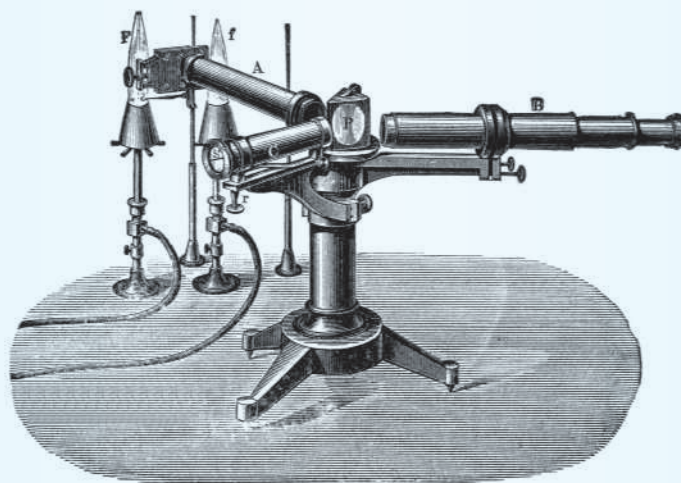


Figure 24F-2 Bunsen burner of the type used in early spectroscopic studies with a prism spectroscope of type used by Kirchhoff. (From H. Kayser, *Handbuch der Spectroscopie*, Stuttgart, Germany: S. Hirzel Verlag GmbH, 1900.)

In spectroscopy, **attenuate** means to decrease the energy per unit area of a beam of radiation. In terms of the photon model, attenuate means to decrease the number of photons per second in the beam.

The term **monochromatic radiation** refers to radiation of a single color; that is, a single wavelength or frequency. In practice, it is virtually impossible to produce a single color of light. We discuss the practical problems associated with producing monochromatic radiation in Chapter 25.

Percent transmittance = % T

$$= \frac{P}{P_0} \times 100\%.$$

Absorbance can be calculated from percent transmittance as follows:

$$T = \frac{\%T}{100\%}$$

$$A = -\log T$$

$$= -\log \%T + \log 100$$

$$= 2 - \log \%T$$

Figure 24-7 Attenuation of a beam of radiation by an absorbing solution. The larger arrow on the incident beam signifies a higher radiant power P_0 than that transmitted by the solution P . The path length of the absorbing solution is b and the concentration is c .

24C ABSORPTION OF RADIATION

Every molecular species is capable of absorbing its own characteristic frequencies of electromagnetic radiation, as described in Figure 24-5. This process transfers energy to the molecule and results in a decrease in the intensity of the incident electromagnetic radiation. Absorption of the radiation thus **attenuates** the beam in accordance with the absorption law as described in Section 24C-1.

24C-1 The Absorption Process

The absorption law, also known as the **Beer-Lambert law** or just **Beer's law**, tells us quantitatively how the amount of attenuation depends on the concentration of the absorbing molecules and the path length over which absorption occurs. As light traverses a medium containing an absorbing analyte, the intensity decreases as the analyte becomes excited. For an analyte solution of a given concentration, the longer the length of the medium through which the light passes (path length of light), the more absorbers are in the path, and the greater the attenuation. Similarly, for a given path length of light, the higher the concentration of absorbers, the stronger the attenuation.

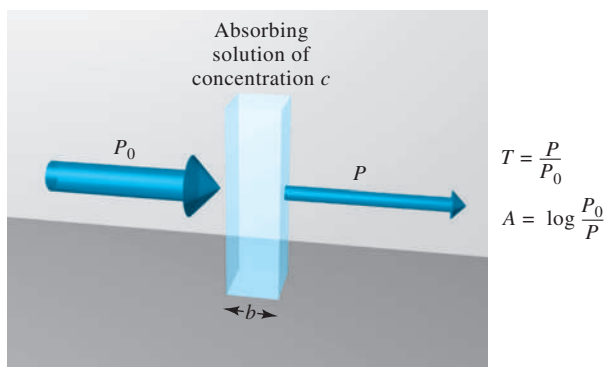
Figure 24-7 depicts the attenuation of a parallel beam of **monochromatic radiation** as it passes through an absorbing solution of thickness b cm and concentration c moles per liter. Because of interactions between the photons and absorbing particles (recall Figure 24-5), the radiant power of the beam decreases from P_0 to P . The **transmittance** T of the solution is the fraction of incident radiation transmitted by the solution, as shown in Equation 24-4. Transmittance is often expressed as a percentage and called the **percent transmittance**.

$$T = P/P_0 \quad (24-4)$$

Absorbance

The **absorbance**, A , of a solution is related to the transmittance in a logarithmic manner as shown in Equation 24-5. Notice that as the absorbance of a solution increases, the transmittance decreases. The relationship between transmittance and absorbance is illustrated by the conversion spreadsheet shown in **Figure 24-8**. The scales on earlier instruments were linear in transmittance or sometimes in absorbance. In modern instruments, a computer calculates absorbance from measured quantities.

$$A = -\log T = -\log \frac{P}{P_0} = \log \frac{P_0}{P} \quad (24-5)$$



Unless otherwise noted, all content on this page is © Cengage Learning.

	A	B	C	D
1	Calculation of Absorbance from Transmittance			
2	<i>T</i>	% <i>T</i>	<i>A</i> = -log <i>T</i>	<i>A</i> = 2·log % <i>T</i>
3	0.001	0.1	3.000	3.000
4	0.010	1.0	2.000	2.000
5	0.050	5.0	1.301	1.301
6	0.075	7.5	1.125	1.125
7	0.100	10.0	1.000	1.000
8	0.200	20.0	0.699	0.699
9	0.300	30.0	0.523	0.523
10	0.400	40.0	0.398	0.398
11	0.500	50.0	0.301	0.301
12	0.600	60.0	0.222	0.222
13	0.700	70.0	0.155	0.155
14	0.800	80.0	0.097	0.097
15	0.900	90.0	0.046	0.046
16	1.000	100.0	0.000	0.000
17				
18	Spreadsheet Documentation			
19	Cell B3=A3*100			
20	Cell C3=LOG10(A3)			
21	Cell D3=2·LOG10(B3)			

Figure 24-8 Conversion spreadsheet relating transmittance T , percent transmittance % T , and absorbance A . The transmittance data to be converted are entered in cells A3 through A16. The percent transmittance is calculated in cells B3 by the formula shown in the documentation section, cell A19. This formula is copied into cells B4 through B16. The absorbance is calculated from $-\log T$ in cells C3 through C16 and from $2 - \log \%T$ in cells D3 through D16. The formulas for the first cell in the C and D columns are shown in cells A20 and A21.

Measuring Transmittance and Absorbance

Transmittance and absorbance, as defined by Equations 24-4 and 24-5 and depicted in Figure 24-7, usually cannot be measured as shown because the solution to be studied must be held in a container (cell or cuvette). Reflection and scattering losses can occur at the cell walls, as shown in Figure 24-9. These losses can be substantial. For example, about 8.5% of a beam of yellow light is lost by reflection when it passes through a glass cell. Light can also be scattered in all directions from the surface of large molecules or particles, such as dust, in the solvent, and this scattering can cause further attenuation of the beam as it passes through the solution.

To compensate for these effects, the power of the beam transmitted through a cell containing the analyte solution is compared with one that traverses an identical cell containing only the solvent, or a reagent blank. An experimental absorbance that closely approximates the true absorbance for the solution is thus obtained, that is,

$$A = \log \frac{P_0}{P} \approx \log \frac{P_{\text{solvent}}}{P_{\text{solution}}} \quad (24-6)$$

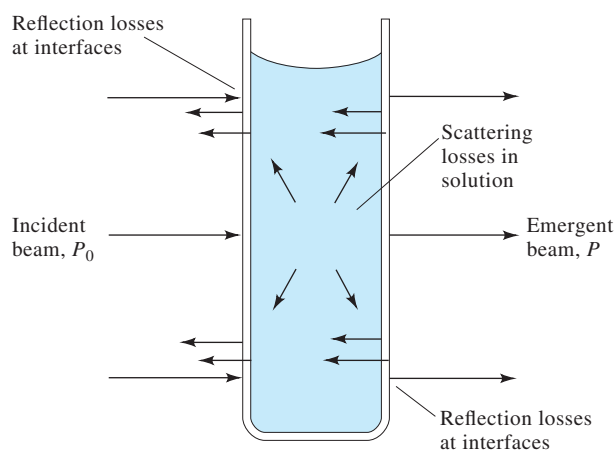


Figure 24-9 Reflection and scattering losses with a solution contained in a typical glass cell. Losses by reflection can occur at all the boundaries that separate the different materials. In this example, the light passes through the following boundaries, called interfaces: air-glass, glass-solution, solution-glass, and glass-air.

Because of this close approximation, the terms P_0 and P will henceforth refer to the power of a beam that has passed through cells containing the solvent (or blank) and the analyte solution, respectively.

Beer's Law

According to Beer's law, absorbance is directly proportional to the concentration of the absorbing species, c , and to the path length, b , of the absorbing medium as expressed by Equation 24-7.

$$A = \log(P_0/P) = abc \quad (24-7)$$

The molar absorptivity of a species at an absorption maximum is characteristic of that species. Peak molar absorptivities for many organic compounds range from 10 or less to 10,000 or more. Some transition metal complexes have molar absorptivities of 10,000 to 50,000. High molar absorptivities are desirable for quantitative analysis because they lead to high analytical sensitivity.



In Equation 24-7, a is a proportionality constant called the **absorptivity**. Because absorbance is a unitless quantity, the absorptivity must have units that cancel the units of b and c . If, for example, c has the units of g L^{-1} and b has the units of cm , absorptivity has the units of $\text{L g}^{-1} \text{cm}^{-1}$.

When we express the concentration in Equation 24-7 in moles per liter and b in cm , the proportionality constant is called the **molar absorptivity** and is given the symbol ϵ . Thus,

$$A = \epsilon bc \quad (24-8)$$

where ϵ has the units of $\text{L mol}^{-1} \text{cm}^{-1}$.

FEATURE 24-2

Deriving Beer's Law

To derive Beer's law, we consider the block of absorbing matter (solid, liquid, or gas) shown in **Figure 24F-3**. A beam of parallel monochromatic radiation with power P_0 strikes the block perpendicular to a surface; after passing through a length b of the material, which contains n absorbing particles (atoms, ions, or molecules), its power is decreased to P as a result of absorption. Consider now a cross section of the block having an area S and an infinitesimal thickness dx . Within this section, there are dn absorbing particles. Associated with each particle, we can imagine a surface at which photon capture will occur, that is, if a photon reaches one of these

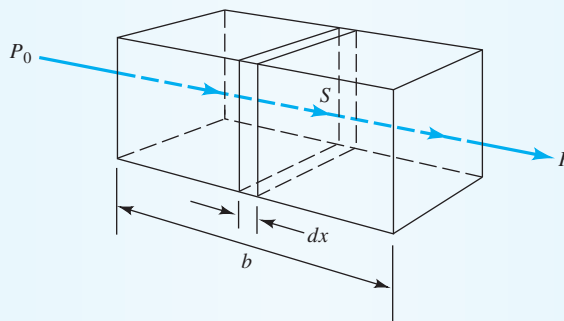


Figure 24F-3 Attenuation of a beam of electromagnetic radiation with initial power P_0 by a solution containing c mol/L of absorbing solute and a path length of b cm. The transmitted beam has a radiant power P ($P < P_0$).

areas by chance, absorption will follow immediately. The total projected area of these capture surfaces within the section is designated as dS ; the ratio of the capture area to the total area then is dS/S . On a statistical average, this ratio represents the probability for the capture of photons within the section. The power of the beam entering the section, P_x , is proportional to the number of photons per square centimeter per second, and dP_x represents the quantity removed per second within the section. The fraction absorbed is then $-dP_x/P_x$, and this ratio also equals the average probability for capture. The term is given a minus sign to indicate that *the* radiant power undergoes a decrease. Thus,

$$-\frac{dP_x}{P_x} = \frac{dS}{S} \quad (24-9)$$

Recall now that dS is the sum of the capture areas for particles within the section. It must, therefore, be proportional to the number of particles, or

$$dS = a \times dn \quad (24-10)$$

where dn is the number of particles and a is a proportionality constant, which is called the *capture cross section*. By combining Equations 24-9 and 24-10 and integrating over the interval between 0 and n , we obtain

$$-\int_{P_x}^P \frac{dP_x}{P_x} = \int_0^n \frac{a \times dn}{S}$$

which, when integrated, gives

$$-\ln \frac{P}{P_0} = \frac{an}{S}$$

We then convert to base 10 logarithms, invert the fraction to change the sign, and obtain

$$\log \frac{P_0}{P} = \frac{an}{2.303 S} \quad (24-11)$$

where n is the total number of particles within the block shown in Figure 24F-3. The cross-sectional area S can be expressed in terms of the volume of the block V in cm^3 and its length b in cm. Thus,

$$S = \frac{V}{b} \text{ cm}^2$$

By substituting this quantity into Equation 24-11, we find

$$\log \frac{P_0}{P} = \frac{anb}{2.303 V} \quad (24-12)$$

Notice that n/V has the units of concentration (that is, number of particles per cubic centimeter). To convert n/V to moles per liter, we find the number of moles by

$$\text{number mol} = \frac{n \text{ particles}}{6.022 \times 10^{23} \text{ particles/mol}}$$

(continued)

The concentration c in mol/L is then

$$c = \frac{n}{6.022 \times 10^{23}} \text{ mol} \times \frac{1000 \text{ cm}^3/\text{L}}{V \text{ cm}^3}$$

$$= \frac{1000n}{6.022 \times 10^{23}} \text{ mol/L}$$

By combining this relationship with Equation 24-12, we have

$$\log \frac{P_0}{P} = \frac{6.022 \times 10^3 abc}{2.303 \times 1000}$$

Finally, the constants in this equation can be collected into a single term ϵ to give

$$A = \log \frac{P_0}{P} = \epsilon bc \quad (24-13)$$

which is Beer's law.

Terms Used in Absorption Spectrometry

In addition to the terms we have introduced to describe absorption of radiant energy, you may encounter other terms in the literature or with older instruments. The terms, symbols, and definitions given in **Table 24-3** are recommended by the Society for Applied Spectroscopy and the American Chemical Society. The third column contains the older names and symbols. Because a standard nomenclature is highly desirable to avoid ambiguities, we urge you to learn and use the recommended terms and symbols and to avoid the older terms.

TABLE 24-3

Important Terms and Symbols Employed in Absorption Measurements

Term and Symbol*	Definition	Alternative Name and Symbol
Incident radiant power, P_0	Radiant power in watts incident on sample	Incident intensity, I_0
Transmitted radiant power, P	Radiant power transmitted by sample	Transmitted intensity, I
Absorbance, A	$\log(P_0/P)$	Optical density, D ; extinction, E
Transmittance, T	P/P_0	Transmission, T
Path length of sample, b	Length over which attenuation occurs	l, d
Absorptivity [†] , a	$A/(bc)$	α, k
Molar absorptivity [‡] , ϵ	$A/(bc)$	Molar absorption coefficient

*Compilation of terminology recommended by the American Chemical Society and the Society for Applied Spectroscopy (*Appl. Spectrosc.*, **2012**, 66, 132).

[†] c may be expressed in g L^{-1} or in other specified concentration units; b may be expressed in cm or other units of length.

[‡] c is expressed in mol L^{-1} ; b is expressed in cm.

Using Beer's Law

Beer's law, as expressed in Equations 24-6 and 24-8, can be used in several different ways. We can calculate molar absorptivities of species if the concentration is known, as shown in Example 24-3. We can use the measured value of absorbance to obtain concentration if absorptivity and path length are known. Absorptivities, however, are functions of such variables as solvent, solution composition, and temperature. Because of variations in absorptivity with conditions, it is never a good idea to depend on literature values for quantitative work. Hence, a standard solution of the analyte in the same solvent and at a similar temperature is used to obtain the absorptivity at the time of the analysis. Most often, we use a series of standard solutions of the analyte to construct a calibration curve, or working curve, of A versus c or to obtain a linear regression equation (for the method of external standards and linear regression, see Section 8D-2). It may also be necessary to duplicate closely the overall composition of the analyte solution in order to compensate for matrix effects. Alternatively, the method of standard additions (see Section 8D-3 and Section 26A-3) is used for the same purpose.

EXAMPLE 24-3

A 7.25×10^{-5} M solution of potassium permanganate has a transmittance of 44.1% when measured in a 2.10-cm cell at a wavelength of 525 nm. Calculate (a) the absorbance of this solution and (b) the molar absorptivity of KMnO_4 .

Solution

- (a) $A = -\log T = -\log 0.441 = -(-0.356) = 0.356$
 (b) From Equation 24-8,

$$\begin{aligned}\epsilon &= A/bc = 0.356/(2.10 \text{ cm} \times 7.25 \times 10^{-5} \text{ mol L}^{-1}) \\ &= 2.34 \times 10^3 \text{ L mol}^{-1} \text{ cm}^{-1}\end{aligned}$$



Spreadsheet Summary In the first exercise in Chapter 12 of *Applications of Microsoft® Excel in Analytical Chemistry*, 2nd ed., a spreadsheet is developed to calculate the molar absorptivity of permanganate ion. A plot of absorbance versus permanganate concentration is constructed, and least-squares analysis of the linear plot is carried out. The data are analyzed statistically to determine the uncertainty of the molar absorptivity. In addition, other spreadsheets are presented for calibration in quantitative spectrophotometric experiments and for calculating concentrations of unknown solutions.

Applying Beer's Law to Mixtures

Beer's law also applies to solutions containing more than one kind of absorbing substance. Provided that there is no interaction among the various species, the total

absorbance for a multicomponent system at a single wavelength is the sum of the individual absorbances. In other words,

Absorbances are additive if the absorbing species do not interact.



$$A_{\text{total}} = A_1 + A_2 + \cdots + A_n = \epsilon_1 b c_1 + \epsilon_2 b c_2 + \cdots + \epsilon_n b c_n \quad (24-14)$$

where the subscripts refer to absorbing components 1, 2, . . . , n .

A bit of Latin. One plot of absorbance versus wavelength is called a **spectrum**; two or more plots are called **spectra**.



24C-2 Absorption Spectra

An **absorption spectrum** is a plot of absorbance versus wavelength, as illustrated in **Figure 24-10**. Absorbance could also be plotted against wavenumber or frequency. Modern scanning spectrophotometers produce such an absorption spectrum directly. Older instruments sometimes displayed transmittance and produced plots of T or $\%T$ versus wavelength. Occasionally plots with $\log A$ as the ordinate are used. The logarithmic axis leads to a loss of spectral detail, but it is convenient for comparing solutions of widely different concentrations. A plot of molar absorptivity ϵ as a function of wavelength is independent of concentration. This type of spectral plot is characteristic for a given molecule and is sometimes used to aid in identifying or confirming the identity of a particular species. The color of a solution is related to its absorption spectrum (see Feature 24-3).

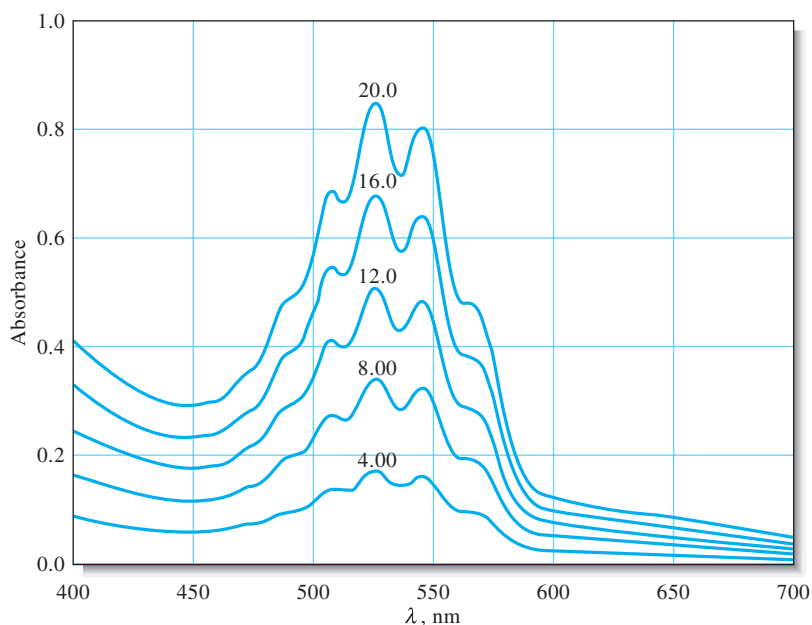


Figure 24-10 Typical absorption spectra of potassium permanganate at five different concentrations. The numbers adjacent to the curves indicate concentration of manganese in ppm, and the absorbing species is permanganate ion, MnO_4^- . The cell path length b is 1.00 cm. A plot of absorbance at the peak wavelength at 525 nm versus concentration of permanganate is linear and thus the absorber obeys Beer's law.

FEATURE 24-3

Why Is a Red Solution Red?

An aqueous solution of the complex $\text{Fe}(\text{SCN})^{2+}$ is not red because the complex adds red radiation to the solvent. Instead, it absorbs green from the incoming white radiation and transmits the red component (see Figure 24F-4). Thus, in a colorimetric determination of iron based on its thiocyanate complex, the maximum change in absorbance with concentration occurs with green radiation; the absorbance change with red radiation is negligible. In general, then, the radiation used for a colorimetric analysis should be the complementary color of the analyte solution. The following table shows this relationship for various parts of the visible spectrum.

The Visible Spectrum

Wavelength Region Absorbed, nm	Color of Light Absorbed	Complementary Color Transmitted
400–435	Violet	Yellow-green
435–480	Blue	Yellow
480–490	Blue-green	Orange
490–500	Green-blue	Red
500–560	Green	Purple
560–580	Yellow-green	Violet
580–595	Yellow	Blue
595–650	Orange	Blue-green
650–750	Red	Green-blue

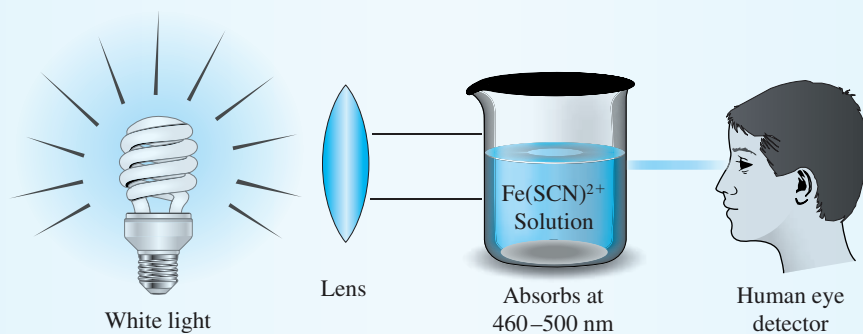


Figure 24F-4 Color of a solution. White light from a lamp or the sun strikes an aqueous solution of $\text{Fe}(\text{SCN})^{2+}$. The fairly broad absorption spectrum shows a maximum absorbance in the 460 to 500 nm range (see Figure 26-4a). The complementary red color is transmitted.

Atomic Absorption

When a beam of polychromatic ultraviolet or visible radiation passes through a medium containing gaseous atoms, only a few frequencies are attenuated by absorption, and when recorded on a very high resolution spectrometer, the spectrum consists of a number of very narrow absorption lines.

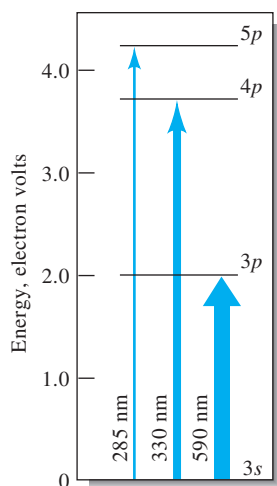


Figure 24-11 Partial energy level diagram for sodium, showing the transitions resulting from absorption at 590, 330, and 285 nm.

The **electron volt (eV)** is a unit of energy. When an electron with charge $q = 1.60 \times 10^{-19}$ coulombs is moved through a potential difference of 1 volt = 1 joule/coulomb, the energy expended (or released) is then equal to $E = qV = (1.60 \times 10^{-19} \text{ coulombs})(1 \text{ joule/coulomb}) = 1.60 \times 10^{-19} \text{ joule} = 1 \text{ eV}$.

$$\begin{aligned} 1 \text{ eV} &= 1.60 \times 10^{-19} \text{ J} \\ &= 3.83 \times 10^{-20} \text{ calories} \\ &= 1.58 \times 10^{-21} \text{ L atm} \end{aligned}$$

In an **electronic transition**, an electron moves from one orbital to another. Transitions occur between atomic orbitals in atoms and between molecular orbitals in molecules.

Vibrational and rotational transitions occur with polyatomic species because only this type of species has vibrational and rotational states with different energies.

The **ground state** of an atom or a molecular species is the minimum energy state of the species. At room temperature, most atoms and molecules are in their ground state.

Figure 24-11 is a partial energy level diagram for sodium that shows the major atomic absorption transitions. The transitions, shown as colored arrows between levels, occur when the single outer electron of sodium is excited from its room temperature or ground state $3s$ orbital to the $3p$, $4p$, and $5p$ orbitals. These excitations are brought on by absorption of photons of radiation whose energies exactly match the differences in energies between the excited states and the $3s$ ground state. Transitions between two different orbitals are termed **electronic transitions**. Atomic absorption spectra are not usually recorded because of instrumental difficulties. Instead, atomic absorption is measured at a single wavelength using a very narrow, nearly monochromatic source (see Section 28D).

EXAMPLE 24-4

The energy difference between the $3p$ and the $3s$ orbitals in Figure 24-11b is 2.107 eV. Calculate the wavelength of radiation that would be absorbed in exciting the $3s$ electron to the $3p$ state ($1 \text{ eV} = 1.60 \times 10^{-19} \text{ J}$).

Solution

Rearranging Equation 24-3 gives

$$\begin{aligned} \lambda &= \frac{hc}{E} \\ &= \frac{6.63 \times 10^{-34} \text{ J}\cdot\text{s} \times 3.00 \times 10^{10} \text{ cm/s} \times 10^7 \text{ nm/cm}}{2.107 \text{ eV} \times 1.60 \times 10^{-19} \text{ J/eV}} \\ &= 590 \text{ nm} \end{aligned}$$

Molecular Absorption

Molecules undergo three types of quantized transitions when excited by ultraviolet, visible, and infrared radiation. For ultraviolet and visible radiation, excitation occurs when an electron residing in a low-energy molecular or atomic orbital is promoted to a higher-energy orbital. We mentioned previously that the energy $h\nu$ of the photon must be exactly the same as the energy difference between the two orbital energies.

In addition to electronic transitions, molecules exhibit two other types of radiation-induced transitions: **vibrational transitions** and **rotational transitions**. Vibrational transitions occur because a molecule has a multitude of quantized energy levels, or vibrational states, associated with the bonds that hold the molecule together.

Figure 24-12 is a partial energy level diagram that depicts some of the processes that occur when a polyatomic species absorbs infrared, visible, and ultraviolet radiation. The energies E_1 and E_2 , two of the several electronically excited states of a molecule, are shown relative to the energy of the ground state E_0 . In addition, the relative energies of a few of the many vibrational states associated with each electronic state are indicated by the lighter horizontal lines.

You can get an idea of the nature of vibrational states by picturing a bond in a molecule as a vibrating spring with atoms attached to both ends. In **Figure 24-13a**, two types of stretching vibration are shown. With each vibration, atoms first approach and then move away from one another. The potential energy of such a system at any instant depends on the extent to which the spring is stretched or compressed. For a real-world macroscopic spring, the energy of the system varies continuously and

reaches a maximum when the spring is fully stretched or fully compressed. In contrast, the energy of a spring system of atomic dimensions (a chemical bond) can have only certain discrete energies called vibrational energy levels.

Figure 24-13b shows four other types of molecular vibrations. The energies associated with these vibrational states usually differ from one another and from the energies associated with stretching vibrations. Some of the vibrational energy levels associated with each of the electronic states of a molecule are depicted by the lines labeled 1, 2, 3, and 4 in **Figure 24-12** (the lowest vibrational levels are labeled 0). Note that the differences in energy among the vibrational states are significantly smaller than among energy levels of the electronic states (typically an order of magnitude smaller). Although they are not shown, a molecule has many quantized rotational states that are associated with the rotational motion of a molecule around its center of gravity. These rotational energy states are superimposed on each of the vibrational states shown in the energy diagram. The energy differences among these states are smaller than those among vibrational states by an order of magnitude and so are not shown in the diagram. The total energy E associated with a molecule is then given by

$$E = E_{\text{electronic}} + E_{\text{vibrational}} + E_{\text{rotational}} \quad (24-15)$$

where $E_{\text{electronic}}$ is the energy associated with the electrons in the various outer orbitals of the molecule, $E_{\text{vibrational}}$ is the energy of the molecule as a whole due to interatomic vibrations, and $E_{\text{rotational}}$ accounts for the energy associated with rotation of the molecule about its center of gravity.

Infrared Absorption. Infrared radiation generally is not energetic enough to cause electronic transitions, but it can induce transitions in the vibrational and rotational states associated with the ground electronic state of the molecule. Four of these

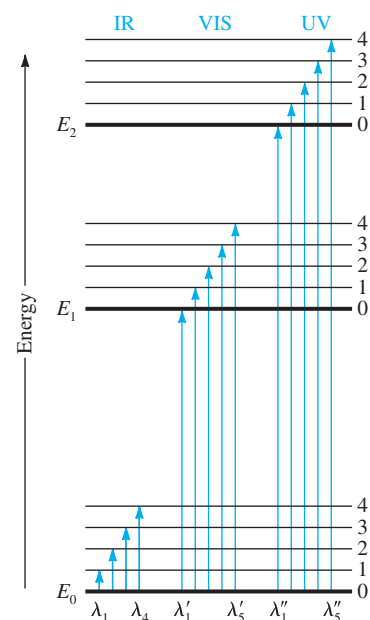
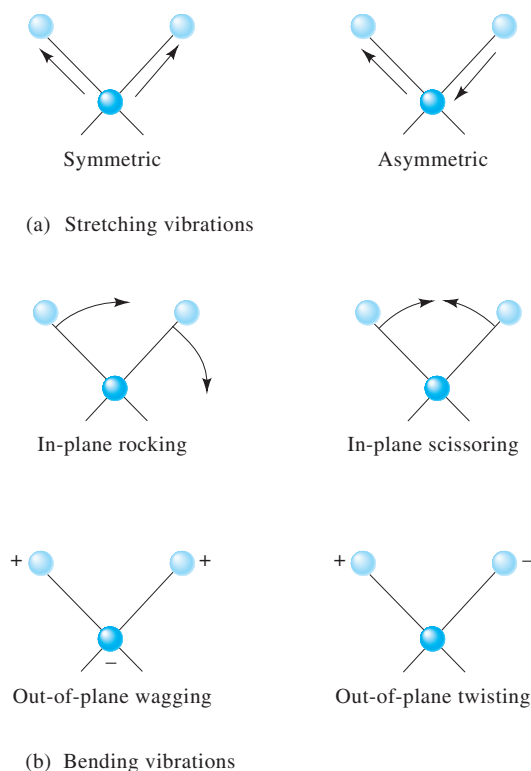


Figure 24-12 Energy level diagram showing some of the energy changes that occur during absorption of infrared (IR), visible (VIS), and ultraviolet (UV) radiation by a molecular species. Note that with some molecules a transition from E_0 to E_1 may require UV radiation instead of visible radiation. With other molecules, the transition from E_0 to E_2 may occur with visible radiation instead of UV radiation. Only a few vibrational levels (0–4) are shown. The rotational levels associated with each vibrational level are not shown because they are too closely spaced.

Figure 24-13 Types of molecular vibrations. The plus sign indicates motion out of the page; the minus sign indicates motion into the page.

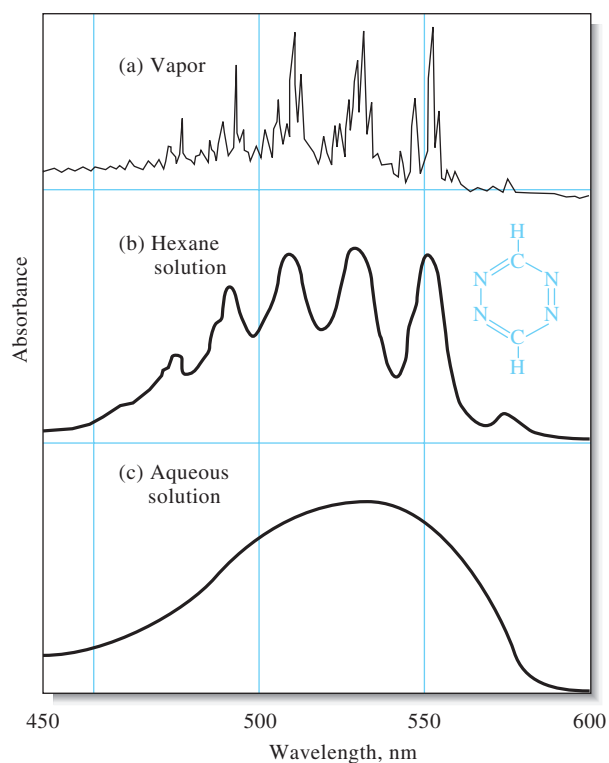
transitions are depicted in the lower left part of Figure 24-12 (λ_1 to λ_4). For absorption to occur, the radiation source has to emit frequencies corresponding exactly to the energies indicated by the lengths of the four arrows.

Absorption of Ultraviolet and Visible Radiation. The center arrows in Figure 24-12 suggest that the molecules under consideration absorb visible radiation of five wavelengths (λ'_1 to λ'_5), thereby promoting electrons to the five vibrational levels of the excited electronic level E_1 . Ultraviolet photons that are more energetic are required to produce the absorption indicated by the five arrows to the right.

Figure 24-12 suggests that molecular absorption in the ultraviolet and visible regions produces **absorption bands** made up of closely spaced lines. A real molecule has many more energy levels than can be shown in the diagram. Thus, a typical absorption band consists of a large number of lines. In a solution, the absorbing species are surrounded by solvent molecules, and the band nature of molecular absorption often becomes blurred because collisions tend to spread the energies of the quantum states, giving smooth and continuous absorption peaks.

Figure 21-14 shows visible spectra for 1,2,4,5-tetrazine that were obtained under three different conditions: gas phase, nonpolar solvent, and polar solvent (aqueous solution). Notice that in the gas phase (see Figure 24-14a), the individual tetrazine molecules are sufficiently separated from one another to vibrate and rotate freely so that many individual absorption peaks resulting from transitions among the various vibrational and rotational states appear in the spectrum. In the liquid state and in nonpolar solvents (see Figure 24-14b), however, tetrazine molecules are unable to rotate freely so that we see no fine structure in the spectrum. Furthermore, in a polar solvent such as water (see Figure 24-14c), frequent collisions and interactions between tetrazine and water molecules cause the vibrational levels to be modified

Figure 24-14 Typical visible absorption spectra. The compound is 1,2,4,5-tetrazine. In (a), the spectrum is shown in the gas phase where many lines due to electronic, vibrational, and rotational transitions are seen. In a nonpolar solvent (b), the electronic transitions can be observed, but the vibrational and rotational structure has been lost. In a polar solvent (c), the strong intermolecular forces have caused the electronic peaks to blend together to give only a single smooth absorption peak. (Reproduced from S. F. Mason, *J. Chem. Soc.*, **1959**, 1263, DOI: 10.1039/JR9590001263, with permission of The Royal Society of Chemistry.)



Unless otherwise noted, all content on this page is © Cengage Learning.

energetically in an irregular way. Hence, the spectrum appears as a single broad peak. The trends shown in the spectra of tetrazine in this figure are typical of UV-visible spectra of other molecules recorded under similar conditions.

24C-3 Limits to Beer's Law

There are few exceptions to the linear relationship between absorbance and path length at a fixed concentration. We frequently observe deviations from the direct proportionality between absorbance and concentration, however, when the path length b is a constant. Some of these deviations, called **real deviations**, are fundamental and represent real limitations to the law. Others are a result of the method that we use to measure absorbance (**instrumental deviations**) or from chemical changes that occur when the concentration changes (**chemical deviations**).

Real Limitations to Beer's Law

Beer's law describes the absorption behavior only of dilute solutions and in this sense is a **limiting law**. At concentrations exceeding about 0.01 M, the average distances between ions or molecules of the absorbing species are diminished to the point where each particle affects the charge distribution and thus the extent of absorption of its neighbors. Because the extent of interaction depends on concentration, the occurrence of this phenomenon causes deviations from the linear relationship between absorbance and concentration. A similar effect sometimes occurs in dilute solutions of absorbers that contain high concentrations of other species, particularly electrolytes. When ions are very close to one another, the molar absorptivity of the analyte can be altered because of electrostatic interactions which can lead to departures from Beer's law.

Chemical Deviations

As shown in Example 24-5, deviations from Beer's law appear when the absorbing species undergoes association, dissociation, or reaction with the solvent to give products that absorb differently from the analyte. The extent of such departures can be predicted from the molar absorptivities of the absorbing species and the equilibrium constants for these equilibria. Unfortunately, since we are usually unaware that such processes are affecting the analyte, there is often no opportunity to correct the measurement. Typical equilibria that give rise to this effect include monomer-dimer equilibria, metal complexation equilibria where more than one complex is present, acid/base equilibria, and solvent-analyte association equilibria.

EXAMPLE 24-5

Solutions containing various concentrations of the acidic indicator HIn with $K_a = 1.42 \times 10^{-5}$ were prepared in 0.1 M HCl and 0.1 M NaOH. In both media, plots of absorbance at either 430 nm or 570 nm versus the total indicator concentration are nonlinear. However, in both media, the individual species HIn or In^- obey Beer's law at 430 nm and 570 nm. Hence, if we knew the equilibrium concentrations of HIn and In^- , we could compensate for the fact that dissociation of HIn occurs. Usually, though, the individual concentrations are unknown, and only the total concentration $c_{\text{total}} = [\text{HIn}] + [\text{In}^-]$ is known. Let us now calculate the absorbance for a solution with $c_{\text{total}} = 2.00 \times 10^{-5}$ M. The magnitude of the

(continued)

Limiting laws in science are those that hold under limiting conditions such as dilute solutions. In addition to Beer's law, the Debye-Hückel law (see Chapter 10) and the law of independent migration that describes the conductance of electricity by ions are limiting laws.

acid dissociation constant suggests that, for all practical purposes, the indicator is entirely in the undissociated form (HIn) in the HCl solution and completely dissociated as In^- in NaOH. The molar absorptivities at the two wavelengths were found to be

	ϵ_{430}	ϵ_{570}
HIn (HCl solution)	6.30×10^2	7.12×10^3
In^- (NaOH solution)	2.06×10^4	9.60×10^2

We would now like to find the absorbances (1.00-cm cell) of unbuffered solutions of the indicator ranging in concentration from 2.00×10^{-5} M to 16.00×10^{-5} M. Let us first find the concentration of HIn and In^- in the unbuffered 2×10^{-5} M solution. From the equation for the dissociation reaction, we know that $[\text{H}^+] = [\text{In}^-]$. Furthermore, the mass-balance expression for the indicator tells us that $[\text{In}^-] + [\text{HIn}] = 2.00 \times 10^{-5}$ M. By substituting these relationships into the K_a expression, we find that

$$\frac{[\text{In}^-]^2}{2.00 \times 10^{-5} - [\text{In}^-]} = 1.42 \times 10^{-5}$$

This equation can be solved to give $[\text{In}^-] = 1.12 \times 10^{-5}$ M and $[\text{HIn}] = 0.88 \times 10^{-5}$ M. The absorbances at the two wavelengths are found by substituting the values for ϵ , b , and c into Equation 24-13 (Beer's Law). The result is that $A_{430} = 0.236$ and $A_{570} = 0.073$. We could similarly calculate A for several other values of c_{total} . Additional data, obtained in the same way, are shown in Table 24-4. Figure 24-15 shows plots at the two wavelengths that were constructed from data obtained in a similar manner.

CHALLENGE: Perform calculations to confirm that $A_{430} = 0.596$ and $A_{570} = 0.401$ for a solution in which the analytical concentration of HIn is 8.00×10^{-5} M.

The plots of Figure 24-15 illustrate the kinds of departures from Beer's law that occur when the absorbing system undergoes dissociation or association. Notice that the direction of curvature is opposite at the two wavelengths.

TABLE 24-4

Absorbance Data for Several Concentrations of the Indicator in Example 24-5

c_{HIn}, M	[HIn]	$[\text{In}^-]$	A_{430}	A_{570}
2.00×10^{-5}	0.88×10^{-5}	1.12×10^{-5}	0.236	0.073
4.00×10^{-5}	2.22×10^{-5}	1.78×10^{-5}	0.381	0.175
8.00×10^{-5}	5.27×10^{-5}	2.73×10^{-5}	0.596	0.401
12.0×10^{-5}	8.52×10^{-5}	3.48×10^{-5}	0.771	0.640
16.0×10^{-5}	11.9×10^{-5}	4.11×10^{-5}	0.922	0.887

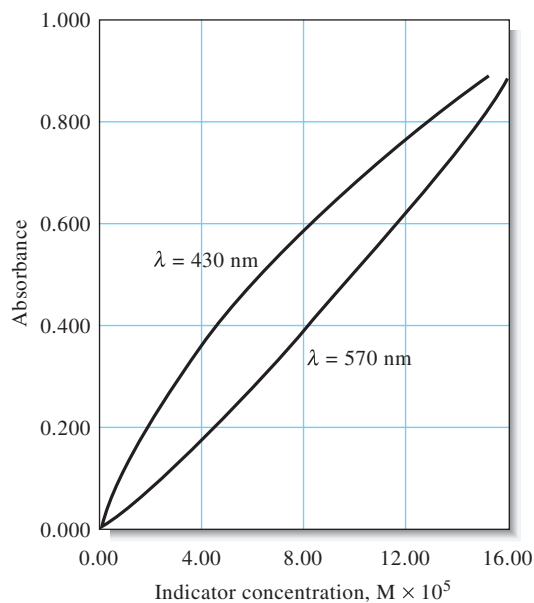


Figure 24-15 Chemical deviations from Beer's law for unbuffered solutions of the indicator HIn. The absorbance values were calculated at various indicator concentrations, as shown in Example 24-5. Note that there are positive deviations at 430 nm and negative deviations at 570 nm. At 430 nm, the absorbance is primarily due to the ionized In^- form of the indicator and is in fact proportional to the fraction ionized. The fraction ionized varies nonlinearly with total concentration. At lower total concentrations ($[\text{HIn}] + [\text{In}^-]$), the fraction ionized is larger than at high total concentrations. Hence, a positive error occurs. At 570 nm, the absorbance is due principally to the undissociated acid HIn. The fraction in this form begins as a low amount and increases nonlinearly with the total concentration, giving rise to the negative deviation shown.

Instrumental Deviations: Polychromatic Radiation

Beer's law strictly applies only when measurements are made with monochromatic source radiation. In practice, polychromatic sources that have a continuous distribution of wavelengths are used in conjunction with a grating or a filter to isolate a nearly symmetric band of wavelengths surrounding the wavelength to be employed (see Chapter 25, Section 25A-3).

The following derivation shows the effect of polychromatic radiation on Beer's law. Consider a beam of radiation consisting of just two wavelengths λ' and λ'' . Assuming that Beer's law applies strictly for each wavelength, we may write for λ'

$$A' = \log \frac{P'_0}{P'} = \varepsilon'bc$$

or

$$\frac{P'_0}{P'} = 10^{\varepsilon'bc}$$

where P'_0 is the incident power and P' is the resultant power at λ' . The symbols b and c are the path length and concentration of the absorber, and ε' is the molar absorptivity at λ' . Then,

$$P' = P'_0 10^{-\varepsilon'bc}$$

Similarly, for λ'' ,

$$P'' = P''_0 10^{-\varepsilon''bc}$$

When an absorbance measurement is made with radiation composed of both wavelengths, the power of the beam emerging from the solution is the sum of the powers

Deviations from Beer's law often occur when polychromatic radiation is used to measure absorbance.

emerging at the two wavelengths $P' + P''$. Likewise, the total incident power is the sum $P'_0 + P''_0$. Therefore, the measured absorbance A_m is

$$A_m = \log\left(\frac{P'_0 + P''_0}{P' + P''}\right)$$

We then substitute for P' and P'' and find that

$$A_m = \log\left(\frac{P'_0 + P''_0}{P'_0 10^{-\varepsilon'bc} + P''_0 10^{-\varepsilon''bc}}\right)$$

or

$$A_m = \log(P'_0 + P''_0) - \log(P'_0 10^{-\varepsilon'bc} + P''_0 10^{-\varepsilon''bc})$$

We see that, when $\varepsilon' = \varepsilon''$, this equation simplifies to

$$\begin{aligned} A_m &= \log(P'_0 + P''_0) - \log[(P'_0 + P''_0)(10^{-\varepsilon'bc})] \\ &= \log(P'_0 + P''_0) - \log(P'_0 + P''_0) - \log(10^{-\varepsilon'bc}) \\ &= \varepsilon'bc = \varepsilon''bc \end{aligned}$$

High-quality spectrophotometers produce narrow bands of radiation and are less likely to suffer deviations from Beer's law due to polychromatic radiation than low-quality instruments.

Polychromatic light, literally multicolored light, is light of many wavelengths, such as that from a tungsten light bulb. Light that is essentially monochromatic can be produced by filtering, diffracting, or refracting polychromatic light, as discussed in Chapter 25, Section 25A-3.

and Beer's law is followed. As shown in **Figure 24-16**, however, the relationship between A_m and concentration is no longer linear when the molar absorptivities differ. In addition, as the difference between ε' and ε'' increases, the deviation from linearity increases. When this derivation is expanded to include additional wavelengths, the effect remains the same.

If the band of wavelengths selected for spectrophotometric measurements corresponds to a region of the absorption spectrum in which the molar absorptivity of the analyte is essentially constant, departures from Beer's law will be minimal. Many molecular bands in the UV/visible region of the spectrum fit this description. For these bands, Beer's law is obeyed, as demonstrated by Band A in **Figure 24-17**. On the other hand, some absorption bands in the UV-visible region and many in the IR region are very narrow, and departures from Beer's law are common, as illustrated for Band B in **Figure 24-17**. To avoid such deviations, it is best to select a wavelength

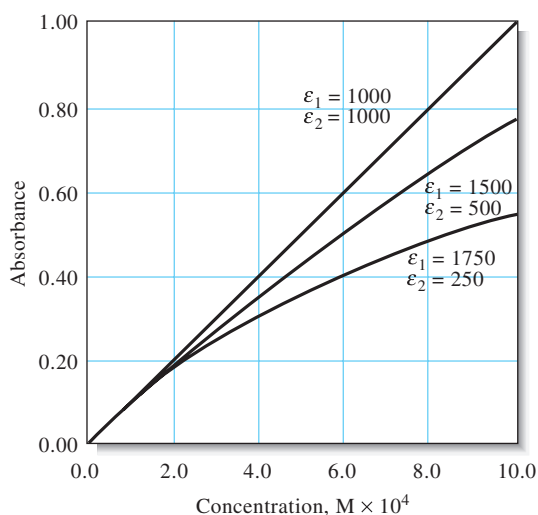


Figure 24-16 Deviations from Beer's law with polychromatic radiation. The absorber has the indicated molar absorptivities at the two wavelengths λ' and λ'' .

band near the wavelength of maximum absorption where the analyte absorptivity changes little with wavelength. Atomic absorption lines are so narrow that they require special sources to obtain adherence to Beer's law as discussed in Chapter 25, Section 25A-2.

Instrumental Deviations: Stray Light

Stray radiation, commonly called **stray light**, is defined as radiation from the instrument that is outside the nominal wavelength band chosen for the determination. This stray radiation often is the result of scattering and reflection off the surfaces of gratings, lenses or mirrors, filters, and windows. When measurements are made in the presence of stray light, the observed absorbance A' is given by

$$A' = \log\left(\frac{P_0 + P_s}{P + P_s}\right)$$

where P_s is the radiant power of the stray light. **Figure 24-18** shows a plot of the apparent absorbance A' versus concentration for various levels of P_s , relative to P_0 . Stray light always causes the apparent absorbance to be lower than the true absorbance. The deviations due to stray light are most significant at high absorbance values. Because stray radiation levels can be as high as 0.5% in modern instruments, absorbance levels above 2.0 are rarely measured unless special precautions are taken or special instruments with extremely low stray light levels are used. Some inexpensive filter instruments show deviations from Beer's law at absorbances as low as 1.0 because of high stray light levels and/or the presence of polychromatic light.

Mismatched Cells

Another almost trivial, but important, deviation from adherence to Beer's law is caused by mismatched cells. If the cells holding the analyte and blank solutions are not of equal path length and equivalent in optical characteristics, an intercept will occur in the calibration curve, and $A = \epsilon bc + k$ will be the equation for the

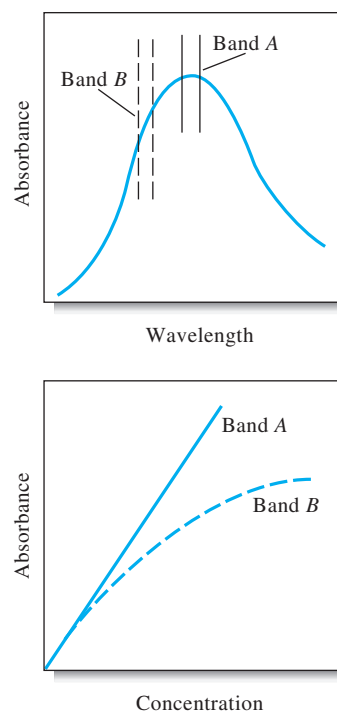


Figure 24-17 The effect of polychromatic radiation on Beer's law. In the absorption spectrum at the top, the absorptivity of the analyte is seen to be nearly constant over Band A from the source. Note in the Beer's law plot at the bottom that using Band A gives a linear relationship. In the spectrum, band B coincides with a region of the spectrum over which the absorptivity of the analyte changes. Note the dramatic deviation from Beer's law that results in the lower plot.

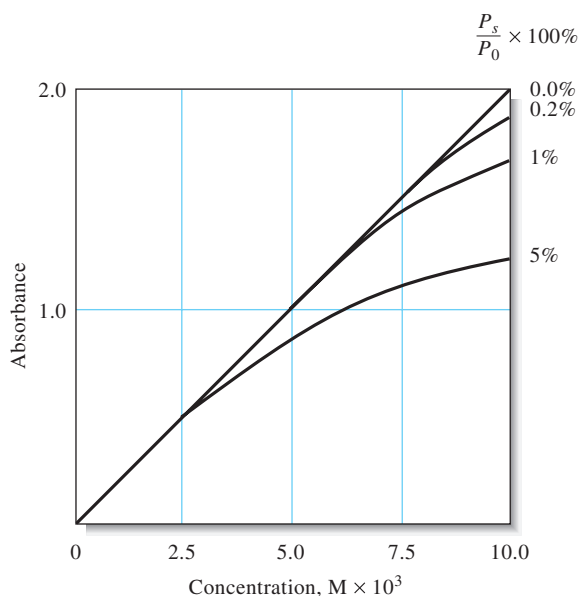


Figure 24-18 Deviation from Beer's law caused by various levels of stray light. Note that absorbance begins to level off with concentration at high stray light levels. Stray light always limits the maximum absorbance that can be obtained because, when the absorbance is high, the radiant power transmitted through the sample can become comparable to or lower than the stray light level.

curve instead of Equation 24-8. This error can be avoided either by using carefully matched cells or by using a linear regression procedure to calculate both the slope and intercept of the calibration curve. In most cases, linear regression is the best strategy because an intercept can also occur if the blank solution does not totally compensate for interferences. Another way to avoid the mismatched-cell problem with single beam instruments is to use only one cell and keep it in the same position for both blank and analyte measurements. After obtaining the blank reading, the cell is emptied by aspiration, washed, and filled with analyte solution.



Spreadsheet Summary In Chapter 12 of *Applications of Microsoft® Excel in Analytical Chemistry*, 2nd ed., spreadsheets are presented for modeling the effects of chemical equilibria and stray light on absorption measurements. Chemical and physical variables may be changed to observe their effects on instrument readouts.

Chemical species can be caused to emit light by (1) bombardment with electrons; (2) heating in a plasma, flame, or an electric arc; or (3) irradiation with a beam of light.

24D EMISSION OF ELECTROMAGNETIC RADIATION

Atoms, ions, and molecules can be excited to one or more higher energy levels by any of several processes, including bombardment with electrons or other elementary particles; exposure to a high-temperature plasma, flame, or electric arc; or exposure to a source of electromagnetic radiation. The lifetime of an excited species is generally transitory (10^{-9} to 10^{-6} s), and relaxation to a lower energy level or the ground state takes place with a release of the excess energy in the form of electromagnetic radiation, heat, or perhaps both.

24D-1 Emission Spectra

Radiation from a source is conveniently characterized by means of an emission spectrum, which usually takes the form of a plot of the relative power of the emitted radiation as a function of wavelength or frequency. **Figure 24-19** illustrates a typical emission spectrum, which was obtained by aspirating a brine solution into an oxyhydrogen flame. Three types of spectra are superimposed in the figure: a **line spectrum**, a **band spectrum**, and a **continuum spectrum**. The line spectrum, marked lines in **Figure 24-19**, consists of a series of sharp, well-defined spectral lines caused by excitation of individual atoms. The band spectrum, marked bands, is comprised of several groups of lines so closely spaced that they are not completely resolved. The source of the bands is small molecules or radicals in the source flame. Finally, the continuum spectrum, shown as a green dashed line in the figure, is responsible for the increase in the background that appears above about 350 nm. The line and band spectra are superimposed on this continuum. The source of the continuum is described on page 677.

The line widths of atoms in a medium such as a flame or plasma are about 0.1–0.01 Å. The wavelengths of atomic lines are unique for each element and are often used for qualitative analysis.

Line Spectra

Line spectra occur when the radiating species are individual atoms or ions that are well separated, as in a gas. The individual particles in a gaseous medium behave independently of one another, and the spectrum in most media consists of a series of sharp lines with widths of 10^{-1} – 10^{-2} Å (10^{-2} – 10^{-3} nm). In **Figure 24-19**, lines for sodium, potassium, strontium, calcium, and magnesium are identified.

The energy level diagram in **Figure 24-20** shows the source of three of the lines that appear in the emission spectrum of **Figure 24-19**. The horizontal line labeled $3s$ in **Figure 24-20** corresponds to the lowest, or ground state, energy of the atom E_0 . The horizontal lines labeled $3p$, $4p$, and $4d$ are three higher-energy electronic levels

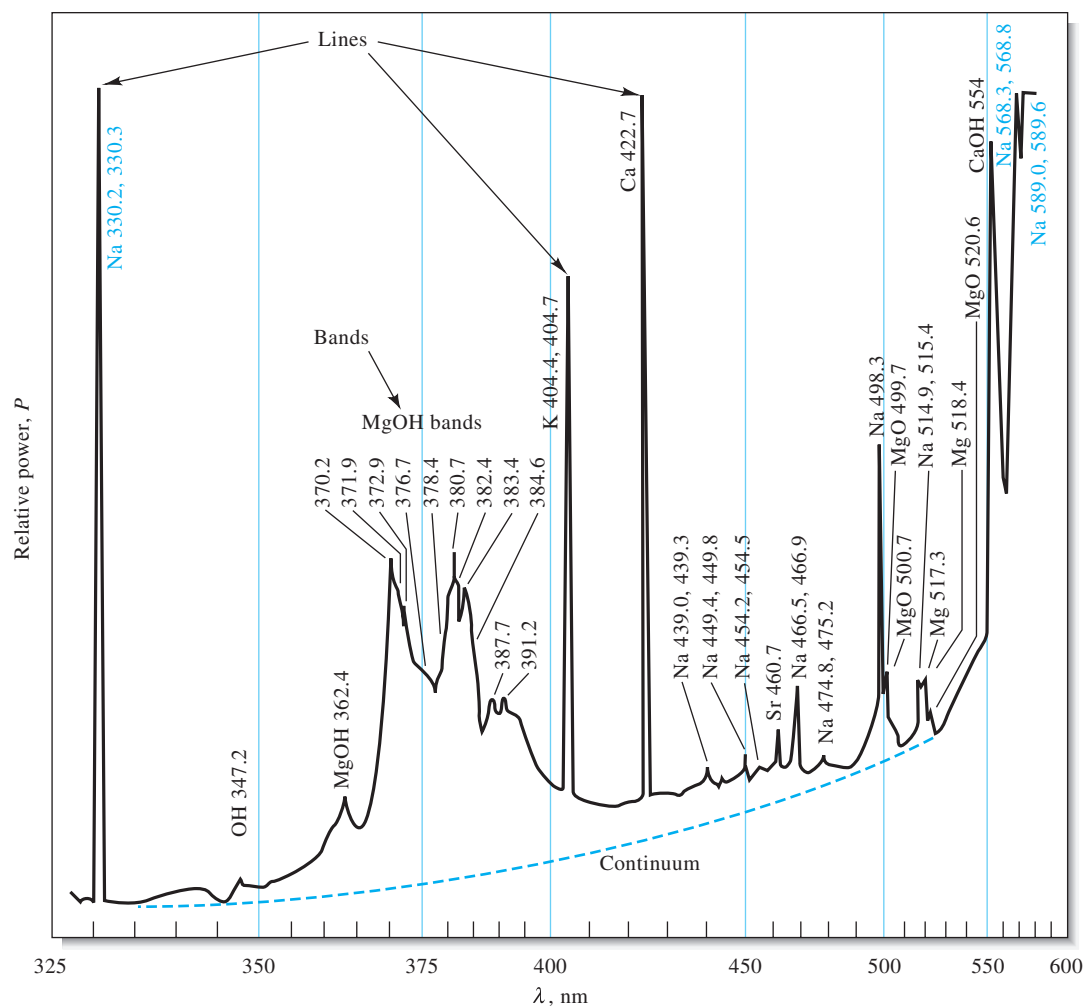


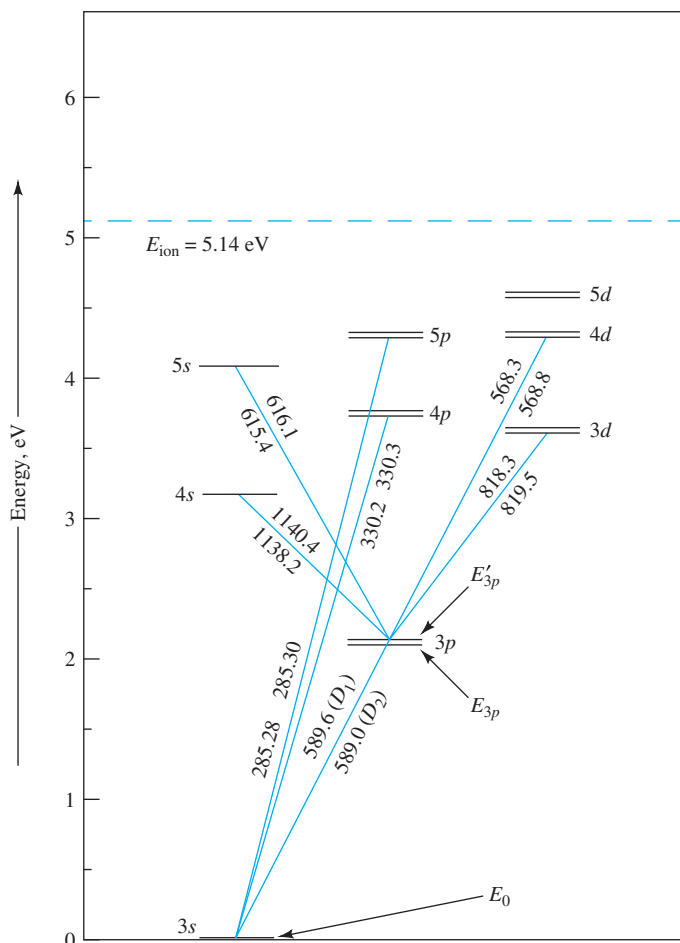
Figure 24-19 Emission spectrum of a brine sample obtained with an oxyhydrogen flame. The spectrum consists of the superimposed line, band, and continuum spectra of the constituents of the sample and flame. The characteristic wavelengths of the species contributing to the spectrum are listed beside each feature. (R. Hermann and C. T. J. Alkemade, *Chemical Analysis by Flame Photometry*, 2nd ed., New York: Interscience, 1979, p. 484.)

of sodium. Note that each of the p and d states are split into two closely spaced energy levels as a result of electron spin. The single outer shell electron in the ground state $3s$ orbital of a sodium atom can be excited into either of these levels by absorption of thermal, electrical, or radiant energy. Energy levels E_{3p} and E'_{3p} then represent the energies of the atom when this electron has been promoted to the two $3p$ states by absorption. The promotion to these states is depicted by the green line between the $3s$ and the two $3p$ levels in Figure 24-20. A few nanoseconds after excitation, the electron returns from the $3p$ state to the ground state, emitting a photon whose wavelength is given by Equation 24-3.

$$\lambda_1 = \frac{hc}{(E_{3p} - E_0)} = 589.6 \text{ nm}$$

In a similar way, relaxation from the $3p'$ state to the ground state yields a photon with $\lambda_2 = 589.0 \text{ nm}$. This emission process is once again shown by the green line between the $3s$ and $3p$ levels in Figure 24-20. The result is that the emission process from the two closely spaced $3p$ levels produces two corresponding closely spaced lines

Figure 24-20 Energy level diagram for sodium in which the horizontal lines represent the atomic orbitals, which are identified with their respective labels. The vertical scale is orbital energy in electron volts (eV), and the energies of excited states relative to the ground state 3s orbital can be read from the vertical axis. The lines in color show the allowed transitions resulting in emission of various wavelengths (in nm), indicated adjacent to the lines. The horizontal dashed line represents the ionization energy of sodium. (INGLE, JAMES D., CROUCH, STANLEY R., *SPECTROCHEMICAL ANALYSIS*, 1st Edition, © 1988, p.206. Reprinted by permission of Pearson Education, Inc., Upper Saddle River, NJ.)



in the emission spectrum called a **doublet**. These lines, indicated by the transitions labeled D_1 and D_2 in Figure 24-20, are the famous Fraunhofer “D” lines discussed in Feature 24-1. They are so intense that they are completely off scale in the upper right corner of the emission spectrum of Figure 24-19.

The transition from the more energetic 4p state to the ground state (see Figure 24-20) produces a second doublet at a shorter wavelength. The line appearing at about 330 nm in Figure 24-19 results from these transitions. The 4d-to-3p transition provides a third doublet at about 568 nm. Notice that all three of these doublets appear in the emission spectrum of Figure 24-19 as just single lines. This is a result of the limited resolution of the spectrometer used to produce the spectrum, as discussed in Sections 25A-3 and 28A-4. It is important to note that the emitted wavelengths are identical to the wavelengths of the absorption peaks for sodium (see Figure 24-11) because the transitions are between the same pairs of states.

At first glance, it may appear that radiation could be absorbed and emitted by atoms between any pair of the states shown in Figure 24-20, but in fact, only certain transitions are allowed, while others are forbidden. The transitions that are allowed and forbidden to produce lines in the atomic spectra of the elements are determined by the laws of quantum mechanics in what are called **selection rules**. These rules are beyond the scope of our discussion.⁴

⁴See J. D. Ingle, Jr., and S. R. Crouch, *Spectrochemical Analysis*, Upper Saddle River, NJ: Prentice-Hall, 1988, p. 205.

Band Spectra

Band spectra are often produced in spectral sources because of the presence of gaseous radicals or small molecules. For example, in Figure 24-19, bands for OH, MgOH, and MgO are labeled and consist of a series of closely spaced lines that are not fully resolved by the instrument used to obtain the spectrum. Bands arise from the numerous quantized vibrational levels that are superimposed on the ground state electronic energy level of a molecule. For further discussion of band spectra, see Section 28B-3.

Continuum Spectrum

As shown in Figure 24-21, a spectral continuum of radiation is produced when solids such as carbon and tungsten are heated to incandescence. Thermal radiation of this kind, which is called **blackbody radiation**, is more characteristic of the temperature of the emitting surface than of its surface material. Blackbody radiation is produced by the innumerable atomic and molecular oscillations excited in the condensed solid by the thermal energy. Note that the energy peaks in Figure 24-21 shift to shorter wavelengths with increasing temperature. As the figure shows, very high temperatures are required to cause a thermally excited source to emit a substantial fraction of its energy as ultraviolet radiation.

Part of the continuum background radiation in the flame spectrum shown in Figure 24-19 is probably thermal emission from incandescent particles in the flame. Note that this background decreases rapidly as the wavelength approaches the ultraviolet region of the spectrum.

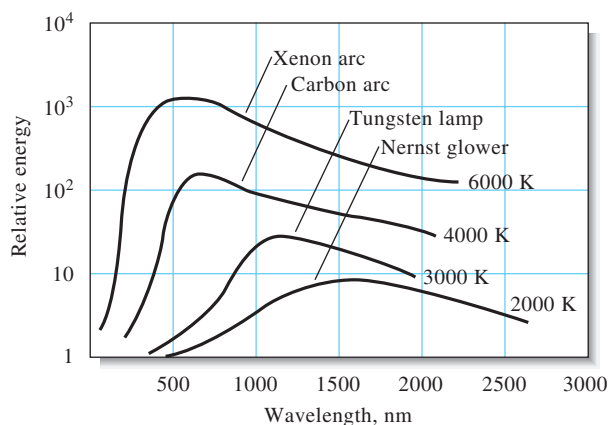
Heated solids are important sources of infrared, visible, and longer-wavelength ultraviolet radiation for analytical instruments, as we will see in Chapter 25.

Effect of Concentration on Line and Band Spectra

The radiant power P of a line or a band depends directly on the number of excited atoms or molecules, which in turn is proportional to the total concentration c of the species present in the source. Thus, we can write

$$P = kc \quad (24-16)$$

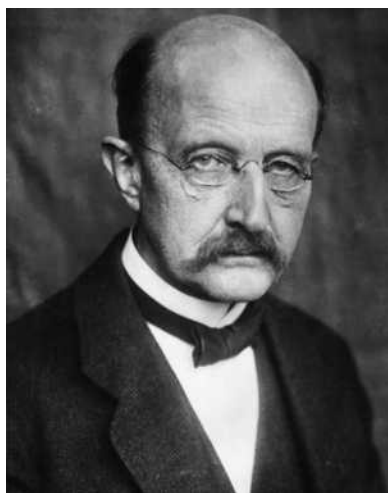
where k is a proportionality constant. This relationship is the basis of quantitative emission spectroscopy, which is described in some detail in Section 28C.



◀ An emission band spectrum is made up of many closely spaced lines that are difficult to resolve.

◀ A spectral continuum has no line character and is generally produced by heating solids to a high temperature.

Figure 24-21 Blackbody radiation curves for various light sources. Note the shift in the wavelengths of maximum emission as the temperature of the sources changes.



© Bettmann/CORBIS

In 1900, Max Planck (1858–1947) discovered a formula (now often called the Planck radiation law) that modeled curves like those shown in Figure 24-21 nearly perfectly. He followed this discovery by developing a theory that made two bold assumptions regarding the oscillating atoms or molecules in blackbody radiators. He assumed (1) that these species could have only discrete energies and (2) that they could absorb or emit energy in discrete units, or quanta. These assumptions, which are implicit in Equation 24-3, laid the foundation for the development of quantum theory.

Resonance fluorescence is radiation that is identical in wavelength to the radiation that excited the fluorescence.

24D-2 Emission by Fluorescence and Phosphorescence

Fluorescence and phosphorescence are analytically important emission processes in which atoms or molecules are excited by the absorption of a beam of electromagnetic radiation. The excited species then relax to the ground state, giving up their excess energy as photons. Fluorescence takes place much more rapidly than phosphorescence and is generally complete in 10^{-5} s or less from the time of excitation. Phosphorescence emission may extend for minutes or even hours after irradiation has ceased. Fluorescence is considerably more important than phosphorescence in analytical chemistry, so our discussions focus primarily on fluorescence.

Atomic Fluorescence

Gaseous atoms fluoresce when they are exposed to radiation that has a wavelength that exactly matches that of one of the absorption (or emission) lines of the element in question. For example, gaseous sodium atoms are promoted to the excited energy state, E_{3p} , shown in Figure 24-20 through absorption of 589-nm radiation. Relaxation may then take place by reemission of radiation of the identical wavelength. When excitation and emission wavelengths are the same, the resulting emission is called **resonance fluorescence**. Sodium atoms could also exhibit resonance fluorescence when exposed to 330-nm or 285-nm radiation. In addition, however, the element could also produce nonresonance fluorescence by first relaxing from E_{5p} or E_{4p} to energy level E_{3p} through a series of nonradiative collisions with other species in the medium. Further relaxation to the ground state can then take place either by the emission of a 589-nm photon or by further collisional deactivation.

Molecular Fluorescence

Fluorescence is a photoluminescence process in which atoms or molecules are excited by absorption of electromagnetic radiation, as shown in Figure 24-22a. The excited species then relax back to the ground state, giving up their excess energy as photons. As we have noted, the lifetime of an excited species is brief because there are several mechanisms for an excited atom or molecule to give up its excess energy and relax to its ground state. Two of the most important of these mechanisms, **nonradiative relaxation** and **fluorescence emission**, are illustrated in Figures 24-22b and c.

Nonradiative Relaxation. Two types of nonradiative relaxation are shown in Figure 24-22b. **Vibrational deactivation**, or **relaxation**, depicted by the short wavy arrows between vibrational energy levels, takes place during collisions between excited molecules and molecules of the solvent. During the collisions, the excess vibrational energy is transferred to solvent molecules in a series of steps as indicated in the figure. The gain in vibrational energy of the solvent is reflected in a tiny increase in the temperature of the medium. Vibrational relaxation is such an efficient process that the average lifetime of an excited vibrational state is only about 10^{-15} s. Nonradiative relaxation between the lowest vibrational level of an excited electronic state and the upper vibrational level of another electronic state can also occur. This type of relaxation, which is called **internal conversion**, depicted by the two longer wavy arrows in Figure 24-22b, is much less efficient than vibrational relaxation so that the average lifetime of an electronic excited state is between 10^{-9} and 10^{-6} s. The mechanisms by which this type of relaxation occurs are not fully understood, but the net effect is again a very small rise in the temperature of the medium.

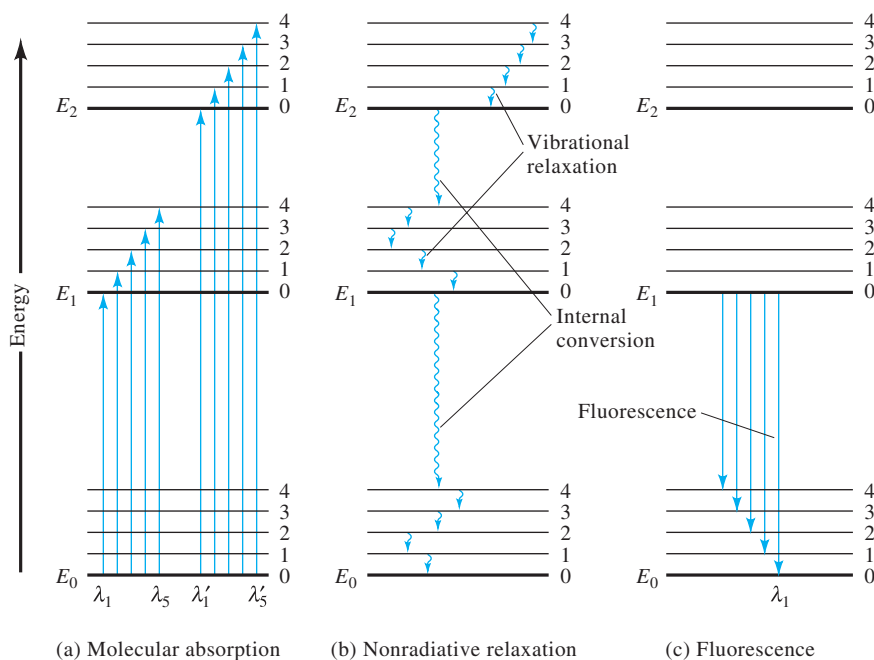


Figure 24-22 Energy level diagram showing some of the energy changes that occur during absorption, nonradiative relaxation, and fluorescence by a molecular species.

Fluorescence. The relative number of molecules that fluoresce is small because fluorescence requires structural features that slow the rate of the nonradiative relaxation processes illustrated in Figure 24-22b and enhance the rate of fluorescence emission shown in Figure 24-22c. Most molecules lack these features and undergo nonradiative relaxation at a rate that is significantly greater than the radiative relaxation rate, and so fluorescence does not occur. As shown in Figure 24-22c, bands of radiation are produced when molecules relax from the lowest-lying vibrational state of an excited state, E_1 , to the many vibrational levels of the ground state, E_0 . Like molecular absorption bands, molecular fluorescence bands are made up of a large number of closely spaced lines that are usually difficult to resolve. Notice that the transition from E_1 to the lowest-lying vibrational state of the ground state (λ_1) has the highest energy of all of the transitions in the band. As a result, all of the other lines that terminate in higher vibrational levels of the ground state are lower in energy and produce fluorescence emission at longer wavelengths than λ_1 . In other words, molecular fluorescence bands consist largely of lines that are longer in wavelength than the band of absorbed radiation responsible for their excitation. This shift in wavelength is called the **Stokes shift**. A more detailed discussion of molecular fluorescence is given in Chapter 27.

The **Stokes shift** refers to fluorescence radiation that occurs at wavelengths that are longer than the wavelength of radiation used to excite the fluorescence.

WEB WORKS

To learn more about Beer's law, use a search engine to find the IUPAC "Glossary of Terms Used in Photochemistry." Find how the molar absorptivity (the IUPAC "Glossary" uses **molar absorption coefficient**) of a compound (ϵ) relates to the absorption cross section (σ). Multiply the absorption cross section by Avogadro's number and note the result. How would the result change if absorbance were expressed as $A = -\ln(P/P_0)$ rather than the usual definition in terms of base 10 logarithms? What are the units of σ ? Which of the quantities ϵ or σ is a macroscopic quantity? Which of the terms, molar absorptivity or molar absorption coefficient, is most descriptive? Explain and justify your answer.

QUESTIONS AND PROBLEMS

- *24-1.** In a solution of pH 5.3, the indicator bromocresol purple exhibits a yellow color, but when the pH is 6.0, the indicator solution changes to purple. Discuss why these colors are observed in terms of the wavelength regions and colors absorbed and transmitted.
- 24-2.** What is the relationship between
 *(a) absorbance and transmittance?
 (b) absorptivity a and molar absorptivity ϵ ?
- *24-3.** Identify factors that cause the Beer's law relationship to be nonlinear.
- 24-4.** Describe the differences between "real" deviations from Beer's law and those due to instrumental or chemical factors.
- 24-5.** How does an electronic transition resemble a vibrational transition? How do they differ?
- 24-6.** Calculate the frequency in hertz of
 *(a) an X-ray beam with a wavelength of 2.65 Å.
 (b) an emission line for copper at 211.0 nm.
 *(c) the line at 694.3 nm produced by a ruby laser.
 (d) the output of a CO₂ laser at 10.6 μm.
 *(e) an infrared absorption peak at 19.6 μm.
 (f) a microwave beam at 1.86 cm.
- 24-7.** Calculate the wavelength in centimeters of
 *(a) an airport tower transmitting at 118.6 MHz.
 (b) a VOR (radio navigation aid) transmitting at 114.10 kHz.
 *(c) an NMR signal at 105 MHz.
 (d) an infrared absorption peak with a wavenumber of 1210 cm⁻¹.
- 24-8.** A sophisticated ultraviolet/visible/near-IR instrument has a wavelength range of 185 to 3000 nm. What are its wavenumber and frequency ranges?
- *24-9.** A typical simple infrared spectrophotometer covers a wavelength range from 3 to 15 μm. Express its range (a) in wavenumbers and (b) in hertz.
- 24-10.** Calculate the frequency in hertz and the energy in joules of an X-ray photon with a wavelength of 2.70 Å.
- *24-11.** Calculate the wavelength and the energy in joules associated with a signal at 220 MHz.
- 24-12.** Calculate the wavelength of
 *(a) the sodium line at 589 nm in an aqueous solution with a refractive index of 1.35.
 (b) the output of a ruby laser at 694.3 nm when it is passing through a piece of quartz that has a refractive index of 1.55.
- 24-13.** What are the units for absorptivity when the path length is given in centimeters and the concentration is expressed in
 *(a) parts per million?
 (b) micrograms per liter?
 *(c) mass-volume percent?
 (d) grams per liter?
- 24-14.** Express the following absorbances in terms of percent transmittance
 *(a) 0.0356
 (b) 0.895
 *(c) 0.379
 (d) 0.167
 *(e) 0.485
 (f) 0.753
- 24-15.** Convert the accompanying transmittance data to absorbances.
 *(a) 27.2%
 (b) 0.579
 *(c) 30.6%
 (d) 3.98%
 *(e) 0.093
 (f) 63.7%
- 24-16.** Calculate the percent transmittance of solutions that have twice the absorbance of the solutions in Problem 24-14.
- 24-17.** Calculate the absorbances of solutions with half the transmittance of those in Problem 24-15.
- 24-18.** Evaluate the missing quantities in the accompanying table. Where needed, use 200 for the molar mass of the analyte.

	A	$\%T$	ϵ L mol ⁻¹ cm ⁻¹	a cm ⁻¹ ppm ⁻¹	b cm	c M	ppm
*(a)	0.172		4.23×10^3		1.00		
(b)		44.9		0.0258		1.35×10^{-4}	
*(c)	0.520		7.95×10^3		1.00		
(d)		39.6		0.0912			1.76
*(e)			3.73×10^3		0.100	1.71×10^{-3}	
(f)		83.6			1.00	8.07×10^{-6}	
*(g)	0.798				1.50		33.6
(h)		11.1	1.35×10^4			7.07×10^{-5}	
*(i)		5.23	9.78×10^3				5.24
(j)	0.179				1.00	7.19×10^{-5}	

Unless otherwise noted, all content on this page is © Cengage Learning.

- 24-19.** A solution containing 4.48 ppm KMnO_4 exhibits 85.9% T in a 1.00-cm cell at 520 nm. Calculate the molar absorptivity of KMnO_4 at this wavelength.
- 24-20.** Beryllium(II) forms a complex with acetylacetone (166.2 g/mol). Calculate the molar absorptivity of the complex, given that a 2.25 ppm solution has a transmittance of 37.5% when measured in a 1.00-cm cell at 295 nm, the wavelength of maximum absorption.
- *24-21.** At 580 nm, the wavelength of its maximum absorption, the complex $\text{Fe}(\text{SCN})^{2+}$ has a molar absorptivity of $7.00 \times 10^3 \text{ L cm}^{-1} \text{ mol}^{-1}$. Calculate
- the absorbance of a $3.40 \times 10^{-5} \text{ M}$ solution of the complex at 580 nm in a 1.00-cm cell.
 - the absorbance of a solution in which the concentration of the complex is twice that in (a).
 - the transmittance of the solutions described in (a) and (b).
 - the absorbance of a solution that has half the transmittance of that described in (a).
- 24-22.** A 2.50-mL aliquot of a solution that contains 4.33 ppm iron(III) is treated with an appropriate excess of KSCN and diluted to 50.0 mL. What is the absorbance of the resulting solution at 580 nm in a 2.50-cm cell? See Problem 24-21 for absorptivity data.
- *24-23.** A solution containing the complex formed between Bi(III) and thiourea has a molar absorptivity of $9.32 \times 10^3 \text{ L cm}^{-1} \text{ mol}^{-1}$ at 470 nm.
- What is the absorbance of a $5.67 \times 10^{-5} \text{ M}$ solution of the complex at 470 nm in a 1.00-cm cell?
 - What is the percent transmittance of the solution described in (a)?
 - What is the molar concentration of the complex in a solution that has the absorbance described in (a) when measured at 470 nm in a 2.50-cm cell?
- 24-24.** The complex formed between Cu(I) and 1,10-phenanthroline has a molar absorptivity of $7000 \text{ L cm}^{-1} \text{ mol}^{-1}$ at 435 nm, the wavelength of maximum absorption. Calculate
- the absorbance of a $6.17 \times 10^{-5} \text{ M}$ solution of the complex when measured in a 1.00-cm cell at 435 nm.
 - the percent transmittance of the solution in (a).
 - the concentration of a solution that in a 5.00-cm cell has the same absorbance as the solution in (a).
 - the path length through a $3.13 \times 10^{-5} \text{ M}$ solution of the complex that is needed for an absorbance that is the same as the solution in (a).
- *24-25.** A solution with a “true” absorbance [$A = -\log(P_0/P)$] of 2.10 was placed in a spectrophotometer with a stray light percentage (P_s/P_0) of 0.75. What absorbance A' would be measured? What percentage error would result?
- 24-26.** A compound X is to be determined by UV/visible spectrophotometry. A calibration curve is constructed from standard solutions of X with the following results: 0.50 ppm, $A = 0.24$; 1.5 ppm, $A = 0.36$; 2.5 ppm, $A = 0.44$; 3.5 ppm, $A = 0.59$; and 4.5 ppm, $A = 0.70$. Find the slope and intercept of the calibration curve, the standard error in Y, the concentration of the solution of unknown X concentration, and the standard deviation in the concentration of X. Construct a plot of the calibration curve and determine the unknown concentration by hand from the plot.
- 24-27.** One common way to determine phosphorus in urine is to treat the sample after removing the protein with molybdenum (VI) and then reducing the resulting 12-molybdophosphate complex with ascorbic acid to give an intense blue-colored species called molybdenum blue. The absorbance of molybdenum blue can be measured at 650 nm. A 24-hour urine sample was collected, and the patient produced 1122 mL in 24 hours. A 1.00 mL aliquot of the sample was treated with Mo(VI) and ascorbic acid and diluted to a volume of 50.00 mL. A calibration curve was prepared by treating 1.00 mL aliquots of phosphate standard solutions in the same manner as the urine sample. The absorbances of the standards and the urine sample were obtained at 650 nm and the following results obtained:

Solution	Absorbance at 650 nm
1.00 ppm P	0.230
2.00 ppm P	0.436
3.00 ppm P	0.638
4.00 ppm P	0.848
Urine sample	0.518

- Find the slope, intercept, and standard error in y of the calibration curve. Construct a calibration curve. Determine the concentration number of phosphorus in ppm in the urine sample and its standard deviation from the least-squares equation of the line. Compare the unknown concentration to that obtained manually from a calibration curve.
- What mass in grams of phosphorus was eliminated per day by the patient?
- What is the phosphate concentration in urine in mM?

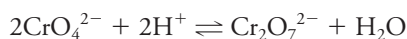
- 24-28.** Nitrite is commonly determined by a colorimetric procedure using a reaction called the Griess reaction. In this reaction, the sample containing nitrite is reacted with sulfanilimide and N-(1-Naphthyl) ethylenediamine to form a colored species that absorbs at 550 nm. Using an automated flow analysis

instrument, the following results were obtained for standard solutions of nitrite and for a sample containing an unknown amount:

Solution	Absorbance at 550 nm
2.00 μM	0.065
6.00 μM	0.205
10.00 μM	0.338
14.00 μM	0.474
18.00 μM	0.598
Unknown	0.402

- Find the slope, intercept, and standard deviation of the calibration curve.
- Construct the calibration curve.
- Determine the concentration of nitrite in the sample and its standard deviation.

24-29. The equilibrium constant for the reaction



is 4.2×10^{14} . The molar absorptivities for the two principal species in a solution of K_2CrO_7 are

λ , nm	ϵ_1 (CrO_4^{2-})	ϵ_2 ($\text{Cr}_2\text{O}_7^{2-}$)
345	1.84×10^3	10.7×10^2
370	4.81×10^3	7.28×10^2
400	1.88×10^3	1.89×10^2

Four solutions were prepared by dissolving 4.00×10^{-4} , 3.00×10^{-4} , 2.00×10^{-4} , and 1.00×10^{-4} moles of $\text{K}_2\text{Cr}_2\text{O}_7$ in water and diluting to 1.00 L with a pH 5.60 buffer. Calculate theoretical absorbance values (1.00-cm cells) for each solution and plot the data for (a) 345 nm; (b) 370 nm; and (c) 400 nm.

24-30. Challenge Problem: NIST maintains a database of the spectra of the elements at http://www.nist.gov/pml/data/asd_contents.cfm. The following energy levels for neutral lithium were obtained from this database:

Electronic Configuration	Level, eV
$1s^2 2s^1$	0.00000
$1s^2 2p^1$	1.847818 1.847860
$1s^2 3s^1$	3.373129
$1s^2 3p^1$	3.834258 3.834258
$1s^2 3d^1$	3.878607 3.878612
$1s^2 4s^1$	4.340942
$1s^2 4p^1$	4.521648 4.521648
$1s^2 4d^1$	4.540720 4.540723

- Construct a partial energy level diagram similar to the one in Figure 24-20. Label each energy level with its corresponding orbital.
- Browse to the NIST website and click on the Physical Reference Data link. Locate and click on the link for the Atomic Spectral Database and click on the Lines icon. Use the form to retrieve the spectral lines for Li I between 300 nm and 700 nm, including energy level information. Note that the retrieved table contains wavelength, relative intensity, and changes in electron configuration for the transitions that give rise to each line. Add connecting lines to the partial energy level diagram from (a) to illustrate the transitions and label each line with the wavelength of the emission. Which of the transitions in your diagram are doublets?
- Use the intensity versus wavelength data that you retrieved in (b) to sketch an emission spectrum for lithium. If you placed a sample of LiCO_3 in a flame, what color would the flame be?
- Describe how the flame spectrum of an ionic lithium compound, such as LiCO_3 , displays the spectrum of neutral lithium atoms.
- There appear to be no emission lines for lithium between 544 nm and 610 nm. Why is this?
- Describe how the information obtained in this problem could be used to detect the presence of lithium in urine. How would you determine the amount of lithium quantitatively?



Instrumentation for Fluorescence Spectroscopy

The success of fluorescence experiments requires attention to experimental details and an understanding of the instrumentation. There are also many potential artifacts that can distort the data. Light can be detected with high sensitivity. As a result, the gain or amplification of instruments can usually be increased to obtain observable signals, even if the sample is nearly nonfluorescent. These signals seen at high amplification may not originate with the fluorophore of interest. Instead, the interference can be due to background fluorescence from the solvents, light leaks in the instrumentation, emission from the optical components, stray light passing through the optics, light scattered by turbid solutions, and Rayleigh and/or Raman scatter, to name a few interference sources.

An additional complication is that there is no ideal spectrofluorometer. The available instruments do not yield true excitation or emission spectra. This is because of the nonuniform spectral output of the light sources and the wavelength-dependent efficiency of the monochromators and detector tubes. The polarization or anisotropy of the emitted light can also affect the measured fluorescence intensities because the efficiency of gratings depends on polarization. It is important to understand and control these numerous factors. In this chapter we will discuss the properties of the individual components in a spectrofluorometer, and how these properties affect the observed spectral data. These instrumental factors can affect the excitation and emission spectra, as well as the measurement of fluorescence lifetimes and anisotropies. Additionally, the optical properties of the samples—such as optical density and turbidity—can also affect the spectral data. Specific examples are given to clarify these effects and the means to avoid them.

2.1. SPECTROFLUOROMETERS

2.1.1. Spectrofluorometers for Spectroscopy Research

With most spectrofluorometers it is possible to record both excitation and emission spectra. An emission spectrum is the wavelength distribution of an emission measured at a single constant excitation wavelength. Conversely, an excitation spectrum is the dependence of emission intensity, measured at a single emission wavelength, upon scanning the excitation wavelength. Such spectra can be presented on either a wavelength scale or a wavenumber scale. Light of a given energy can be described in terms of its wavelength λ , frequency ν , or wavenumber. The usual units for wavelength are nanometers, and wavenumbers are given in units of cm^{-1} . Wavelengths and wavenumbers are easily interconverted by taking the reciprocal of each value. For example, 400 nm corresponds to $(400 \times 10^{-7} \text{ cm})^{-1} = 25,000 \text{ cm}^{-1}$. The presentation of fluorescence spectra on the wavelength or wavenumber scale has been a subject of debate. Admittedly, the wavenumber scale is linear in energy. However, most commercially available instrumentation yields spectra on the wavelength scale, and such spectra are more familiar and thus easier to interpret visually. Since corrected spectra are not needed on a routine basis, and since accurately corrected spectra are difficult to obtain, we prefer to use the directly recorded technical or uncorrected spectra on the wavelength scale.

For an ideal instrument, the directly recorded emission spectra would represent the photon emission rate or power emitted at each wavelength, over a wavelength interval determined by the slit widths and dispersion of the emission

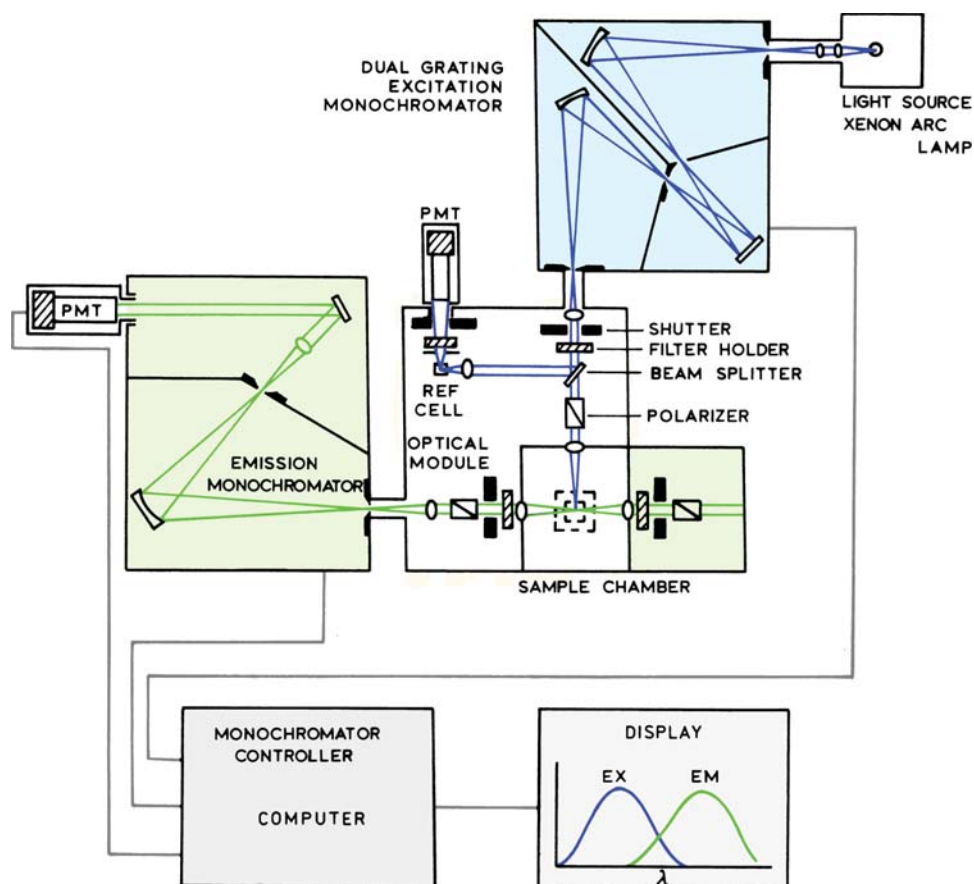


Figure 2.1. Schematic diagram of a spectrofluorometer [1].

monochromator. Similarly, the excitation spectrum would represent the relative emission of the fluorophore at each excitation wavelength. For most fluorophores the quantum yields and emission spectra are independent of excitation wavelength. As a result, the excitation spectrum of a fluorophore can be superimposable on its absorption spectrum. However, such identical absorption and excitation spectra are rarely observed because the excitation intensity is different at each wavelength. Even under ideal circumstances such correspondence of the excitation and absorption spectra requires the presence of only a single type of fluorophore, and the absence of other complicating factors, such as a nonlinear response resulting from a high optical density of the sample or the presence of other chromophores in the sample. Emission spectra recorded on different instruments can be different because of the wavelength-dependent sensitivities of the instruments.

Figure 2.1 shows a schematic diagram of a general-purpose spectrofluorometer: this instrument has a xenon

lamp as a source of exciting light. Such lamps are generally useful because of their high intensity at all wavelengths ranging upward from 250 nm. The instrument shown is equipped with monochromators to select both the excitation and emission wavelengths. The excitation monochromator in this schematic contains two gratings, which decreases stray light, that is, light with wavelengths different from the chosen one. In addition, these monochromators use concave gratings, produced by holographic means to further decrease stray light. In subsequent sections of this chapter we will discuss light sources, detectors and the importance of spectral purity to minimize interference due to stray light. Both monochromators are motorized to allow automatic scanning of wavelength. The fluorescence is detected with photomultiplier tubes and quantified with the appropriate electronic devices. The output is usually presented in graphical form and stored digitally.

The instrument schematic also shows the components of the optical module that surrounds the sample holder. Ver-

satiate and stable optical components are indispensable for a research spectrofluorometer. The module shown in Figure 2.1 contains a number of convenient features that are useful on a research instrument. Shutters are provided to eliminate the exciting light or to close off the emission channel. A beam splitter is provided in the excitation light path. This splitter reflects part of the excitation light to a reference cell, which generally contains a stable reference fluorophore. The beam splitter consists of a thin piece of clear quartz, which reflects about 4% of the incident light. This amount is generally adequate for a reference channel that frequently contains a highly fluorescent quantum counter (Section 2.8.1). The intensity from the standard solution is typically isolated with a bandpass filter, and is proportional to the intensity of the exciting light. Changes in the intensity of the arc lamp may be corrected for by division of the intensity from the sample by that of the reference fluorophore.

Polarizers are present in both the excitation and emission light paths. Generally, the polarizers are removable so that they can be inserted only for measurements of fluorescence anisotropy, or when it is necessary to select for particular polarized components of the emission and/or excitation. Accurate measurement of fluorescence anisotropies requires accurate angular positioning of the polarizers. The polarizer mounts must be accurately indexed to determine the angular orientation. The optical module shown in Figure 2.1 has an additional optical path on the right side of the sample holder. This path allows measurement of fluorescence anisotropy by the T-format method (Chapter 10). There are many occasions where the additional light path is necessary or convenient for experiments, but with modern electronics it is usually not necessary to use the T-format for anisotropy measurements.

The present trend is toward small compact spectrofluorometers, with all the optical components in a single enclosure. Such instruments are easy to maintain because there is little opportunity to alter the configuration. A modular instrument has some advantages in a spectroscopy laboratory. For instance, if the xenon lamp and monochromator are removable, a laser source can be used in place of the arc lamp. On some occasions it is desirable to bypass the emission monochromator and use bandpass filters to collect as much of the emission as possible. Such experiments are possible if the emission monochromator is removable. If the monochromator cannot be removed the gratings can act like mirrors if set at the zero-order diffraction or a wavelength of zero. If the wavelength is set to zero the monochromator

typically transmits all wavelengths. Filters can be used to isolate the desired range of wavelengths.

It is convenient if the instrument has a versatile sample holder. If the research involves anisotropy measurements it will often be necessary to measure the fundamental anisotropy (r_0) in the absence of rotational diffusion. This is accomplished at low temperature, typically -50°C in glycerol. Low temperature can only be achieved if the sample holder is adequately sized for a high rate of coolant flow, has good thermal contact with the cuvette, and is insulated from the rest of the instrument. Many cuvette holders can maintain a temperature near room temperature, but may not be able to maintain a temperature much above or below that.

Another useful feature is the ability to place optical filters into the excitation or emission light path. Filters are often needed, in addition to monochromators, to remove unwanted wavelengths in the excitation beam, or to remove scattered light from the emission channel.

2.1.2. Spectrofluorometers for High Throughput

At present the design of fluorescence experiments is changing toward a multi-sample approach. Instead of detailed experiments on a single sample, the experiments are designed to include many samples. Such experiments can include binding studies, quenching, and cell-based assays. High-throughput screening assays are used in drug discovery, often using numerous microplates, each with 384 or more wells. Such measurements are typically performed using microplate readers (Figure 2.2). The samples are contained in the wells of the microplates, which are taken inside the instrument for the measurements. Such an instrument may not provide the detailed information available using an instrument designed for spectroscopy (Figure 2.1) but can rapidly provide measurements on numerous samples.

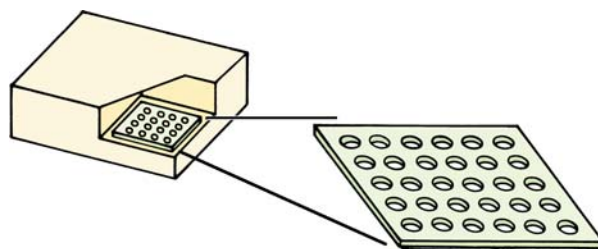


Figure 2.2. Fluorescence microplate reader.

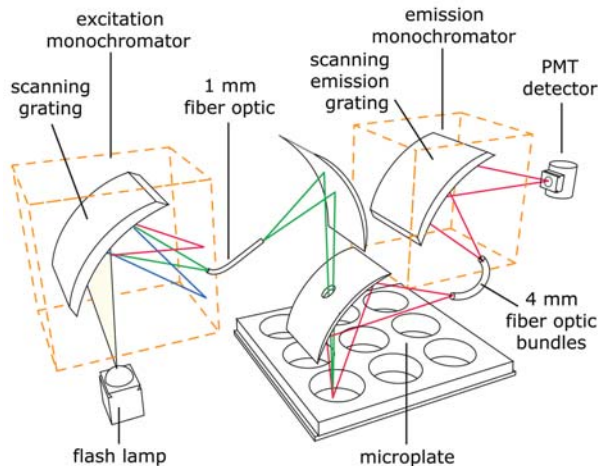


Figure 2.3. Optical path for a microplate reader [2].

The optics used in microplate readers are different than in an instrument designed for use with a cuvette. Microwell plates must remain horizontal, and it is not possible to use right-angle observation as can be used with a cuvette. Figure 2.3 shows a typical optical path for microplate readers. The light source is a xenon flash lamp, which is becoming more common in fluorescence instruments. The desired excitation wavelength is selected using a monochromator. A unique feature is the mirror with a hole to transmit the excitation. The fluorescence, which occurs in all directions, is directed toward the detector optics by the same mirror. Typically, the microplate is moved to position each well in the observation path by an x - y scanning stage. Some microplate readers include a second mirror under the microplate to facilitate cell-based assays or absorption measurements. Microplate readers are typically used for intensity measurements on a large number of samples. Microplate readers have become available for research spectrofluorometers allowing collection of spectra, anisotropies, and lifetimes.

2.1.3. An Ideal Spectrofluorometer

In an ideal case the recorded excitation and emission spectra would represent the relative photon intensity per wavelength interval. To obtain such "corrected" emission spectra the individual components must have the following characteristics:

1. the light source must yield a constant photon output at all wavelengths;
2. the monochromator must pass photons of all wavelengths with equal efficiency;

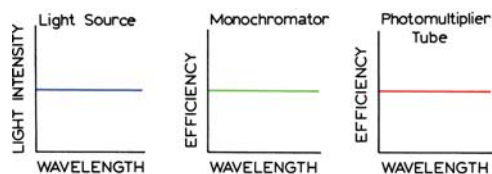


Figure 2.4. Properties of the ideal components of a spectrofluorometer.

3. the monochromator efficiency must be independent of polarization; and
4. the detector (photomultiplier tube) must detect photons of all wavelengths with equal efficiency.

These characteristics for ideal optical components are illustrated in Figure 2.4. Unfortunately, light sources, monochromators, and photomultiplier tubes with such ideal characteristics are not available. As a result, one is forced to compromise on the selection of components and to correct for the nonideal response of the instrument.

An absorption spectrophotometer contains these same components, so why is it possible to record correct absorption spectra? In recording an absorption spectrum the intensity of light transmitted by the sample is measured relative to that transmitted by the blank. Comparative measurements are performed with the same components, at the same wavelengths. The nonideal behavior of the components cancels in the comparative measurements. In contrast to absorption measurements, fluorescence intensity measurements are absolute, not relative. Comparison of the sample fluorescence with a blank is not useful because the blank, in principle, displays no signal. Also, the weak background signal has an unknown spectral distribution, and thus cannot be used for correction of the wavelength dependence of the optical components. Hence, the opportunity for internal compensation is limited. As will be described below, a limited number of standard spectra are available for correction purposes. Corrected emission spectra are provided in Appendix I.

2.1.4. Distortions in Excitation and Emission Spectra

To record an excitation spectrum, the emission monochromator is set at the desired wavelength, generally the emission maximum. The excitation monochromator is then scanned through the absorption bands of the fluorophore. The observed signal is distorted for several reasons:

1. The light intensity from the excitation source is a function of wavelength. Even if the intensity of the exciting light is monitored via the beam splitter shown in Figure 2.1, and corrected by division, the response of the reference solution or detector may be dependent upon wavelength.
2. The transmission efficiency of the excitation monochromators is a function of wavelength.
3. The optical density of the sample may exceed the linear range, which is about 0.1 absorbance units, depending upon sample geometry.

Emission spectra are recorded by choosing an appropriate excitation wavelength and scanning wavelength with the emission monochromator. In addition to the factors discussed above, the emission spectrum is further distorted by the wavelength-dependent efficiency of the emission monochromator and photomultiplier. The emission spectrum can also be distorted by absorption of the sample.

2.2. LIGHT SOURCES

We now describe the individual components of a spectrofluorometer. The general characteristics of these components are considered along with the reason for choosing specific components. Understanding the characteristics of these components allows one to understand the capabilities and limitations of spectrofluorometers. We will first consider light sources.

2.2.1. Arc and Incandescent Xenon Lamps

At present the most versatile light source for a steady-state spectrofluorometer is a high-pressure xenon (Xe) arc lamp. These lamps provide a relatively continuous light output from 250 to 700 nm (Figure 2.5), with a number of sharp lines occurring near 450 nm and above 800 nm. Xenon arc lamps emit a continuum of light as a result of recombination of electrons with ionized Xe atoms. These ions are generated by collisions of Xe atoms with the electrons that flow across the arc. Complete separation of the electrons from the atoms yields the continuous emission. Xe atoms that are in excited states but not ionized yield lines rather than broad emission bands. The peaks near 450 nm are due to these excited states. The output intensity drops rapidly below 280 nm. Furthermore, many Xe lamps are classified as being ozone-free, meaning that their operation does not generate

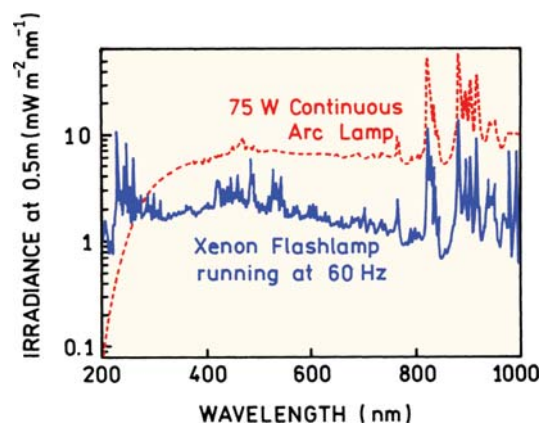


Figure 2.5. Spectral output of a continuous xenon arc lamp and a xenon flash lamp. Revised from [3]. Courtesy of Newport Corp.

ozone in the surrounding air. The quartz envelope used in such ozone-free lamps does not transmit light with wavelengths shorter than 250 nm, and the output of such lamps decreases rapidly with decreasing wavelength.

The wavelength-dependent output of Xe lamps is a major reason for distortion of the excitation spectra of compounds that absorb in the visible and ultraviolet. To illustrate this effect Figure 2.6 shows corrected and uncorrected excitation fluorescein spectra. The uncorrected spectra are recorded emission intensities with no correction for wavelength-dependent excitation intensity. The uncorrected excitation spectrum displays a number of peaks near 450 nm. These peaks are due to the output of the Xe lamp, which also displays peaks near 450 nm (Figure 2.5). Also shown in Figure 2.6 is the excitation spectrum, corrected for the wavelength-dependent output of the Xe arc lamp. A

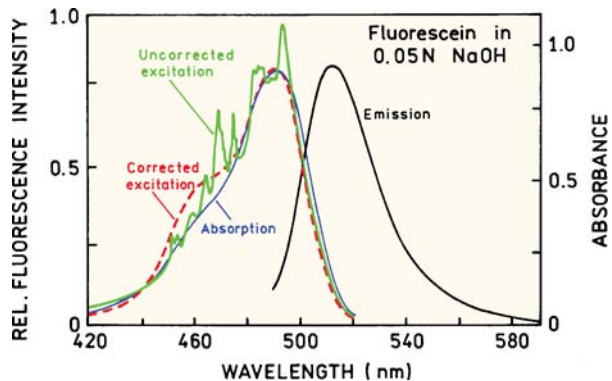


Figure 2.6. Corrected and uncorrected excitation spectra of fluorescein. From [4].

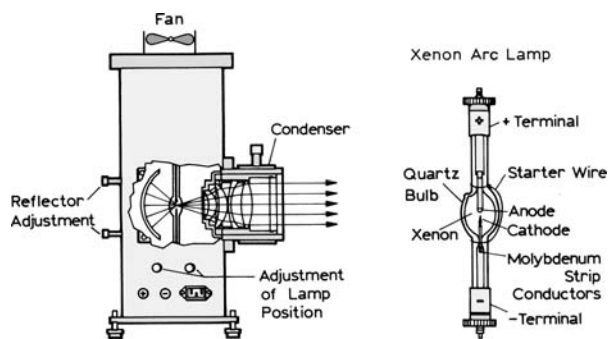


Figure 2.7. Xenon air lamp and a typical lamp housing. Revised from [5]. Courtesy of Newport Corp.

quantum counter was used in the reference channel to provide a signal proportional to the lamp intensity, and the intensity of the sample was divided by this reference intensity (Section 2.8.1). The peaks are no longer apparent in the corrected excitation spectrum, and this spectrum corresponds more closely with the absorption spectrum of fluorescein. The marked difference between the corrected and uncorrected spectra illustrates how the spectral output of the lamp influences the shape of the excitation spectra.

Xenon lamps are usually contained within specially designed housings. The arc lamp housing serves several important functions (Figure 2.7). The gas in xenon lamps is under high pressure (about 10 atmospheres), and explosion is always a danger. The housing protects the user from the lamp and also from its intense optical output. The housing also directs air over the lamp and removes excess heat and ozone. A xenon lamp that is on should never be observed directly. The extreme brightness will damage the retina, and the ultraviolet light can damage the cornea.

Another important role of the housing is for collecting and collimating lamp output, which is then focused into the entrance slit of the monochromator. Some lamp houses have mirrors behind the lamp to direct additional energy toward the output. Most of the light output originates from the small central region between the electrodes, and this spot needs to be focused on the optical entrance slit of the excitation monochromator.

Because of the heat and high intensity of a running xenon lamp, it is not practical to adjust the position of an uncovered lamp. Hence the lamp housing should have external provisions for position adjustment and focusing. The useful life of a xenon lamp is about 2000 hours. Safety glasses should be worn when handling these lamps. The

quartz envelope should not be touched, and if touched should be cleaned with a solvent such as ethanol. The fingerprint residues will char, resulting in hot spots on the quartz envelope and possible lamp failure. To protect the next person handling the disposed lamp, one should wrap the lamp in heavy paper and break the quartz envelope. It is important to pay close attention to mounting lamps in the proper orientation, which can be different for different types of lamps.

The power supplies of arc lamps are extremely dangerous, generating 25 amps at 20 volts, for a typical 450-watt lamp. Starting the lamps requires high-voltage pulses of 20 to 40 kV. This voltage can penetrate the skin, and the following high current could be lethal. Starting of xenon lamps can damage nearby sensitive electronics. The high-voltage starting pulse can destroy sensitive amplifiers or confuse computers. If possible, it is preferable to start a lamp first, and then turn on other electronic devices.

Xenon arc lamps have become more compact (Figure 2.8). These lamps typically have the arc within a parabolic reflector, which collects a large solid angle and provides a collimated output.⁶ In addition to improved light collection efficiency, these lamps are compact, and as a result are found in commercial spectrofluorometers.

When using a xenon arc lamp it is important to remember the lamps emit a large amount of infrared radiation, extending beyond the wavelength range of Figure 2.5. Because of the infrared output, the lamp output cannot be passed directly through most optical filters. The filter will heat and/or crack, and the samples will be heated. When passed through a monochromator the optical components and housing serve as a heat sink. If the xenon lamp output is to be used directly, one should use a heat filter made of heat-resistant glass, which absorbs the infrared.

2.2.2. Pulsed Xenon Lamps

At present compact fluorometers and plate readers often use xenon flash lamps. The output of a xenon flash lamp is more structured than a continuous lamp (Figure 2.5). The output of a flash lamp is higher in the UV. The output intensities in Figure 2.5 are the time-averaged output of the lamp. The peak intensity of the pulses is usually higher than that of the continuous arcs. The flash lamps consume less power and generate less heat. In some cases the lack of continuous excitation can minimize photodamage to the sample.

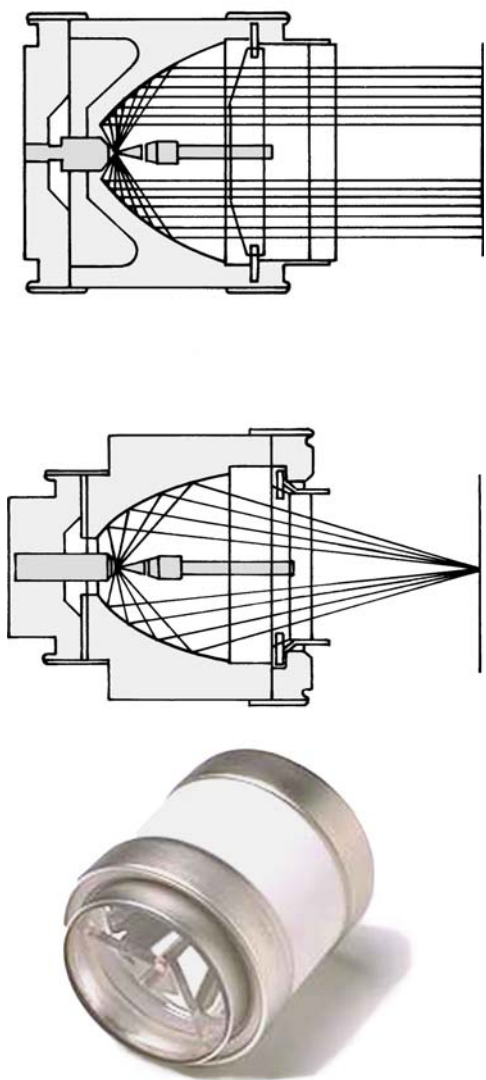


Figure 2.8. Compact xenon arc lamps. Reprinted from Cermax lamp engineering guide.

2.2.3. High-Pressure Mercury (Hg) Lamps

In general Hg lamps have higher intensities than Xe lamps, but the intensity is concentrated in lines. It is usually better to choose the excitation wavelengths to suit the fluorophore, rather than vice versa. These lamps are only useful if the Hg lines are at suitable wavelengths for excitation.

2.2.4. Xe–Hg Arc Lamps

High-pressure mercury–xenon lamps are also available. These have higher intensities in the ultraviolet than Xe lamps, and the presence of Xe tends to broaden the spectral

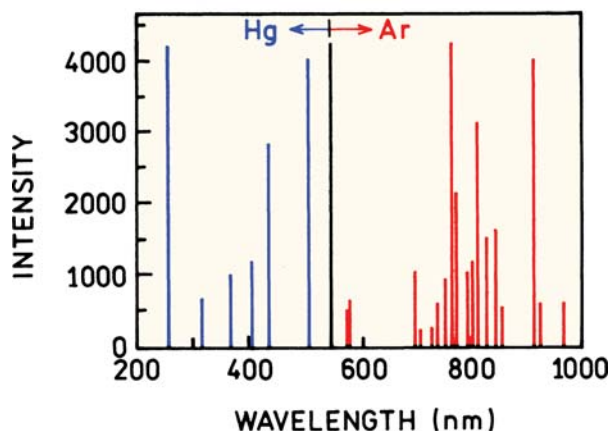


Figure 2.9. Spectral output of a low pressure mercury–argon lamp. Revised from [7]. Courtesy of Ocean Optics Inc.

output. The output of these lamps is dominated by the Hg lines. The Hg–Xe lamp has slightly more output between the Hg lines. When first started the Hg–Xe lamp output is due mostly to Xe. As the lamp reaches operating temperature all the Hg becomes vaporized, and the Hg output increases.

2.2.5. Quartz–Tungsten Halogen (QTH) Lamps

These lamps provide continuous output in the visible and IR regions of the spectrum. Previously such lamps were not useful for fluorescence because they have low output below 400 nm, and are thus not useful for excitation of UV absorbing fluorophores. However, there is presently increasing interest in fluorophores absorbing in the red and near infrared (NIR), where the output of a QTH lamp is significant.

2.2.6. Low-Pressure Hg and Hg–Ar Lamps

These lamps yield very sharp line spectra that are useful primarily for calibration purposes (Figure 2.9). Previously the lamps contained only mercury. Some lamps now contain both mercury and argon. The mercury lines are below 600 nm and the argon lines are above 600 nm (Table 2.1). The use of these lamps for wavelength calibration is described in Section 2.3.5.

2.2.7. LED Light Sources

LEDs are just beginning to be used as light sources in spectrofluorometers.^{8–9} A wide range of wavelengths are available with LEDs (Figure 2.10, see also Figure 4.13). In order

Table 2.1. Strong Emission Lines from a Mercury–Argon Calibration Source^a

Mercury lines (nm)			Argon lines (nm)	
253.7	404.7	696.5	763.5	842.5
296.7	407.8	706.7	772.4	852.1
302.2	435.8	710.7	794.8	866.8
313.2	546.1	727.3	800.6	912.3
334.1	577.0	738.0	811.5	922.6
365.0	579.1	750.4	826.5	

^aData from [7].

to obtain a wide range of wavelengths an array of LEDs can be used.⁸ LEDs can be placed close to the samples, and if needed the excitation wavelength can be defined better by the use of an excitation filter. Unlike a xenon lamp, LEDs do not generate significant infrared, so that an additional heat filter is not needed. There are ongoing efforts to develop white LEDs, which are already found in LED flashlights. These LEDs contain phosphors to provide a wider range of wavelengths.⁹ LEDs have the advantage of long life and low power consumption. The use of LEDs as an excitation source is likely to broaden in the near future.

2.2.8. Laser Diodes

Another light source is the laser diode. In contrast to LEDs, laser diodes emit monochromatic radiation. Laser diodes are available with wavelengths ranging from about 405 to 1500 nm. Laser diodes are convenient because the output is easily focused and manipulated. In contrast to arc lamps or incandescent lamps, the output of LEDs and laser diodes can be pulsed or modulated. LEDs can be amplitude modulated up to about 100 MHz, and laser diodes can be modulated to several GHz. The use of these light sources

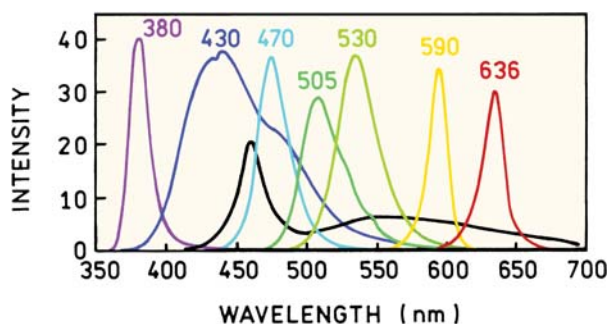


Figure 2.10. Spectral output of light-emitting diodes [8]. The black line shows the output of a white LED [7].

for time-resolved measurements is described in Chapters 4 and 5.

2.3. MONOCHROMATORS

Monochromators are used to disperse polychromatic or white light into the various colors or wavelengths. This dispersion can be accomplished using prisms or diffraction gratings. The monochromators in most spectrofluorometers use diffraction gratings rather than prisms. The performance specifications of a monochromator include dispersion, efficiency, and stray light levels. Dispersion is usually given in nm/mm. The slit width is sometimes expressed in mm, which requires knowledge of the dispersion. A monochromator for fluorescence spectroscopy should have low stray light levels to avoid problems due to scattered or stray light. By stray light we mean light transmitted by the monochromator at wavelengths outside the chosen wavelength and bandpass. Monochromators are also chosen for high efficiency to maximize the ability to detect low light levels. Resolution is usually of secondary importance since emission spectra rarely have peaks with line widths less than 5 nm. The slit widths are generally variable, and a typical monochromator will have both an entrance and exit slit. The light intensity that passes through a monochromator is approximately proportional to the square of the slit width. Larger slit widths yield increased signal levels, and therefore higher signal-to-noise ratios. Smaller slit widths yield higher resolution, but at the expense of light intensity. If the entrance slit of the excitation monochromator is already wide enough to accept the focused image of the arc, then the intensity will not be increased significantly with a wider slit width. If photobleaching of the sample is a problem, this factor can sometimes be minimized by decreasing the excitation intensity. Gentle stirring of the sample can also minimize photobleaching. This is because only a fraction of the sample is illuminated and the bleached portion of the sample is continuously replaced by fresh solution.

Monochromators can have planar or concave gratings (Figure 2.11). Planar gratings are usually produced mechanically. Concave gratings are usually produced by holographic and photoresist methods. Imperfections of the gratings are a source of stray light transmission by the monochromators, and of ghost images from the grating. Ghost images can sometimes be seen within an open monochromator as diffuse spots of white light on the inside surfaces. Monochromators sometimes contain light blocks to intercept these ghost images. Monochromators based on

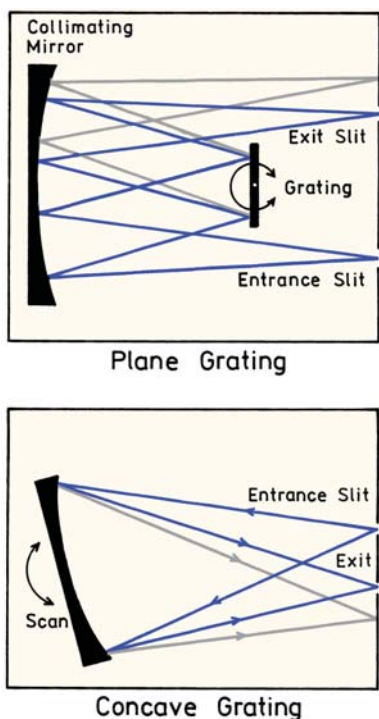


Figure 2.11. Monochromators based on a plane (top) or concave (bottom) grating. Revised from [7].

concave gratings can have fewer reflecting surfaces, lower stray light, and can be more efficient. A concave grating can serve as both the diffraction and focusing element, resulting on one instead of three reflecting surfaces. For these reasons the holographic gratings are usually preferable for fluorescence spectroscopy.

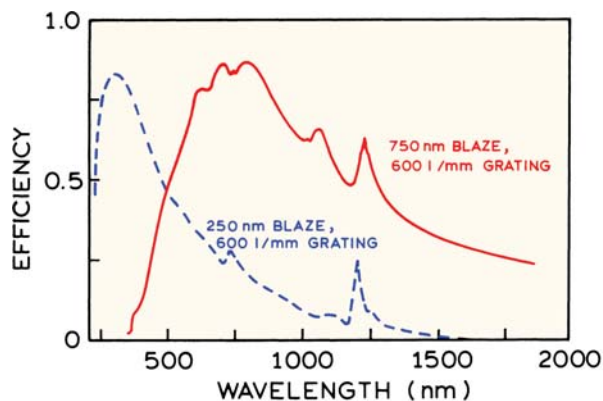


Figure 2.12. Efficiency of two-ruled grating blazed for different wavelengths. Redrawn from [5]. Courtesy of Newport Corp.

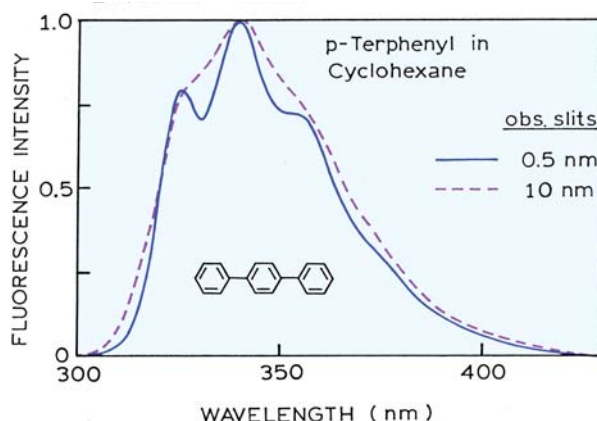


Figure 2.13. Emission spectra of p-terphenyl collected with a spectral resolution of 0.5 and 10 nm. From [10].

The transmission efficiency of a grating and monochromator is dependent on wavelength and on the design of the grating. Examples are shown in Figures 2.12 and 2.13. For a mechanically produced plane grating the efficiency at any given wavelength can be maximized by choice of blaze angle, which is determined by the shape and angle of the tool used to produce the grating. By choice of this angle one may obtain maximum diffraction efficiency for a given wavelength region, but the efficiency is less at other wavelengths. For the examples shown in Figure 2.12 the efficiency was optimized for 250 or 750 nm. Generally, the excitation monochromator is chosen for high efficiency in the ultraviolet and an emission monochromator for high efficiency at visible wavelengths.

2.3.1. Wavelength Resolution and Emission Spectra

The emission spectra of most fluorophores are rather broad and devoid of structure. Hence, the observed emission spectra are typically independent of spectral resolution. For fluorophores that display structured emission, it is important to maintain adequate wavelength resolution, which is adjusted by the slit widths on the monochromator. Emission spectra of p-terphenyl are shown in Figure 2.13. They display vibrational structure when recorded with a resolution of 0.5 nm. However, this structure is nearly lost when the resolution is 10 nm. Although not important for steady-state measurements, the transit time through a monochromator can depend on wavelength (Section 4.6.5).

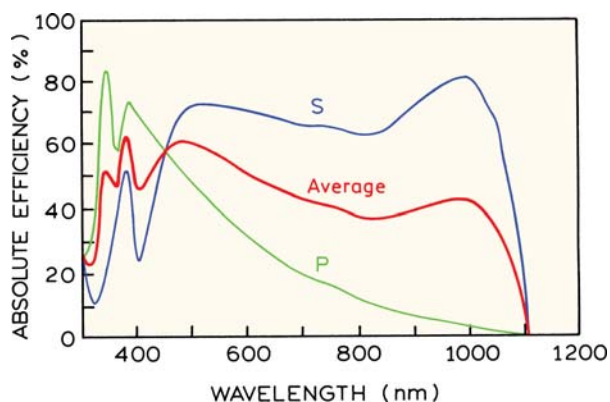


Figure 2.14. Grating efficiency for a 1800 line/mm holographic grating, optimized for the UV. The bold line is the average, and the other lines are for differently (S and P) polarized light, defined in Figure 2.39. Redrawn from [11].

2.3.2. Polarization Characteristics of Monochromators

For a grating monochromator the transmission efficiency depends upon the polarization of the light. This is illustrated in Figure 2.14 for a concave grating. For this reason, the observed fluorescence intensities can be dependent upon the polarization displayed by the fluorescence emission. The emission spectrum can be shifted in wavelength and altered in shape, depending upon the polarization conditions chosen to record the emission spectrum. For example, consider an emission spectrum recorded with the grating shown in Figure 2.14, and through a polarizer oriented vertically (\parallel) or horizontally (\perp). Assume that the dotted transmission curve corresponds to vertically polarized light. The spectrum recorded through the vertically oriented polarizer would appear shifted to shorter wavelengths relative to that recorded with the polarizer in the horizontal position. This is because the transmission efficiency for vertically polarized light is higher at shorter wavelengths. This spectral shift would be observed irrespective of whether its emission was polarized or not polarized.

The polarization properties of concave gratings can have a dramatic effect on the appearance of emission spectra. This is shown in Figure 2.15 for a probe bound to DNA. The emission spectrum shows a dramatic decrease near 630 nm when the emission polarizer is in the horizontal position. This drop is not seen when the emission polarizer is in a vertical orientation. In addition to this unusual dip in the spectrum, the emission maximum appears to be different for each polarizer orientation. These effects are due to the polarization properties of this particular grating, which dis-

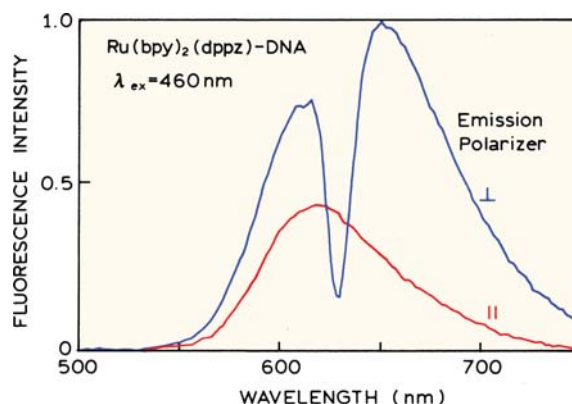


Figure 2.15. Emission spectra of $[\text{Ru}(\text{bpy})_2(\text{dppz})]^{2+}$ bound to DNA. This probe is described in chapter 20. Excitation at 460 nm. Except for intensity, the same spectral distributions was observed for vertically as horizontally polarized excitation. From [12].

plays a minimum in efficiency at 630 nm for horizontally polarized light. Such effects are due to the emission monochromator, and are independent of the polarization of the excitation beam.

The polarization characteristics of monochromators have important consequences in the measurement of fluorescence anisotropy. Such measurements must be corrected for the varying efficiencies of each optical component. This correction is expressed as the G factor (Section 10.4). However, the extreme properties of the concave gratings (Figure 2.14) can cause difficulties in the measurement of fluorescence polarization. For example, assume that the polarization is to be measured at an excitation wavelength of 450 nm. The excitation intensities will be nearly equal with the excitation polarizers in each orientation, which makes it easier to compare the relative emission intensities. If the emission is unpolarized the relative intensities with parallel (\parallel) and perpendicular (\perp) excitation intensities will be nearly equal. However, suppose the excitation is at 340 nm, in which case the intensities of the polarized excitation will be very different. In this case it is more difficult to accurately measure the relative emission intensities because of the larger difference in the excitation intensities. Measurement of the G factor is generally performed using horizontally polarized light, and the intensity of this component would be low.

2.3.3. Stray Light in Monochromators

The stray light level of the monochromator is a critical parameter for fluorescence measurements. Stray light is

defined as any light that passes through the monochromator besides the desired wavelength. Consider the excitation monochromator. The entire output from the light source enters the monochromator. Ultraviolet wavelengths are frequently used for excitation, and the ultraviolet intensity may be 100-fold less than the visible output of the Xe lamp. Stray light at longer wavelengths can be passed by the excitation monochromator, and can easily be as intense as the fluorescence itself. Fluorescence intensities are frequently low, and many biological samples possess significant turbidity. The incident stray light at the emission wavelength can be scattered, and can interfere with measurements of the fluorescence intensity. For these reasons, double-grating monochromators are frequently used, especially for excitation. Stray light levels for such monochromators are frequently 10^{-8} to 10^{-12} of the peak intensities. However, double-grating monochromators are less efficient, and sensitivity must be sacrificed.

The stray light properties of the emission monochromator are also important. Generally, only a low percentage of the exciting light is absorbed by the fluorophores, and fluorescence quantum yields can be small. It is not unusual for the fluorescence signal to be 1000-fold less intense than the exciting light. Now consider a turbid suspension of membranes, from which we wish to observe the fluorescence of membrane-bound proteins. The excitation and emission wavelengths would be near 280 and 340 nm, respectively. Since the emission monochromator is imperfect, some of the scattered light at 280 nm can pass through the emission monochromator set at 340 nm. Assume that the emission monochromator, when set at 340 nm, discriminates against 280 nm by a factor of 10^{-4} . The intensity of scattered light at 280 nm can easily be 10^3 -fold more intense than the fluorescence at 340 nm. Hence 10% of the "fluorescence" at 340 nm may actually be due to scattered exciting light at 280 nm. It is also important to recognize that scattered light is highly polarized, typically 100%. This means that the scattered light will contribute to the vertical intensity but not to the horizontal intensity. Stray scattered light can easily invalidate measurements of fluorescence anisotropy.

The stray light rejection of holographic gratings is superior to that of the mechanically produced ruled gratings. It appears that the passage of stray light depends upon imperfections in the gratings, resulting in ghost images which can escape from the monochromators. Fewer such images are present with the holographic gratings because

they are produced optically and have fewer imperfections. In addition, monochromators with holographic gratings generally have fewer reflecting surfaces within the monochromators (Figure 2.11). This is because the concave grating can also act as an imaging device, and thus additional concave mirrors are not required for focusing. With fewer reflecting surfaces there is a decreased probability of stray light escaping from the monochromator.

2.3.4. Second-Order Transmission in Monochromators

Another source of unwanted light is higher-order light diffraction by the monochromator. Light diffraction at the grating can occur as a first, second- or higher-order process. These diffraction orders frequently overlap (Figure 2.16). Suppose the excitation monochromator is set at 600 nm. The xenon light source contains output of both 300 and 600 nm. When the monochromator is set at 600 nm, some 300-nm light can be present at the exit slit due to second-order diffraction.

Transmission of second-order diffraction can also result in extraneous light passing through the emission monochromators. Suppose the excitation is at 300 nm and the emission monochromator is scanned through 600 nm. If the sample is strongly scattering, then some of the scattered light at 300 nm can appear as second-order diffraction when the emission monochromator is set to 600 nm. The emission spectrum from a turbid solution can have a peak at twice the excitation wavelength due to 2nd-order transmission through the emission monochromator. Bandpass excitation filters can be used to remove unwanted wavelengths from the excitation beam.

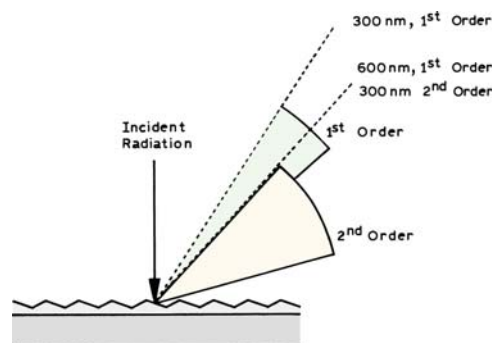


Figure 2.16. First- and second-order diffraction off a diffraction grating. The region where there is no overlap of the 1st- and 2nd-order diffraction is called the free spectral range.

2.3.5. Calibration of Monochromators

The wavelength calibration of monochromators should be checked periodically. Calibration can be performed using a low pressure mercury or mercury–argon lamp. These lamps are shaped like a cylinder, about 5 mm in diameter, and conveniently fit into the cuvette holder. These lamps provide a number of sharp lines that can be used for calibration (Figure 2.9). The lamp can be held stationary with a block of metal in which the lamp fits snugly. This holder is the same size as a cuvette. A pinhole on the side of this holder allows a small amount of the light to enter the emission monochromator. A small slit width is used to increase the precision of wavelength determination and to decrease light intensity. It is important to attenuate the light so that the photomultiplier tube and/or amplifiers are not damaged. Following these precautions, the dominant Hg lines are located using the emission monochromator. The measured wavelengths are compared with the known values, which are listed in Table 2.1. Since there are multiple Hg lines, it is necessary to observe three or more lines to be certain a line is assigned the correct wavelength. If the observed wavelengths differ from the known values by a constant amount, one recalibrates the monochromator to obtain coincidence. A more serious problem is encountered if the wavelength scale is nonlinear.

After calibration of the emission monochromator, the excitation monochromator can be calibrated against this new standard. The slits on both monochromators should be set to the same small value, consistent with the available light intensity. A dilute suspension of glycogen or Ludox is placed in the cuvette holder to scatter the exciting light. The emission monochromator is set to some arbitrary wavelength. If the excitation monochromator is properly calibrated, then the maximum intensity of the scattered light is seen when the indicated wavelengths are identical. The linearity of the wavelength scale can be determined by setting the emission monochromator at various wavelengths. One advantage of this procedure is that there is no need to remove the light source. The mercury light can be used in place of the xenon lamp to calibrate the excitation monochromator, but then the xenon lamp must be removed.

2.4. OPTICAL FILTERS

2.4.1. Colored Filters

While spectrofluorometers have monochromators for wavelength selection, it is often important to use optical filters in

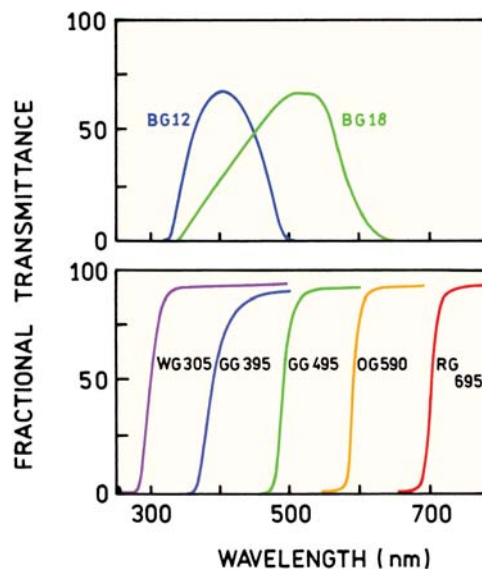


Figure 2.17. Transmission spectra of some typical colored glass filters. From [13].

addition to monochromators. Optical filters are used to compensate for the less-than-ideal behavior of monochromators. Also, when the spectral properties of a fluorophore are known, maximum sensitivity is often obtained using filters rather than monochromators. A large range of filters are available. The manufacturers typically provide the transmission spectra of the filters. Before the advances in thin film technology, most filters were colored-glass filters. Colored-glass filters can transmit a range of wavelengths (Figure 2.17, top). Some color filters are called long-pass filters and transmit all wavelengths above some particular wavelength (bottom). The names of the filters divide them into classes according to their colors (BG, blue glass, GG, green glass, etc.).

The transmission spectra shown in Figure 2.17 are visually pleasing but may not provide all the needed information. In turbid or dilute samples the scattered light can be orders of magnitude more intense than the fluorescence. This is also true for two-photon excitation when the excitation wavelength is longer than the emission wavelength. For these reasons transmission curves are often presented on a logarithm scale, which makes it possible to determine if the filter transmits 1% or much less than 1% of the light at any given wavelength (Figure 2.18). These curves also show transmission at longer wavelengths, where there may be interference from scattered light from the higher-order transmission of monochromators.

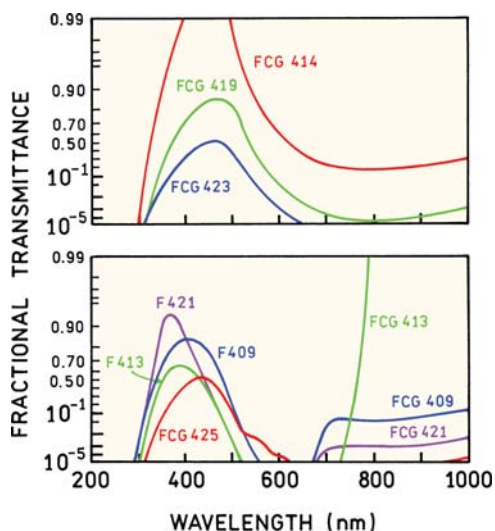


Figure 2.18. Transmission spectra of colored-glass filters. Top: in order of increasing wavelength FCG 414, 419, and 423. Bottom: FCG 409, 413, 421, and 425. From [13].

An important consideration in the use of bandpass filters is the possibility of emission from the filter itself. Many filters are luminescent when illuminated with UV light, which can be scattered from the sample. For this reason it is usually preferable to locate the filter further away from the sample, rather than directly against the sample. Glass filters of the type shown in Figures 2.17 and 2.18 are highly versatile, effective, and inexpensive, and a wide selection is needed in any fluorescence laboratory. Excitation and emission filters can be used in all experiments, even those using monochromators, to reduce the possibility of undesired wavelengths corrupting the data.

2.4.2. Thin-Film Filters

A wide variety of colored-glass filters are available, but the transmission curves are not customized for any given application. During the past ten years there have been significant advances in the design of thin-film optical filters.¹⁴ Almost any desired transmission curve can be obtained. Filters are now being designed for specific applications, rather than choosing the colored-glass filter that best suits an application. Long-pass filters are an example of this type filter (Figure 2.19). These filters have a sharp cut on the transmission above 325 nm or 488 nm, which are wavelengths available from a helium–cadmium or argon ion laser, respectively. The transmission above the cut-on wavelength is close to 100% to provide maximum sensitivity.

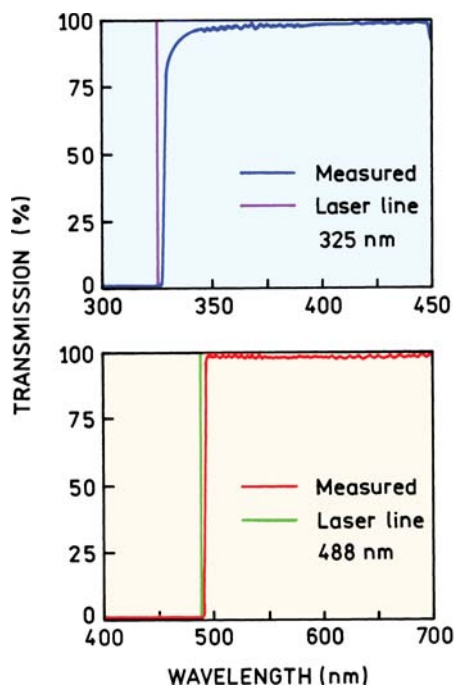


Figure 2.19. Long-pass filters designed to reject light from a helium-cadmium laser at 325 nm or an argon ion laser at 488 nm. Revised from [15].

Thin-film filters are also available to specifically transmit or reject laser lines. Laser light can contain additional wavelengths in addition to the main laser line. This emission is referred to as the plasma emission, which typically occurs over a range of wavelengths and is not strongly directional. The light can be made more monochromatic by passing the laser beam through a laser line filter, such as the one shown for a helium–neon laser at 633 nm (Figure 2.20). Alternatively, it may be necessary to eliminate scattered light at the laser wavelength. This can be accomplished with a notch filter which transmits all wavelengths except the laser wavelengths. These filters are sometimes called Raman notch filters because of their use in Raman spectroscopy.

Emission can usually be selected using a long-pass filter. However, there may be additional emission at longer wavelengths, such as the acceptor emission in an energy transfer experiment. In these cases it is useful to have a filter that transmits a selected range of wavelengths or auto-fluorescence from the sample. Figure 2.21 shows examples of bandpass filters that transmit from 460 to 490 nm or from 610 to 700 nm. The width of transmission can be made narrower or wider. Such filters are often referred to as interference filters.

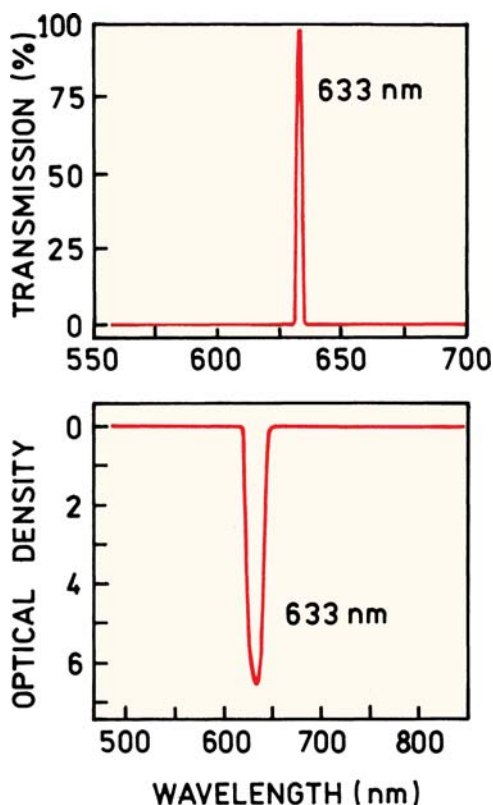


Figure 2.20. Laser line filter to transmit only the laser wavelength (top) and a notch filter to reject the laser wavelength. From [15].

2.4.3. Filter Combinations

While one can obtain almost any desired filter with modern coating technology, the design of custom filters for each experiment is usually not practical. If a single filter is not

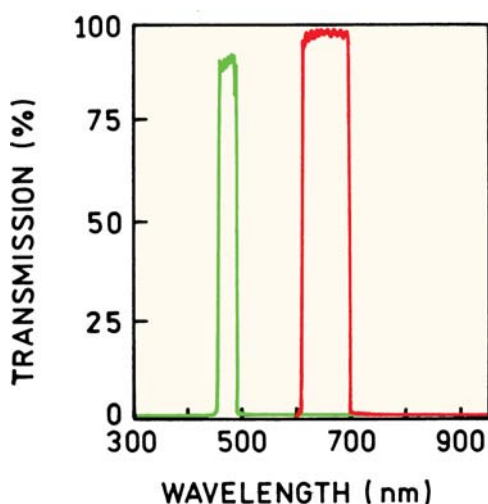


Figure 2.21. Interference filter to transmit selected wavelengths. From [15].

INSTRUMENTATION FOR FLUORESCENCE SPECTROSCOPY

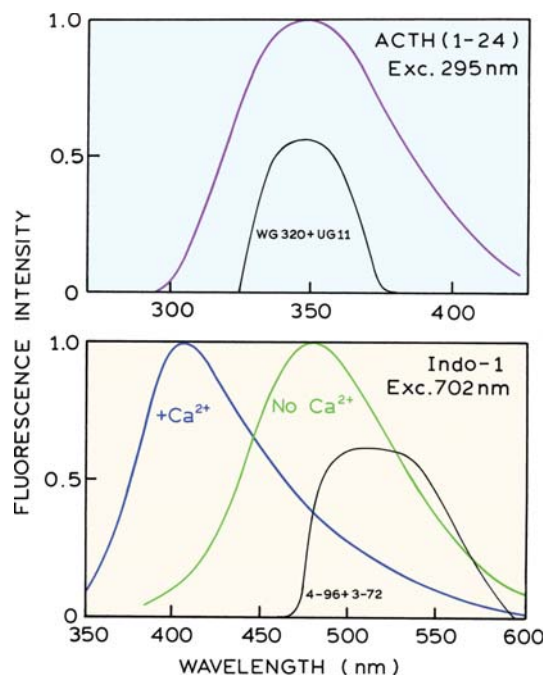


Figure 2.22. Transmission profile of a combination of Corning and Schott filters used to isolate protein fluorescence (top) and Indo-1 fluorescence (bottom). Lower panel from [17].

adequate for a given experiment, it is often possible to combine two or more bandpass filters to obtain the desired spectral properties. This possibility is shown in Figure 2.22. The UG-11 and WG-320 filters are often used in our laboratory to isolate protein fluorescence.¹⁶ For probes emitting near 450 nm, we often use a combination of Corning 4-96 and 3-72 filters.¹⁷ In this example the filter was selected to reject 702 nm, which was the excitation wavelength for two-photon excitation of Indo-1.¹⁷ This example illustrates an important aspect in selecting filters. Filters should be selected not only for their ability to transmit the desired wavelength, but perhaps more importantly for their ability to reject possible interfering wavelengths.

2.4.4. Neutral-Density Filters

Neutral-density filters are used to attenuate light equally at all wavelengths. They are typically composed of sheets of glass or quartz coated with a metal to obtain the desired optical density. Quartz transmits in the UV and is preferred unless no experiments will be done using wavelengths below 360 nm. Neutral-density filters are described by their optical density, and can typically be obtained in increments of 0.1, up to optical densities of 4. It is often necessary to adjust or match the intensity of two signals, which is conveniently accomplished using neutral-density filters.

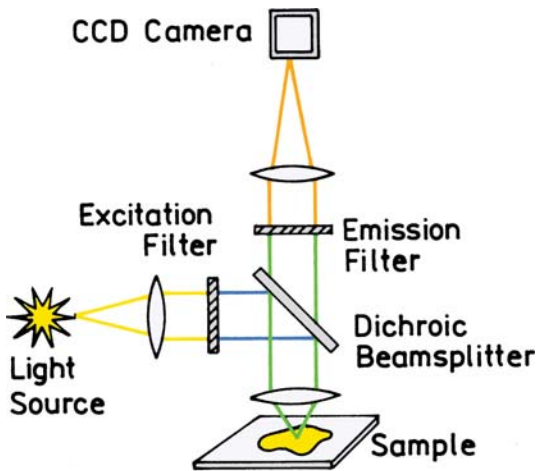


Figure 2.23. Filter geometry used for epifluorescence microscopy.

2.4.5. Filters for Fluorescence Microscopy

Fluorescence microscopy relies on optical filters rather than monochromators for wavelength selection. Most fluorescence microscopy is performed using the epifluorescence configuration. The term epifluorescence refers to excitation and emission passing through the same objective (Figure 2.23). This configuration has the advantage of most of the excitation traveling away from the detector. Additionally, the excitation can be observed for the same location. Even though most of the excitation passes through the sample, a substantial fraction of the excitation is reflected or scattered back into the objective.

Observation of the fluorescence image requires specially designed sets of filters. A set contains an excitation filter, an emission filter, and a dichroic beam splitter. The function of such filters can be understood by examination of their transmission spectra (Figure 2.24). The excitation filter selects a range of wavelengths from a broadband source to excite the sample. The emission filter transmits the emission and rejects the excitation wavelengths. The unusual component is the dichroic beam splitter, which serves a dual function. It reflects the excitation wavelengths into the objective, and transmits the emission and allows it to reach the eyepiece or detector. Filter sets for microscopy are now often named for use with specific fluorophores rather than wavelengths.

Fluorescence microscopy is often performed using multiple fluorophores to label different regions of the cell, allowing the region to be identified by the emission wavelength. Emission filters have been designed to pass the emission from multiple fluorophores. Figure 2.25 shows

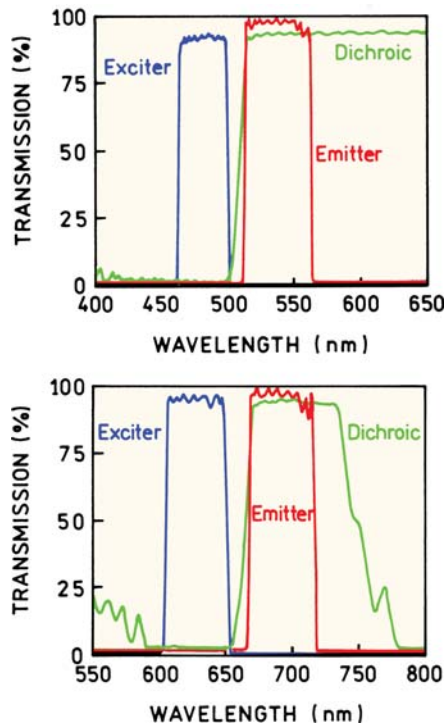


Figure 2.24. Epifluorescence filter sets for fluorescein or Cy5. From [15].

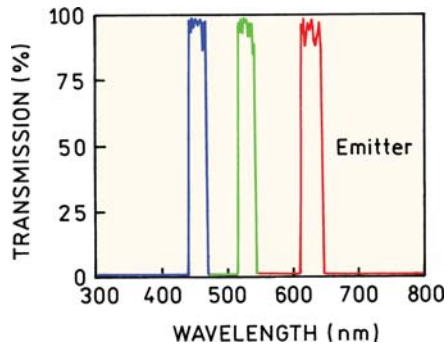


Figure 2.25. Multi-bandpass filter designed to transmit the emission of DAPI, fluorescein and Texas Red. Note that this is a single filter with three bandpasses. From [15].

the transmission curve of a filter designed to pass the emission from DAPI near 460 nm, fluorescein near 530 nm, and Texas Red at 630 nm. The availability of such filters has greatly expanded the capabilities of fluorescence microscopy.

2.5. OPTICAL FILTERS AND SIGNAL PURITY

A major sources of errors in all fluorescence measurements is interference due to scattered light, stray light, or sample

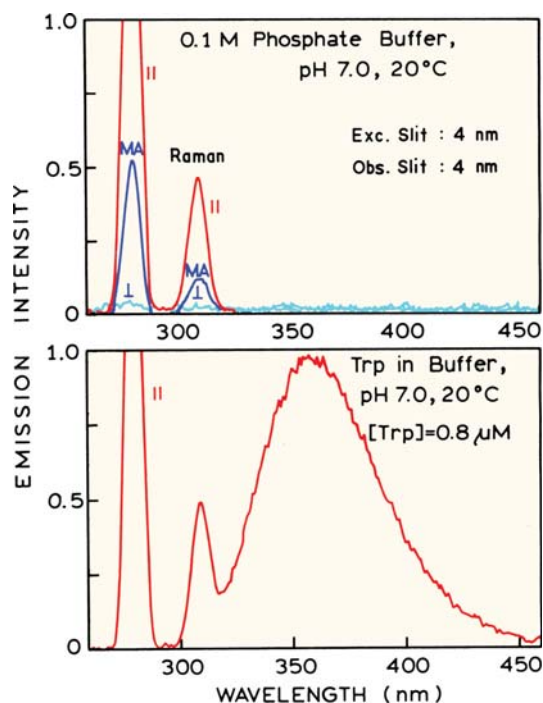


Figure 2.26. Emission spectrum of a $0.8\text{-}\mu\text{M}$ solution of tryptophan (bottom) in 0.1 M phosphate buffer, $\text{pH } 7.0$. The observation polarizer was vertically oriented. Top: emission spectrum of a blank buffer solution under the same optical conditions. The emission polarizer was vertical (II), horizontal (\perp) or at the 54.7° magic angle (MA) position. From [10].

impurities. These problems can be minimized by careful selection of the emission filter, the use of optical filters in addition to the excitation and emission monochromators, and by control experiments designed to reveal the presence of unwanted components. The use of optical filters and control experiments to avoid such artifacts is best illustrated by specific examples.

Figure 2.26 (bottom) shows the emission spectrum of a dilute solution of tryptophan in aqueous buffer. The large sharp peak on the left is due to scattered excitation, the broad peak at 360 nm is the tryptophan fluorescence, and the small sharp peak at 310 nm is the Raman scatter. Raman scatter will occur from all solvents. For water, the Raman peak appears at a wavenumber 3600 cm^{-1} lower than the incident wavenumber. For excitation at 280 nm , the Raman peak from water occurs at 311 nm . Highly fluorescent samples generally overwhelm the Raman peak. However, if the gain of the instrument is increased to compensate for a dilute solution or a low quantum yield, the Raman scatter may become significant and distort the emission spectrum. Raman scatter always occurs at a constant wavenumber dif-

ference from the incident light, and can be identified by changing the excitation wavelength. Also, the spectral width of the Raman peak will be determined by the resolution of the monochromators.

In microscopy and in assays the fluorescence may be observed without a monochromator. The emission can be observed through a filter that is presumed to remove the scattered light. Observation through a filter rather than a monochromator increases the sensitivity because the band-pass of the observation is increased and the attenuation due to the monochromator is removed. The signal level can often be 50-fold higher when observed through filters rather than a monochromator. Lifetime measurements are usually performed using long-pass filters to observe the entire emission. Under these conditions it is important to choose an emission filter that eliminates both the scattered incident light and the Raman scatter.

In any fluorescence experiment it is essential to examine blank samples, which are otherwise identical to the sample but do not contain the fluorophore. These control samples allow the presence of Rayleigh and Raman scatter to be determined. Control samples can also reveal the presence of fluorescent impurities. An emission spectrum of the buffer blank for the dilute tryptophan solution is shown in Figure 2.26 (top). The gain of the instrument should be the same when recording the emission spectrum of the sample and that of the blank. These control spectra are recorded under the same conditions, because the only meaningful consideration is whether the blank contributes to the emission under the conditions of a given experiment. In this case the blank spectrum above 320 nm is essentially zero, showing that the peak at 360 nm (bottom) is in fact due to the sample. While this may seem like a trivial result, the presence of background fluorescence and/or scattered light is the most common error in fluorescence measurements. Examination of the blank sample also allows identification of the peak at 310 nm as due to the buffer and not to the sample.

The most appropriate blank solution is one that is identical to the sample, but does not contain the fluorophore. This can be difficult to accomplish with protein or membrane solutions, where the macromolecules themselves are the source of the signal. Such solutions will typically be more strongly scattering than the buffer blanks. In these cases it is useful to add glycogen or colloidal silica (Ludox) to the buffer blank, to mimic the amount of scattering from the sample. This allows selection of filters that are adequate to reject scattered light from the sample.

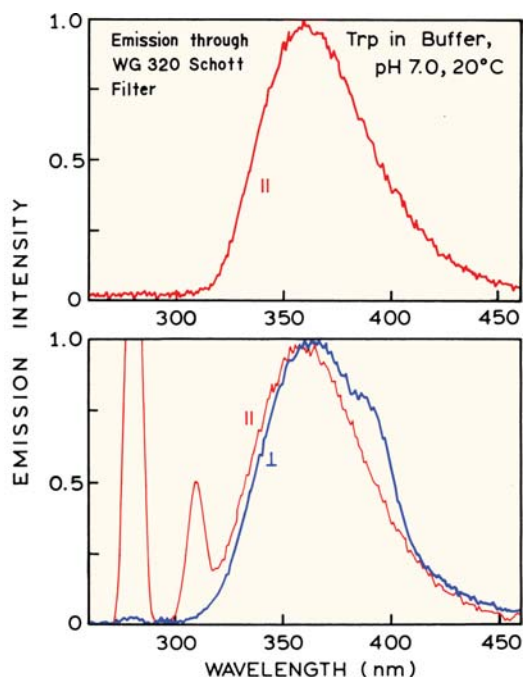


Figure 2.27. Rejection of scattered light from the 0.8- μ M tryptophan solution using a bandpass filter (top) or a polarizer but no bandpass filter (bottom). The emission polarizer was oriented vertically (||) or horizontally (\perp). From [10].

2.5.1. Emission Spectra Taken through Filters

Suppose you wanted to measure the lifetime of the tryptophan sample in Figure 2.26 (bottom) and the measurements are to be performed using a bandpass filter to isolate the emission. How can one know the scattered light has been rejected by the emission filter? This control is performed by collecting an emission spectrum through the filter used to measure the lifetime (Figure 2.27, top). In this case the Schott WG320 filter rejected both the scattered light and the Raman scatter, as seen by the zero intensity from 280 to 310 nm. In some cases the filter itself can be a source of background emission. The use of an equivalent scattering solution is preferred, as this provides the most rigorous test of the filter for rejecting scattered light and for displaying minimal fluorescence.

It is important to remember that scattered light is usually 100% polarized ($p = r = 1.0$). This is the reason the emission polarizer was vertical in Figure 2.27 (top), which is the worst-case situation. If the emission spectrum was recorded with the polarizer in the horizontal position, then the scattered light would be rejected by the polarizer (Figure 2.27, bottom). If the sample is then measured with a vertical polarizer, scattered light may be detected. When

examining spectra for the presence of scattered light, it is preferable to keep both polarizers in the vertical position, and thereby maximize the probability that the interfering signal will be observed. Conversely, a horizontal emission polarizer can be used to minimize the scattered light if only the emission spectrum needs to be recorded.

The emission spectra in Figure 2.27 (bottom) illustrate how the polarization-dependent transmission properties of the monochromator can distort the emission spectra. For these spectra the excitation was polarized vertically, and the emission spectra were recorded through a polarizer oriented vertically (||) or horizontally (\perp). These spectra are clearly distinct. The spectrum observed through the vertically oriented polarizer is blue shifted relative to the spectrum observed when the emission polarizer is in the horizontal orientation. The extra shoulder observed at 390 nm is due to the transmission properties of the monochromator. These results illustrate the need for comparing only those spectra that were recorded under identical conditions, including the orientation of the polarizers. The emission spectra for the same fluorophore can differ slightly if the emission is polarized or unpolarized.

One way to avoid these difficulties is to use a defined orientation of the polarizers when recording emission spectra. One preferred method is to use the so-called "magic angle" conditions. This is vertically polarized excitation and an emission polarizer oriented 54.7° from the vertical. In effect, the use of this condition results in a signal proportional to the total fluorescence intensity (I_τ) which is given by $I_\parallel + 2I_\perp$, where I_\parallel and I_\perp are the intensities of vertically and horizontally polarized emission. Such precautions are generally taken only when necessary. If the excitation source is unpolarized, the presence of polarizers in both the excitation and emission light paths results in an approximate fourfold decrease in signal level.

Polarization or anisotropy measurements are frequently performed using filters rather than monochromators. Scattered light is 100% polarized ($r = 1.0$). Hence, a small percentage of scatter can result in serious errors. For example, assume 10% of the observed intensity is due to Raman scatter. Furthermore, assume that the actual anisotropy of a sample, in the absence of scatter, is 0.10. The observed anisotropy is then given by

$$r_{\text{obs}} = f_s r_s + f_F r_F \quad (2.1)$$

where the f_s value represents the fractional contribution of the scattered light, f_F is the fractional contribution of the flu-

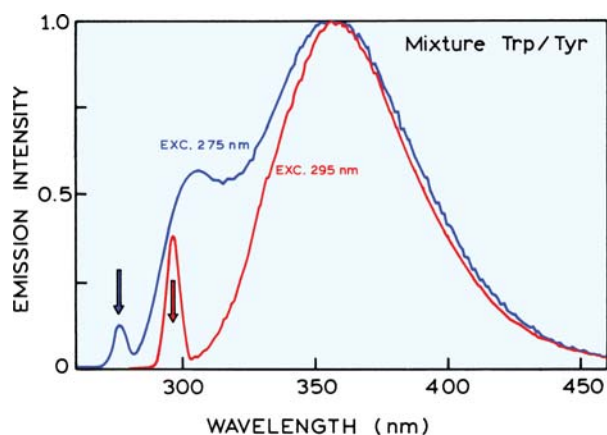


Figure 2.28. Emission spectra of tryptophan with a trace impurity of tyrosine, for excitation at 275 and 295 nm. From [10].

orescence, r_F is the anisotropy of the fluorescence, and r_s is the anisotropy of the scattered light. Substitution into eq. 2.1 yields $r_{\text{obs}} = 0.19$. Hence, a 10% contribution from scattered light can result in an almost twofold error in the measured anisotropy. The relative error would be still larger if r_F was smaller. These considerations apply to both Raman and Rayleigh scattering.

When measuring tryptophan or protein emission it is important to recognize that Raman scatter can be mistaken for tyrosine emission. This possibility is shown in Figure 2.28, which shows the emission spectrum of a tryptophan solution that contains a minor amount of tyrosine. Upon excitation at 275 nm the tyrosine results in a peak near 300 nm. The fact that this peak is due to tyrosine is shown by the spectrum obtained for 295-nm excitation, which shows only the tryptophan emission. If the emission spectrum of tryptophan alone was recorded at lower resolution, one can readily imagine how the broadened Raman line would become visually similar to tyrosine emission (Figure 2.28).

2.6. PHOTOMULTIPLIER TUBES

Almost all fluorometers use photomultiplier tubes (PMTs) as detectors, and it is important to understand their capabilities and limitations. A PMT is best regarded as a current source. The current is proportional to the light intensity. A PMT responds to individual photons, and the pulses can be detected as an average signal or counted as individual photons.

A PMT vacuum tube consists of a photocathode and a series of dynodes which are the amplification stages (Figure

INSTRUMENTATION FOR FLUORESCENCE SPECTROSCOPY

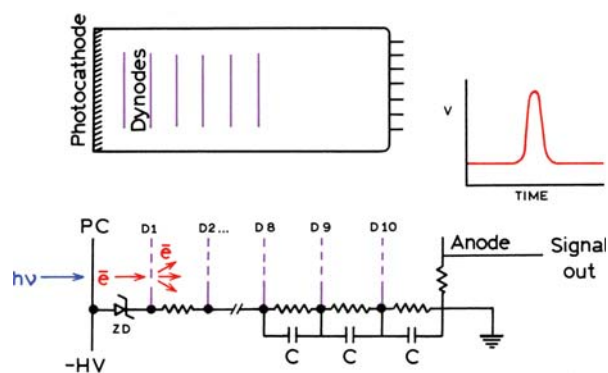


Figure 2.29. Schematic diagram of a photomultiplier tube and its dynode chain.

2.29). The photocathode is a thin film of metal on the inside of the window. Incident photons cause electrons to be ejected from this surface. The generation efficiency of photoelectrons is dependent upon the incident wavelength. The photocathode is held at a high negative potential, typically -1000 to -2000 volts. The dynodes are also held at negative potentials, but these potentials decrease toward zero along the dynode chain. The potential difference between the photocathode and the first dynode potential is generally fixed at a constant voltage by a Zener diode, at values ranging from -50 to -200 volts. This potential difference causes an ejected photoelectron to be accelerated toward the first dynode. Upon collision with the first dynode the photoelectron causes 5 to 20 additional electrons to be ejected, depending on the voltage difference to this dynode. This process continues down the dynode chain until a current pulse arrives at the anode. The size of this pulse depends upon the overall voltage applied to the PMT. Higher voltages result in an increased number of electrons ejected from each dynode, and hence higher amplification. PMTs are useful for low-level light detection because they are low-noise amplifiers. Little additional noise is created as the electrons pass through the PMT. Amplification outside of the PMT generally results in more noise being added to the signal.

For quantitative measurements, the anode current must be proportional to the light intensity. A nonlinear response can result from an excessive current being drawn from the photocathode. Under high-intensity illumination the electrical potential of the photocathode can be decreased because of its limited current-carrying capacity. This decreases the voltage difference between the photocathode and the first dynode, and also decreases the gain. Excessive photocurrents can damage the light-sensitive photocathodes, result-

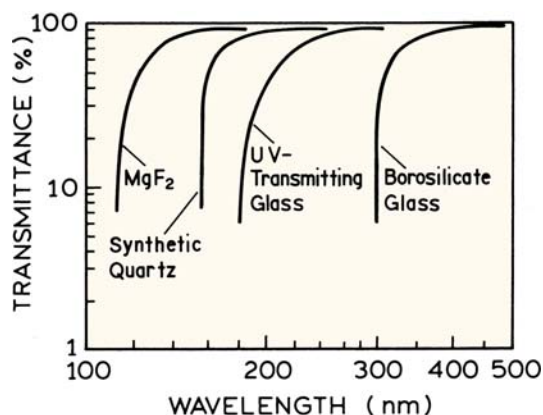


Figure 2.30. Typical transmittance of PMT window materials.

ing in loss of gain and excessive dark currents. The dark current from a PMT is the current in the absence of incident light.

A linear response also requires that the dynode voltages remain constant, irrespective of the incident light level and anode current. Dynode chains are designed so that the total current through the chain is at least 100-fold greater than the maximum anode current. Consider the 10-stage tube shown in Figure 2.29. Using resistors with $R = 100 \text{ k}\Omega$, the dynode current would be 1.0 Ma at 1000 volts total voltage across the PMT. Hence $10 \mu\text{A}$ should be the maximum anode current. There are often capacitors placed between the higher-numbered dynodes to provide a source of current during a single photoelectron pulse or periods of high illumination. Constant amplification by a PMT requires careful control of the high voltage. A typical PMT will yield a threefold increase in gain for each 100 volts. Hence, a small change in voltage can result in a significant change in the signal. The high voltage supply needs to provide a constant, ripple-free voltage that is stable for long periods of time. Photomultiplier tubes are available in a wide variety of types. They can be classified in various ways, such as according to the design of the dynode chain, size, and shape, spectral response, or temporal response.

2.6.1. Spectral Response of PMTs

The sensitivity of a PMT depends upon the incident wavelength. The spectral response is determined by the type of transparent material used for the window, and the chemical composition of the photocathode. Only light that enters the PMT can generate photocurrent. The input windows must be transparent to the desired wavelengths. The transmission

curves of typical windows material are shown in Figure 2.30. UV transmitting glass is frequently used and transmits all wavelengths above 200 nm. Synthetic quartz can be used for detection deeper into the UV. MgF_2 windows are only selected for work in the vacuum ultraviolet. Since atmospheric oxygen absorbs strongly below 200 nm, there is little reason for selecting MgF_2 unless the apparatus is used in an oxygen-free environment. For this reason the spectral region below 200 nm is called the vacuum ultraviolet.

The second important factor is the material used for the photocathode. Numerous types of photocathodes are available, and the spectral responses of just a few are shown in Figure 2.31. The quantum efficiency is not constant over any reasonable range of wavelengths. This is one origin of the nonideal wavelength response of spectrofluorometers. Most photocathodes are sensitive in the UV, blue and green (300–500 nm) regions of the spectrum. The differences in photocathode material are important mostly for wavelengths above 600 nm. One of the most commonly used is the bialkali photocathode (Figure 2.31), which provides high sensitivity and low dark current. One disadvantage of the bialkali photocathode is the rapid decrease in sensitivity above 600 nm. Given the current emphasis on red and

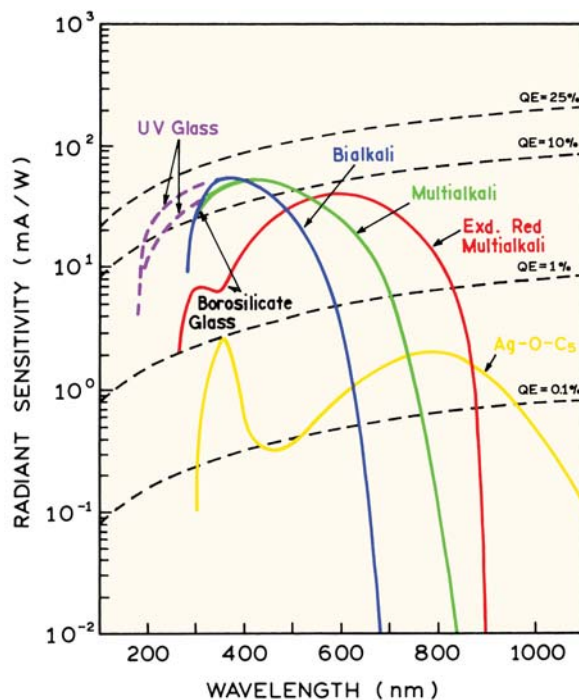


Figure 2.31. Spectral response curves of typical photocathodes. From [18].

Table 2.2. Characteristics of Typical Photomultiplier Tubes^a

Type	R446 Side window	R2560 Head-on	R3809 Head-on	R3811 Subminiature
Dynode chain	Circular cage	Linear plate	Microchannel cage	Circular cage
Photocathode	Multi-alkali	Bialkali	Multi-alkali S-20	Multi-alkali
Wavelength range (nm)	185–870	300–650	160–185	185–850
Amplification	5×10^6	6×10^6	2×10^5	1.3×10^6
Rise time (ns)	2.2	2.2	0.15	1.4
Transit time (ns)	22	26	0.55	15
Bandwidth (MHz) (estimate)	200	200	2000	300

^a The number refers to types provided by Hamamatsu Inc.¹⁸

NIR fluorescence, the bialkali photocathode is becoming less useful.

The sensitivity above 500 nm has been increased by the introduction of multi-alkali and extended red multi-alkali photocathodes, which provide good sensitivity to 700 or 800 nm (Figure 2.31). Red-sensitive PMTs typically have higher dark current, but for most multi-alkali photocathodes the dark current is not a problem. Sensitivity to still longer wavelengths can be obtained using Ag–O–Cs or S-1 photocathodes. However, their quantum efficiency is uniformly poor, and it is often difficult to detect the signal above the dark current with an S-1 PMT. In fact, these PMTs are rarely used without cooling to reduce the dark current.

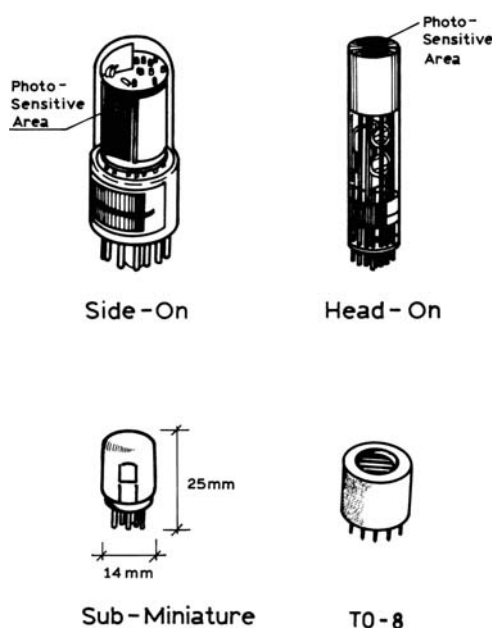


Figure 2.32. Types of photomultiplier tubes.

2.6.2. PMT Designs and Dynode Chains

The major types of PMTs and dynode chains used in fluorescence are shown in Figures 2.32 and 2.33. A commonly used PMT is the side-window or side-on tube. A large number of variants are available, and all are descendants of one of the earliest PMTs, the 1P-28. These side-on tubes used a circular cage dynode chain, sometimes referred to as a squirrel cage (Figure 2.33). The specifications of one side-on tube are listed in Table 2.2. The multi-alkali photocathode of the R446 is sensitive from 185 to 870 nm. This type of circular cage PMT has evolved into the subminiature PMTs. Because of their compact design the time response is excellent (Table 2.2). PMTs are also available in the compact TO-8 format, which is 16 mm in diameter. Small PMTs are available complete with a high voltage supply and dynode chain, all in a compact package. These compact high-sensitivity detectors have appeared in many research and clinical instruments.

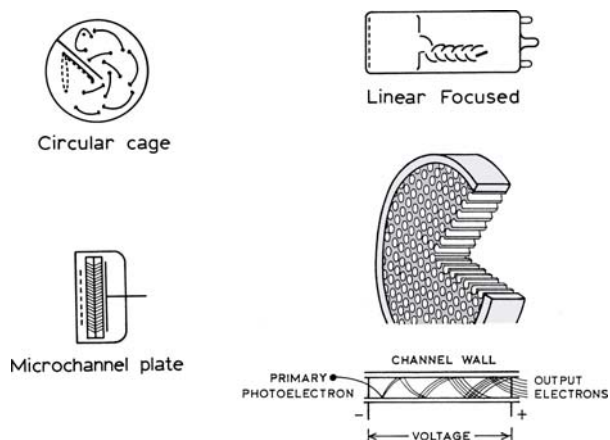


Figure 2.33. Types of PMT dynode chains. From [14].

Another type of PMT is the head-on design (Figure 2.32). This design is used with various types of dynode chains, such as the box and grid, blind and mesh design. For time-resolved fluorescence the head-on PMTs typically use a linear-focused dynode chain (Figure 2.33). The purpose of this design is to minimize the transit time spread and thus improve the time response of the PMT. The use of a head-on design allows the dynode chain to be extended as long as desired, so that the highest amplification is usually available with this type of PMT.

The final type of PMT is the microchannel plate PMT (MCP-PMT). In place of a dynode chain the MCP-PMT has plates that contain numerous small holes (Figure 2.33). The holes in these plates are the microchannels, which are lined with a secondary emissive dynode material. The electrons are amplified as they drop down the voltage gradient across the microchannel plate. Because of the short distances for electron travel, and the restricted range of electron paths, this type of PMT shows the fastest time response and is used in the most demanding time-resolved measurements. MCP-PMTs are available with one, two, or three stages of microchannel plates. The amplification is generally lower than for PMTs with discrete dynode chains. Also, the maximum photocurrent is typically 100 nA, as compared with 10 to 100 μ A for a dynode PMT.

2.6.3. Time Response of Photomultiplier Tubes

For steady-state measurements the time response of a PMT is not important. The PMT time response is important for lifetime measurements. There are three main timing characteristics of PMT—the transit time, the rise time, and the transit time spread (Figure 2.34). The transit time of a PMT is the time interval between the arrival of a photon at the cathode and the arrival of the amplified pulse at the anode. Typical transit times range from 20 to 50 ns. The rise time is the time required for the PMT anode signal to rise from 10 to 90% of its final level. The rise time is determined primarily by the transit time variation in the PMT, that is, the scatter around the average transit time.

The transit time spread is the most important specification for time-resolved measurements. These timing variations result from the different geometric paths that the electrons can take from the photocathode to the anode. The photoelectrons can originate from different parts of the photocathode, or can have different trajectories from the same region of the photocathode. The electrons subsequently ejected from the dynodes can take slightly different geo-

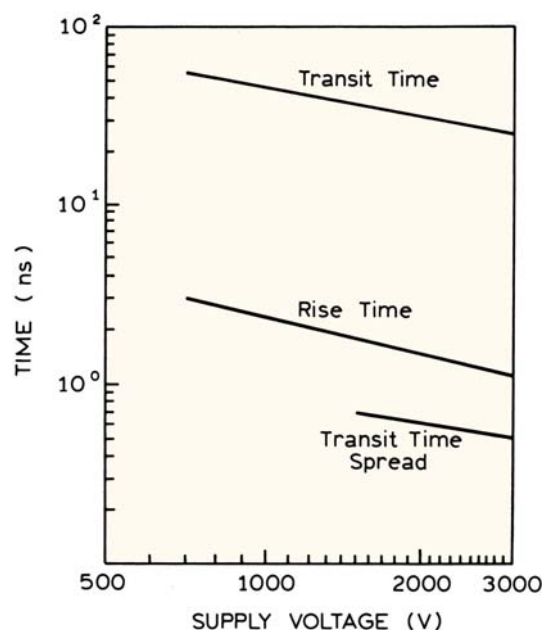


Figure 2.34. Time response of a typical PMT. The data are for a R2059, head on, 12-stage linear focused PMT. Revised from [18].

metric paths through the PMT. This can be seen in Figure 2.29 from the various ejection angles of electrons coming off the first dynode. Transit time spread can be decreased by using photocathode and dynode geometries which minimize the number of different trajectories. This can be accomplished by the use of small illuminated areas, or a dynode designed to direct the flight of the electrons along a defined trajectory.

The most dramatic advance in high-speed PMTs has been the introduction of the MCP-PMT. In this case the photoelectrons are proximity focused into the MCP (Figure 2.33). There is very little variation in terms of electron trajectory within the MCP. For this reason MCP-PMTs have transit time spreads tenfold smaller than those of standard PMTs (Table 2.2).

A second source of the time dependence of a PMT results from the photocathode itself. Typically, its time response is dependent upon the wavelength incident on the photocathode. This property is called the color effect. The energy of the ejected electrons is dependent upon the incident wavelength, and the energy affects the path an electron takes through the phototube. Color effects are not important for steady-state measurements. Color effects were a significant source of error in lifetime measurements, but color effects seem to be smaller in the current generation of fast PMTs.

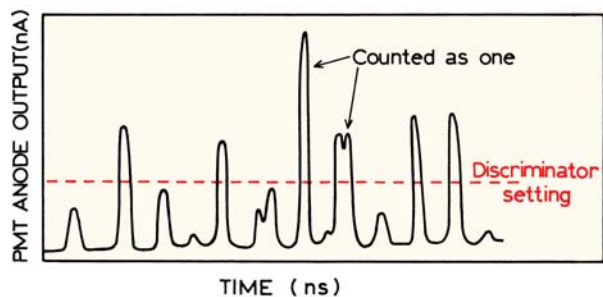


Figure 2.35. Photon-counting detection using a PMT. From [19].

2.6.4. Photon Counting versus Analog Detection of Fluorescence

A PMT is capable of detecting individual photons. Each photoelectron results in a burst of 10^5 to 10^6 electrons, which can be detected as individual pulses at the anode (Figure 2.35). Hence, PMTs can be operated as photon counters, or can be used in the analog mode in which the average photocurrent is measured. Note that we are considering steady-state measurements. Time-correlated photon counting for lifetime measurements will be discussed in Chapter 4. In photon-counting mode, the individual anode pulses due to each photon detected and counted. As a result, the detection system is operating at the theoretical limits of sensitivity. Noise or dark current in the PMT frequently results from electrons that do not originate at the photocathode, but from further down the dynode chain. Such anode pulses from these electrons are smaller, and can be ignored by setting the detection threshold high enough to count only fully amplified primary photoelectrons. Besides increased sensitivity, the stability of the detection system can be increased. Because the PMT is operated at a constant high voltage, small drifts in the voltage do not result in significant changes in the efficiency with which each photon is counted. Photon-counting detection is frequently used when signal levels are low, and when it is necessary to average repetitive wavelength scans to increase the signal-to-noise ratio.

There can be disadvantages to photon counting for steady-state measurements. The gain of the PMT cannot be varied by changing the applied voltage. Photon-counting detection can be inconvenient when signal levels are high. To stay within the linear range, one must adjust the slit widths or the fluorescence intensities (using neutral-density filters). Another disadvantage of photon counting is the limited range of intensity over which the count rate is linear. If

two pulses arrive at the anode closely spaced in time, they will be counted as a single pulse. Anode pulses resulting from a single photon are typically 5 ns wide. This limits the response of the PMT to 200 MHz, or 2×10^8 Hz for a periodic signal. For random events, the count rates need to be about 100-fold less to avoid the simultaneous arrival of two photons. Hence, count rates are limited to several MHz. Manufacturers often specify count rates of 50 MHz or higher. However, these count rates apply to uniformly spaced pulses, and the pulse widths of the detector may be too wide to distinguish pulses which occur too close together. In practice, the count rates often become sublinear before the theoretical upper limit is reached (Figure 2.36). Higher count rates can be obtained with PMTs which show shorter pulse widths. Additionally, the signal-to-noise ratio becomes unsatisfactory at count rates below 10,000 photons per second. The linear dynamic range can be as small as 3 log units (Figure 2.36).²⁰ This limited intensity range is a drawback of photon-counting detection for steady-state measurements of fluorescence, unless the highest sensitivity is required.

In analog mode the individual pulses are averaged. Since the current from each pulse contributes to the average anode current, the simultaneous arrival of pulses is not a problem. When using analog detection the gain of the detection system can be varied by changing either the amplifier gain or the voltage on the photomultiplier tube. As a result, a wider range of signal levels can be detected without concerns about a nonlinear response. The precision of the individual measurements can be higher than for photon counting measurements, because of the higher overall sig-

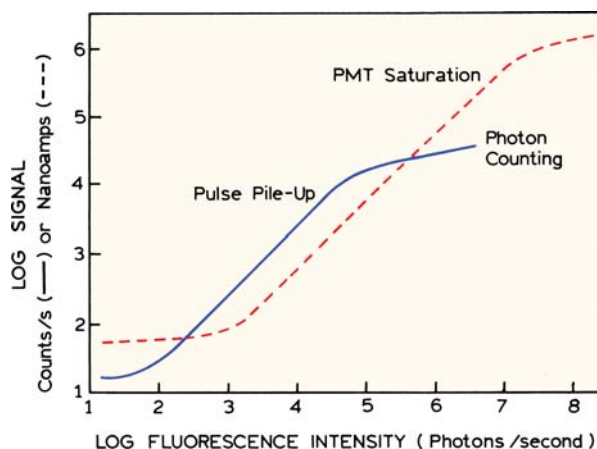


Figure 2.36. Dynamic range available with photon counting and analogue detection. From [19].

nal levels. However, even the analog measurements have a limited range because all PMTs display saturation above a certain light level if one exceeds the capacity of the photocathode to carry the photocurrent, or an ability of the dynode chain to maintain a constant voltage.

2.6.5. Symptoms of PMT Failure

Photomultiplier tubes should be handled with care. Their outer surfaces should be free of dust and fingerprints, and should not be touched with bare hands. The photocathode is light sensitive, and it is best to perform all manipulations in dim light. It is convenient to know the common signs of PMT failure. One may observe pulses of current when the applied voltage is high. At lower voltages this symptom may appear as signal instability. For instance, the gain may change 20% to several-fold over a period of 2–20 seconds. The origin of this behavior is frequently, but not always, a leakage of gas into the tube. The tube cannot be fixed and replacement is necessary. In some instances the tube may perform satisfactory at lower voltages.

A second symptom is high dark current. This appears as an excessive amount of signal when no light is incident on the PMT. The origin of high dark currents is usually excessive exposure of the tube to light. Such exposure is especially damaging if voltage is applied to the tube at the same time. Again, there is no remedy except replacement or the use of lower voltages.

Signal levels can be unstable for reasons other than a failure of the photomultiplier tube. If unstable signals are observed one should determine that there are no light leaks in the instrument, and that the high voltage supplies and amplifiers are functioning properly. In addition, the pins and socket connections of the PMT should be checked, cleaned, and tightened, as necessary. Over a period of years, oxide accumulation can result in decreased electrical contact. Photobleaching of a sample may give the appearance of an instrument malfunction. For example, the fluorescence intensity may show a time-dependent decrease due to bleaching, and then an increase in intensity due to convection currents which replenish the bleached portion of the sample.

2.6.6. CCD Detectors

There is a growing usefulness of charge-coupled devices (CCDs) in fluorescence spectroscopy.^{21–22} CCDs are imaging detectors with remarkable sensitivity and linear dynam-

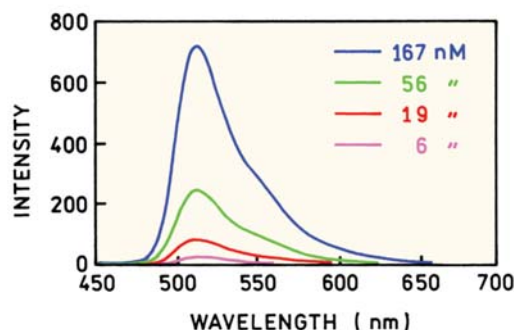


Figure 2.37. CCD spectrofluorometer and emission spectra of fluorescein. The light source for the fluorescein spectra was a 450 nm blue LED. From [25]. Image courtesy of Ocean Optics Inc.

ic range. CCDs typically contain 10^6 or more pixels. Each pixel acts as an accumulating detector where charge accumulates in proportion to total light exposure. The charge at each pixel point can be read out when desired, to obtain a two-dimensional image. CCDs are used widely in fluorescence microscopy.^{23–24}

Small spectrofluorometers using CCDs are commercially available.²⁵ These devices are conveniently interfaced via a USB cable and have no moving parts. The sensitivity can be rather good, as seen from the fluorescein emission spectra (Figure 2.37). The signal is easily brought to the device using a fiber-optic cable. When combined with an LED light source the entire instrument becomes a solid-state device. These spectrofluorometers are convenient for bringing the instrument to the experiment, rather than vice versa.

2.7. POLARIZERS

When discussing polarizers it is useful to recall a few conventional definitions. The laboratory vertical-axis is typically referred to as the z -axis. Light can be described as

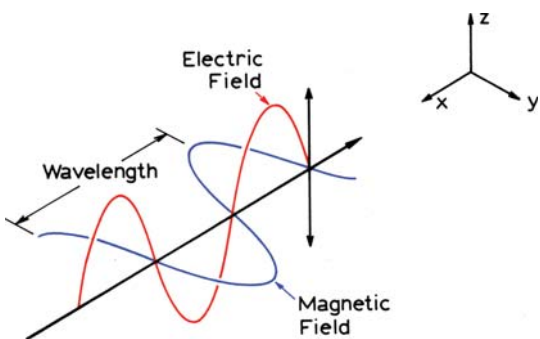


Figure 2.38. Vertically polarized light.

having a direction for its electrical component. Unpolarized light, of the type from incandescent or arc lamp sources, has equal amplitudes of the electric vector normal to the direction of light propagation. Polarized light has greater amplitude in one of the directions. Light with its electrical vector directed along the z -axis is said to be vertically polarized (Figure 2.38). Light with its electrical vector at right angles to the z -axis is said to be horizontally polarized.

In a discussion of polarization, the terms "S" and "P" polarization are often used. These terms are defined relative to the normal to the plane of incidence of the light on the optical interface. The plane of incidence is the plane defined by the light ray and the axis normal to the surface. If the electrical vector is in the plane of incidence the ray is said to be "P" polarized (Figure 2.39). If the electrical vector is perpendicular to the plane of incidence this ray is said to be "S" polarized.

Polarizers transmit light when the electric vector is aligned with the polarization axis, and block light when the

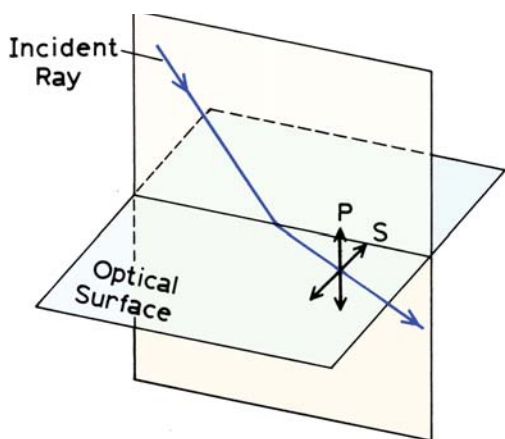


Figure 2.39. Definition of S and P polarization. P-polarized light has the electric field polarized parallel to the plane of incidence. S-polarized light has the electric field polarized perpendicular to the plane of incidence.

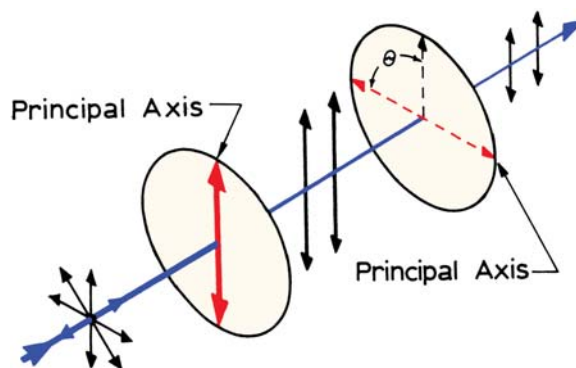


Figure 2.40. Transmission of light through polarizers. The incident beam is unpolarized. Only vertically polarized light passes through the first polarizer. Transmission through the second polarizer is proportional to $\cos^2 \theta$.

electric vector is rotated 90° . These principles are shown in Figure 2.40. The incident light is unpolarized. About 50% of the light is transmitted by the first polarizer, and this beam is polarized along the principal axis of the polarizer. If the second polarizer is oriented in the same direction, then all the light is transmitted except for reflection losses. If the second polarizer is rotated through an angle θ the intensity is given by

$$I = I_{\max} \cos^2 \theta \quad (2.2)$$

where I_{\max} corresponds to $\theta = 0$. Polarizers are frequently characterized by their extinction ratios. If the first polarizer is illuminated with linearly polarized light along the principal axis, the extinction ratio is the ratio of intensities for parallel ($\theta = 0^\circ$) and crossed polarizers ($\theta = 90^\circ$). A slightly different definition is used if the first polarizer is illuminated with unpolarized light. Extinction ratios range from 10^3 to 10^6 .

For general use in fluorescence spectroscopy a UV-transmitting Glan-Thompson polarizer has the best all-around properties (Figure 2.41). These polarizers consist of calcite prisms, which are birefringent, meaning the refractive index is different along each optical axis of the crystal. The angle of the crystal is cut so that one polarized component undergoes total internal reflection at the interface, and the other continues along its optical path. The reflected beam is absorbed by the black material surrounding the calcite. The purpose of the second prism is to ensure that the desired beam exits the polarizer in the same direction as the entering beam. For high-power laser applications an exit port is provided to allow the reflected beam to escape.

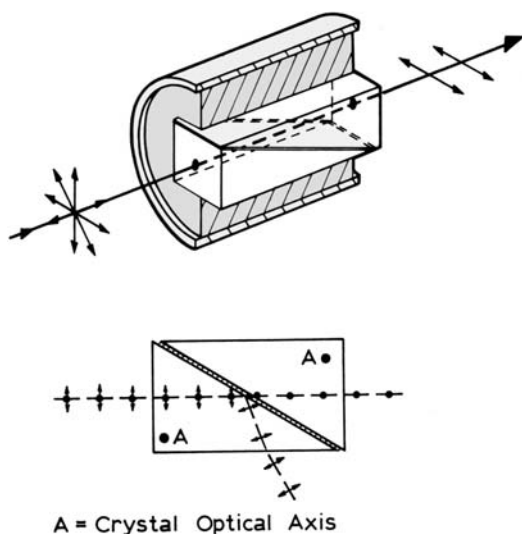


Figure 2.41. Glan-Thompson polarizer (top) and light paths (bottom).

Calcite transmits well into the UV, and the transmission properties of the polarizer are determined by the material between the two prisms, which can be air or some type of cement. An air space is usually used for UV transmission. The polarizers are typically mounted in 1 inch diameter cylinders for ease of handling. Glan-Thompson polarizers provide high extinction coefficients near 10^6 , but that is not the reason they are used in fluorescence. Glan-Thompson polarizers have a high acceptance angle, 10-15°, allowing them to be used where the beams are not well collimated. Another advantage is the low UV and visible absorbance of calcite, providing high transmission efficiency.

Another type of polarizer used in fluorescence are film polarizers, the same type used in polaroid glasses. These are thin films of a stretched polymer that transmit the light polarized in one direction and absorb the light polarized in another direction (Figure 2.40). Because the light is absorbed they are easily damaged by intense laser beams. They have a wide acceptance angle, but overall transmission is poor, especially in the ultraviolet. A wide variety of other polarizers are available. Most of the others, such as Wallaston polarizers and Rochon prism polarizers, split the unpolarized light into two beams, which must then be spatially selected.

2.8. CORRECTED EXCITATION SPECTRA

The development of methods to obtain excitation and emission spectra, corrected for wavelength-dependent effects,

has been the subject of numerous investigations. None of these methods are completely satisfactory, especially if the corrected spectra are needed on a regular basis. Prior to correcting spectra, the researcher should determine if such corrections are necessary. Frequently, it is only necessary to compare emission spectra with other spectra collected on the same instrument. Such comparisons are usually made between the technical (or uncorrected) spectra. Furthermore, the response of many spectrofluorometers is similar because of the similar components, and comparison with spectra in the literature can frequently be made. Of course, the spectral distributions and emission maxima will differ slightly, but rigorous overlap of spectra obtained in different laboratories is rarely a necessity.

Modern instruments with red-sensitive PMTs and with gratings comparable to that shown in Figure 2.41 can provide spectra that are not very distorted, particularly in the visible to red region of the spectrum. Corrected spectra are needed for calculation of quantum yields and overlap integrals (Chapter 13). We briefly describe the methods judged to be most useful.

2.8.1. Corrected Excitation Spectra Using a Quantum Counter

Excitation spectra are distorted primarily by the wavelength dependence of the intensity of the exciting light. This intensity can be converted to a signal proportional to the number of incident photons by the use of a quantum counter. Rhodamine B (RhB) in ethylene glycol (3 g/l) is the best-known quantum counter,²⁶ and to this day remains the most generally reliable and convenient quantum counter. This concentrated solution absorbs virtually all incident light from 220 to 600 nm. The quantum yield and emission maximum (≈ 630 nm) of rhodamine B are essentially independent of excitation wavelength from 220 to 600 nm.

The principle of a quantum counter is illustrated in Figure 2.42, which shows the ratio of the intensities observed from the RhB quantum counter and a thermopile. It is seen that the ratio remains constant at varying wavelengths. Since the emission spectrum of rhodamine B is independent of excitation wavelength, the quantum counter circumvents the wavelength-dependent sensitivity of the reference phototube. Hence, this solution provides a signal of constant emission wavelength and this signal, which is proportional to the photon flux of the exciting light. Quantum counters can also be made using moderately concentrated solutions of quinine sulfate or fluorescein. Quinine sulfate (4 g/l in 1

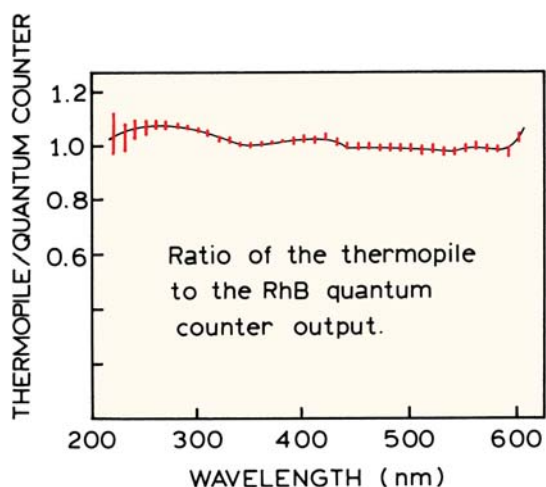


Figure 2.42. Comparison of the thermopile and the rhodamine B quantum counter as radiation detectors. Redrawn from [26].

$\text{N H}_2\text{SO}_4$) is useful at excitation wavelengths ranging from 220 to 340 nm and fluorescein (2 g/l in 0.1 N NaOH) is useful over this same range, but is less reliable from 340 to 360 nm,²⁶ where absorption of fluorescein is weaker.

To record corrected excitation spectra, the quantum counter is placed in the reference channel of the spectrofluorometer (Figure 2.1). Because of the high optical density, the reference cell holder is modified so that the emission is observed from the same surface of the quantum counter that is being illuminated. Alternatively, quantum counters can be used in a transmission mode by observing the fluorescent light exiting the back surface of the illuminated cuvette.²⁷ In either case an optical filter is placed between the quantum counter and the PMT, which eliminates incident light but transmits the fluorescence. With a quantum counter in place, a corrected excitation spectrum may be obtained by scanning the excitation monochromator and measuring the ratio of the fluorescence intensity from the sample to that from the quantum counter. The wavelength-dependent response of the emission monochromator and phototube are not important because the emission wavelength is unchanged during a scan of the excitation wavelength. This procedure was used to record the corrected excitation spectrum of fluorescein shown in Figure 2.6.

Other quantum counters have been described, and are summarized in Table 2.3. The long wavelength dye HITC extends the range to 800 nm, but its response is not as flat as RhB. Unfortunately, there is no perfect quantum counter, and for most applications RhB appears to be the best choice.

Table 2.3. Quantum Counters

Solution	Range (nm)	Flatness	Reference
3 g/l Rhodamine B in ethylene glycol	220–580	±5%	26
8 g/l Rhodamine B in ethylene glycol ^a	250–600	±4%	27
2 g/l Fluorescein in 0.1 N NaOH	240–400 ^b	±5%	26
4 g/l quinine sulfate in 1 N H_2SO_4	220–340	±5%	26
Rhodamine in polyvinyl alcohol (PVA) films	360–600	±3%	28 ^c
Coumarins in PVA films	360–480	±3%	28 ^c
5 g/l $\text{Ru}(\text{bpy})_3^{2+}$ in methanol	360–540	1.1%	29
$\text{Ru}(\text{bpy})_3^+$ in PVA films	360–530	1%	29 ^d
8 g/l HITC ^e in acetonitrile	320–800 ^f	±10%	30

^aA higher concentration of RhB is claimed to be preferred for use in transmission mode. See [27].

^bResponse may be 15% lower from 340 to 360 nm.

^cSee [28] for details on the rhodamines, coumarins, and PVA film preparations.

^dSee [29] for details.

^eHITC, 1,1',3,3',3',3'-hexamethylindotricarbocyanine.

^fDeviation up to 20% occurs near 470 nm.

2.9. CORRECTED EMISSION SPECTRA

2.9.1. Comparison with Known Emission Spectra

It is necessary to know the wavelength-dependent efficiency of the detection system to calculate the corrected emission spectra. It is difficult and time consuming to measure the correction factors for any given spectrofluorometer. Even after careful corrections are made the results are only accurate to ±10%. For this reason the observed technical spectra are usually reported. If corrected spectra are necessary, one simple and reliable method of obtaining the necessary correction factors is to compare the observed emission spectrum of a standard substance with the known corrected spectrum for this same substance. Such spectra have been published for a variety of readily available fluorophores including quinine sulfate, β -naphthol, 3-aminophthalimide, 4-dimethylamino-4'-nitrostilbene, and *N,N*-dimethylamino-*m*-nitrobenzene.^{31–36} The emission wavelengths of these compounds cover the range from 300 to 800 nm and the data are presented in graphical and numerical form. Corrected spectra have been published for a series of harmine derivatives, covering the range 400–600

nm.³⁷ For convenience some of these corrected spectra are given in Appendix I, Corrected Emission Spectra.

To obtain correction factors the emission spectrum of a standard compound is recorded and compared to the data for a standard compound. This simple comparative method avoids the difficulties inherent in the more rigorous procedures described below. β -Naphthol should probably not be used as a standard because, under the conditions described, both naphthol and naphtholate emission are observed. The dual emission is a result of an excited state reaction, the extent of which is difficult to control. Quinine sulfate has been questioned as a standard, because its intensity decay may not be a single exponential and its quantum yield may be somewhat dependent on excitation wavelength.³⁸ However, it seems to be an acceptable standard for most circumstances. One should remember that quinine sulfate is collisionally quenched by chloride,³⁹ so solutions of quinine used as a quantum yield standard should not contain chloride. A potentially superior standard is β -carboline, whose spectral characteristics are similar to quinine sulfate and which displays a single exponential decay time.⁴⁰ The emission spectra of quinine sulfate and β -carboline are similar.

2.9.2. Corrections Using a Standard Lamp

The correction factors can also be obtained by observing the wavelength-dependent output from a calibrated light source. The wavelength distribution of the light from a tungsten filament lamp can be approximated by that of a black body of equivalent temperature. Standard lamps of known color temperature are available from the National Bureau of Standards and other secondary sources. Generally one uses the spectral output data provided with the lamp ($L(\lambda)$) because the black-body equation is not strictly valid for a tungsten lamp. The detection system is then calibrated as follows:

1. The intensity of the standard lamp versus wavelength $I(\lambda)$ is measured using the detection system of the spectrofluorometer.
2. The sensitivity of the detection system $S(\lambda)$ is calculated using

$$S(\lambda) = I(\lambda)/L(\lambda) \quad (2.3)$$

where $L(\lambda)$ is the known output of the lamp.

3. The corrected spectra are then obtained by dividing the measured spectra by these sensitivity factors.

It is important to recognize that the operation of a standard lamp requires precise control of the color temperature. In addition, the spectral output of the lamp can vary with age and usage of the lamp.

2.9.3. Correction Factors Using a Quantum Counter and Scatterer

Another method to obtain the correction factors for the emission monochromator and PMT is to calibrate the xenon lamp in the spectrofluorometer for its spectral output.²⁶ The relative photon output ($L(\lambda)$) can be obtained by placing a quantum counter in the sample compartment. Once this intensity distribution is known, the xenon lamp output is directed onto the detector using a magnesium oxide scatterer. MgO is assumed to scatter all wavelengths with equal efficiency. Correction factors are obtained as follows:

1. The excitation wavelength is scanned with the quantum counter in the sample holder. The output yields the lamp output $L(\lambda)$.
2. The scatterer is placed in the sample compartment and the excitation and emission monochromators are scanned in unison. This procedure yields the product $L(\lambda) S(\lambda)$, where $S(\lambda)$ is the sensitivity of the detector system.
3. Division of $S(\lambda) \cdot L(\lambda)$ by $L(\lambda)$ yields the sensitivity factors $S(\lambda)$.

A critical aspect of this procedure is obtaining a reliable scatterer. The MgO must be freshly prepared and be free of impurities. Although this procedure seems simple, it is difficult to obtain reliable correction factors. It is known that the reflectivity of MgO changes over time, and with exposure to UV light, particularly below 400 nm.⁴¹ In addition to changes in reflectivity, it seems probable that the angular distribution of the scattered light and/or collection efficiency changes with wavelength, and one should probably use an integrating sphere at the sample location to avoid spatial effects. Given the complications and difficulties of this procedure, the use of emission spectrum standards is the preferred method when corrected emission spectra are needed.

2.9.4. Conversion Between Wavelength and Wavenumber

Occasionally, it is preferable to present spectra on the wavenumber scale ($\bar{\nu}$) rather than on the wavelength scale

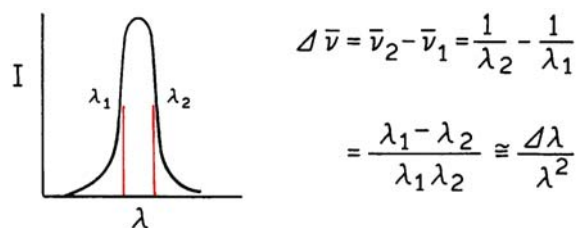


Figure 2.43. Relationship between spectral resolution in wavelength (λ) or wavenumber ($\bar{\nu}$).

(λ). Wavelengths are easily converted to wavenumbers (cm^{-1}) simply by taking the reciprocal. However, the bandpass in wavenumbers is not constant when the spectrum is recorded with constant wavelength resolution, as is usual with grating monochromators. For example, consider a constant bandpass $\Delta\lambda = \lambda_2 - \lambda_1$, where λ_1 and λ_2 are wavelengths on either side of the transmission maximum (Figure 2.43). At 300 nm a bandpass ($\Delta\lambda$) of 2 nm is equivalent to 222 cm^{-1} . At 600 nm, this same bandpass is equivalent to a resolution (Δ) of 55 cm^{-1} . As the wavelength is increased, the bandpass (in cm^{-1}) decreases as the square of the exciting wavelength. From $\bar{\nu} = 1/\lambda$, it follows that $|\Delta\bar{\nu}| = |\Delta\lambda|/\lambda^2$. Therefore, if spectra are obtained in the usual form of intensity per wavelength interval $I(\lambda, \lambda + \Delta\lambda)/\Delta\lambda$ and $I(\bar{\nu}) = I(\bar{\nu}, \bar{\nu} + \Delta\bar{\nu})$, then conversion to the wavenumber scale requires^{38–40} that each intensity be multiplied by λ^2 :

$$I(\bar{\nu}) = \lambda^2 I(\lambda) \quad (2.4)$$

The effect of this wavelength-to-wavenumber conversion is illustrated in Appendix I. Multiplication by λ^2 results in selective enhancement of the long-wavelength side of the emission, and there is a shift in the apparent emission maximum. It should be noted that even after this correction is performed the resolution of the spectrum still varies with wavenumber.

2.10. QUANTUM YIELD STANDARDS

The easiest way to estimate the quantum yield of a fluorophore is by comparison with standards of known quantum yield. Some of the most used standards are listed in Table 2.4. The quantum yields of these compounds are mostly independent of excitation wavelength, so the standards can be used wherever they display useful absorption.

Determination of the quantum yield is generally accomplished by comparison of the wavelength integrated intensity of the unknown to that of the standard. The optical density is kept below 0.05 to avoid inner filter effects, or the optical densities of the sample and reference (r) are matched at the excitation wavelength. The quantum yield of the unknown is calculated using

$$Q = Q_R \frac{I}{I_R} \frac{OD_R n^2}{OD n_R^2} \quad (2.5)$$

Table 2.4. Quantum Yield Standards

Compound	Solvent	λ_{ex} (nm)	$^{\circ}\text{C}$	Q	Reference
Quinine sulfate	0.1 M H_2SO_4	350	22	0.577	45
		366	–	0.53 ± 0.023	46
β -Carboline ^a	1 N H_2SO_4	350	25	0.60	40
Fluorescein	0.1 M NaOH	496	22	0.95 ± 0.03	47
9,10-DPA ^b	cyclohexane	–	–	0.95	48
9,10-DPA	"	366	–	1.00 ± 0.05	49–50
POPOP ^c	cyclohexane	–	–	0.97	48
2-Aminopyridine	0.1 N H_2SO_4	285	–	0.60 ± 0.05	50–51
Tryptophan	water	280	–	0.13 ± 0.01	52
Tyrosine	water	275	23	0.14 ± 0.01	52
Phenylalanine	water	260	23	0.024	52
Phenol	water	275	23	0.14 ± 0.01	52
Rhodamine 6G	ethanol	488	–	0.94	53
Rhodamine 101	ethanol	450–465	25	1.0	54
Cresyl Violet	methanol	540–640	22	0.54	55

^a β -carboline is 9H-pyrido[3,4- β]-indole.

^b9,10-DPA, 9,10-diphenylanthracene.

^cPOPOP, 2,2'-(1,4-phenylene)bis[5-phenyloxazole].

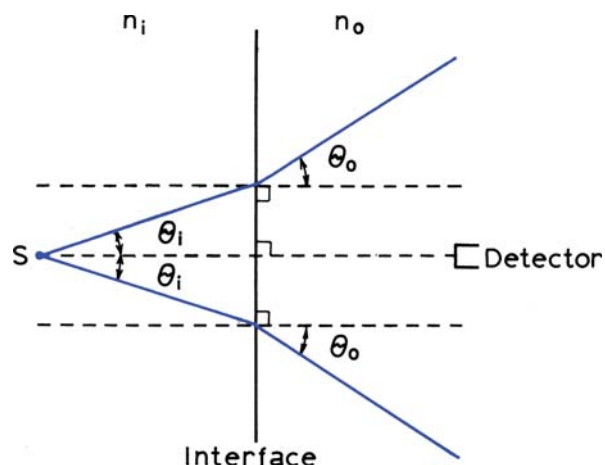


Figure 2.44. Refractive index effects in quantum yield measurements. The point source, S , is in a medium of refractive index n_i , the detector in a medium of refractive index n_o . $n_o < n_i$. Reprinted with permission from [42], copyright © 1971, American Chemical Society.

where Q is the quantum yield, I is the integrated intensity, OD is the optical density, and n is the refractive index. The subscript R refers to the reference fluorophore of known quantum yield. In this expression it is assumed that the sample and reference are excited at the same wavelength, so that it is not necessary to correct for the different excitation intensities of different wavelengths.

This expression is mostly intuitive, except for the use of the ratio of refractive indices of the sample (n) and reference (n_R). This ratio has its origin in consideration of the intensity observed from a point source in a medium of refractive index n_i , by a detector in a medium of refractive index n_o (Figure 2.44). The observed intensity is modified⁴²⁻⁴³ by the ratio $(n_i/n_o)^2$. While the derivation was for a point source, the use of the ratio was found to be valid for many detector geometries.⁴⁴

2.11. EFFECTS OF SAMPLE GEOMETRY

The apparent fluorescence intensity and spectral distribution can be dependent upon the optical density of the sample, and the precise geometry of sample illumination. The most common geometry used for fluorescence is right-angle observation of the center of a centrally illuminated cuvette (Figure 2.45, top left). Other geometric arrangements include front-face and off-center illumination. Off-center illumination decreases the path length, which can also be accomplished by using cuvettes with path lengths less than 1 cm. These methods are generally used to

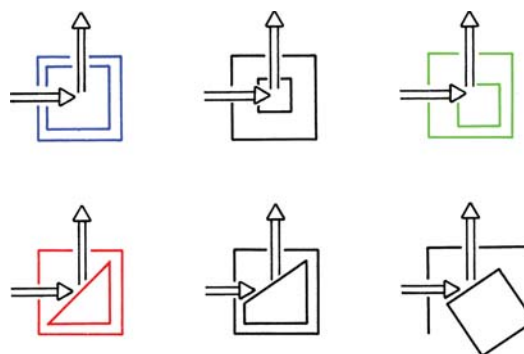


Figure 2.45. Various geometric arrangements for observation of fluorescence.

decrease the inner filtering effects due to high optical densities or to sample turbidity.

Frequently, front-face illumination is performed using either triangular cuvettes or square cuvettes oriented at 30 to 60° relative to the incident beam (Figure 2.45). In our opinion, an angle of 45° should be discouraged. A large amount of light is reflected directly into the emission monochromator, increasing the chance that stray light will interfere with the measurements. With front-face illumination we prefer to orient the illuminated surface about 30° from the incident beam. This procedure has two advantages. First, less reflected light enters the emission monochromator. Second, the incident light is distributed over a larger surface area, decreasing the sensitivity of the measurement to the precise placement of the cuvette within its holder. One disadvantage of this orientation is a decreased sensitivity because a larger fraction of the incident light is reflected off the surface of the cuvette.

It is important to recognize that fluorescence intensities are proportional to the concentration over only a limited range of optical densities. Consider a 1 x 1 cm cuvette that is illuminated centrally and observed at a right angle (Figure 2.45, top left). Assume further that the optical density at the excitation wavelength is 0.1. Using the definition of optical density ($\log I_0/I = OD$), the light intensity at the center of the cuvette (I) is $0.88I_0$, where I_0 is the intensity of the light incident to the cuvette. Since the observed fluorescence intensity is proportional to the intensity of the exciting light, the apparent quantum yield will be about 10% less than that observed for an infinitely dilute solution. This is called an inner filter effect. These effects may decrease the intensity of the excitation at the point of observation, or decrease the observed fluorescence by absorption of the fluorescence. The relative importance of each process depends

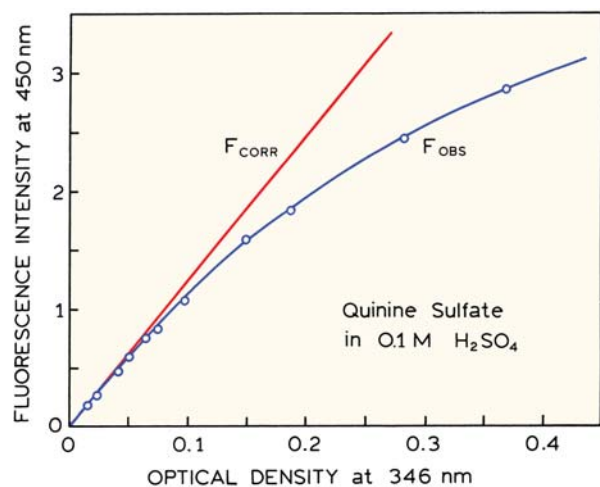


Figure 2.46. Effects of optical density on the fluorescence intensity of quinine sulfate. The solid line (—) shows the measured intensities, and the dashed line (---) indicates the corrected intensities, according to equation (2.6) with $OD_{em} = 0$. These data were obtained in a 1-cm² cuvette that was centrally illuminated.

upon the optical densities of the sample at the excitation and emission wavelengths.

The data for quinine sulfate in Figure 2.46 illustrates the effect of optical density on fluorescence intensity. The measured intensity is proportional to optical density only to an optical density of 0.05. The linear range of the fluorescence intensities could be expanded by using off-center illumination, which reduces the effective light path. These intensities can be approximately corrected for the inner filter effects as follows. Suppose the sample has a significant optical density at both the excitation and emission wavelengths, OD_{ex} and OD_{em} , respectively. These optical densities attenuate the excitation and emission by $10^{-0.5OD_{ex}}$ and $10^{-0.5OD_{em}}$, respectively. Attenuation due to absorption of the incident light or absorption of the emitted light are sometimes called the primary and secondary inner filter effects, respectively.⁵⁶⁻⁵⁷ The corrected fluorescence intensity is given approximately by

$$F_{corr} = F_{obs} \text{antilog} \left(\frac{OD_{ex} + OD_{em}}{2} \right) \quad (2.6)$$

The corrected intensities for quinine sulfate are shown in Figure 2.46, and these calculated values are seen to match the initial linear portion of the curve. For precise corrections it is preferable to prepare calibration curves using the precise compounds and conditions that will be used for the actual experimentation. Empirical corrections are typi-

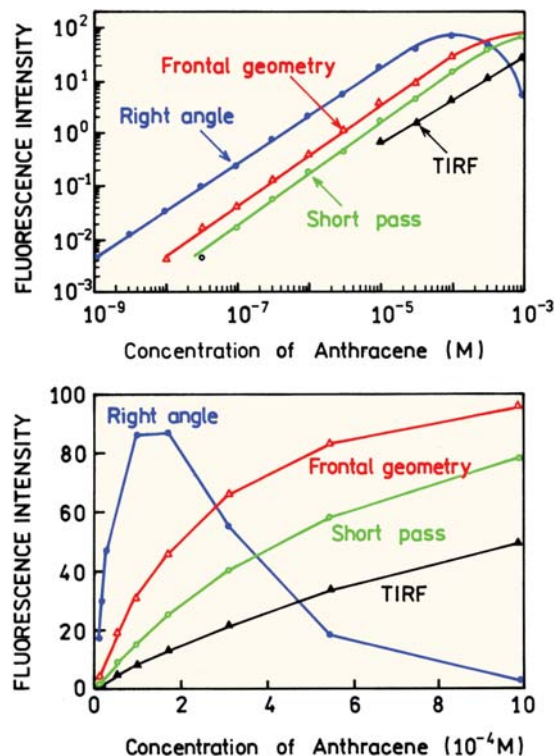


Figure 2.47. Effect of concentrations on the intensity of anthracene. Short pass refers to a 1 mm x 10 mm cuvette. Revised from [61].

cally used in most procedures to correct for sample absorbance.⁵⁶⁻⁶⁰

Figure 2.47 shows the effect of anthracene concentration on its emission intensity as observed for several geometries. TIRF refers to total internal reflection, which is described in Chapter 23. Short pass refers to a cuvette, 1 by 10 mm in dimension. The highest signal levels were obtained with the standard right-angle geometry. The linear range can be somewhat extended by using other geometries. Intuitively we may expect that with the front-face geometry the intensity will become independent of fluorophore concentration at high concentrations.^{60,62} Under these conditions all the incident light is absorbed near the surface of the cuvette. Front-face illumination is also useful for studies of optically dense samples such as whole blood, or a highly scattering solution. The intensity is expected to be proportional to the ratio of the optical density of the fluorophore to that of the sample.⁶³ When front-face illumination is used the total optical density can be very large (20 or larger). However, high fluorophore concentrations can result in quenching due to a variety of interactions, such as radiative and non-radiative transfer and excimer formation. Fluor-

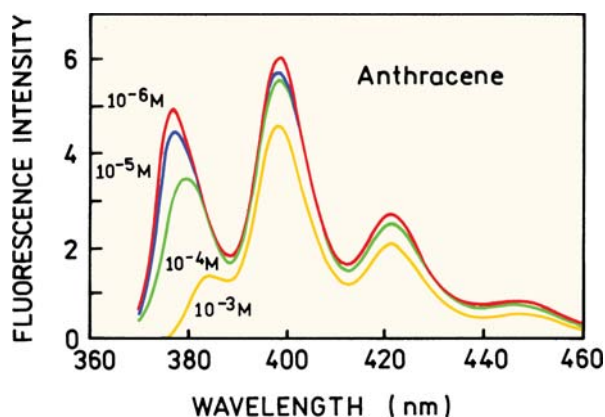


Figure 2.48. Effects of self-absorption of anthracene on its emission spectrum. A 1-cm² cuvette was used with right-angle observation. Revised from [61].

rophores like fluorescein with a small Stokes shift are particularly sensitive to concentration quenching.

High optical densities can distort the emission spectra as well as the apparent intensities. For example, when right-angle observation is used, the short-wavelength emission bands of anthracene are selectively attenuated (Figure 2.48). This occurs because these shorter wavelengths are absorbed by anthracene. Attenuation of the blue edge of the emission is most pronounced for fluorophores that have significant overlap of the absorption and emission spectra. Fluorophores that display a large Stokes shift are less sensitive to this phenomenon.

A dramatic effect of concentration can be seen with fluorophores that display a small Stokes shift. Figure 2.49 shows a photograph of three bottles of rhodamine 6G on a light box, with the concentration increasing from left to right. The color changes from green to orange. This effect is due to reabsorption of the shorter wavelength part of the emission. The emission spectra shift dramatically to longer wavelengths at higher concentrations.

2.12. COMMON ERRORS IN SAMPLE PREPARATION

It is valuable to summarize some of the difficulties that can be encountered with any given sample (Figure 2.50). The sample can be too concentrated, in which case all the light is absorbed at the surface facing the light source. In fact, this is one of the more common errors. With highly absorbing solutions and right-angle observations the signal levels can be very low. Other problems are when the sample contains a fluorescent impurity, or the detected light is contam-

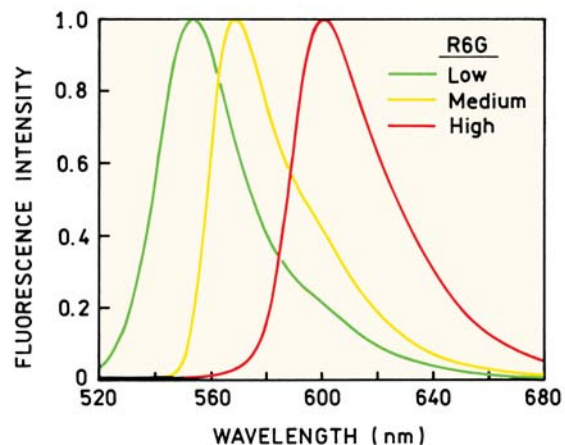
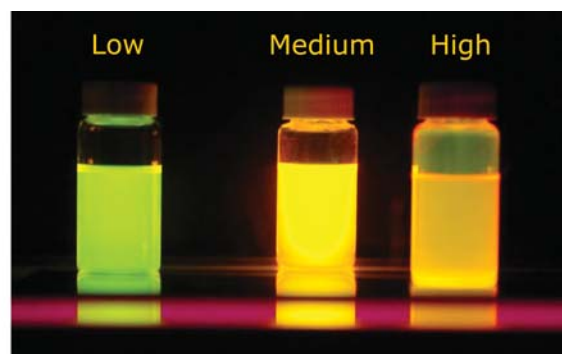


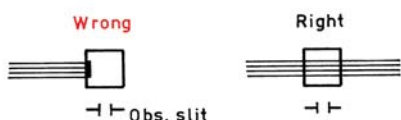
Figure 2.49. Effect of concentrations on the color and emission spectra of rhodamine 6G. The concentrations of R6G are 5×10^{-6} , 1.6×10^{-4} , and 5.7×10^{-3} M. From [64].

inated by Rayleigh or Raman scatter. Sometimes the signal may seem too noisy given the signal level. Intensity fluctuations can be due to particles that drift through the laser beam, and fluoresce or scatter the incident light.

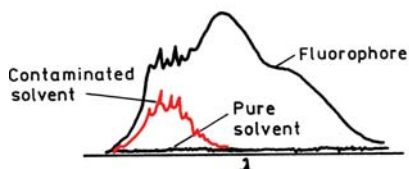
Even if the fluorescence is strong, it is important to consider the possibility of two or more fluorophores, that is, an impure sample. Emission spectra are usually independent of excitation wavelength.⁶⁵ Hence it is useful to determine if the emission spectrum remains the same at different excitation wavelengths.

One example of a mixture of fluorophores is shown in Figure 2.51, which contains a mixture of coumarin 102 (C102) and coumarin 153 (C153). For a pure solution of C102 the same emission spectrum is observed for excitation at 360 and 420 nm (top). For a mixture of C102 and C153, one finds an increased intensity above 500 nm for excitation at 420 (bottom, dashed). This peak at 520 nm is due to C153, which can be seen from its emission spectrum (dot-

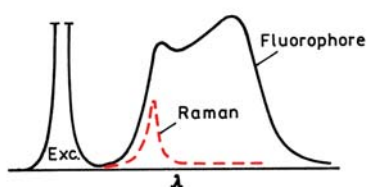
Fluorophore concentration too high



Contaminated solvent and/or cuvette



Scattered light



Particles in solution

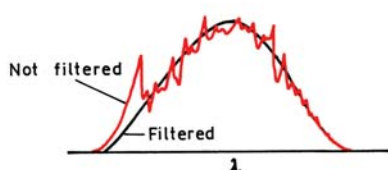


Figure 2.50. Common errors in sample preparation.

ted). Whenever the emission spectrum changes with excitation wavelength one should suspect an impurity.

It is interesting to note the significant change in the emission spectra of these two coumarin derivatives for a small change in structure. The fluorine-substituted coumarin (C153) appears to be more sensitive to solvent polarity. This effect is probably due to an increased charge separation in C153, due to movement of these amino electrons toward the $-\text{CF}_3$ group in the excited state. These effects are described in Chapter 6.

2.13. ABSORPTION OF LIGHT AND DEVIATION FROM THE BEER-LAMBERT LAW

A fundamental aspect of fluorescence spectroscopy is the measurement of light absorption. While the theory of light absorption is well known, a number of factors can result in

INSTRUMENTATION FOR FLUORESCENCE SPECTROSCOPY

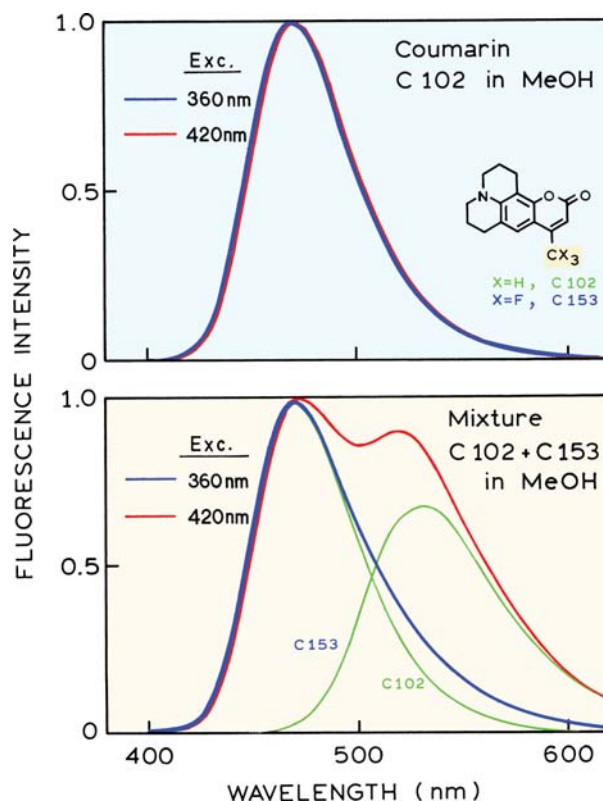


Figure 2.51. Emission spectra of C102 (top) and a mixture of C102 and C153 (bottom) excited at 360 and 420 nm. From [66].

misleading measurements of light absorption. We will first derive the Beer-Lambert Law, and then describe reasons for deviations from this law.

Consider a thin slab of solution of thickness dx that contains n light-absorbing molecules/cm³ (Figure 2.52). Let σ be the effective cross-section for absorption in cm². The light intensity dI absorbed per thickness dx is proportional to the intensity of the incident light I and to both σ and n , where n is the number of molecules per cm³:

$$\frac{dI}{dx} = -I\sigma n \quad (2.7)$$

Rearrangement and integration, subject to the boundary condition $I = I_0$ at $x = 0$, yields

$$\ln \frac{I_0}{I} = \sigma nd \quad (2.8)$$

where d is the thickness of the sample. This is the Beer-Lambert equation, which is generally used in an alternative form:

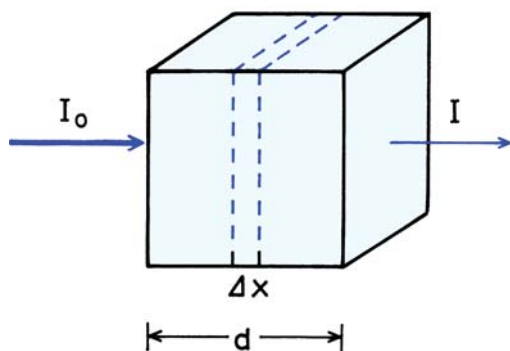


Figure 2.52. Light absorption.

$$\log \frac{I_0}{I} = \epsilon cd = \text{optical density} \quad (2.9)$$

where ϵ is the decadic molar extinction coefficient (in $M^{-1} \text{ cm}^{-1}$) and c is the concentration in moles/liter. Combination of eqs. 2.8 and 2.9 yields the relationship between the extinction coefficient and the cross-section for light absorption:

$$\sigma = 2.303 \frac{\epsilon c}{n} \quad (2.10)$$

Since $n = Nc/10^3$ (where N is Avogadro's number), we obtain

$$\sigma = 3.82 \times 10^{-21} \epsilon \quad (\text{in } \text{cm}^2) \quad (2.11)$$

It is interesting to calculate the absorption cross-section for typical aromatic compounds. The extinction coefficients of anthracene are 160,000 and 6,300 $M^{-1} \text{ cm}^{-1}$ at 253 and 375 nm, respectively. These values correspond to cross-sections of 6.1 and 0.24 \AA^2 , respectively. Assuming the molecular cross-section of anthracene to be 12 \AA^2 , we see that anthracene absorbs about 50% of the photons it encounters at 253 nm and 2% of the photons at 375 nm.

Occasionally one encounters the term "oscillator strength." This term represents the strength of absorption relative to a completely allowed transition. The oscillator strength (f) is related to the integrated absorption of a transition by

$$f = \frac{4.39 \times 10^{-9}}{n} \int \epsilon(\bar{\nu}) d\bar{\nu} \quad (2.12)$$

where n is the refractive index.

2.13.1. Deviations from Beer's Law

Beer's Law predicts that the optical density is directly proportional to the concentration of the absorbing species. Deviations from Beer's law can result from both instrumental and intrinsic causes. Biological samples are frequently turbid because of macromolecules or other large aggregates that scatter light. The optical density resulting from scatter will be proportional to $1/\lambda^4$ (Rayleigh scattering), and may thus be easily recognized as a background absorption that increases rapidly with decreasing wavelength.

If the optical density of the sample is high, and if the absorbing species is fluorescent, the emitted light cannot reach the detector. This effect yields deviations from Beer's law that are concave toward the concentration axis. The fluorescence is omnidirectional, whereas the incident light is collimated along an axis. Hence, this effect can be minimized by keeping the detector distant from the sample, and thereby decreasing the efficiency with which the fluorescence emission is collected.

If the absorbing species is only partially soluble, it may aggregate in solutions at high concentrations. The absorption spectra of the aggregates may be distinct from the monomers. An example is the common dye bromophenol blue. At concentrations around 10 mg/ml it appears as a red solution, whereas at lower concentrations it appears blue. Depending upon the wavelength chosen for observation, the deviations from Beer's law may be positive or negative.

The factors described above were due to intrinsic properties of the sample. Instrumental artifacts can also yield optical densities that are nonlinear with concentration. This is particularly true at high optical densities. For example, consider a solution of indole with an optical density of 5 at 280 nm. In order to accurately measure this optical density, the spectrophotometer needs to accurately quantify the intensity of I_0 and I , the latter of which is 10^{-5} less intense than the incident light I_0 . Generally, the stray light passed by the monochromator, at wavelengths where the compound does not absorb, are larger than this value. As a result, one cannot reliably measure such high optical densities unless considerable precautions are taken to minimize stray light.

2.14. CONCLUSIONS

At first glance it seems easy to perform fluorescence experiments. However, there are numerous factors that can compromise the data and invalidate the results. One needs to be constantly aware of the possibility of sample contamina-

tion, or contamination of the signal from scattered or stray light. Collection of emission spectra, and examination of blank samples, is essential for all experiments. One cannot reliably interpret intensity values, anisotropy, or lifetimes without careful examination of the emission spectra.

REFERENCES

- Revised from commercial literature provided by SLM Instruments.
- Revised from commercial literature provided by Molecular Devices, <http://www.moleculardevices.com/pages/instruments/gemini.html>.
- Revised from commercial literature from Spectra Physics, www.spectra-physics.com.
- Laczko G, Lakowicz JR, unpublished observations.
- Oriel Corporation, 250 Long Beach Blvd., PO Box 872, Stratford, CT 06497: Light Sources, Monochromators and Spectrographs, Detectors and Detection Systems, Fiber Optics.
- ILC Technology Inc. 399 West Joan Drive, Sunnyvale, CA 94089: Cermac Product Specifications for collimated and focused xenon lamps.
- Ocean Optics product literature, <http://www.oceanoptics.com/products/>
- Hart SJ, JiJi RD. 2002. Light emitting diode excitation emission matrix fluorescence spectroscopy. *Analyst* **127**:1643–1699.
- Landgraf S. 2004. Use of ultrabright LEDs for the determination of static and time-resolved fluorescence information of liquid and solid crude oil samples. *J Biochem Biophys Methods* **61**:125–134.
- Gryczynski I, Lakowicz JR, unpublished observations.
- Optometrics USA Inc., Nemco Way, Stony Brook Industrial Park, Ayer, MA 01432: 1996 Catalog Optical Components and Instruments.
- Castellano P, Lakowicz JR, unpublished observations.
- Melles Griot product literature, <http://shop.mellesgriot.com/products/optics/>
- Macleod HA. 2001. *Thin-film optical filters*, 3rd ed. Institute of Physics, Philadelphia.
- Semrock Inc., Rochester, NY, www.semrock.com.
- Gryczynski I, Malak H, Lakowicz JR, Cheung HC, Robinson J, Umeda PK. 1996. Fluorescence spectral properties of troponin C mutant F22W with one-, two- and three-photon excitation. *Biophys J* **71**:3448–3453.
- Szmacinski H, Gryczynski I, Lakowicz JR. 1993. Calcium-dependent fluorescence lifetimes of Indo-1 for one- and two-photon excitation of fluorescence. *Photochem Photobiol* **58**:341–345.
- Hamamatsu Photonics K.K., Electron Tube Center, (1994), 314-5, Shimokanzo, Toyooka-village, Iwata-gun, Shizuoka-ken, 438-01 Japan: Photomultiplier Tubes.
- Provided by Dr. R. B. Thompson
- Leaback DH. 1997. Extended theory, and improved practice for the quantitative measurement of fluorescence. *J Fluoresc* **7**(1):55S–57S.
- Epperson PM, Denton MB. 1989. Binding spectral images in a charge-coupled device. *Anal Chem* **61**:1513–1519.
- Bilhorn RB, Sweedler JV, Epperson PM, Denton MB. 1987. Charge-transfer device detectors for analytical optical spectroscopy—operation and characteristics. *Appl Spectrosc* **41**:1114–1124.
- Hiraoka Y, Sedat JW, Agard DA. 1987. The use of a charge-coupled device for quantitative optical microscopy of biological structures. *Science* **238**:36–41.
- Aikens RS, Agard DA, Sedat JW. 1989. Solid-state imagers for microscopy. *Methods Cell Biol* **29**:291–313.
- Ocean Optics Inc., http://www.oceanoptics.com/products/usb2000_flg.asp.
- Melhuish WH. 1962. Calibration of spectrofluorometers for measuring corrected emission spectra. *J Opt Soc Am* **52**:1256–1258.
- Yguerabide J. 1968. Fast and accurate method for measuring photon flux in the range 2500–6000 Å. *Rev Sci Instrum* **39**(7):1048–1052.
- Mandal K, Pearson TDL, Demas JN. 1980. Luminescent quantum counters based on organic dyes in polymer matrices. *Anal Chem* **52**:2184–2189.
- Mandal K, Pearson TDL, Demas NJ. 1981. New luminescent quantum counter systems based on a transition-metal complex. *Inorg Chem* **20**:786–789.
- Nothnagel EA. 1987. Quantum counter for correcting fluorescence excitation spectra at 320- and 800-nm wavelengths. *Anal Biochem* **163**:224–237.
- Lippert E, Nagelle W, Siebold-Blakenstein I, Staiger U, Voss W. 1959. Messung von fluoreszenzspektren mit hilfe von spektralphotometern und vergleichsstandards. *Zeitschr Anal Chem* **17**:1–18.
- Schmillen A, Legler R. 1967. *Landolt-Borstein*. Vol 3: Lumineszenz Organischer Substanzen. Springer-Verlag, New York.
- Argauer RJ, White CE. 1964. Fluorescent compounds for calibration of excitation and emission units of spectrofluorometer. *Anal Chem* **36**:368–371.
- Melhuish WH. 1960. A standard fluorescence spectrum for calibrating spectrofluorometers. *J Phys Chem* **64**:762–764.
- Parker CA. 1962. Spectrofluorometer calibration in the ultraviolet region. *Anal Chem* **34**:502–505.
- Velapoldi RA. 1973. Considerations on organic compounds in solution and inorganic ions in glasses as fluorescent standard reference materials. *Proc Natl Bur Stand* **378**:231–244.
- Pardo A, Reyman D, Poyato JML, Medina F. 1992. Some β -carboline derivatives as fluorescence standards. *J Lumines* **51**:269–274.
- Chen RF. 1967. Some characteristics of the fluorescence of quinine. *Anal Biochem* **19**:374–387.
- Verity B, Bigger SW. 1996. The dependence of quinine fluorescence quenching on ionic strength. *Int J Chem Kinet* **28**(12):919–923.
- Ghiggino KP, Skilton PF, Thistlethwaite PJ. 1985. β -Carboline as a fluorescence standard. *J Photochem* **31**:113–121.
- Middleton WEK, Sanders CL. 1951. The absolute spectral diffuse reflectance of magnesium oxide. *J Opt Soc Am* **41**(6):419–424.
- Demas JN, Crosby GA. 1971. The measurement of photoluminescence quantum yields: a review. *J Phys Chem* **75**(8):991–1025.
- Birks JB. 1970. *Photophysics of aromatic molecules*. Wiley-Interscience, New York.
- Hermans JJ, Levinson S. 1951. Some geometrical factors in light-scattering apparatus. *J Opt Soc Am* **41**(7):460–465.
- Eastman JW. 1967. Quantitative spectrofluorimetry—the fluorescence quantum yield of quinine sulfate. *Photochem Photobiol* **6**:55–72.
- Adams MJ, Highfield JG, Kirkbright GF. 1977. Determination of absolute fluorescence quantum efficiency of quinine bisulfate in aqueous medium by optoacoustic spectrometry. *Anal Chem* **49**:1850–1852.
- Brannon JH, Magde D. 1978. Absolute quantum yield determination by thermal blooming: fluorescein. *J Phys Chem* **82**(6):705–709.
- Mardelli M, Olmsted J. 1977. Calorimetric determination of the 9,10-diphenyl-anthracene fluorescence quantum yield. *J Photochem* **7**:277–285.
- Ware WR, Rothman W. 1976. Relative fluorescence quantum yields using an integrating sphere: the quantum yield of 9,10-diphenylanthracene in cyclohexane. *Chem Phys Lett* **39**(3):449–453.
- Testa AC. 1969. Fluorescence quantum yields and standards. *Fluoresc News* **4**(4):1–3.

51. Rusakowicz R, Testa AC. 1968. 2-aminopyridine as a standard for low-wavelength spectrofluorometry. *J Phys Chem* **72**:2680–2681.
52. Chen RF. 1967. Fluorescence quantum yields of tryptophan and tyrosine. *Anal Lett* **1**:35–42.
53. Fischer M, Georges J. 1996. Fluorescence quantum yield of rhodamine 6G in ethanol as a function of concentration using thermal lens spectrometry. *Chem Phys Lett* **260**:115–118.
54. Karstens T, Kobe K. 1980. Rhodamine B and Rhodamine 101 as reference substances for fluorescence quantum yield measurements. *J Phys Chem* **84**:1871–1872.
55. Magde D, Brannon JH, Cremers TL, Olmsted J. 1979. Absolute luminescence yield of cresyl violet: a standard for the red. *J Phys Chem* **83**(6):696–699.
56. Kubista M, Sjöback R, Eriksson S, Albinsson B. 1994. Experimental correction for the inner-filter effect in fluorescence spectra. *Analyst* **119**:417–419.
57. Yappert MC, Ingle JD. 1989. Correction of polychromatic luminescence signals for inner-filter effects. *Appl Spectros* **43**(5):759–767.
58. Wiechelmann KJ. 1986. Empirical correction equation for the fluorescence inner filter effect. *Am Lab* **18**:49–53.
59. Puchalski MM, Morra MJ, von Wandruszka R. 1991. Assessment of inner filter effect corrections in fluorimetry. *Fresenius J Anal Chem* **340**:341–344.
60. Guilbault GG, ed. 1990. *Practical fluorescence*. Marcel Dekker, New York.
61. Kao S, Asanov AN, Oldham PB. 1998. A comparison of fluorescence inner-filter effects for different cell configurations. *Instrum Sci Tech* **26**(4):375–387.
62. Eisinger J. 1969. A variable temperature, UV luminescence spectrograph for small samples. *Photochem Photobiol* **9**:247–258.
63. Eisinger J, Flores J. 1979. Front-face fluorometry of liquid samples. *Anal Biochem* **94**:15–21.
64. Courtesy of Drs. Joanna Lukomska and Ignacy Gryczynski.
65. Kasha M. 1960. Paths of molecular excitation. *Radiat Res* **2**:243–275.
66. Gryczynski I, unpublished observations.

PROBLEMS

- P2.1. *Measurement of High Optical Densities*: Suppose you wish to determine the concentration of a 10^{-4} M solution of rhodamine B, which has an extinction coefficient near $100,000 \text{ M}^{-1} \text{ cm}^{-1}$ at 590 nm. The monochromator in your spectrophotometer is imperfect, and the incident light at 590 nm contains 0.01% of light at longer wavelengths, not absorbed by rhodamine B. What is the true optical density of the solution? Which is the apparent optical density measured with your spectrophotometer? Assume the path length is 1 cm.
- P2.2. *Calculation of Concentrations by Absorbance*: Suppose a molecule displays an extinction coefficient of $30,000 \text{ M}^{-1} \text{ cm}^{-1}$, and that you wish to determine its concentration from the absorbance. You have two solutions, with actual optical densities of 0.3 and 0.003 in a 1-cm cuvette. What are the concentrations of the two solutions? Assume the measurement error in percent transmission is 1%. How does the 1% error affect determination of the concentrations?



Introduction to Fluorescence

During the past 20 years there has been a remarkable growth in the use of fluorescence in the biological sciences. Fluorescence spectroscopy and time-resolved fluorescence are considered to be primarily research tools in biochemistry and biophysics. This emphasis has changed, and the use of fluorescence has expanded. Fluorescence is now a dominant methodology used extensively in biotechnology, flow cytometry, medical diagnostics, DNA sequencing, forensics, and genetic analysis, to name a few. Fluorescence detection is highly sensitive, and there is no longer the need for the expense and difficulties of handling radioactive tracers for most biochemical measurements. There has been dramatic growth in the use of fluorescence for cellular and molecular imaging. Fluorescence imaging can reveal the localization and measurements of intracellular molecules, sometimes at the level of single-molecule detection.

Fluorescence technology is used by scientists from many disciplines. This volume describes the principles of fluorescence that underlie its uses in the biological and chemical sciences. Throughout the book we have included examples that illustrate how the principles are used in different applications.

1.1. PHENOMENA OF FLUORESCENCE

Luminescence is the emission of light from any substance, and occurs from electronically excited states. Luminescence is formally divided into two categories—fluorescence and phosphorescence—depending on the nature of the excited state. In excited singlet states, the electron in the excited orbital is paired (by opposite spin) to the second electron in the ground-state orbital. Consequently, return to the ground state is spin allowed and occurs rapidly by emission of a photon. The emission rates of fluorescence are typically 10^8 s^{-1} , so that a typical fluorescence lifetime is near 10 ns ($10 \times 10^{-9} \text{ s}$). As will be described in Chapter 4, the lifetime (τ) of a fluorophore is the average time between its excitation and return to the ground state. It is valuable to consider a 1-ns lifetime within the context of the speed of

light. Light travels 30 cm, or about one foot, in one nanosecond. Many fluorophores display subnanosecond lifetimes. Because of the short timescale of fluorescence, measurement of the time-resolved emission requires sophisticated optics and electronics. In spite of the added complexity, time-resolved fluorescence is widely used because of the increased information available from the data, as compared with stationary or steady-state measurements. Additionally, advances in technology have made time-resolved measurements easier, even when using microscopes.

Phosphorescence is emission of light from triplet excited states, in which the electron in the excited orbital has the same spin orientation as the ground-state electron. Transitions to the ground state are forbidden and the emission rates are slow (10^3 to 10^0 s^{-1}), so that phosphorescence lifetimes are typically milliseconds to seconds. Even longer lifetimes are possible, as is seen from "glow-in-the-dark" toys. Following exposure to light, the phosphorescence substances glow for several minutes while the excited phosphors slowly return to the ground state. Phosphorescence is usually not seen in fluid solutions at room temperature. This is because there exist many deactivation processes that compete with emission, such as non-radiative decay and quenching processes. It should be noted that the distinction between fluorescence and phosphorescence is not always clear. Transition metal–ligand complexes (MLCs), which contain a metal and one or more organic ligands, display mixed singlet–triplet states. These MLCs display intermediate lifetimes of hundreds of nanoseconds to several microseconds. In this book we will concentrate mainly on the more rapid phenomenon of fluorescence.

Fluorescence typically occurs from aromatic molecules. Some typical fluorescent substances (fluorophores) are shown in Figure 1.1. One widely encountered fluorophore is quinine, which is present in tonic water. If one observes a glass of tonic water that is exposed to sunlight, a faint blue glow is frequently visible at the surface. This glow is most apparent when the glass is observed at a right

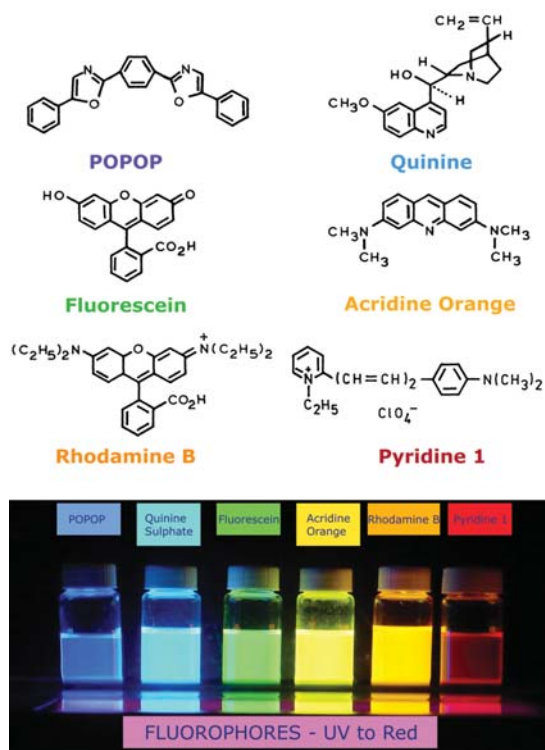


Figure 1.1. Structures of typical fluorescent substances.

angle relative to the direction of the sunlight, and when the dielectric constant is decreased by adding less polar solvents like alcohols. The quinine in tonic water is excited by the ultraviolet light from the sun. Upon return to the ground state the quinine emits blue light with a wavelength near 450 nm. The first observation of fluorescence from a quinine solution in sunlight was reported by Sir John Frederick William Herschel (Figure 1.2) in 1845.¹ The following is an excerpt from this early report:

On a case of superficial colour presented by a homogeneous liquid internally colourless. By Sir John Frederick William Herschel, Philosophical Translation of the Royal Society of London (1845) 135:143–145. Received January 28, 1845 — Read February 13, 1845.

"The sulphate of quinine is well known to be of extremely sparing solubility in water. It is however easily and copiously soluble in tartaric acid. Equal weights of the sulphate and of crystallised tartaric acid, rubbed up together with addition of a very little water, dissolve entirely and immediately. It is this solution, largely diluted, which exhibits the optical phenomenon in question. Though perfectly transparent and colourless when held between the eye and the



Figure 1.2. Sir John Fredrich William Herschel, March 7, 1792 to May 11, 1871. Reproduced courtesy of the Library and Information Centre, Royal Society of Chemistry.

light, or a white object, it yet exhibits in certain aspects, and under certain incidences of the light, an extremely vivid and beautiful celestial blue colour, which, from the circumstances of its occurrence, would seem to originate in those strata which the light first penetrates in entering the liquid, and which, if not strictly superficial, at least exert their peculiar power of analysing the incident rays and dispersing those which compose the tint in question, only through a very small depth within the medium.

To see the colour in question to advantage, all that is requisite is to dissolve the two ingredients above mentioned in equal proportions, in about a hundred times their joint weight of water, and having filtered the solution, pour it into a tall narrow cylindrical glass vessel or test tube, which is to be set upright on a dark coloured substance before an open window exposed to strong daylight or sunshine, but with no cross lights, or any strong reflected light from behind. If we look down perpendicularly into the vessel so that the visual ray shall graze the internal surface of the glass through a great part of its depth, the whole of that surface of the liquid on which the light first strikes will appear of a lively blue, ...

If the liquid be poured out into another vessel, the descending stream gleams internally from all

its undulating inequalities, with the same lively yet delicate blue colour, ... thus clearly demonstrating that contact with a denser medium has no share in producing this singular phenomenon.

The thinnest film of the liquid seems quite as effective in producing this superficial colour as a considerable thickness. For instance, if in pouring it from one glass into another, ... the end of the funnel be made to touch the internal surface of the vessel well moistened, so as to spread the descending stream over an extensive surface, the intensity of the colour is such that it is almost impossible to avoid supposing that we have a highly coloured liquid under our view."

It is evident from this early description that Sir Herschel recognized the presence of an unusual phenomenon that could not be explained by the scientific knowledge of the time. To this day the fluorescence of quinine remains one of the most used and most beautiful examples of fluorescence. Herschel was from a distinguished family of scientists who lived in England but had their roots in Germany.² For most of his life Sir Herschel did research in astronomy, publishing only a few papers on fluorescence.

It is interesting to notice that the first known fluorophore, quinine, was responsible for stimulating the development of the first spectrofluorometers that appeared in the 1950s. During World War II, the Department of War was interested in monitoring antimalaria drugs, including quinine. This early drug assay resulted in a subsequent program at the National Institutes of Health to develop the first practical spectrofluorometer.³

Many other fluorophores are encountered in daily life. The green or red-orange glow sometimes seen in antifreeze is due to trace quantities of fluorescein or rhodamine, respectively (Figure 1.1). Polynuclear aromatic hydrocarbons, such as anthracene and perylene, are also fluorescent, and the emission from such species is used for environmental monitoring of oil pollution. Some substituted organic compounds are also fluorescent. For example 1,4-bis(5-phenyloxazol-2-yl)benzene (POPOP) is used in scintillation counting and acridine orange is often used as a DNA stain. Pyridine 1 and rhodamine are frequently used in dye lasers.

Numerous additional examples of probes could be presented. Instead of listing them here, examples will appear throughout the book, with a description of the spectral properties of the individual fluorophores. An overview of fluorophores used for research and fluorescence sensing is presented in Chapter 3. In contrast to aromatic organic mol-

ecules, atoms are generally nonfluorescent in condensed phases. One notable exception is the group of elements commonly known as the lanthanides.⁴ The fluorescence from europium and terbium ions results from electronic transitions between *f* orbitals. These orbitals are shielded from the solvent by higher filled orbitals. The lanthanides display long decay times because of this shielding and low emission rates because of their small extinction coefficients.

Fluorescence spectral data are generally presented as emission spectra. A fluorescence emission spectrum is a plot of the fluorescence intensity versus wavelength (nanometers) or wavenumber (cm^{-1}). Two typical fluorescence emission spectra are shown in Figure 1.3. Emission spectra vary widely and are dependent upon the chemical structure of the fluorophore and the solvent in which it is dissolved. The spectra of some compounds, such as perylene, show significant structure due to the individual vibrational energy levels of the ground and excited states. Other compounds, such as quinine, show spectra devoid of vibrational structure.

An important feature of fluorescence is high sensitivity detection. The sensitivity of fluorescence was used in 1877 to demonstrate that the rivers Danube and Rhine were connected by underground streams.⁵ This connection was demonstrated by placing fluorescein (Figure 1.1) into the Danube. Some sixty hours later its characteristic green fluorescence appeared in a small river that led to the Rhine. Today fluorescein is still used as an emergency marker for locating individuals at sea, as has been seen on the landing of space capsules in the Atlantic Ocean. Readers interested in the history of fluorescence are referred to the excellent summary by Berlman.⁵

1.2. JABLONSKI DIAGRAM

The processes that occur between the absorption and emission of light are usually illustrated by the Jablonski⁶ diagram. Jablonski diagrams are often used as the starting point for discussing light absorption and emission. Jablonski diagrams are used in a variety of forms, to illustrate various molecular processes that can occur in excited states. These diagrams are named after Professor Alexander Jablonski (Figure 1.4), who is regarded as the father of fluorescence spectroscopy because of his many accomplishments, including descriptions of concentration depolarization and defining the term "anisotropy" to describe the polarized emission from solutions.^{7,8}

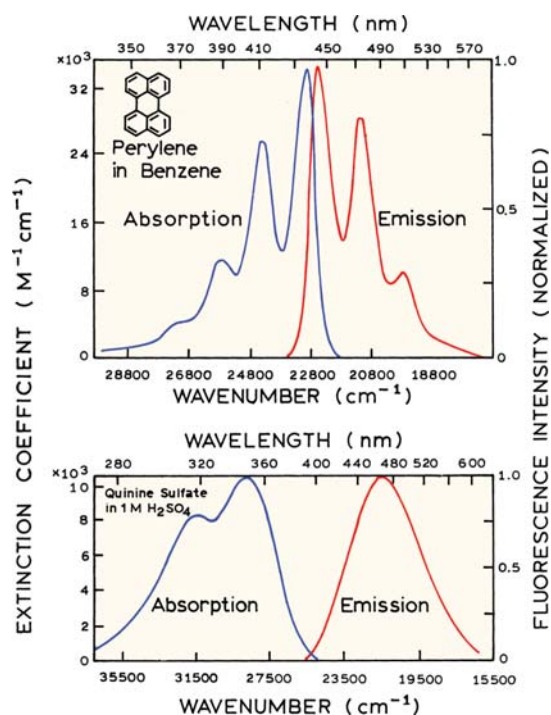


Figure 1.3. Absorption and fluorescence emission spectra of perylene and quinine. Emission spectra cannot be correctly presented on both the wavelength and wavenumber scales. The wavenumber presentation is correct in this instance. Wavelengths are shown for convenience. See Chapter 3. Revised from [5].

Brief History of Alexander Jablonski

Professor Jablonski was born February 26, 1898 in Voskresenovka, Ukraine. In 1916 he began his study of atomic physics at the University of Kharkov, which was interrupted by military service first in the Russian Army and later in the newly organized Polish Army during World War I. At the end of 1918, when an independent Poland was re-created after more than 120 years of occupation by neighboring powers, Jablonski left Kharkov and arrived in Warsaw, where he entered the University of Warsaw to continue his study of physics. His study in Warsaw was again interrupted in 1920 by military service during the Polish-Bolshevik war.

An enthusiastic musician, Jablonski played first violin at the Warsaw Opera from 1921 to 1926 while studying at the university under Stefan Pienkowski. He received his doctorate in 1930 for work "On the influence of the change of wavelengths of excitation light on the fluorescence spectra." Although Jablonski left the opera in 1926 and devoted himself entirely to scientific work, music remained his great passion until the last days of his life.



Figure 1.4. Professor Alexander Jablonski (1898–1980), circa 1935. Courtesy of his daughter, Professor Danuta Frackowiak.

Throughout the 1920s and 30s the Department of Experimental Physics at Warsaw University was an active center for studies on luminescence under S. Pienkowski. During most of this period Jablonski worked both theoretically and experimentally on the fundamental problems of photoluminescence of liquid solutions as well as on the pressure effects on atomic spectral lines in gases. A problem that intrigued Jablonski for many years was the polarization of photoluminescence of solutions. To explain the experimental facts he distinguished the transition moments in absorption and in emission and analyzed various factors responsible for the depolarization of luminescence.

Jablonski's work was interrupted once again by a world war. From 1939 to 1945 Jablonski served in the Polish Army, and spent time as a prisoner of first the German Army and then the Soviet Army. In 1946 he returned to Poland to chair a new Department of Physics in the new Nicholas Copernicus University in Torun. This beginning occurred in the very difficult postwar years in a country totally destroyed by World War II. Despite all these difficulties, Jablonski with great energy organized the Department of Physics at the university, which became a scientific center for studies in atomic and molecular physics.

His work continued beyond his retirement in 1968. Professor Jablonski created a spectroscopic school of thought that persists today through his numerous students, who now occupy positions at universities in Poland and elsewhere. Professor Jablonski died on September 9, 1980. More complete accounts of his accomplishments are given in [7] and [8].

A typical Jablonski diagram is shown in Figure 1.5. The singlet ground, first, and second electronic states are depicted by S_0 , S_1 , and S_2 , respectively. At each of these electronic energy levels the fluorophores can exist in a number of vibrational energy levels, depicted by 0, 1, 2, etc. In this Jablonski diagram we excluded a number of interactions that will be discussed in subsequent chapters, such as quenching, energy transfer, and solvent interactions. The transitions between states are depicted as vertical lines to illustrate the instantaneous nature of light absorption. Transitions occur in about 10^{-15} s, a time too short for significant displacement of nuclei. This is the Franck-Condon principle.

The energy spacing between the various vibrational energy levels is illustrated by the emission spectrum of perylene (Figure 1.3). The individual emission maxima (and hence vibrational energy levels) are about 1500 cm^{-1} apart. At room temperature thermal energy is not adequate to significantly populate the excited vibrational states. Absorption and emission occur mostly from molecules with the lowest vibrational energy. The larger energy difference between the S_0 and S_1 excited states is too large for thermal population of S_1 . For this reason we use light and not heat to induce fluorescence.

Following light absorption, several processes usually occur. A fluorophore is usually excited to some higher vibrational level of either S_1 or S_2 . With a few rare exceptions, molecules in condensed phases rapidly relax to the lowest vibrational level of S_1 . This process is called internal conversion and generally occurs within 10^{-12} s or less. Since fluorescence lifetimes are typically near 10^{-8} s, internal conversion is generally complete prior to emission. Hence, fluorescence emission generally results from a thermally equilibrated excited state, that is, the lowest energy vibrational state of S_1 .

Return to the ground state typically occurs to a higher excited vibrational ground state level, which then quickly (10^{-12} s) reaches thermal equilibrium (Figure 1.5). Return to an excited vibrational state at the level of the S_0 state is the reason for the vibrational structure in the emission spectrum of perylene. An interesting consequence of emission to higher vibrational ground states is that the emission spec-

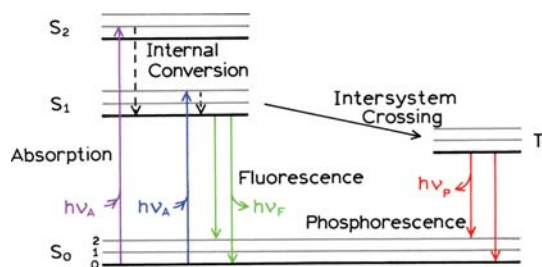


Figure 1.5. One form of a Jablonski diagram.

trum is typically a mirror image of the absorption spectrum of the $S_0 \rightarrow S_1$ transition. This similarity occurs because electronic excitation does not greatly alter the nuclear geometry. Hence the spacing of the vibrational energy levels of the excited states is similar to that of the ground state. As a result, the vibrational structures seen in the absorption and the emission spectra are similar.

Molecules in the S_1 state can also undergo a spin conversion to the first triplet state T_1 . Emission from T_1 is termed phosphorescence, and is generally shifted to longer wavelengths (lower energy) relative to the fluorescence. Conversion of S_1 to T_1 is called intersystem crossing. Transition from T_1 to the singlet ground state is forbidden, and as a result the rate constants for triplet emission are several orders of magnitude smaller than those for fluorescence. Molecules containing heavy atoms such as bromine and iodine are frequently phosphorescent. The heavy atoms facilitate intersystem crossing and thus enhance phosphorescence quantum yields.

1.3. CHARACTERISTICS OF FLUORESCENCE EMISSION

The phenomenon of fluorescence displays a number of general characteristics. Exceptions are known, but these are infrequent. Generally, if any of the characteristics described in the following sections are not displayed by a given fluorophore, one may infer some special behavior for this compound.

1.3.1. The Stokes Shift

Examination of the Jablonski diagram (Figure 1.5) reveals that the energy of the emission is typically less than that of absorption. Fluorescence typically occurs at lower energies or longer wavelengths. This phenomenon was first observed by Sir. G. G. Stokes in 1852 at the University of Cambridge.⁹ These early experiments used relatively simple

instrumentation (Figure 1.6). The source of ultraviolet excitation was provided by sunlight and a blue glass filter, which was part of a stained glass window. This filter selectively transmitted light below 400 nm, which was absorbed by quinine (Figure 1.6). The incident light was prevented from reaching the detector (eye) by a yellow glass (of wine) filter. Quinine fluorescence occurs near 450 nm and is therefore easily visible.

It is interesting to read Sir George's description of the observation. The following is from his report published in 1852:⁹

On the Change of Refrangibility of Light. By G. G. Stokes, M.A., F.R.S., Fellow of Pembroke College, and Lucasian Professor of Mathematics in the University of Cambridge. *Phil. Trans. Royal Society of London* (1852) pp. 463-562.
Received May 11, — Read May 27, 1852.

"The following researches originated in a consideration of the very remarkable phenomenon discovered by Sir John Herschel in a solution of sulphate of quinine, and described by him in two papers printed in the Philosophical Transactions for 1845, entitled "On a Case of Superficial Colour presented by a Homogeneous Liquid internally colourless," and "On the Epipolic Dispersion of Light." The solution of quinine, though it appears to be perfectly transparent and colourless, like water, when viewed by transmitted light, exhibits nevertheless in certain aspects, and under certain incidences of the light, a beautiful celestial blue colour. It appears from the experiments of Sir John Herschel that the blue colour comes only from a stratum of fluid of small but finite thickness adjacent to the surface by which the light enters. After passing through this stratum, the incident light, though not sensibly enfeebled nor coloured, has lost the power of producing the same effect, and therefore may be con-

sidered as in some way or other qualitatively different from the original light."

Careful reading of this paragraph reveals several important characteristics of fluorescent solutions. The quinine solution is colorless because it absorbs in the ultraviolet, which we cannot see. The blue color comes only from a region near the surface. This is because the quinine solution was relatively concentrated and absorbed all of the UV in the first several millimeters. Hence Stokes observed the inner filter effect. After passing through the solution the light was "enfeebled" and no longer capable of causing the blue glow. This occurred because the UV was removed and the "enfeebled" light could no longer excite quinine. However, had Sir George used a second solution of fluorescein, rather than quinine, it would have still been excited because of the longer absorption wavelength of fluorescein.

Energy losses between excitation and emission are observed universally for fluorescent molecules in solution. One common cause of the Stokes shift is the rapid decay to the lowest vibrational level of S_1 . Furthermore, fluorophores generally decay to higher vibrational levels of S_0 (Figure 1.5), resulting in further loss of excitation energy by thermalization of the excess vibrational energy. In addition to these effects, fluorophores can display further Stokes shifts due to solvent effects, excited-state reactions, complex formation, and/or energy transfer.

Brief History of Sir. G. G. Stokes:

Professor Stokes was born in Ireland, August 3, 1819 (Figure 1.7). He entered Pembroke College, Cambridge, in 1837, and was elected as a fellow of Pembroke immediately upon his graduation in 1841. In 1849 Stokes became Lucasian Professor at Cambridge, a chair once held by Newton. Because of poor endowment for the chair, he also worked in the Government School of Mines.

Stokes was involved with a wide range of scientific problems, including hydrodynamics, elasticity of solids, and diffraction of light. The wave theory of light was already known when he entered Cambridge. In his classic paper on quinine, he understood that light of a higher "refrangibility" or frequency was responsible for the blue glow of lower refrangibility or frequency. Thus invisible ultraviolet rays were absorbed to produce the blue light at the surface. Stokes later suggested using optical properties such as absorption, colored reflection, and fluorescence, to identify organic substances.

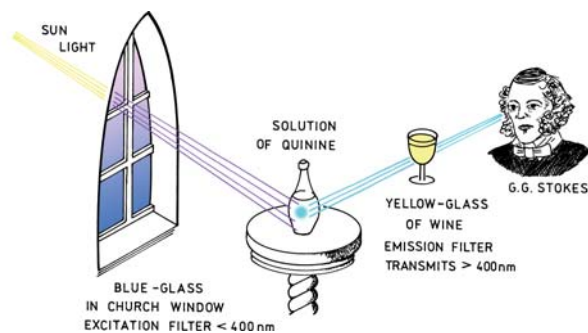


Figure 1.6. Experimental schematic for detection of the Stokes shift.

Later in life Stokes was universally honored with degrees and medals. He was knighted in 1889 and became Master of Pembroke College in 1902. After the 1850s, Stokes became involved in administrative matters, and his scientific productivity decreased. Some things never change. Professor Stokes died February 1, 1903.

1.3.2. Emission Spectra Are Typically Independent of the Excitation Wavelength

Another general property of fluorescence is that the same fluorescence emission spectrum is generally observed irrespective of the excitation wavelength. This is known as Kasha's rule,¹⁰ although Vavilov reported in 1926 that quantum yields were generally independent of excitation wavelength.⁵ Upon excitation into higher electronic and vibrational levels, the excess energy is quickly dissipated, leaving the fluorophore in the lowest vibrational level of S_1 . This relaxation occurs in about 10^{-12} s, and is presumably a result of a strong overlap among numerous states of nearly equal energy. Because of this rapid relaxation, emission spectra are usually independent of the excitation wavelength. Exceptions exist, such as fluorophores that exist in two ionization states, each of which displays distinct absorption and emission spectra. Also, some molecules are known to emit from the S_2 level, but such emission is rare and generally not observed in biological molecules.

It is interesting to ask why perylene follows the mirror-image rule, but quinine emission lacks the two peaks seen in its excitation spectrum at 315 and 340 nm (Figure 1.3). In the case of quinine, the shorter wavelength absorption peak is due to excitation to the second excited state (S_2), which relaxes rapidly to S_1 . Emission occurs predominantly from the lowest singlet state (S_1), so emission from S_2 is not observed. The emission spectrum of quinine is the mirror image of the $S_0 \rightarrow S_1$ absorption of quinine, not of its total absorption spectrum. This is true for most fluorophores: the emission is the mirror image of $S_0 \rightarrow S_1$ absorption, not of the total absorption spectrum.

The generally symmetric nature of these spectra is a result of the same transitions being involved in both absorption and emission, and the similar vibrational energy levels of S_0 and S_1 . In most fluorophores these energy levels are not significantly altered by the different electronic distributions of S_0 and S_1 . Suppose the absorption spectrum of a fluorophore shows distinct peaks due to the vibrational energy levels. Such peaks are seen for anthracene in Figure



Figure 1.7. Sir George Gabriel Stokes, 1819–1903, Lucasian Professor at Cambridge. Reproduced courtesy of the Library and Information Centre, Royal Society of Chemistry.

1.8. These peaks are due to transitions from the lowest vibrational level of the S_0 state to higher vibrational levels of the S_1 state. Upon return to the S_0 state the fluorophore can return to any of the ground state vibrational levels. These vibrational energy levels have similar spacing to those in the S_1 state. The emission spectrum shows the same vibrational energy spacing as the absorption spectrum. According to the Franck-Condon principle, all electronic transitions are vertical, that is, they occur without change in the position of the nuclei. As a result, if a particular transition probability (Franck-Condon factor) between the 0th and 1st vibrational levels is largest in absorption, the reciprocal transition is also most probable in emission (Figure 1.8).

A rigorous test of the mirror-image rule requires that the absorption and emission spectra be presented in appropriate units.¹² The closest symmetry should exist between the modified spectra $\epsilon(\bar{\nu})/\bar{\nu}$ and $F(\bar{\nu})/\bar{\nu}^3$, where $\epsilon(\bar{\nu})$ is the extinction coefficient at wavenumber ($\bar{\nu}$), and $F(\bar{\nu})$ is the relative photon flux over a wavenumber increment $\Delta\bar{\nu}$. Agreement between these spectra is generally found for polynuclear aromatic hydrocarbons.

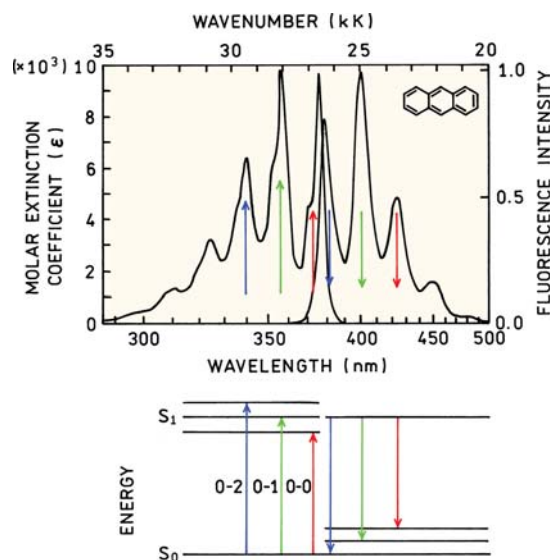


Figure 1.8. Mirror-image rule and Franck-Condon factors. The absorption and emission spectra are for anthracene. The numbers 0, 1, and 2 refer to vibrational energy levels. From [11].

1.3.3. Exceptions to the Mirror-Image Rule

Although often true, many exceptions to the mirror-image rule occur. This is illustrated for the pH-sensitive fluorophore 1-hydroxypyrene-3,6,8-trisulfonate (HPTS) in Figure 1.9. At low pH the hydroxyl group is protonated. The absorption spectrum at low pH shows vibrational structure typical of an aromatic hydrocarbon. The emission spectrum shows a large Stokes shift and none of the vibrational structure seen in the absorption spectrum. The difference between the absorption and emission spectra is due to ionization of the hydroxyl group. The dissociation constant (pK_a) of the hydroxyl group decreases in the excited state, and this group becomes ionized. The emission occurs from a different molecular species, and this ionized species displays a broad spectrum. This form of HPTS with an ionized hydroxyl group can be formed at pH 13. The emission spectrum is a mirror image of the absorption of the high pH form of HPTS.

Changes in pK_a in the excited state also occur for biochemical fluorophores. For example, phenol and tyrosine each show two emissions, the long-wavelength emission being favored by a high concentration of proton acceptors. The pK_a of the phenolic hydroxyl group decreases from 11 in the ground state to 4 in the excited state. Following excitation, the phenolic proton is lost to proton acceptors in the solution. Depending upon the concentration of these acceptors, either the phenol or the phenolate emission may dominate the emission spectrum.

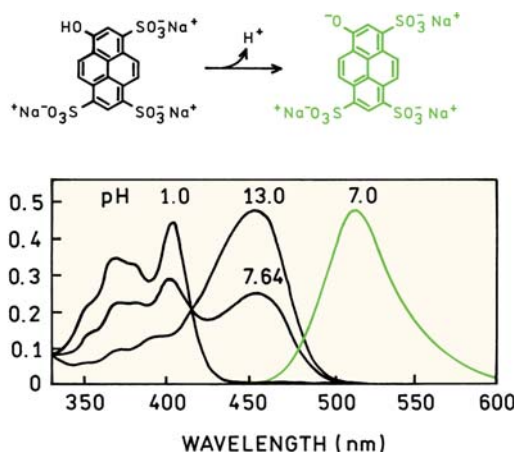


Figure 1.9. Absorption (pH 1, 7.64, and 13) and emission spectra (pH 7) of 1-hydroxypyrene-3,6,8-trisulfonate in water. From [11].

Excited-state reactions other than proton dissociation can also result in deviations from the mirror symmetry rule. One example is shown in Figure 1.10, which shows the emission spectrum of anthracene in the presence of diethylaniline.¹³ The structured emission at shorter wavelengths is a mirror image of the absorption spectrum of anthracene. The unstructured emission at longer wavelengths is due to formation of a charge-transfer complex between the excited state of anthracene and diethylaniline. The unstructured emission is from this complex. Many polynuclear aromatic hydrocarbons, such as pyrene and perylene, also form charge-transfer complexes with amines. These excited-state complexes are referred to as exciplexes.

Some fluorophores can also form complexes with themselves. The best known example is pyrene. At low concentrations pyrene displays a highly structured emission (Figure 1.11). At higher concentrations the previously invisible UV emission of pyrene becomes visible at 470 nm. This long-wavelength emission is due to excimer formation. The term "excimer" is an abbreviation for an excited-state dimer.

1.4. FLUORESCENCE LIFETIMES AND QUANTUM YIELDS

The fluorescence lifetime and quantum yield are perhaps the most important characteristics of a fluorophore. Quantum yield is the number of emitted photons relative to the number of absorbed photons. Substances with the largest quantum yields, approaching unity, such as rhodamines, display the brightest emissions. The lifetime is also important, as it determines the time available for the fluorophore

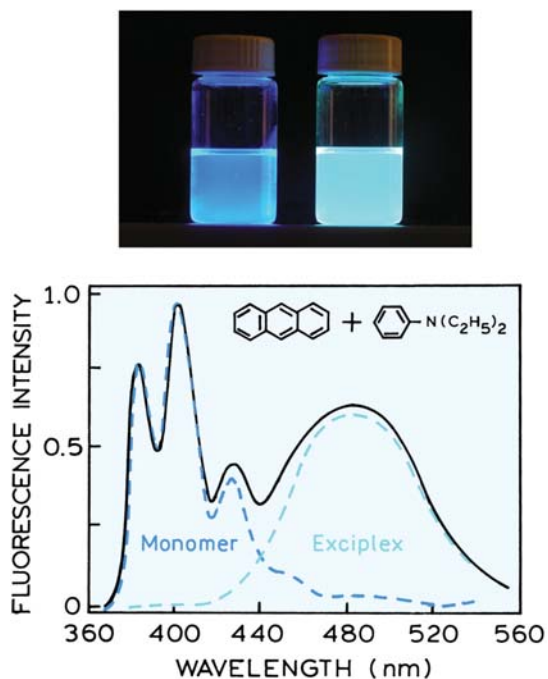


Figure 1.10. Emission spectrum of anthracene in toluene containing 0.2 M diethylaniline. The dashed lines show the emission spectra of anthracene or its exciplex with diethylaniline. Figure revised from [13], photo from [14].

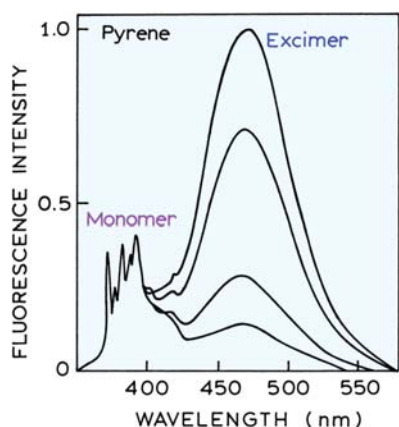


Figure 1.11. Emission spectra of pyrene and its excimer. The relative intensity of the excimer peak (470 nm) decreases as the total concentration of pyrene is decreased from 6×10^{-3} M (top) to 0.9×10^{-4} M (bottom). Reproduced with permission from John Wiley and Sons Inc. From [12].

to interact with or diffuse in its environment, and hence the information available from its emission.

The meanings of quantum yield and lifetime are best represented by a simplified Jablonski diagram (Figure 1.12). In this diagram we do not explicitly illustrate the

individual relaxation processes leading to the relaxed S_1 state. Instead, we focus on those processes responsible for return to the ground state. In particular, we are interested in the emissive rate of the fluorophore (Γ) and its rate of non-radiative decay to S_0 (k_{nr}).

The fluorescence quantum yield is the ratio of the number of photons emitted to the number absorbed. The rate constants Γ and k_{nr} both depopulate the excited state. The fraction of fluorophores that decay through emission, and hence the quantum yield, is given by

$$Q = \frac{\Gamma}{\Gamma + k_{nr}} \quad (1.1)$$

The quantum yield can be close to unity if the radiationless decay rate is much smaller than the rate of radiative decay, that is $k_{nr} < \Gamma$. We note that the energy yield of fluorescence is always less than unity because of Stokes losses. For convenience we have grouped all possible non-radiative decay processes with the single rate constant k_{nr} .

The lifetime of the excited state is defined by the average time the molecule spends in the excited state prior to return to the ground state. Generally, fluorescence lifetimes are near 10 ns. For the fluorophore illustrated in Figure 1.12 the lifetime is

$$\tau = \frac{1}{\Gamma + k_{nr}} \quad (1.2)$$

Fluorescence emission is a random process, and few molecules emit their photons at precisely $t = \tau$. The lifetime is an average value of the time spent in the excited state. For a single exponential decay (eq. 1.13) 63% of the molecules have decayed prior to $t = \tau$ and 37% decay at $t > \tau$.

An example of two similar molecules with different lifetimes and quantum yields is shown in Figure 1.13. The differences in lifetime and quantum yield for eosin and erythrosin B are due to differences in non-radiative decay rates. Eosin and erythrosin B have essentially the same extinction coefficient and the same radiative decay rate (see eq. 1.4). Heavy atoms such as iodine typically result in shorter lifetimes and lower quantum yields.

The lifetime of the fluorophore in the absence of non-radiative processes is called the intrinsic or natural lifetime, and is given by

$$\tau_n = \frac{1}{\Gamma} \quad (1.3)$$

In principle, the natural lifetime τ_n can be calculated from the absorption spectra, extinction coefficient, and

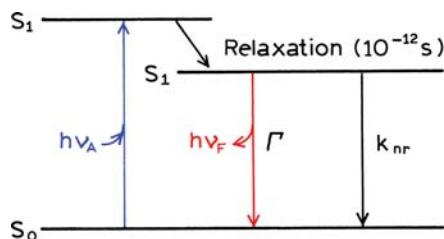


Figure 1.12. A simplified Jablonski diagram to illustrate the meaning of quantum yields and lifetimes.

emission spectra of the fluorophore. The radiative decay rate Γ can be calculated using^{15,16}

$$\begin{aligned} \Gamma &\approx 2.88 \times 10^9 n^2 \frac{\int F(\bar{\nu}) d\bar{\nu}}{\int F(\bar{\nu}) d\bar{\nu} / \bar{\nu}^3} \int \frac{\epsilon(\bar{\nu})}{\bar{\nu}} d\bar{\nu} \\ &= 2.88 \times 10^9 n^2 \langle \bar{\nu}^{-3} \rangle^{-1} \int \frac{\epsilon(\bar{\nu}) d\bar{\nu}}{\bar{\nu}} \end{aligned} \quad (1.4)$$

where $F(\bar{\nu})$ is the emission spectrum plotted on the wavenumber (cm^{-1}) scale, $\epsilon(\bar{\nu})$ is the absorption spectrum, and n is the refractive index of the medium. The integrals are calculated over the $S_0 \rightarrow S_1$ absorption and emission spectra. In many cases this expression works rather well, particularly for solutions of polynuclear aromatic hydrocarbons. For instance, the calculated value¹⁵ of Γ for perylene is $1.8 \times 10^8 \text{ s}^{-1}$, which yields a natural lifetime of 5.5 ns. This value is close to that observed for perylene, which displays a quantum yield near unity. However, there are numerous reasons why eq. 1.4 can fail. This expression assumes no interaction with the solvent, does not consider changes in the refractive index (n) between the absorption

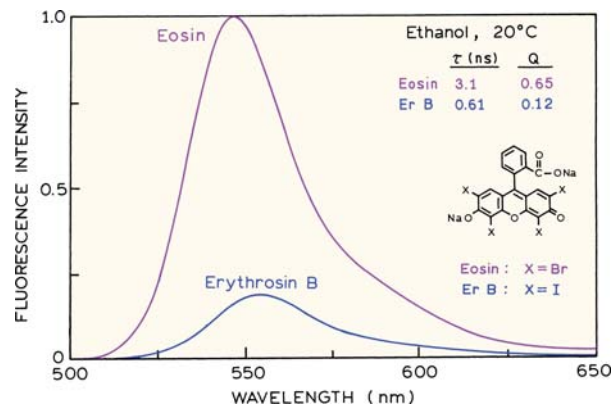


Figure 1.13. Emission spectra of eosin and erythrosin B (ErB).

and emission wavelength, and assumes no change in excited-state geometry. A more complete form of eq. 1.4 (not shown) includes a factor $G = g_l/g_u$ on the right-hand side, where g_l and g_u are the degeneracies of the lower and upper states, respectively. For fluorescence transitions $G = 1$, for phosphorescence transitions $G = 1/3$.

The natural lifetime can be calculated from the measured lifetime (τ) and quantum yield

$$\tau_n = \tau / Q \quad (1.5)$$

which can be derived from eqs. 1.2 and 1.3. Many biochemical fluorophores do not behave as predictably as unsubstituted aromatic compounds. Hence, there is often poor agreement between the value of τ_n calculated from eq. 1.5 and that calculated from its absorption and emission spectra (eq. 1.4). These discrepancies occur for a variety of unknown and known reasons, such as a fraction of the fluorophores located next to quenching groups, which sometimes occurs for tryptophan residues in proteins.

The quantum yield and lifetime can be modified by factors that affect either of the rate constants (Γ or k_{nr}). For example, a molecule may be nonfluorescent as a result of a large rate of internal conversion or a slow rate of emission. Scintillators are generally chosen for their high quantum yields. These high yields are a result of large Γ values. Hence, the lifetimes are generally short: near 1 ns. The fluorescence emission of aromatic substances containing $-\text{NO}_2$ groups are generally weak, primarily as a result of large k_{nr} values. The quantum yields of phosphorescence are extremely small in fluid solutions at room temperature. The triplet-to-singlet transition is forbidden by symmetry, and the rates of spontaneous emission are about 10^3 s^{-1} or smaller. Since k_{nr} values are near 10^9 s^{-1} , the quantum yields of phosphorescence are small at room temperature. From eq. 1.1 one can predict phosphorescence quantum yields of 10^{-6} .

Comparison of the natural lifetime, measured lifetime, and quantum yield can be informative. For example, in the case of the widely used membrane probe 1,6-diphenyl-1,3,5-hexatriene (DPH) the measured lifetime near 10 ns is much longer than that calculated from eq. 1.4, which is near 1.5 ns.¹⁷ In this case the calculation based on the absorption spectrum of DPH is incorrect because the absorption transition is to a state of different electronic symmetry than the emissive state. Such quantum-mechanical effects are rarely seen in more complex fluorophores with heterocyclic atoms.

1.4.1. Fluorescence Quenching

The intensity of fluorescence can be decreased by a wide variety of processes. Such decreases in intensity are called quenching. Quenching can occur by different mechanisms. Collisional quenching occurs when the excited-state fluorophore is deactivated upon contact with some other molecule in solution, which is called the quencher. Collisional quenching is illustrated on the modified Jablonski diagram in Figure 1.14. In this case the fluorophore is returned to the ground state during a diffusive encounter with the quencher. The molecules are not chemically altered in the process. For collisional quenching the decrease in intensity is described by the well-known Stern-Volmer equation:

$$\frac{F_0}{F} = 1 + K[Q] = 1 + k_q\tau_0[Q] \quad (1.6)$$

In this expression K is the Stern-Volmer quenching constant, k_q is the bimolecular quenching constant, τ_0 is the unquenched lifetime, and $[Q]$ is the quencher concentration. The Stern-Volmer quenching constant K indicates the sensitivity of the fluorophore to a quencher. A fluorophore buried in a macromolecule is usually inaccessible to water-soluble quenchers, so that the value of K is low. Larger values of K are found if the fluorophore is free in solution or on the surface of a biomolecule.

A wide variety of molecules can act as collisional quenchers. Examples include oxygen, halogens, amines, and electron-deficient molecules like acrylamide. The mechanism of quenching varies with the fluorophore–quencher pair. For instance, quenching of indole by acrylamide is probably due to electron transfer from indole to acrylamide, which does not occur in the ground state. Quenching by halogen and heavy atoms occurs due to spin–orbit coupling and intersystem crossing to the triplet state (Figure 1.5).

Aside from collisional quenching, fluorescence quenching can occur by a variety of other processes. Fluorophores can form nonfluorescent complexes with quenchers. This process is referred to as static quenching since it occurs in the ground state and does not rely on diffusion or molecular collisions. Quenching can also occur by a variety of trivial, i.e., non-molecular mechanisms, such as attenuation of the incident light by the fluorophore itself or other absorbing species.

1.4.2. Timescale of Molecular Processes in Solution

The phenomenon of quenching provides a valuable context for understanding the role of the excited-state lifetime in

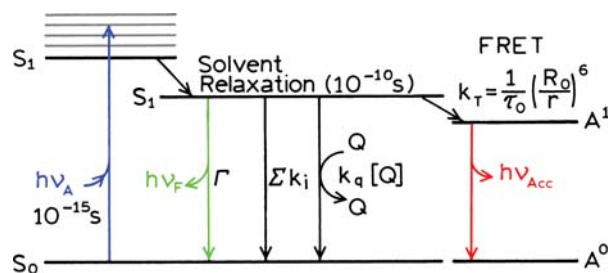


Figure 1.14. Jablonski diagram with collisional quenching and fluorescence resonance energy transfer (FRET). The term Σk_i is used to represent non-radiative paths to the ground state aside from quenching and FRET.

allowing fluorescence measurements to detect dynamic processes in solution or in macromolecules. The basic idea is that absorption is an instantaneous event. According to the Franck-Condon principle, absorption occurs so fast that there is no time for molecular motion during the absorption process. Absorption occurs in the time it takes a photon to travel the length of a photon: in less than 10^{-15} s. As a result, absorption spectroscopy can only yield information on the average ground state of the molecules that absorb light. Only solvent molecules that are immediately adjacent to the absorbing species will affect its absorption spectrum. Absorption spectra are not sensitive to molecular dynamics and can only provide information on the average solvent shell adjacent to the chromophore.

In contrast to absorption, emission occurs over a longer period of time. The length of time fluorescent molecules remain in the excited state provides an opportunity for interactions with other molecules in solution. Collisional quenching of fluorescence by molecular oxygen is an excellent example of the expansion of time and distance provided by the fluorescence lifetime. If a fluorophore in the excited state collides with an oxygen molecule, then the fluorophore returns to the ground state without emission of a photon. The diffusion coefficient (D) of oxygen in water at 25°C is $2.5 \times 10^{-5} \text{ cm}^2/\text{s}$. Suppose a fluorophore has a lifetime of 10 ns. Although 10 ns may appear to be a brief time span, it is in fact quite long relative to the motions of small molecules in fluid solution. The average distance $(\Delta x^2)^{1/2}$ an oxygen molecule can diffuse in 10^{-8} s or 10 ns is given by the Einstein equation:

$$\Delta x^2 = 2D\tau \quad (1.7)$$

The distance is about 70 \AA , which is comparable to the thickness of a biological membrane or the diameter of a protein. Some fluorophores have lifetimes as long as 400

ns, and hence diffusion of oxygen molecules may be observed over distances of 450 Å. Absorption measurements are only sensitive to the immediate environment around the fluorophore, and then only sensitive to the instantaneously averaged environment.

Other examples of dynamic processes in solution involve fluorophore–solvent interactions and rotational diffusion. As was observed by Stokes, most fluorophores display emission at lower energies than their absorption. Most fluorophores have larger dipole moments in the excited state than in the ground state. Rotational motions of small molecules in fluid solution are rapid, typically occurring on a timescale of 40 ps or less. The relatively long timescale of fluorescence allows ample time for the solvent molecules to reorient around the excited-state dipole, which lowers its energy and shifts the emission to longer wavelengths. This process is called solvent relaxation and occurs within 10^{-10} s in fluid solution (Figure 1.14). It is these differences between absorption and emission that result in the high sensitivity of emission spectra to solvent polarity, and the smaller spectral changes seen in absorption spectra. Solvent relaxation can result in substantial Stokes shifts. In proteins, tryptophan residues absorb light at 280 nm, and their fluorescence emission occurs near 350 nm.

1.5. FLUORESCENCE ANISOTROPY

Anisotropy measurements are commonly used in the biochemical applications of fluorescence. Anisotropy measurements provide information on the size and shape of proteins or the rigidity of various molecular environments. Anisotropy measurements have been used to measure protein–protein associations, fluidity of membranes, and for immunoassays of numerous substances.

Anisotropy measurements are based on the principle of photoselective excitation of fluorophores by polarized light. Fluorophores preferentially absorb photons whose electric vectors are aligned parallel to the transition moment of the fluorophore. The transition moment has a defined orientation with respect to the molecular axis. In an isotropic solution, the fluorophores are oriented randomly. Upon excitation with polarized light, one selectively excites those fluorophore molecules whose absorption transition dipole is parallel to the electric vector of the excitation (Figure 1.15). This selective excitation results in a partially oriented population of fluorophores (photoselection), and in partially polarized fluorescence emission. Emission also occurs with the light polarized along a fixed axis in the fluorophore. The

relative angle between these moments determines the maximum measured anisotropy [r_0 , see eq. 10.19]. The fluorescence anisotropy (r) and polarization (P) are defined by

$$r = \frac{I_{\parallel} - I_{\perp}}{I_{\parallel} + 2I_{\perp}} \quad (1.8)$$

$$P = \frac{I_{\parallel} - I_{\perp}}{I_{\parallel} + I_{\perp}} \quad (1.9)$$

where I_{\parallel} and I_{\perp} are the fluorescence intensities of the vertically (\parallel) and horizontally (\perp) polarized emission, when the sample is excited with vertically polarized light. Anisotropy and polarization are both expressions for the same phenomenon, and these values can be interchanged using eqs. 10.3 and 10.4.

Several phenomena can decrease the measured anisotropy to values lower than the maximum theoretical values. The most common cause is rotational diffusion (Figure 1.15). Such diffusion occurs during the lifetime of the excited state and displaces the emission dipole of the fluorophore. Measurement of this parameter provides information about the relative angular displacement of the fluorophore between the times of absorption and emission. In fluid solution most fluorophores rotate extensively in 50 to 100 ps. Hence, the molecules can rotate many times during the 1–10 ns excited-state lifetime, and the orientation of the polarized emission is randomized. For this reason fluorophores in non-viscous solution typically display anisotropies near zero. Transfer of excitation between fluorophores also results in decreased anisotropies.

The effects of rotational diffusion can be decreased if the fluorophore is bound to a macromolecule. For instance, it is known that the rotational correlation time for the protein human serum albumin (HSA) is near 50 ns. Suppose HSA is covalently labeled with a fluorophore whose lifetime is 50 ns. Assuming no other processes result in loss of anisotropy, the expected anisotropy is given by the Perrin equation:¹⁸

$$r = \frac{r_0}{1 + (\tau/\theta)} \quad (1.10)$$

where r_0 is the anisotropy that would be measured in the absence of rotational diffusion, and θ is the rotational correlation time for the diffusion process. In this case binding of the fluorophore to the protein has slowed the probe's rate of rotational motion. Assuming $r_0 = 0.4$, the anisotropy is expected to be 0.20. Smaller proteins have shorter correla-

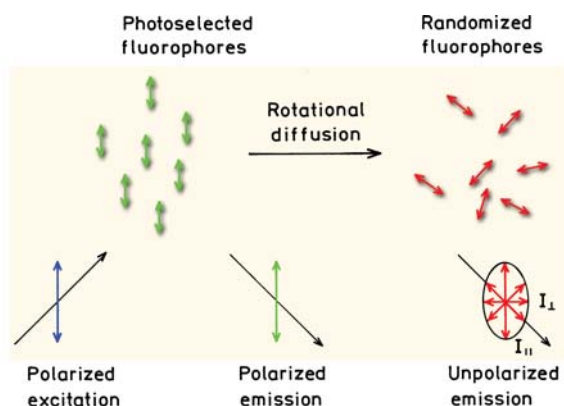


Figure 1.15. Effects of polarized excitation and rotational diffusion on the polarization or anisotropy of the emission.

tion times and are expected to yield lower anisotropies. The anisotropies of larger proteins can also be low if they are labeled with long-lifetime fluorophores. The essential point is that the rotational correlation times for most proteins are comparable to typical fluorescence lifetimes. As a result, measurements of fluorescence anisotropy will be sensitive to any factor that affects the rate of rotational diffusion. The rotational rates of fluorophores in cell membranes also occur on the nanoscale timescale, and the anisotropy values are thus sensitive to membrane composition. For these reasons, measurements of fluorescence polarization are widely used to study the interactions of biological macromolecules.

1.6. RESONANCE ENERGY TRANSFER

Another important process that occurs in the excited state is resonance energy transfer (RET). This process occurs whenever the emission spectrum of a fluorophore, called the donor, overlaps with the absorption spectrum of another molecule, called the acceptor.¹⁹ Such overlap is illustrated in Figure 1.16. The acceptor does not need to be fluorescent. It is important to understand that RET does not involve emission of light by the donor. RET is not the result of emission from the donor being absorbed by the acceptor. Such reabsorption processes are dependent on the overall concentration of the acceptor, and on non-molecular factors such as sample size, and thus are of less interest. There is no intermediate photon in RET. The donor and acceptor are coupled by a dipole–dipole interaction. For these reasons the term RET is preferred over the term fluorescence resonance energy transfer (FRET), which is also in common use.

The extent of energy transfer is determined by the distance between the donor and acceptor, and the extent of spectral overlap. For convenience the spectral overlap (Figure 1.16) is described in terms of the Förster distance (R_0). The rate of energy transfer $k_T(r)$ is given by

$$k_T(r) = \frac{1}{\tau_D} \left(\frac{R_0}{r} \right)^6 \quad (1.11)$$

where r is the distance between the donor (D) and acceptor (A) and τ_D is the lifetime of the donor in the absence of energy transfer. The efficiency of energy transfer for a single donor–acceptor pair at a fixed distance is

$$E = \frac{R_0^6}{R_0^6 + r^6} \quad (1.12)$$

Hence the extent of transfer depends on distance (r). Fortunately, the Förster distances are comparable in size to biological macromolecules: 30 to 60 Å. For this reason energy transfer has been used as a "spectroscopic ruler" for measurements of distance between sites on proteins.²⁰ The value of R_0 for energy transfer should not be confused with the fundamental anisotropies (r_0).

The field of RET is large and complex. The theory is different for donors and acceptors that are covalently linked, free in solution, or contained in the restricted geometries of membranes or DNA. Additionally, depending on donor lifetime, diffusion can increase the extent of energy transfer beyond that predicted by eq. 1.12.

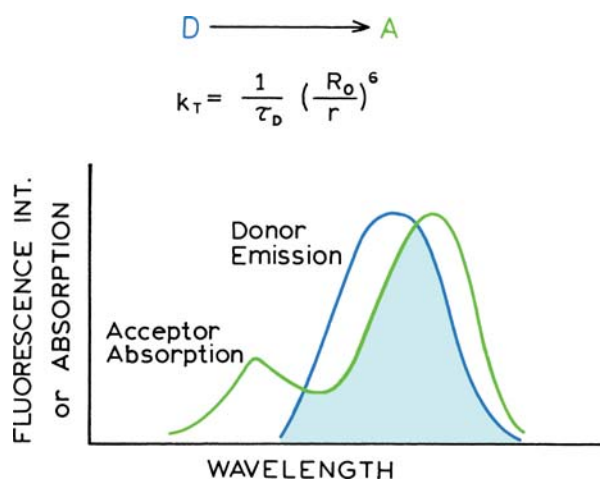


Figure 1.16. Spectral overlap for fluorescence resonance energy transfer (RET).

1.7. STEADY-STATE AND TIME-RESOLVED FLUORESCENCE

Fluorescence measurements can be broadly classified into two types of measurements: steady-state and time-resolved. Steady-state measurements, the most common type, are those performed with constant illumination and observation. The sample is illuminated with a continuous beam of light, and the intensity or emission spectrum is recorded (Figure 1.17). Because of the ns timescale of fluorescence, most measurements are steady-state measurements. When the sample is first exposed to light, steady state is reached almost immediately.

The second type of measurement is time-resolved, which is used for measuring intensity decays or anisotropy decays. For these measurements the sample is exposed to a pulse of light, where the pulse width is typically shorter than the decay time of the sample (Figure 1.17). This intensity decay is recorded with a high-speed detection system that permits the intensity or anisotropy to be measured on the ns timescale.

It is important to understand the relationship between steady-state and time-resolved measurements. A steady-state observation is simply an average of the time-resolved phenomena over the intensity decay of the sample. For instance, consider a fluorophore that displays a single decay time (τ) and a single rotational correlation time (θ). The intensity and anisotropy decays are given by

$$I(t) = I_0 e^{-t/\tau} \quad (1.13)$$

$$r(t) = r_0 e^{-t/\theta} \quad (1.14)$$

where I_0 and r_0 are the intensities and anisotropies at $t = 0$, immediately following the excitation pulse, respectively.

Equations 1.13 and 1.14 can be used to illustrate how the decay time determines what can be observed using fluorescence. The steady-state anisotropy (r) is given by the average of $r(t)$ weighted by $I(t)$:

$$r = \frac{\int_0^\infty r(t)I(t) dt}{\int_0^\infty I(t) dt} \quad (1.15)$$

In this equation the denominator is present to normalize the anisotropy to be independent of total intensity. In the numerator the anisotropy at any time t contributes to the steady-state anisotropy according to the intensity at time t .

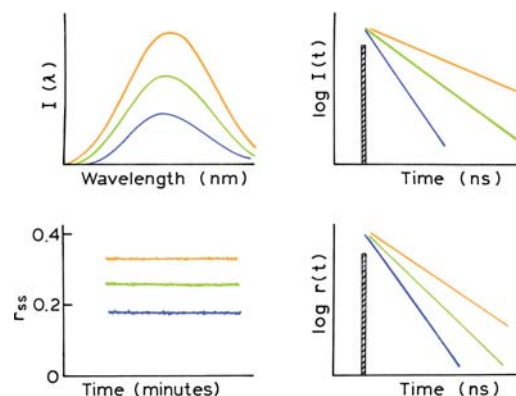


Figure 1.17. Comparison of steady-state and time-resolved fluorescence spectroscopy.

Substitution of eqs. 1.13 and 1.14 into 1.15 yields the Perrin equation, 1.10.

Perhaps a simpler example is how the steady-state intensity (I_{SS}) is related to the decay time. The steady-state intensity is given by

$$I_{SS} = \int_0^\infty I_0 e^{-t/\tau} dt = I_0 \tau \quad (1.16)$$

The value of I_0 can be considered to be a parameter that depends on the fluorophore concentration and a number of instrumental parameters. Hence, in molecular terms, the steady-state intensity is proportional to the lifetime. This makes sense in consideration of eqs. 1.1 and 1.2, which showed that the quantum yield is proportional to the lifetime.

1.7.1. Why Time-Resolved Measurements?

While steady-state fluorescence measurements are simple, nanosecond time-resolved measurements typically require complex and expensive instrumentation. Given the relationship between steady-state and time-resolved measurements, what is the value of these more complex measurements? It turns out that much of the molecular information available from fluorescence is lost during the time averaging process. For example, anisotropy decays of fluorescent macromolecules are frequently more complex than a single exponential (eq. 1.14). The precise shape of the anisotropy decay contains information about the shape of the macromolecule and its flexibility. Unfortunately, this shape information is lost during averaging of the anisotropy over the decay time (eq. 1.15). Irrespective of the form of $r(t)$, eq. 1.15 yields a

single steady-state anisotropy. In principle, the value of r still reflects the anisotropy decay and shape of the molecule. In practice, the information from r alone is not sufficient to reveal the form of $r(t)$ or the shape of the molecule.

The intensity decays also contain information that is lost during the averaging process. Frequently, macromolecules can exist in more than a single conformation, and the decay time of a bound probe may depend on conformation. The intensity decay could reveal two decay times, and thus the presence of more than one conformational state. The steady-state intensity will only reveal an average intensity dependent on a weighted averaged of the two decay times.

There are numerous additional reasons for measuring time-resolved fluorescence. In the presence of energy transfer, the intensity decays reveal how acceptors are distributed in space around the donors. Time-resolved measurements reveal whether quenching is due to diffusion or to complex formation with the ground-state fluorophores. In fluorescence, much of the molecular information content is available only by time-resolved measurements.

1.8. BIOCHEMICAL FLUOROPHORES

Fluorophores are divided into two general classes—intrinsic and extrinsic. Intrinsic fluorophores are those that occur naturally. Extrinsic fluorophores are those added to a sample that does not display the desired spectral properties. In proteins, the dominant fluorophore is the indole group of tryptophan (Figure 1.18). Indole absorbs near 280 nm, and emits near 340 nm. The emission spectrum of indole is highly sensitive to solvent polarity. The emission of indole may be blue shifted if the group is buried within a native protein (N), and its emission may shift to longer wavelengths (red shift) when the protein is unfolded (U).

Membranes typically do not display intrinsic fluorescence. For this reason it is common to label membranes with probes which spontaneously partition into the nonpolar side chain region of the membranes. One of the most commonly used membrane probes is diphenylhexatriene (DPH). Because of its low solubility and quenched emission in water, DPH emission is only seen from membrane-bound DPH (Figure 1.18). Other lipid probes include fluorophores attached to lipid or fatty acid chains.

While DNA contains nitrogenous bases that look like fluorophores, DNA is weakly or nonfluorescent. However, a wide variety of dyes bind spontaneously to DNA—such as acridines, ethidium bromide, and other planar cationic species. For this reason staining of cells with dyes that bind to DNA is widely used to visualize and identify chromosomes. One example of a commonly used DNA probe is

4',6-diamidino-2-phenolindole (DAPI). There is a wide variety of fluorophores that spontaneously bind to DNA.

A great variety of other substances display significant fluorescence. Among biological molecules, one can observe fluorescence from reduced nicotinamide adenine dinucleotide (NADH), from oxidized flavins (FAD, the adenine dinucleotide, and FMN, the mononucleotide), and pyridoxyl phosphate, as well as from chlorophyll. Occasionally, a species of interest is not fluorescent, or is not fluorescent in a convenient region of the UV visible spectrum. A wide variety of extrinsic probes have been developed for labeling the macromolecules in such cases. Two of the most widely used probes, dansyl chloride DNS-Cl, which stands for 1-dimethylamino-5-naphthylsulfonyl chloride, and fluorescein isothiocyanate (FITC), are shown in Figure 1.19. These probes react with the free amino groups of proteins, resulting in proteins that fluoresce at blue (DNS) or green (FITC) wavelengths.

Proteins can also be labeled on free sulfhydryl groups using maleimide reagents such as Bodipi 499/508 maleimide. It is frequently useful to use longer-wavelength probes such as the rhodamine dye Texas Red. Cyanine dyes are frequently used for labeling nucleic acids, as shown for the labeled nucleotide Cy3-4-dUTP. A useful fluorescent probe is one that displays a high intensity, is stable during continued illumination, and does not substantially perturb the biomolecule or process being studied.

1.8.1. Fluorescent Indicators

Another class of fluorophores consists of the fluorescent indicators. These are fluorophores whose spectral properties are sensitive to a substance of interest. One example is Sodium Green, which is shown in Figure 1.20. This fluorophore contains a central azacrown ether, which binds Na^+ . Upon binding of sodium the emission intensity of Sodium Green increases, allowing the amount of Na^+ to be determined. Fluorescent indicators are presently available for a variety of substances, including Ca^{2+} , Mg^{2+} , Na^+ , Cl^- , and O_2 , as well as pH. The applications of fluorescence to chemical sensing is described in Chapter 19.

1.9. MOLECULAR INFORMATION FROM FLUORESCENCE

1.9.1. Emission Spectra and the Stokes Shift

The most dramatic aspect of fluorescence is its occurrence at wavelengths longer than those at which absorption occurs. These Stokes shifts, which are most dramatic for

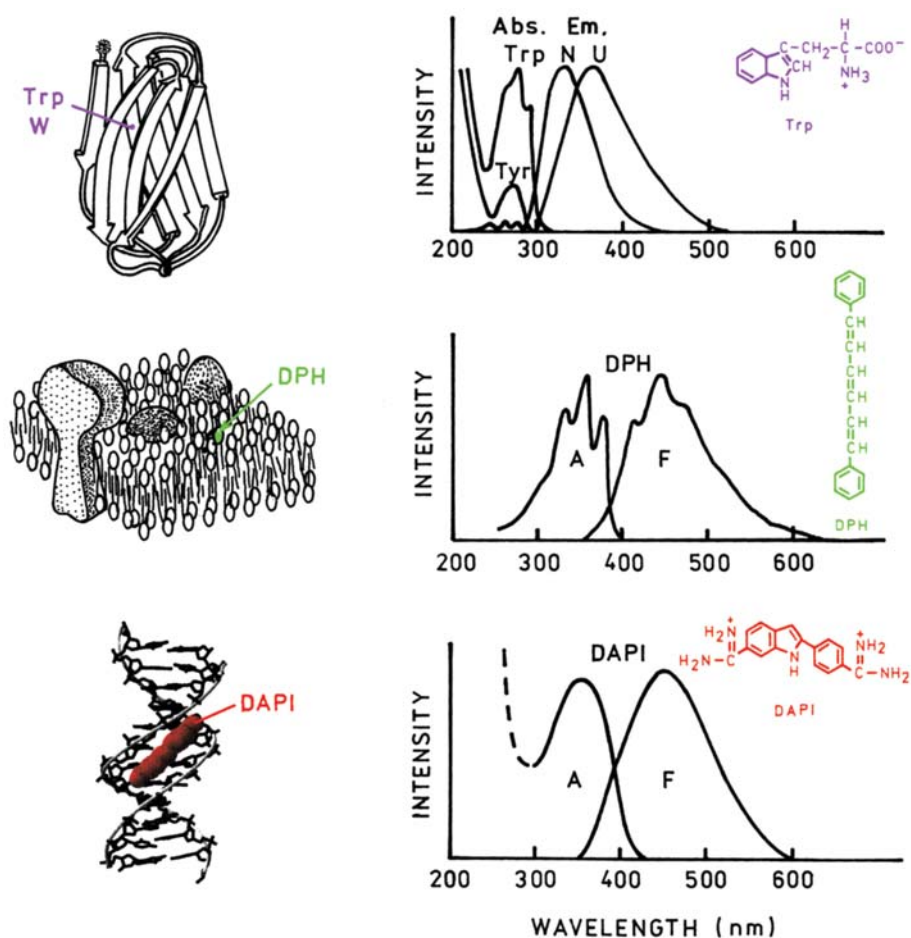


Figure 1.18. Absorption and emission spectra of biomolecules. Top, tryptophan emission from proteins. Middle, spectra of extrinsic membrane probe DPH. Bottom, spectra of the DAPI bound to DNA (---). DNA itself displays very weak emission. Reprinted with permission by Wiley-VCH, STM. From [21].

polar fluorophores in polar solvents, are due to interactions between the fluorophore and its immediate environment. The indole group of tryptophan residues in proteins is one such solvent-sensitive fluorophore, and the emission spectra of indole can reveal the location of tryptophan residues in proteins. The emission from an exposed surface residue will occur at longer wavelengths than that from a tryptophan residue in the protein's interior. This phenomenon was illustrated in the top part of Figure 1.18, which shows a shift in the spectrum of a tryptophan residue upon unfolding of a protein and the subsequent exposure of the tryptophan residue to the aqueous phase. Prior to unfolding, the residue is shielded from the solvent by the folded protein.

A valuable property of many fluorophores is their sensitivity to the surrounding environment. The emission spectra and intensities of extrinsic probes are often used to determine a probe's location on a macromolecule. For example, one of the widely used probes for such studies is

6-(p-toluidinyl)naphthalene-2-sulfonate (TNS), which displays the favorable property of being very weakly fluorescent in water (Figure 1.21). The green emission of TNS in the absence of protein is barely visible in the photographs. Weak fluorescence in water and strong fluorescence when bound to a biomolecule is a convenient property shared by other widely used probes, including many DNA stains. The protein apomyoglobin contains a hydrophobic pocket that binds the heme group. This pocket can also bind other non-polar molecules. Upon the addition of apomyoglobin to a solution of TNS, there is a large increase in fluorescence intensity, as well as a shift of the emission spectrum to shorter wavelengths. This increase in TNS fluorescence reflects the nonpolar character of the heme-binding site of apomyoglobin. TNS also binds to membranes (Figure 1.21). The emission spectrum of TNS when bound to model membranes of dimyristoyl-L- α -phosphatidylcholine (DMPC) is somewhat weaker and at longer wavelengths

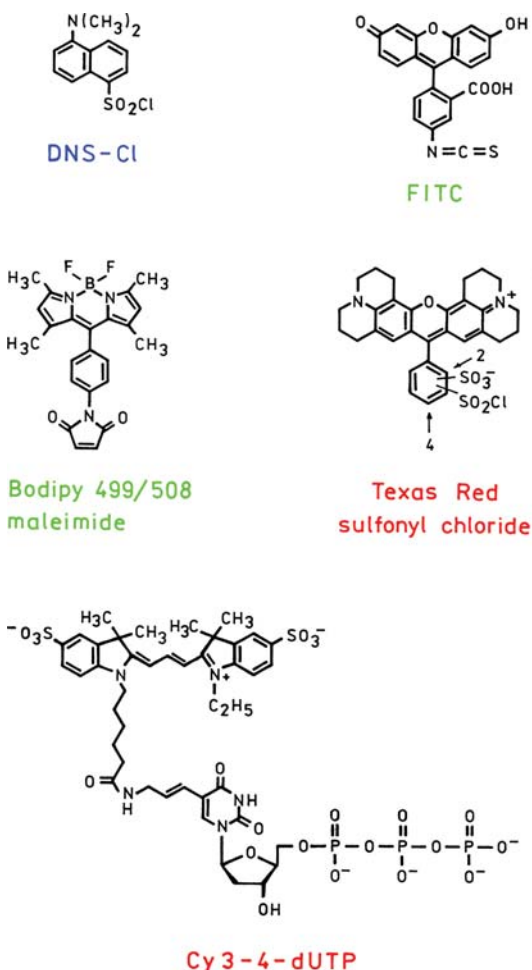


Figure 1.19. Fluorophores for covalent labeling of biomolecules.

compared to that of apomyoglobin. This indicates that the TNS binding sites on the surface of the membrane are more polar. From the emission spectrum it appears that TNS binds to the polar head group region of the membranes, rather than to the nonpolar acyl side chain region. Hence, the emission spectra of solvent-sensitive fluorophores provide information on the location of the binding sites on the macromolecules.

1.9.2. Quenching of Fluorescence

As described in Section 1.4.1, a wide variety of small molecules or ions can act as quenchers of fluorescence, that is, they decrease the intensity of the emission. These substances include iodide (I^-), oxygen, and acrylamide. The accessibility of fluorophores to such quenchers can be used to determine the location of probes on macromolecules, or the porosity of proteins and membranes to quenchers. This

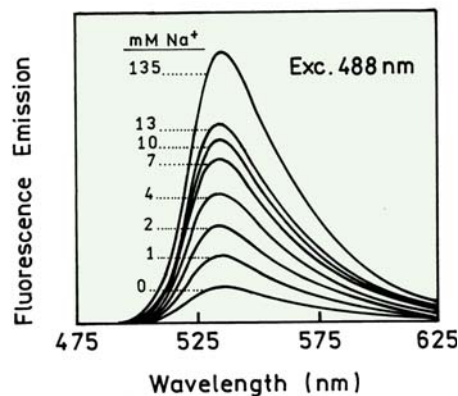
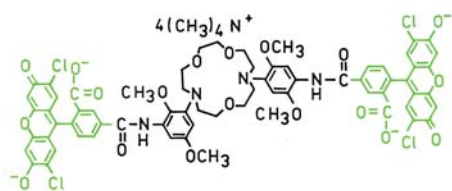


Figure 1.20. Effects of sodium on the emission of Sodium Green. From [22].

concept is illustrated in Figure 1.22, which shows the emission intensity of a protein- or membrane-bound fluorophore in the presence of the water-soluble quencher iodide, I^- . As shown on the right-hand side of the figure, the emission intensity of a tryptophan on the protein's surface (W_2), or on the surface of a cell membrane (P_2 , right), will be decreased in the presence of a water-soluble quencher. The intensity of a buried tryptophan residue (W_1) or of a probe in the membrane interior (P_1) will be less affected by the dissolved iodide (left). The iodide Stern-Volmer quenching constant K in eq. 1.6 will be larger for the exposed fluorophores than for the buried fluorophores. Alternatively, one can add lipid-soluble quenchers, such as brominated fatty acids, to study the interior acyl side chain region of membranes, by measurement from the extent of quenching by the lipid-soluble quencher.

1.9.3. Fluorescence Polarization or Anisotropy

As described in Section 1.5, fluorophores absorb light along a particular direction with respect to the molecular axes. For example, DPH only absorbs light polarized along its long axis (Figure 1.18). The extent to which a fluorophore rotates during the excited-state lifetime determines its polarization or anisotropy. The phenomenon of fluorescence polarization can be used to measure the apparent vol-

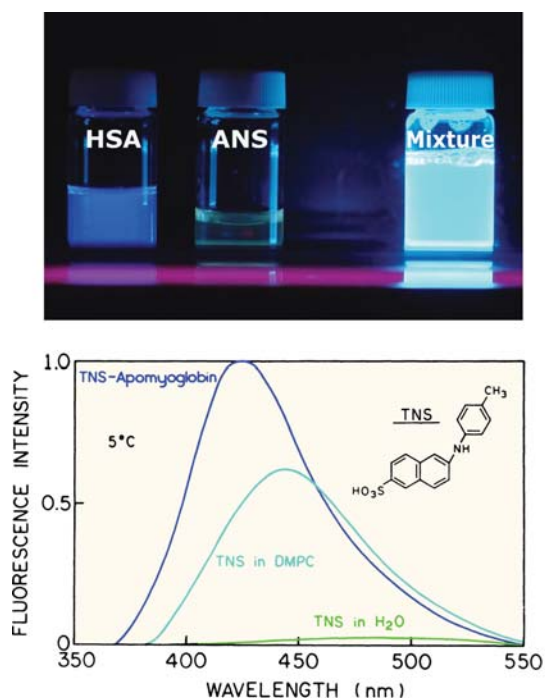


Figure 1.21. Emission spectra of TNS in water, bound to apomyoglobin, and bound to lipid vesicles.

ume (or molecular weight) of proteins. This measurement is possible because larger proteins rotate more slowly. Hence, if a protein binds to another protein, the rotational rate decreases, and the anisotropy(s) increases (Figure 1.23). The rotational rate of a molecule is often described by its rotational correlation time θ , which is related to

$$\theta = \frac{\eta V}{RT} \quad (1.17)$$

where η is the viscosity, V is the molecular volume, R is the gas constant, and T is the temperature in $^{\circ}\text{K}$. Suppose a protein is labeled with DNS-Cl (Figure 1.23). If the protein associates with another protein, the volume increases and so does the rotational correlation time. This causes the anisotropy to increase because of the relationship between the steady-state anisotropy r to the rotational correlation time θ (eq. 1.10).

Fluorescence polarization measurements have also been used to determine the apparent viscosity of the side chain region (center) of membranes. Such measurements of microviscosity are typically performed using a hydrophobic probe like DPH (Figure 1.23), which partitions into the membrane. The viscosity of membranes is known to decrease in the presence of unsaturated fatty acid side

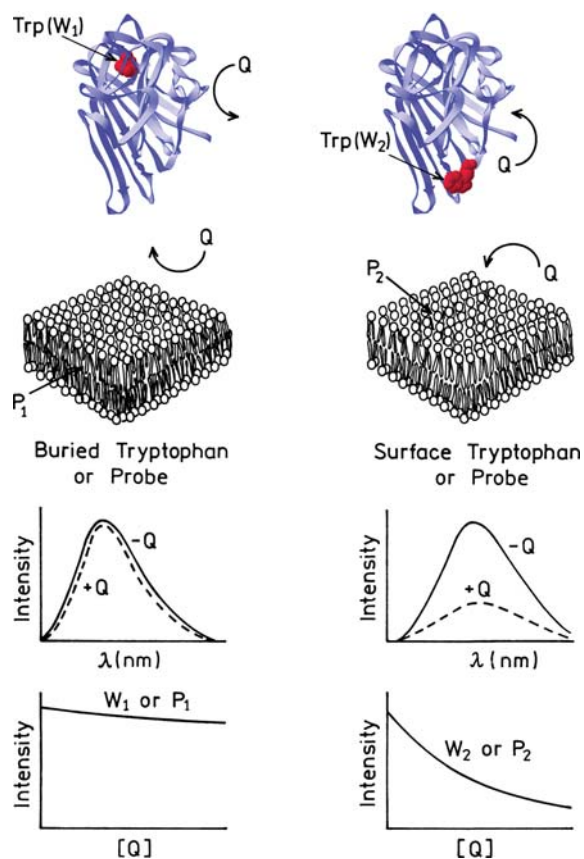


Figure 1.22. Accessibility of fluorophores to the quencher (Q). Reprinted with permission by Wiley-VCH, STM. From [21].

chains. Hence, an increase in the amount of unsaturated fatty acid is expected to decrease the anisotropy. The apparent microviscosity of the membrane is determined by comparing the polarization of the probe measured in the membrane with that observed in solutions of known viscosity.

Anisotropy measurements are widely used in biochemistry, and are even used for clinical immunoassays. One reason for this usage is the ease with which these absolute values can be measured and compared between laboratories.

1.9.4. Resonance Energy Transfer

Resonance energy transfer (RET), sometimes called fluorescence resonance energy transfer (FRET), provides an opportunity to measure the distances between sites on macromolecules. Förster distances are typically in the range of 15 to 60 Å, which is comparable to the diameter of many proteins and to the thickness of membranes. According to eq. 1.12, the distance between a donor and acceptor can be calculated from the transfer efficiency.

The use of RET to measure protein association and distance is shown in Figure 1.24 for two monomers that associate to form a dimer. Suppose one monomer contains a tryptophan residue, and the other a dansyl group. The Förster distance is determined by the spectral overlap of the trp donor emission with the dansyl acceptor absorption. Upon association RET will occur, which decreases the intensity of the donor emission (Figure 1.24). The extent of donor quenching can be used to calculate the donor-to-acceptor distance in the dimer (eq. 1.12). It is also important to notice that RET provides a method to measure protein association because it occurs whenever the donor and acceptor are within the Förster distance.

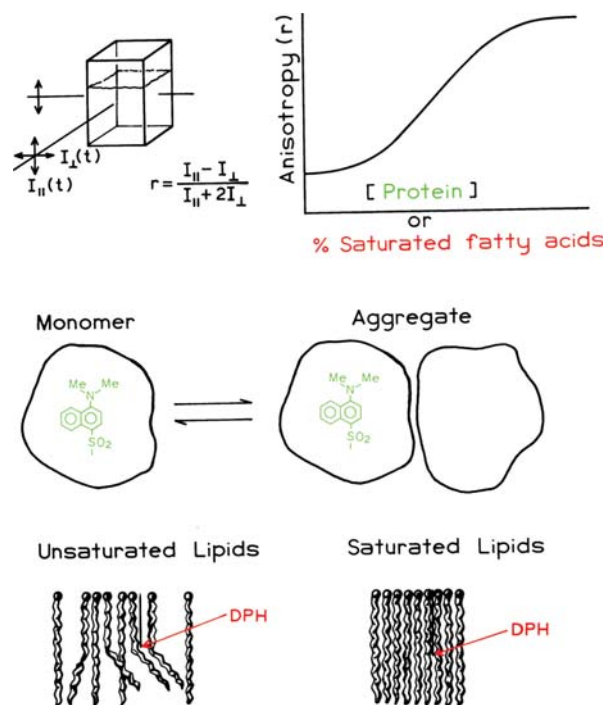


Figure 1.23. Effect of protein association and membrane microviscosity on the fluorescence anisotropy. From [21].

1.10. BIOCHEMICAL EXAMPLES OF BASIC PHENOMENA

The uses of fluorescence in biochemistry can be illustrated by several simple examples. The emission spectra of proteins are often sensitive to protein structure. This sensitivity is illustrated by melittin,²³ which is a 26-amino-acid peptide containing a single tryptophan residue. Depending upon the solution conditions, melittin can exist as a monomer or self-associate to form a tetramer. When this occurs the tryptophan emission maximum shifts to shorter wavelengths (Figure 1.25). These spectra show that a protein association reaction can be followed in dilute solution using simple measurements of the emission spectra.

Association reactions can also be followed by anisotropy measurements. Figure 1.26 shows anisotropy measurements of melittin upon addition of calmodulin.²⁴ Calmodulin does not contain any tryptophan, so the total tryptophan emission is only due to melittin. Upon addition of calmodulin the melittin anisotropy increases about twofold. This effect is due to slower rotational diffusion of the melittin–calmodulin complex as compared to melittin alone. The emission spectra of melittin show that the tryptophan residue becomes shielded from the solvent upon binding to calmodulin. The tryptophan residue is probably located at the interface between the two proteins.

Resonance energy transfer can also be used to study DNA hybridization.²⁵ Figure 1.27 shows complementary DNA oligomers labeled with either fluorescein (Fl) or rhodamine (Rh). Hybridization results in increased RET from fluorescein to rhodamine, and decreased fluorescein intensities (lower panel). Disassociation of the oligomers results in less RET and increased fluorescein intensities. The extent of hybridization can be followed by simple intensity measurements.

RET can also be used to study gene expression. One approach is to use donor- and acceptor-labeled DNA oligomers (Figure 1.28). If a complementary mRNA is present, the oligomers can bind close to each other.²⁶ The RET will result in increased emission intensity from the acceptor. The lower panels show fluorescence microscopy images of human dermal fibroblasts. The cells on the left were not stimulated and did not produce the K-ras gene product. The cells on the right were stimulated to cause expression of the K-ras oncogene. Mutations in the gene are associated with human colorectal cancer.²⁷ The images show the emission intensity of the acceptor. Significant acceptor intensity is only found in the stimulated cells where the mRNA for K-ras is present. RET is now widely used in cellular imaging to detect many types of gene expression and the intracellular proximity of biomolecules.

1.11. NEW FLUORESCENCE TECHNOLOGIES

1.11.1. Multiphoton Excitation

During the past several years technological advances have provided new uses of fluorescence. These technologies have been quickly adopted and are becoming mainstream methods. One of these technologies is two-photon or multi-

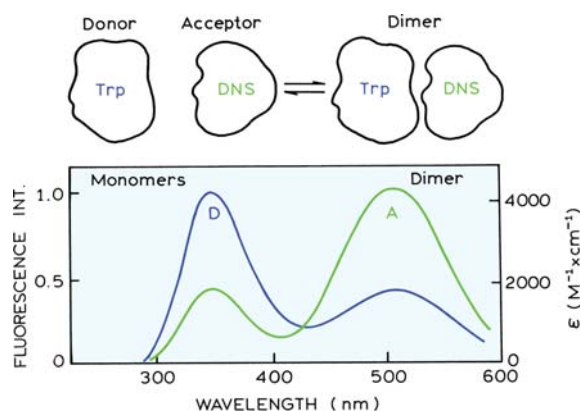


Figure 1.24. Energy transfer between donor- (D) and acceptor- (A) labeled monomers, which associate to form a dimer. In this case the donor is tryptophan and the acceptor DNS.

photon excitation and multiphoton microscopy.^{28–30} Fluorescence is usually excited by absorption of a single photon with a wavelength within the absorption band of the fluorophore. Pulse lasers with femtosecond pulse widths can excite fluorophores by two-photon absorption. Such lasers have become easy to use and available with microscopes. If the laser intensity is high, a fluorophore can simultaneously absorb two long-wavelength photons to reach the first singlet state (Figure 1.29). This process depends strongly on the light intensity and occurs only at the focal point of the laser beam. This can be seen in the photo, where emission is occurring only from a single spot within the sample. Fluorophores outside the focal volume are not excited.

Localized excitation from two-photon excitation has found widespread use in fluorescence microscopy. Multiphoton excitations allow imaging from only the focal plane of a microscope. This is an advantage because fluorescence

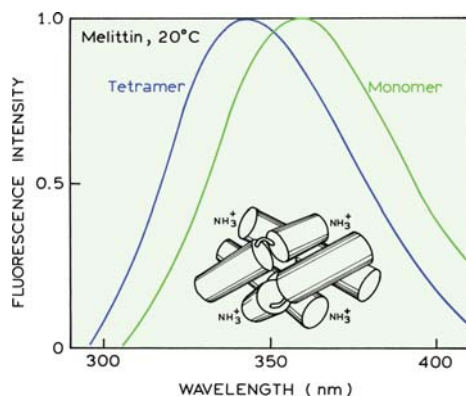


Figure 1.25. Emission spectra of melittin monomer and tetramer. Excitation was at 295 nm. In the schematic structure, the tryptophans are located in the center between the four helices. From [23].

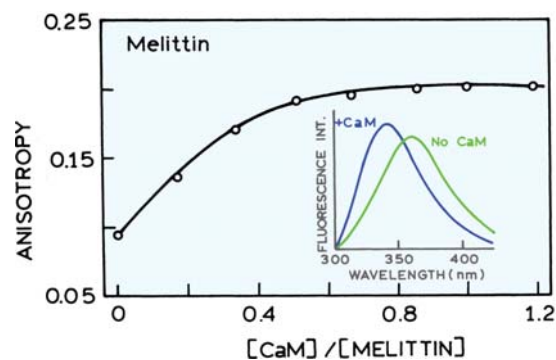


Figure 1.26. Effect of melittin–calmodulin association on the anisotropy of melittin. **Inset:** Emission spectra of melittin in the presence and absence of calmodulin (CaM). Modified from [24].

images are otherwise distorted from fluorescence from above and below the focal plane. Figure 1.30 shows an example of the remarkably sharp images obtainable with multiphoton excitation. The cells were labeled with three probes: DAPI for DNA, Patman for membranes, and tetramethylrhodamine for mitochondria. A single excitation wavelength of 780 nm was used. This wavelength does not excite any of the fluorophores by one-photon absorption, but 780 nm is absorbed by all these fluorophores through a multiphoton process. The images are sharp because there is no actual phase fluorescence that decreases the contrast in non-confocal fluorescence microscopy. Such images are now being obtained in many laboratories.

1.1.1.2. Fluorescence Correlation Spectroscopy

Fluorescence correlation spectroscopy (FCS) has rapidly become a widely used tool to study a wide range of association reactions.³¹ FCS is based on the temporal fluctuations occurring in a small observed volume. Femtoliter volumes can be obtained with localized multiphoton excitation or using confocal optics (Figure 1.31, top). Bursts of photons are seen as single fluorophores diffuse in and out of the laser beam. The method is highly sensitive since only a few fluorophores are observed at one time. In fact, FCS cannot be performed if the solution is too concentrated and there are many fluorophores in the observed volume. Less fluorophores result in more fluctuations, and more fluorophores result in smaller fluctuations and a more constant average signal.

FCS is performed by observing the intensity fluctuations with time (Figure 1.31, middle panel). The rate of fluctuation depends on the rate of fluorophore diffusion. The intensity increases and decreases more rapidly if the

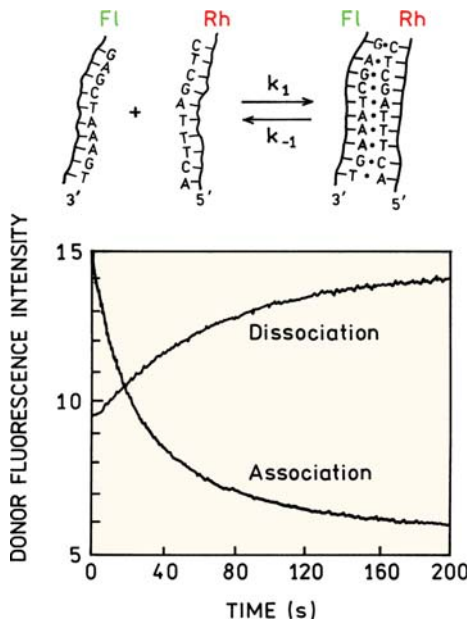


Figure 1.27. DNA hybridization measured by RET between fluorescein (Fl) and rhodamine (Rh). The lower panel shows the fluorescein donor intensities. Revised from [25].

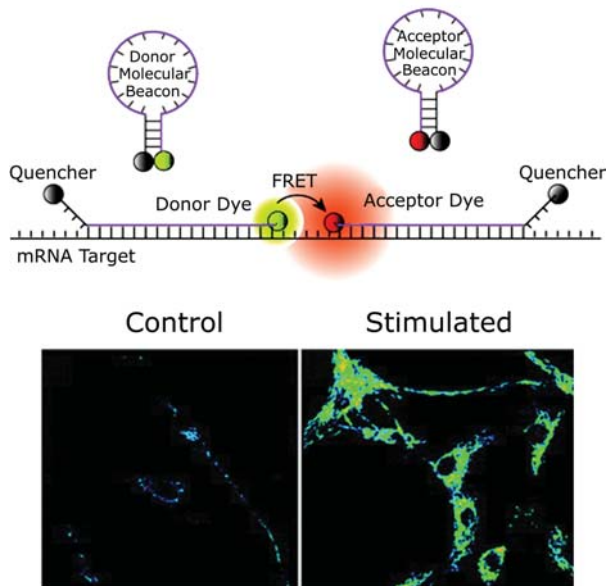


Figure 1.28. Detection of mRNA with RET and molecular beacons. The lower panels show acceptor intensity images of control cells and stimulated fibroblasts expressing the K-ras gene. Revised from [26].

fluorophores diffuse rapidly. If the fluorophores diffuse slowly they remain in the observed volume for a longer period of time and the intensity fluctuations occur more slowly. The amplitude and speed of the fluctuations are used to calculate the correlation function (lower panel). The height of the curve is inversely proportional to the average

number of fluorophores being observed. The position of the curve on the time axis indicates the fluorophore's diffusion coefficient.

Figure 1.32 shows how FCS can be used to study ligand bindings to a single neuronal cell. The ligand was an Alexa-labeled benzodiazepine.³² Benzodiazepines are used to treat anxiety and other disorders. FCS curves are shown for Alexa-Bz in solution and when bound to its receptor. The receptors were present on the membrane of a single neuronal cell where the laser beam was focused. The FCS curve clearly shows binding of Alexa-Bz to the receptor by a 50-fold increase in the diffusion time. Such measurements can be performed rapidly with high sensitivity. FCS will be used increasingly in drug discovery and biotechnology, as well as biochemistry and biophysics.

1.11.3. Single-Molecule Detection

Observations on single molecules represent the highest obtainable sensitivity. Single-molecule detection (SMD) is now being performed in many laboratories.³³⁻³⁴ At present

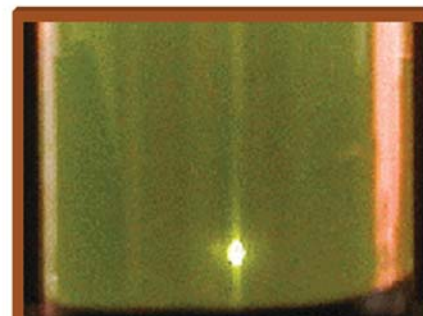
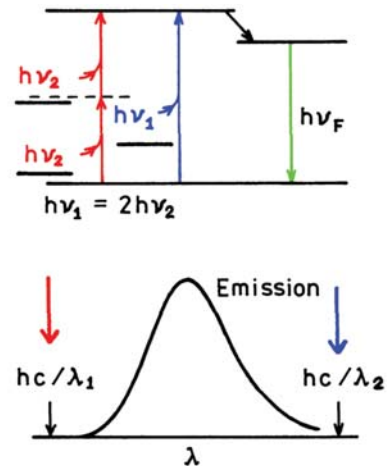


Figure 1.29. Jablonski diagram for two-photon excitation. The photo shows localized excitation at the focal point of the laser beam.

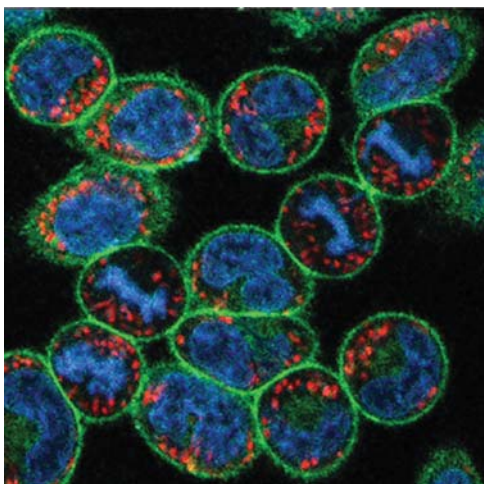


Figure 1.30. Fluorescence image of RBL-3H3 cells stained with DAPI (blue), Patman (green), and tetramethylrhodamine (red). Courtesy of Dr. W. Zipfel and Dr. W. Webb, Cornell University. Reprinted with permission from [30].

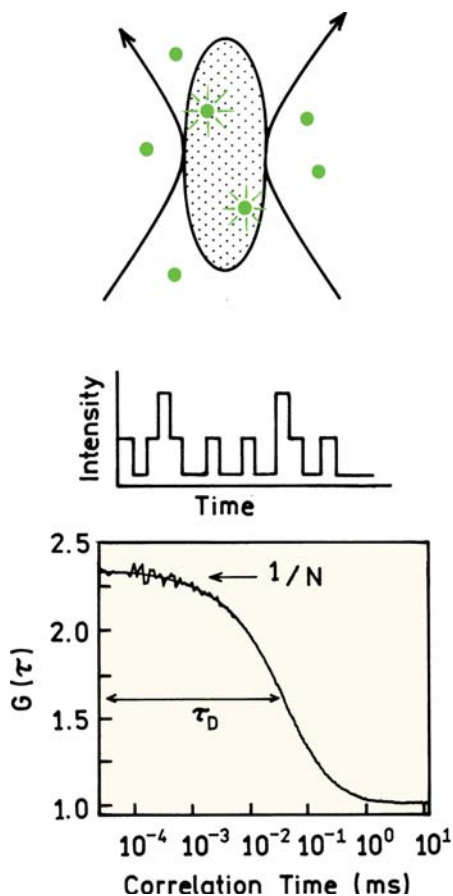


Figure 1.31. Fluorescence correlation spectroscopy. **Top:** observed volume shown as a shaded area. **Middle:** intensity fluctuations. **Bottom:** correlation function.

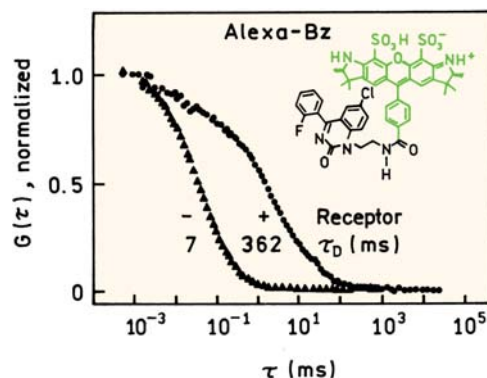


Figure 1.32. FCS of an Alexa-labeled benzodiazepine (Alexa-Bz) in solution and on a single neuronal cell. Revised from [32].

most single-molecule experiments are performed on immobilized fluorophores, with fluorophores chosen for their high quantum yields and photostability (Chapter 23). A typical instrument for SMD consists of laser excitation through microscope objective, a scanning stage to move the sample and confocal optics to reject unwanted signals. SMD is now being extended to include UV-absorbing fluorophores, which was considered unlikely just a short time ago. The probe 2,2'-dimethyl-p-quaterphenyl (DMQ) has an absorption maximum of 275 nm and an emission maximum of 350 nm. Figure 1.33 (left) shows intensity images of DMQ on a quartz cover slip.³⁵ The spots represent the individual DMQ molecules, which can yield signals as high as 70,000 photons per second. The technology for SMD has advanced so rapidly that the lifetimes of single molecules can also be measured at the same time the intensity images are being collected (right). The individual DMQ molecules all display lifetimes near 1.1 ns.

Without the use of SMD, almost all experiments observe a large number of molecules. These measurements reveal the ensemble average of the measured properties. When observing a single molecule there is no ensemble averaging, allowing for the behavior of a single molecule to be studied. Such an experiment is shown in Figure 1.34 for a hairpin ribozyme labeled with a donor and acceptor. Steady-state measurements on a solution of the labeled ribozyme would yield the average amount of energy transfer, but would not reveal the presence of subpopulations showing different amounts of energy transfer. Single-molecule experiments show that an individual ribozyme molecule fluctuates between conformations with lower or higher amounts of energy transfer.³⁶ These conformational changes are seen from simultaneous increases and decreases

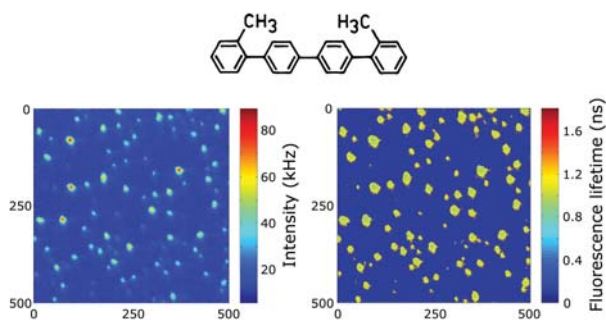


Figure 1.33. Single-molecule intensities and lifetimes of DMQ in a quartz slide. Excitation at 266 nm. Figure courtesy of Dr. S. Seeger, University of Zürich. Reprinted with permission from [35].

es in donor and acceptor emission. The single-molecule experiments also reveal the rate of the conformational changes. Such detailed information is not available from ensemble measurements.

At present single-molecule experiments are mostly performed using cleaned surfaces to minimize background. However, SMD can be extended to intracellular molecules if they are not diffusing too rapidly. One such experiment is detection of single molecules of the oncogen product Ras within cells.³⁷ Ras was labeled with yellow fluorescent pro-

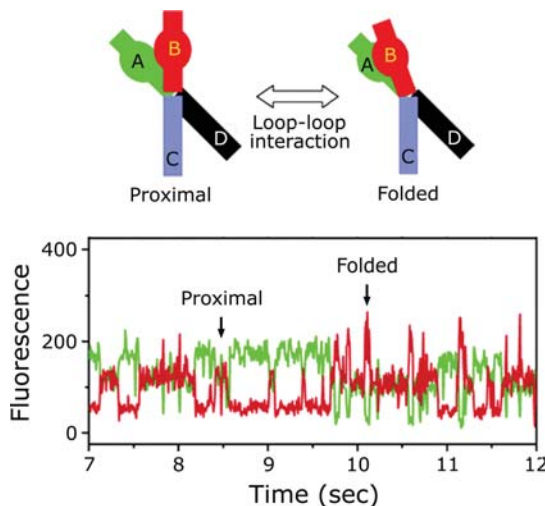


Figure 1.34. Single-molecule RET between a donor (green) and acceptor (red) on a hairpin ribozyme. Revised from [36].

tein (YFP). Upon activation Ras binds GTP (Figure 1.35). In this experiment activated Ras binds GTP labeled with a fluorophore called Bodipy TR. Single molecules of YFP-Ras were imaged on a plasma membrane (lower left). Upon activation of Ras, fluorescent red spots appeared that were

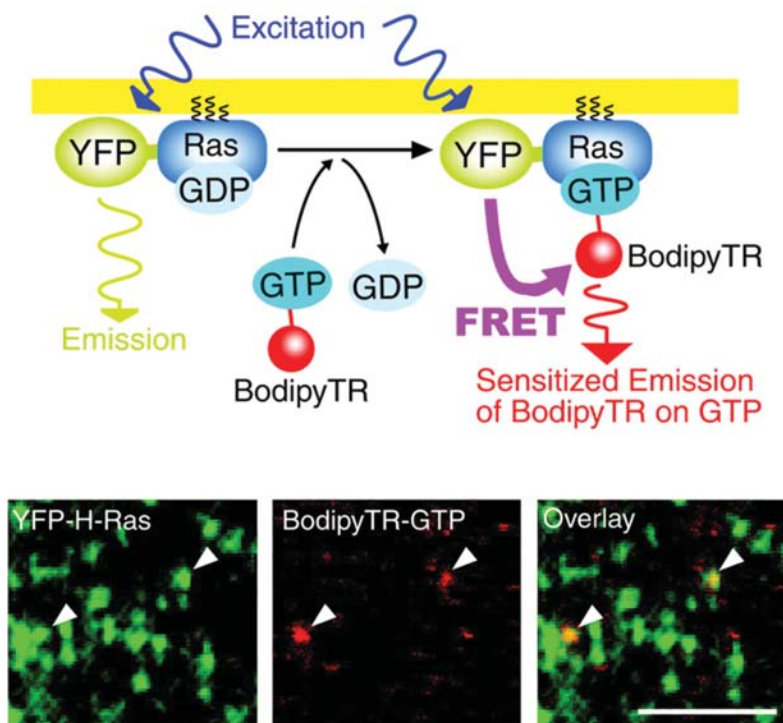


Figure 1.35. Binding of Bodipy TR-labeled GTP to activated YFP-Ras. The lower panels show single-molecule images of YFP-Ras and Bodipy TR-labeled GTP. The overlay of both images shows the location of activated Ras from the plasma membrane of KB cells. Bar = 5 μm. Revised from [37].

due to binding of Bodipy TR-GTP. The regions where emission from both YFP and Bodipy TR is observed corresponds to single copies of the activated Ras protein.

I.12. OVERVIEW OF FLUORESCENCE SPECTROSCOPY

Fluorescence spectroscopy can be applied to a wide range of problems in the chemical and biological sciences. The measurements can provide information on a wide range of molecular processes, including the interactions of solvent molecules with fluorophores, rotational diffusion of biomolecules, distances between sites on biomolecules, conformational changes, and binding interactions. The usefulness of fluorescence is being expanded by advances in technology for cellular imaging and single-molecule detection. These advances in fluorescence technology are decreasing the cost and complexity of previously complex instruments. Fluorescence spectroscopy will continue to contribute to rapid advances in biology, biotechnology and nanotechnology.

REFERENCES

- Herschel, Sir JFW. 1845. On a case of superficial colour presented by a homogeneous liquid internally colourless. *Phil Trans Roy Soc (London)* **135**:143–145.
- Gillispie CC, ed. 1972. John Frederick William Herschel. In *Dictionary of scientific biography*, Vol. 6, pp. 323–328. Charles Scribner's Sons, New York.
- Undenfriend S. 1995. Development of the spectrofluorometer and its commercialization. *Protein Sci* **4**:542–551.
- Martin BR, Richardson F. 1979. Lanthanides as probes for calcium in biological systems. *Quart Rev Biophys* **12**:181–203.
- Berlman IB. 1971. *Handbook of fluorescence spectra of aromatic molecules*, 2nd ed. Academic Press, New York.
- Jablonski A. 1935. Über den Mechanismus des Photolumineszenz von Farbstoffphosphoren. *Z Phys* **94**:38–46.
- Szudy J, ed. 1998. *Born 100 years ago: Aleksander Jablonski (1898–1980)*, Uniwersytet Mikołaja Kopernika, Torun, Poland.
- Acta Physica Polonica. 1978. Polska Akademia Nauk Instytut Fizyki. *Europhys J*, Vol. A65(6).
- Stokes GG. 1852. On the change of refrangibility of light. *Phil Trans R Soc (London)* **142**:463–562.
- Kasha M. 1950. Characterization of electronic transitions in complex molecules. *Disc Faraday Soc* **9**:14–19.
- Courtesy of Dr. Ignacy Gryczynski.
- Birks JB. 1970. *Photophysics of aromatic molecules*. John Wiley & Sons, New York.
- Lakowicz JR, Balter A. 1982. Analysis of excited state processes by phase-modulation fluorescence spectroscopy. *Biophys Chem* **16**:117–132.
- Photo courtesy of Dr. Ignacy Gryczynski and Dr. Zygmunt Gryczynski.
- Birks JB. 1973. *Organic molecular photophysics*. John Wiley & Sons, New York.
- Strickler SJ, Berg RA. 1962. Relationship between absorption intensity and fluorescence lifetime of molecules. *J Chem Phys* **37**(4):814–822.
- See [12], p. 120.
- Berberan-Santos MN. 2001. Pioneering contributions of Jean and Francis Perrin to molecular luminescence. In *New trends in fluorescence spectroscopy: applications to chemical and life sciences*, Vol. 18, pp. 7–33. Ed B Valeur, J-C Brochon. Springer, New York.
- Förster Th. 1948. Intermolecular energy migration and fluorescence (Transl RS Knox). *Ann Phys (Leipzig)* **2**:55–75.
- Stryer L. 1978. Fluorescence energy transfer as a spectroscopic ruler. *Annu Rev Biochem* **47**:819–846.
- Lakowicz JR. 1995. Fluorescence spectroscopy of biomolecules. In *Encyclopedia of molecular biology and molecular medicine*, pp. 294–306. Ed RA Meyers. VCH Publishers, New York.
- Haugland RP. 2002. LIVE/DEAD BacLight bacterial viability kits. In *Handbook of fluorescent probes and research products*, 9th ed., pp. 626–628. Ed J Gregory. Molecular Probes, Eugene, OR.
- Gryczynski I, Lakowicz JR. Unpublished observations.
- Lakowicz JR, Gryczynski I, Laczko G, Wiczak W, Johnson ML. 1994. Distribution of distances between the tryptophan and the N-terminal residue of melittin in its complex with calmodulin, troponin, C, and phospholipids. *Protein Sci* **3**:628–637.
- Morrison LE, Stols LM. 1993. Sensitive fluorescence-based thermodynamic and kinetic measurements of DNA hybridization in solution. *Biochemistry* **32**:3095–3104.
- Santangelo PJ, Nix B, Tsourkas A, Bao G. 2004. Dual FRET molecular beacons for mRNA detection in living cells. *Nucleic Acids Res* **32**(6):e57.
- Alberts B, Johnson A, Lewis J, Raff M, Roberts K, Walter P. 2002. *Molecular biology of the cell*, 4th ed. Garland Science, New York.
- Diaspro A, ed. 2002. *Confocal and two-photon microscopy, foundations, applications, and advances*. Wiley-Liss, New York.
- Masters BR, Thompson BJ, eds. 2003. *Selected papers on multiphoton excitation microscopy*. SPIE Optical Engineering Press, Bellingham, Washington.
- Zipfel WR, Williams RM, Webb WW. 2003. Nonlinear magic: multiphoton microscopy in the biosciences. *Nature Biotechnol* **21**(11):1369–1377.
- Rigler R, Elson ES. 2001. *Fluorescence correlation spectroscopy*. Springer, Berlin.
- Hegener O, Jordan R, Häberlein H. 2004. Dye-labeled benzodiazepines: development of small ligands for receptor binding studies using fluorescence correlation spectroscopy. *J Med Chem* **47**:3600–3605.
- Rigler R, Orrit M, Basché T. 2001. *Single molecule spectroscopy*. Springer, Berlin.
- Zander Ch, Enderlein J, Keller RA, eds. 2002. *Single molecule detection in solution, methods and applications*. Wiley-VCH, Darmstadt, Germany.
- Li Q, Ruckstuhl T, Seeger S. 2004. Deep-UV laser-based fluorescence lifetime imaging microscopy of single molecules. *J Phys Chem B* **108**:8324–8329.
- Ha T. 2004. Structural dynamics and processing of nucleic acids revealed by single-molecule spectroscopy. *Biochemistry* **43**(14):4055–4063.
- Murakoshi H, Iino R, Kobayashi T, Fujiwara T, Ohshima C, Yoshimura A, Kusumi A. 2004. Single-molecule imaging analysis of Ras activation in living cells. *Proc Natl Acad Sci USA* **101**(19):7317–7322.
- Kasha M. 1960. Paths of molecular excitation. *Radiation Res* **2**:243–275.
- Hagag N, Birnbaum ER, Darnall DW. 1983. Resonance energy transfer between cysteine-34, tryptophan-214, and tyrosine-411 of human serum albumin. *Biochemistry* **22**:2420–2427.
- O'Neil KT, Wolfe HR, Erickson-Viitanen S, DeGrado WF. 1987. Fluorescence properties of calmodulin-binding peptides reflect alpha-helical periodicity. *Science* **236**:1454–1456.
- Johnson DA, Leathers VL, Martinez A-M, Walsh DA, Fletcher WH. 1993. Fluorescence resonance energy transfer within a heterochromatic cAMP-dependent protein kinase holoenzyme under equilibri-

um conditions: new insights into the conformational changes that result in cAMP-dependent activation. *Biochemistry* 32:6402–6410.

A glossary of mathematical terms and commonly used acronyms is located at the end of this volume.

PROBLEMS

P1.1. *Estimation of Fluorescence and Phosphorescence Quantum Yields:* The quantum yield for fluorescence is determined by the radiative and non-radiative decay rates. The non-radiative rates are typically similar for fluorescence and phosphorescence states, but the emissive rates (Γ) vary greatly. Emission spectra, lifetimes (τ) and quantum yields (Q) for eosin and erythrosin B (ErB) are shown in Figure 1.13.

- Calculate the natural lifetime (τ_n) and the radiative and non-radiative decay rates of eosin and ErB. What rate accounts for the lower quantum yield of ErB?
- Phosphorescence lifetimes are typically near 1–10 ms. Assume that the natural lifetime for phosphorescence emission of these compounds is 10 ms, and that the non-radiative decay rates of the two compounds are the same for the triplet state as for the singlet state. Estimate the phosphorescence quantum yields of eosin and ErB at room temperature.

P1.2. *Estimation of Emission from the S_2 State:* When excited to the second singlet state (S_2) fluorophores typically relax to the first singlet state within 10^{-13} s.³⁸ Using the radiative decay rate calculated for eosin (problem 1.1), estimate the quantum yield of the S_2 state.

P1.3. *Thermal Population of Vibrational Levels:* The emission spectrum of perylene (Figure 1.3) shows equally spaced peaks that are due to various vibrational states, as illustrated. Use the Boltzmann distribution to estimate the fraction of the ground-state molecules that are in the first vibrationally excited state at room temperature.

P1.4. *Anisotropy of a Labeled Protein:* Naphthylamine sulfonic acids are widely used as extrinsic labels of proteins. A number of derivatives are available. One little known but particularly useful derivative is 2-diethylamino-5-naphthalenesulfonic acid (DENS), which displays a lifetime near 30 ns, longer than that of most similar molecules. Absorption and emission spectra of DENS are shown in Figure 1.36.

- Suppose the fundamental anisotropy of DENS is 0.30 and that DENS is bound to a protein with a rotational correlation time of 30 ns. What is the anisotropy?
- Assume now that the protein is bound to an antibody with a molecular weight of 160,000 and a rotational correlation time of 100 ns. What is the anisotropy of the DENS-labeled protein?

P1.5. *Effective Distance on the Efficiency of FRET:* Assume the presence of a single donor and acceptor and that the distance between them (r) can be varied.

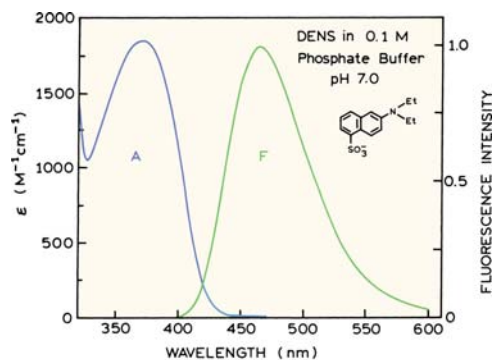


Figure 1.36. Absorption and emission spectra of DENS. The quantum yield relative to quinine sulfate is 0.84, and its lifetime is near 30 ns.

- Plot the dependence of the energy transfer efficiency on the distance between the donor and the acceptor.
 - What is the transfer efficiency when the donor and the acceptor are separated by $0.5R_0$, R_0 , and $2R_0$?
- P1.6. *Calculation of a Distance from FRET Data:* The protein human serum albumin (HSA) has a single tryptophan residue at position 214. HSA was labeled with an anthraniloyl group placed covalently on cysteine-34.³⁹ Emission spectra of the labeled and unlabeled HSA are shown in Figure 1.37. The Förster distance for Trp to anthraniloyl transfer is 30.3 Å. Use the emission spectra in Figure 1.37 to calculate the Trp to anthraniloyl distance.
- P1.7. *Interpretation of Tryptophan Fluorescence from a Peptide:* Figure 1.38 shows a summary of spectral data for a peptide from myosin light-chain kinase (MLCK). This peptide contained a single tryptophan residue, which was placed at positions 1 through 16 in the peptide. This peptide binds to the hydrophobic patch of calmodulin. Explain the changes in emission maxima, Stern-Volmer quenching constant for acrylamide (K), and anisotropy (r).

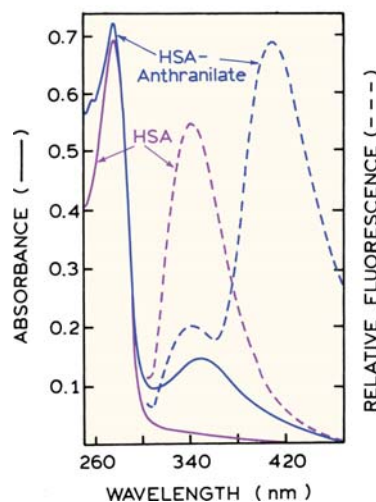


Figure 1.37. Absorption and fluorescence spectra of human serum albumin (HSA) and anthraniloyl-HSA. From [39].

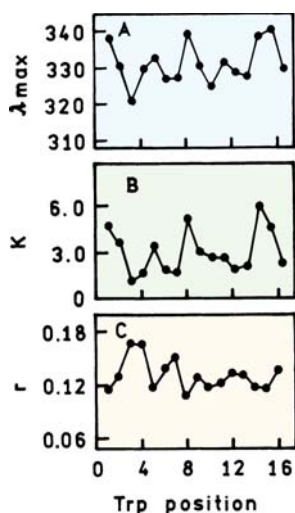


Figure 1.38. Dependence of the emission maxima (A), acrylamide quenching constants (B), and steady-state anisotropies (C) of MLCK peptides bound to calmodulin on the position of tryptophan residue. Reprinted, with permission, from [40]. (O'Neil KT, Wolfe HR, Erickson-Vitanen S, DeGrado WF. 1987. Fluorescence properties of calmodulin-binding peptides reflect alpha-helical periodicity. *Science* **236**:1454–1456, Copyright © 1987, American Association for the Advancement of Science.)

- P1.8. *Interpretation of Resonance Energy Transfer Between Protein Subunits:* Figure 1.39 shows emission spectra of fluorescein (Fl) and rhodamine (Rh) when covalently attached to the catalytic (C) or regulator (R) subunit of a cAMP-dependent protein kinase (PK).⁴¹ When the subunits are associated, RET occurs from Fl to Rh. The associated form is C_2R_2 . Figure 1.40 shows emission spectra of both subunits without any additives, in the presence of cAMP, and in the presence of protein kinase inhibitor (PKI). Suggest an interpretation of these spectra. Your interpretation should be consistent with the data, but it may not be the only possible interpretation.

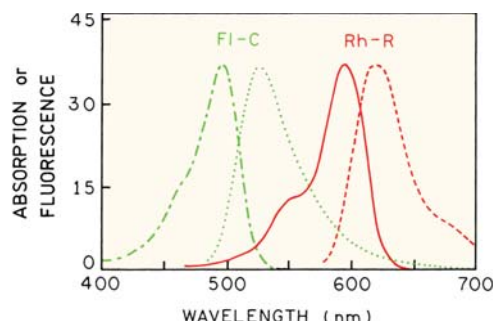


Figure 1.39. Spectral overlap of the fluorescein-labeled catalytic subunit (FI-C) and the Texas red-labeled regulator subunit (Rh-R) of a cAMP-dependent protein kinase. Revised and reprinted with permission from [41]. (Copyright © 1993, American Chemical Society.)

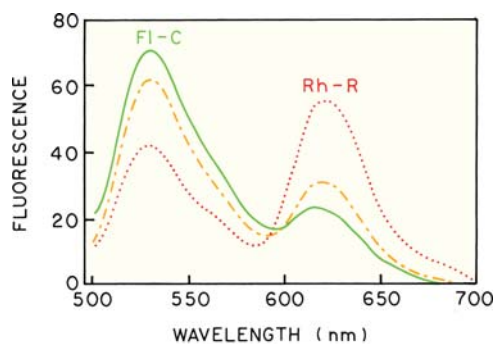


Figure 1.40. Effect of cAMP and the protein kinase inhibitor on the emission spectra of the donor and acceptor labeled holoenzyme. Emission spectra are shown without cAMP or PK (•••••), and the following addition of cAMP (---•---), and PKI (—). Revised and reprinted with permission from [41]. (Copyright © 1993, American Chemical Society.)

3

Characteristics of Fluorescence Emission

Though perfectly transparent and colorless when held between the eye and the light, it [an acid quinine solution] yet exhibits in certain aspects, and under certain incidences of the light, an extremely vivid and beautiful celestial blue color.

Sir John Herschel (1845)

This chapter describes the characteristics of the fluorescence emission of an excited molecule in solution. We do not consider here the photophysical processes involving interactions with other molecules (electron transfer, proton transfer, energy transfer, excimer or exciplex formation, etc.). These processes will be examined in Chapter 6.

3.1

Radiative and Nonradiative Transitions between Electronic States

The Perrin–Jablonski diagram (Figure 3.1) is convenient for visualizing in a simple way the possible processes: photon absorption, internal conversion, fluorescence, intersystem crossing, phosphorescence, delayed fluorescence, and triplet–triplet transitions. The singlet electronic states are denoted by S_0 (fundamental electronic state), S_1 , S_2 , . . . and the triplet states, T_1, T_2 , . . . Vibrational levels are associated with each electronic state. It is important to note that absorption is very fast ($\approx 10^{-15}$ s) with respect to all other processes (so that there is no concomitant displacement of the nuclei according to the Franck–Condon principle; see Chapter 2).

The vertical arrows corresponding to absorption start from the 0 (lowest) vibrational energy level of S_0 because the majority of molecules are in this level at room temperature, as shown in Box 3.1. Absorption of a photon can bring a molecule to one of the vibrational levels of S_1 , S_2 , . . . The subsequent possible de-excitation processes will now be examined.

However, it should be noted that most fluorescent molecules exhibit broad and structureless absorption and emission bands, which means that each electronic state consists of an almost continuous manifold of vibrational levels. If the energy difference between the 0 and 1 vibrational levels of S_0 (and S_1) is, for instance,

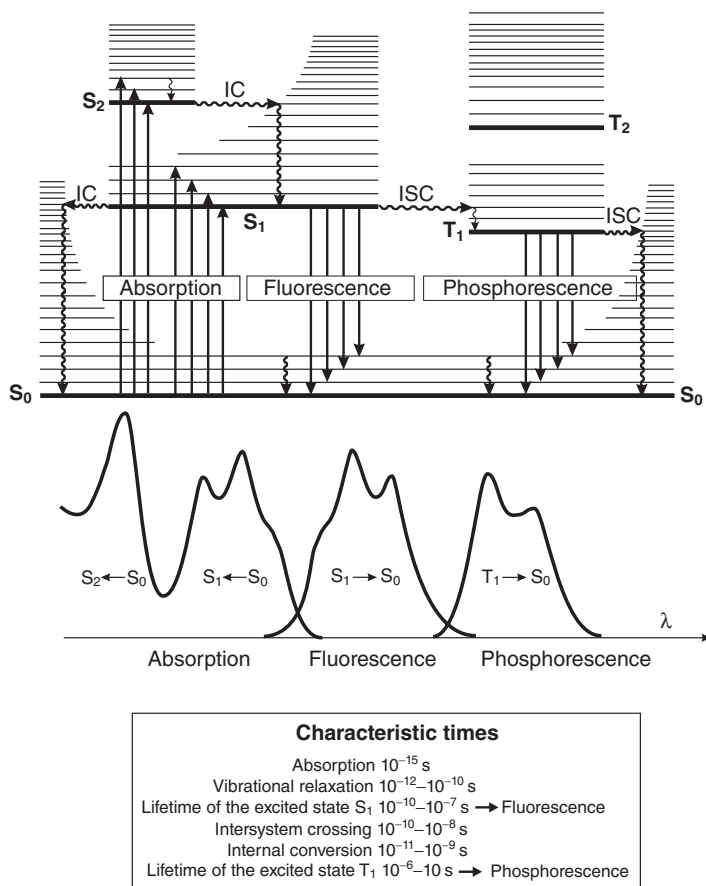


Figure 3.1 Perrin–Jablonski diagram and illustration of the relative positions of absorption, fluorescence, and phosphorescence spectra. Straight arrows represent radiative processes, whereas wavy arrows stand for nonradiative ones. In this book, when denoting a transition, the spectroscopic

convention (recommended by IUPAC) of always placing the higher energy state in the first place is followed. The orientation of the arrow then immediately tells if the transition corresponds to an absorption process (←) or to an emission process (→).

only about 500 cm⁻¹, the ratio N_1/N_0 becomes about 0.09. Consequently, excitation can then occur from a vibrationally excited level of the S₀ state. This explains why the absorption spectrum can partially overlap the fluorescence spectrum (see Section 3.1.2).

In all cases, the energy gap between S₀ and S₁ is of course much larger than between the vibrational levels, so the probability of finding a molecule in S₁ at room temperature as a result of thermal energy is nearly zero ($E_{S_1} - E_{S_0} \approx 4 \times 10^{-19}$ J, compared with $kT \approx 4 \times 10^{-21}$ J).

Box 3.1 Relative populations of molecules in the vibrational energy levels according to the Boltzmann law

For some aromatic hydrocarbons such as naphthalene, anthracene, and perylene, the electronic absorption and fluorescence spectra exhibit vibronic structure, that is, well-defined transitions between vibrational levels of the so-called active normal modes of vibration can be clearly seen. The energy spacing between the vibrational levels and the Franck–Condon factors (see Chapter 2) that determine the relative intensities of the vibronic bands are similar in S_0 and S_1 so that the emission spectrum often appears to be symmetrical to the absorption spectrum (“mirror image” rule), as illustrated in Figure B3.1.1. It is interesting to note that the absorption spectrum reflects the vibrational spacing in S_1 , whereas the fluorescence spectrum reflects the vibrational spacing in S_0 . These are frequently slightly different.

The ratio of the numbers of molecules N_1 and N_0 in the 1 and 0 vibrational levels of energy E_1 and E_0 , respectively, is given by the Boltzmann law:

$$N_1/N_0 = \exp[-(E_1 - E_0)/kT]$$

where k is the Boltzmann constant ($k = 1.3807 \times 10^{-23} \text{ J K}^{-1}$) and T is the absolute temperature.

For instance, the absorption and emission spectra of anthracene show a wavenumber spacing of about 1400 cm^{-1} , that is, an energy spacing of $2.8 \times 10^{-20} \text{ J}$, between consecutive vibrational levels. In this case, the ratio N_1/N_0 at room temperature (298 K) is about 0.001.

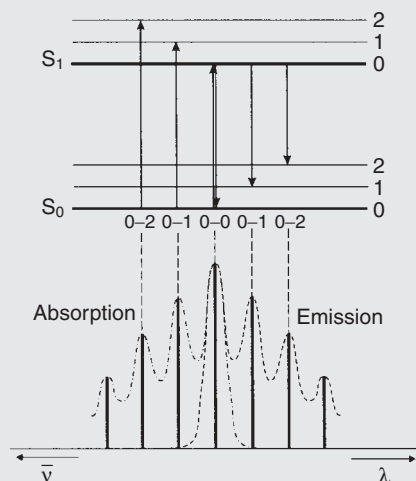


Figure B3.1.1 Illustration of the vibrational bands in the absorption and fluorescence spectra of aromatic hydrocarbons. Broadening of the bands is explained in Section 5.1.

As a last note, it should be kept in mind that the Perrin–Jablonski diagram presupposes that the excited-state Franck–Condon and relaxed geometries and respective electron densities are the same, which is not always observed. For this reason, geometry or charge distribution changes in the excited state often lead to a breakdown of the mirror image relationship between absorption and emission.

3.1.1

Internal Conversion

Internal conversion is a nonradiative transition between two electronic states of the same spin multiplicity. In solution, this process is followed by a vibrational relaxation toward the lowest vibrational level of the final electronic state. The excess vibrational energy can be indeed transferred to the solvent during collisions of the excited molecule with the surrounding solvent molecules.

When a molecule is excited to an energy level higher than the lowest vibrational level of the first electronic state, vibrational relaxation (and internal conversion if the singlet excited state is higher than S_1) leads the excited molecule towards the 0 vibrational level of the S_1 singlet state with a time-scale of 10^{-13} – 10^{-11} s.

From S_1 , internal conversion to S_0 is possible but is less efficient than conversion from S_2 to S_1 , because of the much larger energy gap between S_1 and S_0 .¹⁾ Therefore, internal conversion from S_1 to S_0 can compete with emission of photons (fluorescence) and intersystem crossing to the triplet state from which emission of photons (phosphorescence) can possibly be observed.

3.1.2

Fluorescence

Emission of photons accompanying the $S_1 \rightarrow S_0$ relaxation is called fluorescence. It should be emphasized that, apart from a few exceptions,²⁾ fluorescence emission occurs from S_1 and therefore its characteristics (except polarization) do not depend on the excitation wavelength (provided of course that only one species exists in the ground state).

The 0–0 transition is usually the same for absorption and fluorescence. However, the fluorescence spectrum is located at higher wavelengths (lower energy) than the absorption spectrum because of the energy loss in the excited state due to vibrational relaxation (Figure 3.1). According to the Stokes rule (an empirical observation predating the Perrin–Jablonski diagram), the wavelength of a fluorescence emission should always be higher than that of absorption. However in most cases, the absorption spectrum partly overlaps the fluorescence spectrum, that is, a fraction of light is emitted at shorter wavelengths than the absorbed light. Such

- | | |
|--|---|
| 1) The smaller the energy gap between the initial and final electronic states, the larger the efficiency of internal conversion. | from S_1 and S_2 in the case of indole in some solvents. Minor but measurable emission from S_2 in some metal porphyrins. |
| 2) For instance, dominant emission from S_2 in the case of azulene; simultaneous emission | |

an observation seems to be, at first sight, in contradiction to the principle of energy conservation. However, such an “energy defect” is compensated for (as stated by Einstein for the first time) by the fact that at room temperature, a small fraction of molecules are in a vibrational level higher than level 0 (distribution among the energy levels fulfilling the Boltzmann law; see Box 3.1) in the ground state as well as in the excited state. At low temperature, this departure from the Stokes law should disappear.

In general, the differences between the vibrational levels are similar in the ground and excited states, so that the fluorescence spectrum often resembles the first absorption band (“mirror image” rule). The gap (expressed in wavenumbers) between the maximum of the first absorption band and the maximum of fluorescence is called the Stokes shift.

It should be noted that emission of a photon is as fast as absorption of a photon ($\approx 10^{-15}$ s). However, excited molecules stay in the S_1 state for a certain time (a few tens of picoseconds to a few hundreds of nanoseconds, depending on the type of molecule and the medium) before emitting a photon or undergoing other de-excitation processes (internal conversion, intersystem crossing). Thus, after excitation of a population of molecules by a very short pulse of light, the fluorescence intensity decreases exponentially with a characteristic time, reflecting the average lifetime of the molecules in the S_1 excited state (excited-state lifetime; see Section 3.2.1). Such an intensity decay is formally comparable with a radioactive decay that is also exponential, with a characteristic time, called the radioactive period, reflecting the average lifetime of a radioelement before disintegration.

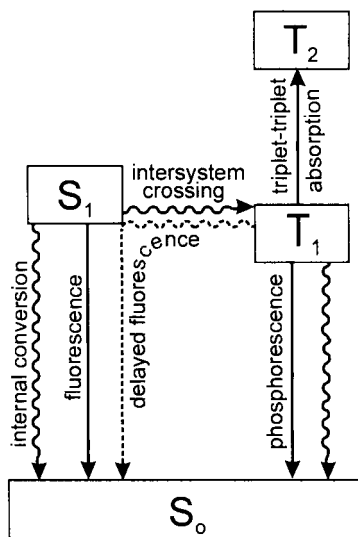
The emission of fluorescence photons just described is a spontaneous process. Under certain conditions, stimulated emission can occur (e.g., dye lasers) (see Box 3.2).

3.1.3

Intersystem Crossing and Subsequent Processes

A third possible de-excitation process from S_1 is intersystem crossing toward the T_1 triplet state followed by other processes, according to Scheme 3.1.

It might be expected that, for a given wavelength, increasing the radiation density (hence departing from thermal equilibrium) could render stimulated emission dominant. This is indeed observed. However, a radiation density increase also corresponds to an increase in the rate of absorption, and in the limit of very high density (neglecting other effects) the population of the two levels (with identical degeneracy) becomes identical (saturation), and no net gain in emission is observed, although stimulated emission largely dominates over spontaneous emission. A necessary condition for net gain (more output radiation than input radiation, i.e., amplification) is that the population of the upper state is larger than that of the lower state. In other words, an inversion of population ($N_{S_1} > N_{S_0}$) is required. This inversion can only be attained with three-level and four-level schemes. Inversion is achieved using optical pumping by an intense light source (flash lamps or



Scheme 3.1

lasers); dye and solid-state lasers work in this way. Alternatively, electrical discharge in a gas (gas lasers, copper vapor lasers) can be used.

In contrast to spontaneous emission, induced emission (also called stimulated emission) is coherent, that is, all emitted photons have the same physical characteristics—they have the same direction, the same phase, and the same polarization. These properties are characteristic of laser emission (L.A.S.E.R. = Light Amplification by Stimulated Emission of Radiation). The term induced emission comes from the fact that de-excitation is triggered by the interaction of an incident photon with an excited atom or molecule, which induces emission of a second photon having the same characteristics as those of the incident photon.

3.1.3.1 Intersystem Crossing

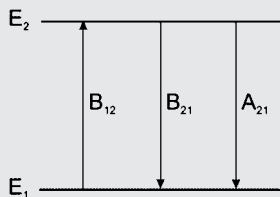
Intersystem crossing³⁾ is a nonradiative transition between two isoenergetic vibrational levels belonging to electronic states of different multiplicities. For example, an excited molecule in the 0 vibrational level of the S_1 state can move to the isoenergetic vibrational level of the T_n triplet state; then vibrational relaxation brings it into the lowest vibrational level of T_1 . Intersystem crossing may be fast enough

3) The word “crossing” comes from the fact that the intersection between the potential energy surfaces corresponding to the S_1 and T_n states allows a molecule to cross from the S_1 state to the T_n state. The smaller the difference between the crossing point of these two surfaces and the minimum

energy of the S_1 state, the more likely the crossing. If the difference in energy between the S_1 and T_1 states is small, molecules may return to the S_1 state. The subsequent emission from this state is called delayed fluorescence (see Section 3.1.3.3).

Box 3.2 Spontaneous and stimulated emissions

The Einstein coefficients characterize the probability of transition of a molecule between two energy levels E_1 and E_2 (Scheme B3.2.1). B_{12} is the induced absorption coefficient (see Chapter 2), B_{21} is the induced emission coefficient, and A_{21} is the spontaneous emission coefficient. The emission-induced process $E_2 \rightarrow E_1$ occurs at exactly the same rate as the absorption-induced process $E_2 \leftarrow E_1$, so that $B_{12} = B_{21}$.



Scheme B3.2.1

The number of molecules in states 1 and 2 is N_1 and N_2 , respectively. These numbers must satisfy the Boltzmann law:

$$\frac{N_1}{N_2} = \exp[-(E_1 - E_2)/kT] = \exp(+h\nu/kT)$$

where h is Planck's constant.

The rate of absorption from state 1 to state 2 is $N_1 B_{12} \rho(\nu)$, where $\rho(\nu)$ is the energy density incident on the sample at frequency ν . The rate of emission from state 2 to state 1 is $N_2 (A_{21} + B_{21} \rho(\nu))$. At equilibrium, these two rates are equal; hence,

$$\frac{N_1}{N_2} = \frac{B_{21} \rho(\nu) + A_{21}}{B_{12} \rho(\nu)} = 1 + \frac{A_{21}}{B_{12} \rho(\nu)}$$

The radiation density $\rho(\nu)$ is given by Planck's black body radiation law:

$$\rho(\nu) = \frac{8\pi h\nu^3}{c^3 [\exp(+h\nu/kT) - 1]}$$

The three equations above lead to

$$A_{21} = \frac{8\pi h\nu^3}{c^3} B_{21}$$

Note that the ratio A_{21}/B_{21} is proportional to the cube of the frequency. For this reason, while in the visible region essentially all emission is spontaneous or the usual radiation levels, the same is not true for longer wavelengths (e.g., radiofrequencies), where spontaneous emission is negligible.

(10^{-7} – 10^{-9} s) to compete with other pathways of de-excitation from S_1 (fluorescence and internal conversion $S_1 \rightarrow S_0$).

Crossing between states of different multiplicity is in principle forbidden, but spin–orbit coupling (i.e., coupling between the orbital magnetic moment and the spin magnetic moment) (see Chapter 2) can be large enough to make it possible. The probability of intersystem crossing depends on the singlet and triplet states involved. If the transition $S_1 \leftarrow S_0$ is of $n \rightarrow \pi^*$ type for instance, intersystem crossing is often efficient. It should also be noted that the presence of heavy atoms (i.e., whose atomic number is large, e.g., Br, Pb, Pt) increases spin–orbit coupling and thus favors intersystem crossing.

3.1.3.2 Phosphorescence versus Nonradiative De-Excitation

In solution at room temperature, nonradiative de-excitation from the triplet state T_1 is predominant over radiative de-excitation called phosphorescence. In fact, the transition $T_1 \rightarrow S_0$ is forbidden (but it can be observed because of spin–orbit coupling), and the radiative rate constant is thus very low. During such a slow process, the numerous collisions with solvent molecules favor intersystem crossing and vibrational relaxation in S_0 .

On the contrary, at low temperatures and/or in a rigid medium, phosphorescence can be observed. The lifetime of the triplet state may, under these conditions, be long enough to observe phosphorescence on a time-scale up to seconds, even minutes or more.

The phosphorescence spectrum is located at wavelengths longer than the fluorescence spectrum (Figure 3.1) because the energy of the lowest vibrational level of the triplet state T_1 is lower than that of the singlet state S_1 .

3.1.3.3 Delayed Fluorescence

Thermally activated delayed fluorescence reverse intersystem crossing $S_1 \leftarrow T_1$ can occur when the energy difference between S_1 and T_1 is small and when the lifetime of T_1 is long enough. This results in emission with the same spectral distribution as normal fluorescence but with a much longer decay time constant because the molecules stay in the triplet state before emitting from S_1 . This fluorescence emission is thermally activated; consequently, its efficiency increases with increasing temperature.

It is also called delayed fluorescence of E-type because it was observed for the first time with eosin. It does not normally occur in aromatic hydrocarbons because of the relatively large difference in energy between S_1 and T_1 . In contrast, delayed fluorescence is very efficient in fullerenes.

Triplet–triplet annihilation in concentrated solutions, a collision between two molecules in the T_1 state can provide enough energy to allow one of them to return to the S_1 state. Such a triplet–triplet annihilation thus leads to a delayed fluorescence emission (also called delayed fluorescence of P-type because it was observed for the first time with pyrene). The decay time constant of the delayed fluorescence process is half the lifetime of the triplet state in dilute solution, and the intensity has a characteristic quadratic dependence on excitation light intensity.

3.1.3.4 Triplet–Triplet Transitions

Once a molecule is excited and reaches the triplet state T_1 , it can absorb another photon at a different wavelength because triplet–triplet transitions are spin allowed. These transitions can be observed provided that the population of molecules in the triplet state is large enough, which can be achieved by illumination with an intense pulse of light.

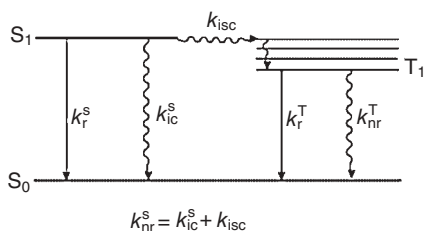
3.2

Lifetimes and Quantum Yields

3.2.1

Excited-State Lifetimes

The rate constants for the various processes are denoted as follows (see Scheme 3.2):



Scheme 3.2

k_r^S : rate constant for radiative deactivation $S_1 \rightarrow S_0$ with emission of fluorescence.

k_{ic}^S : rate constant for internal conversion $S_1 \rightarrow S_0$.

k_{isc} : rate constant for intersystem crossing.

Regarding the two latter nonradiative pathways of de-excitation from S_1 , it is convenient to introduce the overall nonradiative rate constant k_{nr}^S such that

$$k_{nr}^S = k_{ic}^S + k_{isc}$$

For deactivation from T_1 , we have

k_r^T : rate constant for radiative deactivation $T_1 \rightarrow S_0$ with emission of phosphorescence.

k_{nr}^T : rate constant for nonradiative deactivation (intersystem crossing) $T_1 \rightarrow S_0$.

De-excitation processes resulting from intermolecular interactions are not considered in this chapter; they will be described in Chapter 6.

Let us consider a dilute solution of a fluorescent species A whose concentration is $[A]$ (in mol L^{-1}). A very short pulse of light⁴⁾ (i.e., whose duration is short with

4) Strictly speaking, the light pulse is a δ -function (Dirac). The response of the system in terms of fluorescence intensity will thus be called a δ -pulse response.

respect to the reciprocal of the involved rate constants) at time 0 brings a certain number of molecules A to the S_1 excited state by absorption of photons. These excited molecules then return to S_0 , either radiatively or nonradiatively, or undergo intersystem crossing. As in classical chemical kinetics, the rate of disappearance of excited molecules is expressed by the following differential equation:

$$-\frac{d[{}^1A^*]}{dt} = (k_r^S + k_{nr}^S)[{}^1A^*] \quad (3.1)$$

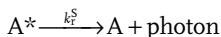
Integration of this equation yields the time evolution of the concentration of excited molecules $[{}^1A^*]$. Let $[{}^1A^*]_0$ be the concentration of excited molecules at time 0 resulting from pulse light excitation. Integration leads to

$$[{}^1A^*] = [{}^1A^*]_0 \exp\left(-\frac{t}{\tau_s}\right) \quad (3.2)$$

where τ_s , the lifetime of excited state S_1 , is given by

$$\tau_s = \frac{1}{k_r^S + k_{nr}^S} \quad (3.3)$$

The fluorescence intensity is defined as the amount of photons (in mol, or its equivalent, in einsteins; 1 einstein = 1 mole of photons) emitted per unit time (s) and per unit volume of solution (liter: L) according to



The fluorescence intensity i_F at time t after excitation by a very short pulse of light at time 0 is proportional, at any time, to the instantaneous concentration of molecules still excited $[{}^1A^*]$; the proportionality factor is the rate constant for radiative de-excitation k_r^S :

$$i_F(t) = k_r^S [{}^1A^*] = k_r^S [{}^1A^*]_0 \exp\left(-\frac{t}{\tau_s}\right) \quad (3.4)$$

$i_F(t)$, the δ -pulse response of the system, decreases according to a single exponential.

It should be emphasized that, in any practical measurement of fluorescence intensity, the measured quantity is proportional to i_F , the proportionality factor depending on instrumental conditions (see Chapter 9). The “measured” fluorescence intensity will be denoted by I_F . It will be helpful to keep in mind that the numerical value of I_F is obtained on an arbitrary scale, depending on the experimental settings.

If the only way of de-excitation from S_1 to S_0 was fluorescence emission, the lifetime would be $1/k_r^S$; this is called the radiative lifetime (in preference to natural lifetime) and denoted by τ_r .⁵⁾ The radiative lifetime can be theoretically

5) It is interesting to note that for a resonant transition (i.e., coinciding absorption and emission frequencies), the reciprocal of the radiative lifetime is equal to the Einstein coefficient A_{21} for spontaneous emission (see Box 3.2).

calculated from the absorption and fluorescence spectra using the Strickler–Berg relation.⁶⁾

The lifetime of a homogeneous population of fluorophores is very often independent of the excitation wavelength, as happens with the emission spectrum (but there are some exceptions). In fact, internal conversion and vibrational relaxation are always very fast in solution and emission arises from the lowest vibrational level of the state S_1 .

The fluorescence decay time τ_s is one of the most important characteristics of a fluorescent molecule because it defines the time window of observation of dynamic phenomena. As illustrated in Figure 3.2, no accurate information on the rate of phenomena occurring at time-scales shorter than about $\tau/100$ (“private life” of the molecule) or longer than about 10τ (“death” of the molecule) can be obtained, whereas at intermediate times (“public life” of the molecule) the time evolution of phenomena can be followed. It is interesting to note that a similar situation is found in the use of radioisotopes for dating: the period (i.e., the time constant of the exponential radioactive decay) must be of the same order of magnitude as the age of the object to be dated (Figure 3.2).

Following a δ -pulse excitation, a fraction of excited molecules can reach the triplet state, from which they return to the ground state either radiatively or non-radiatively. The concentration of molecules in the triplet state decays exponentially with a time constant t_T representing the lifetime of the triplet state

$$\tau_T = \frac{1}{k_r^T + k_{nr}^T} \quad (3.5)$$

For organic molecules, the lifetime of the singlet state ranges from tens of picoseconds to hundreds of nanoseconds, whereas the triplet lifetime is much longer (microseconds to seconds). However, such a difference cannot by itself be used to make a distinction between fluorescence and phosphorescence because borderline cases exist.

Monitoring of phosphorescence or delayed fluorescence enables us to study much slower phenomena.

Examples of lifetimes of singlet and triplet states for some aromatic hydrocarbons are given in Table 3.1. The lifetime of compounds that can be used as standards are given in Chapter 10 (Table 10.1). Other values of lifetimes can be found in the Appendix at the end of the book.

- 6) The Strickler–Berg relation (*J. Chem. Phys.*, 37, 814 [1962]) is

$$\begin{aligned} \frac{1}{\tau_r} &= \frac{8\pi \times 230c_0 n^2}{N_a} \int \frac{F_{\bar{\nu}_F}(\bar{\nu}_F) d\bar{\nu}_F}{\bar{\nu}_F^3 F_{\bar{\nu}_F}(\bar{\nu}_F)} \int \frac{\epsilon(\bar{\nu}_A) d\bar{\nu}_A}{\bar{\nu}_A} \\ &= 2.88 \times 10^{-9} n^2 \int \frac{F_{\bar{\nu}_F}(\bar{\nu}_F) d\bar{\nu}_F}{\bar{\nu}_F^3 F_{\bar{\nu}_F}(\bar{\nu}_F)} \int \frac{\epsilon(\bar{\nu}_A) d\bar{\nu}_A}{\bar{\nu}_A} \end{aligned}$$

where n is the index of refraction, c_0 is the speed of light, ϵ is the molar absorption coefficient, and $F_{\bar{\nu}_F}(\bar{\nu}_F)$ is defined by Eq.

(3.21) (see later). The Strickler–Berg equation yields values of τ_r that are often in agreement with the experimental ones, but it fails in a number of cases, especially when the interactions with the solvent cannot be ignored and when there is a change in the excited-state geometry. An important consequence of this equation is that the lower the molar absorption coefficient, the longer the radiative lifetime, that is, the lower the rate of the radiative process.

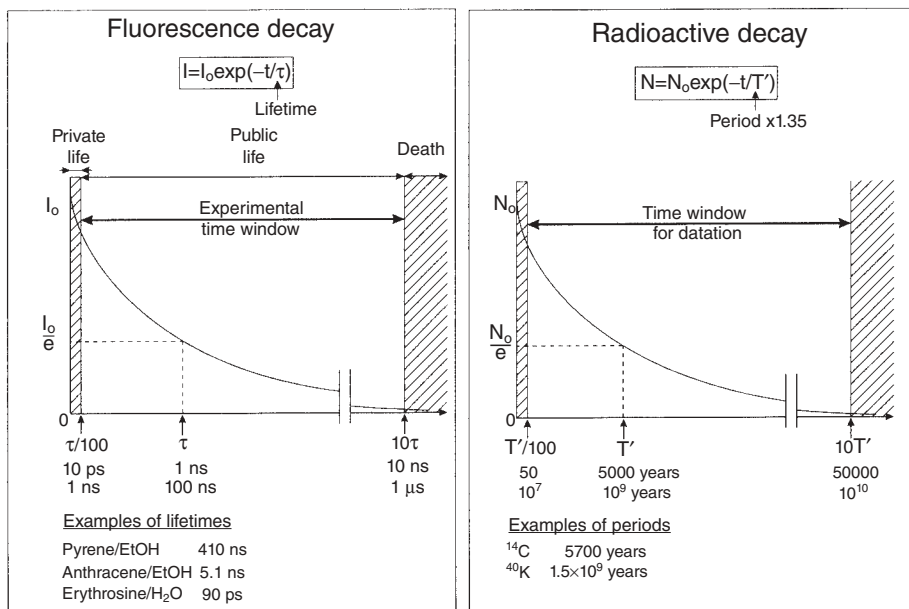


Figure 3.2 Decay of fluorescence intensity and analogy with radioactive decay. Note that the lifetime τ is the time needed for the concentration of molecular entities to decrease to $1/e$ of its original value, whereas

the radioactive period T is the time needed for the number of radioactive entities to decrease to $1/2$ of its original value. Therefore, T' (the decay time constant equivalent to the lifetime) is equal to $1.35 T$.

3.2.2

Quantum Yields

The fluorescence quantum yield Φ_F is the fraction of excited molecules that return to the ground state S_0 with emission of fluorescence photons:

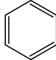
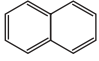
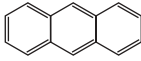
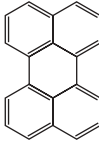
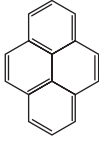
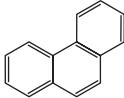
$$\Phi_F = \frac{k_r^S}{k_r^S + k_{nr}^S} = k_r^S \tau_S \quad (3.6)$$

In other words, the fluorescence quantum yield is the ratio of the number of emitted photons (over the whole duration of the decay) to the number of absorbed photons, hence the qualifier “quantum.” Owing to the Stokes law, a fluorescence yield expressed in terms of energy is always lower than unity. According to Eq. (3.4), the ratio of the δ -pulse response $i_F(t)$ to the number of absorbed photons is given by

$$\frac{i_F(t)}{[{}^1A^*]_0} = k_r^S \exp\left(-\frac{t}{\tau_S}\right) \quad (3.7)$$

and integration of this relation over the whole duration of the decay (mathematically from 0 to infinity) yields Φ_F :

Table 3.1 Quantum yields for fluorescence, phosphorescence, and intersystem crossing and lifetimes of singlet and triplet states for some aromatic hydrocarbons (Mainly from Birks, J.B. (1970) *Photophysics of Aromatic Molecules*, Wiley-Interscience, London).

Compound	Formula	Solvent (temperature)	Φ_F	τ_S (ns)	Φ_{isc}	Φ_P	τ_T (s)
Benzene		Ethanol (293 K) EPA ^{a)} (77 K)	0.04	31		0.17	7.0
Naphthalene		Ethanol (293 K)	0.21	2.7	0.79		
		Cyclohexane (293 K) EPA (77 K)	0.19	96		0.06	2.6
Anthracene		Ethanol (293 K)	0.30	5.5	0.72		
		Cyclohexane (293 K)	0.30	4.9			
		EPA (77 K)					0.09
Perylene		<i>n</i> -Hexane	0.98		0.02		
		Cyclohexane (293 K)	0.78	6			
Pyrene		Ethanol (293 K)	0.65	475	0.38		
		Cyclohexane (293 K)	0.65	450			
Phenanthrene		Ethanol (293 K)	0.13		0.85		
		<i>n</i> -Heptane (293 K)	0.16	60			
		EPA (77 K)				0.31	3.3
		Polymer film	0.12		0.88		0.11

a) EPA: mixture of ethanol, isopentane, diethyl ether 2:5:5 v/v/v.

$$\frac{1}{[^1A^*]_0} \int_0^\infty i_F(t) dt = k_r^S \tau_S = \Phi_F \quad (3.8)$$

The quantum yields of intersystem crossing (Φ_{isc}) and phosphorescence (Φ_P) are given by

$$\Phi_{isc} = \frac{k_{isc}}{k_r^S + k_{nr}^S} = k_{isc} \tau_S \quad (3.9)$$

$$\Phi_P = \frac{k_r^T}{k_r^T + k_{nr}^T} \Phi_{isc} \quad (3.10)$$

Using the radiative lifetime, as previously defined, the fluorescence quantum yield can also be written as

$$\Phi_F = \frac{\tau_S}{\tau_r} \quad (3.11)$$

Following an external perturbation, the fluorescence quantum yield can remain proportional to the lifetime of the excited state (e.g., in the case of dynamic quenching (see Chapter 6), variation in temperature, etc.). However, such a proportionality may not be valid if de-excitation pathways—different from those described above—result from interactions with other molecules. A typical case where the fluorescence quantum yield is affected without any change in excited-state lifetime is the formation of a ground-state complex that is nonfluorescent (static quenching; see Chapter 6).

It is interesting to note that when the fluorescence quantum yield and the excited-state lifetime of a fluorophore are measured under the same conditions, the nonradiative and radiative rate constants can be easily calculated by means of the following relations:

$$k_r^s = \frac{\Phi_F}{\tau_s} \quad k_{nr}^s = \frac{1}{\tau_s} (1 - \Phi_F)$$

Examples of quantum yields of fluorescence, phosphorescence, and intersystem crossing for some aromatic hydrocarbons are reported in Table 3.1. The fluorescence quantum yields of compounds that can be used as standards are given in Chapter 9 (Table 9.1). Other values can be found in the Appendix at the end of the book.

It is well known that dioxygen quenches fluorescence (and phosphorescence) (see Chapter 6), but its effect on quantum yields and lifetimes strongly depends on the nature of the compound and the medium. Oxygen quenching is a collisional process and is therefore diffusion-controlled. Consequently, compounds of long lifetime, such as naphthalene and pyrene, are particularly sensitive to the presence of oxygen. Moreover, oxygen quenching is less efficient in media of high viscosity. Oxygen quenching can be avoided by bubbling nitrogen or argon in the solution; however, the most efficient method (used particularly in phosphorescence studies) is to perform a number of freeze-pump-thaw cycles.

3.2.3

Effect of Temperature

Generally, an increase in temperature results in a decrease in the fluorescence quantum yield and the lifetime because the nonradiative processes related to thermal agitation (collisions with solvent molecules, intramolecular vibrations and rotations, etc.) are more efficient at higher temperatures. Experiments are often in good agreement with the empirical linear variation of $\ln(1/\Phi_F - 1)$ versus $1/T$. Delayed fluorescence, on the other hand, increases with temperature within a certain range, as back-intersystem crossing is an activated process.

As mentioned above, phosphorescence is observed only under certain conditions because the triplet states are very efficiently deactivated by collisions with solvent molecules (or oxygen and impurities) because their lifetime is long. These effects can be reduced and may even disappear when the molecules are in a frozen solvent, or in a rigid matrix (e.g., polymer) at room temperature. The increase in

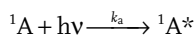
phosphorescence quantum yield by cooling can reach a factor of 10^3 , whereas this factor is generally not larger than 10 or so for the fluorescence quantum yield.

In conclusion, lifetimes and quantum yields are characteristics of major importance. Obviously, the larger the fluorescence quantum yield, the easier it is to observe a fluorescent compound, especially a fluorescent probe. It should be emphasized that, in the condensed phase, many parameters can affect the quantum yields and lifetimes: temperature, pH, polarity, viscosity, hydrogen bonding, presence of quenchers, etc. Attention should be paid to possible erroneous interpretation arising from the simultaneous effects of several factors (for instance, changes in viscosity due to a variation in temperature).

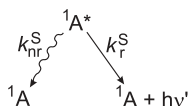
3.3 Emission and Excitation Spectra

3.3.1 Steady-State Fluorescence Intensity

Emission and excitation spectra are recorded using a spectrofluorometer (see Chapter 9). The light source is a lamp emitting a constant photon flow, that is, a constant amount of photons per unit time, whatever their energy. Let us denote by N_0 the constant amount of incident photons entering, during a given time, a unit volume of the sample where the fluorophore concentration is $[A]$ (N_0 and $[A]$ in mol L^{-1}). αN_0 represents the amount of absorbed photons per unit volume involved in the excitation process



Let us recall that the pseudo-first-order rate constant for this process is very large ($k_a \approx 10^{15} \text{ s}^{-1}$) whereas the subsequent steps of de-excitation occur with much lower rate constants (k_r^S and $k_{nr}^S \approx 10^7 - 10^{10} \text{ s}^{-1}$), according to



Under continuous illumination, the concentration $[{}^1A^*]$ remains constant, which means that ${}^1A^*$ is in a steady state. Measurements under these conditions are then called steady-state measurements.

The rate of change of $[{}^1A^*]$ is equal to zero:

$$\frac{d[{}^1A^*]}{dt} = 0 = k_a \alpha N_0 - (k_r^S + k_{nr}^S)[{}^1A^*] \quad (3.12)$$

$k_a \alpha N_0$ represents the amount of absorbed photons per unit volume and per unit time. It can be rewritten as αI_0 where I_0 represents the intensity of the incident light (in moles of photons per liter and per second).

The constant concentration [$^1A^*$] is given by

$$[{}^1A^*] = \frac{\alpha I_0}{k_r^S + k_{nr}^S} \quad (3.13)$$

The amount of fluorescence photons emitted per unit time and per unit volume, that is, the steady-state fluorescence intensity, is then given by

$$i_F = k_r^S [{}^1A^*] = \alpha I_0 \frac{k_r^S}{k_r^S + k_{nr}^S} = \alpha I_0 \Phi_F \quad (3.14)$$

This expression shows that the steady-state fluorescence intensity per absorbed photon $i_F/\alpha I_0$ is the fluorescence quantum yield.⁷⁾

3.3.2

Emission Spectra

We have so far considered all emitted photons, whatever their energy. We now focus our attention on the energy distribution of the emitted photons. With this in mind, it is convenient to express the steady-state fluorescence intensity per absorbed photon as a function of the wavelength of the emitted photons, denoted by $F_\lambda(\lambda_F)$ (in m^{-1} or nm^{-1}) and satisfying the relationship

$$\int_0^\infty F_\lambda(\lambda_F) d\lambda_F = \Phi_F \quad (3.15)$$

where Φ_F is the fluorescence quantum yield defined above. $F_\lambda(\lambda_F)$ represents the fluorescence spectrum or emission spectrum: it reflects the distribution of the probability of the various transitions from the lowest vibrational level of S_1 to the various vibrational levels of S_0 . The emission spectrum is characteristic of a given compound.

In practice, the steady-state fluorescence intensity $I_F(\lambda_F)$ measured at wavelength λ_F (selected by a monochromator with a certain wavelength bandpass $\Delta\lambda_F$) is proportional to $F_\lambda(\lambda_F)$ and to the number of photons absorbed at the excitation wavelength λ_E (selected by a monochromator). It is convenient to replace this number of photons by the absorbed intensity $I_A(\lambda_E)$, defined as the difference between the intensity of the incident light $I_0(\lambda_E)$ and the intensity of the transmitted light $I_T(\lambda_E)$:

$$I_A(\lambda_E) = I_0(\lambda_E) - I_T(\lambda_E) \quad (3.16)$$

7) It is worth noting that integration of the δ -pulse response $i_F(t)$ of the fluorescence intensity over the whole duration of the decay (Eq. (3.8)) yields

$$\int_0^\infty i_F(t) dt = k_r^S \tau_S [{}^1A^*]_0 = [{}^1A^*]_0 \Phi_F$$

This quantity is the total amount of photons emitted per unit volume under steady-state

conditions which, divided by time, yields the above expression for i_F . An exciting light of constant intensity can then be considered as an infinite sum of infinitely short light pulses.

The fluorescence intensity can thus be written as

$$I_F(\lambda_E, \lambda_F) = kF_\lambda(\lambda_F)I_A(\lambda_A) \quad (3.17)$$

The proportionality factor k depends on several parameters, in particular on the optical configuration for observation (i.e., the solid angle through which the instrument collects fluorescence, which is in fact emitted in all directions) and on the bandwidth of the monochromators (i.e., the entrance and exit slit widths; see Chapter 9).

Furthermore, the intensity of the transmitted light can be expressed using the Beer–Lambert law (see Chapter 2):

$$I_T(\lambda_E) = I_0(\lambda_E)\exp[-2.3\varepsilon(\lambda_E)lc] \quad (3.18)$$

where $\varepsilon(\lambda_E)$ denotes the molar absorption coefficient of the fluorophore at wavelength λ_E (in $\text{L mol}^{-1}\text{cm}^{-1}$), l the optical path in the sample (in cm), and c the concentration (in mol L^{-1}). The quantity $\varepsilon(\lambda_E)lc$ represents the absorbance $A(\lambda_E)$ at wavelength λ_E .

Equations (3.16)–(3.18) lead to

$$I_F(\lambda_E, \lambda_F) = kF_\lambda(\lambda_F)I_0(\lambda_E)\{1 - \exp[-2.3\varepsilon(\lambda_E)lc]\} \quad (3.19)$$

In practice, measurement of the variations in I_F as a function of wavelength λ_F , for a fixed excitation wavelength λ_E , reflects the variations in $F_\lambda(\lambda_F)$ and thus provides the fluorescence spectrum.⁸⁾ Because the proportionality factor k is generally unknown, the numerical value of the measured intensity I_F has no meaning, and generally speaking, I_F is expressed in arbitrary units. In the case of low concentrations, the following expansion can be used in Eq. (3.17):

$$1 - \exp(-2.3\varepsilon lc) = 2.3\varepsilon lc - \frac{1}{2}(2.3\varepsilon lc)^2 + \dots$$

In highly diluted solutions, the terms of higher order become negligible. By keeping only the first term, we obtain

$$I_F(\lambda_E, \lambda_F) \cong kF_\lambda(\lambda_F)I_0(\lambda_E)[2.3\varepsilon(\lambda_E)lc] = 2.3kF_\lambda(\lambda_F)I_0(\lambda_E)A(\lambda_E) \quad (3.20)$$

This relation shows that the fluorescence intensity is proportional to the concentration only for low absorbances. Deviation from a linear variation increases with increasing absorbance (Table 3.2).

Moreover, when the concentration of fluorescent compound is high, inner filter effects reduce the fluorescence intensity depending on the observation conditions (see Chapter 9). In particular, the photons emitted at wavelengths corresponding to the overlap between the absorption and emission spectra can be reabsorbed (radiative transfer). Consequently, when fluorometry is used for a quantitative evaluation of the concentration of a species, it should be kept in mind that the

8) It will be shown in Chapter 6 that k depends on the wavelength because the transmission of the monochromator and the sensitivity of the detector are wavelength dependent. Therefore, correction of spectra is necessary for quantitative measurements.

Table 3.2 Deviation from linearity in the relation between fluorescence intensity and concentration for various absorbances.

Absorbance	Deviation (%)
10^{-3}	0.1
10^{-2}	1.1
0.05	5.5
0.10	10.6
0.20	19.9

fluorescence intensity is proportional to the concentration only for dilute solutions.

Equation (3.20) can be integrated over the emission wavelengths to give

$$I_F(\lambda_E) \cong 2.3k\Phi_F I_0(\lambda_E)[\varepsilon(\lambda_E)lc] \quad (3.21)$$

This equation shows that when comparing the fluorescence of different compounds at equal concentrations and for the same experimental setup, the respective total intensity is determined not only by the fluorescence quantum yield but also by the absorption coefficient at the excitation wavelength. This gives rise to a figure of merit often used, the *brightness* of a fluorophore, which is simply the product $\varepsilon(\lambda_E)\Phi_F$. High fluorescence quantum yields are usually associated with high $S_1 \leftarrow S_0$ absorption coefficients (the Einstein coefficients A and B being proportional), and hence to a good brightness for that band, but not necessarily for other excitation wavelengths. Furthermore, a compound whose fluorescence quantum yield is relatively small but still significant may be useless *per se* if the respective absorption coefficient is low for all practical excitation wavelengths, that is, if its brightness is low for the entire excitation range. This is for instance the case of the luminescent lanthanide ions, whose f - f transitions are very weak (see Chapter 4). In this case, absorption is enhanced by the use of appropriate aromatic ligands that are good absorbers and act as antennas, and also transfer the absorbed energy to the emitting metal, hence increasing its effective brightness (see Chapter 4).

Brightness is an important parameter for fluorophores used as tracers, especially in biology (see Chapter 15). Some values are also given in the Appendix at the end of the book.

This is because the fluorescence intensity is measured above a low background level whereas in the measurement of low absorbances, two large signals that are slightly different are compared. Thanks to outstanding progress in instrumentation, it is now possible in some cases to even detect a single fluorescent molecule (see Chapter 12).

The fluorescence spectrum of a compound may be used in some cases for the identification of species, especially when the spectrum exhibits vibronic bands

(e.g., in the case of aromatic hydrocarbons), but the spectra of most fluorescent probes (in the condensed phase) exhibit broad bands.

Equations (3.15)–(3.20) have been written using wavelengths, but they could also have been written using wavenumbers. For example, the integral in Eq. (3.15) is found to be written in some books using wavenumbers instead of wavelengths:

$$\int_{\infty}^0 F_{\bar{\nu}}(\bar{\nu}_F) d\bar{\nu}_F = \Phi_F \quad (3.22)$$

Where $F_{\bar{\nu}}(\bar{\nu}_F)$ is the fluorescence intensity per unit wavenumber.

Comments should be made here on the theoretical equivalence between Eqs. (3.15) and (3.22). The fluorescence quantum yield Φ_F , that is, the number of photons emitted over the whole fluorescence spectrum divided by the number of absorbed photons, must of course be independent of the representation of the fluorescence spectrum in the wavelength scale (Eq. (3.15)) or the wavenumber scale (Eq. (3.22)):

$$\Phi_F = \int_0^{\infty} F_{\lambda}(\lambda_F) d\lambda_F = \int_{\infty}^0 F_{\bar{\nu}}(\bar{\nu}_F) d\bar{\nu}_F \quad (3.23)$$

However, as shown in Box 3.3, it should be emphasized that $F_{\lambda}(\lambda_F)$ is not equal to $F_{\bar{\nu}}(\bar{\nu}_F)$ and this has practical consequences.

From the theoretical point of view, the important consequence of Eq. (3.23) is that the conversion of an integral from the wavenumber form to the wavelength form simply consists of replacing $F_{\bar{\nu}}(\bar{\nu}_F)$ by $F_{\lambda}(\lambda_F)$, and $d\bar{\nu}_F$ by $d\lambda_F$. However, from the practical point of view, because all spectrofluorometers are equipped with grating monochromators, calculation of the integral must be performed with the wavelength form. The fluorescence spectrum is then recorded on a linear wavelength scale at constant wavelength bandpass $\Delta\lambda_F$ (which is the integration step) (see Box 3.3).

3.3.3

Excitation Spectra

The variations in fluorescence intensity as a function of the excitation wavelength λ_E for a fixed observation wavelength λ_F represents the excitation spectrum. According to Eq. (3.20), these variations reflect the evolution of the product $I_0(\lambda_E)A(\lambda_E)$. If we can compensate for the wavelength dependence of the incident light (see Chapter 9), the sole term to be taken into consideration is $A(\lambda_E)$, which represents the absorption spectrum. The corrected excitation spectrum is thus identical in shape to the absorption spectrum, provided that there is a single species in the ground state. In contrast, when several species are present, or when a sole species exists in different forms in the ground state (aggregates, complexes, tautomeric forms, etc.), the excitation and absorption spectra are no longer superimposable. Comparison of absorption and excitation spectra often provides useful information.

Box 3.3 Determination of fluorescence quantum yields from fluorescence spectra: wavelength scale or wavenumber scale?

Fluorescence quantum yields are usually determined by integration of the fluorescence spectrum (and subsequent normalization using a standard of known fluorescence quantum yield in order to get rid of the instrumental factor k appearing in Eq. (3.17) or (3.18); see Chapter 9). In practice, attention should be paid to the method of integration.

When the emission monochromator of the spectrofluorometer is set at a certain wavelength λ_f with a bandpass $\Delta\lambda_f$, the reading is proportional to the number of photons emitted in the wavelength range from λ_f to $\lambda_f + \Delta\lambda_f$, or in the corresponding wavenumber range from $1/\lambda_f$ to $1/(\lambda_f + \Delta\lambda_f)$. The number of detected photons satisfies the relationship

$$F_\lambda(\lambda_f)\Delta\lambda_f = F_{\bar{\nu}}(\bar{\nu}_f)\Delta\bar{\nu}_f$$

where $\Delta\bar{\nu}_f$ must be positive and is thus defined as $1/\lambda_f - 1/(\lambda_f + \Delta\lambda_f)$. Hence,

$$F_\lambda(\lambda_f) = F_{\bar{\nu}}(\bar{\nu}_f) \frac{1}{\lambda_f(\lambda_f + \Delta\lambda_f)}$$

Because $\Delta\lambda_f \ll \lambda_f$, this equation becomes

$$F_\lambda(\lambda_f)\lambda_f^2 = F_{\bar{\nu}}(\bar{\nu}_f)$$

which clearly shows that $F_\lambda(\lambda_f)$ is not equal to $F_{\bar{\nu}}(\bar{\nu}_f)$.

If a grating monochromator is used to record the fluorescence spectrum, the bandpass $\Delta\lambda_f$ is constant and the scale is linear in wavelength. Therefore, after correction of the spectrum (see Chapter 9), the integral should be calculated with the wavelength form (Eq. (3.13)). Some workers convert the wavelength scale into the wavenumber scale before integration, but this procedure is incorrect. In some cases, the consequence might be that the quantum yield calculated by comparison with a fluorescent standard is found to be greater than 1!

It should be noted that no such difficulty appears with the integral of an absorption spectrum because the absorption coefficient is proportional to the logarithm of a ratio of intensities, so that $\varepsilon(\lambda) = \varepsilon(\bar{\nu})$. For instance, in the calculation of an oscillator strength (defined in Chapter 2), integration can be done either in the wavelength scale or in the wavenumber scale.

3.3.4 Stokes Shift

The Stokes shift is the gap between the maximum of the first absorption band and the maximum of the fluorescence spectrum (expressed in wavenumbers), $\Delta\bar{\nu} = \bar{\nu}_a - \bar{\nu}_f$ (Figure 3.3).

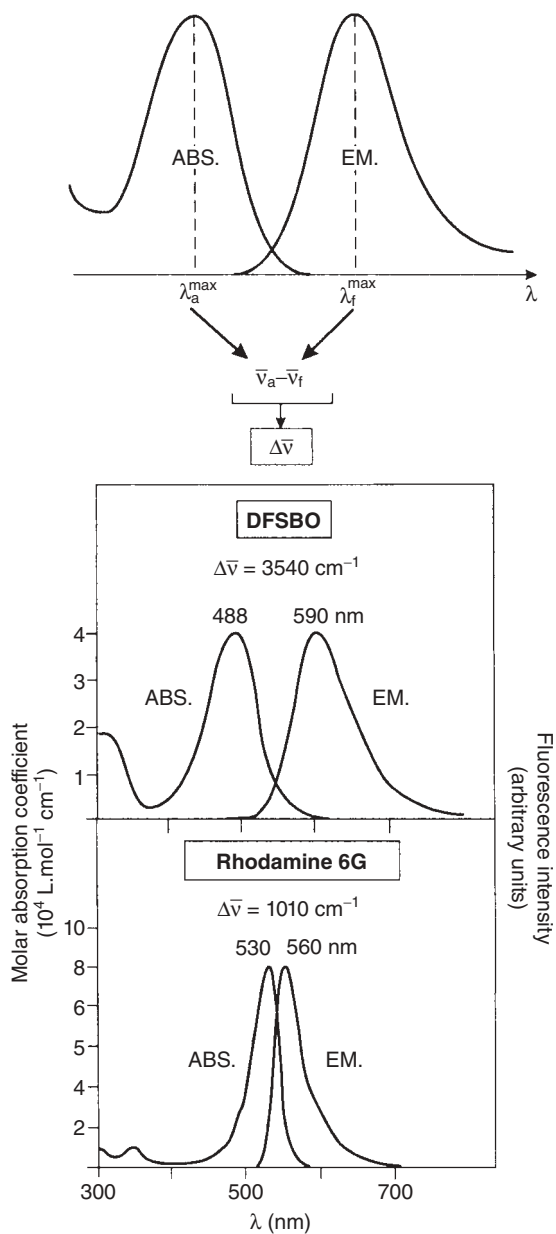


Figure 3.3 Definition of the Stokes shift. Examples of Stokes shifts: rhodamine 6G and a benzoxazinone derivative (DFSBO) (Fery-Forgues, S. *et al.* (1992) *J. Phys. Chem.* **96**, 701).

This important parameter can provide information on the excited states. For instance, when the dipole moment of a fluorescent molecule is higher in the excited state than in the ground state, the Stokes shift increases with solvent polarity (Chapter 5) which allows estimation of this parameter using fluorescent polarity probes (Chapter 13).

From a practical point of view, the detection of a fluorescent species is of course easier when the Stokes shift is larger.

Bibliography

See the general books on fluorescence spectroscopy cited at the end of Chapter 1.

11

Fluorescence Microscopy

Quelle source délicieuse et inépuisable de plaisirs réels peut nous procurer un bon Microscope ! Il n'est pas une science pratique qui ne lui doive un grand nombre de perfectionnements. Combien n'a-t-il pas fait jaillir de faits importants (. . .)! Combien de trésors inépuisables restent encore à découvrir!

[Which delicious and inexhaustible source of real pleasures can get us a good Microscope. There is no practical science that does not owe it a large number of improvements. It disclosed so many important facts (. . .)! How many inexhaustible treasures still remain to discover!]

Noël Paymal Lerebours, 1846

Fluorescence microscopy is a powerful tool for the study of micro- and nanostructured systems, be they living cells and biological tissues, or colloids, liquid crystals, polymers, and fibers. In classical fluorescence microscopy (wide-field microscopy), the full field is viewed simultaneously, but in many studies, the submicrometer level of detail requires a sequential scanning of the area (or volume) of interest. This is accomplished with confocal and two-photon microscopies that allow 3D imaging. A higher lateral resolution can still be attained with special (superresolution) techniques like scanning near-field optical microscopy (SNOM), stimulated emission depletion (STED), and stochastic optical reconstruction microscopy (STORM). Inclusion of the time dimension in fluorescence microscopy is accomplished with fluorescence lifetime imaging (FLIM) techniques, both in the time domain and in the frequency domain. This chapter will focus on all these fluorescence microscopy techniques.

11.1

Wide-Field (Conventional), Confocal, and Two-Photon Fluorescence Microscopies

11.1.1

Wide-Field (Conventional) Fluorescence Microscopy

In a common optical microscope (*bright field microscope*), the sample is illuminated with a light source and it is this same light that is analyzed, after interaction (absorption, reflection, scattering, diffraction, refraction, and so on) with the sample. In a *fluorescence microscope*, the collected light originates from the sample itself. A wide-field fluorescence microscope differs from a standard optical microscope by the light source (LED, mercury, or xenon lamp), which produces UV-visible light. The excitation wavelength is selected by an interference filter or a monochromator.

Excitation of the sample and observation of its fluorescence are usually done through the same objective, that is, with a front-face (ca. 0°) geometry (*epifluorescence microscope*, Figure 11.1). Observation of the fluorescence is made by eye or with a charge-coupled device (CCD) camera.

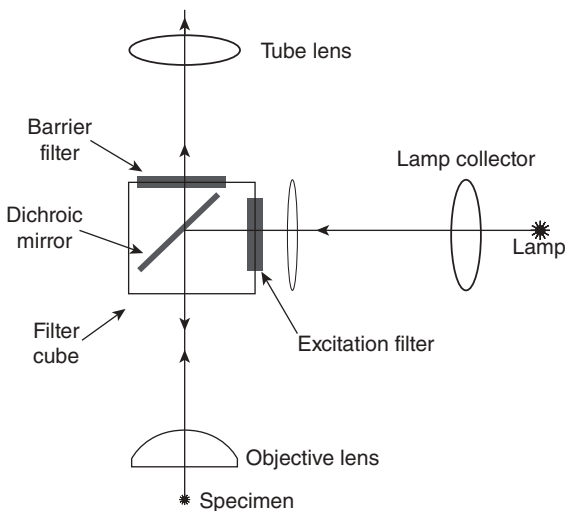


Figure 11.1 Epifluorescence wide-field microscope. The heart of an epifluorescence microscope is a “filter cube” (also used in other microscopes) housing two filters and a dichroic mirror. Excitation light (from a lamp) goes through the excitation filter and is reflected by the dichroic mirror. In wide-field microscopy, an image of the source is formed at the back focal plane of the objective, producing uniform illumination of the sample.

The fluorescence emitted is collected by the objective and is transmitted by the dichroic mirror toward the detector. Backward reflected excitation light is removed with the barrier (emission) filter. Different cubes are used for different excitation/emission wavelengths, hence for different fluorophores (reproduced with permission from Parker I. (2003) *Meth. Enzymol.*, **360**, 345).

Fluorescence microscopes can have two different configurations, *upright* and *inverted*, according to the position of the objective: in the upright configuration, it is located above the sample, whereas in the inverted one, it is below the sample. The last one is usually preferred when working with biological samples or with additional techniques like SNOM (see Section 11.2.1) and atomic force microscopy (AFM).

A very important parameter in microscopy is the *resolution* (or *critical dimension*), which is the minimum distance at which two distinct and neighboring features or objects (in the xy -plane) can still be identified as separate entities. For conventional fluorescence microscopes, the resolution is approximately equal to half the wavelength of the radiation used (diffraction or Abbe's limit), that is, about 200–400 nm for visible radiation. In order to understand the origin of this limitation, one must first consider the image that a continuously emitting and isotropic point source (for our purposes, a subnanometer-sized source) from the sample produces at the plane where it is detected and recorded. The scaled image, called the (*detection*) *point-spread function* (PSF), is much broader than the original, and is, in the simplest case, a disk with a bright center and progressively fainter concentric rings (Airy pattern), whose effective radius (e.g., 200 nm) is defined by the collection optics (lenses, pinholes, etc.). The center of the disk can be usually determined within 10–20 nm, and so, in principle, fluorophores can also be located with this precision. However, when two or more fluorophores are viewed as being within 200–400 nm (in the best case) from each other, the respective PSF overlaps in such a way that a single spot is obtained for the ensemble, when excited, and individual contributions (individual disks) can no longer be recognized in the image (“optical crowding,” determined not only by concentration but also by depth of field, see below). The diffraction limit is attained.

Another important optical parameter is the *depth of field* (thickness of the z - or optical axis layer). In a conventional fluorescence microscope, it is 2–3 μm . This may be too high for samples that are microscopically heterogeneous along the optical axis. Furthermore, for samples thicker than the depth of field, the images are blurred by out-of-focus fluorescence. Corrections for the last effect using appropriate software are possible, but other techniques such as confocal microscopy and two-photon excitation microscopy are generally preferred *that allow viewing finer details along the z -axis, hence obtaining 3D images if desired*. It is also possible to overcome the resolution limit imposed by diffraction using techniques like scanning near-field optical microscopy (SNOM) and other super-resolution (subdiffraction) techniques, all far-field, under the common designation of “photoswitching” microscopies (Section 11.2.3).

11.1.2

Confocal Fluorescence Microscopy

In a confocal microscope, invented in the mid-1950s, but mainly developed from 1978 onward (Sheppard and Wilson), a focused spot of light scans the specimen. As in conventional fluorescence microscopy, the fluorescence emitted by the

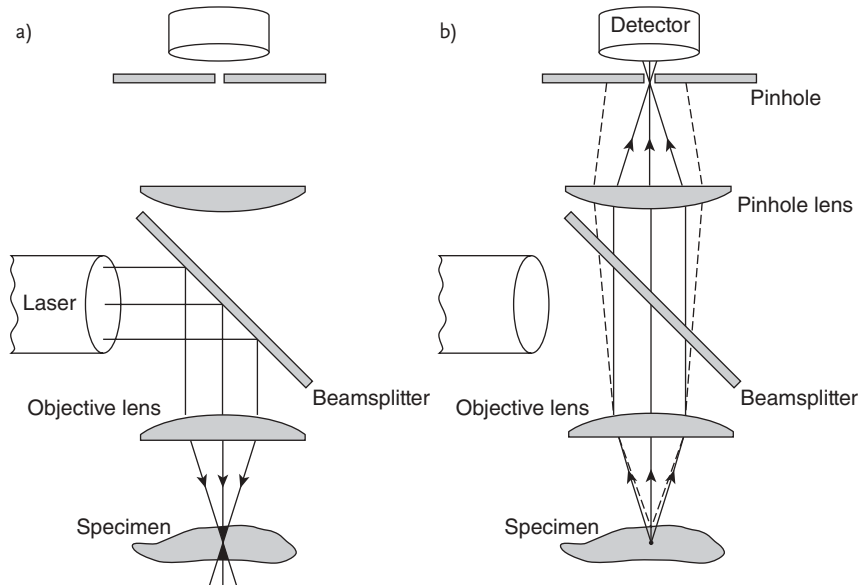


Figure 11.2 Diagram of a confocal fluorescence microscope. (a) The laser beam is focused to a diffraction-limited spot on the sample, but fluorophores are excited within the whole cone. (b) Fluorescence generated at the focus is imaged through a pinhole onto the detector. Fluorescence coming from other parts of the excitation cone is blocked. It is implicit in the drawing that a contact fluid

with a refractive index matching that of the specimen is used. Use of two detectors and an additional dichroic mirror allows simultaneous detection at two emission wavelengths (reproduced with permission from Jonkman, J.E.N., Swoger, J., Kress, H., Rohrbach, A., and Stelzer, E.H.K. (2003) *Meth. Enzymol.*, **360**, 416).

specimen is directed to a detector (usually an avalanche photodiode (APD)). Apart from the scanning mode, the two major differences are the excitation source, which is a laser, and the existence of a pinhole aperture. Fluorescence from out-of-focus planes above and below the specimen strikes the aperture wall and cannot pass through the pinhole (Figure 11.2).

The principle is somewhat similar to the reading of a compact disk: a focused laser beam is reflected by the microscopic pits (embedded inside a plastic layer) toward a small photodiode so that scratches and dust have no effect (rotation of the disk is in this case the equivalent of scanning). In confocal fluorescence microscopy, scanning is achieved using vibrating mirrors or a rotating disk containing multiple pinholes in a spiral arrangement (Nipkow disk). Images are obtained pixel by pixel, stored on a computer and displayed on a monitor, whereas in wide-field microscopy, all pixels for the whole image are recorded simultaneously with a CCD.

One of the distinctive features of confocal microscopy is that it can produce optical slices of defined thickness through thick specimens (Figure 11.2). Using a lens of high numerical aperture (NA), thickness of the confocal sections can reach

a theoretical limit of about 500 nm (z -axis or axial resolution). Therefore, by moving the specimen up and down, a three-dimensional (3D) image is obtained. The achievable lateral (xy -plane) resolution is similar to that of conventional microscopy (ca. 200–400 nm).

In order to get a better understanding of the magnitudes involved, it is interesting to consider a homogeneous distribution of point particles (e.g., fluorophores) in a transparent 3D matrix. For a depth of field Δz , the effective number of particles per unit area (2D number density) viewed in the microscope's field is $\sigma = n\Delta z$, where n is the number density (number of particles per unit volume). The corresponding mean lateral distance L is $L = 1/(2\sigma^{1/2})$. Using $\Delta z = 500$ nm, L attains 290 nm (a typical resolution value) for a concentration as low as 10^{-8} M. In order to individualize (resolve) 90% of the fluorophores in the field of view, the 3D concentration cannot exceed 10^{-9} M. These simple calculations show that avoidance of optical crowding requires very dilute 3D homogeneous solutions, or their local equivalent. These are important considerations for single molecule spectroscopy of immobilized molecules (Chapter 12).

It should be noted that, because confocal microscopy collects only a fraction of the total fluorescence emitted by a sample, the excitation energy required to image this fluorescence must be higher than in conventional fluorescence microscopy. Therefore, the amount of photobleaching per detected photon is higher. Photobleaching should be minimized by using stable fluorophores and by operating the confocal microscope at low laser power, high detector sensitivity, and maximum objective numerical aperture.

Confocal fluorescence microscopy can be combined with time-domain and frequency-domain techniques to produce lifetime imaging (see Section 11.2.3).

11.1.3

Two-Photon Excitation Fluorescence Microscopy

In conventional fluorescence spectroscopy, a fluorophore is excited by absorption of one photon whose energy corresponds to the energy difference between the ground state and the excited state. The simultaneous absorption of two red photons can excite a molecule whose absorption spectrum is the UV (see Chapter 2). For instance, absorption of two photons in the red light can excite a molecule that gets absorbed in the UV. Two-photon excitation is a nonlinear process; there is a quadratic dependence of absorption on excitation light intensity.

Two-photon excitation fluorescence microscopy was introduced in 1990 by Watt Webb and coworkers. When a single laser is used, the two photons are of identical wavelength, and the technique is called two-photon excitation fluorescence microscopy. When the photons are of different wavelengths λ_1 and λ_2 (so that $1/\lambda_1 + 1/\lambda_2 = 1/\lambda_0$), the technique is called two-color excitation fluorescence microscopy.

The probability of two-photon absorption depends on both spatial and temporal overlap of the incident photons (the photons must arrive within 10^{-18} s). For most molecules, the cross-sections for two-photon absorption are small (see Chapter 2). Consequently, only fluorophores located in a region of very large photon flux can be

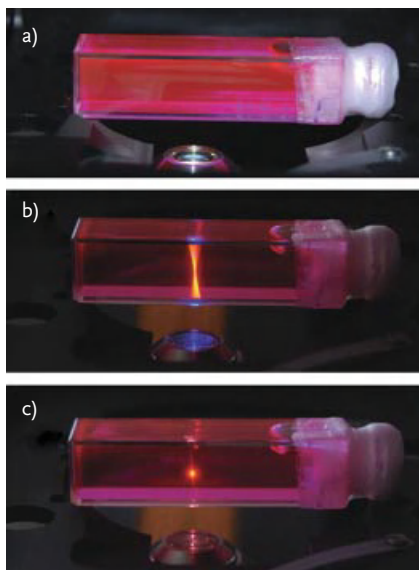


Figure 11.3 Experimental excitation profile corresponding to confocal (b) and two-photon (c) excitation (fluorescence microscope from CQFM-IST). In both cases a cell with a rhodamine B solution (red fluorescence) is placed above the microscope objective. In the confocal case, excitation occurs throughout the path of the beam, and the exciting blue

light (460 nm) is also seen. In the two-photon case (800 nm) excitation takes place only within a localized 3D spot. The spot is however slightly broader than the narrowest confocal region. For comparison, whole cell front-face fluorescence in response to the camera flash is also shown (a).

excited (Figure 11.3). Mode-locked, high-peak power lasers like titanium-sapphire lasers can provide enough intensity for two-photon excitation in microscopy.

Because the excitation intensity varies as the square of the distance from the focal plane, the probability of two-photon absorption outside the focal region falls off with the fourth power of the distance along the z optical axis. Excitation of fluorophores can occur only at the focal point. Using an objective with a numerical aperture of 1.25 and an excitation beam at 780 nm, more than 80% of total fluorescence intensity is confined to within 1 μm of the focal plane. The excitation volume is of the order of 0.1–1 fL. Compared to conventional fluorimeters, this represents a reduction by a factor of 10^{10} of the excitation volume.

Two-photon excitation provides intrinsic 3D resolution in laser scanning fluorescence microscopy. The 3D sectioning effect is comparable to that of confocal microscopy, but lateral (xy -plane) resolution is slightly lower, as the excitation wavelength has twice the value for one-photon excitation.

Two-photon excitation fluorescence microscopy has at least two advantages with respect to the confocal one: (i) there is *no out-of-focus photobleaching* and (ii) the *excitation beam is not attenuated by out-of-focus absorption*, which results in increased penetration depth of the excitation light. In biological samples, the longer excita-

tion wavelength used also means: (iii) *negligible autofluorescence* and (iv) an additional increase in the penetration depth owing to *decreased light scattering of the excitation beam*.

In addition to these advantages, two-photon fluorescence microscopy also allows exciting UV-absorbing fluorophores, whereas confocal fluorescence microscopy usually relies on fluorophores that absorb in the visible.

However, photobleaching within the in-focus area can be somewhat higher than in confocal microscopy, depending on the fluorophore. The major technical limitation of two-photon fluorescence microscopy is the need of photostable fluorophores with significant two-photon absorption cross-sections, and one of the major strengths is the possibility of obtaining deep images of biological tissues (Box 11.1).

Two-photon fluorescence microscopy can be combined with time-domain and frequency-domain techniques to produce lifetime imaging (see Section 11.2.4). As with wide-field and confocal microscopy, simultaneous detection at two emission wavelengths (channels) is possible.

11.1.4

Fluorescence Polarization Measurements in Microscopy

Polarization imaging is best carried out with linearly polarized excitation and requires the measurement of two polarized components for each pixel. A polarizing beam splitter, sending each component to a different detector, can be used. Sequential acquisition of each component is also possible, by rotating the excitation or emission polarizer through 90° . A problem with respect to the absolute values of the anisotropy is the effect of aperture. The usual formulas for the anisotropy assume normal incidence for the excitation as well as observation of fluorescence normal to the surface (Chapter 7).

However, fluorescence coming from the focal point is collected within a cone (the maximum acceptance angle θ defines the numerical aperture, $NA = n \sin \theta$, where n is the refractive index of the medium in contact with the objective). The effect can be significant; for example, for a typical numerical aperture of 1.3, the measured anisotropy can be 0.22, instead of 0.35 measured with the low NA of fluorimeters (see Yan and Marriot, in Marriot and Parker, 2003). It should also be reminded that two-photon excitation has different rules with respect to the anisotropy values (see Chapter 7).

11.2

Super-Resolution (Subdiffraction) Techniques

11.2.1

Scanning Near-Field Optical Microscopy (SNOM)

As mentioned, the maximal spatial resolution of a conventional microscope is set by diffraction and is approximately $\lambda/2$, λ being the wavelength. Nevertheless, this

Box 11.1 Two-photon fluorescence microscopy of biological tissues

With very few exceptions, biological tissues scatter light strongly, rendering impossible the use of confocal microscopy for deep imaging. Two-photon excitation spectroscopy allows imaging biological tissues nondestructively down to 1 mm deep, whereas confocal microscopy attains at most tens of micrometers [1]. Out-of-focus scattering not only blurs confocal images but also greatly reduces the signal strength. In the case of two-photon absorption, scattering is less serious a problem, nevertheless it has the effect of broadening the laser pulses, hence reducing the absorption efficiency for a given intensity. Fluorescence from deep regions is also severely attenuated by scattering, and this is usually the limiting factor with respect to the maximum achievable imaging depth.

Two-photon excitation fluorescence imaging of several intact organs of living animals is presently used. Unless the structures of interest are autofluorescent, labeling of some sort is needed. Fluorescent dyes can be injected into the blood stream, or used for direct staining. Fluorescent proteins can also be expressed, and transgenic animals are studied. An example of live tissue (mouse neocortex) imaging is shown in Figure B11.1.1 [1].

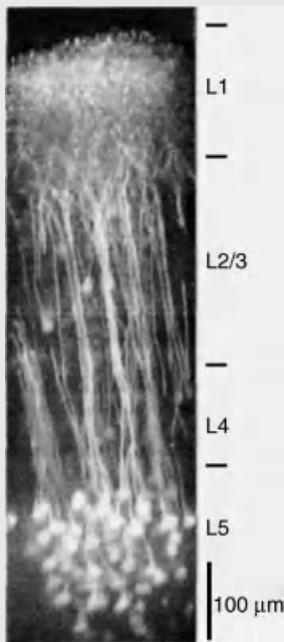


Figure B11.1.1 Neocortex (brain tissue) image of a live transgenic mouse expressing a fluorescent chloride indicator. Skull bone is removed locally. Data taken with a 10W pumped Ti:sapphire laser using a $40\times$ NA 0.8 water-immersion objective (reproduced with permission from Helmchen, F., and Denk, W. (2005) *Nat. Methods*, 2, 932–940).

1 Helmchen, F. and Denk, W. (2005) *Nat. Methods*, 2, 932–940.

limit applies only to far-field radiation, and can be overcome by using a subwavelength light source and by placing the sample very close to this source (at distances shorter than the wavelength, i.e., in the near field). The relevant domain is near-field optics (as opposed to far-field conventional optics), which has been applied to microscopy, spectroscopy, and optical sensors. In particular, scanning near-field optical microscopy (SNOM or NSOM) has proved to be a powerful tool in physical, chemical, and life sciences.

The idea of near-field optics to bypass the diffraction limit was proposed by Syngé in 1928. Syngé's idea is illustrated in Figure 11.4. Incident light passes

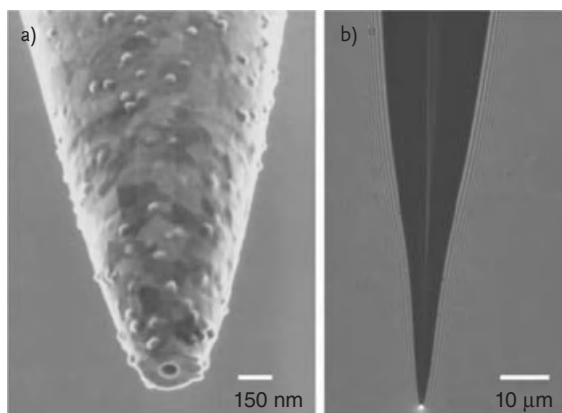
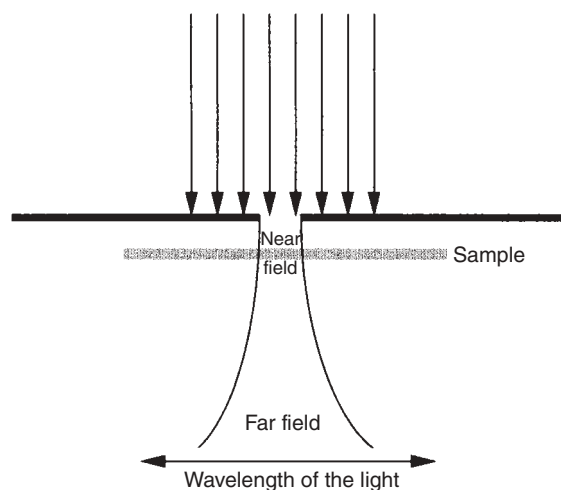


Figure 11.4 (Top) Principle of near-field optics according to Syngé's idea for overcoming the diffraction limit. (Bottom) Actual images of an aluminum-coated tip: In (a), the aperture is

clearly seen, whereas in (b), the spot of light emerging from the aperture is observed (reproduced with permission from Dickenson *et al.* (2010) *Anal. Bioanal. Chem.*, **396**, 31).

through a subwavelength hole in an opaque screen. The surface of the sample is positioned in close proximity to the hole so that the emerging light is forced to interact with it. The hole acts as a subwavelength-sized light probe that can be used to image a specimen before the light is diffracted out. The first measurement using this idea was reported half a century later, and today SNOM is used in many fields, but remains a much less popular technique than the far-field fluorescence microscopies.

As intensity cannot be increased above a certain threshold, owing to tip damage, very small holes also imply very few excitation photons, putting a limit on resolution typically at 50–100 nm (but down to 30 nm in favorable cases). In addition to its high lateral resolution, SNOM has an outstanding sensitivity that permits single-molecule measurements (see Section 11.2.2).

Most SNOM devices are built as additional accessories to an inverted fluorescence microscope (180° geometry, see Figure 11.5) that offers the advantage of providing images in confocal or two-photon modes (by exclusively using the objective for both excitation and detection) and allowing the region to be studied to be located with the higher resolution SNOM mode (Figure 11.5). A laser beam passes through a single-mode optical fiber whose end is fashioned into a near-field tip (Figure 11.4). The tip is held in a z -piezo head. An xy -piezo stage on which the sample is mounted permits the scanning of the sample. Light from the tip excites the sample whose emitted fluorescence is collected from below by an objective with a high numerical aperture and detected through a filter (to remove residual laser excitation light) and a detector (e.g., avalanche photodiode or optical multichannel analyzer (OMA)). This mode is called the illumination mode. Alternatively, in the collection mode, the sample is illuminated from the far field, and fluorescence is collected by the SNOM tip.

The systems that scan the piezos and record the image are similar to those used in atomic force microscopy.

The SNOM tip is obtained by heating and pulling a single-mode optical fiber down to a fine point. A reflective metal coating (aluminum, silver, or gold) is deposited by vacuum evaporative techniques in order to guide the light.

Precise positioning of the tip within nanometers of the sample surface is required to obtain high-resolution images. This can be achieved by a feedback mechanism that is generally based on the shear-force method: the tip is dithered laterally at one of its resonating frequencies with an amplitude of about 2–5 nm. As the tip comes within the van der Waals force field of the sample, the shear forces dampen the amplitude of the tip vibration. This amplitude can be monitored and used to generate a feedback signal to control the distance between the sample and the tip during imaging.

SNOM has a higher resolution than confocal and two-photon microscopy, but not higher than that of far-field super-resolution techniques (see Section 11.2.2). One of the major limitations of SNOM is the fact that the maximum depth (z -axis) cannot exceed a few tens of nanometers; hence, its 3D imaging capability is very limited. Another important drawback of SNOM is the quality and reproducibility of the tips.

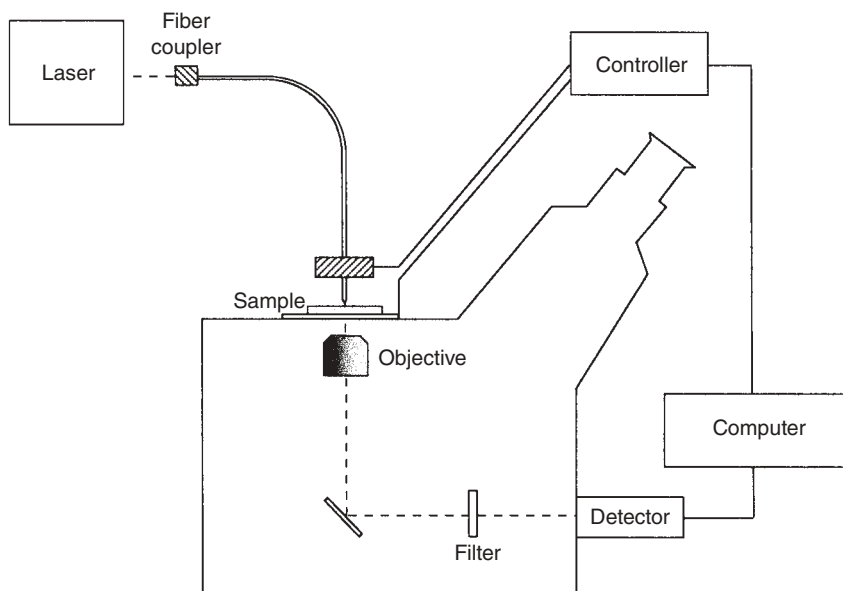


Figure 11.5 Schematic of a SNOM instrument built around an inverted fluorescence microscope and operating according to the illumination mode.

Two-photon excitation in SNOM has been shown to be possible with uncoated fiber tips in shared aperture arrangement. A recent development intended to overcome the minimum hole size limitation is the use of a nanoantenna instead of a hollow tip.

As with other microscopies, discrimination of species in complex samples can be made via lifetime measurements using the single-photon timing method coupled to SNOM. However, the presence of the tip in the close vicinity of the excited fluorophore (1–2 nm) may affect its decay rate, for example, via FRET.

11.2.2

Far-Field Techniques

As mentioned in Section 11.1, analysis of the individual PSF intensity profile allows locating a fluorophore within 10–20 nm (or down to 1–2 nm in optimized conditions—when the fluorophore is highly photostable and many counts are possible¹). However, if the distance between fluorophores is shorter than 200–400 nm,

- 1) Each photon collected corresponds to a given location (pixel). Successive counts (detector hits) allow building a histogram of the (detection) PSF. In particular, the average position gives the approximate location of the center of the disk: if σ is the PSF standard deviation (usually ca. 100–200 nm), then the standard deviation of

the mean is σ/\sqrt{N} where N is the number of counts. A photostable fluorophore may allow thousands of counts before bleaching. In practice, this increases the measurement time, and a few hundred counts are used, producing localizations with uncertainties of 10–20 nm. Note that localization cannot be better than the pixel size.

only a single, collective fluorescence spot is observed. For this to occur, fluorophores in this area need not be simultaneously excited. If they are excited at random, after a few accumulations contributions from all will add up to give a single, broad spot. Individualization of fluorophores can nevertheless be achieved by the temporary suppression of the emission of all surrounding fluorophores within a 200–400 nm radius, during a time sufficient to acquire enough photons to define the “uncontaminated” PSF of a specific fluorophore. The process is then repeated by exciting one of the previously “dark” fluorophores, and simultaneously rendering nonemissive the previously excited one. Repetition of the process allows locating all fluorophores, one at a time (in a given spot area). This can be achieved in a number of ways, all falling under the “photoswitching” category, as first discussed by Hell and Wichmann (1994). For this process to be feasible, all fluorophores must exist in at least two forms, one of which is emissive, and the other is nonemissive, and a transition between the two may be induced with light of two different wavelengths (one wavelength for each direction; one of the steps can even be spontaneous). An ingenious method for this purpose is the STED (stimulated emission depletion) technique (Figure 11.6).

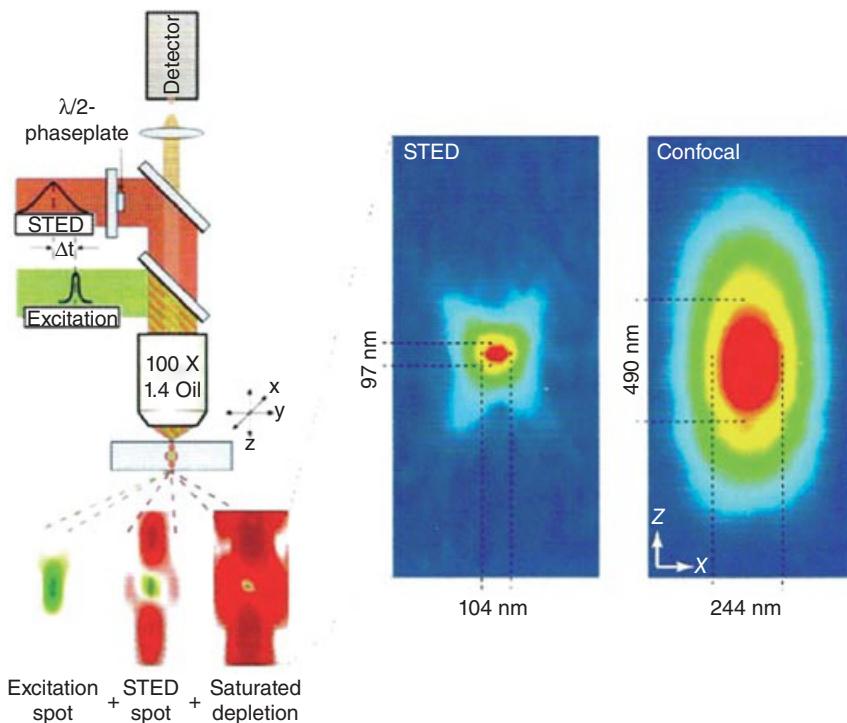


Figure 11.6 The principle of the STED method. The experimental setup is shown, along with the spots resulting from the excitation beam (green) and from the

depletion beam (red). The resulting reduction of the excited area is displayed on the right (reproduced with permission from Hell, S.W. (2003) *Nat. Biotechnol.*, 21, 1347).

In this technique, devised and put into practice by Stefan Hell and coworkers, a first pulse (excitation pulse), with a narrow circular cross-section and duration of a few picoseconds, excites several neighboring fluorophores. By itself, it would give rise to an unresolved, diffraction-limited fluorescence spot. However, after a delay of a few hundred picoseconds, while most of the initially excited fluorophores are still in the excited state, a second pulse (depletion pulse) of a slightly longer wavelength and much higher intensity is fired over the same area. The intensity distribution of this second beam is torus-shaped, hence stimulated emission occurs almost exclusively in the torus area, leaving a subdiffraction disk of excited fluorophores in the central area. The radius of this smaller disk may be enough to individualize a single excited fluorophore. Repeated sequences of excitation–depletion pulses during a certain dwell time allow accumulating a certain number of counts. Scanning in the proximity allows to obtain the PSF and to localize the fluorophore. While theoretically the localization of a fluorophore by STED can be extremely precise, photodegradation and other processes put a limit on the intensity of the depletion pulse. Notwithstanding, localizations with uncertainties of 20–50 nm have been attained. Using luminescent diamonds, whose centers are extremely photostable (see Chapter 4), a value as low as 6 nm was reported (see Rittweger *et al.*, 2009). CW laser sources were also shown to be effective in STED microscopy, as well as supercontinuum lasers, covering the entire spectral range required.

In the STED method, the nonemissive state (dark or off-state) is the ground state. However, with suitable fluorophores, the off-state can be a nonemissive photoproduct that relaxes slowly (thermally) to the original ground state. In this case, the torus (donut)-shaped pulse has the appropriate wavelength to generate the photoproduct and operates at a much lower intensity than that required for stimulated emission.

Other methods that can also break the diffraction limit are inherently stochastic and are based on single-molecule fluorescence. These methods, essentially equivalent, and proposed in 2006, are known under acronyms such as PALM (photoactivated localization microscopy) and STORM (stochastic optical reconstruction microscopy). The basic principle is the selection of a sparse subset of fluorophores. This is accomplished by initially shelving most of fluorophores in a dark state. Only a few, randomly selected, and on the average at distances between each other larger than the diffraction limit, remain excitable. Repeated excitation of these fluorophores allows obtaining the respective single-molecule PSF, and therefore the respective locations. The neighboring fluorophores are optically silent as they remain in the dark state. The system is then reset, and a new set of excitable fluorophores, randomly selected, is produced. These are next repeatedly excited until the respective positions are defined to a specified accuracy. Continuation of the sequence random activation-localization-bleaching allows obtaining enough individual locations (typically between 10^3 and 10^6 , each within 50–100 nm) to define a spatial pattern for the distribution of fluorophores (see Figure 11.7).

STORM usually relies on organic dyes such as Alexa647 and Cy5, whereas PALM uses fluorescent proteins. Dark states are obtained by bleaching, and

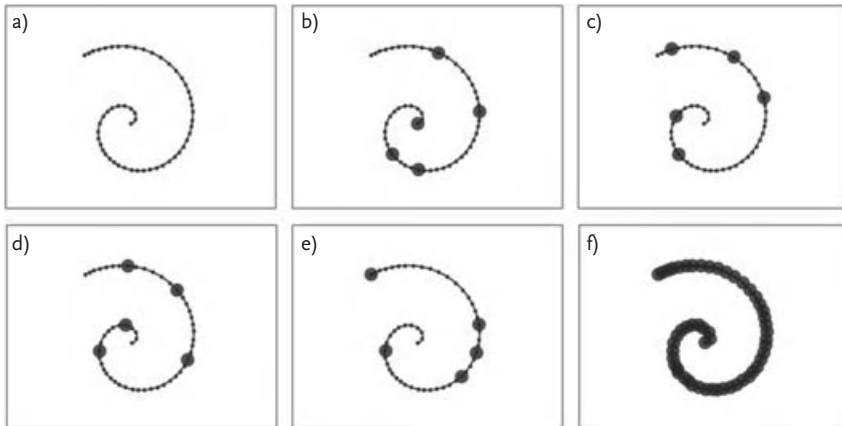


Figure 11.7 The principle of super-resolution stochastic methods such as STORM and PALM. (a) A flat unidimensional chain is labeled with photoactivatable fluorophores (small circles). (b–e) Consecutive and selective excitation of sparse sets of fluorophores, allows their sub-diffraction localization (large circles), typically with a resolution of tens of nm, that is, at least one order of magnitude higher than fluorophore dimensions. (f) Addition of the obtained sets allows reconstructing the original pattern.

activation is achieved with UV radiation. The main disadvantage of the stochastic methods is the long time (up to hours) needed to build the high-resolution image.

11.3 Fluorescence Lifetime Imaging Microscopy (FLIM)

Fluorescence lifetime imaging uses differences in the excited-state lifetime of fluorophores as a contrast technique for imaging. As emphasized in several chapters of this book, the excited-state lifetime of a fluorophore is sensitive to its microenvironment. Therefore, imaging of the lifetimes provides complementary information on local physical parameters (e.g., microviscosity) and chemical parameters (e.g., pH and ion concentration), and even on the identity of the fluorophore, in addition to information obtained from steady-state characteristics (fluorescence spectra, excitation spectra, and polarization). The origin of lifetime imaging is almost as old as that of lifetime measurements. The original Becquerel phosphoroscope (see Chapter 1) allowed direct observation of a macroscopic sample with varying time delays. However, lateral discrimination of lifetimes was not the purpose of the studies. It was Newton Harvey (1942) who built the first lifetime imaging microscope, still based on Becquerel's phosphoroscope. Fluorescence lifetime measurements in optical microscopes started in 1959, but the great impulse on FLIM happened only in the late 1980s, when CCDs and confocal microscopes became available (see Chen and Clegg, 2009).

Both time-domain and frequency-domain methods can be used in FLIM.

11.3.1

Time-Domain FLIM

Lifetime imaging is possible by a combination of the single-photon timing technique with scanning techniques, and is available as an option in some confocal and two-photon commercial microscopes. Simultaneous detection at two emission wavelengths (channels) is possible. However, collecting at each pixel a number of photons similar to that used with macroscopic samples is not feasible. In the first place, owing to the time required for obtaining a full FLIM image, a high resolution scan may lead to prohibitive acquisition times. Second, owing to photobleaching, as the same small subset of immobile fluorophores is repeatedly excited, whereas in macroscopic samples, usually liquid, there is a constant renewal by diffusion, and the intensity of the excitation beam can also be smaller. For these reasons, usually no more than a few thousand photons/pixel are collected. The small number of counts per pixel imposes severe limits on the accuracy of the results: As little as 200 photons can be satisfactory in the single exponential case, but several thousand or more may be needed to resolve double exponential decays. The small number of counts also restricts the number of channels in the decay histogram, which are typically between 32 and 128, compared to 1024 or 2048 for macroscopic samples. Measurement of very short lifetimes (tens of picoseconds) is usually not possible.

If accurate determination of decay curves is not the purpose, and a simple estimation of average lifetime suffices, but instead fast (up to real time) acquisition of images is essential, then the *rapid lifetime imaging* (RLI) method that uses time-gated detection can be used. Laser or LED pulses are used to periodically illuminate the entire field of view via an optical fiber and a lens of large numerical aperture, and two time windows ΔT at delay times t_1 and t_2 are defined on a gated CCD. For a single exponential decay of the form $\alpha \exp(-t/\tau)$, with a lifetime much larger than the pulse width, the corresponding fluorescence signals are proportional to

$$D_1 = \int_{t_1}^{t_1+\Delta T} \alpha \exp\left(-\frac{t}{\tau}\right) dt \quad (11.1)$$

$$D_2 = \int_{t_2}^{t_2+\Delta T} \alpha \exp\left(-\frac{t}{\tau}\right) dt \quad (11.2)$$

The lifetime corresponding to each pixel can then be calculated by means of the following expression:

$$\tau = \frac{t_2 - t_1}{\ln(D_1 / D_2)} \quad (11.3)$$

This procedure requires the determination of only two parameters per pixel, and lifetime images can be obtained very quickly. If the decay is complex, then Eq. (11.3) only approximately returns the average lifetime. Confocal and two-photon implementation of RLI is also possible.

11.3.2

Frequency-Domain FLIM

In frequency-domain FLIM, the optics and detection system (MCP image intensifier and slow scan CCD camera) are similar to those of time-domain FLIM, except for the light source, which consists of a LED or CW laser and an acousto-optical modulator instead of a pulsed source. The principle of lifetime measurement is the same as that described in Chapter 10 (Section 10.1.2). The phase shift and modulation depth are measured relative to a known fluorescence standard or to scattering of the excitation light. The most used detection mode is the homodyne one, that is, the modulation frequency of the excitation light is the same as that of the image intensifier (see Chen and Clegg, 2009). A single frequency is often used. The method is very fast and can be carried out at real time (video frequency).

In the case of a single exponential decay, the lifetime can be rapidly calculated by either the phase shift Φ or the modulation ratio M by means of the following equations established in Chapter 10 (Section 10.3.1):

$$\tau_{\Phi} = \frac{1}{\omega} \tan \Phi \quad (11.4)$$

$$\tau_M = \frac{1}{\omega} \left(\frac{1}{M^2} - 1 \right)^{1/2} \quad (11.5)$$

If the values calculated in these two ways are identical, the fluorescence decay is indeed a single exponential. Otherwise, for a multicomponent decay, $\tau_{\Phi} < \tau_M$. In this case, several series of images have to be acquired at different frequencies (at least five for a triple exponential decay because three lifetimes and two fractional amplitudes are to be determined), which is a challenging computational problem. For this reason, qualitative approaches are very useful such as the polar plot introduced in Chapter 10 and further discussed in Box 11.1.

11.4**Applications**

Fluorescence confocal microscopy is by far the most common high-resolution fluorescence imaging technique, and it is in particular extensively used in membrane and cell studies. Single living cells can indeed be studied by this technique: visualization of organelles, distribution of electrical potential, pH imaging, Ca^{2+} imaging, etc. Some interesting applications in chemistry and materials science have also been reported in the fields of colloids, liquid crystals, and polymer blends. In the last field, resolution down to the molecular level is usually desirable,

and for this reason not many studies using fluorescence microscopy exist, except at the single molecule level (see Chapter 12). An important exception is the characterization of microdomains in polymer-based luminescence oxygen sensors (Bowman *et al.*, 2003).

Two-photon excited fluorescence microscopy is increasingly used because of the specific advantages mentioned in Section 11.1.3. It is well suited to the study of highly scattering samples like biological tissues. An interesting application of both confocal and two-photon microscopies is the characterization of domains in giant unilamellar vesicles (GUV) composed of binary mixtures of phospholipids, with and without cholesterol, where the photoselection effect (see Chapter 7) is also clearly visualized (Bagatolli, 2006; Fidorra *et al.*, 2009).

SNOM is a remarkable tool for the analysis of thin films such as electroluminescent polymers J-aggregates, liquid crystals, and Langmuir-Blodgett films, but has not found widespread use thus far. Photosynthetic systems, protein localization, chromosome mapping, and membrane microstructure are examples of systems that have been successfully investigated by SNOM (see Dickenson *et al.*, 2010). Imaging of fixed biological samples in aqueous environments is in fact possible, but the study of unfixed cells is problematic, as it is that of corrugated samples.

FLIM is an outstanding tool for the study of single cells with the possibility of coupling multiparameter imaging of cellular structures with spectral information. Discrimination of autofluorescence of living cells from true fluorescence is possible on the basis of lifetime differences (see Box 11.2). Various applications have been reported: calcium (or other chemical) imaging; membrane fluidity, transport, and fusion; DNA sequencing; and clinical imaging (e.g., use of antibodies and nucleic acids labeled with fluorophores for quantitative measurements of multiple disease markers in individual cells of patient specimens). Additional characterization of microdomains in luminescence oxygen sensors was carried out using FLIM (López-Gejo, Haigh, and Orellana, 2010).

As already mentioned, Förster resonance energy transfer (FRET) is a popular process for imaging interactions in biological systems because it allows quantifying the distance between two species labeled with two different fluorophores. Studies can be done on the basis of intensities (intensity FRET) or lifetimes (FRET-FLIM). Whenever donor and acceptor are close by, quenching by energy transfer occurs, the donor intensity is decreased and the donor lifetime is reduced. In many applications, a qualitative picture suffices (see, e.g., Spoelgen *et al.*, 2009 for a combined intensity FRET and FRET-FLIM two-photon excitation study). If the acceptor is also fluorescent, its intensity will increase. As with solution studies, care must be taken to discard both direct excitation of the acceptor and emission of the donor at the acceptor emission wavelength.

Box 11.2 The polar plot in fluorescence microscopy

As described in Chapter 10 (Section 10.3.1), the single exponential decay locus in a polar (or phasor) plot is a half-circle, the precise location being a function of frequency and lifetime. The representation applies directly to the phase-modulation technique, but is also valid for time-resolved measurements, as the sine and cosine Fourier transforms of the (deconvoluted) decay can be numerically computed. In such a case, the frequency value is in principle chosen according to convenience. The polar plot approach is useful in conjunction with FLIM measurements, as it is fast, allows handling complex decays, and processes such as quenching and energy transfer can be identified by characteristic trajectories in the plane [1, 2]. Diagrams are used for selected pixels only.

In the case of multiexponential decays, it follows immediately from Eqs. (10.21) and (10.22) that the coordinates P and Q are given by

$$P = \sum_{i=1}^n f_i P_i \quad (\text{B.2.1})$$

$$Q = \sum_{i=1}^n f_i Q_i \quad (\text{B.2.2})$$

where the P_i and Q_i are the coordinates of each component, and the f_i are the respective weights. The point corresponding to the multiexponential decay is thus located at an average distance from those of the components. In the case of a two-exponential decay with positive amplitudes, for instance, the corresponding point falls on a straight line connecting the two components (Figure B11.2.1).

Similarly, a decay that results from contributions of different species can be positioned with respect to the corresponding points. If these species have

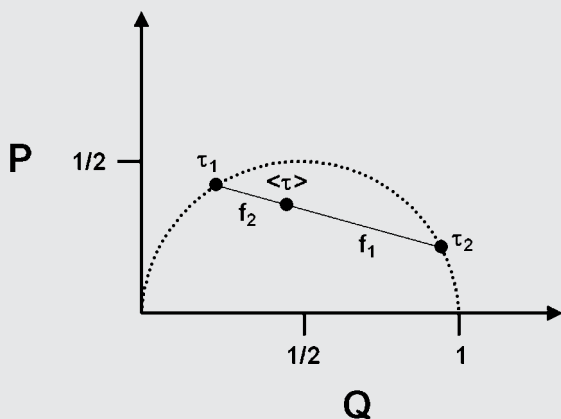


Figure B11.2.1 The polar plot for a two-exponential decay (with positive amplitudes). Analogously to the lever rule of thermodynamic phase diagrams, the fractional contribution of a given component is given by

the length of the segment connecting the decay point (“average lifetime”) to the opposite component, divided by the length of the full segment uniting the two extreme points (components).

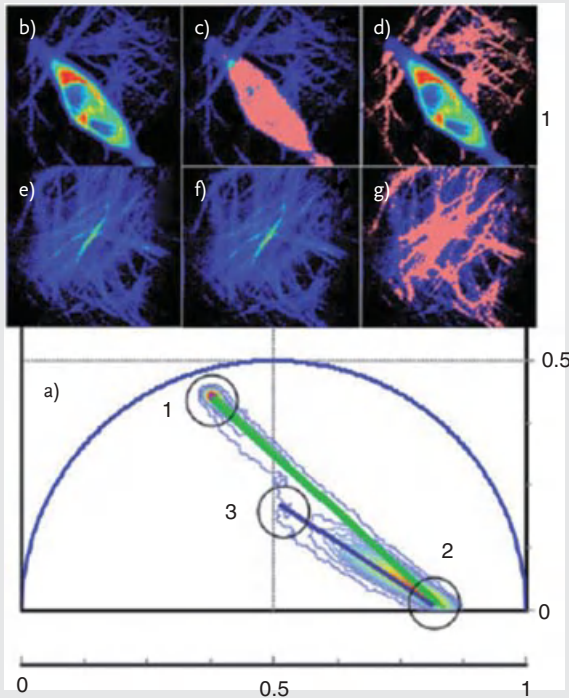


Figure B11.2.2 The polar plot for CHO-K1 cells transfected with paxillin EGFP (upper images) in a three-dimensional collagen matrix (upper and lower images). Phase plot (a) of the two images, produced with a two-photon microscope operating in the time domain. Data from neighboring pixels do not fall exactly on the same point, but rather define clusters. Region of the sample with a transfected cell (b) and with the collagen matrix (e). Pixels in the image selected at position 1 (c, EGFP) are highlighted in pink. It is seen that the EGFP decay is not single

exponential, as it lies inside the circle. (d and g) Pixels selected at position 2 (collagen) are highlighted in pink. The decay of collagen is seen to result from very long and very short components. Position 3 represents weak background fluorescence (with complex decay). Pixels with multiple contributions lie along the line joining the EGFP (1) and the collagen points (2) (green line) or the background autofluorescence (3) and the collagen point (2) (black line) (reproduced with permission from Caiolfa *et al.* (2008) *Biophys. J.*, **94**, L14).

themselves complex decays, the corresponding points define a polygon, located inside the circle, with the decay point lying in turn inside the polygon.

Several applications of the polar plot approach are described by Digman *et al.* [2, 3] One of these is displayed in Figure B11.2.2.

- 1 Redford, G.I. and Clegg, R.M. (2005) *J. Fluoresc.*, **15**, 805; Chen, Y.-C., and Clegg, R.M. (2009) *Photosynth. Res.*, **102**, 143.
- 2 Digman, M.A., Caiolfa, V.R., Zamai, M., and Gratton, E. (2008) *Biophys. J.*, **94**, L14.
- 3 Digman, M.A. and Gratton, E. (2012) The phasor approach to FLIM: exploiting

phasor linear properties, in *Fluorescence Lifetime Spectroscopy and Imaging: Principles and Applications in Biomedical Diagnostics* (ed. L. Marcu, P.M.W. French, and D.S. Elson) CRC Press.

Bibliography

Books on Fluorescence Microscopy

- Diaspro, A. (2002) *Confocal and Two Photon Microscopy. Foundations, Applications and Advances*, John Wiley & Sons, Inc., New York.
- Diaspro, A. (ed.) (2010) *Nanoscopy and Multidimensional Optical Fluorescence Spectroscopy*, CRC Press, Boca Raton, FL.
- Gadella, T.W.J. (ed.) (2008) *FRET and FLIM Techniques*, Elsevier, Amsterdam.
- Kotyk, A. (ed.) (1999) *Fluorescence Microscopy and Fluorescent Probes (Proceedings of the Third Conference Held in Prague on June 20–23, 1999)*, Espero Publishing, Prague.
- Marriot, G. and Parker, I. (eds) (2003) *Biophotonics, Part A, Methods in Enzymology*, vol. 360. Academic Press, Amsterdam.
- Periasamy, A. and Day, R.N. (eds) (2005) *Molecular Imaging. FRET Microscopy and Spectroscopy*, Oxford University Press, New York.
- Periasamy, A. and Clegg, R.M. (eds) (2009) *FLIM Microscopy in Medicine and Biology*, Taylor and Francis, Boca Raton.
- Sauer, M., Hofkens, J., and Enderlein, J. (2011) *Handbook of Fluorescence Spectroscopy and Imaging*, Wiley-VCH Verlag GmbH, Weinheim.
- Zayats, A. and Richards, D. (2009) *Nano-Optics and Near-Field Optical Microscopy*, Artech House, Boston.
- Jameson, D. and Ross, J.A. (2010) Fluorescence polarization/anisotropy in diagnostics and imaging. *Chem. Rev.*, **110**, 2685–2708.
- Confocal and Two-Photon Microscopies**
- Bagatolli, L.A. (2006) To see or not to see: lateral organization of biological membranes and fluorescence microscopy. *Biochim. Biophys. Acta*, **1758**, 1541–1556, and references therein.
- Bowman, R.D., Kneas, K.A., Demas, J.N., and Periasamy, A. (2003) Conventional, confocal and two-photon fluorescence microscopy investigations of polymer-supported oxygen sensors. *J. Microsc.*, **211**, 112–120.
- Diaspro, A., Chirico, G., and Collini, M. (2005) Two-photon fluorescence excitation and related techniques in biological microscopy. *Q. Rev. Biophys.*, **38**, 97–166.
- Denk, W., Strickler, J.H., and Webb, W.W. (1990) Two-photon laser scanning fluorescence microscopy. *Science*, **248**, 73–76.
- Eggeling, C., Volkmer, A., and Seidel, C.A.M. (2005) Molecular photobleaching kinetics of rhodamine 6G by one- and two-photon induced confocal fluorescence microscopy. *Chemphyschem*, **6**, 791–804.
- Ellis-Davies, G.C.R. (2011) Two-photon microscopy for chemical neuroscience. *ACS Chem. Neurosci.*, **2**, 185–197.
- Fidorra, M., Garcia, A., Ipsen, J.H., Härtel, S., and Bagatolli, L.A. (2009) Lipid domains in giant unilamellar vesicles and their correspondence with equilibrium thermodynamic phases: a quantitative fluorescence microscopy imaging approach. *Biochim. Biophys. Acta*, **1788**, 2142–2149.
- Helmchen, F. and Denk, W. (2005) Deep-tissue two-photon microscopy. *Nat. Methods*, **2**, 932–940.
- Prasad, V., Semwogerere, D., and Weeks, E.R. (2007) Confocal microscopy of colloids. *J. Phys. Cond. Mat.*, **19**, 113102.
- Rubart, M. (2004) Two-photon microscopy of cells and tissue. *Circ. Res.*, **95**, 1154–1166.
- Sheppard, C.J.R. and Wilson, T. (1978) Image formation in scanning microscopes with partially coherent source and detector. *Opt. Acta*, **25**, 315–325.
- SO, P.T.C., Dong, C.Y., Masters, B.R., and Berland, K.M. (2000) Two-photon excitation fluorescence microscopy. *Annu. Rev. Biomed. Eng.*, **2**, 399–429.
- Svoboda, K. and Yasuda, R. (2006) Principles of two-photon excitation microscopy and its applications to neuroscience. *Neuron*, **50**, 823–839.
- Webb, R.H. (1996) Confocal optical microscopy. *Rep. Prog. Phys.*, **59**, 427–471.

White, J.G., Amos, W.B., and Fordham, M. (1987) An evaluation of confocal versus conventional imaging of biological structures by fluorescence light microscopy. *J. Cell. Biol.*, **105**, 41–48.

SNOM

Dickenson, N.E., Armendariz, K.P., Huckabay, H.A., Livanec, P.W., and Dunn, R.C. (2010) Near-field scanning optical microscopy: a tool for nanometric exploration of biological membranes. *Anal. Bioanal. Chem.*, **396**, 31–43.

Dunn, R.C. (1999) Near-field scanning optical microscopy. *Chem. Rev.*, **99**, 2891–2927.

Hecht, B., Sick, B., Wild, U.P., Deckert, V., Zenobi, R., Martin, O.J.F., and Pohl, D.W. (2000) Scanning near-field optical microscopy with aperture probes: fundamentals and applications. *J. Chem. Phys.*, **112**, 7761–7774.

Rasmussen, A. and Deckert, V. (2005) New dimension in nano-imaging: breaking through the diffraction limit with scanning near-field optical microscopy. *Anal. Bioanal. Chem.*, **381**, 165–172.

Synge, E.H. (1928) A suggested method for extending microscopic resolution into the ultra-microscopic region. *Phil. Mag.*, **6**, 356–362.

STED, PALM, STORM, and Other Super-Resolution Techniques

Heilemann, M., Dedecker, P., Hofkens, J., and Sauer, M. (2009) Photoswitches: key molecules for subdiffraction-resolution fluorescence imaging and molecular quantification. *Laser Photon. Rev.*, **3**, 180–202.

Hell, S.W. and Wichmann, J. (1994) Breaking the diffraction resolution limit by stimulated emission: stimulated emission depletion fluorescence microscopy. *Opt. Lett.*, **19**, 780–782.

Patterson, G., Davidson, M., Manley, S., and Lippincott-Schwartz, J. (2010) Super-resolution imaging using single-molecule localization. *Annu. Rev. Phys. Chem.*, **61**, 345–367.

Rittweger, E., Han, K.Y., Irvine, S.E., Eggeling, C., and Hell, S.W. (2009) STED

microscopy reveals crystal colour centres with nanometric resolution. *Nat. Photon.*, **3**, 144–147.

Thompson, R.E., Larson, D.R., and Webb, W.W. (2002) Precise nanometer localization analysis for individual fluorescent probes. *Biophys. J.*, **82**, 2775–2783.

Yildiz, A. and Selvin, P.R. (2005) Fluorescence imaging with one nanometer accuracy: application to molecular motors. *Acc. Chem. Res.*, **38**, 574–582.

FLIM and Polar Plots

Berezin, M.Y. and Achilefu, S. (2010) Fluorescence lifetime measurements and biological imaging. *Chem. Rev.*, **110**, 2641–2684.

Chen, Y.-C. and Clegg, R.M. (2009) Fluorescence lifetime-resolved imaging. *Photosynth. Res.*, **102**, 143–155.

Clayton, A.H.A., Hanley, Q.S., and Verveer, P.J. (2004) Graphical representation and multicomponent analysis of single-frequency fluorescence lifetime imaging microscopy data. *J. Microsc.*, **213**, 1–5.

Digman, M.A., Caiolfa, V.R., Zamai, M., and Gratton, E. (2008) The phasor approach to fluorescence lifetime imaging analysis. *Biophys. J.*, **94**, L14–L16.

Digman, M.A. and Gratton, E. (2012) The phasor approach to FLIM: exploiting phasor linear properties, in *Fluorescence Lifetime Spectroscopy and Imaging: Principles and Applications in Biomedical Diagnostics* (ed. L. Marcu, P.M.W. French, and D.S. Elson) CRC Press.

Hanley, Q.S. and Clayton, A.H.A. (2005) AB-plot assisted determination of fluorophore mixtures in a fluorescence lifetime microscope using spectra or quenchers. *J. Microsc.*, **218**, 62–67.

Herman, B., Wang, X.F., Wodnicki, P., Perisamy, A., Mahajan, N., Berry, G., and Gordon, G. (1999) Fluorescence lifetime imaging microscopy, in *Applied Fluorescence in Chemistry, Biology and Medicine* (eds W. Rettig, et al.), Springer-Verlag, Berlin, pp. 491–507.

Köllner, M. and Wolfrum, J. (1992) How many photons are necessary for fluorescence-lifetime measurements?

- Chem. Phys. Lett.*, **200**, 199–204; Liebsch G., Klimant I., Frank B., Holst G., and Wolfbeis O.S. (2000) Luminescence lifetime imaging of oxygen, pH, and carbon dioxide distribution using optical sensors, *Appl. Spectrosc.*, **54**, 548–559.
- López-Gejo, J., Haigh, D., and Orellana, G. (2010) Relationship between the microscopic and macroscopic world in optical oxygen sensing: a luminescence lifetime study. *Langmuir*, **26**, 2144–2150.
- Redford, G.I. and Clegg, R.M. (2005) Polar plot representation for frequency-domain analysis of fluorescence lifetimes. *J. Fluoresc.*, **15**, 805–815.
- Spoelgen, R., Adams, K.W., Koker, M., Thomas, A.V., Andersen, O.M., Hallett, P.J., Bercury, K.K., Joyner, D.F., Deng, M., Stoothoff, W.H., Strickland, D.K., Willnow, T.E., and Hyman, B.T. (2009) Interaction of the apolipoprotein E receptors low density lipoprotein receptor-related protein and sorLA/LR11. *Neuroscience*, **158**, 1460–1468.
- Wang, X.F., Periasamy, A., Wodnicki, P., Gordon, G.W., and Herman, B. (1996) Time-resolved fluorescence lifetime imaging microscopy: instrumentation and biomedical applications, in *Fluorescence Imaging Spectroscopy and Microscopy, Chemical Analysis Series*, vol. 137. (eds X.F. Wang and B. Herman), John Wiley & Sons, Inc., New York., pp. 313–350.

Basic Principles

1. ELECTROMAGNETIC RADIATION

All light (including infrared) is classified as electromagnetic radiation and consists of alternating electric and magnetic fields and is described classically by a continuous sinusoidal wave like motion of the electric and magnetic fields. Typically, for IR and Raman spectroscopy we will only consider the electric field and neglect the magnetic field component. Figure 2.1 depicts the electric field amplitude of light as a function of time.

The important parameters are the wavelength (λ , length of 1 wave), frequency (ν , number cycles per unit time), and wavenumbers ($\bar{\nu}$, number of waves per unit length) and are related to one another by the following expression:

$$\bar{\nu} = \frac{\nu}{(c/n)} = \frac{1}{\lambda}$$

where c is the speed of light and n the refractive index of the medium it is passing through. In quantum theory, radiation is emitted from a source in discrete units called photons where the photon frequency, ν , and photon energy, E_p , are related by

$$E_p = h\nu$$

where h is Planck's constant (6.6256×10^{-27} erg sec). Photons of specific energy may be absorbed (or emitted) by a molecule resulting in a transfer of energy. In absorption spectroscopy this will result in raising the energy of molecule from ground to a specific excited state

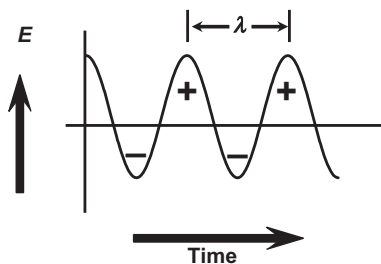


FIGURE 2.1 The amplitude of the electric vector of electromagnetic radiation as a function of time. The wavelength is the distance between two crests.

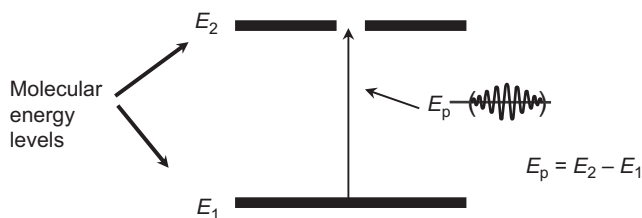


FIGURE 2.2 Absorption of electromagnetic radiation.

as shown in Fig. 2.2. Typically the rotational (E_{rot}), vibrational (E_{vib}), or electronic (E_{el}) energy of molecule is changed by ΔE :

$$\Delta E = E_p = h\nu = hc\bar{\nu}$$

In the absorption of a photon the energy of the molecule increases and ΔE is positive. To a first approximation, the rotational, vibrational, and electronic energies are additive:

$$E_T = E_{\text{el}} + E_{\text{vib}} + E_{\text{rot}}$$

We are concerned with photons of such energy that we consider E_{vib} alone and only for condensed phase measurements. Higher energy light results in electronic transitions (E_{el}) and lower energy light results in rotational transitions (E_{rot}). However, in the gas-state both IR and Raman measurements will include $E_{\text{vib}} + E_{\text{rot}}$.

2. MOLECULAR MOTION/DEGREES OF FREEDOM

2.1. Internal Degrees of Freedom

The molecular motion that results from characteristic vibrations of molecules is described by the internal degrees of freedom resulting in the well-known $3n - 6$ and $3n - 5$ rule-of-thumb for vibrations for non-linear and linear molecules, respectively. Figure 2.3 shows the fundamental vibrations for the simple water (non-linear) and carbon dioxide (linear) molecules.

The internal degrees of freedom for a molecule define n as the number of atoms in a molecule and define each atom with 3 degrees of freedom of motion in the X , Y , and Z directions resulting in $3n$ degrees of motional freedom. Here, three of these degrees are translation, while three describe rotations. The remaining $3n - 6$ degrees (non-linear molecule) are motions, which change the distance between atoms, or the angle between bonds. A simple example of the $3n - 6$ non-linear molecule is water (H_2O) which has $3(3) - 6 = 3$ degrees of freedom. The three vibrations include an in-phase and out-of-phase stretch and a deformation (bending) vibration. Simple examples of $3n - 5$ linear molecules include H_2 , N_2 , and O_2 which all have $3(2) - 5 = 1$ degree of freedom. The only vibration for these simple molecules is a simple stretching vibration. The more complicated CO_2 molecule has $3(3) - 5 = 4$ degrees of freedom and therefore four vibrations. The four vibrations include an in-phase and out-of-phase stretch and two mutually perpendicular deformation (bending) vibrations.

The molecular vibrations for water and carbon dioxide as shown in Fig. 2.3 are the normal mode of vibrations. For these vibrations, the Cartesian displacements of each atom in molecule

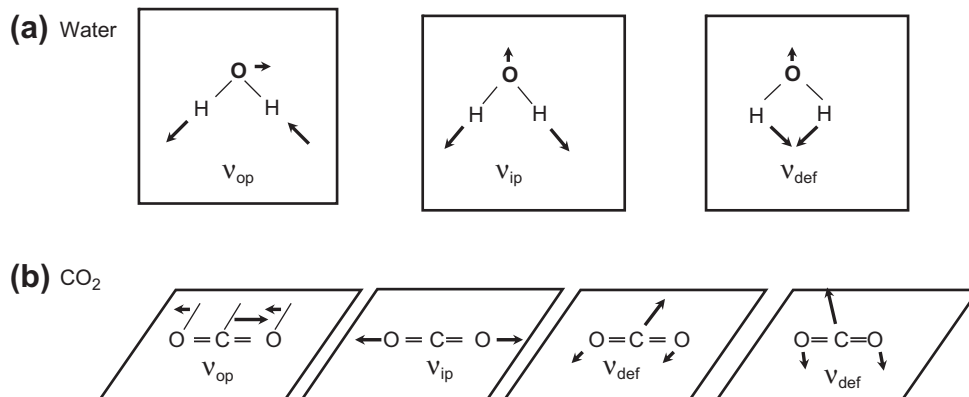


FIGURE 2.3 Molecular motions which change distance between atoms for water and CO₂.

change periodically with the same frequency and go through equilibrium positions simultaneously. The center of the mass does not move and the molecule does not rotate. Thus in the case of harmonic oscillator, the Cartesian coordinate displacements of each atom plotted as a function of time is a sinusoidal wave. The relative vibrational amplitudes may differ in either magnitude or direction. Figure 2.4 shows the normal mode of vibration for a simple diatomic such as HCl and a more complex totally symmetric CH stretch of benzene.

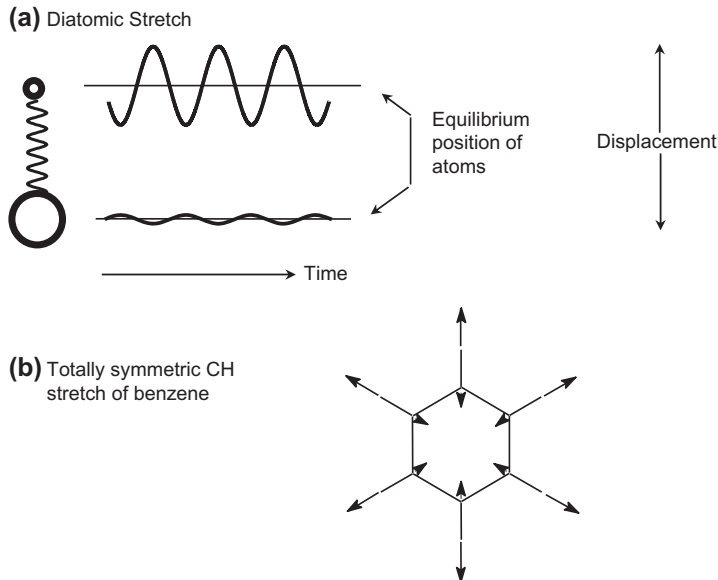


FIGURE 2.4 Normal mode of vibration for a simple diatomic such as HCl (a) and a more complex species such as benzene (b). The displacement versus time is sinusoidal, with equal frequency for all the atoms. The typical Cartesian displacement vectors are shown for the more complicated totally symmetric CH stretch of benzene.

3. CLASSICAL HARMONIC OSCILLATOR

To better understand the molecular vibrations responsible for the characteristic bands observed in infrared and Raman spectra it is useful to consider a simple model derived from classical mechanics.¹ Figure 2.5 depicts a diatomic molecule with two masses m_1 and m_2 connected by a massless spring. The displacement of each mass from equilibrium along the spring axis is X_1 and X_2 . The displacement of the two masses as a function of time for a harmonic oscillator varies periodically as a sine (or cosine) function.

In the above diatomic system, although each mass oscillates along the axis with different amplitudes, both atoms share the same frequency and both masses go through their equilibrium positions simultaneously. The observed amplitudes are inversely proportional to the mass of the atoms which keeps the center of mass stationary

$$\frac{X_1}{X_2} = \frac{m_2}{m_1}$$

The classical vibrational frequency for a diatomic molecule is:

$$\nu = \frac{1}{2\pi} \sqrt{K \left(\frac{1}{m_1} + \frac{1}{m_2} \right)}$$

where K is the force constant in dynes/cm and m_1 and m_2 are the masses in grams and ν is in cycles per second. This expression is also encountered using the reduced mass where

$$\frac{1}{\mu} = \frac{1}{m_1} + \frac{1}{m_2} \quad \text{or} \quad \mu = \frac{m_1 m_2}{m_1 + m_2}$$

In vibrational spectroscopy wavenumber units, $\bar{\nu}$ (waves per unit length) are more typically used

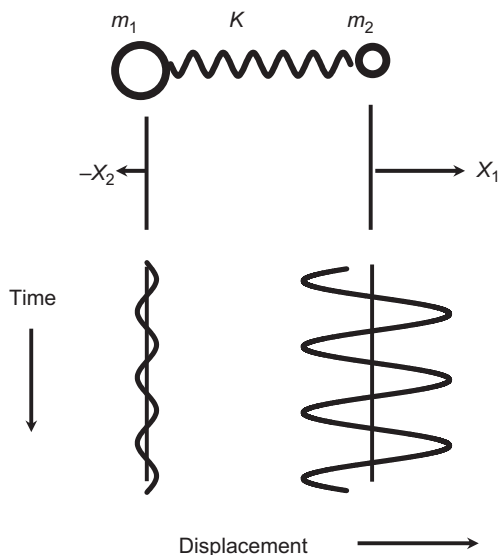


FIGURE 2.5 Motion of a simple diatomic molecule. The spring constant is K , the masses are m_1 and m_2 , and X_1 and X_2 are the displacement vectors of each mass from equilibrium where the oscillator is assumed to be harmonic.

$$\bar{\nu} = \frac{1}{2\pi c} \sqrt{K \left(\frac{1}{m_1} + \frac{1}{m_2} \right)}$$

where $\bar{\nu}$ is in waves per centimeter and is sometimes called the frequency in cm^{-1} and c is the speed of light in cm/s .

If the masses are expressed in unified atomic mass units (u) and the force constant is expressed in millidynes/Ångström then:

$$\bar{\nu} = 1303 \sqrt{K \left(\frac{1}{m_1} + \frac{1}{m_2} \right)}$$

where $1303 = [N_a \times 10^5]^{1/2} / 2\pi c$ and N_a is Avogadro's number ($6.023 \times 10^{23} \text{ mole}^{-1}$)

This simple expression shows that the observed frequency of a diatomic oscillator is a function of

1. the force constant K , which is a function of the bond energy of a two atom bond (see Table 2.1)
2. the atomic masses of the two atoms involved in the vibration.

TABLE 2.1 Approximate Range of Force Constants for Single, Double, and Triple Bonds

Bond type	K (millidynes/Ångström)
Single	3–6
Double	10–12
Triple	15–18

Table 2.1 shows the approximate range of the force constants for single, double, and triple bonds.

Conversely, knowledge of the masses and frequency allows calculation of a diatomic force constant. For larger molecules the nature of the vibration can be quite complex and for more accurate calculations the harmonic oscillator assumption for a diatomic will not be appropriate.

The general wavenumber regions for various diatomic oscillator groups are shown in Table 2.2, where Z is an atom such as carbon, oxygen, nitrogen, sulfur, and phosphorus.

TABLE 2.2 General Wavenumber Regions for Various Simple Diatomic Oscillator Groups

Diatomic oscillator	Region (cm^{-1})
Z–H	4000–2000
$\text{C}\equiv\text{C}$, $\text{C}\equiv\text{N}$	2300–2000
$\text{C}=\text{O}$, $\text{C}=\text{N}$, $\text{C}=\text{C}$	1950–1550
$\text{C}-\text{O}$, $\text{C}-\text{N}$, $\text{C}-\text{C}$	1300–800
$\text{C}-\text{Cl}$	830–560

4. QUANTUM MECHANICAL HARMONIC OSCILLATOR

Vibrational spectroscopy relies heavily on the theoretical insight provided by quantum theory. However, given the numerous excellent texts discussing this topic only a very cursory review is presented here. For a more detailed review of the quantum mechanical principles relevant to vibrational spectroscopy the reader is referred elsewhere.²⁻⁵

For the classical harmonic oscillation of a diatomic the potential energy (PE) is given by

$$\text{PE} = \frac{1}{2} KX^2$$

A plot of the potential energy of this diatomic system as a function of the distance, X between the masses, is thus a parabola that is symmetric about the equilibrium internuclear distance, X_e . Here X_e is at the energy minimum and the force constant, K is a measure of the curvature of the potential well near X_e .

From quantum mechanics we know that molecules can only exist in quantized energy states. Thus, vibrational energy is not continuously variable but rather can only have certain discrete values. Under certain conditions a molecule can transit from one energy state to another ($\Delta v = \pm 1$) which is what is probed by spectroscopy.

Figure 2.6 shows the vibrational levels in a potential energy diagram for the quantum mechanical harmonic oscillator. In the case of the harmonic potential these states are equidistant and have energy levels E given by

$$E_i = \left(v_i + \frac{1}{2} \right) h\nu \quad v_i = 0, 1, 2, \dots$$

Here, ν is the classical vibrational frequency of the oscillator and v is a quantum number which can have only integer values. This can only change by $\Delta v = \pm 1$ in a harmonic oscillator model. The so-called zero point energy occurs when $v = 0$ where $E = \frac{1}{2} h\nu$ and this vibrational energy cannot be removed from the molecule.

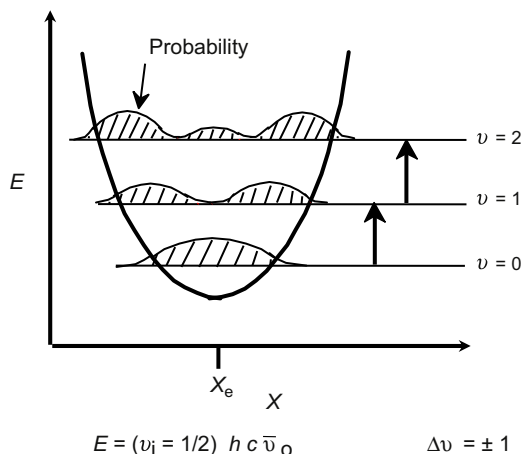


FIGURE 2.6 Potential energy, E , versus internuclear distance, X , for a diatomic harmonic oscillator.

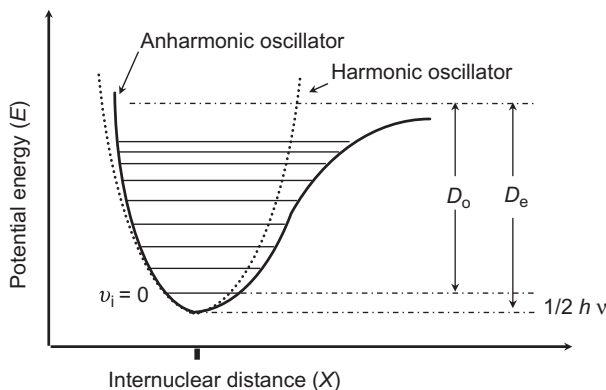


FIGURE 2.7 The potential energy diagram comparison of the anharmonic and the harmonic oscillator. Transitions originate from the $\nu = 0$ level, and D_0 is the energy necessary to break the bond.

Figure 2.6 shows the curved potential wells for a harmonic oscillator with the probability functions for the internuclear distance X , within each energy level. These must be expressed as a probability of finding a particle at a given position since by quantum mechanics we cannot be certain of the position of the mass during the vibration (a consequence of Heisenberg's uncertainty principle).

Although we have only considered a harmonic oscillator, a more realistic approach is to introduce anharmonicity. Anharmonicity results if the change in the dipole moment is not linearly proportional to the nuclear displacement coordinate. Figure 2.7 shows the potential energy level diagram for a diatomic harmonic and anharmonic oscillator. Some of the features introduced by an anharmonic oscillator include the following.

The anharmonic oscillator provides a more realistic model where the deviation from harmonic oscillation becomes greater as the vibrational quantum number increases. The separation between adjacent levels becomes smaller at higher vibrational levels until finally the dissociation limit is reached. In the case of the harmonic oscillator only transitions to adjacent levels or so-called fundamental transitions are allowed (i.e., $\Delta v = \pm 1$) while for the anharmonic oscillator, overtones ($\Delta v = \pm 2$) and combination bands can also result. Transitions to higher vibrational states are far less probable than the fundamentals and are of much weaker intensity. The energy term corrected for anharmonicity is

$$E_\nu = h\nu_e \left(\nu + \frac{1}{2} \right) - h\chi_e \nu_e \left(\nu + \frac{1}{2} \right)^2$$

where $\chi_e \nu_e$ defines the magnitude of the anharmonicity.

5. IR ABSORPTION PROCESS

The typical IR spectrometer broad band source emits all IR frequencies of interest simultaneously where the near-IR region is $14,000\text{--}4000\text{ cm}^{-1}$, the mid-IR region is

4000–400 cm^{-1} , and the far-IR region is 400–10 cm^{-1} . Typical of an absorption spectroscopy, the relationship between the intensities of the incident and transmitted IR radiation and the analyte concentration is governed by the Lambert–Beer law. The IR spectrum is obtained by plotting the intensity (absorbance or transmittance) versus the wavenumber, which is proportional to the energy difference between the ground and the excited vibrational states.

Two important components to the IR absorption process are the radiation frequency and the molecular dipole moment. The interaction of the radiation with molecules can be described in terms of a resonance condition where the specific oscillating radiation frequency matches the natural frequency of a particular normal mode of vibration. In order for energy to be transferred from the IR photon to the molecule via absorption, the molecular vibration must cause a change in the dipole moment of the molecule. This is the familiar selection rule for IR spectroscopy, which requires a change in the dipole moment during the vibration to be IR active.

The dipole moment, μ , for a molecule is a function of the magnitude of the atomic charges (e_i) and their positions (r_i)

$$\mu = \sum e_i r_i$$

The dipole moments of uncharged molecules derive from partial charges on the atoms, which can be determined from molecular orbital calculations. As a simple approximation, the partial charges can be estimated by comparison of the electronegativities of the atoms. Homonuclear diatomic molecules such as H_2 , N_2 , and O_2 have *no* dipole moment and are IR inactive (but Raman active) while heteronuclear diatomic molecules such as HCl , NO , and CO do have dipole moments and have IR active vibrations.

The IR absorption process involves absorption of energy by the molecule if the vibration causes a change in the dipole moment, resulting in a change in the vibrational energy level. Figure 2.8 shows the oscillating electric field of the IR radiation generates forces on the

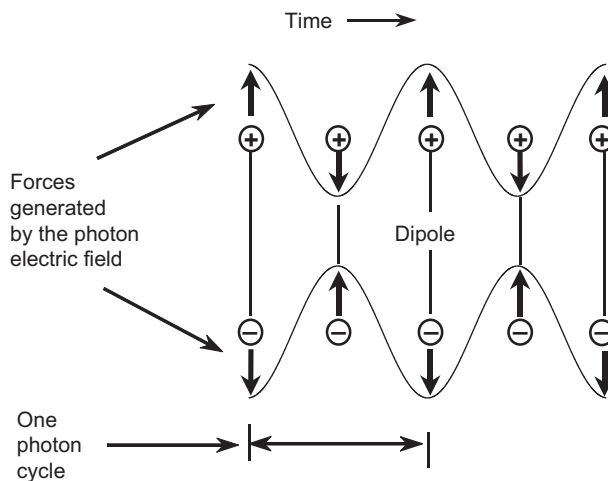


FIGURE 2.8 The oscillating electric field of the photon generates oscillating, oppositely directed forces on the positive and negative charges of the molecular dipole. The dipole spacing oscillates with the same frequency as the incident photon.

molecular dipole where the oscillating electric field drives the oscillation of the molecular dipole moment and alternately increases and decreases the dipole spacing.

Here, the electric field is considered to be uniform over the whole molecule since λ is much greater than the size of most molecules. In terms of quantum mechanics, the IR absorption is an electric dipole operator mediated transition where the change in the dipole moment, μ , with respect to a change in the vibrational amplitude, Q , is greater than zero.

$$\left(\frac{\partial\mu}{\partial Q}\right)_0 \neq 0$$

The measured IR band intensity is proportional to the square of the change in the dipole moment.

6. THE RAMAN SCATTERING PROCESS

Light scattering phenomena may be classically described in terms of electromagnetic (EM) radiation produced by oscillating dipoles induced in the molecule by the EM fields of the incident radiation. The light scattered photons include mostly the dominant Rayleigh and the very small amount of Raman scattered light.⁶ The induced dipole moment occurs as a result of the molecular polarizability α , where the polarizability is the deformability of the electron cloud about the molecule by an external electric field.

Figure 2.9 shows the response of a non-polar diatomic placed in an oscillating electric field. Here we represent the static electric field by the plates of a charged capacitor. The negatively charged plate attracts the nuclei, while the positively charged plate attracts the least tightly

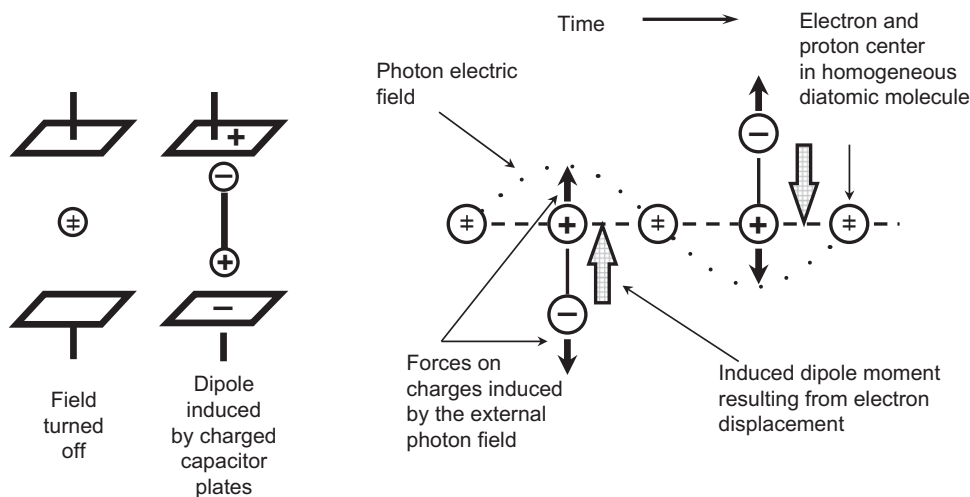


FIGURE 2.9 Induced dipole moment of a homonuclear diatomic originating from the oscillating electric field of the incident radiation. The field relative to the proton center displaces the electron center. The charged plates of a capacitor, which induces a dipole moment in the polarizable electron cloud, can represent the electric field.

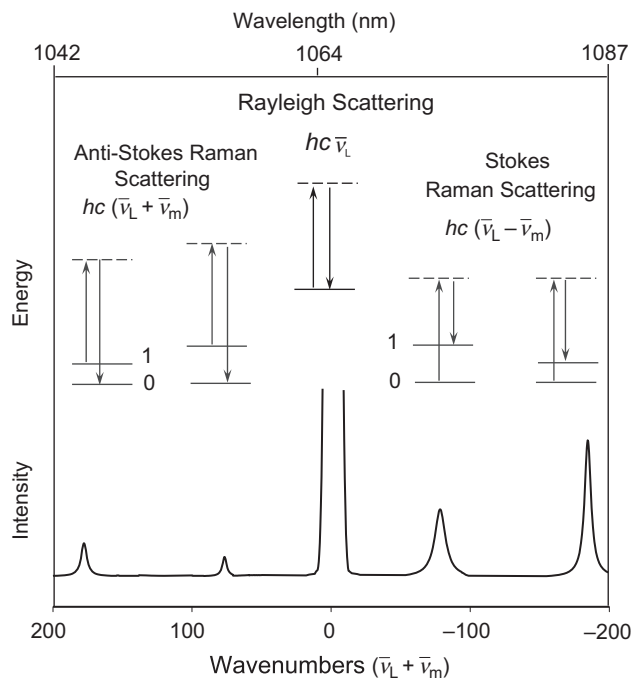


FIGURE 2.10 Schematic illustration of Rayleigh scattering as well as Stokes and anti-Stokes Raman scattering. The laser excitation frequency (ν_L) is represented by the upward arrows and is much higher in energy than the molecular vibrations. The frequency of the scattered photon (downward arrows) is unchanged in Rayleigh scattering but is of either lower or higher frequency in Raman scattering. The dashed lines indicate the “virtual state.”

bound outer electrons resulting in an induced dipole moment. This induced dipole moment is an off-resonance interaction mediated by an oscillating electric field.

In a typical Raman experiment, a laser is used to irradiate the sample with monochromatic radiation. Laser sources are available for excitation in the UV, visible, and near-IR spectral region (785 and 1064 nm). Thus, if visible excitation is used, the Raman scattered light will also be in the visible region. The Rayleigh and Raman processes are depicted in Fig. 2.10. No energy is lost for the elastically scattered Rayleigh light while the Raman scattered photons lose some energy relative to the exciting energy to the specific vibrational coordinates of the sample. In order for Raman bands to be observed, the molecular vibration must cause a change in the polarizability.

Both Rayleigh and Raman are two photon processes involving scattering of incident light ($hc\bar{\nu}_L$), from a “virtual state.” The incident photon is momentarily absorbed by a transition from the ground state into a virtual state and a new photon is created and scattered by a transition from this virtual state. Rayleigh scattering is the most probable event and the scattered intensity is ca. 10^{-3} less than that of the original incident radiation. This scattered photon results from a transition from the virtual state back to the ground state and is an elastic scattering of a photon resulting in no change in energy (i.e., occurs at the laser frequency).

Raman scattering is far less probable than Rayleigh scattering with an observed intensity that is ca. 10^{-6} that of the incident light for strong Raman scattering. This scattered photon results from a transition from the virtual state to the first excited state of the molecular vibration. This is described as an inelastic collision between photon and molecule, since the molecule acquires different vibrational energy ($\bar{\nu}_m$) and the scattered photon now has different energy and frequency.

As shown in Fig. 2.10 two types of Raman scattering exist: Stokes and anti-Stokes. Molecules initially in the ground vibrational state give rise to Stokes Raman scattering $hc(\bar{\nu}_L - \bar{\nu}_m)$ while molecules initially in vibrational excited state give rise to anti-Stokes Raman scattering, $hc(\bar{\nu}_L + \bar{\nu}_m)$. The intensity ratio of the Stokes relative to the anti-Stokes Raman bands is governed by the absolute temperature of the sample, and the energy difference between the ground and excited vibrational states. At thermal equilibrium Boltzmann's law describes the ratio of Stokes relative to anti-Stokes Raman lines. The Stokes Raman lines are much more intense than anti-Stokes since at ambient temperature most molecules are found in the ground state.

The intensity of the Raman scattered radiation I_R is given by:

$$I_R \propto \nu^4 I_o N \left(\frac{\partial \alpha}{\partial Q} \right)^2$$

where I_o is the incident laser intensity, N is the number of scattering molecules in a given state, ν is the frequency of the exciting laser, α is the polarizability of the molecules, and Q is the vibrational amplitude.

The above expression indicates that the Raman signal has several important parameters for Raman spectroscopy. First, since the signal is concentration dependent, quantitation is possible. Secondly, using shorter wavelength excitation or increasing the laser flux power density can increase the Raman intensity. Lastly, only molecular vibrations which cause a change in polarizability are Raman active. Here the change in the polarizability with respect to a change in the vibrational amplitude, Q , is greater than zero.

$$\left(\frac{\partial \alpha}{\partial Q} \right) \neq 0$$

The Raman intensity is proportional to the square of the above quantity.

7. CLASSICAL DESCRIPTION OF THE RAMAN EFFECT

The most basic description of Raman spectroscopy describes the nature of the interaction of an oscillating electric field using classical arguments.⁶ Figure 2.11 schematically represents this basic mathematical description of the Raman effect.

As discussed above, the electromagnetic field will perturb the charged particles of the molecule resulting in an induced dipole moment:

$$\mu = \alpha E$$

where α is the polarizability, E is the incident electric field, and μ is the induced dipole moment. Both E and α can vary with time. The electric field of the radiation is oscillating

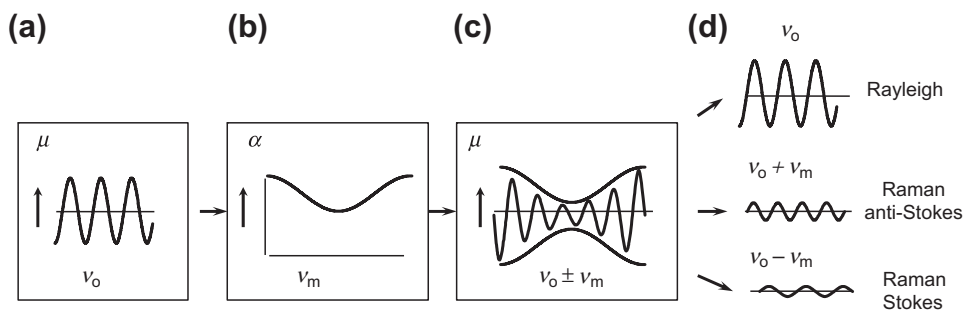


FIGURE 2.11 Schematic representing Rayleigh and Raman scattering. In (a) the incident radiation makes the induced dipole moment of the molecule oscillate at the photon frequency. In (b) the molecular vibration can change the polarizability, α , which changes the amplitude of the dipole moment oscillation. The result as shown in (c) is an amplitude modulated dipole moment oscillation. The image (d) shows the components with steady amplitudes which can emit electromagnetic radiation.

as a function of time at a frequency ν_0 , which can induce an oscillation of the dipole moment μ of the molecule at this same frequency, as shown in Fig. 2.11a. The polarizability α of the molecule has a certain magnitude whose value can vary slightly with time at the much slower molecular vibrational frequency ν_m , as shown in Fig. 2.11b. The result is seen in Fig. 2.11c, which depicts an amplitude modulation of the dipole moment oscillation of the molecule. This type of modulated wave can be resolved mathematically into three steady amplitude components with frequencies ν_0 , $\nu_0 + \nu_m$, and $\nu_0 - \nu_m$ as shown in Fig. 2.11d. These dipole moment oscillations of the molecule can emit scattered radiation with these same frequencies called Rayleigh, Raman anti-Stokes, and Raman Stokes frequencies. If a molecular vibration did not cause a variation in the polarizability, then there would be no amplitude modulation of the dipole moment oscillation and there would be no Raman Stokes or anti-Stokes emission.

8. SYMMETRY: IR AND RAMAN ACTIVE VIBRATIONS

The symmetry of a molecule, or the lack of it, will define what vibrations are Raman and IR active.⁵ In general, symmetric or in-phase vibrations and non-polar groups are most easily studied by Raman while asymmetric or out-of-phase vibrations and polar groups are most easily studied by IR. The classification of a molecule by its symmetry enables understanding of the relationship between the molecular structure and the vibrational spectrum. Symmetry elements include planes of symmetry, axes of symmetry, and a center of symmetry.

Group Theory is the mathematical discipline, which applies symmetry concepts to vibrational spectroscopy and predicts which vibrations will be IR and Raman active.^{1,5} The symmetry elements possessed by the molecule allow it to be classified by a point group and vibrational analysis can be applied to individual molecules. A thorough discussion of Group Theory is beyond the scope of this work and interested readers should examine texts dedicated to this topic.⁷

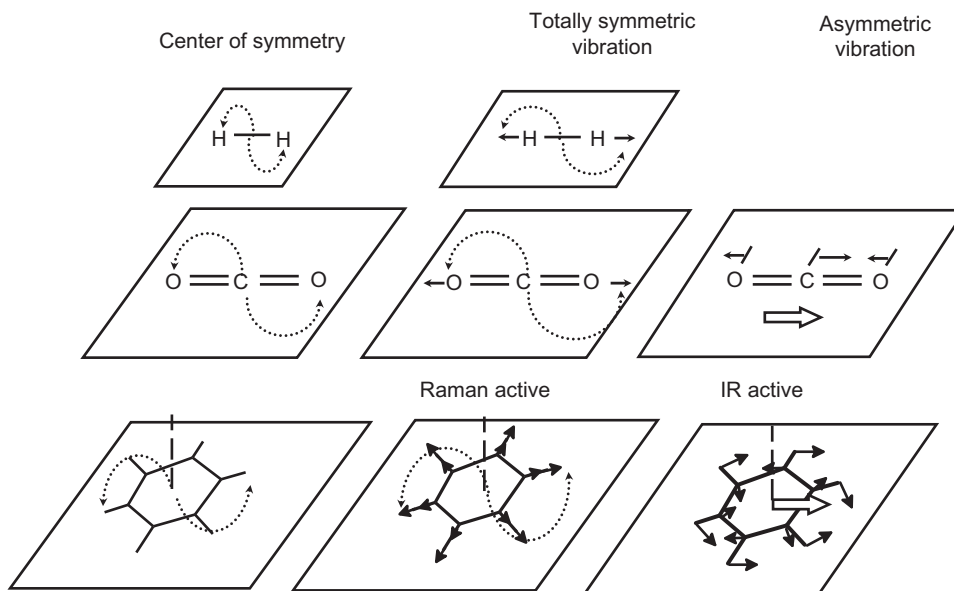


FIGURE 2.12 The center of symmetry for H₂, CO₂, and benzene. The Raman active symmetric stretching vibrations above are symmetric with respect to the center of symmetry. Some IR active asymmetric stretching vibrations are also shown.

For small molecules, the IR and Raman activities may often be determined by a simple inspection of the form of the vibrations. For molecules that have a center of symmetry, the rule of mutual exclusion states that no vibration can be active in both the IR and Raman spectra. For such highly symmetrical molecules vibrations which are Raman active are IR inactive and vice versa and some vibrations may be both IR and Raman inactive.

Figure 2.12 shows some examples of molecules with this important symmetry element, the center of symmetry. To define a center of symmetry simply start at any atom, go in a straight line through the center and an equal distance beyond to find another, identical atom. In such cases the molecule has no permanent dipole moment. Examples shown below include H₂, CO₂, and benzene and the rule of mutual exclusion holds.

In a molecule with a center of symmetry, vibrations that retain the center of symmetry are IR inactive and may be Raman active. Such vibrations, as shown in Fig. 2.12, generate a change in the polarizability during the vibration but no change in a dipole moment. Conversely, vibrations that do not retain the center of symmetry are Raman inactive, but may be IR active since a change in the dipole moment may occur.

For molecules without a center of symmetry, some vibrations can be active in both the IR and Raman spectra.

Molecules that do not have a center of symmetry may have other suitable symmetry elements so that some vibrations will be active only in Raman or only in the IR. Good examples of this are the in-phase stretches of inorganic nitrate and sulfate shown in Fig. 2.13. These are Raman active and IR inactive. Here, neither molecule has a center of symmetry but the negative oxygen atoms move radially simultaneously resulting in no dipole moment change.

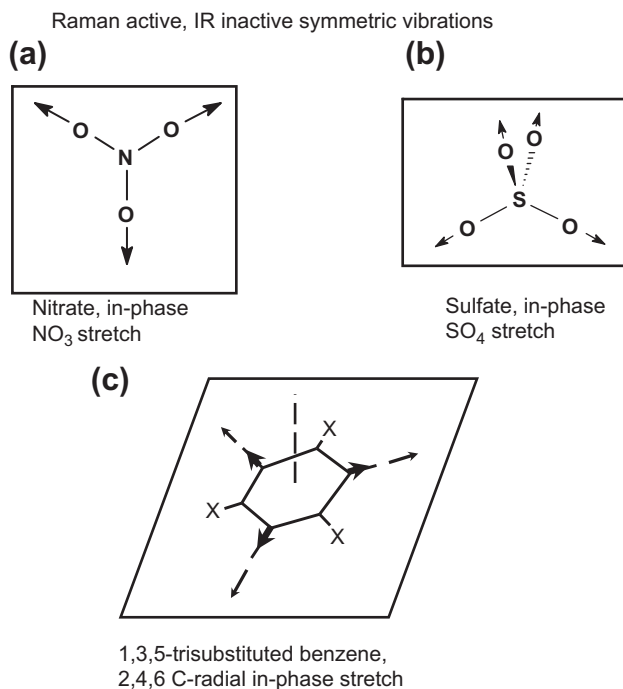


FIGURE 2.13 Three different molecules, nitrate, sulfate, and 1,3,5-trisubstituted benzene molecules that do not have a center of symmetry. The in-phase stretching vibrations of all three result in Raman active, but IR inactive vibrations.

Another example is the 1,3,5-trisubstituted benzene where the C-Radial in-phase stretch is Raman active and IR inactive.

In **Figure 2.14** some additional symmetry operations are shown, other than that for a center of symmetry for an XY₂ molecule such as water. These include those for a plane of symmetry, a two-fold rotational axis of symmetry, and an identity operation (needed for group theory) which makes no change. If a molecule is symmetrical with respect to a given symmetry element, the symmetry operation will not make any discernible change from the original configuration. As shown in **Fig. 2.14**, such symmetry operations are equivalent to renumbering the symmetrically related hydrogen (Y) atoms.

Figure 2.15 shows the Cartesian displacement vectors (arrows) of the vibrational modes Q₁, Q₂, and Q₃ of the bent triatomic XY₂ molecule (such as water), and shows how they are modified by the symmetry operations C₂, σ_v, and σ'_v. For non-degenerate modes of vibration such as these, the displacement vectors in the first column (the identity column, I) are multiplied by either (+1) or (−1) as shown to give the forms in the other three columns. Multiplication by (+1) does not change the original form so the resulting form is said to be symmetrical with respect to that symmetry operation. Multiplication by (−1) reverses all the vectors of the original form and the resulting form is said to be anti-symmetrical with respect to that symmetry element. As seen in **Fig. 2.15**, Q₁ and Q₂ are both totally

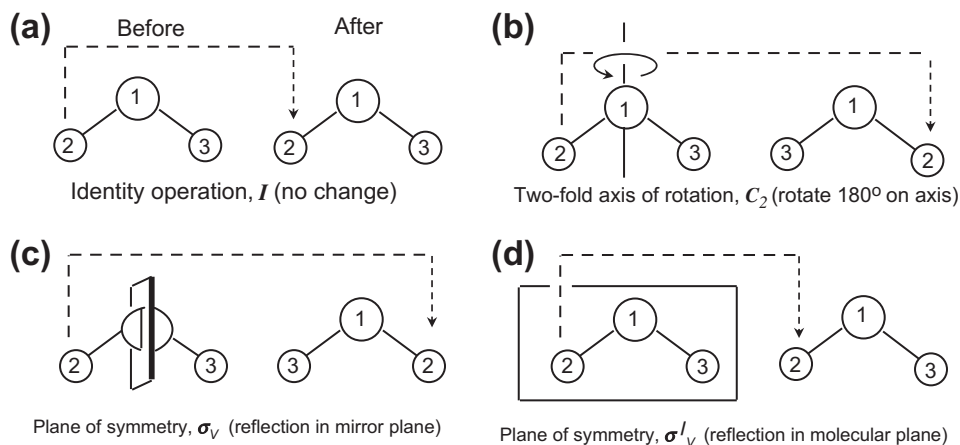


FIGURE 2.14 Symmetry operations for an XY_2 bent molecule such as water in the equilibrium configuration.

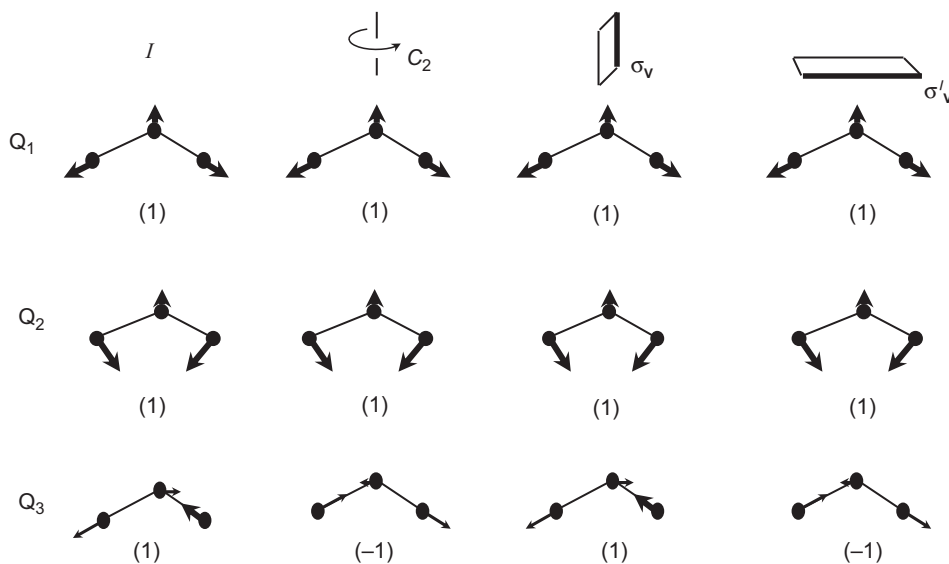
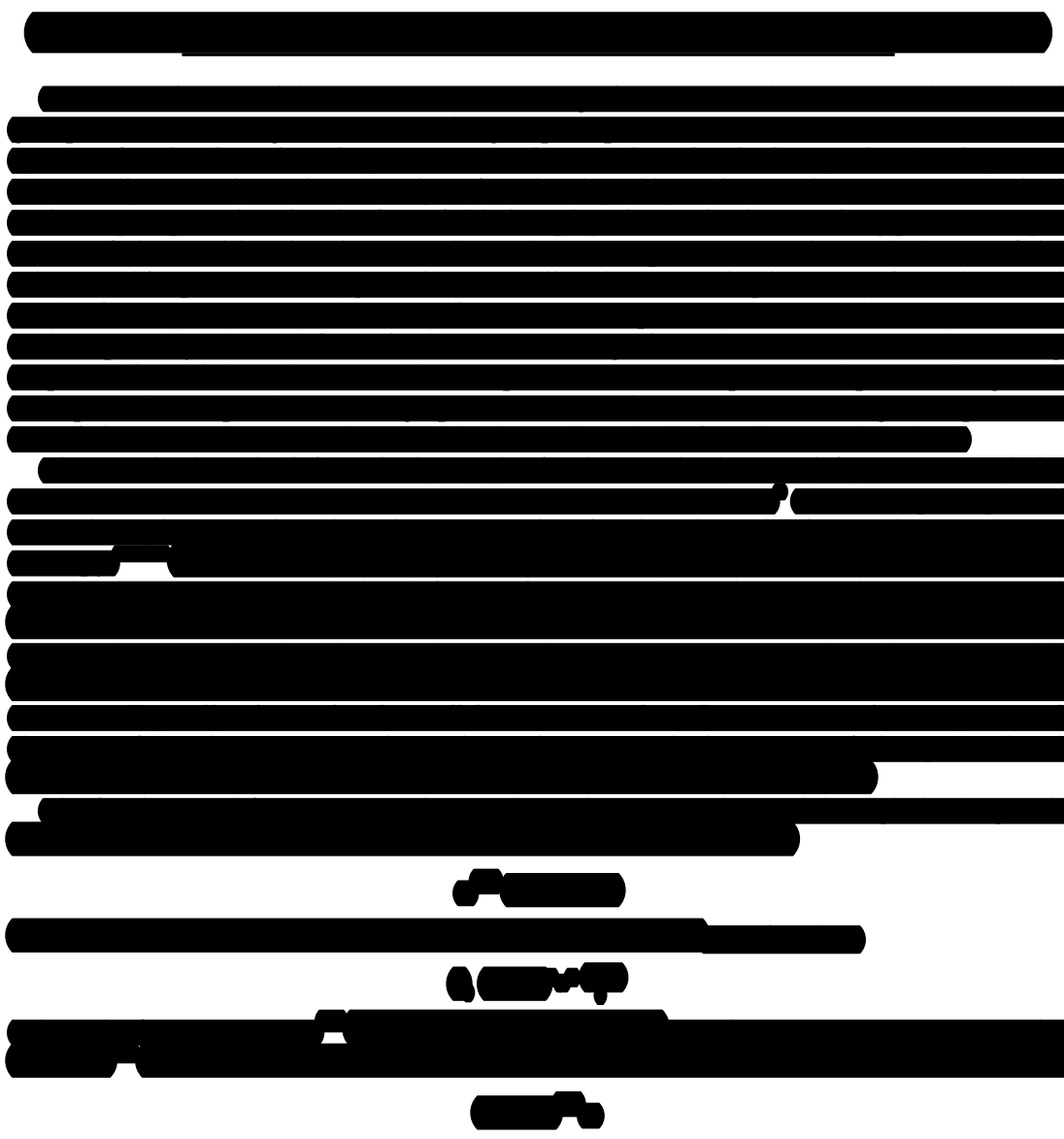


FIGURE 2.15 The bent symmetrical XY_2 molecule such as H_2O performing the three fundamental modes Q_1 , Q_2 , and Q_3 . The vectors in column one (identity I) are transformed by the C_2 , σ_v , and σ'_v operations into the forms in the remaining columns, where the vectors are like those in column one multiplied by (+1) symmetrical or (-1) anti-symmetrical.

symmetric modes (i.e., symmetric to all symmetry operations), whereas Q_3 is symmetric with respect to the σ'_v operation but anti-symmetric with respect to the C_2 and σ_v operations. The transformation numbers (+1 and -1) are used in group theory to characterize the symmetries of non-degenerate vibrational modes. From these symmetries one can deduce that Q_1 , Q_2 , and Q_3 are all active in both the IR and Raman spectra. In addition,

the dipole moment change in Q_1 and Q_2 is parallel to the C_2 axis and in Q_3 it is perpendicular to the C_2 axis and the σ_v plane.

Doubly degenerate modes occur when two different vibrational modes have the same vibrational frequency as a consequence of symmetry. A simple example is the C–H bending vibration in Cl_3C-H molecule where the C–H bond can bend with equal frequency in two mutually perpendicular directions. The treatment of degenerate vibrations is more complex and will not be discussed here.



Chapter 1

Introduction, Basic Theory and Principles

1.1 INTRODUCTION

The main spectroscopies employed to detect vibrations in molecules are based on the processes of infrared absorption and Raman scattering. They are widely used to provide information on chemical structures and physical forms, to identify substances from the characteristic spectral patterns ('fingerprinting'), and to determine quantitatively or semi-quantitatively the amount of a substance in a sample. Samples can be examined in a whole range of physical states; for example, as solids, liquids or vapours, in hot or cold states, in bulk, as microscopic particles, or as surface layers. The techniques are very wide ranging and provide solutions to a host of interesting and challenging analytical problems. Raman scattering is less widely used than infrared absorption, largely due to problems with sample degradation and fluorescence. However, recent advances in instrument technology have simplified the equipment and reduced the problems substantially. These advances, together with the ability of Raman spectroscopy to examine aqueous solutions, samples inside glass containers and samples without any preparation, have led to a rapid growth in the application of the technique.

In practice, modern Raman spectroscopy is simple. Variable instrument parameters are few, spectral manipulation is minimal and a simple interpretation of the data may be sufficient. This chapter and Chapter 2 aim to set out the basic principles and experimental methods to give the reader a firm understanding of the basic theory and practical considerations so that the technique

can be applied at the level often required for current applications. However, Raman scattering is an underdeveloped technique, with much important information often not used or recognized. Later chapters will develop the minimum theory required to give a more in-depth understanding of the data obtained and to enable comprehension of some of the many more advanced techniques which have specific advantages for some applications.

1.1.1 History

The phenomenon of inelastic scattering of light was first postulated by Smekal in 1923 [1] and first observed experimentally in 1928 by Raman and Krishnan [2]. Since then, the phenomenon has been referred to as Raman spectroscopy. In the original experiment sunlight was focussed by a telescope onto a sample which was either a purified liquid or a dust-free vapour. A second lens was placed by the sample to collect the scattered radiation. A system of optical filters was used to show the existence of scattered radiation with an altered frequency from the incident light – the basic characteristic of Raman spectroscopy.

1.2 BASIC THEORY

When light interacts with matter, the photons which make up the light may be absorbed or scattered, or may not interact with the material and may pass straight through it. If the energy of an incident photon corresponds to the energy gap between the ground state of a molecule and an excited state, the photon may be absorbed and the molecule promoted to the higher energy excited state. It is this change which is measured in absorption spectroscopy by the detection of the loss of that energy of radiation from the light. However, it is also possible for the photon to interact with the molecule and scatter from it. In this case there is no need for the photon to have an energy which matches the difference between two energy levels of the molecule. The scattered photons can be observed by collecting light at an angle to the incident light beam, and provided there is no absorption from any electronic transitions which have similar energies to that of the incident light, the efficiency increases as the fourth power of the frequency of the incident light.

Scattering is a commonly used technique. For example, it is widely used for measuring particle size and size distribution down to sizes less than 1 μm . One everyday illustration of this is that the sky is blue because the higher energy blue light is scattered from molecules and particles in the atmosphere more efficiently than the lower energy red light. However, the main scattering technique used for molecular identification is Raman scattering.

The process of absorption is used in a wide range of spectroscopic techniques. For example it is used in acoustic spectroscopy where there is a very small energy difference between the ground and excited states and in X-ray absorption spectroscopy where there is a very large difference. In between these extremes are many of the common techniques such as NMR, EPR, infrared absorption, electronic absorption and fluorescence emission, and vacuum ultraviolet (UV) spectroscopy. Figure 1.1 indicates the wavelength ranges of some commonly used types of radiation.

Radiation is often characterized by its wavelength (λ). However, in spectroscopy, because we are interested in the interaction of radiation with states of the molecule being examined and this being usually discussed in terms of energy, it is often useful to use frequency (ν) or wavenumber ($\bar{\omega}$) scales, which are linearly related with energy. The relationships between these scales are given below:

$$\lambda = c/\nu \quad (1.1)$$

$$\nu = \Delta E/h \quad (1.2)$$

$$\bar{\omega} = \nu/c = 1/\lambda \quad (1.3)$$

It is clear from Equations (1.1)–(1.3) that the energy is proportional to the reciprocal of wavelength and therefore the highest energy region is on the left in Figure 1.1 and the longest wavelength on the right.

The way in which radiation is employed in infrared and Raman spectroscopies is different. In infrared spectroscopy, infrared energy covering a range of frequencies is directed onto the sample. Absorption occurs where the frequency of the incident radiation matches that of a vibration so that the molecule is promoted to a vibrational excited state. The loss of this frequency of radiation from the beam after it passes through the sample is then detected. In contrast, Raman spectroscopy uses a single frequency of radiation to irradiate the sample and it is the radiation scattered from the molecule, one vibrational unit of energy different from the incident beam, which is detected. Thus, unlike infrared absorption, Raman scattering does not require matching of the incident radiation to the energy difference between the ground and excited states. In Raman scattering, the light interacts with the molecule and distorts (polarizes) the cloud of electrons round the nuclei to form a short-lived state

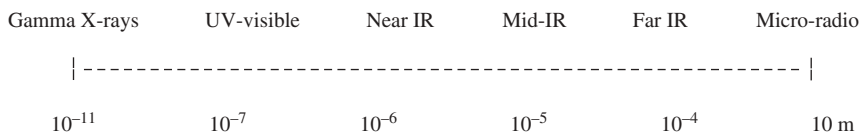


Figure 1.1. The electromagnetic spectrum on the wavelength scale in metres.

called a ‘virtual state’, which is discussed in Chapter 3. This state is not stable and the photon is quickly re-radiated.

The energy changes we detect in vibrational spectroscopy are those required to cause nuclear motion. If only electron cloud distortion is involved in scattering, the photons will be scattered with very small frequency changes, as the electrons are comparatively light. This scattering process is regarded as elastic scattering and is the dominant process. For molecules it is called Rayleigh scattering. However, if nuclear motion is induced during the scattering process, energy will be transferred either from the incident photon to the molecule or from the molecule to the scattered photon. In these cases the process is inelastic and the energy of the scattered photon is different from that of the incident photon by one vibrational unit. This is Raman scattering. It is inherently a weak process in that only one in every 10^6 – 10^8 photons which scatter is Raman scattered. In itself this does not make the process insensitive since with modern lasers and microscopes, very high power densities can be delivered to very small samples but it does follow that other processes such as sample degradation and fluorescence can readily occur.

Figure 1.2 shows the basic processes which occur for one vibration. At room temperature, most molecules, but not all, are present in the lowest energy vibrational level. Since the virtual states are not real states of the molecule but are created when the laser interacts with the electrons and causes polarization, the energy of these states is determined by the frequency of the light source used. The Rayleigh process will be the most intense process since most photons scatter this way. It does not involve any energy change and consequently the light returns to the same energy state. The Raman scattering process from the ground vibrational state m leads to absorption of energy by the molecule and its promotion to a higher energy excited vibrational state (n). This is called Stokes

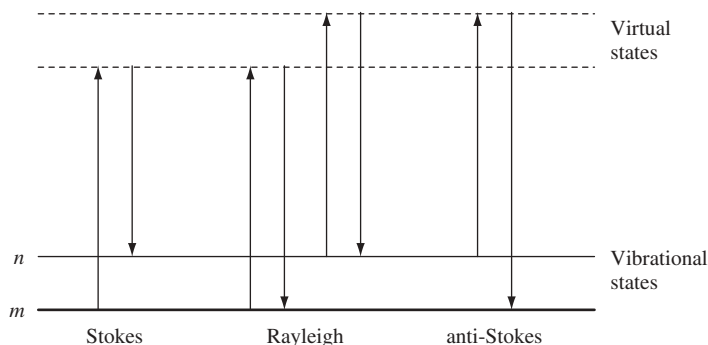


Figure 1.2. Diagram of the Rayleigh and Raman scattering processes. The lowest energy vibrational state m is shown at the foot with states of increasing energy above it. Both the low energy (upward arrows) and the scattered energy (downward arrows) have much larger energies than the energy of a vibration.

scattering. However, due to thermal energy, some molecules may be present in an excited state such as n in Figure 1.2. Scattering from these states to the ground state m is called anti-Stokes scattering and involves transfer of energy to the scattered photon. The relative intensities of the two processes depend on the population of the various states of the molecule. The populations can be worked out from the Boltzmann equation (Chapter 3) but at room temperature, the number of molecules expected to be in an excited vibrational state other than any really low-energy ones will be small.

Thus, compared to Stokes scattering, anti-Stokes scattering will be weak and will become weaker as the frequency of the vibration increases, due to decreased population of the excited vibrational states. Further, anti-Stokes scattering will increase relative to Stokes scattering as the temperature rises. Figure 1.3 shows a typical spectrum of Stokes and anti-Stokes scattering from cyclohexane separated by the intense Rayleigh scattering which should be off-scale close to the point where there is no energy shift. However there is practically no signal close to the frequency of the exciting line along the x -axis. This is because filters in front of the spectrometer remove almost all light within about 200 cm^{-1} of the exciting line. Some breakthrough of the laser light can be seen where there is no energy shift at all.

Usually, Raman scattering is recorded only on the low-energy side to give Stokes scattering but occasionally anti-Stokes scattering is preferred. For example, where there is fluorescence interference, this will occur at a lower energy than the excitation frequency and consequently anti-Stokes scattering can be used to avoid interference. The difference in intensities of Raman bands in Stokes and anti-Stokes scattering can also be used to measure temperature.

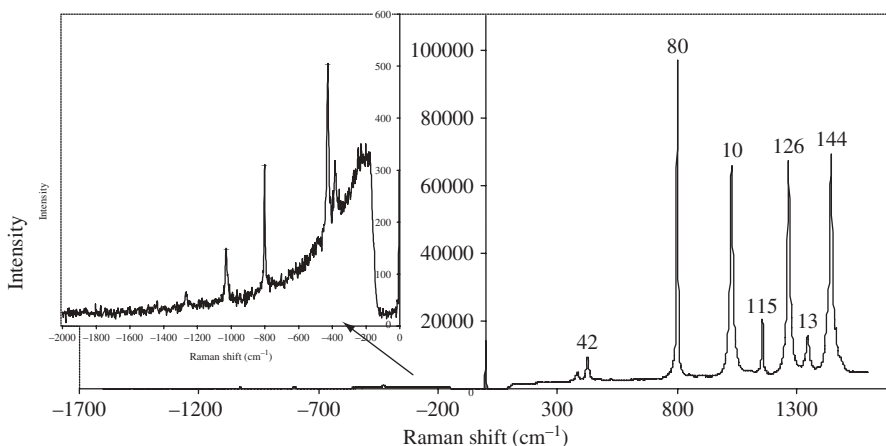


Figure 1.3. Stokes and anti-Stokes scattering for cyclohexane. To show the weak anti-Stokes spectrum, the y -axis has been extended in the inset.

Figure 1.2 illustrates one key difference between infrared absorption and Raman scattering. As described above, infrared absorption would involve direct excitation of the molecule from state m to state n by a photon of exactly the energy difference between them. In contrast, Raman scattering uses much higher energy radiation and measures the difference in energy between n and m by subtracting the energy of the scattered photon from that of the incident beam (the two vertical arrows in each case).

The cyclohexane spectrum in Figure 1.3 shows that there is more than one vibration which gives effective Raman scattering (i.e. is Raman active); the nature of these vibrations will be discussed in Section 1.3. However, there is a basic selection rule which is required to understand this pattern. Intense Raman scattering occurs from vibrations which cause a change in the polarizability of the electron cloud round the molecule. Usually, symmetric vibrations cause the largest changes and give the greatest scattering. This contrasts with infrared absorption where the most intense absorption is caused by a change in dipole and hence asymmetric vibrations which cause this are the most intense. As will be seen later, not all vibrations of a molecule need, or in some cases can, be both infrared and Raman active and the two techniques usually give quite different intensity patterns. As a result the two are often complementary and, used together, give a better view of the vibrational structure of a molecule.

One specific class of molecule provides an additional selection rule. In a centrosymmetric molecule, no band can be active in both Raman scattering and infrared absorption. This is sometimes called the mutual exclusion rule. In a centrosymmetric molecule, reflection of any point through the centre will reach an identical point on the other side (C_2H_4 is centrosymmetric, CH_4 is not). This distinction is useful particularly for small molecules where a comparison of the spectra obtained from infrared absorption and Raman scattering can be used to differentiate *cis* and *trans* forms of a molecule in molecules such as a simple azo dye or a transition metal complex.

Figure 1.4 shows a comparison of the infrared and Raman spectra for benzoic acid. The x -axis is given in wavenumbers for which the unit is cm^{-1} . Wavenumbers are not recommended SI units but the practice of spectroscopy is universally carried out using these and this is unlikely to change. For infrared absorption each peak represents an energy of radiation absorbed by the molecule. The y -axis gives the amount of the light absorbed and is usually shown with the maximum absorbance as the lowest point on the trace. Raman scattering is presented only as the Stokes spectrum and is given as a shift in energy from the energy of the laser beam. This is obtained by subtracting the scattered energy from the laser energy. In this way the difference in energy corresponding to the ground and excited vibrational states (n and m in Figure 1.2) is obtained. This energy difference is what is measured directly by infrared. The scattering is measured as light detected by the spectrometer and the maximum amount of light detected is the highest point on the trace.

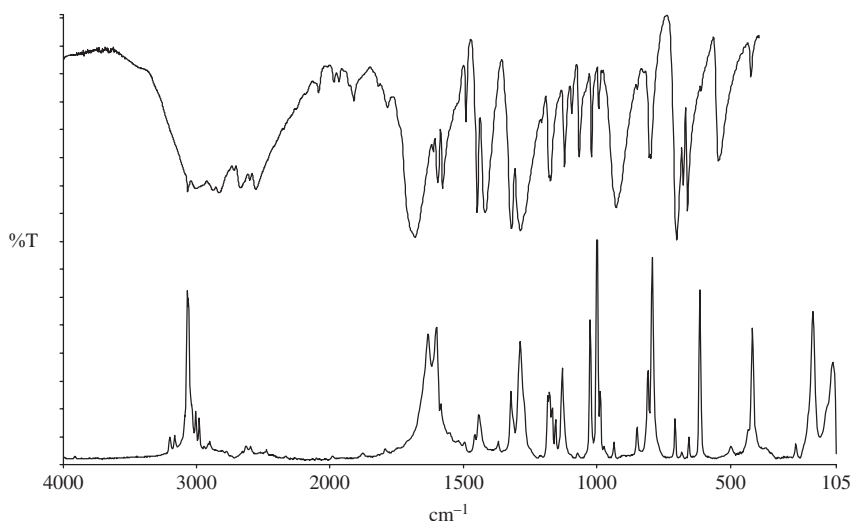


Figure 1.4. Infrared and Raman spectra of benzoic acid. The top trace is infrared absorption given in % transmission (%T) so that the lower the transmission value the greater the absorption. The lower trace is Raman scattering and the higher the peak the greater the scattering.

Strictly speaking, Raman scattering should be expressed as a shift in energy from that of the exciting radiation and should be referred to as Δcm^{-1} but it is often expressed simply as cm^{-1} . This practice is followed in this book for simplicity. Although different energy ranges are possible, the information of interest to most users is in the $3600\text{--}400\text{cm}^{-1}$ (2.8–12 micron) range in infrared spectroscopy and down to 200cm^{-1} in Raman spectroscopy since this includes most modes which are characteristic of a molecule. In some applications, much larger or smaller energy changes are studied and modern Raman equipment can cope with much wider ranges. One specific advantage of Raman scattering is that shifts from the laser line of 50cm^{-1} or lower can easily be recorded with the correct equipment. Many modern machines for reasons of cost and simplicity are not configured in a suitable way to measure shifts below $100\text{--}200\text{cm}^{-1}$. The intensities of the bands in the Raman spectrum are dependent on the nature of the vibration being studied and on instrumentation and sampling factors. Modern instruments should be calibrated to remove the instrument factors but this is not always the case; these factors are dealt with in the next chapter. Sampling has a large effect on the absolute intensities, bandwidths observed and band positions. Again these will be dealt with later. This chapter will concentrate on the effect on Raman scattering of the set of vibrations present in a molecule and set out a step-by-step approach to interpretation based on simple selection rules.

1.3 MOLECULAR VIBRATIONS

Provided that there is no change in electronic energy, for example, by the absorption of a photon and the promotion of an electron to an excited electronic state, the energy of a molecule can be divided into a number of different parts or ‘degrees of freedom’. Three of these degrees of freedom are taken up to describe the translation of the molecule in space and three to describe rotational movement except for linear molecules where only two types of rotation are possible. Thus, if N is the number of atoms in a molecule, the number of vibrational degrees of freedom and therefore the number of vibrations possible is $3N - 6$ for all molecules except linear ones where it is $3N - 5$. For a diatomic molecule, this means there will be only one vibration. In a molecule such as oxygen, this is a simple stretch of the O–O bond. This will change the polarizability of the molecule but will not induce any dipole change since there is no dipole in the molecule and the vibration is symmetric about the centre. Thus the selection rules already discussed would predict, and it is true, that oxygen gas will give a band in the Raman spectrum and no band in the infrared spectrum. However in a molecule such as nitric oxide, NO, there will be only one band but, since there is both a dipole change and a polarizability change, it will appear in both the infrared and Raman spectrum.

A triatomic molecule will have three modes of vibration. They are a symmetrical stretch, a bending or deformation mode and an asymmetrical stretch as shown in Figure 1.5. The very different water (H_2O) and carbon dioxide (CO_2) molecules clearly demonstrate these vibrations. These diagrams use ‘spring and ball’ models. The spring represents the bond or bonds between the atoms. The stronger the bond the higher the frequency. The balls represent the atoms and the heavier they are the lower the frequency. The expression which relates the mass of the atoms and the bond strength to the vibrational frequency is Hooke’s

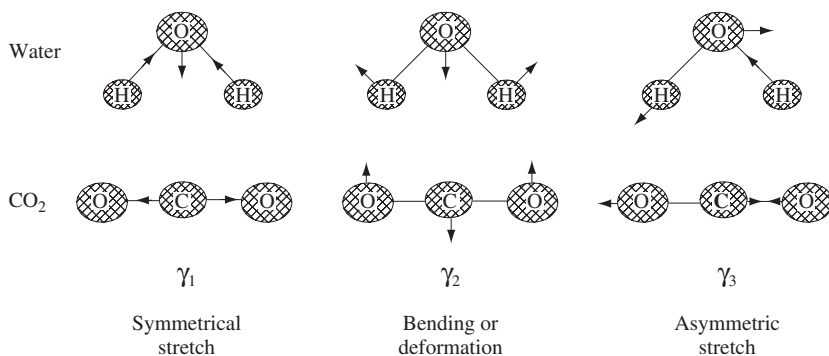


Figure 1.5. Spring and ball model – three modes of vibration for H_2O and CO_2 .

law which is dealt with in Chapter 3, but for the present, it is clear that strong bonds and light atoms will give higher frequencies of vibration and heavy atoms and weak bonds will give lower ones.

This simple model is widely used to interpret vibrational spectra. However, the molecule actually exists as a three-dimensional structure with a pattern of varying electron density covering the whole molecule. A simple depiction of this for carbon dioxide is shown in Figure 1.6. If either molecule vibrates, the electron cloud will alter as the positive nuclei change position and depending on the nature of the change, this can cause a change of dipole moment or polarization. In these triatomic molecules, the symmetrical stretch causes large polarization changes and hence strong Raman scattering with weak or no dipole change and hence weak or no infrared absorption. The deformation mode causes a dipole change but little polarization change and hence strong infrared absorption and weak or non-existent Raman scattering.

As an example of this, Figure 1.7 illustrates the vibrations possible for carbon disulphide along with the corresponding infrared absorption and Raman scattering spectra.

Although this type of analysis is suitable for small molecules, it is more difficult to apply in a more complex molecule. Figure 1.8 shows one vibration from a dye in which a large number of atoms are involved. This is obtained from a theoretical calculation using density functional theory (DFT) which is discussed briefly later. It probably gives a depiction of the vibration which is close to the truth. However, even if it were possible to calculate the spectrum of every molecule quickly in the laboratory, which at present it is not, this type of diagram is only of limited utility to the spectroscopist. A comparison between molecules of similar type is difficult unless a full calculation is available for them all and each subtle change in the nuclear displacements is drawn out or accurately described for each one. This limits the ability to compare large numbers of molecules or to understand the nature of vibrations in molecules for which there is no calculation.

The usual approach to describing vibrations is to simplify the problem and break the displacements down into a number of characteristic features, which

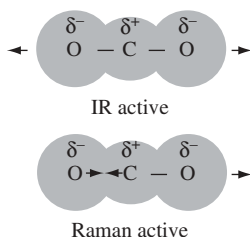


Figure 1.6. Electron cloud model of water and carbon dioxide showing an IR and a Raman active vibrations.

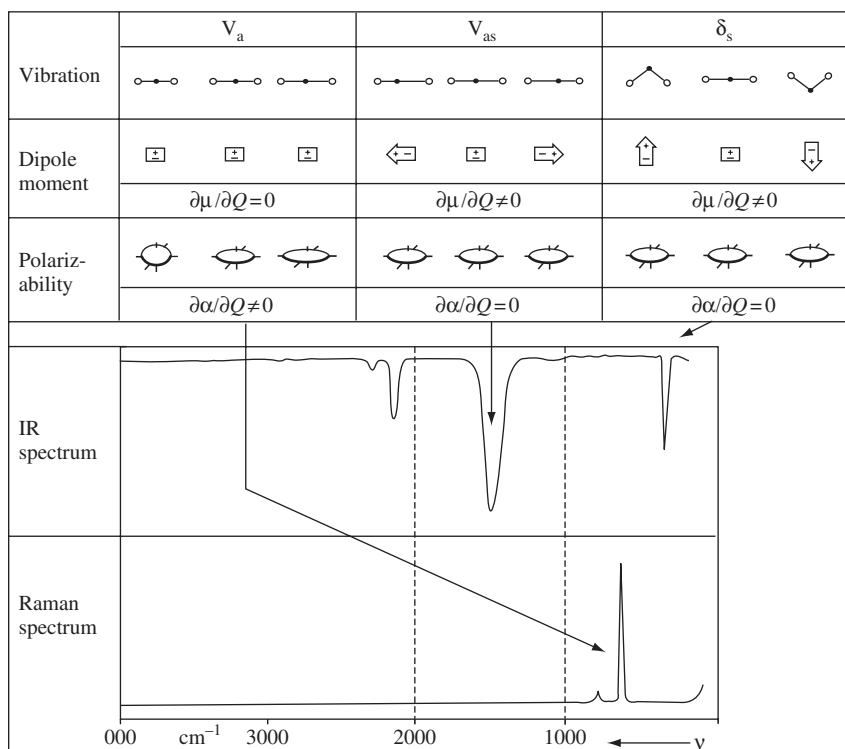


Figure 1.7. Dipole and polarization changes in carbon disulphide, with resultant infrared and Raman spectra. (Reprinted from A. Fadini and F.-M. Schnepel, *Vibrational Spectroscopy: Methods and Applications*, Ellis Horwood Ltd, Chichester, 1989.)

can relate to more than one molecule. In the vibration in Figure 1.8 which comes from a calculation to predict the energies of vibrations each azo dye, the biggest displacements of the heavier atoms is on one of the ring systems. The vibration would almost certainly be labelled vaguely as a ‘ring stretch’. In another vibration not shown the situation was much simpler. Large displacements were found on the two nitrogen atoms which form the azo bond between the rings, and the direction indicated bond lengthening and contracting during the vibrational cycle. Thus this vibration is called the azo stretch, and there is a change in polarizability just as there was for oxygen; so it should be a Raman-active vibration. We can search for these vibrations in the actual spectrum and hopefully match a peak to the vibration. This is called assigning the vibration. Thus, it is possible to describe a vibration in a few helpful words. In some cases this is fairly accurate as for the azo stretch, but in some cases, the description is not adequate to describe the actual movement. However, common bands can be assigned and reasonably described in many molecules.

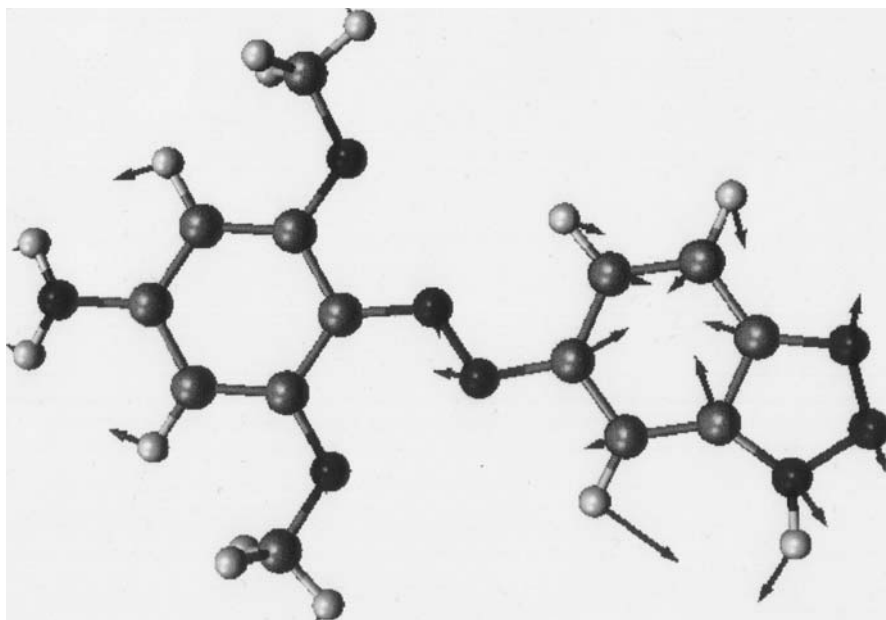


Figure 1.8. A displacement diagram for a vibration at about 1200cm^{-1} in a dye indicating the involvement of a number of atoms. The arrows show the direction of the displacement. Since the equilibrium position of the atoms is shown, during a complete vibration the arrows will reverse in direction.

1.3.1 Group Vibrations

To assign vibrations to spectral peaks it is necessary to realize that two or more bonds which are close together in a molecule and are of similar energies can interact and it is the vibration of the group of atoms linked by these bonds which is observed in the spectrum. For example, the CH_2 group is said to have a symmetric and an anti-symmetric stretch rather than two separate CH stretches (Figure 1.9). It follows from this and from the geometry of the molecule that different types of vibrations are possible for different groups. Selected examples of a few of these for CH_3 and C_6H_6 are shown in Figure 1.9.

In contrast, where there is a large difference in energy between the vibrations in different bonds or if the atoms are well separated in the molecule, they can be treated separately. Thus, for CH_3Br , the C–H bonds in CH_3 must be treated as a group but the C–Br vibration is treated separately. In Figure 1.9, the selected vibrations of benzene are shown in two different ways. Firstly they are shown with the molecule in the equilibrium position with arrows showing the direction of the vibrational displacement. To illustrate what this means, they are also shown with the vibration at the extremes of the vibrational movement. To show

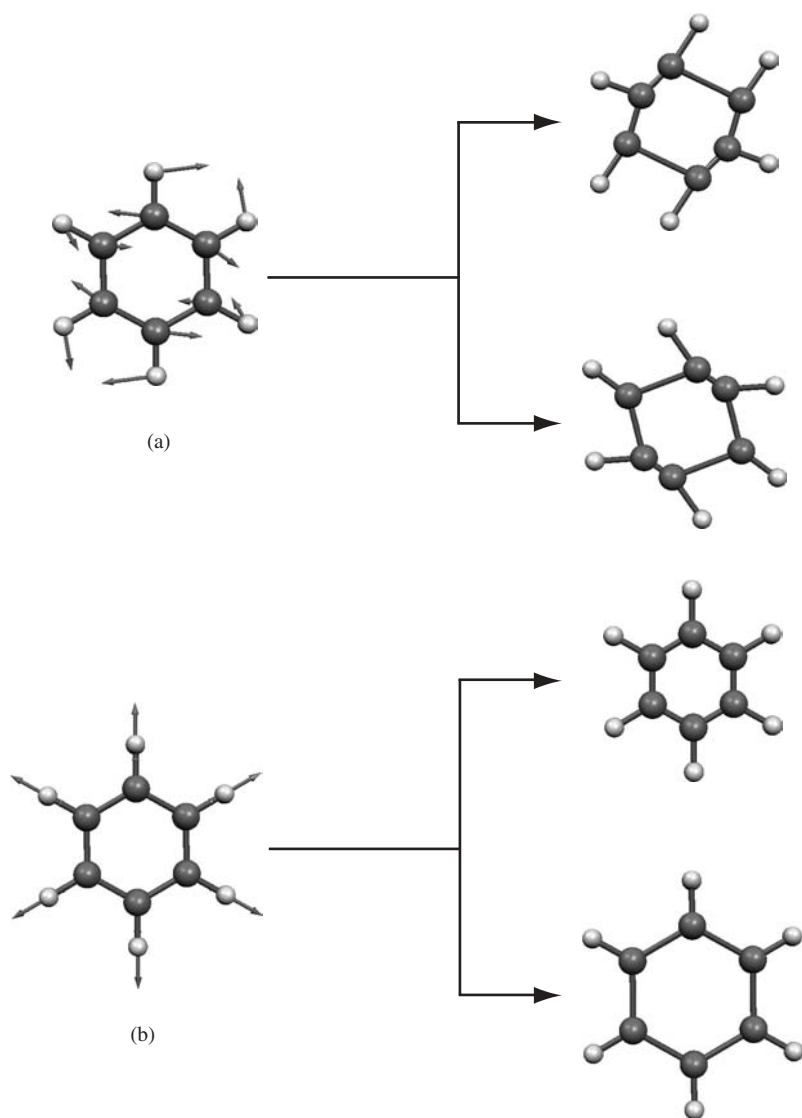


Figure 1.9. Selected displacement diagrams for benzene and for CH_3 in CH_3Br . (a) A quadrant stretch for benzene at about 1600 cm^{-1} . (b) The symmetric breathing mode at just above 1000 cm^{-1} . (c and d) Two C-H vibrations at about 3000 cm^{-1} . (e) The symmetric stretch of CH_3 in CH_3Br at above 3000 cm^{-1} . (f) An asymmetric stretch at above 3000 cm^{-1} . (g) A CH bend at about $1450\text{--}1500\text{ cm}^{-1}$. (h) A low frequency mode at below 600 cm^{-1} .

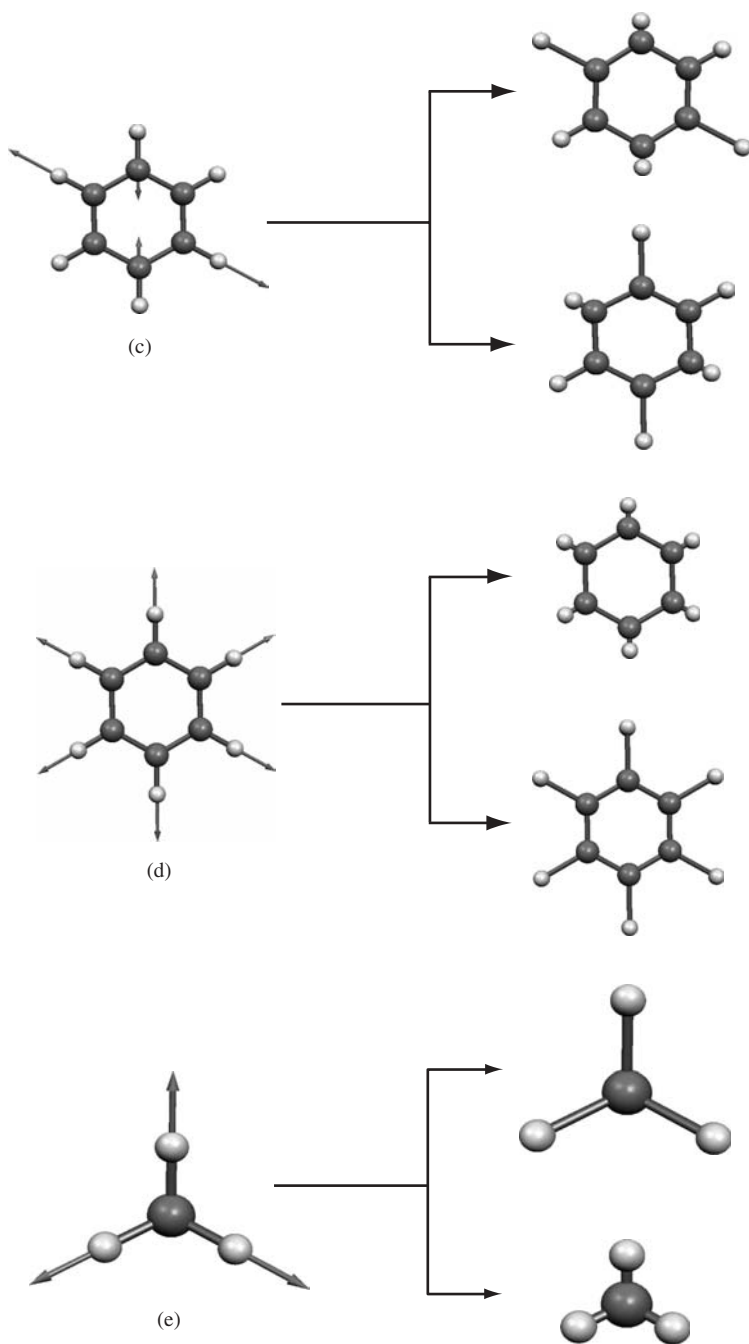


Figure 1.9. Continued.

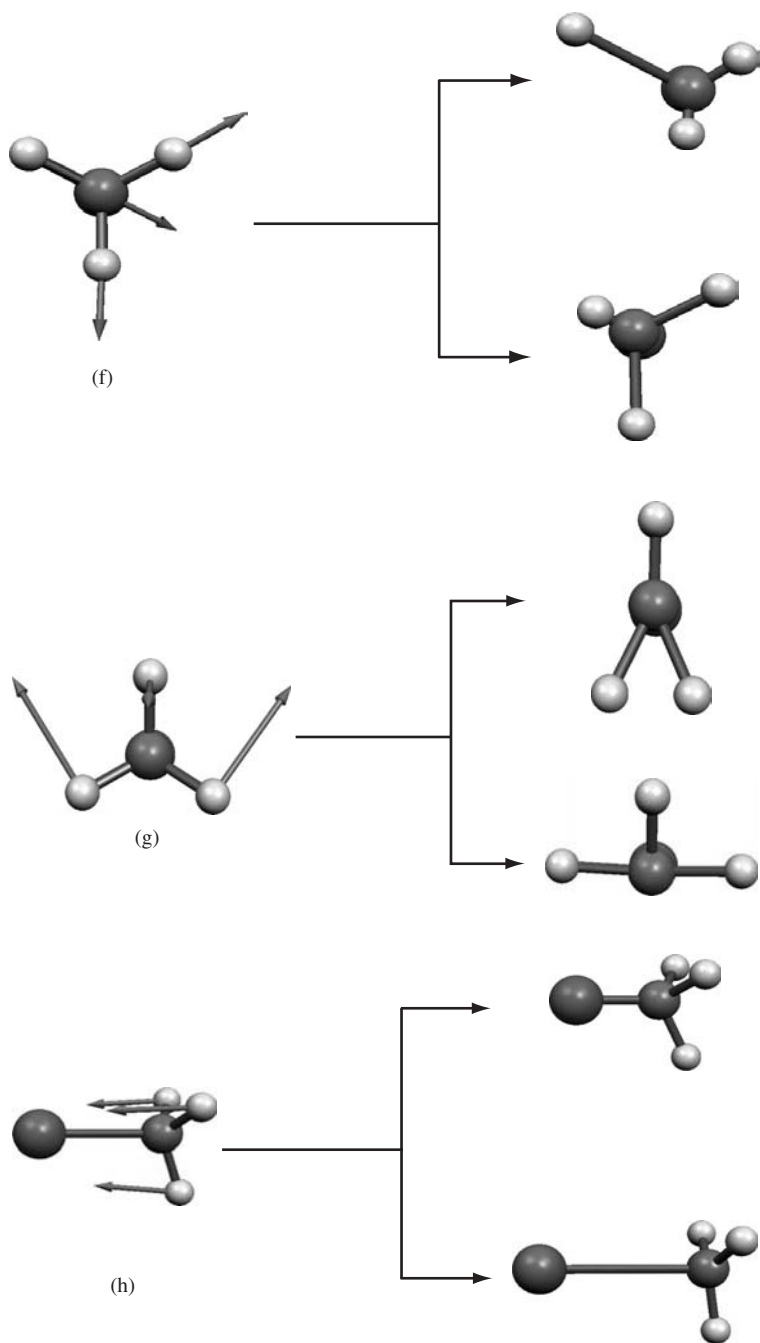


Figure 1.9. Continued.

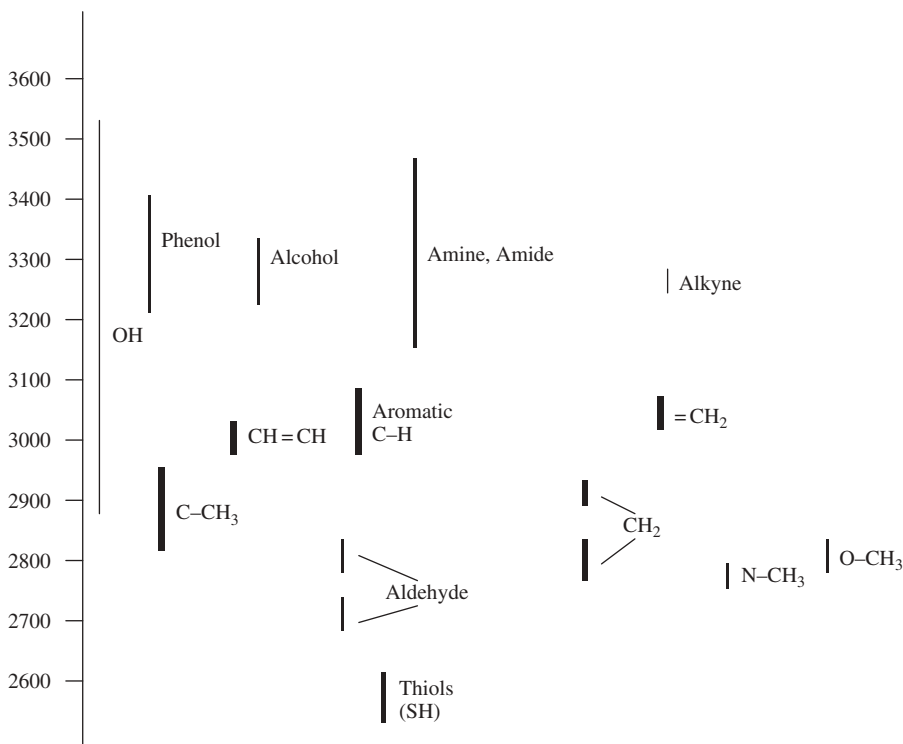
the selected CH_3 group vibrations, the molecule is completed using a bromine. As discussed, the C-Br bond vibrates at a much lower frequency and does not interact appreciably with the high CH_3 displacements shown.

1.3.2 An Approach to Interpretation

It is possible to give energy ranges in which the characteristic frequencies of the most common groups which are strong in either infrared or Raman scattering can occur. The relative intensities of specific peaks help to confirm that the correct vibration has been picked out.

For example, carbonyl groups $>\text{C}=\text{O}$ which are both asymmetric and ionic will have a dipole moment which will change when the group stretches in a manner analogous to oxygen. They have strong bands in the infrared spectrum

Table 1.1. Single vibration and group frequencies and possible intensities of peaks commonly identified in Raman scattering. The length of the vertical line represents the wavenumber range in cm^{-1} in which each type of vibration is normally found and the line thickness gives an indication of intensity with thick lines being the most intense.



but are weaker in the Raman spectrum. They are usually present at $\sim 1700\text{ cm}^{-1}$. Symmetrical groups such as unsaturated bonds ($-\text{C}=\text{C}-$) and disulphide bonds ($-\text{S}-\text{S}-$) are weak infrared absorbers, but strong Raman scatterers. The stretching modes for these vibrations are ~ 1640 and 500 cm^{-1} respectively. There are many more examples. It is the combination of the knowledge of approximate energy and likely relative intensity of particular vibrations which form the basis of the assignment mode used by most spectroscopists. For example, the $4000\text{--}2500\text{ cm}^{-1}$ is the region where single bonds ($\text{X}-\text{H}$) absorb. The $2500\text{--}2000\text{ cm}^{-1}$ is referred to as the multiple bond ($-\text{N}=\text{C}=\text{O}$) region. The $2000\text{--}1500\text{ cm}^{-1}$ region is where double bonds ($-\text{C}=\text{O}$, $-\text{C}=\text{N}$, $-\text{C}=\text{C}-$) occur. Below 1500 cm^{-1} , some groups, e.g. nitro ($\text{O}=\text{N}=\text{O}$) do have specific bands but many molecules have complex patterns of Carbon–Carbon and Carbon–Nitrogen vibrations. The region is generally referred to as the Fingerprint region. Significant bands below 650 cm^{-1} usually arise from inorganic groups, metal-organic groups or lattice vibrations. Tables 1.1–1.5 show the frequency ranges of

Table 1.2. Single vibration and group frequencies and an indication of possible intensities of peaks commonly identified in Raman scattering

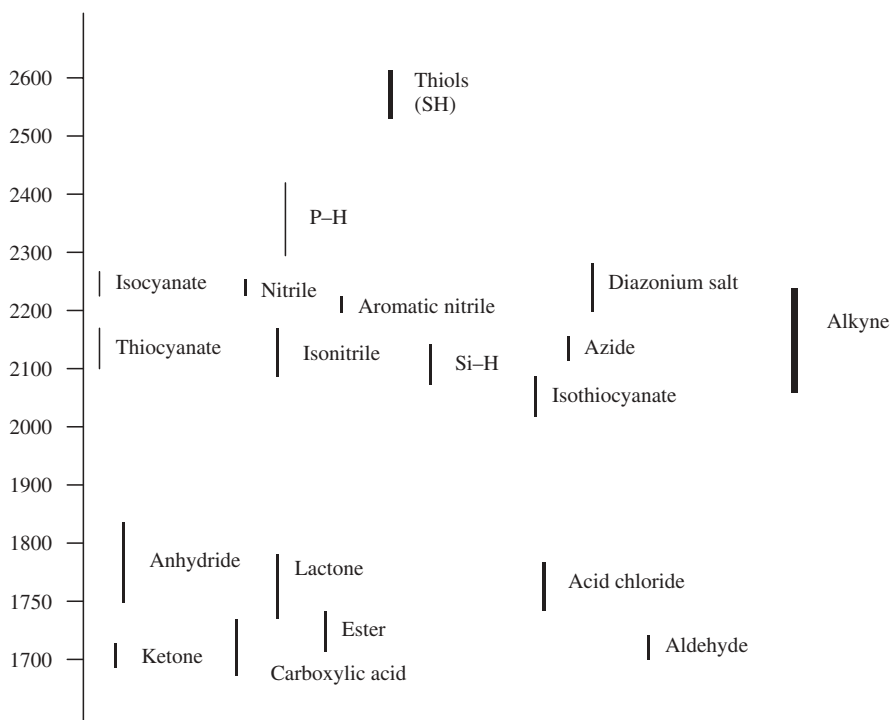
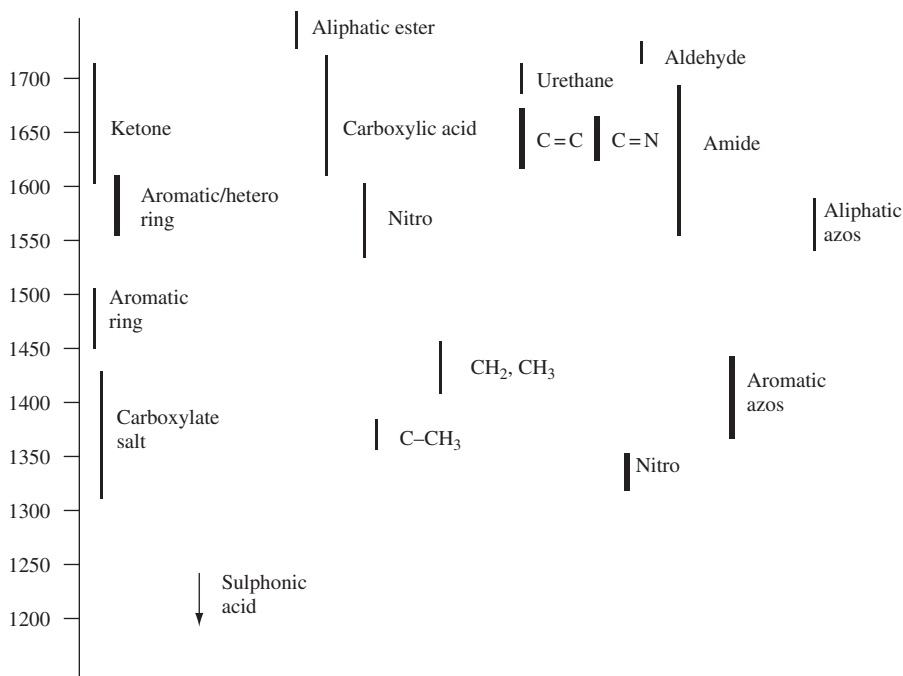
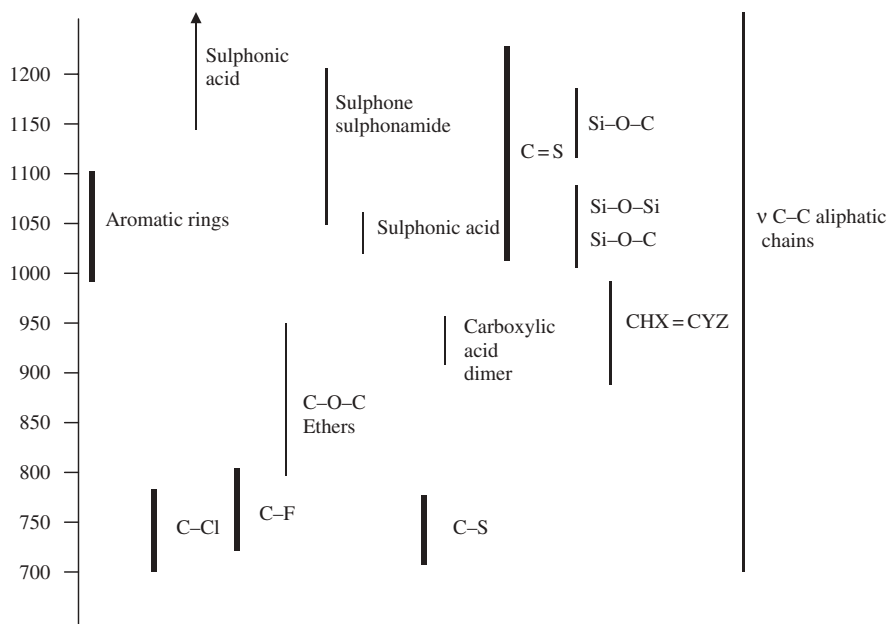


Table 1.3. Single vibration and group frequencies and an indication of possible intensities of peaks commonly identified in Raman scattering

many of the vibrations which give rise to strong bands in either Raman or infrared spectroscopy. The ranges are approximate for the groups in most structures but some groups in unusual structures may give bands outside these ranges. The thickness of the line indicates relative strength. These tables enable a beginning to be made on the assignment of specific bands. A more difficult problem is in estimating the relative intensities of the bands. Earlier in this chapter, we showed that there are reasons why in some circumstances bands which are strong in the infrared spectrum are not strong in the Raman spectrum. However, this cannot be taken as an absolute rule although it is the normal behaviour. Thus, the bands that we would expect to be strong in Raman scattering are the more symmetric bands in the spectrum.

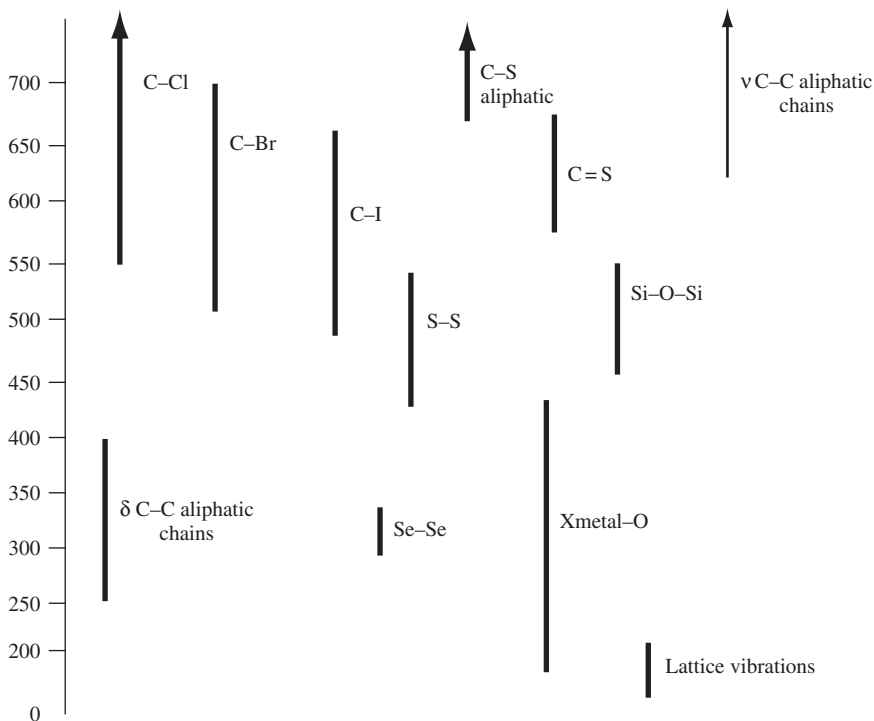
This approach is often used in vibrational spectroscopy. However, to assign specific peaks in the spectrum to specific vibrations, modern laboratories use libraries in which complete spectra are stored electronically. Most spectrometers have software to obtain a computer-generated analysis of the similarities and differences with standards so that specific substances can be identified positively and easily. In other areas, the initial assignment is confirmed by

Table 1.4. Single vibration and group frequencies and an indication of possible intensities of peaks commonly identified in Raman scattering



DFT calculations, where the great advantages are a more accurate assessment of the nature of the vibrations and hence of molecular structure.

Predicting the principal infrared absorption bands for small molecules is relatively simple as shown above, but for large molecules, the number of bands possible is very large. Fortunately, many of these bands overlap and what is observed at room temperature are broad envelopes with recognizable shapes in some energy regions and sharp bands due to specific bonds such as -C=O in some others. Since some vibrations arise from groups of atoms such as the atoms in a carbon chain or from rings linked by bonds of approximately the same energy, the number of peaks and their energies are linked to the overall shape of the molecule. These are called fingerprint bands and the pattern of these bands can help identify a specific molecule *in situ* in a sample. However, for more complex systems, much time can be spent in the assignment of these bands to the bending, stretching or deformation modes but unless the molecule studied is one of a well-understood set such as an alkane chain of a specific length, this more in-depth analysis does not provide much additional help in the majority of first attempts to identify specific materials from the spectrum.

Table 1.5. Single vibration and group frequencies and an indication of possible intensities of peaks commonly identified in Raman scattering

Raman spectra are usually somewhat simpler. The most environmentally sensitive bands, e.g. OH and NH, are broad and weak and the backbone structural bands are strong and sharp. The extent of this difference can be illustrated from the fact that water can be used as a solvent to obtain the Raman spectra of organic molecules. This indicates the relative strength of bands in the organic molecule compared to the weakness of hydrogen bonded species such as the OH bands in water. It is this greater selectivity which leads to the simplicity of Raman spectra compared to infrared spectra. Thus, the Raman spectra of quite large molecules show clear bands. In Figure 1.4 the infrared spectrum is complex and has a strong band just above 1600 cm^{-1} from the carbonyl group due to the C=O vibration. The strong bands in the Raman spectrum are largely due to the aromatic group. The band at 2900 cm^{-1} due to the CH₂ group is hidden under the strong OH bands in the infrared spectrum but can be clearly seen in the Raman spectrum.

The above information makes it possible to start assigning and interpreting Raman spectra. If possible it is always good to run an infrared spectrum for

comparison. The phrase ‘interpretation of Raman spectra’ is used in many different ways. The spectrum of a molecule can be the subject of a full mathematical interpretation in which every band is carefully assigned or of a cursory look to produce the interpretation ‘Yes that is toluene’. However, to be able to carry out a complete, correct and relevant interpretation, the total Raman experiment must be considered. Raman spectroscopists have to make a number of choices in deciding how to examine a sample and the type of answer required may ultimately determine these choices. The simplicity and flexibility of Raman scattering are considerable advantages but if care is not taken in making the correct choices, poor or spurious results can be obtained. Chapter 2 describes the choices and provides the background information to enable the recording and interpretation of Raman scattering in a reliable and secure manner.

1.4 SUMMARY

In this chapter we have attempted to introduce the reader to the basic principles of Raman spectroscopy without going into the theory and details of practice too deeply, with a view to encouraging further interest. Chapter 2 outlines the practical choices to be made in carrying out the Raman experiment in full. Later chapters give the theoretical background required for full analysis of spectra, a guide to ways in which Raman spectroscopy has been successfully employed, and lead to the more sophisticated but less common techniques available to the Raman spectroscopist.

REFERENCES

1. A. Smekal, *Naturwissenschaften*, **43**, 873 (1923).
2. C.V. Raman and K.S. Krishnan, *Nature*, **121**, 501 (1928).

BIBLIOGRAPHY

We have provided a general bibliography. Listed here are a number of publications which the authors have found useful for reference, for theoretical aspects of the spectroscopy and for aids in interpretation.

- J.R. Ferraro and K. Nakamoto, *Introductory Raman Spectroscopy*, Academic Press, San Diego, 1994.
- P. Hendra, C. Jones and G. Warnes, *FT Raman Spectroscopy*, Ellis Horwood Ltd, Chichester, 1991.
- A. Fadini and F.-M. Schnepel, *Vibrational Spectroscopy: Methods and Applications*, Ellis Horwood Ltd, Chichester, 1989.

- N.B. Colthrup, L.H. Daly and S.E. Wiberley, *Introduction to Infrared and Raman Spectroscopy*. 3rd Edition, Academic Press, San Diego, 1990.
- D. Lin-Vien, N.B. Colthrup, W.G. Fateley and J.G. Grasselli, *The Handbook of Infrared and Raman Characteristic Frequencies of Organic Molecules*, John Wiley & Sons, New York, 1991.
- I.A. Degen, *Tables of Characteristic Group frequencies for the Interpretation of Infrared and Raman Spectra*, Acolyte Publications, Harrow, UK, 1997.
- D.M. Adams, *Metal – Ligands and Related Vibrations*, Edward Arnold Ltd, London, 1967.

Chapter 2

Experimental Methods

Learning Objectives

- To understand how an infrared spectrum is obtained from a Fourier-transform instrument.
- To recognize the different methods of sample preparation and sample handling techniques which are used for preparing samples in infrared spectroscopy.
- To recognize poor quality spectra and diagnose their causes.
- To understand the origins of reflectance techniques.
- To understand the origins of infrared microsampling techniques.
- To understand that spectral information may be obtained from combination infrared spectroscopy techniques.
- To select appropriate sample preparation methods for different types of samples.

2.1 Introduction

Traditionally, dispersive instruments, available since the 1940s, were used to obtain infrared spectra. In recent decades, a very different method of obtaining an infrared spectrum has superseded the dispersive instrument. Fourier-transform infrared spectrometers are now predominantly used and have improved the acquisition of infrared spectra dramatically. In this present chapter, the instrumentation required to obtain an infrared spectrum will be described.

Infrared spectroscopy is a versatile experimental technique and it is relatively easy to obtain spectra from samples in solution or in the liquid, solid or gaseous

states. In this chapter, how samples can be introduced into the instrument, the equipment required to obtain spectra and the pre-treatment of samples are examined. First, the various ways of investigating samples using the traditional transmission methods of infrared spectroscopy will be discussed. Reflectance methods, such as the attenuated total reflectance, diffuse reflectance and specular reflectance approaches, as well as photoacoustic spectroscopy, are also explained. Infrared microspectroscopy has emerged in recent years as an effective tool for examining small and/or complex samples; the techniques used are described in this chapter. Infrared spectroscopy has also been combined with other well-established analytical techniques such as chromatography and thermal analysis. Such combination techniques are introduced here.

2.2 Dispersive Infrared Spectrometers

The first dispersive infrared instruments employed prisms made of materials such as sodium chloride. The popularity of prism instruments fell away in the 1960s when the improved technology of grating construction enabled cheap, good-quality gratings to be manufactured.

The dispersive element in dispersive instruments is contained within a monochromator. Figure 2.1 shows the optical path of an infrared spectrometer which uses a grating monochromator. Dispersion occurs when energy falling on the entrance slit is collimated onto the dispersive element and the dispersed radiation is then reflected back to the exit slit, beyond which lies the detector. The dispersed spectrum is scanned across the exit slit by rotating a suitable component within the monochromator. The widths of the entrance and exit slits may be varied and programmed to compensate for any variation of the source energy with wavenumber. In the absence of a sample, the detector then receives radiation of approximately constant energy as the spectrum is scanned.

Atmospheric absorption by CO_2 and H_2O in the instrument beam has to be considered in the design of infrared instruments. Figure 2.2 shows the spectrum of such atmospheric absorptions. These contributions can be taken into account by using a double-beam arrangement in which radiation from a source is divided into two beams. These beams pass through a sample and a reference path of the sample compartment, respectively. The information from these beams is rationed to obtain the required sample spectrum.

A detector must have adequate sensitivity to the radiation arriving from the sample and monochromator over the entire spectral region required. In addition, the source must be sufficiently intense over the wavenumber range and transmittance range. Sources of infrared emission have included the Globar, which is constructed of silicon carbide. There is also the Nernst filament, which is a mixture of the oxides of zirconium, yttrium and erbium. A Nernst filament only conducts electricity at elevated temperatures. Most detectors have consisted of thermocouples of varying characteristics.

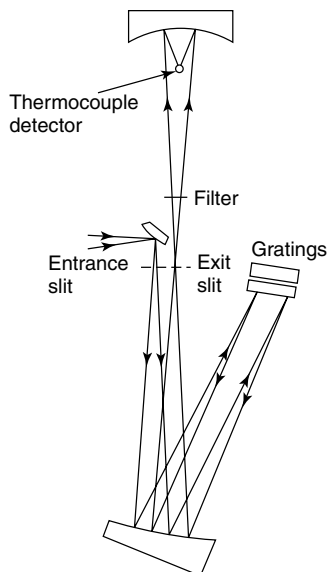


Figure 2.1 Schematic of the optical path of a double-beam infrared spectrometer with a grating monochromator. Reproduced from Brittain, E. F. H., George, W. O. and Wells, C. H. J., *Introduction to Molecular Spectroscopy*, Academic Press, London, Copyright (1975), with permission from Elsevier.

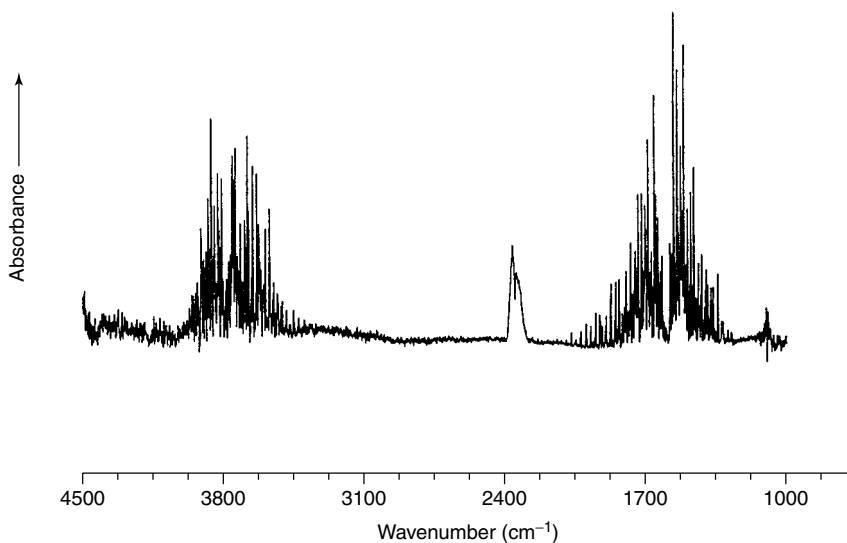


Figure 2.2 Infrared spectrum of atmospheric contributions (e.g. CO_2 and H_2O). From Stuart, B., *Modern Infrared Spectroscopy*, ACOL Series, Wiley, Chichester, UK, 1996. © University of Greenwich, and reproduced by permission of the University of Greenwich.

The essential problem of the dispersive spectrometer lies with its monochromator. This contains narrow slits at the entrance and exit which limit the wavenumber range of the radiation reaching the detector to one resolution width. Samples for which a very quick measurement is needed, for example, in the eluant from a chromatography column, cannot be studied with instruments of low sensitivity because they cannot scan at speed. However, these limitations may be overcome through the use of a Fourier-transform infrared spectrometer.

2.3 Fourier-Transform Infrared Spectrometers

Fourier-transform infrared (FTIR) spectroscopy [1] is based on the idea of the interference of radiation between two beams to yield an *interferogram*. The latter is a signal produced as a function of the change of pathlength between the two beams. The two domains of distance and frequency are interconvertible by the mathematical method of *Fourier-transformation*.

The basic components of an FTIR spectrometer are shown schematically in Figure 2.3. The radiation emerging from the source is passed through an interferometer to the sample before reaching a detector. Upon amplification of the signal, in which high-frequency contributions have been eliminated by a filter, the data are converted to digital form by an analog-to-digital converter and transferred to the computer for Fourier-transformation.

2.3.1 Michelson Interferometers

The most common interferometer used in FTIR spectrometry is a Michelson interferometer, which consists of two perpendicularly plane mirrors, one of which can travel in a direction perpendicular to the plane (Figure 2.4). A semi-reflecting film, the *beamsplitter*, bisects the planes of these two mirrors. The beamsplitter material has to be chosen according to the region to be examined. Materials such as germanium or iron oxide are coated onto an 'infrared-transparent' substrate such as potassium bromide or caesium iodide to produce beamsplitters for the mid- or near-infrared regions. Thin organic films, such as poly(ethylene terephthalate), are used in the far-infrared region.

If a collimated beam of monochromatic radiation of wavelength λ (cm) is passed into an ideal beamsplitter, 50% of the incident radiation will be reflected to one of the mirrors while 50% will be transmitted to the other mirror. The two beams are reflected from these mirrors, returning to the beamsplitter where they recombine and interfere. Fifty percent of the beam reflected from the fixed

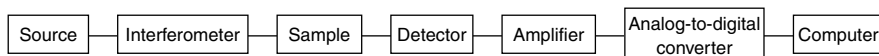


Figure 2.3 Basic components of an FTIR spectrometer.

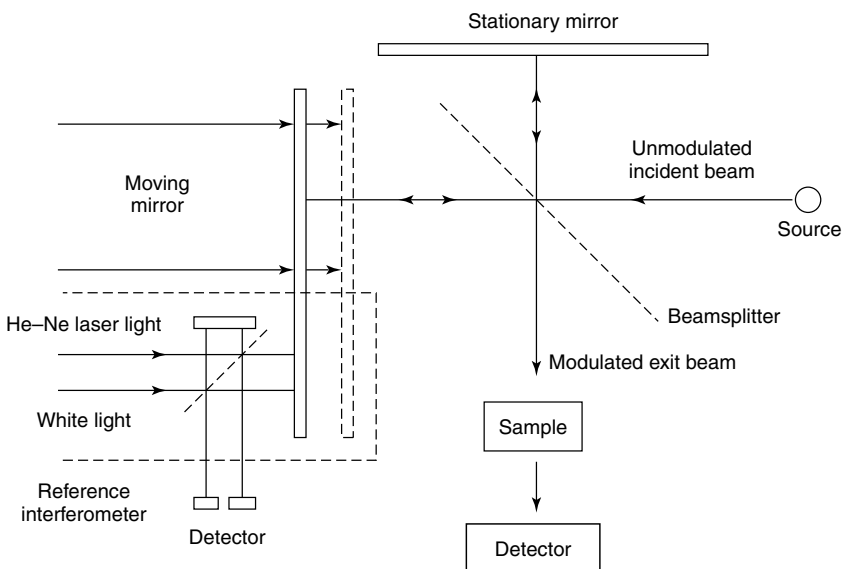


Figure 2.4 Schematic of a Michelson interferometer. From Stuart, B., *Modern Infrared Spectroscopy*, ACOL Series, Wiley, Chichester, UK, 1996. © University of Greenwich, and reproduced by permission of the University of Greenwich.

mirror is transmitted through the beamsplitter while 50% is reflected back in the direction of the source. The beam which emerges from the interferometer at 90° to the input beam is called the transmitted beam and this is the beam detected in FTIR spectrometry.

The moving mirror produces an optical path difference between the two arms of the interferometer. For path differences of $(n + 1/2)\lambda$, the two beams interfere destructively in the case of the transmitted beam and constructively in the case of the reflected beam. The resultant interference pattern is shown in Figure 2.5 for (a) a source of monochromatic radiation and (b) a source of polychromatic radiation (b). The former is a simple cosine function, but the latter is of a more complicated form because it contains all of the spectral information of the radiation falling on the detector.

2.3.2 Sources and Detectors

FTIR spectrometers use a Globar or Nernst source for the mid-infrared region. If the far-infrared region is to be examined, then a high-pressure mercury lamp can be used. For the near-infrared, tungsten-halogen lamps are used as sources.

There are two commonly used detectors employed for the mid-infrared region. The normal detector for routine use is a pyroelectric device incorporating deuterium tryglycine sulfate (DTGS) in a temperature-resistant alkali halide window.

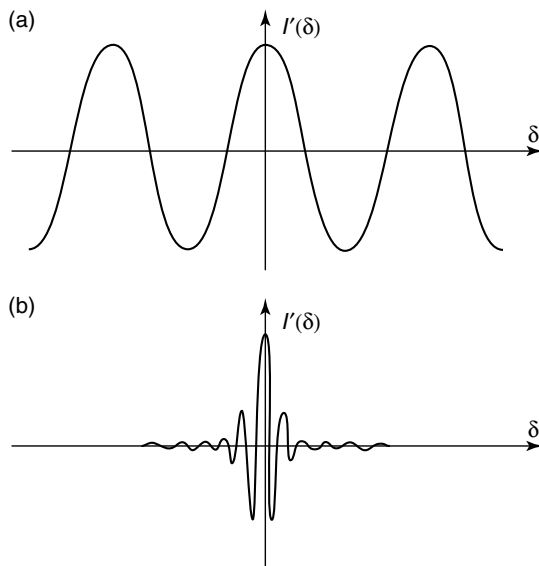


Figure 2.5 Interferograms obtained for (a) monochromatic radiation and (b) polychromatic radiation. Reproduced with permission from Barnes, A. J. and Orville-Thomas, W. J. (Eds), *Vibrational Spectroscopy – Modern Trends*, Elsevier, Amsterdam, Figure 2, p. 55 (1977).

For more sensitive work, mercury cadmium telluride (MCT) can be used, but this has to be cooled to liquid nitrogen temperatures. In the far-infrared region, germanium or indium–antimony detectors are employed, operating at liquid helium temperatures. For the near-infrared region, the detectors used are generally lead sulfide photoconductors.

2.3.3 Fourier-Transformation

The essential equations for a Fourier-transformation relating the intensity falling on the detector, $I(\delta)$, to the spectral power density at a particular wavenumber, $\bar{\nu}$, given by $B(\bar{\nu})$, are as follows:

$$I(\delta) = \int_0^{+\infty} B(\bar{\nu}) \cos(2\pi\bar{\nu}\delta) d\bar{\nu} \quad (2.1)$$

which is one half of a cosine Fourier-transform pair, with the other being:

$$B(\bar{\nu}) = \int_{-\infty}^{+\infty} I(\delta) \cos(2\pi\bar{\nu}\delta) d\delta \quad (2.2)$$

These two equations are interconvertible and are known as a Fourier-transform pair. The first shows the variation in power density as a function of the difference in pathlength, which is an interference pattern. The second shows the variation in intensity as a function of wavenumber. Each can be converted into the other by the mathematical method of *Fourier-transformation*.

The essential experiment to obtain an FTIR spectrum is to produce an interferogram with and without a sample in the beam and transforming the interferograms into spectra of (a) the source with sample absorptions and (b) the source without sample absorptions. The ratio of the former and the latter corresponds to a double-beam dispersive spectrum.

The major advance toward routine use in the mid-infrared region came with a new mathematical method (or algorithm) devised for *fast Fourier-transformation* (FFT). This was combined with advances in computers which enabled these calculations to be carried out rapidly.

2.3.4 Moving Mirrors

The moving mirror is a crucial component of the interferometer. It has to be accurately aligned and must be capable of scanning two distances so that the path difference corresponds to a known value. A number of factors associated with the moving mirror need to be considered when evaluating an infrared spectrum.

The interferogram is an analogue signal at the detector that has to be digitized in order that the Fourier-transformation into a conventional spectrum can be carried out. There are two particular sources of error in transforming the digitized information on the interferogram into a spectrum. First, the transformation carried out in practice involves an integration stage over a finite displacement rather than over an infinite displacement. The mathematical process of Fourier-transformation assumes infinite boundaries. The consequence of this necessary approximation is that the apparent lineshape of a spectral line may be as shown in Figure 2.6, where the main band area has a series of negative and positive side lobes (or pods) with diminishing amplitudes.

The process of *apodization* is the removal of the side lobes (or pods) by multiplying the interferogram by a suitable function before the Fourier-transformation is carried out. A suitable function must cause the intensity of the interferogram to fall smoothly to zero at its ends. Most FTIR spectrometers offer a choice of apodization options and a good general purpose apodization function is the cosine function, as follows:

$$F(D) = [1 + \cos(\pi D)]/2 \quad (2.3)$$

where D is the optical path difference. This cosine function provides a good compromise between reduction in oscillations and deterioration in spectral resolution. When accurate band shapes are required, more sophisticated mathematical functions may be needed.

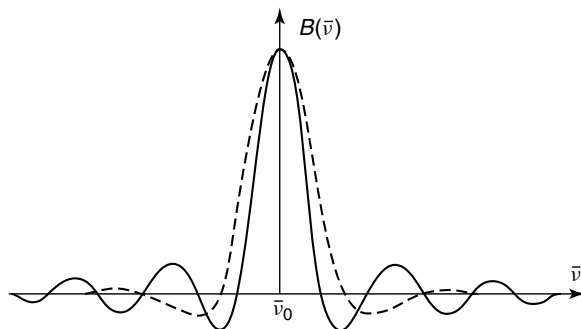


Figure 2.6 Instrument lineshape without apodization. Reproduced with permission from Barnes, A. J. and Orville-Thomas, W. J. (Eds), *Vibrational Spectroscopy – Modern Trends*, Elsevier, Amsterdam, Figure 3, p. 55 (1977).

Another source of error arises if the sample intervals are not exactly the same on each side of the maxima corresponding to zero path differences. Phase correction is required and this correction procedure ensures that the sample intervals are the same on each side of the first interval and should correspond to a path difference of zero.

The resolution for an FTIR instrument is limited by the maximum path difference between the two beams. The limiting resolution in wavenumbers (cm^{-1}) is the reciprocal of the pathlength difference (cm). For example, a pathlength difference of 10 cm is required to achieve a limiting resolution of 0.1 cm^{-1} . This simple calculation appears to show that it is easy to achieve high resolution. Unfortunately, this is not the case since the precision of the optics and mirror movement mechanism become more difficult to achieve at longer displacements of pathlengths.

SAQ 2.1

An FTIR spectrometer is used to record a single-beam spectrum from a single scan with a difference in pathlength (δ) of 100 mm.

- What is the limiting resolution in units of cm^{-1} ?
- How could a limiting resolution of 0.02 cm^{-1} be achieved?

2.3.5 Signal-Averaging

The main advantage of rapid-scanning instruments is the ability to increase the signal-to-noise ratio (SNR) by signal-averaging, leading to an increase of

signal-to-noise proportional to the square root of the time, as follows:

$$\text{SNR} \propto n^{1/2} \quad (2.4)$$

There are diminishing returns for signal-averaging in that it takes an increasingly longer time to achieve greater and greater improvement. The accumulation of a large number of repeat scans makes greater demands on the instrument if it is to exactly reproduce the conditions. It is normal to incorporate a laser monochromatic source in the beam of the continuous source. The laser beam produces standard fringes which can 'line-up' successive scans accurately and can determine and control the displacement of the moving mirror at all times.

2.3.6 Advantages

FTIR instruments have several significant advantages over older dispersive instruments. Two of these are the Fellgett (or multiplex) advantage and the Jacquinot (or throughput) advantage. The *Fellgett advantage* is due to an improvement in the SNR per unit time, proportional to the square root of the number of resolution elements being monitored. This results from the large number of resolution elements being monitored simultaneously. In addition, because FTIR spectrometry does not require the use of a slit or other restricting device, the total source output can be passed through the sample continuously. This results in a substantial gain in energy at the detector, hence translating to higher signals and improved SNRs. This is known as *Jacquinot's advantage*.

Another strength of FTIR spectrometry is its *speed advantage*. The mirror has the ability to move short distances quite rapidly, and this, together with the SNR improvements due to the Fellgett and Jacquinot advantages, make it possible to obtain spectra on a millisecond timescale. In interferometry, the factor which determines the precision of the position of an infrared band is the precision with which the scanning mirror position is known. By using a helium–neon laser as a reference, the mirror position is known with high precision.

2.3.7 Computers

The computer forms a crucial component of modern infrared instruments and performs a number of functions. The computer controls the instrument, for example, it sets scan speeds and scanning limits, and starts and stops scanning. It reads spectra into the computer memory from the instrument as the spectrum is scanned; this means that the spectrum is digitized. Spectra may be manipulated using the computer, for example, by adding and subtracting spectra or expanding areas of the spectrum of interest. The computer is also used to scan the spectra continuously and average or add the result in the computer memory. Complex analyses may be automatically carried out by following a set of pre-programmed commands (described later in Chapter 3). The computer is also used to plot the spectra.

2.3.8 Spectra

Early infrared instruments recorded percentage transmittance over a linear wavelength range. It is now unusual to use wavelength for routine samples and the wavenumber scale is commonly used. The output from the instrument is referred to as a *spectrum*. Most commercial instruments present a spectrum with the wavenumber decreasing from left to right.

The infrared spectrum can be divided into three main regions: the *far-infrared* ($<400\text{ cm}^{-1}$), the *mid-infrared* ($4000\text{--}400\text{ cm}^{-1}$) and the *near-infrared* ($13\,000\text{--}4000\text{ cm}^{-1}$). These regions will be described later in more detail in Chapter 3. Many infrared applications employ the mid-infrared region, but the near- and far-infrared regions also provide important information about certain materials. Generally, there are less infrared bands in the $4000\text{--}1800\text{ cm}^{-1}$ region with many bands between 1800 and 400 cm^{-1} . Sometimes, the scale is changed so that the region between 4000 and 1800 cm^{-1} is contracted and the region between 1800 and 400 cm^{-1} is expanded to emphasize features of interest.

The ordinate scale may be presented in % transmittance with 100% at the top of the spectrum. It is commonplace to have a choice of absorbance or transmittance as a measure of band intensity. The relationship between these two quantities will be described in Chapter 3. Figures 2.7 and 2.8 show the infrared spectra of lactic acid and illustrate the difference in appearance between absorbance and

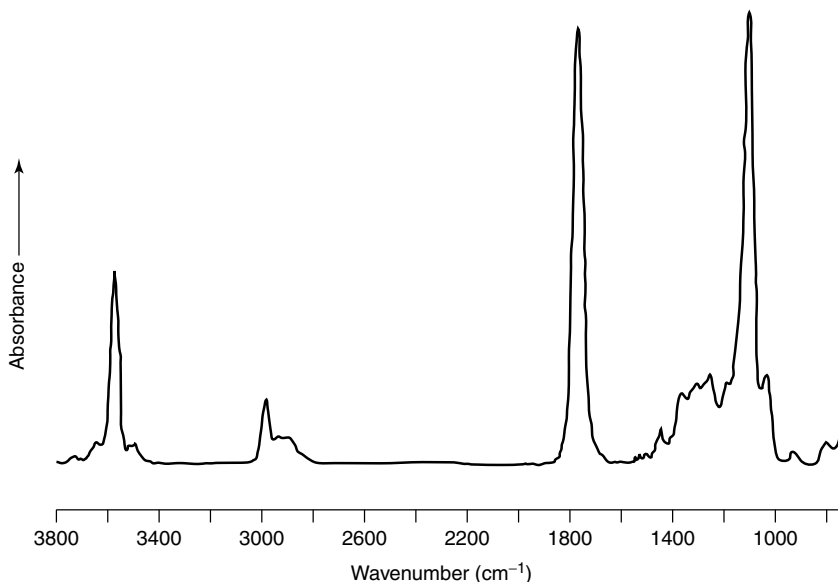


Figure 2.7 Absorbance spectrum of lactic acid. From Stuart, B., *Biological Applications of Infrared Spectroscopy*, ACOL Series, Wiley, Chichester, UK, 1997. © University of Greenwich, and reproduced by permission of the University of Greenwich.

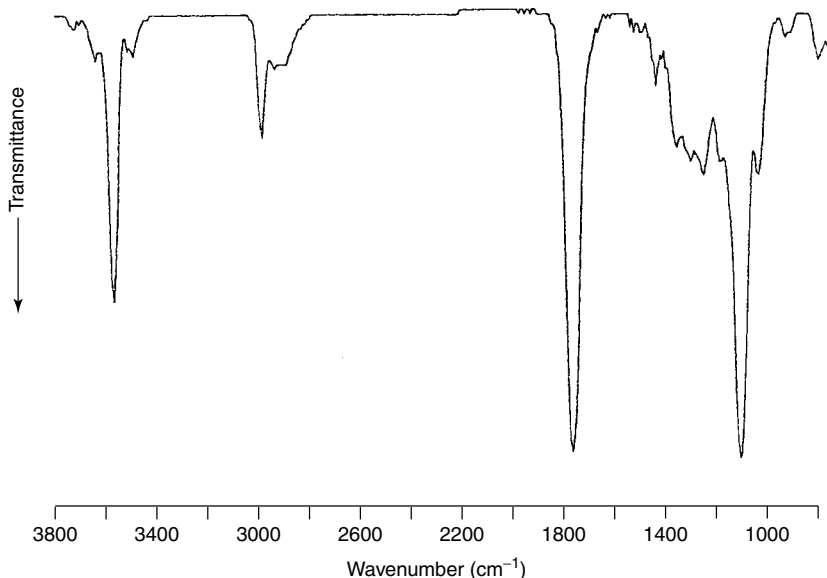


Figure 2.8 Transmittance spectrum of lactic acid. From Stuart, B., *Biological Applications of Infrared Spectroscopy*, ACOL Series, Wiley, Chichester, UK, 1997. © University of Greenwich, and reproduced by permission of the University of Greenwich.

transmittance spectra. It almost comes down to personal preference which of the two modes to use, but the transmittance is traditionally used for spectral interpretation, while absorbance is used for quantitative work.

2.4 Transmission Methods

Transmission spectroscopy is the oldest and most straightforward infrared method. This technique is based upon the absorption of infrared radiation at specific wavelengths as it passes through a sample. It is possible to analyse samples in the liquid, solid or gaseous forms when using this approach.

2.4.1 Liquids and Solutions

There are several different types of transmission solution cells available. Fixed-pathlength sealed cells are useful for volatile liquids, but cannot be taken apart for cleaning. Semi-permanent cells are demountable so that the windows can be cleaned. A semi-permanent cell is illustrated in Figure 2.9. The spacer is usually made of polytetrafluoroethylene (PTFE, known as 'Teflon') and is available in a variety of thicknesses, hence allowing one cell to be used for various pathlengths. Variable pathlength cells incorporate a mechanism for continuously adjusting the pathlength, while a vernier scale allows accurate adjustment. All of these cell

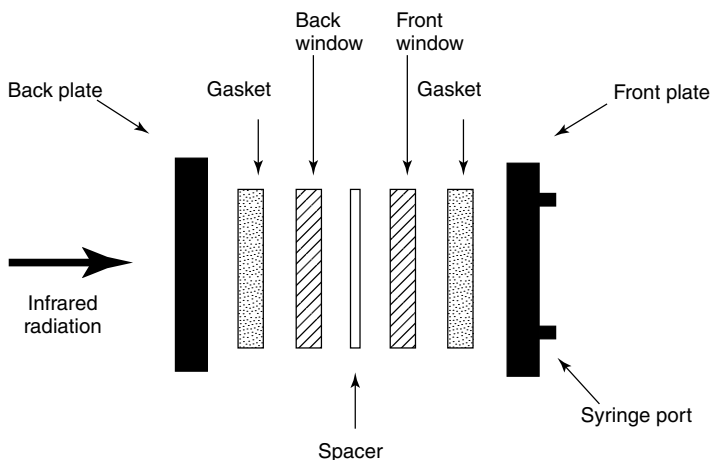


Figure 2.9 Schematic of a typical semi-permanent liquid cell. From Stuart, B., *Biological Applications of Infrared Spectroscopy*, ACOL Series, Wiley, Chichester, UK, 1997. © University of Greenwich, and reproduced by permission of the University of Greenwich.

types are filled by using a syringe and the syringe ports are sealed with PTFE plugs before sampling.

DQ 2.1

Which type of solution cell would you consider to be the easiest to maintain?

Answer

The **demountable** is by far the easiest to maintain as it can be readily dismantled and cleaned. The windows can be repolished, a new spacer supplied and the cell reassembled. The **permanent** cells are difficult to clean and can become damaged by water. The pathlengths need to be calibrated regularly if quantitative work is to be undertaken. Variable pathlength cells suffer from similar disadvantages and they are difficult to take apart. The calibration therefore suffers and the cells have to be calibrated regularly.

An important consideration in the choice of infrared cells is the type of window material. The latter must be transparent to the incident infrared radiation and alkali halides are normally used in transmission methods. The cheapest material is sodium chloride (NaCl), but other commonly used materials are listed in Table 2.1.

Certain difficulties arise when using water as a solvent in infrared spectroscopy. The infrared modes of water are very intense and may overlap with the sample modes of interest. This problem may be overcome by substituting water with deuterium oxide (D₂O). The infrared modes of D₂O occur at different wavenumbers to those observed for water because of the mass dependence of

Table 2.1 Summary of some optical materials used in transmission infrared spectroscopy. From Stuart, B., *Modern Infrared Spectroscopy*, ACOL Series, Wiley, Chichester, UK, 1996. © University of Greenwich, and reproduced by permission of the University of Greenwich

Window material	Useful range (cm ⁻¹)	Refractive index	Properties
NaCl	40 000–600	1.5	Soluble in water; slightly soluble in alcohol; low cost; fair resistance to mechanical and thermal shock; easily polished
KBr	43 500–400	1.5	Soluble in water and alcohol; slightly soluble in ether; hygroscopic; good resistance to mechanical and thermal shock
CaF ₂	77 000–900	1.4	Insoluble in water; resists most acids and bases; does not fog; useful for high-pressure work
BaF ₂	66 666–800	1.5	Insoluble in water; soluble in acids and NH ₄ Cl; does not fog; sensitive to thermal and mechanical shock
KCl	33 000–400	1.5	Similar properties to NaCl but less soluble; hygroscopic
CsBr	42 000–250	1.7	Soluble in water and acids; hygroscopic
CsI	42 000–200	1.7	Soluble in water and alcohol; hygroscopic

the vibrational wavenumber. Table 2.2 lists the characteristic bands observed for both H₂O and D₂O. Where water is used as a solvent, NaCl cannot be employed as a infrared window material as it is soluble in water. Small path-lengths (~ 0.010 mm) are available in liquid cells and help reduce the intensities of the very strong infrared modes produced in the water spectrum. The small path-length also produces a small sample cavity, hence allowing samples in milligram quantities to be examined.

SAQ 2.2

What would be an appropriate material for liquid cell windows if an aqueous solution at pH 7 is to be examined?

Liquid films provide a quick method of examining liquid samples. A drop of liquid may be sandwiched between two infrared plates, which are then mounted in a cell holder.

Table 2.2 The major infrared bands of water and deuterium oxide. From Stuart, B., *Biological Applications of Infrared Spectroscopy*, ACOL Series, Wiley, Chichester, UK, 1997. © University of Greenwich, and reproduced by permission of the University of Greenwich

Wavenumber (cm^{-1})	Assignment
3920	O–H stretching
3490	O–H stretching
3280	O–H stretching
1645	H–O–H bending
2900	O–D stretching
2540	O–D stretching
2450	O–D stretching
1215	D–O–D bending

DQ 2.2

The method of liquid films is normally not used for volatile (with a boiling point less than 100°C) liquids. Why would this be necessary?

Answer

A common problem encountered in obtaining good quality spectra from liquid films is sample volatility. When the spectrum of a volatile sample is recorded, it progressively becomes weaker because evaporation takes place during the recording period. Liquids with boiling points below 100°C should be recorded in solution or in a short-pathlength sealed cell.

Before producing an infrared sample in solution, a suitable solvent must be chosen. In selecting a solvent for a sample, the following factors need to be considered: it has to dissolve the compound, it should be as non-polar as possible to minimize solute–solvent interactions, and it should not strongly absorb infrared radiation.

If quantitative analysis of a sample is required, it is necessary to use a cell of known pathlength. A guide to pathlength selection for different solution concentrations is shown in Table 2.3.

2.4.2 Solids

There are three general methods used for examining solid samples in transmission infrared spectroscopy; i.e. alkali halide discs, mulls and films. The choice of method depends very much on the nature of the sample to be examined. The use of alkali halide discs involves mixing a solid sample with a dry alkali halide powder. The mixture is usually ground with an agate mortar and pestle and

Table 2.3 Pathlength selection for solution cells. From Stuart, B., *Modern Infrared Spectroscopy*, ACOL Series, Wiley, Chichester, UK, 1996. © University of Greenwich, and reproduced by permission of the University of Greenwich

Concentration (%)	Pathlength (mm)
>10	0.05
1–10	0.1
0.1–1	0.2
< 0.1	>0.5

subjected to a pressure of about 10 ton in⁻² (1.575×10^5 kg m⁻²) in an evacuated die. This sinters the mixture and produces a clear transparent disc. The most commonly used alkali halide is potassium bromide (KBr), which is completely transparent in the mid-infrared region. Certain factors need to be considered when preparing alkali halide discs. The ratio of the sample to alkali halide is important; surprisingly little sample is needed and around 2 to 3 mg of sample with about 200 mg of halide is sufficient. The disc must not be too thick or too thin; thin discs are fragile and difficult to handle, while thick discs transmit too little radiation. A disc of about 1 cm diameter made from about 200 mg of material usually results in a good thickness of about 1 mm. If the crystal size of the sample is too large, excessive scattering of radiation results, particularly so at high wavenumbers (this is known as the *Christiansen effect*). The crystal size must be reduced, normally by grinding the solid using a mortar and pestle. If the alkali halide is not perfectly dry, bands due to water appear in the spectrum. Contributions due to water are difficult to avoid, and so the alkali halide should be kept desiccated and warm prior to use in order to minimize this effect.

The mull method for solid samples involves grinding the sample and then suspending this (about 50 mg) in one to two drops of a mulling agent. This is followed by further grinding until a smooth paste is obtained. The most commonly used mulling agent is Nujol (liquid paraffin), with its spectrum being shown in Figure 2.10. Although the mull method is quick and easy, there are some experimental factors to consider. The ratio of the sample to mulling agent must be correct. Too little sample, and there will be no sign of the sample in the spectrum. Too much sample and a thick paste will be produced and no radiation will be transmitted. A rough guide to mull preparation is to use a micro-spatula tip of sample to two to three drops of mulling agent. If the crystal size of the sample is too large, this leads to scattering of radiation, which gets worse at the high-wavenumber end of the spectrum. If the mull is not spread over the whole plate area, the beam of radiation

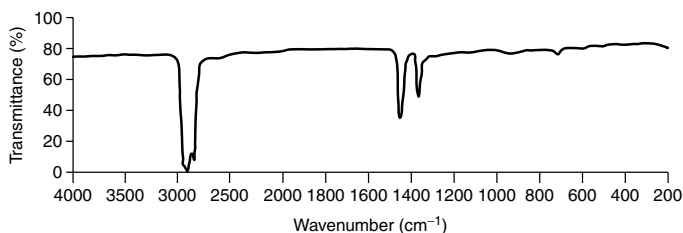


Figure 2.10 Infrared spectrum of Nujol (liquid paraffin). From Stuart, B., *Modern Infrared Spectroscopy*, ACOL Series, Wiley, Chichester, UK, 1996. © University of Greenwich, and reproduced by permission of the University of Greenwich.

passes part through the mull and only part through the plates, hence producing a distorted spectrum. The amount of sample placed between the infrared plates is an important factor; too little leads to a very weak spectrum showing only the strongest absorption bands. Too much mull leads to poor transmission of radiation so that the baseline may be at 50% or less.

It is sometimes possible to reduce the energy of a reference beam to a similar extent by use of an *attenuator*. Beam attenuators are placed in the sample compartment, working somewhat like a venetian blind, and the amount of radiation passing to the detector may be adjusted.

SAQ 2.3

The spectrum of a mull is shown in Figure 2.11. What is the problem with the mull produced and how would one go about remedying the problem?

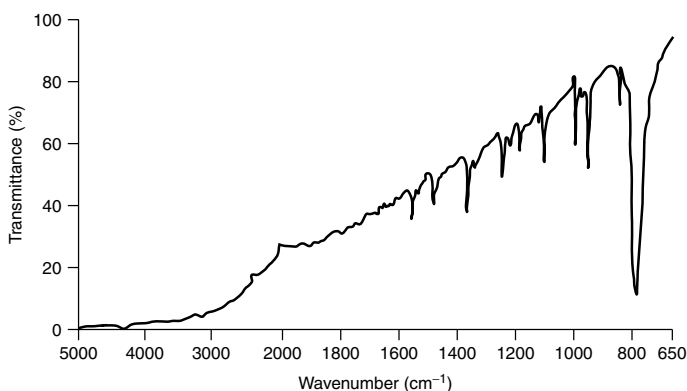


Figure 2.11 Infrared spectrum of a mull (cf. SAQ 2.3). From Stuart, B., *Modern Infrared Spectroscopy*, ACOL Series, Wiley, Chichester, UK, 1996. © University of Greenwich, and reproduced by permission of the University of Greenwich.

Films can be produced by either solvent casting or by melt casting. In solvent casting, the sample is dissolved in an appropriate solvent (the concentration depends on the required film thickness). A solvent needs to be chosen which not only dissolves the sample, but will also produce a uniform film. The solution is poured onto a levelled glass plate (such as a microscope slide) or a metal plate and spread to uniform thickness. The solvent may then be evaporated in an oven and, once dry, the film can be stripped from the plate. However, care must be taken as the heating of samples may cause degradation. Alternatively, it is possible to cast a film straight onto the infrared window to be used. Solid samples which melt at relatively low temperatures without decomposition can be prepared by melt casting. A film is prepared by 'hot-pressing' the sample in a hydraulic press between heated metal plates.

2.4.3 Gases

Gases have densities which are several orders of magnitude less than liquids, and hence pathlengths must be correspondingly greater, usually 10 cm or longer [2]. A typical gas cell is shown in Figure 2.12. The walls are of glass or brass, with the usual choice of windows. The cells can be filled by flushing or from a gas line. To analyse complex mixtures and trace impurities, longer pathlengths are necessary. As the sample compartment size in the instrument is limited, a multi-reflection gas cell is necessary to produce higher pathlengths. In such a cell, the infrared beam is deflected by a series of mirrors which reflect the beam back and forth many times until it exits the cell after having travelled the required

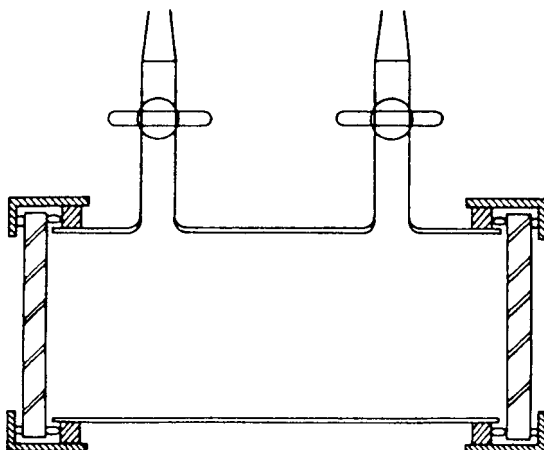


Figure 2.12 Schematic of a typical infrared gas cell. From Stuart, B., *Modern Infrared Spectroscopy*, ACOL Series, Wiley, Chichester, UK, 1996. © University of Greenwich, and reproduced by permission of the University of Greenwich.

equivalent pathlength. This type of cell allows a pathlength of up to 40 m to be attained.

2.4.4 Pathlength Calibration

When using transmission cells it can be useful to know precisely the pathlength of the cell, particularly for quantitative measurements. The cell pathlength can be measured by the method of counting interference fringes. If an empty cell with parallel windows is placed in the spectrometer and a wavelength range scanned, an interference pattern similar to that shown in Figure 2.13 will be obtained. The amplitude of the waveform will vary from 2 to 15%, depending on the state of the windows. The relationship between the pathlength of the cell, L , and the peak-to-peak fringes is given by the following:

$$L = \frac{n}{2(\bar{\nu}_1 - \bar{\nu}_2)} \quad (2.5)$$

where n is the number of complete peak-to-peak fringes between two maxima (or minima) at $\bar{\nu}_1$ and $\bar{\nu}_2$. If the spectrometer is calibrated in wavelengths, the n in Equation (2.5) can be converted to a more convenient form:

$$L = \frac{n(\lambda_1 \times \lambda_2)}{2(\lambda_1 - \lambda_2)} \quad (2.6)$$

where the values of the wavelengths, λ , are expressed in cm.

When a beam of radiation is directed into the face of a cell, most of the radiation will pass straight through (Figure 2.14, beam A). Some of the radiation will undergo a double reflection (beam B) and will, therefore, have travelled an extra distance $2L$ compared to beam A. If this extra distance is equal to a whole number of wavelengths, then beams A and B will be in-phase and the intensity of the transmitted beam (A + B) will be at a maximum. The intensity will be at a minimum when the two component beams are half a wavelength out-of-phase.

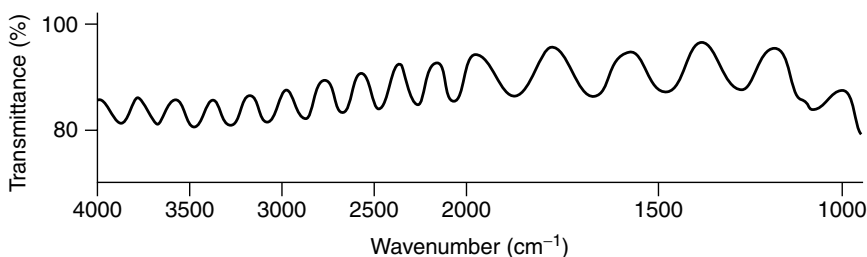


Figure 2.13 Interference pattern recorded with an empty cell in the sample beam. From Stuart, B., *Modern Infrared Spectroscopy*, ACOL Series, Wiley, Chichester, UK, 1996. © University of Greenwich, and reproduced by permission of the University of Greenwich.

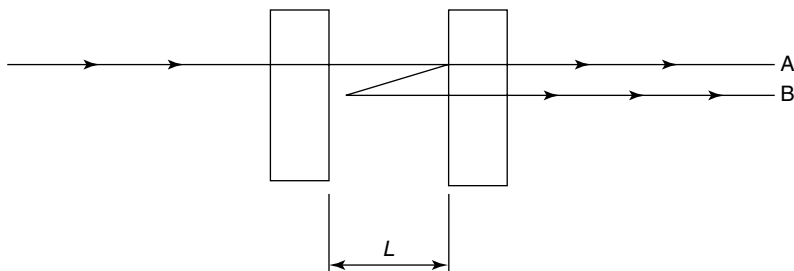


Figure 2.14 Beam of radiation passing through an empty cell.

SAQ 2.4

Using the interference pattern given in Figure 2.13, calculate the pathlength of the cell.

2.5 Reflectance Methods

Reflectance techniques may be used for samples that are difficult to analyse by the conventional transmittance methods. Reflectance methods can be divided into two categories. Internal reflectance measurements can be made by using an attenuated total reflectance cell in contact with the sample. There is also a variety of external reflectance measurements which involve an infrared beam reflected directly from the sample surface.

2.5.1 Attenuated Total Reflectance Spectroscopy

Attenuated total reflectance (ATR) spectroscopy utilizes the phenomenon of *total internal reflection* (Figure 2.15). A beam of radiation entering a crystal will undergo total internal reflection when the angle of incidence at the interface between the sample and crystal is greater than the critical angle, where the latter is a function of the refractive indices of the two surfaces. The beam penetrates a fraction of a wavelength beyond the reflecting surface and when a material that selectively absorbs radiation is in close contact with the reflecting surface, the beam loses energy at the wavelength where the material absorbs. The resultant attenuated radiation is measured and plotted as a function of wavelength by the spectrometer and gives rise to the absorption spectral characteristics of the sample.

The depth of penetration in ATR spectroscopy is a function of the wavelength, λ , the refractive index of the crystal, n_2 , and the angle of incident radiation, θ . The

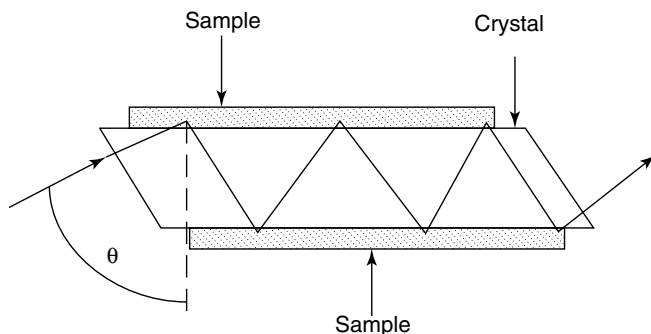


Figure 2.15 Schematic of a typical attenuated total reflectance cell. From Stuart, B., *Modern Infrared Spectroscopy*, ACOL Series, Wiley, Chichester, UK, 1996. © University of Greenwich, and reproduced by permission of the University of Greenwich.

depth of penetration, d_p , for a non-absorbing medium is given by the following:

$$d_p = (\lambda/n_1) / \{2\pi[\sin^2\theta - (n_1/n_2)^2]^{1/2}\} \quad (2.7)$$

where n_1 is the refractive index of the sample.

The crystals used in ATR cells are made from materials that have low solubility in water and are of a very high refractive index. Such materials include zinc selenide (ZnSe), germanium (Ge) and thallium–iodide (KRS-5). The properties of these commonly used materials for ATR crystals are summarized in Table 2.4.

Different designs of ATR cells allow both liquid and solid samples to be examined. It is also possible to set up a flow-through ATR cell by including an inlet and outlet in the apparatus. This allows for the continuous flow of solutions through the cell and permits spectral changes to be monitored with

Table 2.4 Materials used as ATR crystals and their properties. From Stuart, B., *Modern Infrared Spectroscopy*, ACOL Series, Wiley, Chichester, UK, 1996. © University of Greenwich, and reproduced by permission of the University of Greenwich

Window material	Useful range (cm ⁻¹)	Refractive index	Properties
KRS-5 (thallium iodide)	17 000–250	2.4	Soluble in bases; slightly soluble in water; insoluble in acids; soft; highly toxic (handle with gloves)
ZnSe	20 000–500	2.4	Insoluble in water, organic solvents, dilute acids and bases
Ge	5000–550	4.0	Insoluble in water; very brittle

time. Multiple internal reflectance (MIR) and ATR are similar techniques, but MIR produces more intense spectra from multiple reflections. While a prism is usually used in ATR work, MIR uses specially shaped crystals that cause many internal reflections, typically 25 or more.

SAQ 2.5

The spectrum of a polymer film (refractive index, 1.5) was produced by using an ATR cell made of KRS-5 (refractive index, 2.4). If the incident radiation enters the cell crystal at an angle of 60° , what is the depth of penetration into the sample surface at:

- (a) 1000 cm^{-1}
- (b) 1500 cm^{-1}
- (c) 3000 cm^{-1} ?

2.5.2 Specular Reflectance Spectroscopy

In external reflectance, incident radiation is focused onto the sample and two forms of reflectance can occur, i.e. *specular* and *diffuse*. External reflectance measures the radiation reflected from a surface. The material must, therefore, be reflective or be attached to a reflective backing. A particularly appropriate application for this technique is the study of surfaces.

Specular reflectance occurs when the reflected angle of radiation equals the angle of incidence (Figure 2.16). The amount of light reflected depends on the angle of incidence, the refractive index, surface roughness and absorption properties of the sample. For most materials, the reflected energy is only 5–10%, but in regions of strong absorptions, the reflected intensity is greater. The resultant data appear different from normal transmission spectra, as ‘derivative-like’ bands result from the superposition of the normal extinction coefficient spectrum with the refractive index dispersion (based upon Fresnel’s relationships). However, the reflectance spectrum can be corrected by using a *Kramers–Kronig transformation* (K–K transformation). The corrected spectrum then appears like the familiar transmission spectrum.

Increased pathlengths through thin coatings can be achieved by using grazing angles of incidence (up to 85°). Grazing angle sampling accessories allow measurements to be made on samples over a wide range of angles of incidence. Solid samples, particularly coatings on reflective surfaces, are simply placed on a flat surface. The technique is also commonly used for liquid samples that can be poured into a ‘Teflon’ trough. Oriented films on the liquid surface can be investigated by using this method.

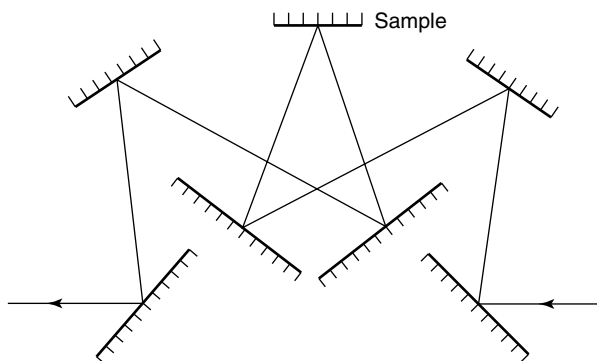


Figure 2.16 Illustration of specular reflectance.

2.5.3 Diffuse Reflectance Spectroscopy

In external reflectance, the energy that penetrates one or more particles is reflected in all directions and this component is called *diffuse reflectance*. In the diffuse reflectance (infrared) technique, commonly called DRIFT, a powdered sample is mixed with KBr powder. The DRIFT cell reflects radiation to the powder and collects the energy reflected back over a large angle. Diffusely scattered light can be collected directly from material in a sampling cup or, alternatively, from material collected by using an abrasive sampling pad. DRIFT is particularly useful for sampling powders or fibres. Figure 2.17 illustrates diffuse reflectance from the surface of a sample.

Kubelka and Munk developed a theory describing the diffuse reflectance process for powdered samples which relates the sample concentration to the scattered radiation intensity. The Kubelka–Munk equation is as follows:

$$(1 - R)^2 / 2R = c/k \quad (2.8)$$

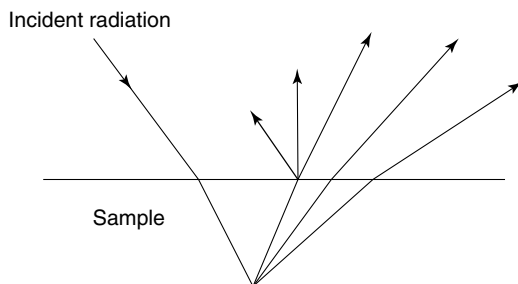


Figure 2.17 Illustration of diffuse reflectance.

where R is the absolute reflectance of the layer, c is the concentration and k is the molar absorption coefficient. An alternative relationship between the concentration and the reflected intensity is now widely used in near-infrared diffuse reflectance spectroscopy, namely:

$$\log (1/R) = k'c \quad (2.9)$$

where k' is a constant.

2.5.4 Photoacoustic Spectroscopy

Photoacoustic spectroscopy (PAS) is a non-invasive reflectance technique with penetration depths in the range from microns down to several molecular monolayers. Gaseous, liquid or solid samples can be measured by using PAS and the technique is particularly useful for highly absorbing samples. The photoacoustic effect occurs when intensity-modulated light is absorbed by the surface of a sample located in an acoustically isolated chamber filled with an inert gas. A spectrum is obtained by measuring the heat generated from the sample due to a re-absorption process. The sample absorbs photons of the modulated radiation,

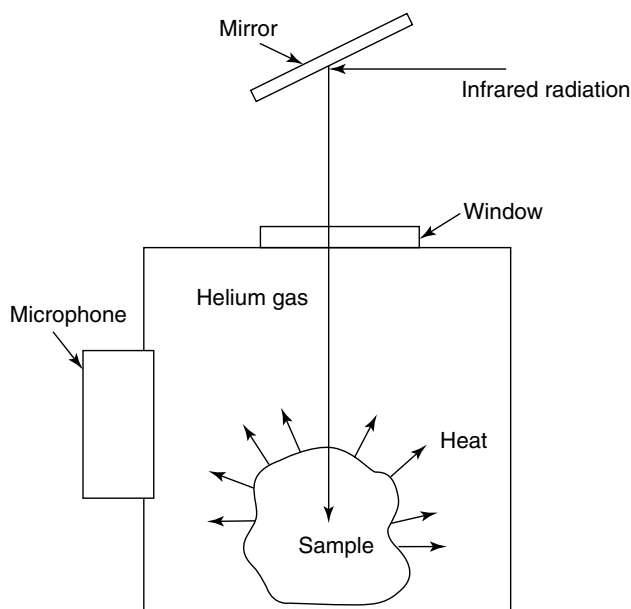


Figure 2.18 Schematic of a typical photoacoustic spectroscopy cell. From Stuart, B., *Modern Infrared Spectroscopy*, ACOL Series, Wiley, Chichester, UK, 1996. © University of Greenwich, and reproduced by permission of the University of Greenwich.

which have energies corresponding to the vibrational states of the molecules. The absorbed energy is released in the form of heat generated by the sample, which causes temperature fluctuations and, subsequently, periodic acoustic waves. A microphone detects the resulting pressure changes, which are then converted to electrical signals. Fourier-transformation of the resulting signal produces a characteristic infrared spectrum. Figure 2.18 shows a schematic diagram of a PAS cell.

2.6 Microsampling Methods

It is possible to combine an infrared spectrometer with a microscope facility in order to study very small samples [3–6]. In recent years, there have been considerable advances in FTIR microscopy, with samples of the order of microns being characterized. In FTIR microscopy, the microscope sits above the FTIR sampling compartment. Figure 2.19 illustrates the layout of a typical infrared microscope assembly. Infrared radiation from the spectrometer is focused onto a sample placed on a standard microscope x – y stage. After passing through the sample, the infrared beam is collected by a Cassegrain objective which produces an image of the sample within the barrel of the microscope. A variable aperture is placed in this image plane. The radiation is then focused on to a small-area mercury cadmium telluride (MCT) detector by another Cassegrain condenser. The microscope also contains glass objectives to allow visual inspection of the sample. In addition, by switching mirrors in the optical train, the microscope can be converted from transmission mode to reflectance mode.

If a microscope facility is not available, there are other special sampling accessories available to allow examination of microgram or microlitre amounts. This is accomplished by using a *beam condenser* so that as much as possible of the beam passes through the sample. Microcells are available with volumes of around $4\ \mu\text{l}$ and pathlengths up to 1 mm. A *diamond anvil cell* (DAC) uses two diamonds to compress a sample to a thickness suitable for measurement and increase the surface area. This technique can be used at normal atmospheric pressures, but it may also be employed to study samples under high pressures and improve the quality of the spectrum of trace samples. Alternatively, a multiple internal reflectance cell may also be used as this technique can produce stronger spectra.

Infrared imaging using FTIR microspectroscopic techniques has emerged as an effective approach for studying complex or heterogeneous specimens [7]. The technique can be used to produce a two- or three-dimensional ‘picture’ of the properties of a sample. This is achievable because, instead of reading the signal of

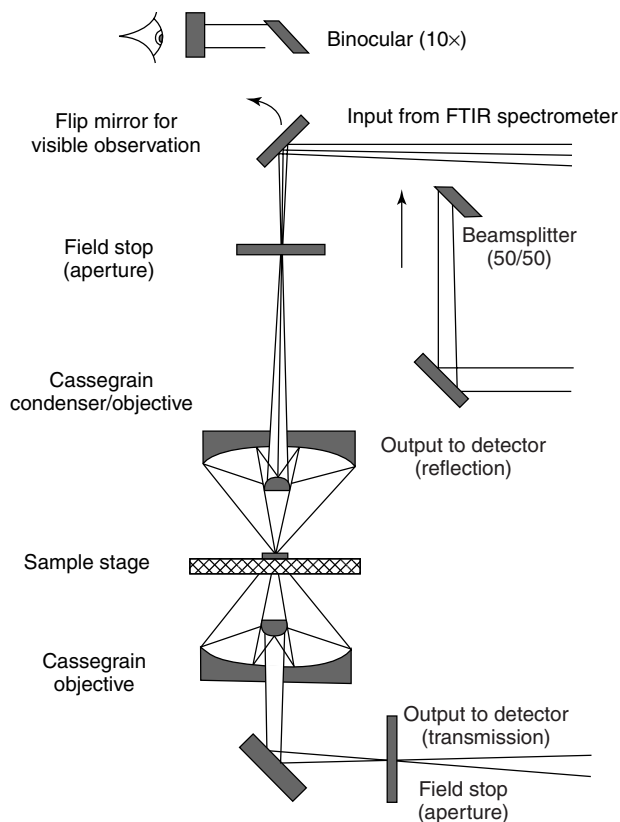


Figure 2.19 Layout of a typical FTIR microspectrometer. Reprinted from Katon, J. E., Sommer, A. J. and Lang, P. L., *Applied Spectroscopy Reviews*, Vol. 25, pp. 173–211 (1989–1990), courtesy of Marcel Dekker, Inc.

only one detector as in conventional FTIR spectroscopy, a large number of detector elements are read during the acquisition of spectra. This is possible due to the development of focal plane array (FPA) detectors. Currently, a step-scanning approach is used which means that the moving mirror does not move continuously during data acquisition, but waits for each detector readout to be completed before moving on to the next position. This allows thousands of interferograms to be collected simultaneously and then transformed into infrared spectra.

Figure 2.20 illustrates the general layout of an FTIR imaging microspectrometer. The infrared beam from a Michelson interferometer is focused onto a sample with a reflective Cassegrain condenser. The light transmitted is collected by a Cassegrain objective and then focused onto an FPA detector. The imaging process

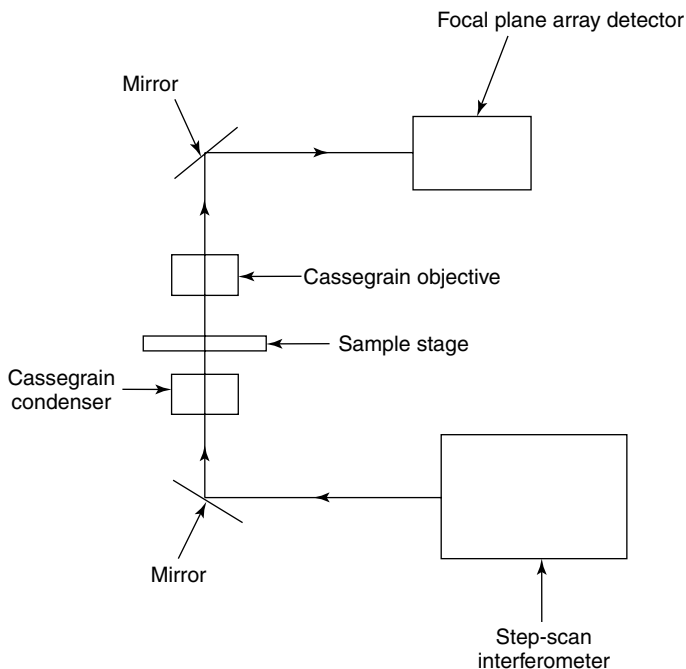


Figure 2.20 Layout of a typical FTIR imaging microspectrometer.

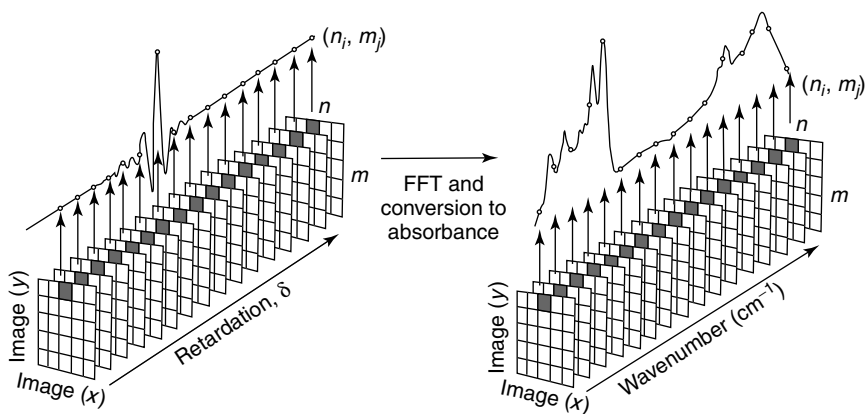


Figure 2.21 FTIR imaging data set. From Kidder, L. H., Levin, I. W. and Lewis, E. N., 'Infrared Spectroscopic Imaging Microscopy: Applications to Biological Systems', in *Proceedings of the 11th International Fourier Transform Spectroscopy Conference*, Athens, GA, USA, August 10–15, 1997, de Haseth, J. A. (Ed.), Figure 1, p. 148, American Institute of Physics, Melville, New York, 1998, pp. 148–158. Reproduced by permission of American Institute of Physics.

is illustrated in Figure 2.21. The data are collected as interferograms with each pixel on the array having a response determined by its corresponding location on the sample. Each point of the interferogram represents a particular moving mirror position and the spectral data are obtained by performing a Fourier-transform for each pixel on the array. Thus, each pixel (or spatial location) is represented by an infrared spectrum.

2.7 Chromatography–Infrared Spectroscopy

Infrared spectroscopy may be combined with each of a number of possible chromatographic techniques, with gas chromatography–infrared spectroscopy (GC–IR) being the most widely used [8, 9]. GC–IR allows for the identification of the components eluting from a gas chromatograph. In GC, the sample in a gaseous mobile phase is passed through a column containing a liquid or solid stationary phase. The retention of the sample depends on the degree of interaction with the stationary phase and its volatility: the higher the affinity of the sample for the stationary phase, then the more the sample partitions into that phase and the longer it takes before it passes through the chromatograph. The sample is introduced into the column, housed in an oven, via injection at one end and a detector monitors the effluent at the other end. A common method for coupling a gas chromatograph to an FTIR spectrometer is to use a light pipe, i.e. a heated flow cell which allows the continuous scanning of the effluent emerging from the GC column. Figure 2.22 shows a schematic diagram of a typical GC–IR system.

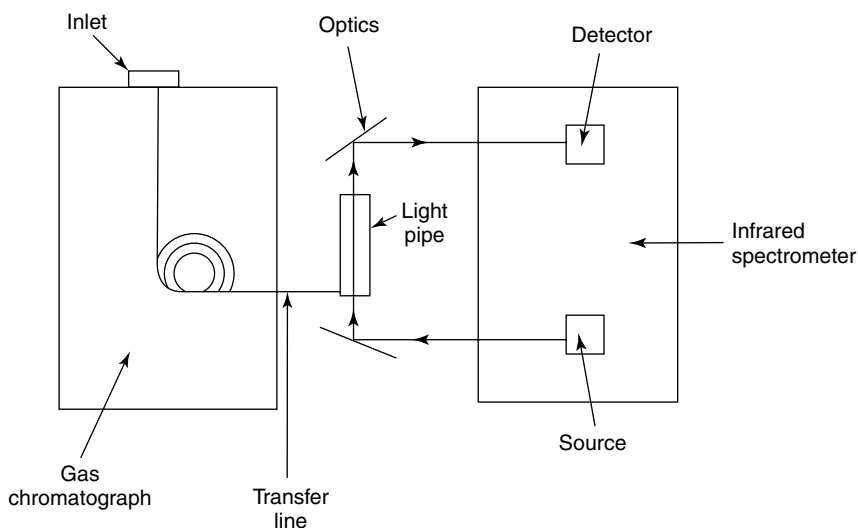


Figure 2.22 Layout of a typical GC–IR system.

The nature of this technique requires that interferograms are collected over short time intervals. Data can be displayed in real time and are commonly monitored as the changing spectrum of the GC effluent and the changing infrared absorption as a function of time. The latter is known as a *Gram–Schmidt chromatogram*.

Liquid chromatography (LC) may also be used in conjunction with infrared spectroscopy [10]. In this technique, the effluent from a liquid chromatograph is passed through a liquid flow-through cell. Supercritical fluid chromatography (SFC), where supercritical CO₂ is commonly used as a mobile phase, can be used with FTIR spectroscopy to improve detection limits.

2.8 Thermal Analysis–Infrared Spectroscopy

Infrared spectrometers may also be combined with thermal analysis instrumentation. Thermal analysis methods provide information about the temperature-dependent physical properties of materials. However, it is not always possible to gain information about the chemical changes associated with changes in temperature by using standard thermal analysis equipment. It is possible to combine thermal analysis apparatus with an infrared spectrometer in order to obtain a complete picture of the chemical and physical changes occurring in various thermal processes [11, 12].

The most common approach is to combine FTIR spectroscopy with a thermal method such as thermogravimetric analysis (TGA) to obtain an evolved gas analysis (EGA). The latter involves the measurement and characterization of the

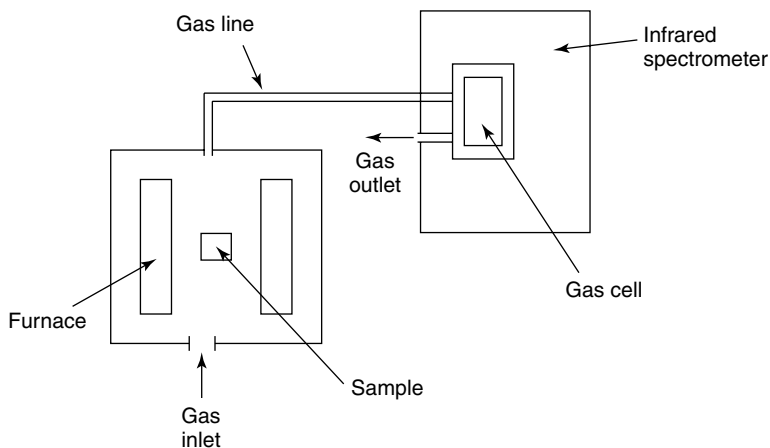


Figure 2.23 Layout of a typical thermal analysis–infrared spectroscopy system.

gaseous products which evolve from a sample when it is heated. Figure 2.23 presents a schematic layout of a typical thermal analysis–infrared spectroscopy system. In this, a sample is placed in a furnace while being suspended from a sensitive balance. The change in sample mass is recorded while the sample is maintained either at a required temperature or while being subjected to a programmed heating sequence. A TGA curve may be plotted as sample mass loss as a function of temperature or in a differential form where the change in sample mass with time is plotted as a function of temperature. The evolved gases can be carried from the furnace to the spectrometer where they can be examined in a long-pathlength gas cell. Data may be illustrated as a function of time by using a Gram–Schmidt plot.

2.9 Other Techniques

Variable-temperature cells, which are controlled to 0.1°C in the range -180 to 250°C , may be used in infrared spectrometers. An electrical heating system is used for temperatures above ambient, and liquid nitrogen with a heater for low temperatures. These cells can be used to study phase transitions and the kinetics of reactions. As well as transmission temperature cells, variable-temperature ATR cells and temperature cells for microsampling are available.

Infrared emission spectroscopy may be carried out by using a heated sample located in the emission port of the FTIR spectrometer as the radiation source.

Optical fibres may be used in conjunction with infrared spectrometers to carry out remote measurements. The fibres transfer the signal to and from a sensing probe and are made of materials that are flexible and ‘infrared-transparent’.

For some samples, dipole moment changes may be in a fixed direction during a molecular vibration and, as such, can only be induced when the infrared radiation is polarized in that direction. Polarized infrared radiation can be produced by using a polarizer consisting of a fine grating of parallel metal wires. This approach is known as *linear infrared dichroism* [13].

SAQ 2.6

Which sampling technique would be the most appropriate in each of the cases listed below?

- (a) A 1 g sample of white powder.
- (b) A $10\ \mu\text{g}$ sample of animal tissue.
- (c) A powder containing a mixture of amphetamines.

Summary

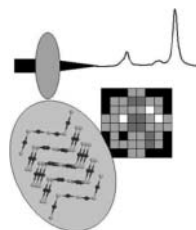
Various aspects of the instrumentation used in infrared spectroscopy were dealt with in this chapter. Traditional dispersive spectrometers were described. The operation and capabilities of Fourier-transform infrared spectrometers were also discussed. Transmission methods for obtaining infrared spectra were also examined. The sampling methods which can be used for solids, solutions, liquids and gases were presented. The different reflectance methods that are now widely available, such as ATR spectroscopy, specular reflectance and diffuse reflectance, along with photoacoustic spectroscopy, were also introduced. The various microsampling techniques, which have emerged as effective methods for investigating small quantities of complex samples, were also described. Infrared spectrometers can also be used in conjunction with other analytical methods such as chromatography and thermal techniques and these were introduced in this chapter.

References

1. Griffiths, P. R. and de Haseth, J. A., *Fourier Transform Infrared Spectrometry*, Wiley, New York, 1986.
2. Günzler, H. and Gremlich, H.-U., *IR Spectroscopy: An Introduction*, Wiley-VCH, Weinheim, Germany, 2002.
3. Sommer, A. J., 'Mid-infrared Transmission Microspectroscopy', in *Handbook of Vibrational Spectroscopy*, Vol. 2, Chalmers, J. M. and Griffiths, P. R. (Eds), Wiley, Chichester, UK, 2002, pp. 1369–1385.
4. Katon, J. E., *Micron*, **27**, 303–314 (1996).
5. Humecki, H. J. (Ed.), *Practical Guide to Infrared Microspectroscopy*, Marcel Dekker, New York, 1999.
6. Messerschmidt, R. G. and Harthcock, M. A. (Eds), *Infrared Microspectroscopy: Theory and Applications*, Marcel Dekker, New York, 1998.
7. Kidder, L. H., Haka, A. S. and Lewis, E. N., 'Instrumentation for FT-IR Imaging', in *Handbook of Vibrational Spectroscopy*, Vol. 2, Chalmers, J. M. and Griffiths, P. R. (Eds), Wiley, Chichester, UK, 2002, pp. 1386–1404.
8. Visser, T., 'Gas Chromatography/Fourier Transform Infrared Spectroscopy', in *Handbook of Vibrational Spectroscopy*, Vol. 2, Chalmers, J. M. and Griffiths, P. R. (Eds), Wiley, Chichester, UK, 2002, pp. 1605–1626.
9. Ragunathan, N., Krock, K. A., Klawun, C., Sasaki, T. A. and Wilkins, C. L., *J. Chromatogr., A*, **856**, 349–397 (1999).
10. Somsen, G. W., Gooijer, C., Velthorst, N. H. and Brinkman, U. A. T., *J. Chromatogr., A*, **811**, 1–34 (1998).
11. Hellgeth, J. W., 'Thermal Analysis–IR Methods', in *Handbook of Vibrational Spectroscopy*, Vol. 2, Chalmers, J. M. and Griffiths, P. R. (Eds), Wiley, Chichester, UK, 2002, pp. 1699–1714.
12. Haines, P. J. (Ed.), *Principles of Thermal Analysis and Calorimetry*, The Royal Society of Chemistry, Cambridge, UK, 2002.
13. Buffeteau, T. and Pezolet, M., 'Linear Dichroism in Infrared Spectroscopy', in *Handbook of Vibrational Spectroscopy*, Vol. 1, Chalmers, J. M. and Griffiths, P. R. (Eds), Wiley, Chichester, UK, 2002, pp. 693–710.

Chapter 4

Raman Instrumentation



Learning Objectives

- To know the main components of Raman instrumentation
- To appreciate the working principle of a laser
- To know the working principle of a CCD-detector
- To be able to name the different types of filters in Raman spectroscopy
- To understand the working principles of the dispersion systems in dispersive and Fourier-transform (FT-) Raman spectrometers
- To explain the working principle of a fibre-optics probehead and the meaning of its filters
- To understand the origin of noise in Raman spectra

In this part, a summary is given of the most important components of the Raman spectrometer. Although many kinds of Raman spectrometers exist, each with their own advantages and disadvantages, a general diagram can be presented (Figure 4.1).

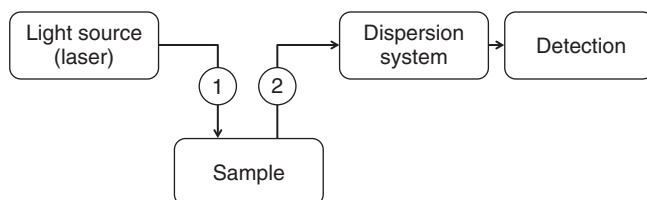


Figure 4.1 General diagram of a (Raman) spectrometer. 1 optics to focus the laser beam on the sample; 2 collection optics for the scattered radiation.

Of course, this diagram is too general to start a detailed study of the different aspects of Raman spectrometers. Components have to be selected according to the tasks and options that are chosen. For example, if a back-scattering geometry is selected, the optics used to focus the laser beam on the sample will be the same as the optics used to transfer the Raman back-scattered light to the spectrometer, where dispersion and detection happen. There are two important types of spectrometers on the market (Figure 4.2), that is, the dispersive spectrometers which use a grating for the separation of the light in its components, and Fourier-transform (FT-) Raman spectrometers, which use a Michelson interferometer. This will be discussed in more detail further in this chapter.

But first, we will discuss the different components of a Raman spectrometer in more detail.

4.1 Lasers

A laser (light amplification through stimulated emission of radiation) is an intense source of monochromatic light which can be used for Raman spectroscopy. There are some important characteristics of a laser which make it extremely suitable for this purpose:

- Lasers are intense
- Lasers are monochromatic
- Lasers have a small divergence
- Lasers are polarised
- Lasers are coherent light sources

In addition, to be suitable for Raman spectroscopy, lasers have to show a high intensity and frequency stability.

In the following paragraphs we will study the different characteristics of lasers and their working principle. But first, we will discuss different ways to classify them.

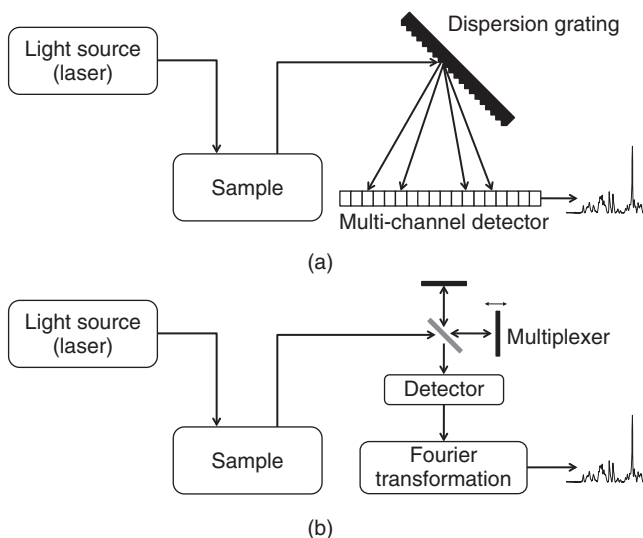


Figure 4.2 General diagram of a dispersive Raman spectrometer (a) and a Fourier-transform (FT-) Raman spectrometer (b).

4.1.1 Classification According to Safety Category

Lasers produce an intense, monochromatic light beam and when they hit a material, they can interact in different ways (see Chapter 2). Thermal, photochemical and mechanical effects (e.g. ablation) can be harmful for the human health, especially for the eyes and skin.

The possible eye damage, besides the intensity, also depends on the laser wavelength. Infrared radiation is mainly absorbed by the moisture which is found on the eye lens, while the UV light is absorbed by the lens itself. Therefore these lasers will mainly damage these parts of the eye. Visible light is focused by our eye lens on our retina. The eye is particularly sensitive in this visible range of the electromagnetic spectrum as this type of laser beam is focused in the eye, and therefore an amplification of 100 000 times occurs. As a result of this a visible laser light will damage the retina. Most of the time the victim will not immediately notice the damage; pain and limited vision will manifest itself after some time. It can take several months before the original vision is restored (almost completely). The focus effects do not apply to the skin; therefore the damage to the skin is usually limited. For certain lasers, however, burning may occur which can result in a pigmented spot.

Depending on the effects on health, lasers can be classified into different categories:

- *Category 1 lasers:* are considered safe.
- *Category 2 lasers:* visible lasers, with limited intensity. Briefly looking into the laser beam for less than 0.25 s is not considered harmful. However, intentionally looking into the laser beam is.
- *Category 3 lasers:* can emit any wavelength, its diffuse reflection on a surface does not cause any harm, except after looking for a long time from a short distance. No increased risk for burning or harm to the skin is expected.

Any *continuous wave* laser (see below) with a capacity lower than 0.5 W is category 3 laser or lower. It is harmful to look into a category 3 laser, and laser precautions need to be taken to make this impossible.

- *Category 4 lasers*: a category 4 laser has a higher power than category 3 lasers. These lasers can cause skin and eye damage, even after diffuse reflection.

Working in a laser laboratory requires a few safety measures. It is good practice to limit free running laser beams and to block them with nonreflecting screens. During outlining of optics it is necessary to wear safety goggles. These are equipped with specific filters, which block the light of this specific wavelength and are transparent for other wavelengths. Special attention should go to reflecting surfaces, when brought in the laser beam. A typical hazard is created when the laser beam hits components of the optical bank (e.g. holders of lenses or mirrors, the back of a mirror, . . .) whereby the reflecting beam is sent uncontrolled through the room. It is obligatory to have a responsible person for laser safety, from laser category 3b or higher. In addition, regular safety drills need to be organised.

4.1.2 The Operating Principle of the Laser

Lasers are very intense, monochromatic light sources. Various types of lasers are available on the market, and depending on their specific optical characteristics, the desired power and wavelength, one or other type is selected.

The laser's performance is based on the amplification of the signal through stimulated emission. The result of the stimulated emission is that all atoms¹ in the laser together emit electromagnetic

¹Note that here we use the word 'atom', where this could be another type of particle. Dependent on the type of laser these particles can be atoms, molecules, ions, etc.

radiation whereby an intense, coherent laser beam is formed. When an atom is found in an electronically excited state, and when it is irradiated with photons of which the energy equals the difference in energy between the ground state and the excited state, this atom will emit two photons with the same energy. Because of this stimulation, both photons have the same frequency (they have the same energy) and are in phase (they are coherent). Therefore, the total intensity of the emitted wave is intense as no interference between the two emitted photons happens. To maximise this effect it is useful to have many atoms/molecules in the excited state. For this reason in lasers a system of population inversion is created. Indeed, if you use a system of spontaneous emission of radiation, you could theoretically expect that the emitted photon provokes a cascade of stimulated emission. In equilibrium conditions, this does not happen, because the odds are very low that the first emitted photon hits a photon in an excited state. Therefore, population inversion is required.

Usually a lower energy level is more occupied than a higher situated level (cf. Boltzmann Distribution). A system with population inversion can be formed in two ways: either by increasing the number of atoms in the excited state, or by decreasing the number of atoms in ground state. According to the Boltzmann Distribution, the addition of thermal energy to the system will increase the average energy of the system, but will not cause a population inversion; one works under thermodynamic equilibrium conditions. The population inversion can be realised by pumping light or electrical energy to the system.

A very common approach is for the atom to be excited to a higher situated energy level, after which it drops down to the energy level of the laser. Intrinsically the population inversion is a kinetic effect, whereby the excitation to the highest level and the decay to the laser level are intrinsically quick processes (Figure 4.3). The highest laser level is a metastable condition whereby the population is highly populated at this energy level and a population inversion

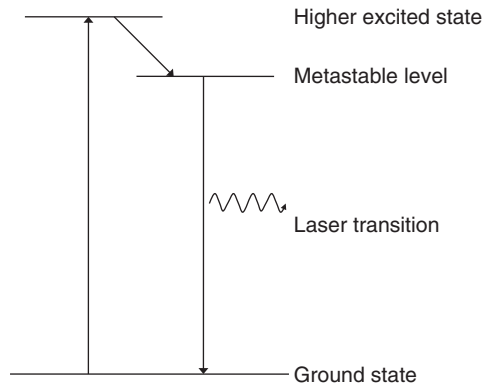


Figure 4.3 3-level energy diagram for laser excitation.

occurs. Typically, the retention time in this metastable condition is 1000 times longer than in the short-lived excited condition. Indirect excitation can be used to excite atoms in an environmental gas mixture, which afterwards transfer their energy to the molecules which cause the laser light.

In practice 4-level laser excitation is often used (Figure 4.4). In this case the population inversion is realised between the metastable level and an excited condition. Thanks to the Boltzmann distribution the lowest laser level is less populated than the ground state, whereby the population inversion occurs more easily. Furthermore the atoms will fall back from the lowest laser level to the ground state, which enables continuous operation.

Apart from the population inversion, there should also be a cavity to amplify the light in that way. Light which was produced by stimulated emission in a laser medium usually has one single wavelength, but needs to be taken out of the medium by an amplifying mechanism. This is done by the resonance cavity which reflects the light back in the laser and amplifies the light intensity by various interactions (Figure 4.5). In this way, after stimulated emission, two

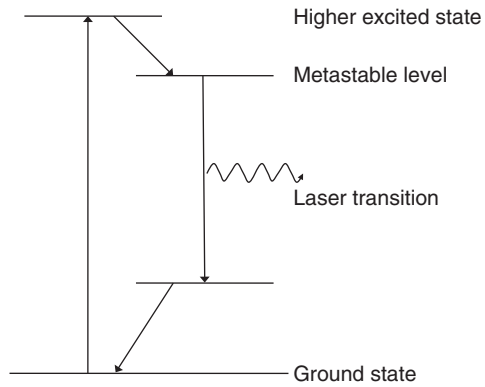


Figure 4.4 4-level energy diagram for laser excitation.

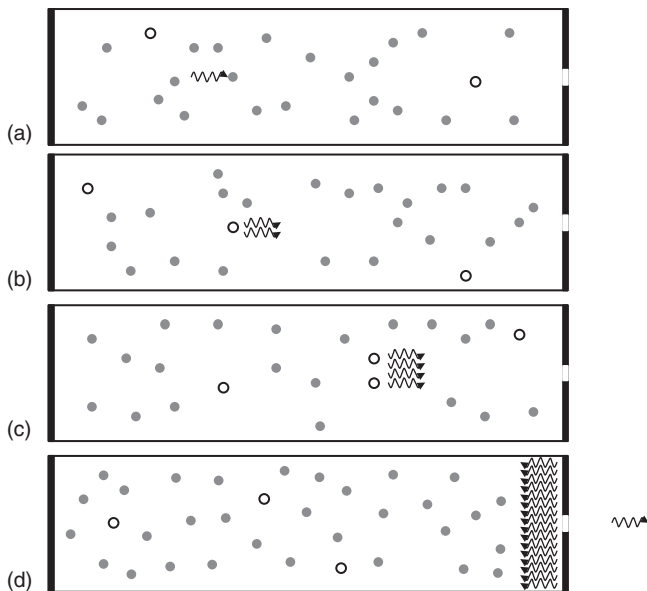


Figure 4.5 Working principle of a laser: stimulated emission in a cavity.

photons are formed with the same frequency, which in turn can de-excite other excited atoms and therefore generate new photons, each with the same energy and phase angle. The number of photons that are generated are proportional to the path length of the light in the laser medium.

INTERMEZZO 4.1 THE HELIUM-NEON LASER

The Helium-Neon laser, is one of the most important gas lasers. Its working principle can be understood by looking at the energy diagram in Figure Intermezzo 4.1).

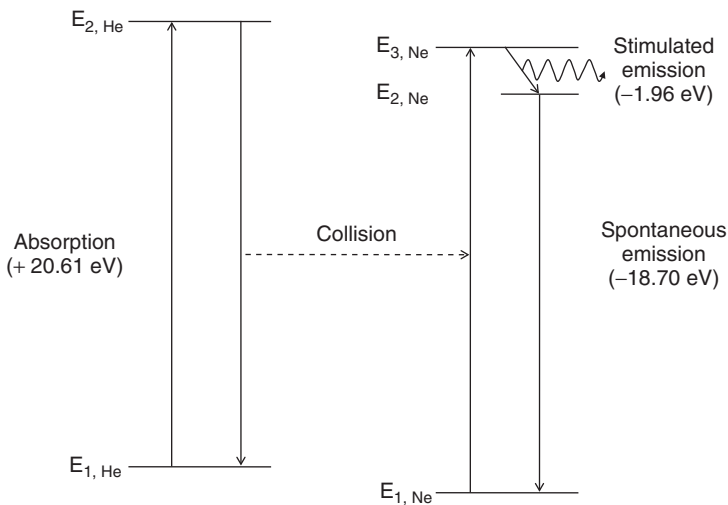


Figure Intermezzo 4.1 The Helium-Neon laser.

By electrical discharge, Helium atoms can be brought to the excited energy level $E_{2, He}$, which is 20.61 eV above the ground state $E_{1, He}$. Neon atoms can be excited from their ground state ($E_{1, Ne}$) to the $E_{3, Ne}$ excited state by collision with the excited He

atoms, as the energy that is required for this excitation almost equals the energy difference between the $E_{2,He}$ and $E_{1,He}$ states. The small excess of energy that is required can be gained from the kinetic (translation) energy of the atoms. One can state that Helium 'pumps' Ne atoms towards the $E_{3,Ne}$ state. Another excited state of Neon, $E_{2,Ne}$, is located in between the $E_{1,Ne}$ and $E_{1,Ne}$ states. As this $E_{2,Ne}$ state normally is unoccupied, population inversion between the $E_{2,Ne}$ and $E_{3,Ne}$ states is easily reached. Stimulated emission between these two states results in red photons of 1.96 eV (632.8 nm). Atoms in the $E_{2,Ne}$ state decay towards the ground state by spontaneous emission.

In gas lasers, such as the HeNe laser, the light is reflected on both ends of a tube filled with the gas, while in solid state lasers, this happens in a solid bar. The waves oscillate back and forth between the ends of the cavity, which is why a laser is sometimes referred to as an oscillator (Figure 4.5). Because of this resonance, increase or extinguishment (interference) occurs according to the length of the cavity in function of the laser wavelength. Because all photons are coherent, the phase difference is constant, after reflection on a mirror. For positive interference twice the cavity length needs to equal a multiple of the laser wavelength. In practice, the laser wavelength is much smaller than the cavity. In addition, a certain band tailing occurs in the laser itself, whereby various wavelengths near to each other are emitted. This is called gain bandwidth. In practice there are different cavity modes (longitudinal modes) which fit in the gain bandwidth. The intensity distribution over the laser beam is defined by the design of the cavity.

From the mechanisms, as shown in Figures 4.3 and 4.4, it is clear that a certain stimulus is needed to excite the atoms: the atoms need to be pumped towards a higher energy level. In most cases several of these excited states are considered, and polychromatic light can be used. In these cases a discharge lamp or a flash light is used.

This process is called optical pumping of a laser. Of course the pumping photons must have a shorter wavelength (higher energy) than the laser light. Sometimes, a primary laser (pump laser) is used to excite the atoms in a second laser.

A second mechanism which is often used is electrical pumping, for example in a gas laser or in a diode laser. In a gas laser an electric current is sent through the gas, whereby the molecules are sent to a higher energy state, to start the decay process in that way. With some gas lasers a continuous current is sent through the gas, whereby a continuous laser output is formed. With other gas lasers short electric pulses are sent, whereby a pulsed output is formed.

Semi-conductors lasers (Figure 4.6) work differently, but also use electrons to generate the population inversion. In these cases the inversion is produced between the current carriers (electrons and electron-hole pairs) in the junctions between the various regions in the semi-conductor. The diode consists basically of a p-junction and an n-junction, with the active layer in between. Electrical leads are connected to both junctions, and the diode is positioned in a heat sink, to remove the generated heat. The light emission in the semi-conductor is concentrated in the active layer and both sides of the semi-conductor crystal act as mirrors for the cavity. The semi-conductor chip and the heat sink are mounted in a protective casing and the light, under the form of an elliptical beam, can escape through a window. The semi-conductor chip reflects sufficient light in the crystal to form an efficient stimulation. The semi-conductor crystal is usually polished, to improve efficiency. The main advantage of diode lasers is that a lower electrical current (and voltage) is needed compared to gas lasers.

4.1.3 Lasers for Raman Spectroscopy

In general, the Raman spectrometers which use lasers with a wavelength shorter than 750 nm are dispersive Raman instruments,

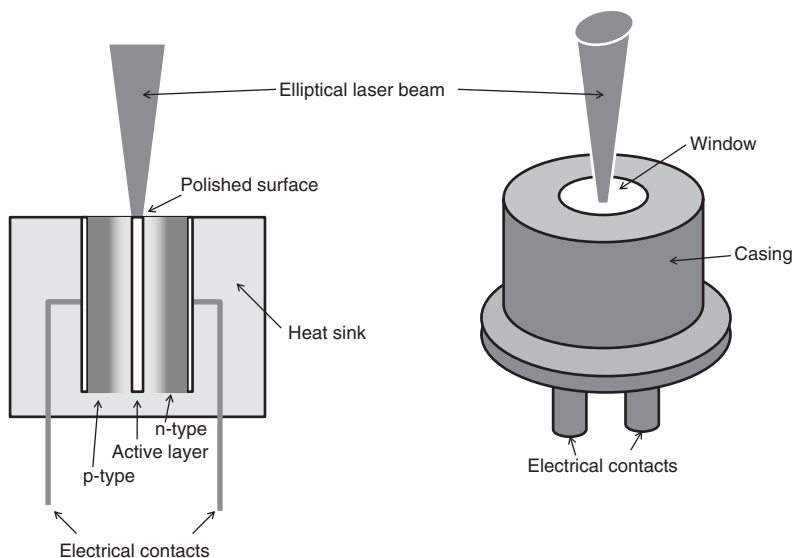


Figure 4.6 Diode laser.

while Fourier-transform (FT) spectrometers are used for longer wavelengths. The reason for this lies with the signal/noise ratio of the used detectors and the sensitivity of the different detectors in specific spectral ranges. In practice, Raman spectroscopy lasers are used, with wavelengths in the UV area (<200 nm) until in the near infrared (1064 nm). A summary of some frequently used laser wavelengths is given in Table 4.1.

QUESTION 4.1

Calculate the wavelength for a (Stokes) Raman band at 3000 cm^{-1} , as detected by using a Nd:YAG laser as well as for a HeNe laser.

Table 4.1 Commonly used lasers for Raman spectroscopy.

Laser type	Frequently used laser wavelengths in Raman spectroscopy (nm)
HeNe laser	632.8
Kr ⁺ laser	413.1, 647.1
Ar ⁺ laser	488.0, 514.5
Diode laser	660–880
Nd:YAG laser	1064
Frequency doubled Nd:YAG laser	532

This summary only discusses continuous wave lasers; there are, however, as well applications of pulsed lasers for Raman spectroscopy. Through their extremely high power density serious safety measures are needed, and the sample may be damaged.

For Raman spectroscopic applications a few conditions need to be complied with:

- Frequency stability: we do not want the laser wavelength to change significantly between two measurements.
- Narrow bandwidth: for most applications a narrow laser line (monochromatic) is required, typically smaller than 1 cm^{-1} , although for some routine-analyses this is not necessary. The bandwidth of the laser line also affects the resolution of the established spectrum.
- Few sidebands (use of band pass filters) gas lasers emit atomic emission lines of the present gases, while solid state lasers can emit luminescence radiation. This radiation can interfere with the sample and cause fluorescence among others.
- Low divergence: especially when no optical fibres are used, this is an important criterion.

- Good definition of the profile of the laser: this is necessary if the spot size on the sample needs to be well defined (cf. confocality, see later).

QUESTION 4.2

When a laserline with a width of 1 cm^{-1} (Raman shift) is required, what is the corresponding width expressed in nm for a 785 nm diode laser? And for a 632.8 nm HeNe laser? And for a 413.1 nm Kr^+ laser?

4.2 Detectors

For Raman spectroscopy, different types of detectors are used. For dispersive instruments we distinguish single-channel detectors and multi-channel detectors, while for Fourier-transform instruments semi-conductor detectors are used (mostly Si, InGaAs or Ge). Different types of detectors are discussed successively.

Taking into account the very weak Raman signals, it is necessary to dispose of sensitive detectors. It is not only important to have a high quantum efficiency (the number of electrons generated per photon), but we also want to have a dark signal as low as possible. This dark signal is formed by spontaneous (thermal) generation of electron–hole pairs in the semi-conductor detector, and involves the introduction of noise (see next chapter). Therefore, these detectors are cooled. As a rule, the longer the wavelength, the less energetic are the photons. Therefore electron–hole pairs are formed less easily and the sensitivity in the infrared region of the electromagnetic spectrum decreases. Detectors that are still sensitive in the near IR only need little energy to create an electron–hole pair and as a consequence a small amount of thermal energy is sufficient

to form an electron–hole pair; therefore, the detector needs to be cooled more and the contribution of the detector background increases.

In regards to detectors a few terms are important:

- Quantum efficiency (quantum yield, detector sensitivity): the number of photo electrons generated per photon that reaches the detector.
- Response curve (quantum efficiency curve): graph which shows the quantum efficiency in function of the wavelength (Raman wavenumber).
- Number of channels: for a multi-channel detector, this is the number of signals/wavelengths that can be measured independently from each other. For the often used charge-coupled device (CCD) detectors this is the number of pixels along the wavenumber axis.
- Dark signal (detector background): the average number of electrons generated in the detector, if the detector is not exposed to light.
- Dark noise and readout noise: noise generated because of the dark signal and by the quantisation by digitalisation respectively. (See next chapter.)

4.2.1 Single-Channel Detectors

Historically, photon multiplier tubes were first used in Raman spectroscopy in the 1960s. The advantage of this approach is their relatively high sensitivity compared to the earlier measurement geometries. The disadvantage of these tubes is their rather high background signal (typically $10\text{ e}^-/\text{s}$) and their sensitivity to permanent damage: if the detectors are exposed to extremely high

light intensities (e.g. laser beam or lights in the room), this could result in permanent damage. Moreover, this approach has the disadvantage that you can only measure at a single wavelength and that the analysis of a complete spectrum needs to be done sequentially, which is time-consuming.

4.2.2 Multi-Channel Detectors

In practice people want to record multiple wavelengths simultaneously. Therefore, usually a multi-channel detector is used. A multi-channel detector is basically a linear array of single-channel detectors. A particular part of the spectrum is projected along the linear axis of the detector, and thus, each channel of the detector corresponds with a different wavelength (or wavenumber). Calibration of this type of spectrometer consists then of assigning a wavenumber to each element of the detector. Linear detectors are often used in small, handheld Raman instruments.

4.2.3 Charge-Coupled Device (CCD) Detectors

Linear detectors often suffer a relatively bad signal to noise ratio. Therefore, in dispersive Raman instruments, another type of multi-channel detector is often used, which consists of a 2-dimensional array of light-sensitive elements: a charge-coupled device (CCD) detector. Usually, the spectrum is projected along one of the dimensions of the CCD, and pixels of the other direction are combined – a method which is named binning. However, some Raman instruments use the full 2-dimensional properties of a CCD, to incorporate spatial information in the analysis (see Chapter 5, Section 5.7 on imaging).

CCD chips usually consist of silica, where photons create electron/hole pairs. In Figure 4.7 a typical response curve for a

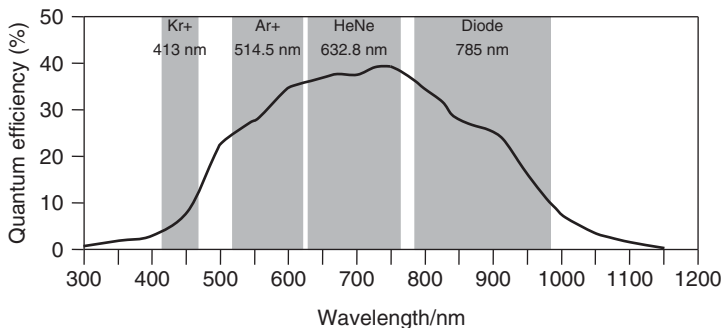


Figure 4.7 Typical response curve of a CCD, with a typical range of a Raman spectrum ($0\text{--}3000\text{ cm}^{-1}$) for different lasers.

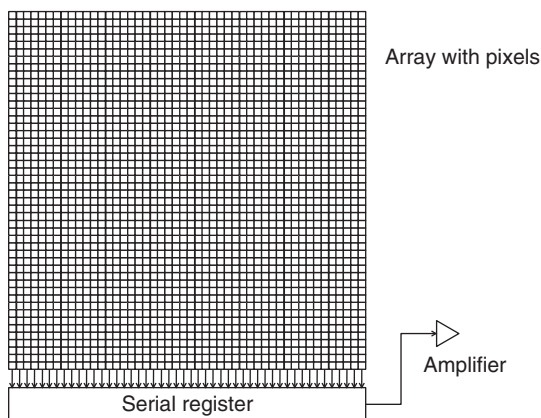


Figure 4.8 Illustration of the design of a CCD-detector.

CCD is shown, with the wavenumber ranges ($0\text{ to }3000\text{ cm}^{-1}$) in relation to various laser wavelengths.

On the chip an electric circuit is printed, consisting of a 2-dimensional matrix of contact points (Figure 4.8), which are kept

at a positive potential. Each contact point corresponds with a small area, which is sensitive to photons. These areas can each contain between 10^4 and 10^6 electrons, before they are saturated (full well capacity). The potential drain therefore functions as an integrator which during a period of time accumulates the electrons which are generated by the photons. Because these potential drains are placed in a two-dimensional array, each column corresponds with a specific wavelength. Often the pixels per column are therefore added up (binning), whereby super pixels are formed. Binning is the combination (before (hardware binning) or after (software binning) readout) of various pixels. During read-out, the charges which are stored in the potential drains are converted to digital entities, whereby the gain (sensitivity) of the detector is the proportionality factor between the digital signal and the number of photoelectrons.

We can distinguish between a front-illuminated and a back-illuminated CCD. The front of a CCD is considered as the side where the electrical circuit is printed. A front-illuminated CCD is illuminated from this side. The electric circuit covers approximately half the area and is not photon-sensitive, therefore the maximum quantum efficiency is ca. 50%. Normally the back of a regular front-illuminated CCD can be partially etched (back-thinned), whereby the thickness is only ca. $15\ \mu\text{m}$. Thus, the electrons which are formed by the irradiation of the back can migrate through the chip to the potential drains at the front of the detector. Because the electric circuit does not cover the CCD now, the quantum efficiency is much higher than with a front-illuminated CCD (typically up to 80–95%). Furthermore, the detector is more sensitive in the UV area, compared with a front-illuminated CCD. This is because, with the making of the electric circuits, people use UV-absorbing coatings (at the circuit side). Back-illuminated CCDs are often covered with an anti-reflective coating. Some typical response curves are shown in Figure 4.9.

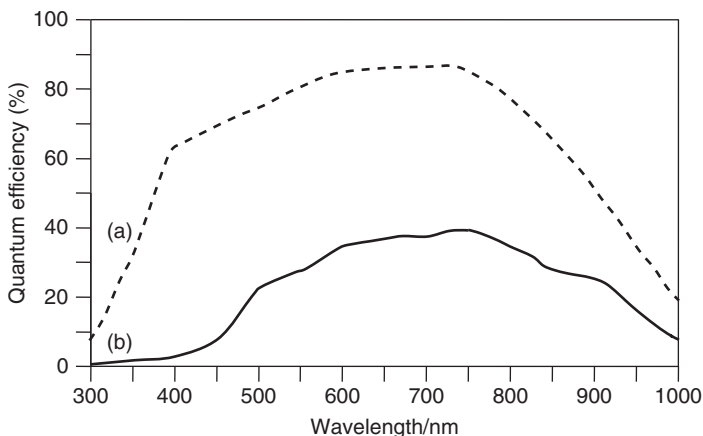


Figure 4.9 Typical response curves for (a) back-illuminated and (b) front-illuminated CCDs.

Although back-illuminated CCDs have a much higher sensitivity than front-illuminated CCDs, there are a few relevant disadvantages:

- Back-illuminated CCDs are more expensive than front-illuminated CCDs.
- Back-illuminated CCDs are thinner and therefore more fragile than front-illuminated CCDs.
- With back-illuminated CCDs light passes through a thin layer of silica and therefore an interference phenomenon can occur. This etaloning effect is reflected in oscillations in the sensitivity and is more pronounced with the use of longer laser wavelengths. Some CCD producers could reduce this effect, but it is best to test the CCD before purchasing it.

Another effect which is used to increase the sensitivity of the detector is the use of a deep depletion CCD. This term refers to the

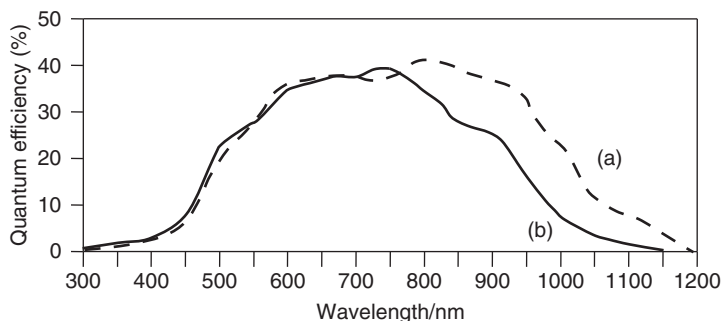


Figure 4.10 Response curve for (a) a typical front-illuminated CCD and (b) a deep-depletion front-illuminated CCD.

use of a doped silica chip, to increase the sensitivity at relatively longer wavelengths (see Figure 4.10).

In conclusion, it is clear that the most appropriate CCD needs to be selected in function of the wavelength area in which you want to work (cf. Figure 4.7).

4.2.4 Semi-conductor Detectors

To avoid fluorescence, it can be useful to use excitation in the infrared region (see Chapter 2). However, as can be seen from the response curves, CCD detectors are not sensitive in this spectral region. Therefore, FT-Raman instruments (with typical wavelength between 1100 and 1700 nm) are usually equipped with semi-conductor detectors with a small band gap (forbidden zone). This band gap should be sufficiently small to allow low energy photons (long wavelengths) to create electron–hole pairs in the semi-conductor. Often indium gallium arsenide (InGaAs) and germanium (Ge) are used. If the forbidden zone is sufficiently small that the low energetic photons can be detected, the detector background will unfortunately increase accordingly, since electron-hole

pairs are generated spontaneously. Therefore, these detectors need to be cooled, as the ‘thermal’ creation of electron–hole pairs is thus reduced. Various factors strongly influence the detection efficiency (e.g. doping and other manufacturing effects); it is therefore usual for Raman manufacturers to select detectors with the highest quantum efficiency or the lowest dark noise from a production batch. Therefore, the instrument sensitivity or the noise can change drastically after the replacement of a detector.

4.3 Filters

A Raman instrument contains a number of filters, each with their own characteristics. In general we can divide the filters into different categories (polarisation filters are not considered here):

- Neutral density filters (grey filters): these absorb the light with a quasi-constant value over the whole wavelength area.
- Long pass filters: These filters reflect the light with a wavelength under a certain limiting value; above this limiting value there is transmission.
- Low pass filters: Light with a wavelength shorter than a certain limiting value will be let through, whereas light with a longer wavelength is reflected.
- Band pass filters: These filters only let light pass of a certain wavelength (within a certain wavelength interval), the other light is reflected.
- Band block filters: These filters block light from a certain wavelength, but let the light through with another wavelength.

An important term when studying filters is the optical density (O.D.). The optical density of a filter is defined as:

$$\text{O.D.} = -\log(\%T)$$

where %T is the percentage of the transmitted light. In other words, if a neutral density filter allows 1% of the light to pass, the optical density of that filter is 2:

$$2 = -\log(0.01)$$

The higher the optical density, the more the filter blocks the light.

QUESTION 4.3

What is the optical density of a 10% and a 25% filter? If a given filter has an optical density of 0.30, what percentage of the light is transmitted?

Since the Raman effect is an intrinsically weak effect, it is important that the Rayleigh signal is suppressed. In the past, people used a double or triple monochromator. Nowadays, holographic filters are often used in Raman instruments. These filters consist of a gelatine-based material in between two glass plates, in which a standing wave pattern is generated. We can consider this filter as a pile of thin layers of gelatine with various densities. If this filter is irradiated with light of a suitable wavelength, destructive interference occurs in this filter, whereby the light of this wavelength is absorbed. It goes beyond saying that to get the optimal effect, the wavelength of the standing wave pattern (i.e. the thickness of the layers) is important. Therefore, during production of these filters this standing wave pattern is generated with a laser of (approximately) the same wavelength as the radiation to be blocked. You can vary the path length in the filter by tilting the filter at a certain angle. Thus, it is possible to adjust the precise position (wavelength) of the absorption band (notch) in the spectrum.

A disadvantage of holographic filters is that they degrade. During functioning, part of the laser light is absorbed, and the energy is released as heat. The standing wave pattern tends to blur

after heating and thus the spectral quality of the filter is reduced. Dielectric edge filters are also available on the market. They are a bit more expensive than holographic filters, but are said to degrade much more slowly. Dielectric films consist of alternating micrometer-thin layers of transparent materials (e.g. TiO_2 , SiO_2) that are sputtered on a glass substrate. Similar to holographic filters, their working principle is interference-based. However, unlike holographic filters, which are a type of band-block filters, dielectric edge filters are long pass filters.

QUESTION 4.4

What is the consequence of using dielectric filters (being long pass filters), when you want to record Stokes and anti-Stokes Raman spectra?

4.4 Dispersion Systems

As outlined in Figures 4.1 and 4.2, all spectrometers need to be able to disperse the light, in function of their wavelength. Light of different wavelengths can be separated either as function of space or in function of time. The first type of spectrometers use the principle of diffraction of light, whereas the second type use Fourier-transformations to obtain the result.

4.4.1 Systems Based on Diffraction of Light

The first type of spectrometer is commonly named ‘dispersive instruments’. The most simple diffraction instrument is a prism, where diffraction is based on the wavelength-dependent (angle of) refraction of the light in the prism. However, in modern spectrometers, usually diffraction gratings are used as dispersion system. A diffraction grating can be considered as a linear

repetition of reflecting (or sometimes transmitting) elements. The distance between the elements (typically referred to as grooves or lines) is similar to the wavelength of the light that needs to be dispersed. Due to the periodic variation in the diffraction grating, the scattered (or transmitted) light undergoes constructive or destructive interference, depending on the wavelength of the light and the angle under which the light is scattered, and thus a spatial resolution of the light, as a function of its wavelength is obtained. Two main types of gratings are differentiated: a reflection grating and a transmission grating. Dispersive gratings consist of a reflective substrate on which a diffraction grating is superimposed. The incident and diffracted light are on the same side of the grating. Opposite to this, when using a transmission grating the incident light beam and the diffracted light are on different sides of the grating (Figure 4.11).

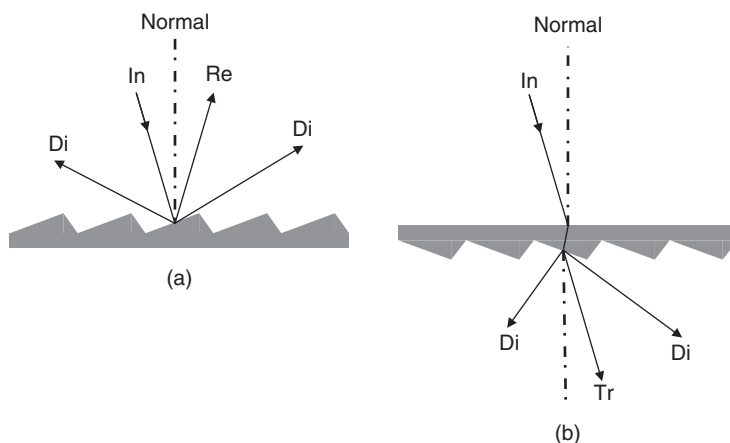


Figure 4.11 Schematic drawing of the lightpaths in (a) a reflection grating and (b) a transmission grating. In: incident beam; Re: reflected beam; Tr: transmitted beam; Di: Diffracted beams.

When monochromatic light is sent under an angle α to a grating, the light is diffracted and under different angles β_n constructive interference can be observed. The angles under which constructive interference is observed are dependent on the angle of incidence, the wavelength of the light and the groove spacing d of the grating. Considering two parallel rays of light, incidenting on a grating (Figure 4.12), constructive interference will only occur when the difference in pathlength between both scattered rays equals an integer number of wavelengths (λ). This is:

$$n \cdot \lambda = d (\sin \alpha - \sin \beta) \quad (4.1)$$

This relationship explains why, for monochromatic light, constructive interference occurs under different angles. The integer n is called the order of diffraction. From this equation it can be seen that the zero-order diffraction corresponds with a situation of reflection ($\alpha = \beta$), which is wavelength-independent. This means that under zero-order conditions the grating acts as a mirror.

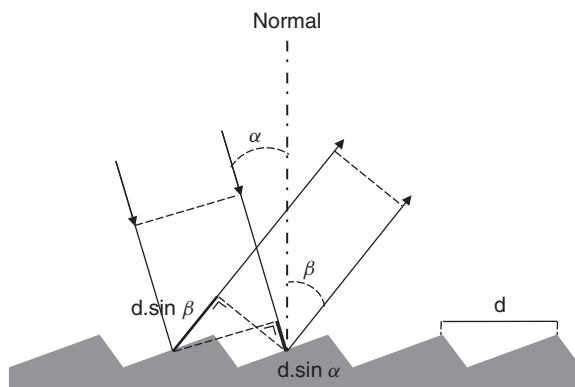


Figure 4.12 Diffraction at a reflective grating. The difference in pathlength between the two rays (in bold), equals $d(\sin \alpha - \sin \beta)$.

When changing the angle of incidence α between the grating and the incident beam (e.g. by rotating the grating), one can select the wavelength(range) that reaches the detector. Indeed, by rotating the grating, the angle between the detector and the normal of the grating, a signal is observed for a particular wavelength, if this angle corresponds with the angle of constructive interference β . The spectral resolution and spectral range, which is projected on the detector, are dependent of the groove spacing d .

However, when selecting a grating for a spectrometer, not only the desired spectral resolution and spectral window are of importance. For a given groove spacing, different gratings can have a different efficiency. Indeed, some materials are better suited than others for dispersion in particular wavelengths. Moreover, gratings can be coated and the exact shape of the grooves can be different. Therefore, it is important to study the efficiency curves of the grating when selecting it for a particular application.

4.4.2 *Fourier-Transform (FT-) Systems*

The central part of an FT-Raman spectrometer is the Michelson interferometer. This set-up (Figure 4.13) consists basically of a beam-splitter and two mirrors, of which one is fixed and the other is translated during the experiment. If we consider a monochromatic light source, which emits light in the interferometer, the light beam is split into two equal parts. 50% of the light is reflected, while 50% of the light passes the semi-transparent mirror. Both of these beams hit a mirror and are sent back to the beam-splitter, where they are combined and sent to the detector. Dependent of the difference in pathlength of these two beams, constructive or destructive interference occurs and the detector registers a signal or not, respectively. When the moving mirror is moved during this experiment, the detector detects, as a function of time (or, if you like, as a function of the position of the moving mirror) a fringe pattern.

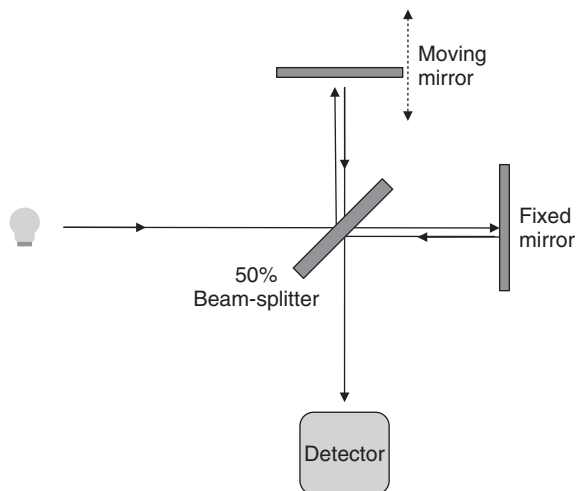


Figure 4.13 Michelson interferometer, the main component of an FT-Raman spectrometer.

During a Raman-experiment, light of different wavelengths (a spectrum) is sent to the interferometer. Each of these wavelengths generates its own fringe pattern and the fringe patterns of all wavelengths that are present in the spectrum are superimposed and detected by the detector. Thus, a so-called interferogram is obtained. Usually, the quality of an interferogram resulting from a single translation of the moving mirror is of poor quality, due to high noise levels. However, to improve the quality of the interferogram, multiple scans (typically a few hundred or thousand) are recorded one after the other and added together. In order to obtain a normal Raman spectrum, a mathematical operation is performed on the interferogram, namely an inverse Fourier-transformation. The spectral resolution that can be obtained with an FT-instrument, is related to the distance the mirror travels per scan. This can be understood by realising that for a given wavelength the number of

fringes that is detected is dependent on the distance that the mirror travels. In order to be able to perform a precise deconvolution, sufficient fringes need to be present. It should be noted that, contrary to dispersive instrumentation, there is no trade-off between spectral resolution and spectral coverage. Often, people mention the multiplex-advantage when discussing FT-Raman spectroscopy. By this term it is meant that all wavelengths are determined simultaneously, although using a single-channel detector. In contrast to this, dispersive spectrometers when using a single-channel detector, need to scan all the wavelengths one after the other. Usually, the movements of the moving mirror are checked with a second laser, which allow for excellent frequency precision.

4.5 Components for Transportation of Light

Apart from the filters, Raman instruments contain other optical components (e.g. mirrors, lenses, etc.) to bring the laser light to the sample, and to lead the scattered light to the Raman spectrometer. In general, two approaches exist for this: the use of a set of lenses and mirrors and/or the use of glass fibre optics. In any case the lenses and mirrors need to be equipped with the appropriate coatings to enable the transmission, respectively the reflection as high as possible. For instance, when working in the infrared region, it is of the utmost importance that the optical components are water-free, as this strongly absorbs infrared radiation, which not only causes less intense spectra and increased noise levels, but the heat which results from the absorbed radiation may cause damage to the components.

The transmission of light through glass fibres is based on the total reflection of the light beam, against the walls of the glass fibre. It is generally thought that the greatest losses with use of glass fibre optics take place at the extremes. There are different parameters which can play a role:

- The material of which the glass fibre is made determines the absorption and therefore also the transmission efficiency of the light. Therefore it is necessary to opt for a glass fibre with few -OH functional groups, because they may absorb the light. The fibre may have to be applied with a suitable coating.
- The diameter of the glass fibre determines how much light can be sent through the cable: it is easier to focus the laser beam in a thick glass fibre than in a thin glass fibre. On the other hand it is true that with a thin fibre you can work in single mode, which means that less band tailing will occur and that the laser spot on the sample will spatially be better defined. This is necessary if you want to work in a confocal way.
- The numerical aperture of the fibre determines the maximum solid angle with which the beam is sent into the fibre and under which the beam leaves the fibre.
- The angle under which the fibre is cleaved determines the direction with which the laser beam leaves the fibre.
- The geometry with which the different fibres are placed also determines the result. It is important that there is an overlap as large as possible between the volume irradiated with exciting beam, as the area which is covered by the collection fibres. There are different measurement geometries possible for the probe heads (Figure 4.14).

When using optical fibres one has to consider that the glass fibres themselves can also initiate a Raman signal or a fluorescence signal. Therefore, filters need to be used to avoid or eliminate these signals (Figure 4.15). In the probe head, before hitting the sample, the laser beam passes through a bandpass filter. Thus, the beam is 'cleaned' and possible signals with other wavelengths are removed, in order that only laser light reaches the sample. The back-scattered light passes through a band rejection filter before entering the collection fibre. There the most intense signal, the Rayleigh line, is removed.

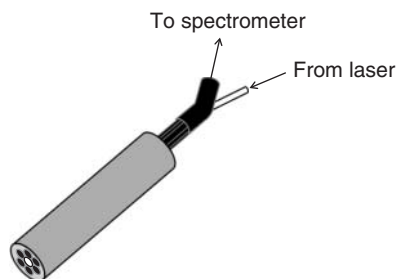


Figure 4.14 Example of a six around one geometry in a glass fibre probehead for Raman spectroscopy.

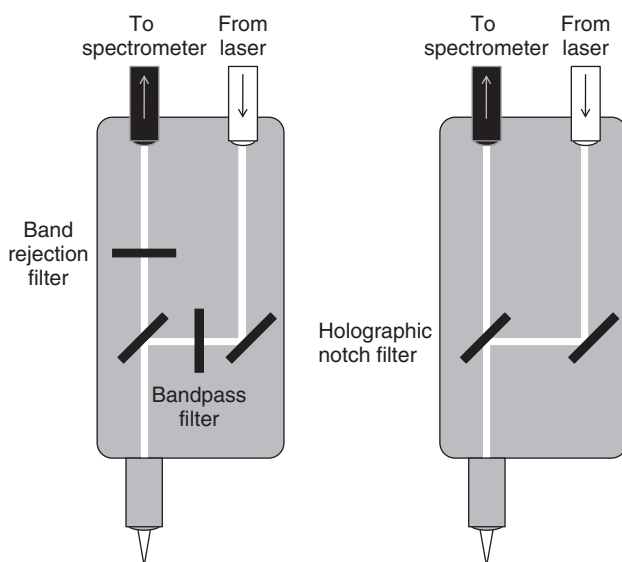
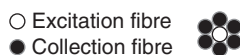


Figure 4.15 Schematic design of two fibre optics probe heads for Raman spectroscopy.

The Rayleigh line does not yield useful information for Raman spectroscopists, but if not removed it would induce a Raman or fluorescence signal in the collection fibre, which would overwhelm the collected Raman spectrum. A more compact design consists of using a single holographic notch filter (or dielectric filter) that acts as a mirror for the laserline, while light of other wavelengths can pass.

4.6 Sample Chambers and Measurement Probes

For Raman spectroscopy, different types of sample chambers and measurement probes were designed. It is impossible to discuss the details here of all types. Therefore we will limit ourselves to some important, general characteristics of this interface between the sample and the spectrometer. These principles will therefore be illustrated through a few examples.

From the formula for the intensity of the Raman signal, it can be concluded that, in order to obtain a signal as intense as possible, various factors are important: the intensity of the laser beam and the number of molecules that are irradiated. Furthermore, the collection of the Raman diffused light needs to be conducted as efficiently as possible. If we perform macroscopic analyses, then the number of analyte molecules (concentration) is a characteristic of the sample in which the analyst usually does not interfere (unless a pre-concentration on a substrate is done).

With macroscopic analysis of transparent materials, it can be interesting to make the path length in the sample as long as possible: this way the laser can interact with as many molecules as possible. This principle is applied when using gas cells, where they let the laser light go back and forth through a sample room filled with gas.

A similar principle is often used with the analysis of liquids, when part of the sample vessel is covered with a reflecting surface.

The intensity of the laser radiation on the sample needs to be as high as possible, without damaging the sample. Therefore it is necessary that the light is sent as efficiently as possible through the Raman spectrometer. The lens, which focuses the laser light on the sample, needs to have a transmission as high as possible. When selecting the objective lenses for these purposes some characteristics are important.

Firstly, the transmission of the laser light through the objective² needs to be as high as possible. Therefore, the objectives need to be made of a suitable type of glass. A typical problem for the use of intense IR lasers is that the lenses and the IR-coating may not contain any water: by absorption the lens warms, whereby small lens deformations may occur and the beam is not well focused. The lenses might be treated with an anti-reflective coating.

In general, there are two types of important image-deformations which can occur to the lenses, namely spherical and chromatic aberration. Spherical aberration occurs with a single lens and is formed by the beams which go through the centre of a lens and are not focussed at the same focal point as beams which are refracted outside the lens axis. It is clear that the larger the solid angle of the lens, the stronger this lens aberration is. Chromatic aberration is formed because the light with different wavelengths is deflected differently by the lens and therefore has a different focal distance. To correct for these aberrations, compound lenses are usually used for microscope lenses: a stack of different lenses, fitted in one housing, tries to correct for these aberrations.

² Objective lens: here the lens which focuses the laser light on the object is named the objective lens, although this lens does not necessarily have to be connected to a microscope. For some Raman measurements, for instance, telescope lenses are used.

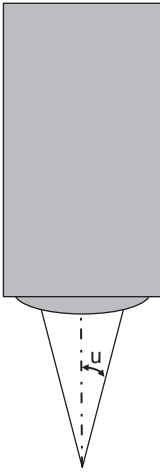


Figure 4.16 Schematic drawing of the aperture cone of an objective lens.

An important parameter, which describes the size of a conical beam of light that can pass through a lens, is the numerical aperture (N.A.). This quantity can be calculated with the formula:

$$\text{N.A.} = n \cdot \sin u \quad (4.2)$$

with n the refractive index of the medium and u the half top angle of the light cone (Figure 4.16). Therefore, the N.A. is a measure for the amount of light which can be collected with the objective lens. In general, it can be said that for most objectives the N.A. becomes greater at a decreasing focal distance. The refractive index n for air is equal to 1; in practice the N.A. for normal objective is 0.95 at the very most. If higher N.A.'s are required, then another medium needs to be present between the objective lens and the object (e.g. water or immersion oil, which have a higher refractive index). Furthermore, certain objectives are corrected for the use of cover slides: these thin layers of glass have an refractive index which is different from 1,

which causes the focal point to be at a different distance than with noncorrected objectives.

Other important characteristics of the objectives are:

- the transmission efficiency: the higher the transmission efficiency, the more light can pass the objective, and the fewer losses occur as a result;
- the enlargement: determines how the laser beam is focused, and therefore which surface is analysed on the object/sample;
- the working distance: the space between the bottom edge of the fitting of the lens and the focal plane;
- the focal distance: the distance between the lens and the focal plane;
- the iris: the diameter of the lens; this one needs to be greater than the diameter of the light beam which is to go through the lens.

One of the often used sample–spectrometer interfaces is a microscope: the laser beam is led into the microscope unit, whereby the microscope objective is used as focusing lens. The same objective lens is used to collect the Raman-diffused light and to send it to the spectrometer. The big advantage hereby is that pieces of sample can be measured with a very small diameter, allowing us to study inhomogeneities.

The lateral resolution is defined according to the Rayleigh criterion, where the resolution δ_p with the illumination of the object with a parallel light source (e.g. laser beam) is given by:

$$\delta_p = 1.22 \cdot \lambda / \text{N.A.} \quad (4.3)$$

with λ the laser wavelength and N.A. the numerical aperture of the lens. This limit value, however, is not reached in practice. Besides the lateral resolution, the depth resolution also plays an important role. This depth resolution can be greatly improved by confocal

measurements. Notice that in what follows, people consider that no significant light refraction nor absorption occurs in the sample, which can seriously change the measured volume.

Opposite to classical microscopy, where the field is illuminated homogenously, with confocal measurements spatial filtering is used, with the use of pinholes or diaphragms. This assembly isolates the light from a specific plane in the sample which coincides with the illuminated part, and eliminates the radiation efficiently coming from other planes which are out of focus. With this set-up it is possible to avoid the Raman signal and the fluorescence contribution of areas which are not in focus. An approximate formula for the maximal obtainable depth resolution is given by:

$$\delta_z \geq \left| \frac{4.4 \cdot n \cdot \lambda}{2\pi \cdot (\text{N.A.})^2} \right| \quad (4.4)$$

An experimental set-up for confocal measurements is shown in Figure 4.17, where it is illustrated how only the radiation of a well-defined depth can pass to the spectrometer. In practice a pinhole or diaphragm is placed in the collected light beam, or the light is led in a glass fibre, where the entrance of the glass fibre functions as the confocal opening.

4.7 Noise in Raman Spectroscopy

Noise is inherent to every spectroscopic technique. With the term ‘noise’ we mean all possible signals that are detected and that do not contain relevant information. Noise can seriously influence the precision of the obtained results. Typical examples of noise in Raman spectra are fluorescence, spikes and background noise. Spikes are said to be caused by cosmic rays that accidentally hit the detector. They result in sharp peaks in the spectrum (typically only few

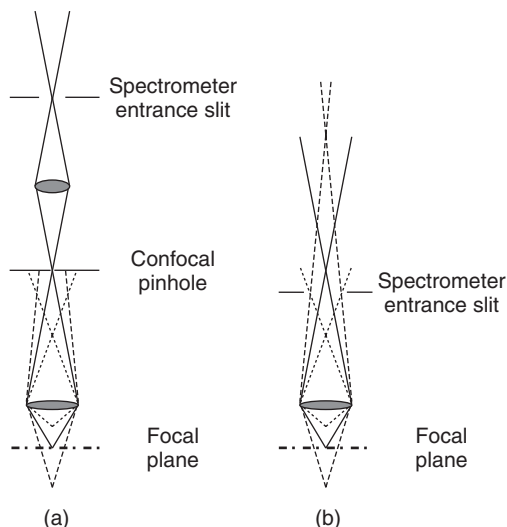


Figure 4.17 Scheme of a confocal (a) and a conventional (b) microscope, coupled to a spectrometer.

pixels wide) and are not reproducible: when recording the same spectrum again, no signal is detected on this spectral position.

The total noise level (σ) contains contributions of different factors, of which some are inherent on the sample (σ_s), some depend on the instrumentation (σ_i) and some on the signal processing (σ_p):

$$\sigma = \sqrt{(\sigma_s^2 + \sigma_i^2 + \sigma_p^2)} \quad (4.5)$$

4.7.1 Noise Originating from the Sample: σ_s

It is a basic rule in spectroscopy that all spectroscopic processes are subject to a certain uncertainty. The uncertainty on a given

spectroscopic signal is fundamental and is, by laws of statistics, given by:

$$\sigma_s = \sqrt{S} \quad (4.6)$$

where S is the signal intensity. This type of noise is commonly referred to as shot noise, and cannot be avoided. Since, for dispersive spectrometers, the total measured signal is proportional to the time measured, it can be said that the shot noise is proportional to the square root of the time. When using an FT-instrument, noise is proportional to the square root of the number of scans.

It should be noted that the shot noise is proportional to the signal intensity. In many cases the signal is composed of different portions, such as the Raman signal of the analyte (in which we are interested), the Raman signal of other components in the sample (matrix), fluorescence detected by the detector, stray light entering in the detector, etc. All these different signals contribute to the total shot noise level. Often it is possible to correct for certain signals, by performing mathematical operations, such as spectral subtraction of a blank to correct for matrix influences or mathematical subtraction of a polynomial to correct for broadband fluorescence signals. However, it is important to understand that it is not possible to correct for the contribution of the shot noise, caused by these interferences.

Since all these signals are proportional to time, one can expect that the signal to noise ratio of a spectrum can always be improved by measuring for a longer time. However, this effect is minimal, since the major contribution to the noise can be due to the background noise.

An important distinction needs to be made between the use of dispersive Raman instruments and the use of FT-spectrometers. In a dispersive instrument, the shot noise on a certain band position corresponds to the square root of the signal, as recorded at that specific pixel. Indeed, the signal on a certain position is not influenced by the signal on another pixel. When recording FT-spectra,

contributions of all wavelengths hit the detector simultaneously. Therefore, the shot noise in an FT-instrument is not only determined by the shot noise of the signal, but is dependent on the total detected signal. This means that a small Raman band at a certain position can be overwhelmed by the noise of the fluorescence in another region of the spectrum.

4.7.2 Noise Originating from the Raman Instrument: σ_i

All components in a Raman instrument can contribute in a way to the Raman spectrum. For the sake of good spectrometer engineering an instrument is designed with low spectrometer noise. If certain components (e.g. glass fibres) give rise to extra signals, shot noise (see previous paragraph) is associated with this contribution.

Detectors are also a source of noise. This is due to the detector dark signal: a certain number of electron–hole pairs are spontaneously generated, even when no photons are present. This thermal generation can be reduced by cooling the detector. This dark signal contributes to the detector shot noise and is also proportional to the square root of measurement time. Detector noise is usually the limit for FT-Raman experiments.

Lasers also contribute to the instrument generated noise level in a spectrum. Some lasers typically do not emit light with a constant intensity, but tend to flicker (depending on the type of laser). FT-instruments are hardly sensitive to this effect, since all wavenumbers are measured simultaneously. Also dispersive spectrometers with a fixed grating are rather insensitive to flicker noise, since the whole spectral range is measured at once. However, when the diffraction grating is tilted and different parts of the spectrum are recorded in sequence – or a single-channel detector is used – the spectrum might suffer some influence of laser flickering.

4.7.3 Noise Originating from the Signal Processing: σ_p

The processing of the electrical signals is also subject to noise. An important type of noise in this context is detector readout noise, which is generated when converting the analogue signal (a number of electrons) to a digital value in the computer. It originates from, amongst others, the amplifiers and other electronical components and the analogue-to-digital-converter. The detector readout noise is not proportional to the measurement time, and detector readout noise is usually only encountered when performing very short measurements or when measuring very weak signals (e.g. gases or monolayers of molecules).

One should as well be aware that mathematical operations on spectra (spectral post-processing) can have an influence on the noise levels. For instance, multiplying the spectral values with a constant (without deviation) changes the absolute noise level, but the signal to noise ratio remains constant. However, adding (or subtracting) a constant (e.g. during baseline subtraction) does not change the absolute noise level, but the signal to noise ratio is influenced (as the signal intensity changes). The rules that apply in these cases are commonly named 'error propagation'.

4.8 Summary

In this chapter, the general structure of Raman instrumentation has been described and each component has been discussed in detail, so that the reader can understand their use. Special attention has been given to the laser, as monochromatic light source and to the CCD detectors and filters. We have discussed in detail the fundamental differences between a dispersive instrument and a Fourier-transform (FT-) Raman spectrometer. Moreover, by now, the reader should

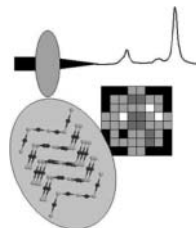
also be able to understand the different sources of noise in a Raman spectrum and see how a dispersive and an FT-Raman spectrum are differently affected by noise.

Further Reading

- Gardiner, D.J. and Graves, P.R. (eds), *Practical Raman Spectroscopy*, Springer, New York, 1988.
- Graselli J.G., Bulkin B.J. (eds), *Analytical Raman Spectroscopy*, John Wiley & Sons, Inc., New York, 1991.
- Laserna, J.J (ed.), *Modern Techniques in Raman Spectroscopy*, John Wiley & Sons Ltd, Chichester, UK, 1996.
- McCreery, R.L., *Raman Spectroscopy for Chemical Analysis*, John Wiley & Sons, Inc., New York, USA, 2000.

Chapter 3

Enhancement of the Raman Signal



Learning Objectives

- To understand the working principle of the Resonance Raman (RR) effect
- To be able to explain the enhancement principles that form the basis for Surface-Enhanced Raman Spectroscopy (SERS)
- To know some major approaches to prepare substrates for SERS

As already mentioned, the Raman effect is an inherently weak effect. Nevertheless, there are several mechanisms that can be used to enhance the Raman signal. The two most important approaches are resonance enhanced Raman spectroscopy (RR) and surface-enhanced Raman spectroscopy (SERS). These two approaches are explained in more detail in the next paragraphs.

3.1 Resonance Raman (RR) Spectroscopy

It can easily be demonstrated that the Raman intensity of a molecule is significantly enhanced when the frequency of the laser corresponds with an allowed transition to an electronic excited state of that molecule. According to the idealised model (see Figure 1.2), this would mean that the virtual state to which the molecule is excited, corresponds with an electronic excited state. Since this (allowed) transition corresponds with a transition to a real state, it is easily understood that this transition is favourable.

The main advantage of this approach is the enhanced sensitivity for specific molecules. On the other hand, this may have the disadvantage that the analyst is focussed on a specific molecule, and that weaker scatterers in the mixture are not easily detected. It is clear that, if someone wants to perform resonance Raman spectroscopy, it is of the utmost importance to select the laser wavelength in function of the molecule on which the research wants to focus.

3.2 Surface-Enhanced Raman Spectroscopy (SERS)

SERS is a technique in which the Raman signal of specific molecules is enhanced by bringing them in contact with certain substrates with a well-defined morphology, usually noble metals (e.g. gold, silver). It is the aim to bring a thin layer of the analyte on the substrate and the Raman signal can in some cases be enhanced with a factor 10^6 . This approach is typically used for the analysis of specific molecules, in solution or gas phase (after adsorption to a substrate), which may lead to the application in sensors. Often, molecules with extended conjugated pi-systems, like aromates, are examined. When using SERS, it is of the utmost importance to select the substrate in a way that the SERS effect is

maximised. Some specific parameters have to be selected carefully, such as the metal (e.g. Au, Ag), the particle size (when using a colloid) or the roughness. Particularly field enhancement (one of the contributing effects, see below) is high with metals with a high reflectivity (e.g. Au, Ag) and the effect is dependent on the type of material in combination with the laser wavelength on hand. Silver substrates tend to be interesting when used in combination with green or blue lasers, while gold substrates tend to perform better when used with red lasers.

3.2.1 Working Principle of SERS

The SERS enhancement is usually ascribed to two different effects, namely field enhancement and chemical enhancement, where the first factor is thought to be the most important. We give a simplified description of the SERS effect, where we try to explain the main factors in an easy to understand way.

(a) Chemical Enhancement

Chemical enhancement counts for an enhancement effect of up to ca. 100 times. It occurs by interaction of the adsorbed molecule and the metal surface. SERS is a surface-effect: i.e. the molecules close to the surface of the substrate are analysed. As the observed Raman signal is related to the number of molecules that are present in the sampling volume, all interactions between the substrate and the molecules that result in a higher analyte concentration close to the surface enhance the obtained Raman signal. Experiments have been performed with polytetrafluorethylene (PTFE, Teflon) coated glass slides, as these have a different polarity than traditional glass slides and thus may cause some preconcentration of compounds. Moreover, when working in an aqueous solution, due to the surface tension of the water, the droplet does not spread

over the whole surface of the slide. Similarly, interactions may take place between metallic surfaces and the analyte molecules. These interactions can be classified as physisorption or chemisorption effects. Physisorption refers to relatively weak interactions (e.g. electrostatic interactions, dipole–dipole effects, Van der Waals interactions, etc.), whereas chemisorption is used to describe the case where a chemical bond is formed between the substrate and the analyte molecule. As a consequence, it may be possible to observe these bonds in the resulting Raman spectrum (different Raman bands are observed compared to the bulk spectra) or bandshifts (compared to the bulk spectrum) may occur due to the interaction.

Another aspect is the orientation effect. As discussed before, for anisotropic molecules, the Raman effect is orientation dependent. Therefore, if the molecules are well aligned, orientation may enhance the Raman effect. Depending on the interaction with the substrate, some molecules can have a preferential orientation, which as such counts for an enhancement effect. For instance, if the substrate interacts with the π -electrons of a benzene molecule, it is likely that the benzene molecule is oriented parallel to the surface of the substrate.

Apart from these preconcentration (chemisorption and/or physisorption) and orientation effects, another chemical enhancement effect may occur, which may be explained by using charge-transfer theory. We will explain this in a rather intuitive way. When describing the resonance Raman effect, we discussed that resonance enhancement occurs when the virtual energy level corresponds with a real state (e.g. an electronic energy level of the molecule). In metals, the orbitals of all the single elements overlap, no longer resulting in relatively narrow energy levels as known for single atoms or even simple molecules. However, we must consider overlapping orbitals, where a certain number is filled with electrons: this is named the conduction band. Because the interaction between the analyte molecule and the energy levels

of the molecule may be shifted, as a result of the interaction of the molecule with the metal, the electron cloud of the molecule may be disturbed. Hence electronic energy levels may shift in such a way that the conditions for resonance enhancement are fulfilled. Moreover, it is also possible that during the Raman experiment, there is an excitement towards an energy level in the conduction band of the metal – which is a real state and thus resonance enhancement may occur between the vibrational ground state of the molecule and the conduction band of the metal.

(b) Field Enhancement (see Figure 3.1)

From the theoretical discussion of the Raman effect, we know that the measured Raman signal is proportional to the strength of the oscillating electromagnetic field (i.e. the intensity of the laser beam). As a consequence, if the molecules are irradiated with a more powerful laser, the signal is increased. Field enhancement increases the electromagnetic field strength as experienced by the analyte molecules and occurs if (rough) metal surfaces are exposed to laser light with a specific wavelength. If a small metallic particle is positioned in an oscillating electromagnetic field (like laser light), the electrons on the surface of the particle undergo forces and are moved from one part to another. If the particles are sufficiently small, the electrons oscillate in phase with the electromagnetic radiation and a (dipolar) surface plasmon is formed. These moving electrons generate an electromagnetic field. As the electrons move in phase with the incident laser beam, the generated electromagnetic field is in its turn oscillating with the same frequency as the movement of the electrons, hence the incident laser beam and is also in phase with it. As a consequence, the analyte molecule not only experiences the electromagnetic field of the laser beam, but also interacts with the generated oscillating field. An analogy can be made with the effects as observed from broadcasting antennas: the

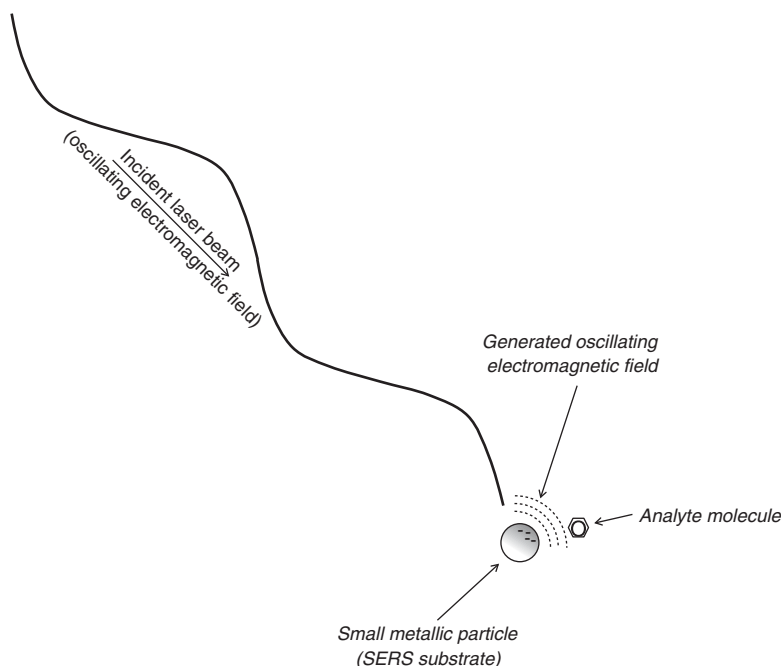


Figure 3.1 Schematic overview of the working principle of field enhancement.

main antenna (laser) emits a signal, that is picked up by an antenna in the field (metal particle). This field antenna (metal particle) emits the signal and acts as an amplifier. The signal is picked up by the antenna on the radio or television set (analyte molecule), where it is transformed into an electrical signal.

From theoretical calculations, based on idealised models (e.g. perfect spherical metal particles, with the same size), it can be understood that the larger the distance between the analyte molecule and the metal particle, the smaller the enhancement is. Indeed, the small metallic particle acts as a spherical source,

emitting a spherical electromagnetic field, and the electromagnetic flux diminishes with the third power of the distance to the source. More precisely, the field enhancement is proportional to $(r/d)^3$, where r is the radius of the particle and d is the distance between the centre of the metal particle and the analyte molecule. Therefore, field enhancement is maximal if there is an intense contact between the analyte and the metal surface (r/d equals 1) and drops if the distance becomes larger. However, this reduction of the effect is less severe, the larger the metallic particles are (for a given d , the ratio $(r/d)^3$ is larger if r is larger). However, the field enhancement theory is only valid if the particles are sufficient small, compared to the laser wavelength (typically $r < (\lambda/10)$).

In general, field enhancement strongly depends on the optical properties of the metal. The metal should have a high reflectivity of the wavelength-range of the laser light. The metal and the laser wavelength need to be adapted. In general, Ag is used when performing SERS experiments with blue or green lasers, whilst Au substrates are used with red lasers. The average size of the metal particles, or the roughness of the metal surface, is critical. As mentioned before, particles should be much smaller than the laser wavelength. But, not only is the average size important: also the particle size distribution can seriously influence the results of the experiment. Moreover, their shape is also of importance: two differently shaped particles may have the same average diameter, but may have a totally different curvature of their surfaces.

3.2.2 Preparation of SERS Substrates

SERS substrates generally have a limited shelf-life: the substrates degrade over time, for instance as particles aggregate to form larger particles, as metal surfaces might oxidise or as atmospheric compounds might contaminate the surface. Therefore, SERS substrates are typically prepared in the analytical lab before the analysis is

performed. Depending on the type of substrate used and the way of preparing it, the substrates can be preserved under an inert atmosphere from a couple of days to a couple of weeks. During the preparation of the SERS substrates, it is of the utmost importance to work with highly pure chemicals and to follow the procedures in a very strict way. If not, the results are hardly predictable: inaccurate procedures might result in differently shaped or sized particles, resulting in lower enhancement factors; impurities may also modify the expected particle shapes, but can also give rise to Raman signals that cannot be attributed to the analyte. In literature, many different procedures are described to produce SERS substrates. A detailed description of these procedures is beyond the scope of this introductory text. However, we will describe here some basic techniques used to produce SERS substrates.

(a) Colloids

A commonly used type of SERS substrate is a colloid of metal particles. As particle size is of the utmost importance to obtain optimal surface enhancement, the particles are kept in suspension and the degree (and speed) of agglomeration is well controlled. During production of the colloid, one typically starts with metal salts that are reduced under controlled circumstances. The quality of the obtained colloid is usually controlled by using UV–VIS absorption spectroscopy – indeed the interaction that causes absorption in the UV–VIS range of the electromagnetic spectrum, is due to transitions between different electronic energy levels and can be related to the phenomena that lead to field enhancement. Typically, the analyte molecules are added to an aqueous suspension of colloidal silver or gold particles or an aliquot of the colloid suspension is spiked to the analyte-bearing solution. Alternatively, the colloid is immobilised on a substrate before the analyte solution is added. Provided the

analytical procedure is well performed and the aggregation times are respected, reproducible results can be obtained.

(b) Sputtering

SERS substrates can be prepared by using sputtering. This is a technique where, under an inert atmosphere, a metal target is ablated under bombardment of ions or photons (e.g. laser sputtering). Thus, metal particles are vaporised and precipitate on a surface. When vaporised silver is deposited on, for instance, a glass substrate, the atoms tend to form small aggregates, so-called silver islands. Obviously, this is only the case when the film thickness is small. Although glass substrates are frequently used, other substrates have also been used to provide silver substrates. After this vapour deposition, the samples are cooled and the substrate is exposed to the analyte solution before analysis. As moisture or oxygen in the atmosphere might modify the SERS surface, the substrates are usually preserved under an inert atmosphere or in vacuum.

(c) Electrochemical Production

A third approach to create a roughened metal surface is based on electrochemical processes. In this case, a silver electrode is used. The approach consists of normal electro-analytical procedures, where the polished electrode is brought in an electrochemical cell containing a KCl solution, with a calomel electrode as counter electrode. The electrode surface is converted into a SERS substrate, by letting the electrode undergo several oxidation-reduction cycles. In the first stage, the silver surface is oxidised towards Ag^+ ions, in the second phase the Ag^+ ions in the solution are reduced at the surface to metallic silver (Ag^0). So, basically, in the first stage of the cycle the metal surface is oxidised and part of the electrode

is brought into solution, while in the second half of the cycle, the ions in solution are precipitated at the surface and reduced. It is obvious that the Ag^+ ions that are reduced at the electrode surface will not be well aligned with the electrode surface and that this way a roughened surface is created. After applying several of these oxidation-reduction cycles, the surface is taken out of the cell, rinsed with water and the analyte is brought into contact with the rough metal surface.

(d) Etching

The previous procedure can be considered as an electrochemical way of etching or roughening the metal surface. Similarly, nitric acid can be used to roughen the surface. This approach is far more simple compared to the electrochemical etching, leading to much higher reproducibility. However, the obtained enhancement factors are lower.

3.2.3 SERS Active Molecules

Theoretically, all types of analyte molecules (as far as they are Raman active) can undergo to a certain extent surface enhancement. However, when studying the literature, some molecules are much more sensitive to SERS than others. Thinking on the two types of enhancement, chemical and field enhancement, it is clear that the first type is determined by the type of analyte molecule that is studied, but that the latter type of enhancement is only slightly affected by the analyte molecule. Indeed, field enhancement is affected by the properties of the metal and the laser. Therefore, properties of the molecules under study that interfere with any of the chemical enhancement processes, increase or decrease the surface enhancement. Typically, molecules with loose bound

electrons (e.g. conjugated systems or aromates) are more likely to be sensitive to charge-transfer interactions. Also, conjugated systems can also interact with the metal surface, to enhance the signal due to physisorption or even chemisorption. Moreover, due to their shape, some molecules may have a preferential orientation towards the surface, which enhances the signal as well.

3.2.4 Advantages and Disadvantages of SERS

The main advantage of SERS is obviously the enhancement of the Raman signal, and as a consequence the lower limits of detection, compared to normal Raman spectroscopy. The approach has definitely proven its value. However, there are also some disadvantages of this approach. Firstly, the approach requires preparation of a substrate, which is a critical step in obtaining good SERS spectra. If quantitative analysis is required, the request for reproducibility can be critical and requires good laboratory skills. Moreover, it is of the utmost importance to work with (ultra-) pure reagents, as contaminants may either change the properties of the produced surface, either produce their own SERS signal. Secondly, critical in the SERS approach is that the analyte molecule is in close contact with the substrate. For solids, this requirement is a bit more difficult to reach, compared to liquid samples. Sometimes, a droplet of colloid suspension has to be positioned over a solid sample, in order to measure this. Generally, sample preparation is more elaborate than for standard Raman experiments. Thirdly, in a mixture not all molecules yield similar enhancement factors and spectra of certain components may overwhelm the spectrum of other products in the mixture. Finally, the obtained SERS spectra are often hard to compare with standard Raman spectra, which can hamper the spectral interpretation and band assignment.

INTERMEZZO 3.1 THE ANALYSIS OF ORGANIC DYES BY SERS

Dye analysis is a very challenging topic in the analysis of cultural heritage objects. Dyes are – opposite to pigments – colouring agents that are soluble in the binding medium that was used. As a consequence, these colorants are not present as single particles. Dyes are usually of organic nature. In the past, they were typically extracted from plants or insects and are, during their application, fixed on the support. Often, this fixation involves some chemical reaction, like an oxidation, or the use of a mordant: a compound that forms a complex together with the dye molecules, and thus fixes them on the support.

The analysis of these organic dyes is a difficult task. Not only are these colorants typically present in very low concentrations, but they are also usually present in mixtures. Plant extracts contain in general a series of molecules and dyes can be deliberately mixed by the artist. Moreover, during history the dyes may have undergone degradation. When performing Raman spectroscopy, the low concentrations lead to very noisy spectra and fluorescence very often hampers the analysis. As a consequence, it is often not possible to identify the dye in an artwork (e.g. on a tapestry) by using normal Raman spectroscopy.

Therefore, surface-enhanced Raman spectroscopy can be used to enhance the Raman signal. When working on artefacts, sampling is usually very limited, as the object cannot be damaged. As a consequence, it is also not possible to apply a silver colloid on the artwork. Therefore, different approaches have been developed, each trying to minimise the amount of sample that is required. One interesting approach is the use of a bead of a polymer hydrogel, loaded with a mixture of water, organic solvent and complexing agent. This bead is brought into contact with the dye on the art object and after removal of the gel bead, a drop of silver colloid is added to the gel, before analysis under the Raman microscope.

In literature, a whole series of procedures can be found. Examples of dyes that were successfully identified include, amongst others, madder (alizarin), turmeric (curcumin), cochineal (carminic acid), etc. A broad range of artists' materials have been studied, including tapestries, water colour paintings, oil paintings, etc.

Further Reading

Brosseau, C.L., Casadio, F., Van Duyne, R.P., *J. Raman Spectrosc.* 42 (2011), 1305–10.

Brosseau, C.L., Rayner, K.S., Casadio, F., Grzywacz, C.M., Van Duyne, R.P., *Anal. Chem.* 17/81 (2009), 7443–7.

Leona, M., Stenger, J., Ferloni, E., *J. Raman Spectrosc.* 37 (2006), 981–92.

Leona, M., Decuzzi, P., Kubic, T.A., Gates, G., Lombardi, J.R., *Anal. Chem.* 83 (2011), 3990–3.

Pozzi, F., Lombardi, J.R., S. Bruni, M. Leona, *Anal. Chem.* 84 (2012), 3751–7.

Whitney, A.V., Van Duyne, R.P., Casadio, F., *J. Raman Spectrosc.* 37 (2006), 993–1002.

3.3 Summary

In this chapter, two important techniques have been described to enhance the Raman signal. The first approach, resonance enhancement, describes how an appropriate selection of the laser wavelength can cause serious enhancement of the Raman signal. In a second approach, surface-enhanced Raman spectroscopy, the analyte can be brought in close contact with a metal substrate, which can yield to chemical and field enhancement of the Raman signal.

Further Reading

Laserna, J.J (Ed.), *Modern Techniques in Raman Spectroscopy*, John Wiley & Sons Ltd, Chichester, UK, 1996.

McCreery, R.L., *Raman Spectroscopy for Chemical Analysis*, John Wiley & Sons, Inc., New York, USA, 2000.

Smith, E. and Dent, G., *Modern Raman Spectroscopy: A Practical Approach*, John Wiley & Sons Ltd, Chichester, UK, 2005.